Stellar Clusters & Associations

A RIA Workshop on Gaia

Proceedings

Granada, Spain, May 23 - 27, 2011

Edited by

Emilio J. Alfaro Navarro[1], A. Teresa Gallego Calvente[1] and María Rosa Zapatero Osorio[2]

[1] Instituto de Astrofísica de Andalucía - CSIC
[2] Centro de Astrobiología, CSIC-INTA

Contents

Preface

Gaia is the ESA scientific mission that the entire Galactic astronomy is awaiting with great eagerness. The huge quantity of objects to be observed and the variety and quality of the data foreseen make this experiment a landmark in the history of astronomy.

The GREAT consortium, financed by the European Science Foundation, was designed to organize the different European teams interested in making use of the Gaia data. In this way, the various meetings, workshops and conferences organized by GREAT have aimed at selecting scientific objectives, discussing exploitation strategies and producing tools that will make for the most rapid and successful use of these data.

Given the great quantity and variety of the data expected from Gaia, the scientific aims of the project comprise almost all of the most burning issues of Galactic physics. This workshop was designed to discuss those problems related with Stellar Clusters.

We do not believe it necessary to emphasise the impact that the study of these objects has on diverse fields of modern astronomy. The majority of the potential readers of these proceedings work on Stellar Clusters and well appreciate this second golden age that we are living through, and we are sure, or at least hope, that those not quite so familiar with these objects will draw this conclusion after reading them.

The SOC took charge of choosing the most relevant lines of investigation that could fit into a meeting of four-and-a-half-working days, and of selecting the astronomers who most represent these areas. Not all of these are here, but all who are here most certainly are. One of us, as chairman of the SOC, wishes here to thank the members of the committee for their availability, work and professionalism. Even though some of them were unable to attend the workshop, they nonetheless participated in its scientific design.

We also wish to thank the work of the LOC, most of which was the responsibility of the IAA's Stellar Systems Group, with the inestimable participation of other members of the Astrophysics Institute of Andalusia (CSIC) and the Astrophysics Institute of the Canaries. They made it seem easy to organize a workshop such as this. Yet there is always at least one difficulty: the funding. GREAT was unable to finance this occasion, but as commitments had already been attained we decided to seek funding from national sources. The Spanish Astronomy Infrastructures Network (RIA) supported the proposal and provided the majority of the budget. The Ministry of Science and Innovation, the Spanish Society of Astronomy, the Astrophysics Institute of Andalusia and the Astrophysics Institute of the Canaries covered the rest of the expenses.

These proceedings are a simple summary, black on white, of the work developed in the workshop, but those of us who experienced it know how great were the number of ideas, collaborations and projects conceived during those days in the Palacio de Congresos (Conference Centre) and in a few of the bars of the city of Granada.

The participating astronomers were the real heroes of the event, some of whom had the responsibility of opening sessions and of guiding the ensuing debates, but all with a praiseworthy zeal for participation. To all of them, to you, thank you for this productive and endearing meeting.

Emilio J. Alfaro, A. Teresa Gallego and María Rosa Zapatero-Osorio
Granada, December 2011

Oral Contributions

List of Topics

1. Gaia Status & Performances
2. Star Formation & Initial Mass Function
    a. Cluster Formation
    b. Embedded Clusters
    c. Initial Mass Function
3. Dynamical Evolution of Stellar Clusters
    a. Cluster Systems in Other Galaxies
    b. Spatial and Kinematic Distributions of Stellar Clusters
    c. Disruption and Destruction Mechanisms
4. Stellar Populations in Clusters
    a. Massive Stars
    b. Low-Mass Stars, Brown Dwarfs and Cluster Exoplanets
    c. Stellar Structure & Evolution
5. Star Clusters as Probes of Galactic Structure
    a. The Formation of the Milky Way
    b. Evolution of the Galactic Disk
    c. Structure of the Halo
6. Surveys Pre and Post Gaia
    a. Spectroscopic & Photometric Surveys
    b. Synergy with Other Space Missions

Chapter 1

Gaia Status and Performances

1.1 Gaia Status & Performances

Timo Prusti[1]

[1] European Space Agency

Abstract

Gaia is an ESA mission performing astrometry, photometry and spectroscopy of about one billion objects in our Milky Way Galaxy and beyond. The prime industrial contractor, EADS Astrium in Toulouse, is in the middle of the qualification and production phase integrating the satellite and payload for launch in 2013. The presentation will give a brief summary of the status of the spacecraft, operational ground segment elements and the launcher. The scientific performance estimates have been consolidated over the last months when more and more design values of hardware have been updated with the true values from tests. The latest performance estimates are available in the Gaia website (www.rssd.esa.int/Gaia) and will be summarized in this contribution.

Introduction

Gaia is the next European astronomy satellite to be launched in 2013. Gaia will perform astrometry, photometry and spectroscopy of more than one billion objects. The main scientific goals address the structure, dynamics and history of our Milky Way Galaxy, but Gaia will impact practically all disciplines of astronomy. The topic of this meeting, Stellar Clusters and Associations, will specifically benefit from Gaia. Fundamental information of distances and members will be gained with the Gaia measurements. Hipparcos made a revolution to cluster studies and Gaia, with a performance increased by orders of magnitude, is anticipated to achieve a new revolution.

As the assembly, integration and testing of Gaia is proceeding, the estimates of the scientific performance are also getting more accurate. In the recent major reviews, Gaia Spacecraft and Gaia Mission, the performance estimates did not significantly change anymore. Therefore the Gaia Science Team decided to update all science performance estimates of Gaia in a form suitable for the wider astronomical community. These estimates can be found on the Gaia web pages and are summarized in this contribution.

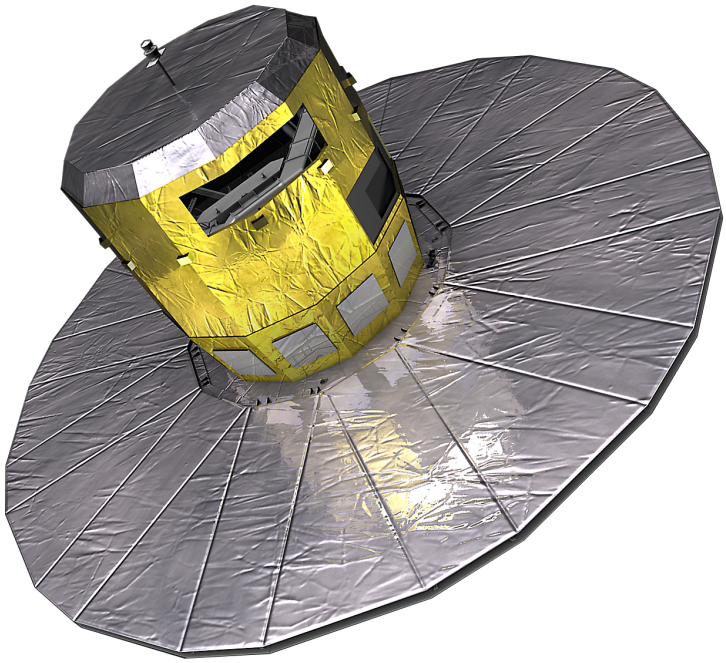

Figure 1.1: The Gaia satellite.

Status

In summer of 2013 the Gaia mirrors (except one of the M2 mirrors) will have been delivered to the prime industrial contractor. Out of the two lines of sight one has been completed in the structural model which has been vibrated successfully.

The Focal Plane Assembly has all CCDs installed marking a major milestone in the development. Also the prisms for the photometre have been delivered and all optical elements of the radial velocity spectrometre have been mounted. With the telescopes and focal plane units the scientific instrumentation of Gaia is getting ready.

In addition to the payload, the development of Gaia requires also new technologies in the service module. The most challenging elements, the Phased Array Antenna and Micropropulsion system, are being finalized for delivery to the prime contractor.

The flight hardware is progressing well, but two additional elements are needed for the mission. The launcher for Gaia will be the new Soyuz facility from French Guyana. The first launch in the Gaia configuration is expected in October 2011. Last but not least, the ground segment for commanding and data reception, done by the Mission Operations Centre, and processing, done by Gaia Data Processing and Analysis Consortium, are getting ready for the launch.

Scientific Performance

Full details of the scientific performance estimates can be found from the Gaia web pages (www.rssd.esa.int/Gaia). A selection of the main figures is presented here.

Astrometric Performance

The astrometric part of the mission is the one which cannot be conducted with ground based facilities due to atmospheric hindrance. Both the hardware of Gaia and the software being built to process the data indicate that the science requirement of an accuracy higher than 10 μarcsec

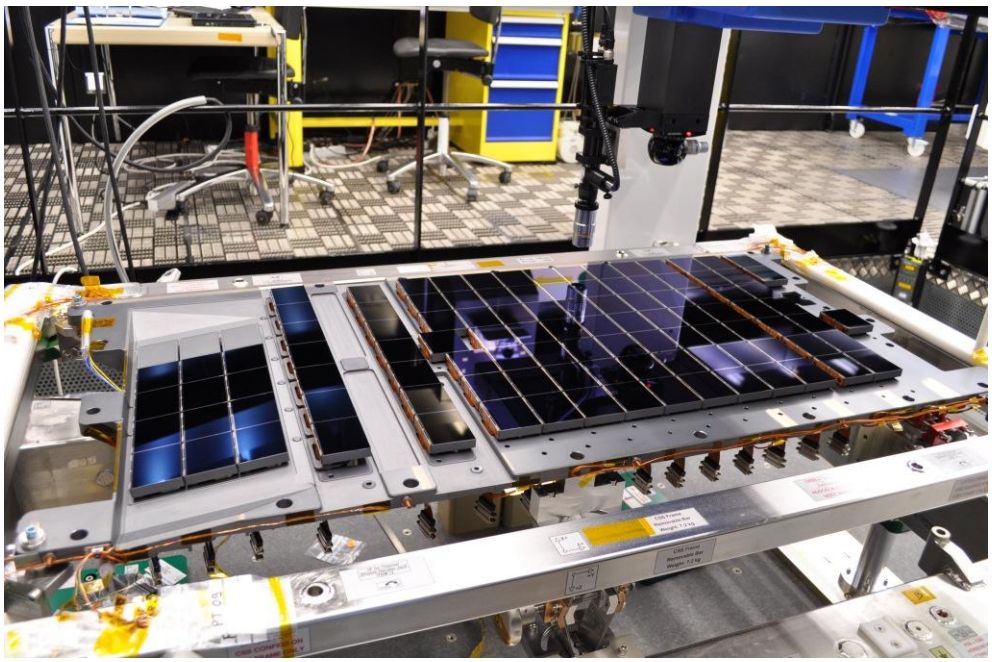

Figure 1.2: Gaia Focal Plane Assembly with all CCDs.

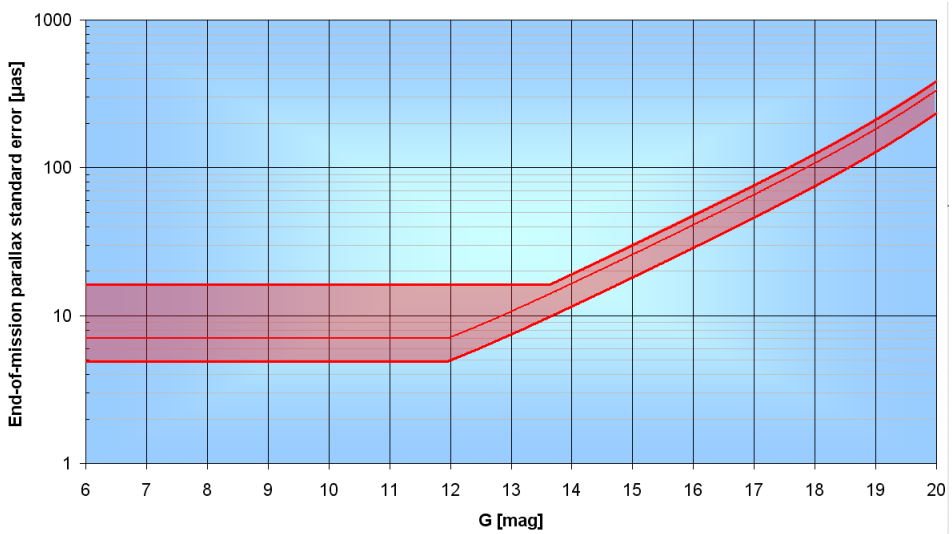

Figure 1.3: Gaia astrometric performance estimate range as a function of object brightness.

for bright star parallaxes can be achieved. The expected performance is plotted in Figure 1.3.

The position and proper motion accuracies can be deduced from the parallax accuracy estimates as detailed in the Gaia web-pages.

Photometric Performance

The photometry on board Gaia is done both with the astrometric instrument as well as spectrophotometry. While the astrometric instrument by definition is broad band (called G-band) to collect the maximum number of photons, also the spectrophotometric part can be used to achieve two broad band integrated measurements. This is due to the fact that the spectrophotometry is divided into red and blue parts which cover both their respective parts of the spectrum.

The end-of-mission photometry accuracy with the G-band is 1 millimag for bright stars and gradually degrading to 3 millimag at the limiting magnitude of 20. The integrated blue and red magnitudes (BP and RP respectively) have for a template G2V type stars end-of-mission accuracies below 10 millimag for stars brighter than 18 mag. For 19 and 20 mag G2V stars the

end-of-mission accuracies are about 0.02 and 0.04 mag respectively.

For astrophysical applications the full power of spectrophotometry will be used and estimates of achievable accuracies can be found from the Gaia web pages.

Radial Velocity Spectrometre

The spectroscopy on board Gaia is specifically tuned to radial velocities. Therefore the scientific performance estimates are focused on this 6th phase space component. For bright objects the accuracy is dominated by systematics with the goal to get accuracies better than 1 km/s. At the faint end, i.e. 16.5 mag for a G2V star, the performance is 13 km/s. These accuracies correspond to end-of-mission results.

In Figure 1.4 the single epoch performance estimates are presented. As can be anticipated from the presented signal to noise ratios, it is possible to deduce astrophysical parameters from spectroscopy for the brightest stars. At the same time, one must notice that for the very faintest objects only an accumulation of spectra from the whole mission can give the radial velocity of these objects and nothing more. The estimates of astrophysical parameters deduced from the radial velocity spectrometre can be found on the Gaia web pages.

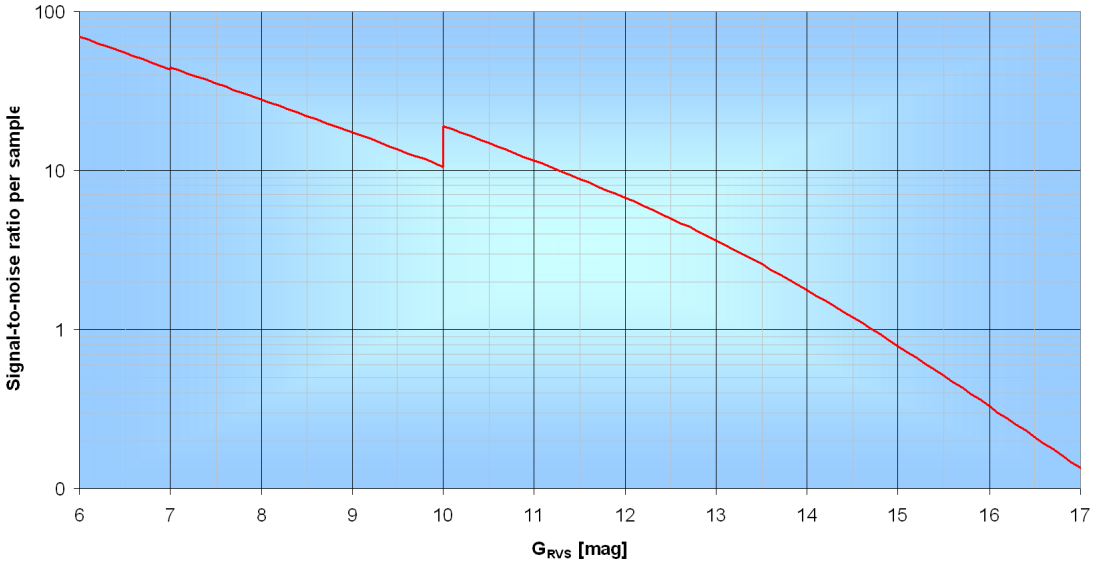

Figure 1.4: Single epoch spectrometre accuracy

Conclusions

Gaia is in a mission on the move. Constant progress is made in all areas relevant for the mission. Any presentation, like this one here, is deemed to be outdated within a few months as the development advances. The community can always consult the Gaia web pages for the latest information.

The scientific performance estimates are expected to be more stable. There are no big unknowns and no major changes are anticipated unless testing gives us some surprises. The summary presented in this contribution is expected not to change before launch, but the Gaia web pages provide again the latest information to be consulted. As the data processing and analysis preparations progress, better and better estimates can be made of deduced astrophysical quantities and their accuracies. These will be provided to the community as soon as they have been established.

All in all the mission is getting shape very well and the anticipated science topics can all be addressed with the Gaia data. In this sense Gaia is on its way to fulfill its promise.

Chapter 2

Star Formation & Initial Mass Function

2.1 Star Cluster Formation and Some Implications for Gaia

Pavel Kroupa[1]

[1] University of Bonn, Auf dem Hügel 71, 53121 Bonn, Germany

Abstract

Stars form in spatially and temporarily correlated star formation events (CSFEs) and the dynamical processes within these "embedded clusters" leave imprints in the stellar populations in galactic fields. Such imprints are correlations in phase space (e.g. gravitationally bound star clusters, tidal streams), in the binary properties of stars and in the present-day stellar mass functions in the surviving clusters. The dynamical processes include expulsion of massive stars from cluster cores, disruption of CSFEs due to residual gas expulsion and energy-equipartition driven evaporation of stars from clusters leading to dark star clusters and cold kinematical streams with epicyclic overdensities. The properties of such phase-space structures in the Milky Way (MW) field depend on the effective gravitational potential of the MW. Gaia data will significantly constrain all of these aspects, and will in particular impact on gravitational dynamics via the properties of cold streams and on star-formation via the constraint on the gas expulsion process through the expanding unbound populations that must be associated with every CSFE.

Introduction

The data generated by the Gaia mission will provide historically unprecedented constraints on the formation and evolution of the MW and will also constrain gravitational theories in the ultra-weak field limit. In order to interpret the Gaia data we will require detailed knowledge on how the stellar phase-space distribution function, which defines the properties of the MW, comes about. This is a complex problem: To interpret the data we will need to compute models of how stars populate phase space. But in which dynamical theory? If we assume Newtonian dynamics the computations can be done today but are equivalent to assuming the concordance cosmological model to be the correct description of reality. The current astronomical constraints already suggest it to be excluded though (Peebles & Nusser [2010]; Kroupa et al.

[2010]), and the so computed model MW would then not match the Gaia constraints unless some additional unknown physics is invoked. Alternatively, perhaps reality follows Modified Newtonian Dynamics (MOND, Milgrom [2009]) or another alternative (e.g. Moffat & Toth [2009]) in which case it may be possible to naturally obtain consistency of the data with the model. But, at present it is not possible to compute a dynamical model of the MW from scratch (i.e. the stars spreading into the field from their birth structures) with Milgrom's dynamics. Until this becomes possible, we will not be able to correctly account for the evolution of the MW, since we will always end up with the trivial solution that the MW is described by Newton's laws plus ad hoc dark unknowns, in order to match the Gaia data.

Irrespective of these issues, here an outline is provided of how the signatures of CSFEs are likely to be contained in astrometric and stellar-population survey data such as will become available with the Gaia mission.

Do all stars form in star clusters?

The phase-space distribution of stars in the MW is not only defined by the effective potential of the MW but also by the dynamical origin of the stars. Here a fundamental QUESTION arises: *Do all stars form in embedded star clusters* (Bressert et al. [2010])? If this were the case then the stellar dynamical processes within the clusters need to be treated first in order to understand the properties of the phase-space distribution function of stars in the MW field. Each cluster of a given energy scale (given by its mass and radius) provides a unique contribution to the stellar population in the field. The concepts of *kinematical population synthesis* (Kroupa [2002]), *dynamical population synthesis* (Kroupa [1995]; Marks & Kroupa [2011]) and of the *integrated galactic initial mass function* (IGIMF) of stars (Kroupa & Weidner [2003]; Weidner et al. [2011b]) arise from the concept of adding up the contributions of all clusters.

Rather than referring to embedded star clusters, the term *Correlated Star Formation Event* (CSFE) is applied here. A CSFE means a group (or "cluster") of stars formed over a spatial scale of about one pc within about one Myr. Observations suggest that these are typical star-forming structures, ranging from the Taurus-Auriga sub-clusters of a dozen binaries in each, through dense-populous young clusters such as the Orion Nebula cluster (ONC), to massive star-bursting embedded clusters with masses $> 10^6$ $M_\odot$. With the work of Larsen [2004] it has become clear that there is no special mode of globular cluster (GC) formation, but that there is as continuous distribution of star-forming events from the smallest to the most massive CSFEs. A CSFE does not have to be gravitationally bound in entirety.

Even if a CSFE were to be formally a gravitationally self bound structure (i.e. a classical star cluster), then a certain fraction of its stars will always be below a density threshold in its outer regions. An observer who applies a density threshold to define "clustered star formation", implying that stars found in regions below this threshold would be termed stars formed in isolation, would thus always find isolated stars in star-forming molecular clouds. For example, an individual cluster represented by a Plummer model in virial equilibrium, i.e. being gravitationally bound, with a Plummer radius of 0.3 pc and with a mass of $20, 100, 1000$ $M_\odot$ has, respectively, 70, 30, 10 per cent of its stars outside a radius at which the projected surface density is 60 stars/pc^2 (Pflamm-Altenburg, priv.comm.). The "efficiency" of clustered star formation thus appears to increase with CSFE mass. A whole population of 0.3 pc Plummer CSFEs ranging from 10 $M_\odot$ to 10^4 $M_\odot$ has a fraction of 30 per cent "isolated" stars. Exponential density profiles (rather than Plummer profiles) or expanding stellar populations after the expulsion of residual gas from initially bound CSFEs would change these numbers such that the fraction may be larger or smaller depending on the characteristic length scale of the CSFEs, such that the observed fraction of star-formation in dense clusters (Bressert et al. [2010]) may be arrived at. The fraction of stars which are apparently formed outside of dense clusters is enhanced due to low-mass embedded clusters dispersing on a few crossing time scales and stars being ejected

from dense regions of their CSFEs (Weidner et al. [2011a]). Despite the significant fraction of "isolated stars", the stellar-dynamics of such CSFEs remains that of an embedded star cluster.

Thus the above QUESTION must be rephrased to the following form: *Do all stars from in CSFEs?*. The answer is yes, because CSFEs are confined to the dense cores of molecular clouds which is where stars form. The least-massive CSFEs can be termed to be non-clustered star formation if these include groups of a few low-mass stars. With this answer, Gaia-relevant modelling can be performed on galaxy scales because the quantities of interest (e.g. velocity and space distributions, binary populations, stellar mass functions) are then given by time-dependent integrals over all CSFEs, once we know the mass and size distribution of the CSFEs.

This contribution touches upon the issue of how star formation in CSFEs affects various aspects of galactic astrophysics. A fundamental concept underlying the approach is that to make a galaxy one merely needs to add up all CSFEs over time (the *cosmological lego*, i.e. the concept that embedded star-clusters are the fundamental building blocks of galaxies Kroupa [2005]).

Formation of CSFEs

It is by now well established observationally that a dense molecular cloud region of a typical scale of a few pc fragments into gas rich sub-clusters with individual diameters of less than a pc (Lada & Lada [2003]). Numerical simulations of turbulent self-gravitating clouds also show this process (e.g. Klessen et al. [2004]). This phase of star-cluster formation takes about 1 Myr by which time between about 10 and 30 per cent of the gas has formed stars with total mass $M_{\rm ecl}$ distributed according to the stellar IMF with a most-massive-star—star-cluster mass relation as a function of the time t, (Bonnell et al. [2004]; Peters et al. [2010, 2011b])

$$m_{\rm max}(t) = 0.39\, M_{\rm ecl}(t)^{2/3}, \tag{2.1}$$

in good agreement with the observed relation, $m_{\rm max} = {\rm fn}(M_{\rm ecl})$, established after star formation has ended (Weidner et al. [2010]).

Once the stellar feedback is sufficient to significantly impact the molecular cloud core the gas is blown out. An issue not fully answered yet is whether gas blow-out is explosive (i.e. faster than a cluster dynamical time) or whether it is adiabatic, and how this depends on cluster mass (see below).

Nevertheless, the theoretical problem of star formation can be divided into two computationally accessible phases. In the first phase, gravo-hydrodynamical simulations can be used to study the collapse and fragmentation of the cloud, while in the second phase purely stellar-dynamical (N-body) methods need to be used to treat the stellar-dynamical processes with high accuracy. The transition between the gas-dominated and the pure N-body dynamics dominated phases occurs at an age of about one Myr and can only be treated with simplifying assumptions, especially if substantial CSFEs with $M_{\rm ecl} > 10^3$ M$_\odot$ are to be studied. Here the sole computationally feasible approach is to model the time-varying gas potential as an additive analytical background potential (e.g. Geyer & Burkert [2001]; Kroupa et al. [2001]) allowing major scans of parameter space (Baumgardt & Kroupa [2007]). Since the formation of each individual star takes about 0.1 Myr, most stars have been born by 1 Myr. For CSFEs with $M_{\rm ecl} >$ few 100 M$_\odot$ they have had enough time to orbit through the CSFE once at least (Kroupa [2005]) such that it can be assumed that such CSFEs are close to dynamical equilibrium when the gas is blown out.

Early stellar dynamical processes

An initially sub-structured stellar population within a CSFE can merge to an embedded cluster on a crossing time scale, or it can disperse into the field, depending on the velocity field of the

cloud and the stellar feedback processes (McMillan et al. [2007]; Clark et al. [2008]; Fellhauer et al. [2009]; Bonnell et al. [2011]). The individual sub-clusters are likely to be initially mass segregated because the most massive stars form in the densest regions (Maschberger et al. [2010]). Even if the overall structure is not mass segregated, the mass segregation time scale is short and of the order of

$$t_{\rm ms} = \mathcal{O}(\frac{m_{\rm av}}{m_{\rm mass}}\, t_{\rm relax}), \tag{2.2}$$

where $m_{\rm av}, m_{\rm mass}$ are the average stellar mass and the mass of the massive star, respectively, while $t_{\rm relax}$ is the two-body relaxation time. For example, for the ONC $t_{\rm relax} \approx 0.6\,$Myr such that $t_{\rm ms} \approx 0.12\,$Myr $\ll$ age of the ONC (Kroupa [2008]).

Once a few massive stars collect in the cluster core the core decays by ejecting the stars on a time scale

$$t_{\rm decay} = \mathcal{O}\left(N_{\rm m}\, t_{\rm core,cross}\right) \tag{2.3}$$

where $N_{\rm m}$ is the number of massive stars in the core and $t_{\rm core,cross}$ is the core-crossing time. For the ONC the core has a radius of about 0.02 pc and the mass of the core is about 150 $M_\odot$ such that $t_{\rm core,cross} \approx 10^4\,$yr and $t_{\rm decay} \approx 10^5\,$yr $\ll$ age of the ONC. Thus, dense clusters are efficient accelerators of massive stars such that a large fraction of them get dispersed into the galactic field as soon as a core of massive stars forms (Pflamm-Altenburg & Kroupa [2006]; Banerjee et al. [2011]; Fujii & Portegies Zwart [2011]; Gvaramadze & Gualandris [2011]). Since most massive stars are born as multiple systems (Sana & Evans [2010]) the dynamical encounters within the cores can be violent.

Indeed, initially mass segregated clusters in which all massive stars are massive binaries eject a large fraction of their massive stars within 3 Myr, as is demonstrated by the extensive young star-cluster N-body library of mass segregated and not mass segregated clusters with and without binaries (Oh et al., in prep.). The primary of an ejected massive binary ultimately explodes as a core-collapse supernova releasing the massive companion into a random direction. About 1 – 4 per cent of all ejected massive stars can therefore not be traced back to their cluster of origin (Pflamm-Altenburg & Kroupa [2010]), while the observed fraction of massive stars that appear to have formed in isolation is about 1 per cent only. Therefore there is no evidence for the formation of massive stars in isolation.

Concerning the binary population in clusters, it is well know from N-body work that binary stars can get disrupted but may also harden through stellar-dynamical encounters (Kroupa [1995]; Portegies Zwart et al. [2001]; Kaczmarek et al. [2011]). It has been shown that a unified invariant birth binary population in which every star with mass $<$ few $M_\odot$ is in a binary naturally evolves into the observed binary population which has a smaller binary fraction (Marks et al. [2011]). By summing all initial populations transformed by all CSFEs the observed period and mass-ratio distributions of the MW field are accounted for naturally through the stellar-dynamical disruptions of the birth population within the individual CSFEs (Marks & Kroupa [2011]).

The expansion of the cluster associated with the dynamical activity of the core is not significant compared to the expansion induced due to the expulsion of residual gas.

The star formation history within a cluster

Some low-mass clusters show evidence for a significant age spread of their stars (Palla et al. [2007]). This can be interpreted to have arisen through a slow formation time-scale of up to 10 Myr and would be in contradiction with cluster formation on a dynamical time-scale (Hartmann et al. [2001]).

There are two processes which naturally lead to an age spread in star clusters such that CSFE formation can occur on a dynamical time but still contain older stars:

1. As the pre-cluster cloud core collapses on a dynamical time scale the potential deepens and young nearby stars from a surrounding older association can be captured to become cluster members. In this way 8 per cent of all ONC stars may be captured older stars (Pflamm-Altenburg & Kroupa [2007]), while 30 per cent or more of stars in ω Cen may be captured from the originally hosting dwarf galaxy (Fellhauer et al. [2006]).

2. After its massive stars have died a young cluster can re-accrete gas if it enters a molecular cloud, because the cluster potential leads to a hydrodynamical instability (Pflamm-Altenburg & Kroupa [2009]).

For massive clusters (about $> 10^6$ $M_\odot$) the gas cannot be removed readily due to the deep potential and shock thermalisation of stellar winds such that successive populations of stars may emerge (Tenorio-Tagle et al. [2003]; Wünsch et al. [2008]). How the observed peculiar chemical compositions in the massive GCs may be accounted for remains an active area of theoretical research (Romano et al. [2007]; Decressin et al. [2009]; de Mink et al. [2009]; Decressin et al. [2010]).

Expulsion of residual gas and initial cluster radii

Observations (Lada & Lada [2003]) show that the star-formation efficiency

$$\epsilon = \frac{M_{\rm ecl}}{M_{\rm ecl} + M_{\rm gas}} \approx 0.3. \tag{2.4}$$

In pure gravo-hydrodynamical simulations of star formation most of the gas can get accreted onto the proto stars (i.e. sink particles in the computations), and ϵ is determined by when the computation is halted. The first simulations of star formation in a turbulent magnetised cloud plus stellar feedback (Price & Bate [2009]; Peters et al. [2011a,b]), however, now demonstrate that ϵ is small on a global cloud scale, because the magnetic field stabilises the cloud on large scales ($> 1\,$pc) while the feedback inhibits fragmentation on small scales. Since virtually all clusters older than about one Myr are free of gas, this can only mean that the residual gas amounting to about 70 per cent of the original cloud core mass is expelled from the cluster within less than one Myr.

A simple estimate of the cloud core binding energy, in comparison with the energy imparted by the feedback energy from massive stars, shows that within less than a crossing time an order of magnitude more energy is deposited in the cloud core. The parameters taken here are a cloud core of radius 1 pc and masses 10^4 and 10^5 $M_\odot$ leading to binding energies of $8.6 \times 10^{48}\,$erg and $8.6 \times 10^{50}\,$erg, respectively. The corresponding crossing times are 0.48 and 0.15 Myr. A single pre-supernova star of 15 $M_\odot$ injects in total $3 \times 10^{50}\,$erg while a single 85 $M_\odot$ star injects $3 \times 10^{50}\,$erg into the cloud, within 0.1 Myr (Maeder [1990]). Thus, the disruption of the nebula is most probably rapid if not explosive, within less than a crossing time scale. Only in massive clusters with $M_{\rm ecl} > 10^5$ $M_\odot$ is a more adiabatic evolution probably the case (Tenorio-Tagle et al. [2003]; Baumgardt et al. [2008b]), because neither individual core-collapse supernovae nor the feedback of all OB stars in the cluster contain sufficient energy to unbind the gas, parts of which shock-thermalises and may form further stars. The effective ϵ probably therefore increases with increasing $M_{\rm ecl} > 10^5$ $M_\odot$.

There is ample observational evidence for explosive gas expulsion. The ONC is super-virial (Kroupa et al. [2001]; Kroupa [2005]), while star clusters appear to show a major expansion in the first 10s Myr of their life time (Bastian & Goodwin [2006]; Goodwin & Bastian [2006]; de Grijs & Parmentier [2007]; Bastian et al. [2008]; Brandner [2008], but see also Gieles et al. [2010]). Very young embedded clusters, or CSFEs, appear to be very compact, with radii of less than a pc, as is inferred from direct observations (Kroupa [2005]) and inverse dynamical population

synthesis (Marks & Kroupa [2012], submitted). Inverse dynamical population synthesis is a potentially powerful tool to infer the initial conditions of star clusters by assuming the initial binary population to be invariant. The present-day binary population stores the dynamical history of the population and the deepest negative energy state of the cluster can be read off from the energy distribution of the present day binary population.

Such work leads to the result that there is a weak embedded-cluster-mass–radius relation for pre-gas-expulsion CSFEs (Marks & Kroupa [2012], submitted)

$$r_h = 0.11^{0.08}_{0.05} M_{\rm ecl}^{0.12\pm0.05}, \tag{2.5}$$

where $M_{\rm ecl}$ is the stellar mass and r_h is the half-mass radius. It will have to be seen how this result, which is obtained by inferring the initial density given the present-day energy distribution of the binary population in each considered cluster, can be made conform to Pfalzner [2009]'s suggestion that there are two sequences of birth CSFEs following different density–radius scaling relations.

Concerning Eq. 2.5, a metallicity dependence also emerges in that metal-poor clusters appear to have had a systematically smaller r_h at a given mass $M_{\rm ecl}$ than metal richer clusters (Marks & Kroupa [2010]). This may suggest that metal-poor gas can collapse to denser states while the more efficient coupling of photons to more metal-enriched gas increases the opacity and thus limits the depth of the collapse while also increasing fragmentation. This is the same physical reason for stellar winds being metal dependent and star-formation theory predicting a bottom heavy stellar IMF for metal rich star-forming conditions (e.g. Bastian et al. [2010]). This finding would imply that metal rich CSFEs with $M_{\rm ecl} > 10^4$ M$_\odot$ are less likely to form bound GCs in present-day galaxy–galaxy encounters, as has been surmised by Forbes et al. [1997], because by forming with larger r_h they are more susceptible to damage from gas expulsion and tidal perturbations.

Taking gas-expulsion into account, it has been shown that one single pre-ONC CSFE evolves, via gas expulsion, through the ONC at an age of about 1 Myr, to the Pleiades at an age of about 100 Myr and then onto to the Hyades and Praesepe at ages of a few hundred Myr (Kroupa et al. [2001]; Portegies Zwart et al. [2001]). Even the binary and stellar populations, as well as the density and velocity profiles come out remarkably well in the models compared to the real clusters. It is remarkable that all these clusters at a mass scale of about 1000 M$_\odot$ are so similar. We will return to this further below (Section *The mass function of CSFEs, of globular clusters and the population II halo*).

Thickening galactic disks, chain galaxies, stellar streams and dark star clusters

The origin of thick disks of galaxies remains unclear, and the reason why the MW thin disk thickened with age also remains unresolved. Gaia data will allow significant constraints to be placed on the acting heating mechanisms through a precise quantification of the phase-space distribution of the various stellar components. A popular hypothesis is that dark-matter sub-clumps and merging dark-matter dominated satellite galaxies thicken the disks. This scenario would be natural for the popular cold- or warm-dark-matter based cosmological models because they are synonymous with hierarchical galaxy formation and imply, by logical necessity, the harassment of thin galactic disks by myriads of dark matter sub clumps. It has proven to be difficult to account for the observed heating though, since the theoretically implied impact of the sub-structures would be far more damaging if not destructive to the thin disks. Sellwood [2010] discusses the various heating processes acting within galactic disks such as heating by bars, transient spiral patterns, molecular clouds, but the full heating has not been accounted for.

Young star clusters that expel their gas explosively loose a dominant fraction of their stellar population which expands, to first order, with the pre-gas-expulsion velocity dispersion. Thus, if the velocity dispersion in the embedded cluster is

$$\sigma \approx \left(\frac{G\,M_{\rm ecl}}{\epsilon\,R}\right)^{\frac{1}{2}}, \tag{2.6}$$

where G is the gravitational constant, then $\sigma > 20\,{\rm km/s}$ if $M_{\rm ecl} > 10^5\,{\rm M}_\odot$ for $\epsilon\,R \approx 1\,{\rm pc}$. These are realistic quantities since $r < 3\,{\rm pc}$ and $\epsilon \approx 0.33$, suggesting that explosive gas expulsion may lead to thickened disks. Kroupa [2002] shows that the thickening history of the MW disk can be accounted for by clustered star formation if the star-formation rate (SFR) decreased over time therewith forming star cluster populations with maximal cluster masses that decrease with decreasing SFR (Weidner et al. [2004]). That the thick disk of the MW could have formed via "popping" CSFEs of mass $\approx 10^6\,{\rm M}_\odot$ has been shown with simulations by Assmann et al. [2011].

This model for the thickening of the MW disk is naturally consistent with the observed *chain galaxies* which show edge-on disk galaxies at high redshift undergoing star formation bursts in many knots within their disks (Elmegreen & Elmegreen [2006]).

The relevance for Gaia is that each CSFE must be associated with a population of stars spreading apart along a thick tidal stream which resulted from the gas-expulsion event. A re-virialised star cluster may be the core of this expanding population, and if the CSFE did yield a bound star cluster then this cluster will be forming a thin kinematically cold tidal stream composed of stars that evaporate from the cluster due to two-body relaxation. These cold streams are of much interest because they may be used to probe how sub-structured the putative dark matter halo of the MW really is. It has already emerged, however, that the observed overdensities in known thin streams can be fully accounted for by *epicyclic overdensities* (Küpper et al. [2010]). A star which is nudged out of its cluster through one of the Lagrange points orbits the MW on a slightly different orbit to that of the cluster and thus the angular separation between the star and the cluster oscillates as the star drifts away from its cluster. Since many stars perform essentially the same motions they accumulate in regions where stars turn around relative to the cluster.

This remarkable development, achieved through high-precision N-body computations that have become possible with Sverre Aarseth's Nbody codes and the GPU-based computing platforms (Aarseth [2008]), opens entirely new and extremely powerful tools for constraining the MW potential and gravitational dynamics in general, since the position and properties of the epicyclic overdensities are a measure of the cluster–MW combined effective potential. It is expected that the Gaia data will contain many thin streams, given that the entire MW field population of stars stems from dissolving CSFEs. It will become possible to measure how the streams diffuse apart with the age of their trace population.

Thus, around each star cluster, such as the Pleiades, the Gaia data ought to reveal two associated kinematical populations. The expanding population and the evaporated population. The total of the expanding population is likely to be about 2/3rds of the initial CSFE membership for the Pleiades (Kroupa et al. [2001], for example).

Furthermore, in each re-virialised post-gas-expulsion star cluster there is a competition of time scales: the remnants of massive stars (neutron stars and black holes) accumulate near the cluster center due to mass segregation. There they eject each other through three-body encounters on a core ejection time-scale. At the same time, low-mass stars evaporate from the cluster on a two-body relaxation time-scale, which is enhanced in stronger tidal fields. It turns out (Banerjee & Kroupa [2011]) that the evaporation time scale is faster than the core-ejection time-scale in star clusters within about 5 kpc distance from the Galactic center. There, clusters with sufficient mass to contain many stellar remnants evolve to black-hole dominated objects with a few stars being bound, the *dark star clusters*. Gaia should find such super-virial ("dark") clusters if they exist. Therewith the typical kick a remnant receives during the supernova

explosion will be constrained to a small value as otherwise the cluster looses the remnants at explosion time. Once the existence of dark clusters has been observationally proven, it will be ascertained that star clusters must be the sources of gravitational wave emission (Banerjee et al. [2010]).

Mining the Gaia data will therefore open entirely new doors into understanding the formation and disruption of CSFEs as well as into gravitational dynamics and the physics of stellar explosions.

The mass function of CSFEs, of globular clusters and the population II halo

Embedded star clusters have been found to have a power-law mass function (ECMF) with power-law index $\beta \approx 2$ (the Salpeter index would be 2.35; Lada & Lada [2003]). If residual gas expulsion is relevant for early cluster evolution, then it follows that the relation between the final mass of the re-virialised young cluster is a fraction of the pre-gas expulsion stellar mass,

$$M_{\rm rev} = f_{\rm st}\, M_{\rm ecl}, \tag{2.7}$$

where $f_{\rm st} < 1$ is the fraction of stars remaining in the re-virialised cluster. Given that $f_{\rm st}$ is likely to be a function of the depth of the potential well,

$$f_{\rm st} = {\rm fn}(M_{\rm ecl}), \tag{2.8}$$

and also of the number of massive stars in the CSFE (being $\propto M_{\rm ecl}$ for an invariant IMF), it follows that $f_{\rm st}$ may have a significant minimum around about $M_{\rm ecl} = 10^4$ M$_\odot$. Here the potential well is still sufficiently shallow while O stars are already present in the population. It is at this mass scale that the expulsion of residual gas may be most damaging and $f_{\rm st}$ may reach a minimum. Such ideas lead to the result that the post-gas expulsion MF of re-virialised young clusters have a structured MF which reflects the variation of $f_{\rm st}$ with $M_{\rm ecl}$.

Kroupa & Boily [2002] show that this ansatz naturally accounts for the turnover of the MF of clusters near 10^5 M$_\odot$ as is observed for the ancient GCs. The gas expulsion process unbinds a large fraction of the embedded cluster population such that the MW halo population II spheroid emerges naturally – it is composed of the quickly dissolved low-mass star clusters that formed together with the present-day GCs plus the stars that were lost from the present day GCs due to residual gas expulsion. Such concepts have been incorporated into N-body modeling of cluster populations by Baumgardt et al. [2008b] and Parmentier et al. [2008].

The post-gas expulsion cluster MF may also have a pronounced peak near $10^3\, M_\odot$ where the ONC, Pleiades, Hyades and Praesepe lie. This may explain why such open clusters may perhaps be overrepresented.

Top-heavy IMF in star bursting clusters

As discussed above, Gaia data will constrain the gas-expulsion process from CSFEs. Constraining the gas-expulsion process is of much importance also for the issue of globular cluster (GC) formation and the possible variation of the stellar IMF with physical cloud conditions. The data will thus touch upon a holy grail of star formation research, namely the finding of conclusive evidence of the long-expected variation of the IMF with star-forming cloud metallicity and cloud density.

The deep observations by De Marchi et al. [2007] of 20 GCs show that the present-day stellar MF (PDMF) becomes increasingly shallower over the stellar mass range $0.3 - 0.8$ M$_\odot$

with decreasing cluster concentration. The same trend holds also with increasing metallicity. Both do not follow readily from theory (Marks & Kroupa [2010]).

That low-concentration clusters are depleted of low mass stars was surprising because the expectation was the opposite, i.e. low-concentration clusters ought to retain their low-mass stars and high concentration (post core collapse) clusters ought to be more evolved dynamically having lost a larger fraction of their low-mass stars. Also, the theoretical expectation has been that low-metallicity clusters ought to have top-heavy IMFs, i.e. should have flatter PDMFs, contrary to the observations.

If clusters were to form mass segregated but with an invariant canonical stellar IMF for < 1 $M_\odot$ and filling their tidal radii then low-mass stars evaporate preferentially immediately and the observed trend between PDMF and concentration can be reproduced (Baumgardt et al. [2008a]). This comes about because by being initially mass segregated, initially tidally-filling clusters loose the most weakly bound (and thus low-mass) stars preferentially. But this ansatz cannot reproduce the trend of the PDMF and of the concentration with metallicity. Also, it is not clear why star clusters should form mass segregated filling their tidal radii, given that the tidal radii of the young clusters are very large (e.g. about 120 pc for a $10^5\,M_\odot$ cluster at a distance of 8 kpc from the MW).

The metallicity trend however gives a clue: If gas expulsion is more efficient for more metal-enriched gas then CSFEs forming out of such material would suffer more damage than low-metallicity CSFEs (compare to metallicity-dependent stellar winds). Indeed, it turns out that low-concentration clusters with flatter PDMFs result naturally if GCs were born mass segregated, had radii of about a pc and expelled their gas at a rate in dependence of the metallicity (Marks et al. [2008]; Marks & Kroupa [2010]). The first ever N-body computation over the entire life-history of a low-mass globular cluster, Pal 14, verifies that a viable re-virialised post-gas-expulsion solution to the low-concentration cluster Pal 14 suggests it may have had a stellar mass function depleted in low mass stars and a large half-mass radius of about 20 pc (Zonoozi et al. [2011]).

The constraints arrived at for the 20 GCs with deep observations imply that in order to actually remove the residual gas a certain amount of feedback needs to be invoked. This feedback is only possible if the IMF was increasingly top heavy with increasing cluster+gas cloud core density and decreasing metallicity (Marks et al. [2012], submitted). This may perhaps be the first ever observationally derived evidence for a density and metallicity dependent IMF variation in consistency with star-formation theory. The onset of this suggested systematic IMF variation is at a pre-cluster cloud-core density $> 10^5$ $M_\odot/pc^3$ and a mass-scale of a CSFE on a pc scale of $> 10^5$ $M_\odot$.

Conclusions

An outline of some of the work done on the physical processes that shape young star clusters and which are relevant for Gaia by leaving imprints in the kinematical field of the MW has been given. An analysis of Gaia astrometric data across the MW is likely to unambiguously constrain the gas expulsion process from CSFEs, because it leaves characteristic signatures in the MW disk. Once the gas expulsion process has been constrained, it will emerge whether galactic disks can be thickened by residual gas expulsion from compact CSFEs and whether the star-cluster MF undergoes the rapid transformation from a power-law embedded cluster MF to a structured MF for older re-virialised clusters. Also, it will then become evident whether the systematic IMF variation, deduced from the careful dynamical analysis of deep GC observations, is supported, since the analysis rests on the notion that residual gas expulsion is a major physical process governing the emergence of star clusters from their embedded phase. It need not be overemphasised that verification of a systematically variable IMF has profound cosmological

implications.

The Gaia mission will thus provide fundamental constraints not only on gravitational dynamics and the potential of the MW, but will also constrain the star-formation process on a pc scale and how it affects the morphology of galaxies.

Acknowledgments

I would like to sincerely thank the organisers for a most memorable conference, and Michael Marks for proof reading this manuscript.

Bibliography

Aarseth, S. J. 2008, in Lecture Notes in Physics, Berlin Springer Verlag, Vol. 760, The Cambridge N-Body Lectures, ed. S. J. Aarseth, C. A. Tout, & R. A. Mardling, 1–4020
Assmann, P., Fellhauer, M., Kroupa, P., Brüns, R. C., & Smith, R. 2011, MNRAS, 415, 1280
Banerjee, S., Baumgardt, H., & Kroupa, P. 2010, MNRAS, 402, 371
Banerjee, S. & Kroupa, P. 2011, ApJ Lett., 741, L12
Banerjee, S., Kroupa, P., & Oh, S. 2011, ArXiv e-prints
Bastian, N., Covey, K. R., & Meyer, M. R. 2010, ARA&A, 48, 339
Bastian, N., Gieles, M., Goodwin, S. P., et al. 2008, MNRAS, 389, 223
Bastian, N. & Goodwin, S. P. 2006, MNRAS, 369, L9
Baumgardt, H., De Marchi, G., & Kroupa, P. 2008a, ApJ, 685, 247
Baumgardt, H. & Kroupa, P. 2007, MNRAS, 380, 1589
Baumgardt, H., Kroupa, P., & Parmentier, G. 2008b, MNRAS, 384, 1231
Bonnell, I. A., Smith, R. J., Clark, P. C., & Bate, M. R. 2011, MNRAS, 410, 2339
Bonnell, I. A., Vine, S. G., & Bate, M. R. 2004, MNRAS, 349, 735
Brandner, W. 2008, in Astronomical Society of the Pacific Conference Series, Vol. 387, Massive Star Formation: Observations Confront Theory, ed. H. Beuther, H. Linz, & T. Henning, 369
Bressert, E., Bastian, N., Gutermuth, R., et al. 2010, MNRAS, 409, L54
Clark, P. C., Bonnell, I. A., & Klessen, R. S. 2008, MNRAS, 386, 3
de Grijs, R. & Parmentier, G. 2007, Chinese Journal of Astronomy and Astrophysic, 7, 155
De Marchi, G., Paresce, F., & Pulone, L. 2007, ApJ Lett., 656, L65
de Mink, S. E., Pols, O. R., Langer, N., & Izzard, R. G. 2009, A&A, 507, L1
Decressin, T., Baumgardt, H., Charbonnel, C., & Kroupa, P. 2010, A&A, 516, A73
Decressin, T., Charbonnel, C., Siess, L., et al. 2009, A&A, 505, 727
Elmegreen, B. G. & Elmegreen, D. M. 2006, ApJ, 650, 644
Fellhauer, M., Kroupa, P., & Evans, N. W. 2006, MNRAS, 372, 338
Fellhauer, M., Wilkinson, M. I., & Kroupa, P. 2009, MNRAS, 397, 954
Forbes, D. A., Brodie, J. P., & Grillmair, C. J. 1997, AJ, 113, 1652
Fujii, M. & Portegies Zwart, S. 2011, ArXiv e-prints
Geyer, M. P. & Burkert, A. 2001, MNRAS, 323, 988
Gieles, M., Sana, H., & Portegies Zwart, S. F. 2010, MNRAS, 402, 1750
Goodwin, S. P. & Bastian, N. 2006, MNRAS, 373, 752
Gvaramadze, V. V. & Gualandris, A. 2011, MNRAS, 410, 304
Hartmann, L., Ballesteros-Paredes, J., & Bergin, E. A. 2001, ApJ, 562, 852
Kaczmarek, T., Olczak, C., & Pfalzner, S. 2011, A&A, 528, A144
Klessen, R. S., Ballesteros-Paredes, J., Li, Y., & Mac Low, M.-M. 2004, in Astronomical Society of the Pacific Conference Series, Vol. 322, The Formation and Evolution of Massive Young Star Clusters, ed. H. J. G. L. M. Lamers, L. J. Smith, & A. Nota, 299
Kroupa, P. 1995, MNRAS, 277, 1491
Kroupa, P. 2002, MNRAS, 330, 707
Kroupa, P. 2005, in ESA Special Publication, Vol. 576, The Three-Dimensional Universe with Gaia, ed. C. Turon, K. S. O'Flaherty, & M. A. C. Perryman, 629
Kroupa, P. 2008, in Lecture Notes in Physics, Berlin Springer Verlag, Vol. 760, The Cambridge N-Body Lectures, ed. S. J. Aarseth, C. A. Tout, & R. A. Mardling, 181
Kroupa, P., Aarseth, S., & Hurley, J. 2001, MNRAS, 321, 699

Kroupa, P. & Boily, C. M. 2002, MNRAS, 336, 1188
Kroupa, P., Famaey, B., de Boer, K. S., et al. 2010, A&A, 523, A32+
Kroupa, P. & Weidner, C. 2003, ApJ, 598, 1076
Küpper, A. H. W., Kroupa, P., Baumgardt, H., & Heggie, D. C. 2010, MNRAS, 401, 105
Lada, C. J. & Lada, E. A. 2003, ARA&A, 41, 57
Larsen, S. S. 2004, ArXiv Astrophysics e-prints
Maeder, A. 1990, A&AS, 84, 139
Marks, M. & Kroupa, P. 2010, MNRAS, 406, 2000
Marks, M. & Kroupa, P. 2011, MNRAS, 417, 1702
Marks, M., Kroupa, P., & Baumgardt, H. 2008, MNRAS, 386, 2047
Marks, M., Kroupa, P., & Oh, S. 2011, MNRAS, 417, 1684
Maschberger, T., Clarke, C. J., Bonnell, I. A., & Kroupa, P. 2010, MNRAS, 404, 1061
McMillan, S. L. W., Vesperini, E., & Portegies Zwart, S. F. 2007, ApJ Lett., 655, L45
Milgrom, M. 2009, Phys. Rev. D, 80, 123536
Moffat, J. W. & Toth, V. T. 2009, MNRAS, 395, L25
Palla, F., Randich, S., Pavlenko, Y. V., Flaccomio, E., & Pallavicini, R. 2007, ApJ Lett., 659, L41
Parmentier, G., Goodwin, S. P., Kroupa, P., & Baumgardt, H. 2008, ApJ, 678, 347
Peebles, P. J. E. & Nusser, A. 2010, Nat, 465, 565
Peters, T., Banerjee, R., Klessen, R. S., & Mac Low, M.-M. 2011a, ApJ, 729, 72
Peters, T., Klessen, R. S., Mac Low, M.-M., & Banerjee, R. 2010, ApJ, 725, 134
Peters, T., Klessen, R. S., Mac Low, M.-M., & Banerjee, R. 2011b, ArXiv e-prints
Pfalzner, S. 2009, A&A, 498, L37
Pflamm-Altenburg, J. & Kroupa, P. 2006, MNRAS, 373, 295
Pflamm-Altenburg, J. & Kroupa, P. 2007, MNRAS, 375, 855
Pflamm-Altenburg, J. & Kroupa, P. 2009, MNRAS, 397, 488
Pflamm-Altenburg, J. & Kroupa, P. 2010, MNRAS, 404, 1564
Portegies Zwart, S. F., McMillan, S. L. W., Hut, P., & Makino, J. 2001, MNRAS, 321, 199
Price, D. J. & Bate, M. R. 2009, MNRAS, 398, 33
Romano, D., Matteucci, F., Tosi, M., et al. 2007, MNRAS, 376, 405
Sana, H. & Evans, C. J. 2010, ArXiv e-prints
Sellwood, J. A. 2010, ArXiv e-prints
Tenorio-Tagle, G., Palouš, J., Silich, S., Medina-Tanco, G. A., & Muñoz-Tuñón, C. 2003, A&A, 411, 397
Weidner, C., Bonnell, I. A., & Moeckel, N. 2011a, MNRAS, 410, 1861
Weidner, C., Kroupa, P., & Bonnell, I. A. 2010, MNRAS, 401, 275
Weidner, C., Kroupa, P., & Larsen, S. S. 2004, MNRAS, 350, 1503
Weidner, C., Kroupa, P., & Pflamm-Altenburg, J. 2011b, MNRAS, 412, 979
Wünsch, R., Tenorio-Tagle, G., Palouš, J., & Silich, S. 2008, ApJ, 683, 683
Zonoozi, A. H., Küpper, A. H. W., Baumgardt, H., et al. 2011, MNRAS, 411, 1989

2.2 The Low–Mass Initial Mass Function in the Orion Nebula Cluster Based on HST/NICMOS III Imaging

Morten Andersen[1], M. R. Meyer[2], M. Robberto[3], I. N. Reid [3], and L. E. Bergeron[3]

[1] Research & Scientific Support Department, ESA ESTEC, Keplerlaan 1, 2200 AG Noordwijk, The Netherlands
[2] Institute for Astronomy ETH, Physics Department, HIT J 22.4, CH-8093 Zurich, Switzerland
[3] Space Telescope Science Institute, Baltimore, MD 21218, USA

Abstract

We present deep HST/NICMOS Camera 3 F110W and F160W imaging of a 26 × 33 arcmin^2, corresponding to 3.1 pc × 3.8 pc, non-contiguous field towards the Orion Nebula Cluster. The main aim is to determine the ratio of low–mass stars (0.08 - 1 $M_\odot$) to brown dwarfs (0.03 - 0.08 $M_\odot$) for the cluster as a function of radius out to a radial distance 1.5 pc. The ratio found for the cluster within a radius of 1.5 pc is $R_{03} = \frac{N(0.08-1M_\odot)}{N(0.03-0.08M_\odot)} = 2.4 \pm 0.2$, after correcting for field stars. The ratio for the central 0.3 pc × 0.3 pc region down to 0.03 $M_\odot$ was previously found to be $R_{03} = 3.3^{+0.8}_{-0.7}$, suggesting the low–mass content of the cluster is mass segregated.

Introduction

A central question in astrophysics is whether the Initial Mass Function (IMF) is universal or is a function of star formation environment. The answer is crucial for our understanding of the buildup of galaxies and provides clues to how stars and brown dwarfs are formed. The stellar part of the IMF appears to be universal based on the comparison of the field IMF (Chabrier [2003]) to clusters within 2 kpc (Meyer et al. [2000]). Bastian et al. [2010] reached the same conclusion with the possible exception of the Taurus Dark Cloud (Luhman et al. [2009]).

The situation is less clear for the brown dwarf part of the IMF. Andersen et al. [2008] analysed the measured IMF's for six nearby star–forming regions and the Pleiades and showed that there is no strong evidence for variations in the derived ratio of low–mass stars to brown dwarfs for the regions and that the combined ratio for the 7 regions showed that the underlying IMF was falling into the brown dwarf regime. Conversely, a handful of studies for OB associations over large areas of the sky have indicated an IMF that does not show evidence for a falling mass function in the brown dwarf regime (e.g. Lodieu et al. [2007];Caballero et al. [2007]). The reason for the apparent discrepancies are not clear but could be due to either differences in the star formation process or to dynamical evolution of the clusters. For several of the clusters compiled by Andersen et al. [2008] only the central regions were studied (e.g. a 0.6 pc square box for the Orion Nebula Cluster (ONC) and 0.24 pc square box for Mon R2) and the measured IMF in the centre can thus be biased if mass segregation is present. Large field of view surveys of young star-forming regions are needed to directly compare with the OB associations.

Here we present HST NICMOS Camera F110W and F160W (similar to the ground–based J and H bands) non–contiguous observations of the ONC, extending studies of the brown dwarf regime to larger radii than previous work. The observations cover the cluster to a radius of 2.55 pc and were obtained as part of the HST Orion Treasury Project (Cycle 13, GO Program 10246 PI Robberto). More details can be found in Andersen et al., (submitted to A&A).

Observations

The non–contiguous nature of the NICMOS Camera 3 observations stems from the fact they were observed in parallel with the ACS and WFPC2 observations from the treasury program. The field–of–view of the

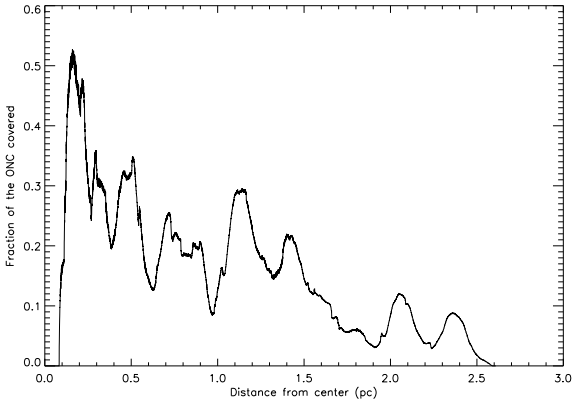

Figure 2.1: The fractional coverage of the ONC by the NICMOS III observations. The fraction covered for annuli around the cluster centre is shown as a function of radial distance from the centre (θ^1 Ori C).

NICMOS Camera 3 is 51.2 × 51.2 arcsec^2 and the pixel scale is 0.2 arcsec.

A total of 102 regions were covered in both the F110W and F160W bands. The regions were typically build up as a 4 piece mosaic in the F160W band and a 5 piece mosaic in the F110W band. In one region a single image was observed in both filters. The integration time for each image was 192 sec in F160W and 256 sec in F110W, resulting in a total integration time per pixel that varies between 192 – 762 sec for the F160W observations and 256 – 1280 sec for the F110W observations.

Sources were visually identified in the F160W mosaics before photometry was performed using an aperture of 2.5 pixels and a sky annulus from 10 to 15 pixels. The radial profile of each source was inspected in order to exclude spurious detections due to nebulosity. We detect a total of 2054 objects. Zero points were adopted from the HST calibration web pages and aperture corrections were determined from bright isolated stars. Objects in common with the dataset by Robberto et al. [2010] were used to calibrate the astrometry of each mosaic and to convert the photometry into the 2MASS system.

The very centre of the cluster is not covered and the majority of the observations are to the south and south–south–west of the cluster centre. Fig. 2.1 shows the fractional area of the ONC covered as a function of distance from the cluster centre. The total area imaged is 162 arcmin^2, corresponding to 2.35 pc^2 for a cluster distance of 414 pc. The coverage extends in radius from 0.05 pc out to 2.55 pc from θ^1 Ori C, assumed to be the centre of the ONC. Due to the large region of sky covered with a small filling factor, the coverage is relatively low, 20–50% within 0.5 pc, 10–30% between 0.5 pc and 1.5 pc, and less at larger distances (see Fig. 2.1).

Results

Fig. 2.2 shows the colour–magnitude diagram for the surveyed region outside 0.35 pc. The data have been divided into the annuli that will be used below to derive the ratio of low–mass stars to brown dwarfs. Overplotted are the 50% completeness limits, a 1 Myr isochrone from Baraffe et al. [1998], and the same isochrone reddened by $A_V = 7$ mag. Most of the objects from 1 $M_\odot$ to the detection limit below 0.01$M_\odot$ are located between the 1 Myr isochrone shifted by the distance modulus to the ONC, and the same isochrone reddened by $A_V = 7$ mag. The objects on the blue side of the 1 Myr isochrone are likely foreground stars or a significantly older population.

One complication in calculating the IMF in young star-forming regions is the presence of differential extinction. Objects are reddened by different amounts due to patchy obscuration along the line of sight. As evident from Fig. 2.2, this is the case for the ONC. Higher mass objects can be detected through larger amounts of extinction than lower mass objects due to their intrinsic brightness. As illustrated in e.g. Andersen et al. [2009] this can potentially introduce a spurious deficit in the derived number of low-mass objects. One approach to avoid this bias is to construct an extinction-limited sample, which is obtained by considering only objects within a certain range of extinction while taking the completeness limit into account. We find that more than 80% of the objects are affected by an extinction of $A_V = 7$ mag or less and use this limit for our extinction limited sample. This sample is complete to below 20 M_{Jup} for a 1 Myr population. The mass of each object is then determined by shifting it along the reddening vector back to the isochrone assumed.

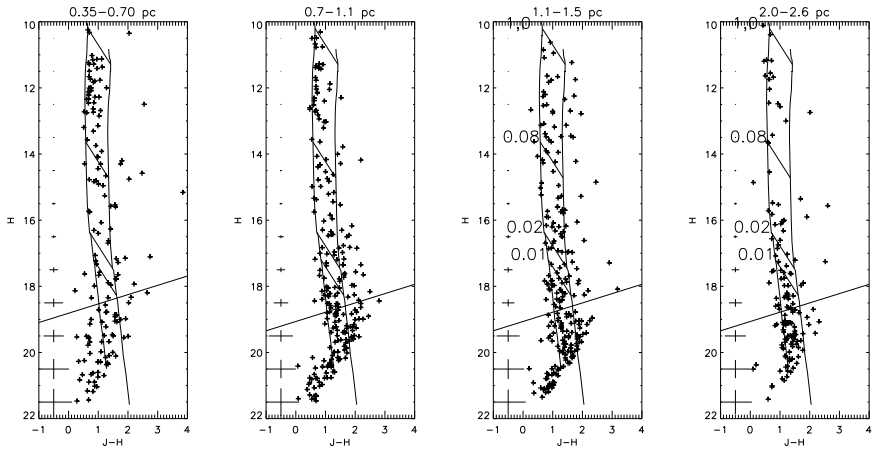

Figure 2.2: The colour–magnitude diagram for the surveyed region. Overplotted are a 1 Myr isochrone from Baraffe et al. [1998] shifted to the distance of the ONC, the same isochrone reddened by $A_V = 7$ mag, and the 50% completeness limit for the data. Masses for a 1 Myr population of 1.0, 0.08, 0.02, and 0.01 $M_\odot$ are indicated on the lower left panel. The region used as control field is shown in the right panel (2.0 – 2.6 pc). The typical photometric and colour error are shown in each diagram as a function of object magnitude.

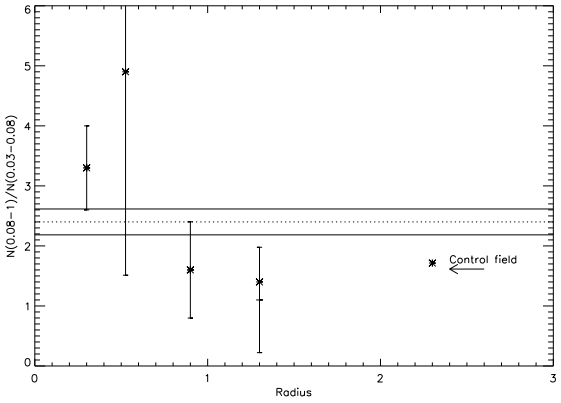

Figure 2.3: The ratio of low–mass stars (0.08 – 1.0 $M_\odot$) to brown dwarfs (0.03 – 0.08 $M_\odot$) for the ONC as a function of radius. The plus signs with error bars indicate the field star corrected measurements whereas the squares indicate the measurements before field star subtraction. The inner data point is from Slesnick et al. [2004] and the horizontal line is the average ratio with the 1 σ error interval provided by the dashed lines.

Due to the relatively large area covered we expect some field star contamination, which has been estimated in the following way. Since the cluster surface density at larger radii decreases as r^{-2} as found in Hillenbrand & Hartmann [1998], we expect the outer region observed (2.0 –2.6 pc) to have a relatively small number of cluster members. Thus, the outer regions can be used as a conservative over–estimate of the field star contamination. However, as we indicate below there appears to be an increase in the relative number of brown dwarfs at larger radii. Any cluster population present at large radii will therefore result in an over subtraction of the brown dwarf content. The derived ratio of stars to brown dwarfs after correction based on the outer regions will thus be an upper limit.

The Mass Function as a function of radius

Following Meyer et al. [2000] and Andersen et al. [2008] we have determined the ratio of low–mass stars (0.08 – 1 $M_\odot$) to brown dwarfs both for the cluster as a whole, and for 3 separate annuli outside a 0.35 pc radius. The ratio of stars to brown dwarfs as a function of radius is shown in Fig. 2.3 where the ratios both with and without field stars subtracted is shown.

The ratio determined at 0.35 – 0.7 pc is consistent with the results by Slesnick et al. [2004] for the central 0.3 pc radius of the cluster. However, for larger distances there is a drop in the ratio of stars to brown dwarfs. Outside a radius 0.7 pc the ratio drops by almost a factor of two compared with the

ratio in the centre, although the error bars for the individual annuli are relatively large. The total ratio of stars to brown dwarfs for the cluster as a whole has been calculated by correcting the source counts in the different annuli by the fraction of the cluster covered by that annulus (derived from Fig. 2.1). As shown by Hillenbrand & Hartmann [1998] the surface density is well represented by a King profile, and thus extends as r^{-2} outside the core radius. Thus, even though the surface density is lower at larger radii, this is compensated by an increase in the area in each annulus. The low ratio far from the centre drives the global ratio to a relatively low value of $R_{03} = \frac{N(0.08-1M_{\odot})}{N(0.03-0.08M_{\odot})} = 2.4 \pm 0.2$, lower than determined in the cluster centre.

The decreasing ratio of stars to brown dwarfs as a function of radius suggests that the cluster is mass segregated. A similar conclusion was found by Hillenbrand & Hartmann [1998] for the massive stars in the cluster centre. However, there was no indication for mass segregation for the lower mass population as their study only extended to 0.3 $M_{\odot}$ and thus compared high-mass stars to low-mass stars. In contrast, we find the sub–stellar members to be segregated compared to the stars as a whole, which are dominated by the lower mass members.

Hillenbrand & Hartmann [1998] concluded that it is possible for the high-mass segregation to have an dynamical origin. This is not the case for the brown dwarfs observed here with the current cluster surface density profile. The half mass relaxation time was estimated in Hillenbrand & Hartmann [1998] to be 6.5 Myr which is much longer than the age of the cluster (1 – 3 Myr) and thus unlikely to cause the variations in the ratio of stars to brown dwarfs through dynamical 2 body evolution (Bonnell et al. [1998]).

A decrease of the ratio of stars to brown dwarfs as a function of radius has been observed in some open clusters as well, e.g. IC 2391 Boudreault & Bailer-Jones [2009] where the brown dwarfs were found to have a flatter distribution than the low–mass stars. Similarly, for IC 348 and central parts of the ONC, Kumar & Schmeja [2007] use the minimum spanning tree method to suggest the brown dwarfs are less centrally concentrated than the stars. A flatter distribution for brown dwarfs compared to stars is what would be expected from an ejection scenario where a fraction of the brown dwarfs are due to ejections in multiple systems during the earliest phases of star formation (see e.g. Reipurth & Clarke [2001]; Bate et al. [2003]).

A smaller ratio of the number of stars to brown dwarfs for the whole cluster compared to the centre region has several implications. Bate [2009] predicted a value of $R_{03} = 1.25$ based on SPH simulations of a spherical collapsing cloud producing a total of 1254 objects, even lower than we determine here for the ONC. It is worth noticing that our value of $R_{03} = 2.4 \pm 0.2$ is not consistent with a Chabrier IMF, which predicts too few brown dwarfs ($R_{03}(Chabrier) = 4.95$). The probability of the ratio to be drawn from an underlying population with a Chabrier distribution is less than 1%. The ratio we determine is in better agreement with a flat or rising IMF into the brown dwarf regime. We stress however, that our IMF is determined from a photometric sample only and that spectroscopic confirmation of the brown dwarf candidates is highly desirable.

The current finding of a possible change in the ratio of stars to brown dwarfs at larger radii suggests further studies of other nearby regions to larger radii than previously surveyed are needed. Also obtaining kinematic data for the individual low–mass members to better characterise any mass segregation would be very valuable. Current near–infrared large field of view capabilities both from the ground and space are well suited for these studies.

Bibliography

Andersen, M., Meyer, M. R., Greissl, J., & Aversa, A. 2008, ApJ Lett., 683, 183
Andersen, M., Zinnecker, H., Moneti, A., et al. 2009, ApJ, 707, 1347
Baraffe, I., Chabrier, G., Allard, F., & Hauschildt, P. H. 1998, A&A, 337, 403
Bastian, N., Covey, K. R., & Meyer, M. R. 2010, ARA&A, 48, 339
Bate, M. R. 2009, MNRAS, 392, 590
Bate, M. R., Bonnell, I. A., & Bromm, V. 2003, MNRAS, 339, 577
Bonnell, I. A., Bate, M. R., & Zinnecker, H. 1998, MNRAS, 298, 93
Boudreault, S. & Bailer-Jones, C. A. L. 2009, ApJ, 706, 1484
Caballero, J. A., Béjar, V. J. S., Rebolo, R., et al. 2007, A&A, 470, 903
Chabrier, G. 2003, PASP, 115, 763
Hillenbrand, L. A. & Hartmann, L. W. 1998, ApJ, 492, 540
Kumar, M. S. N. & Schmeja, S. 2007, A&A, 471, L33

Lodieu, N., Hambly, N. C., Jameson, R. F., et al. 2007, MNRAS, 374, 372
Luhman, K. L., Mamajek, E. E., Allen, P. R., & Cruz, K. L. 2009, ApJ, 703, 399
Meyer, M. R., Adams, F. C., Hillenbrand, L. A., Carpenter, J. M., & Larson, R. B. 2000, in Protostars and Planets IV (Book - Tucson: University of Arizona Press; eds Mannings, V., Boss, A.P., Russell, S. S.), 121
Reipurth, B. & Clarke, C. 2001, AJ, 122, 432
Robberto, M., Soderblom, D. R., Scandariato, G., et al. 2010, AJ, 139, 950
Slesnick, C. L., Hillenbrand, L. A., & Carpenter, J. M. 2004, ApJ, 610, 1045

2.3 Feedback Regulated Star Formation: From Star Clusters to Galaxies

Sami Dib[1]

[1] Astrophysics Group, Blackett Laboratory, Imperial College London, London, SW7 2AZ, United Kingdom; s.dib@imperial.ac.uk

Abstract

This paper summarises results from semi-analytical modelling of star formation in protocluster clumps of different metallicities. In this model, gravitationally bound cores form uniformly in the clump following a prescribed core formation efficiency per unit time. After a contraction timescale which is equal to a few times their free-fall times, the cores collapse into stars and populate the IMF. Feedback from the newly formed OB stars is taken into account in the form of stellar winds. When the ratio of the effective wind energy of the winds to the gravitational energy of the system reaches unity, gas is removed from the clump and core and star formation are quenched. The power of the radiation driven winds has a strong dependence on metallicity and increases with increasing metallicity. Thus, winds from stars in the high metallicity models lead to a rapid evacuation of the gas from the protocluster clump and to a reduced star formation efficiency, SFE_{exp}, as compared to their low metallicity counterparts. By combining SFE_{exp} with the timescales on which gas expulsion occurs, we derive the metallicity dependent star formation rate per unit time in this model as a function of the gas surface density Σ_g. This is combined with the molecular gas fraction in order to derive the dependence of the surface density of star formation Σ_{SFR} on Σ_g. This feedback regulated model of star formation reproduces very well the observed star formation laws extending from low gas surface densities up to the starburst regime. Furthermore, the results show a dependence of Σ_{SFR} on metallicity over the entire range of gas surface densities, and can also explain part of the scatter in the observations.

The SFE in Stellar Clusters and in Galaxies

The star formation efficiency (SFE) is one of the essential quantities that regulates the dynamical evolution and chemical enrichment of stellar clusters, the interstellar medium, and galaxies (e.g., Boissier et al. [2001]; Krumholz & McKee [2005]; Dib et al. [2006]; Dib et al. [2009]; Dib et al. [2011]). The SFE is commonly defined as being the fraction of gas which is converted into stars in a system of a given mass, be it a protocluster molecular clump, an entire giant molecular cloud (GMC), or a galaxy. In an isolated clump, the time evolving SFE is usually defined as being:

$$SFE(t) = \frac{M_{cluster}(t)}{M_{clump}}, \tag{2.9}$$

where $M_{cluster}(t)$ is the cluster mass at time t and M_{clump} is the initial clump mass. In observed protocluster clumps with embedded or semi-embedded clusters, the SFE is usually approximated by:

$$SFE_{obs} = \frac{M_{cluster}}{M_{cluster} + M_{gas}}, \tag{2.10}$$

where M_{gas} is the mass of the star-forming gas. Measured SFEs of nearby embedded clusters, using Eq. 2.10 yield values that fall in the range 0.1 – 0.5 (Wilking & Lada [1983]; Rengarajan [1984]; Wolf et al. [1990]; Pandey et al. [1990]; Lada et al. [1991a,b]; Warin et al. [1996]; Olmi & Testi [2002]). These SFE values are larger than those obtained for entire GMCs which are observed to fall in the range of a few percent (e.g., Duerr et al. [1982], Fukui & Mizuno [1991]; Evans et al. [2009]). On galactic scales, the star formation efficiency is usually defined as being the inverse of the molecular gas consumption time and is given by:

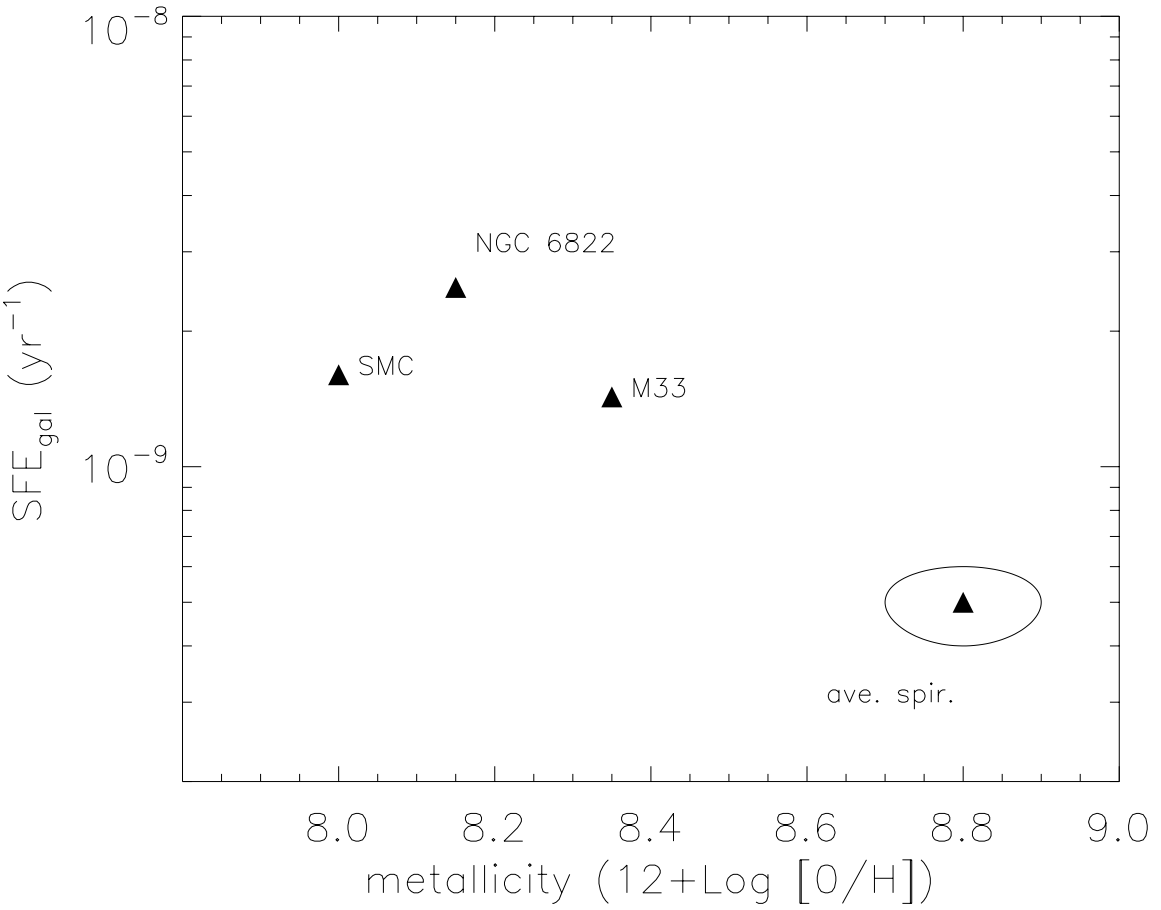

Figure 2.4: Global galactic star formation efficiency SFE_{gal} as a function of the galactic global metallicity. The data for M 33 and NGC 6822 are from Gratier et al. [2010a,b], for the SMC from Leroy et al. [2006], and the average spiral value from the sample of Murgia et al. [2002]. Adapted from Dib et al. [2011].

$$SFE_{gal} = \frac{SFR_{gal}}{M_{H_2}}, \tag{2.11}$$

where SFR_{gal} is the galactic star formation rate (in $M_\odot$ yr^{-1}), and M_{H_2} the mass of the molecular hydrogen gas. In large spiral galaxies $SFE_{gal} \sim 0.5 \times 10^{-9}$ yr^{-1} (e.g., Kennicutt [1998], Murgia et al. [2002]; Leroy et al. [2008]). Fig. 2.4 displays the global SFE_{gal} for a few selected nearby galaxies as a function of their global metallicity. The trend in Fig. 2.4 is strongly suggestive of an SFE_{gal} which increases with decreasing metallicity. Several physical processes regulate the core formation efficiency (CFE) within a star-forming molecular clump/cloud, and as a consequence, the SFE. Supersonic turbulence can provide support against the global collapse of the clump/cloud, or at least delay it (e.g., Vázquez-Semadeni & Passot [1999]). However, on scales smaller than the energy injection scale, but larger than the sonic scales in the cloud, supersonic turbulence produces local compressions (i.e., cores) (e.g., Padoan [1995]; Vázquez-Semadeni et al. [2003]; Dib et al. [2010a]) of which a fraction can be 'captured' by gravity and proceed to collapse into stars (e.g., Vázquez-Semadeni et al. [2005a]; Dib et al. [2007a]; Dib & Kim [2007]; Dib et al. [2008a]; Dib et al. [2010a]). Krumholz & McKee [2005] formulated an analytical theory in which the core formation efficiency per free-fall time, CFE_{ff}, is shown to decrease with an increasing sonic Mach number and an increasing virial parameter and is given by $CFE_{ff} \approx 0.15\alpha_{vir}^{-0.68}\mathcal{M}^{-0.32}$.

Magnetic fields play an important role in determining the fraction of gravitationally bound gas in star-forming clouds/clumps. Results from numerical simulations show that stronger magnetic fields (in terms of magnetic criticality) lower the rate of dense core formation in a star-forming molecular clump/cloud (e.g., Vázquez-Semadeni et al. [2005b]; Price & Bate [2008]; Dib et al. [2008a]; Li et al. [2010]; Dib et al. [2010a]). Dib et al. [2010a] showed that the CFE per unit of the free-fall time of the cloud, CFE_{ff}, are of the order of ~ 6 % and ~ 33 % for clouds with mass-to-magnetic flux ratios of $\mu = 2.2$ and 8.8, respectively (with μ being normalised by the critical mass-to-flux ratio for collapse, see

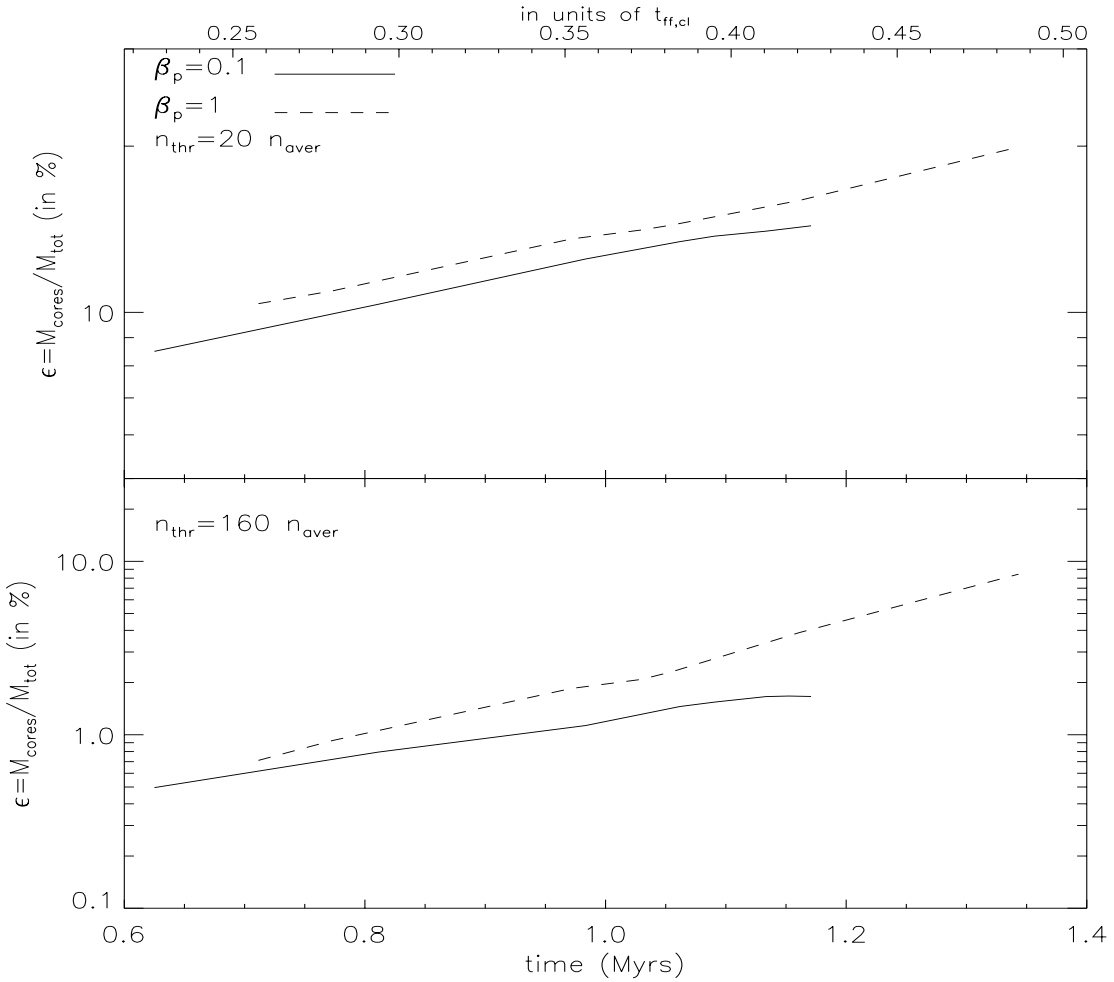

Figure 2.5: Time evolution of the fraction of cloud mass of the cloud that is in dense cores in two 3D numerical simulations of magnetized, turbulent, and self gravitating isothermal molecular cloud (Dib et al. [2010a]). One simulation has a mass-to-magnetic flux ratio of $\mu_B = 2.8$ (mildly supercritical) and the other has $\mu_B = 8.8$ (strongly supercritical). The upper corresponds to cores detected using a density threshold of $n_{thr} = 20\ n_{aver}$ and the lower panel corresponds to cores detected at the density threshold of 160 n_{aver}, where $n_{aver} = 500$ cm^{-3} is the average number density in the cloud. The cores identified at the threshold density of 160 n_{aver} corresponds to a population of gravitationally bound cores. Adapted from Dib et al. [2010a].

Fig. 2.5). The role of stellar feedback in setting the final value of the SFE has been investigated by several authors. The role of protostellar outflows has been studied theoretically by Adams & Fatuzzo [1996], Matzner & McKee [2000] and numerically by Nakamura & Li [2007] and Li et al. [2010]. Supernova explosions are an efficient way of removing gas from the protocluster region (e.g., Parmentier et al. [2008]; Baumgardt et al. [2008]). However, they occur after a few million years from the time massive stars have formed. Another form of stellar feedback is associated with O and B stars, in their main sequence phase, and eventually beyond. OB stars emit UV radiation which ionises the surrounding gas and heats it to temperatures of $\sim 7000 - 10^4$ K. This warm and ionised bubble provides the environment in which particles accelerated from the stellar surface by interaction with some of the stellar radiation propagate outwards. In the following sections, we present a model which describes the co-evolution of the mass function of gravitationally bound cores and the IMF in a protocluster region. In the model, dense cores form in the protocluster clump uniformly in time following a specified core formation efficiency per unit free-fall time of the clump, CFE_{ff}. The dense cores have lifetimes of a few times their free-fall times, after which they collapse to form stars and populate the IMF. Stellar winds from the newly formed massive stars ($M_\star > 5$ M$_\odot$) inject energy into the clump and when the ratio of the effective wind energy to the gravitational energy of the clump reaches unity, gas is removed from the clump and core and star formation are quenched. We discuss the dependence of the final star formation efficiency on the

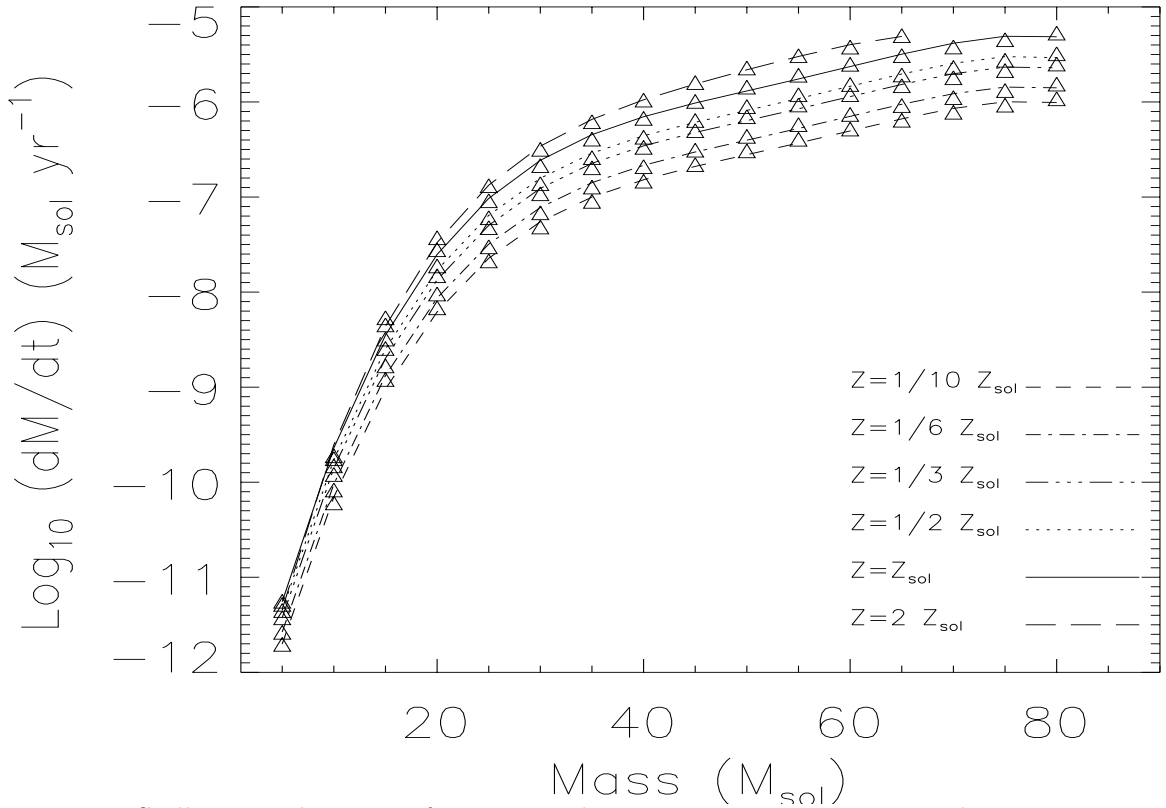

Figure 2.6: Stellar mass loss rates for stars in the mass range 5 – 80 $M_\odot$ on the main sequence, and for various metallicities. The stellar mass loss rates have been calculated using the stellar characteristics (effective temperature, stellar luminosity and radius) computed using the stellar evolution code CESAM coupled to the stellar atmosphere model of Vink et al. [2001]. Overplotted to the data are fourth order polynomial fits. The parameters of the fit functions can be found in Dib et al. [2011]. Adapted from Dib et al. [2011].

metallicity. Finally, we present a derivation of the star formation laws in galaxies in the context of this metallicity dependent, feedback regulated model of star formation.

The Model

Protocluster Clumps

Several studies have established that star clusters form in dense ($> 10^3$ cm^{-3}) clumps embedded in a lower density parental molecular cloud (e.g., Lada & Lada [2003]; Klein et al. [2005]; Rathborne et al. [2006]; Kauffmann & Pillai [2010]; Csengeri et al. [2011]; Hernandez et al. [2011]). Saito et al. [2007] studied, using the $C^{18}O$ molecular emission line, a large sample of cluster-forming clumps whose masses and radii vary between [15 – 1500] $M_\odot$ and [0.14 – 0.61] pc, respectively. The mass-size and velocity dispersion-size relations of clumps in the sample of Saito et al. [2007] were fitted by Dib et al. [2010b]), obtaining:

$$M_{clump}(\mathrm{M}_\odot) = 10^{3.62\pm0.14} R_c^{2.54\pm0.25}(\mathrm{pc}), \tag{2.12}$$

and

$$v_c(\mathrm{km\ s^{-1}}) = 10^{0.45\pm0.08} R_c^{0.44\pm0.14}(\mathrm{pc}), \tag{2.13}$$

where M_{clump} is the mass of the clump, R_c its radius, and v_c the scale dependent gas velocity dispersion. In this work, we adopt a protocluster clump model that follows an r^{-2} density profile:

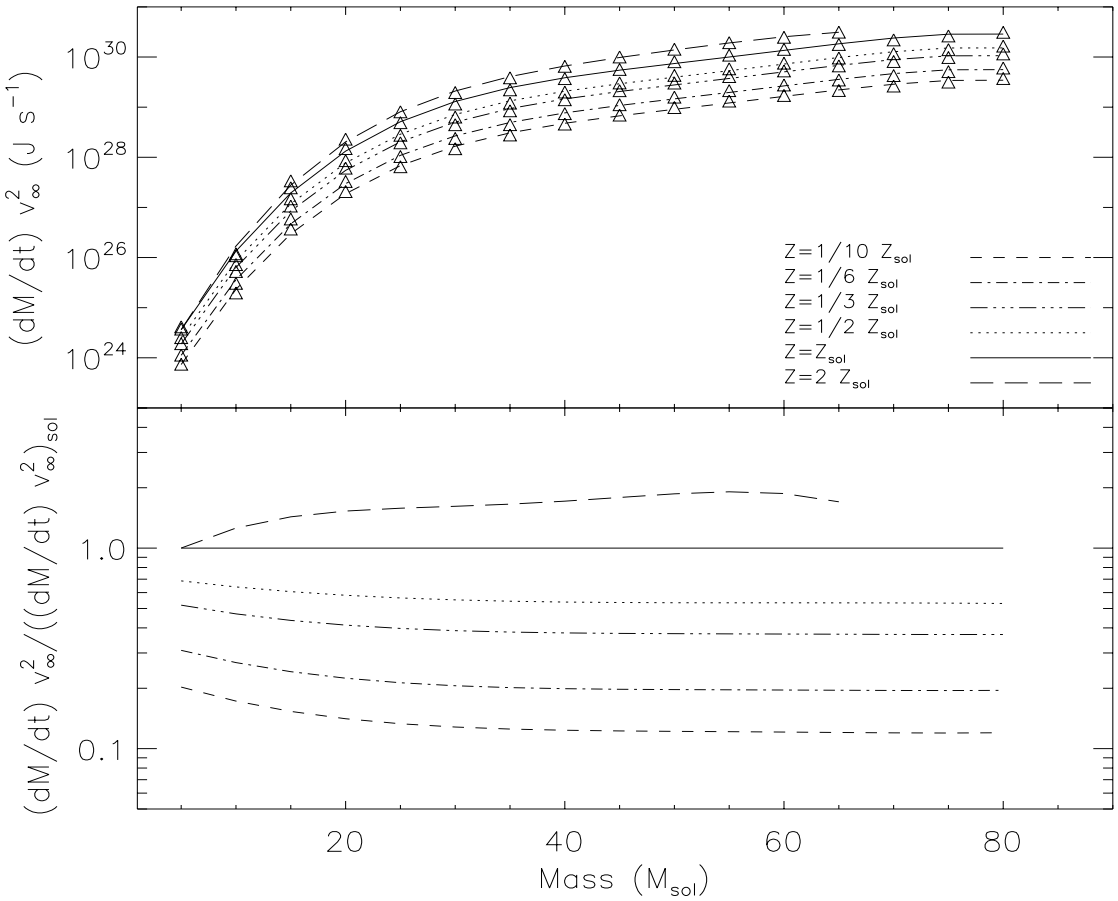

Figure 2.7: The power of the stellar winds, or wind luminosities, for stars in the mass range 5 –80 $M_\odot$ on the main sequence, and for various metallicities. The stellar mass loss rates have been calculated using the stellar characteristics (effective temperature, stellar luminosity and radius) computed using the stellar evolution code CESAM coupled to the stellar atmosphere model of Vink et al. [2001]. The values of v_∞ have been calculated using the derivation by Leitherer et al. [1992]. Over-plotted to the data are fourth order polynomials. The parameters of the fit functions can be found in Dib et al. [2011]. Adapted from Dib et al. [2011].

$$\rho_c(r) = \frac{\rho_{c0}}{1 + (r/R_{c0})^2}, \tag{2.14}$$

where R_{c0} is the clump's core radius, ρ_{c0} is the density at the centre. For a given value of M_{clump}, the central density ρ_{c0} is given by:

$$\rho_{c0} = \frac{M_{clump}}{4\pi R_{c0}^3[(R_c/R_{c0}) - \arctan(R_c/R_{c0})]}. \tag{2.15}$$

The temperatures of the cluster-forming clumps are observed to vary between 15 and 70 K (e.g., Saito et al. [2007]; Rathborne et al. [2010]). In order to further constrain the models and minimise the number of parameters, we relate the sizes of the protocluster clumps to their masses using the mass-size relation of Saito et al. In the absence of detailed information about the velocity dispersion inside the cores in the Saito et al. [2007] study, we assume that the clump-clump velocity dispersion they derived (i.e., Eq. 2.14) is also valid on the scale of the clumps themselves and of their substructure.

Prestellar Cores Model

Whitworth & Ward-Thompson [2001] applied a family of Plummer sphere-like models to the contracting prestellar dense core L 1554, which is representative of the population of gravitationally bound cores in

clumps that are considered in this work. They found a good agreement with the observations of L 1554 if the density profile of the core has the following form:

$$\rho_p(r_p) = \frac{\rho_{p0}}{[1 + (r_p/R_{p0})^2]^2}, \tag{2.16}$$

where ρ_{p0} and R_{p0} are the central density and core radius of the core, respectively. Note that the radius of the core, R_p, depends both on its mass and on its position within the clump. The dependence of R_p on r requires that the density at the edges of the core equals the ambient clump density, i.e., $\rho_p(R_p) = \rho_c(r)$. This would result in smaller radii for cores of a given mass when they are located in their inner parts of the clump. The density contrast between the centre of the core and its edge is given by:

$$\mathcal{C}(r) \equiv \frac{\rho_{p0}}{\rho_c(r)} = \frac{\rho_{p0}}{\rho_{c0}} \left[1 + \left(\frac{r}{R_{c0}}\right)^2\right]. \tag{2.17}$$

Depending on its position r in the clump, the radius of the core of mass M, R_p, can be calculated as being $R_p(r, M) = a(r)\ R_{p0}(r, M)$, where:

$$R_{p0}(r, M) = \left(\frac{M}{2\pi\rho_{p0}}\right)^{1/3} \left(\arctan[a(r)] - \frac{a(r)}{1 + a(r)^2}\right)^{-1/3}, \tag{2.18}$$

and with $a(r) \equiv (\mathcal{C}(r)^{1/2} - 1)^{1/2}$. With our set of parameters, the quantity $\mathcal{C}^{1/2} - 1$ is always guaranteed to be positive. The value $R_p(r, M)$ can be considered as being the radius of the core at the moment of its formation. The radius of the core will decrease as time advances due to gravitational contraction. We assume that the cores contract on a timescale, $t_{cont,p}$ which we take to be a few times their free fall timescale $t_{ff,core}$, and which is parametrised by $t_{cont,p}(r, M) = \nu\, t_{ff,core}(r, M) = \nu\, (3\pi/32\ G\bar{\rho_p}(r, M))^{1/2}$, where G is the gravitational constant, ν is a constant ≥ 1 and $\bar{\rho_p}$ is the radially averaged density of the core of mass M, located at position r in the clump. The time evolution of the radius of a core of mass M, located at position r in the cloud is given by a simple contraction law $R_p(r, M, t) = R_p(r, M, 0)\ e^{-(t/t_{cont,p})}$. Both observational (Jessop & Ward-Thompson [2000]; Ward-Thompson et al. [2007]) and numerical (Vázquez-Semadeni et al. [2005a]; Galván-Madrid et al. [2007]; Dib et al. [2008c]; Gong & Ostriker [2011]) estimates of gravitationally bound cores lifetimes tend to show that they are of the order of a few times their free-fall time. One important issue is the choice of the cores central density, ρ_{p0}. In this work, we first assume that the minimum density contrast that exists between the centre of the core and its edge is of the order of the critical Bonnor-Ebert value and that is > 15. Secondly, we assume that the density contrast between the centre and the edge of the cores depends on their masses following a relation of the type $\rho_{p0} \propto M^{\mu}$. Thus, the density contrast between the centre and the edge for a core with the minimum mass we are considering, M_{min} (typically $M_{min} = 0.1$ M$_\odot$) is 15, whereas for a more massive core of mass M, the density contrast will be equal to $15 \times (M/M_{min})^{\mu}$. Observations show that μ varies in the range $[0 - 0.6]$ (e.g., Johnstone & Bally [2006]).

The Initial Prestellar Cores Distributions

We assume that dense cores form in the clump as a result of its gravo-turbulent fragmentation. The mass distributions of the core formed at every epoch is described using the formulation of Padoan & Nordlund [2002]. Thus, the local mass distributions of cores, $N(r, M)$, are given by:

$$N(r, M)\ d\log\ M = f_0(r)\ M^{-3/(4-\beta)} \times \left[\int_0^M P(M_J) dM_J\right] d\log\ M, \tag{2.19}$$

where β is the exponent of the kinetic energy power spectrum, $E_k \propto k^{-\beta}$, and is related to the exponent α of the size-velocity dispersion relation in the clump with $\beta = 2\alpha + 1$. The local normalisation coefficient $f_0(r)$ is obtained by requiring that $\int_{M_{min}}^{M_{max}} N(r, M)\ dM = 1$ in a shell of width dr, located at distance r from the clump's centre. $P(M_J)$ is the local distribution of Jeans masses given by:

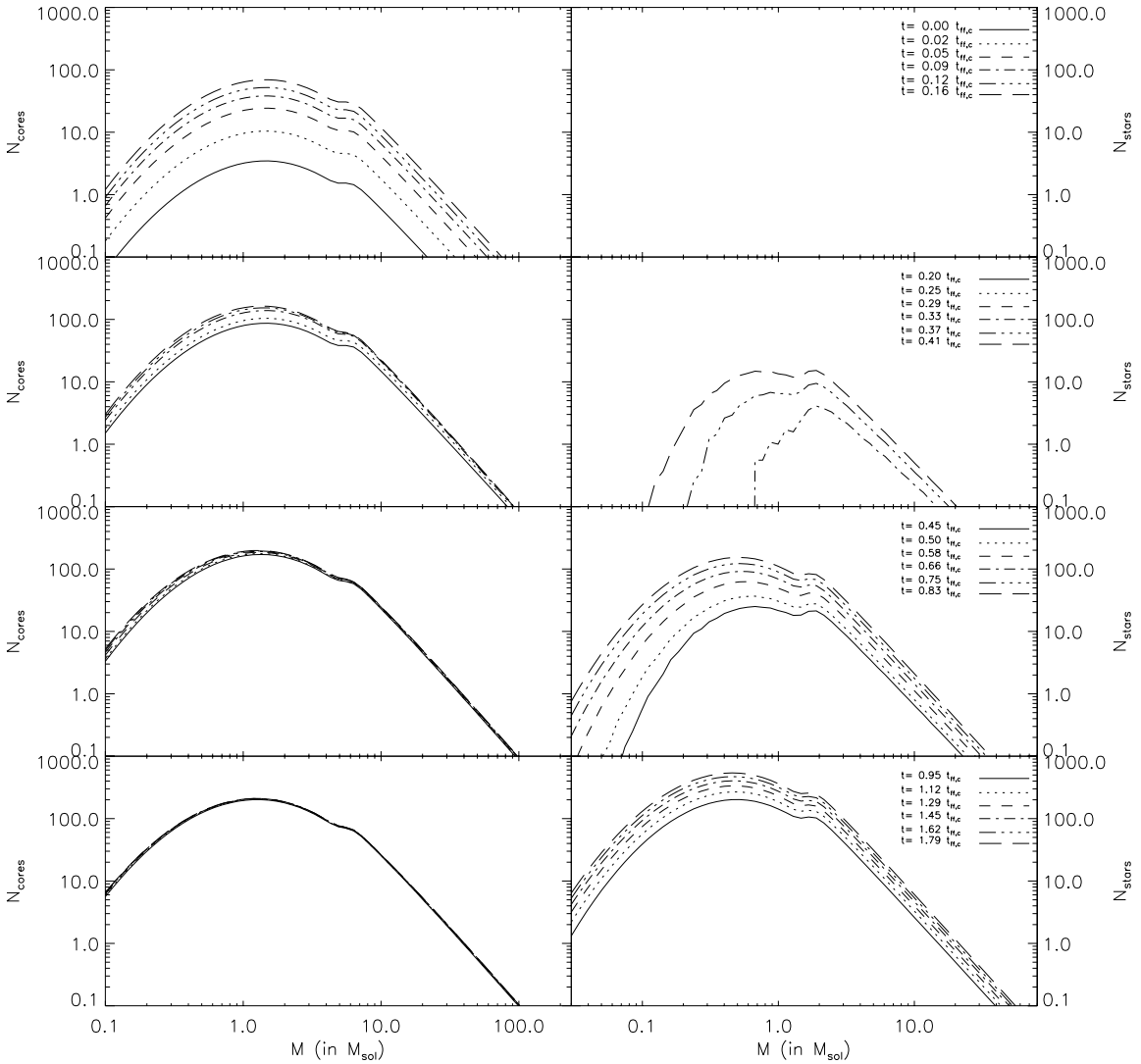

Figure 2.8: Time evolution of the pre-stellar core mass function (left), and stellar mass function (right) in the protocluster clump with the fiducial model parameters. The last time-step shown is 1.79 $t_{ff,c}$ which corresponds to the epoch at which gas is expelled from the protocluster clump. Adapted from Dib et al. [2011].

$$P(M_J)\ dM_J = \frac{2\ M_{J0}^2}{\sqrt{2\pi\sigma_d^2}} M_J^{-3} \exp\left[-\frac{1}{2}\left(\frac{\ln\ M_J - A}{\sigma_d}\right)^2\right] dM_J, \tag{2.20}$$

where M_{J0} is the Jeans mass at the mean local density, and σ_d is the standard deviation of the density distribution which is a function of the local thermal rms Mach number. Therefore, the local distribution of cores generated in the clump, at an epoch τ, $N(r, M, \tau)$, is obtained by multiplying the local normalised function $N(r, M)$ by the local rate of fragmentation such that:

$$N(r, M, \tau)dt = \frac{CFE_{ff}(r)\rho_c(r)}{< M > (r)\ t_{cont,p}(r, M)} \frac{dt}{t_{ff,c}} N(r, M), \tag{2.21}$$

where dt is the time interval between two consecutive epochs, $< M >$ is the average core mass in the local distribution and is calculated by $< M >= \int_{M_{min}}^{M_{max}} M\ N(r, M, 0)\ dM$, and CFE_{ff} is a parameter smaller than unity which describes the local mass fraction of gas that is transformed into cores per free fall time of the protocluster clump, $t_{ff,c}$. In the present study, we assume that CFE_{ff} is independent of r.

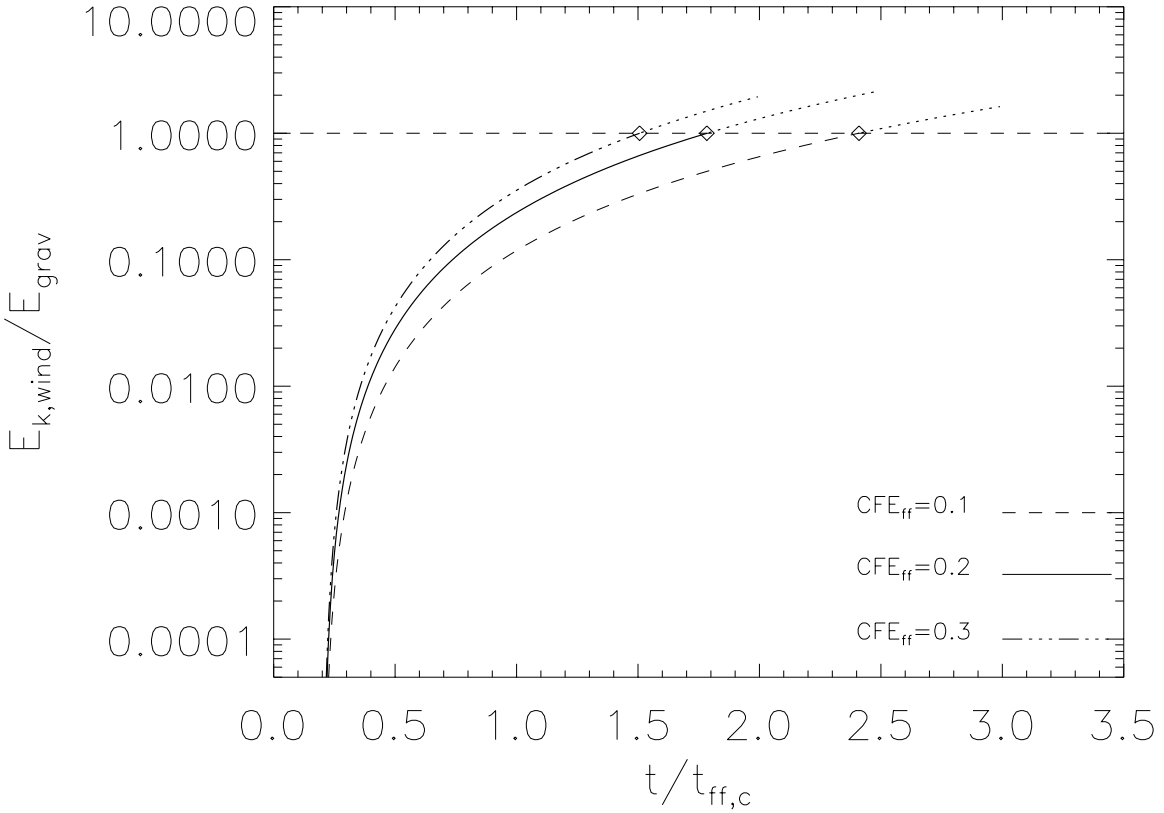

Figure 2.9: Time evolution of the ratio of the effective kinetic energy generated by stellar winds and the gravitational energy of the protocluster clump. Time is shown in units of the protocluster clump free fall timescale $t_{ff,c}$. The horizontal dashed corresponds to $E_{k,wind}/E_{grav} = 1$ with $\kappa = 0.1$. The full line correspond to the fiducial model with the $CFE_{ff} = 0.2$ and the dashed and triple dot-dashed to cases with $CFE_{ff} = 0.1$ and $CFE_{ff} = 0.3$, respectively. Diamonds correspond to the epochs at which the gas is evacuated from the cluster in the three models and the processes of core and star formation are terminated. Adapted from Dib et al. [2011].

Feedback Model

In this model, the formation of cores in the protocluster clump, and consequently star formation, are terminated whenever the fraction of the wind energy stored into motions that oppose gravity exceeds the gravitational energy of the clump. Thus, at any epoch $t < t_{exp}$ (t_{exp} is the epoch at which gas is expelled from the clump), gas is removed from the clump only to be turned into stars. We take into account the feedback generated by the stellar winds of massive stars ($M_\star \geq 5$ M$_\odot$). In order to calculate reliable estimates of the feedback generated by metallicity dependent stellar winds, we proceed in two steps. In the first step, we use a modified version of the stellar evolution code CESAM (see Appendix 1 in Piau et al. [2011]) to calculate a grid of main sequence stellar models for stars in the mass range [5 – 80] M$_\odot$ (with steps of 5 M$_\odot$) at various metallicities $Z/Z_\odot = [1/10, 1/6, 1/3, 1/2, 1, 2]$ ($Z_\odot = 0.0138$). The evolution of massive stars is followed using the CESAM code for ~ 1 Myr, on the main sequence. The characteristic stellar properties, which are the effective temperature T_{eff}, the luminosity $L_\star$, and the stellar radius $R_\star$ are then used in the stellar atmosphere model of Vink et al. [2001] in order to calculate the stellar mass loss rate $\dot{M}_\star$. Vink et al. [2001] did not derive the values of the terminal velocities of the winds (v_∞), therefore, we use instead the derivations of v_∞ obtained by Leitherer et al. [1992]. Fig. 2.6 displays the mass loss rates calculated for OB stars at the various metallicities. The power of the stellar winds is given by $\dot{M}_\star v_\infty^2$. This quantity is displayed in Fig. 2.7 for the models with different metallicities. Both $\log(\dot{M}_\star)$ and $\dot{M}_\star v_\infty^2$ are fitted with fourth order polynomials (overplotted to the data) and whose coefficients are provided in Dib et al. [2011]. The $\dot{M}_\star v_\infty^2 - M_\star$ relations displayed in Fig. 2.7 allow for the calculation of the total wind energy deposited by stellar winds. The total energy from the winds is given by:

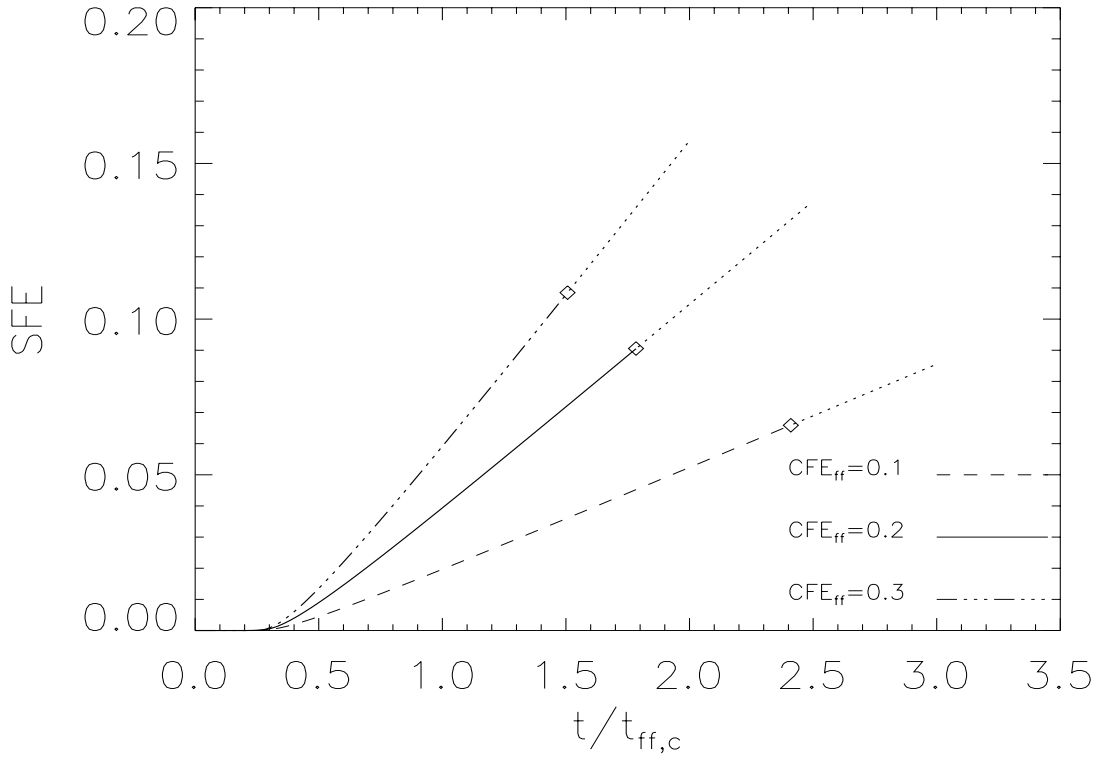

Figure 2.10: Time evolution of the SFE in the protocluster clump. The full line corresponds to the fiducial model with the $CFE_{ff} = 0.2$ and the dashed and triple dot-dashed to cases with $CFE_{ff} = 0.1$ and $CFE_{ff} = 0.3$, respectively. Time is shown in units of the protocluster clump free fall timescale $t_{ff,c}$. Diamonds correspond to the epochs at which the gas is evacuated from the cluster and indicates the final value of the SFE, SFE_f, in the three models. Adapted from Dib et al. [2011].

$$E_{wind} = \int_{t'=0}^{t'=t} \int_{M_\star=5\ \mathrm{M}_\odot}^{M_\star=120\ \mathrm{M}_\odot} \left(\frac{N(M_\star)\dot{M}_\star(M_\star)v_\infty^2}{2} dM_\star \right) dt'. \tag{2.22}$$

We assume that only a fraction of E_{wind} will be transformed into systemic motions that will oppose gravity and participate in the evacuation of the bulk of the gas from the protocluster clump. The rest of the energy is assumed to be dissipated in wind-wind collisions or escape the wind bubble. The effective kinetic wind energy is thus given by:

$$E_{k,wind} = \kappa\ E_{wind}, \tag{2.23}$$

where κ is a quantity ≤ 1. It is currently difficult to estimate κ as its exact value will vary from system to system depending on the number of massive stars, their locations, and their wind interactions. As a conservative guess for the fiducial model, we take $\kappa = 0.1$. $E_{k,wind}$ is compared at every timestep to the absolute value of the gravitational energy, E_{grav}, which is calculated as being:

$$E_{grav} = -\frac{16}{3}\pi^2 G \int_0^{R_c} \rho_c(r)^2 r^4 dr, \tag{2.24}$$

where ρ_c is given by Eq. 2.14.

The co-evolution of the core mass function and of the IMF

Whenever a population of cores of mass M, located at a distance r from the centre of the clump has evolved for a time that is equal to its contraction timescale, it is collapsed into stars. Thus, the local

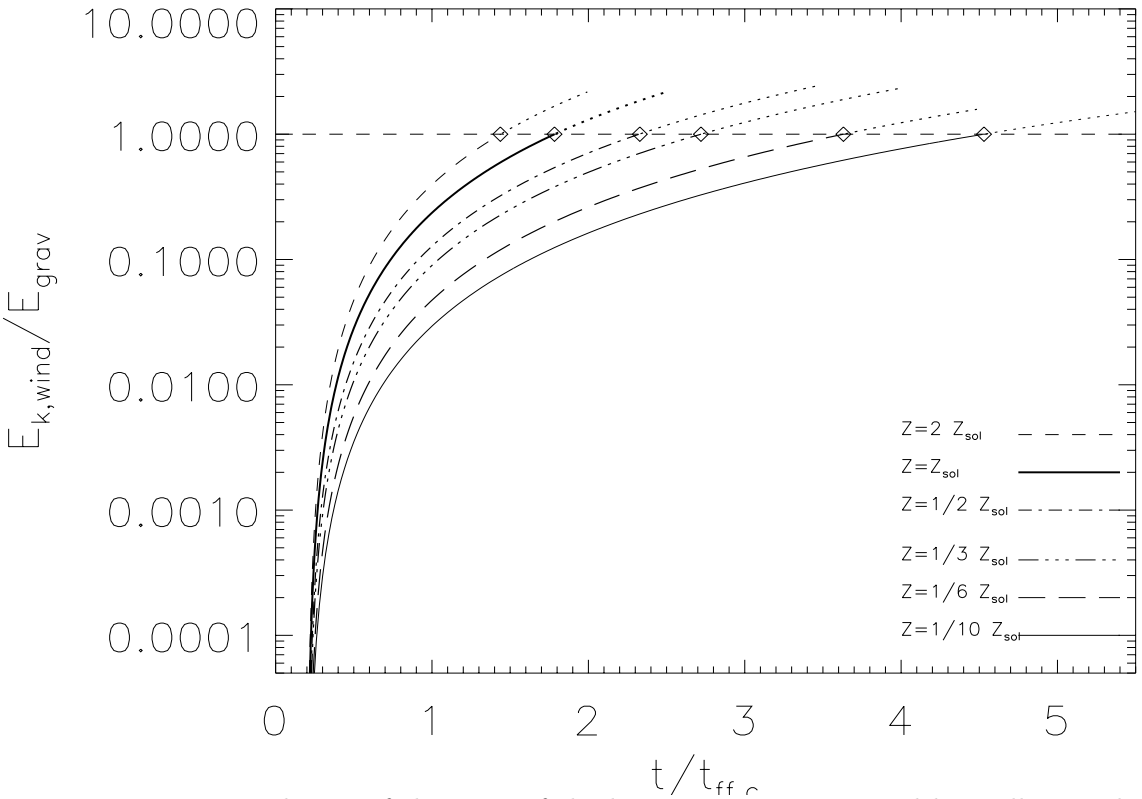

Figure 2.11: Time evolution of the ratio of the kinetic energy generated by stellar winds and the gravitational energy of the protocluster clump. Time is shown in units of the protocluster clump free fall timescale $t_{ff,c}$. The horizontal dashed corresponds to $E_{k,wind}/E_{grav} = 1$ with $\kappa = 0.1$. Diamonds correspond to the epochs at which the gas is evacuated from the cluster in the three models. The mass of the clump in these models is 10^5 $M_\odot$. Adapted from Dib et al. [2011].

number of cores of a given mass, at a given epoch τ, is the sum of all the local populations of cores of the same mass that have formed at all epochs anterior or equal to the considered epoch with the additional step of subtracting from that sum the cores of the same mass that have readily collapsed into stars. The local populations of cores of various ages are evolved separately as they are each in a different phase of their contraction, and will collapse and form stars at various epochs. Thus, the total local number of cores of a given mass M, at a time t, is given by:

$$N(r, M, t) = \sum_{\tau_i \leq t} N(r, M, \tau_i, t). \tag{2.25}$$

We assume that only a fraction of the mass of a core ends up locked in the star. We account for this mass loss in a purely phenomenological way by assuming that the mass of a star which is formed out of a core of mass M is given by $M_\star = \xi M$, where $\xi \leq 1$. Matzner & McKee [2000] showed that ξ can vary in the range $0.25 - 0.75$. In this section, we describe the results for a fiducial model. In this model, the mass of the clump is taken to be $M_{clump} = 10^5$ $M_\odot$, the metallicity is $Z = Z_\odot$, and the CFE is $CFE_{ff} = 0.2$, where $t_{ff,cl}$ is the free-fall time of the clump and is given by $t_{ff,c} = (3\pi/32\ G\bar{\rho}_c)^{1/2}$, and $\bar{\rho}_c$ the average density of the clump. The other quantities have been taken to be equal to the most commonly cited observational determinations and have been set, in the fiducial model as well as in all other models, to the following values: $R_{c0} = 0.2$ pc, $\nu = 3$, $\mu = 0.2$, $\kappa = 0.1$. We also assume that $\xi = 1/3$. Fig. 2.8 displays the time evolution of the CMF (left column) and of the IMF (right column) in the fiducial model. By $t \sim 0.3\ t_{ff,c}$, the first stars form. In this model, since $\mu = 0.2 > 0$, the most massive stars form first, as the most massive cores tend to be, at any given position in the clump, more centrally peaked and thus have shorter lifetimes. As time advances, the IMF becomes fully populated. On the other hand, the CMF ceases to evolve (i.e., there is no accretion or coalescence in this model as in Dib [2007], Dib et al. [2007b]; Dib et al. [2008b]; and Dib et al. [2010a]) as the numbers of cores that are

newly formed at each position in the protocluster clump is balanced by an equal number of cores which collapses and forms stars. The final IMF of the cluster is established at $\sim 1.79\ t_{ff,c}$, which corresponds to the last epoch shown in Fig. 2.8. At this epoch, Fig. 2.9 shows that the ratio $E_{k,wind}/E_{grav}$ reaches unity (full line), and as a consequence, gas is expelled from the protocluster region. Fig. 2.10 displays the time evolution of the SFE in this model (full line). At $t = t_{exp} = 1.79\ t_{ff,c}$, the final value of the SFE is $SFE_{exp} \sim 9.05 \times 10^{-2}$.

In this fiducial model, we have adopted a CFE value of $CFE_{ff} = 0.2$. This is an intermediate value between the values of ~ 0.06 and ~ 0.33 measured by Dib et al. [2010a] in numerical simulations of molecular clouds with two different degrees of magnetisation. At first glance, it may appear that increasing the CFE_{ff} by a given factor will lead to an increase in SFE_{exp} by approximately the same factor. However, for a fully sampled IMF, a larger CFE_{ff} value implies that a larger number of OB stars will be formed and deposit larger amounts of feedback by stellar winds in the protocluster region. This in turn leads to a faster evacuation of the gas and to a limitation of the SFE_{exp}. Fig. 2.9 shows that in two other models similar to the fiducial case but with a different CFE_{ff}, the evacuation of the gas occurs faster for the higher CFE case (i.e., case with $CFE_{ff} = 0.3$) and slower for the low CFE case (i.e., $CFE_{ff} = 0.1$). The time evolution of the SFE in these two additional models is compared to the fiducial case in Fig. 2.10. The final values of the SFE at $t = t_{exp}$ are $SFE_{exp} \sim 6.59 \times 10^{-2}$, $\sim 9.05 \times 10^{-2}$, and ~ 0.11 for the cases with $CFE_{ff} = 0.1, 0.2$, and 0.3 respectively. A factor of 2 and 3 increase in the CFE_{ff} leads to an increase of the SFE_{exp} only by factors of ~ 1.37 and ~ 1.64, respectively. This implies a strong regulation of the effect of a varying CFE by stellar feedback on the resulting SFE_{exp} in protocluster clumps.

The dependence of the star formation efficiency on metallicity

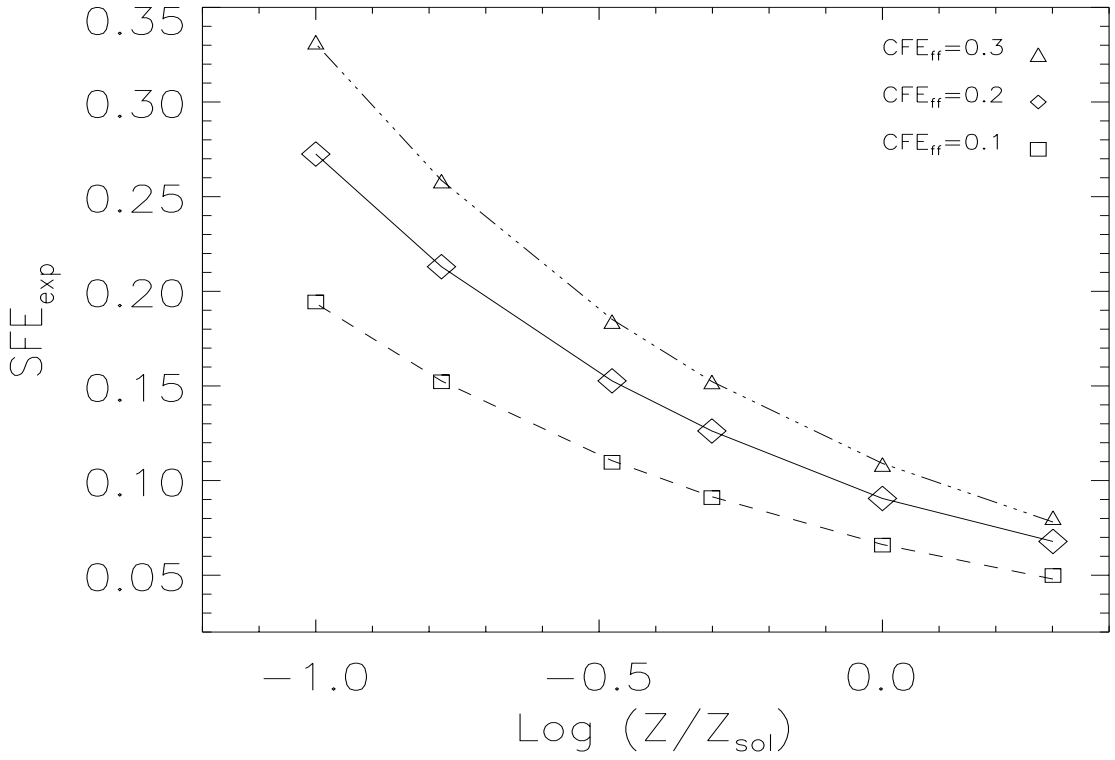

Figure 2.12: SFE_{exp}-Metallicity relations for clumps with the fiducial mass of 10^5 $M_\odot$ and for different core formation efficiencies of $CFE_{ff} = 0.1$, 0.2, and 0.3. Over-plotted to the data are fit functions (Eq. 2.33) whose parameters are given in Dib et al. [2011]. Adapted from Dib et al.[2011].

Fig. 2.11 displays the time evolution of the ratio $E_{k,wind}/E_{grav}$ in models similar to the fiducial case but with metallicities varying between $Z = 0.1\ Z_\odot$ and $Z = 2\ Z_\odot$. All six models have the fiducial value

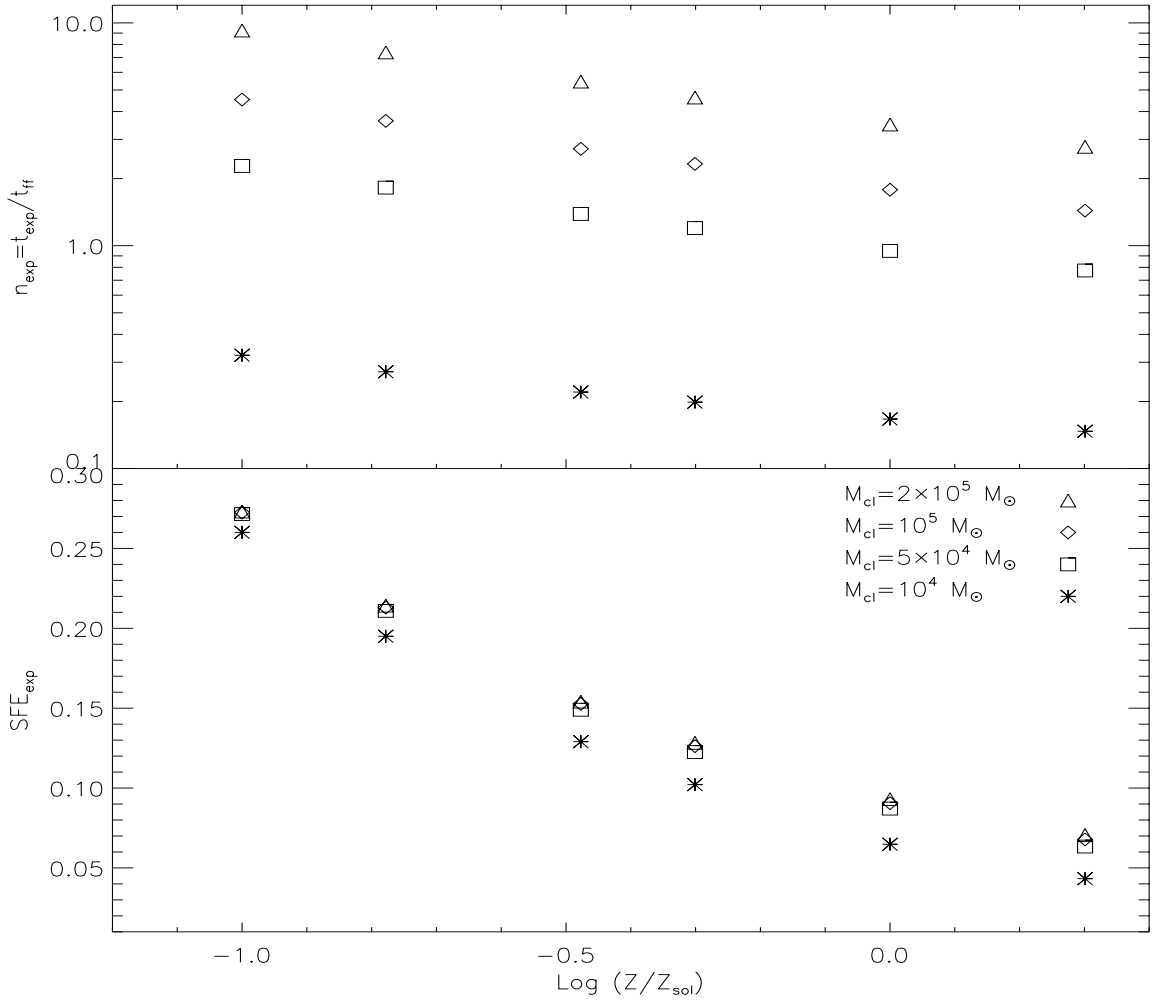

Figure 2.13: Dependence of the quantities SFE_{exp} (final star formation efficiency) and $n_{exp} = t_{exp/t_{ff}}$ (ratio of the expulsion time to the free-fall time) for selected values of the protocluster clump masses and metallicies. Adapted from Dib [2011].

of the CFE, $CFE_{ff} = 0.2$. In models with lower metallicities, the power of the stellar winds in weaker (i.e., Fig. 2.7) and the evacuation of the gas occurs at later epochs as compared to the higher metallicity cases. In the model with $Z = 2\ Z_\odot$, the gas is expelled from the protocluster region at $t \sim 1.4\ t_{ff,c}$ while in the model with $Z = 0.1\ Z_\odot$, the gas expulsion is delayed until $t \sim 4.5\ t_{ff,c}$. For a given CFE_{ff}, longer timescales imply a larger SFE_{exp}. These values are plotted versus metallicity in Fig. 2.12. A clear trend is observed in which the SFE_{exp} increases with decreasing metallicity (diamonds). We fit the $SFE_{exp} - Z$ points in Fig. 2.12 with the following functional form:

$$SFE_f = C_Z\ e^{-\frac{1}{\tau_Z}\log\left(\frac{Z}{Z_\odot}\right)}. \tag{2.26}$$

For the case with $CFE_{ff} = 0.2$, the fit parameters are $C_Z = 0.091 \pm 6.8\times10^{-4}$ and $\tau_Z = 0.91 \pm 7.9\times10^{-3}$. We have also repeated the calculations at the various metallicities using the additional values of $CFE_{ff} = 0.1$ and $CFE_{ff} = 0.3$. The dependence of the SFE_{exp} on metallicity in these cases are also displayed in Fig. 2.12. Fig. 2.12 shows that the SFE_{exp} varies typically by a factor of $\sim 1.3 - 1.4$ and $\sim 1.6 - 1.7$ for variations of the CFE by factors of 2 and 3, respectively. This argues for a strong regulation of the SFE by feedback.

The Kennicutt-Schmidt laws in the feedback regulated model of star formation

Using the above described model, it is possible to derive a metallicity dependent star formation rate (SFR) at a given surface density Σ_g. For a summary on the recent observational determinations of the star formation laws see Kennicutt [2008], Elmegreen [2011], and Dib [2011]. The star formation rate surface density in the feedback regulated mode of star formation is given by:

$$\Sigma_{SFR} = \Sigma_g \ f_{H2} \frac{\langle SFE_{exp} \rangle}{\langle t_{exp} \rangle}, \tag{2.27}$$

where $\langle SFE_{exp} \rangle$ and $\langle t_{exp} \rangle$ are, respectively, the characteristic SFE_{exp} and the epoch at which gas is expelled from the protocluster region for the clump mass distribution associated with a given Σ_g. Writing $\langle t_{exp} \rangle$ in terms of the clumps free-fall time $\langle t_{ff} \rangle$, Eq. 2.10 becomes:

$$\begin{aligned} \Sigma_{SFR} &= \Sigma_g \ f_{H_2} \frac{\langle SFE_{exp} \rangle}{\langle n_{exp} \rangle} \frac{1}{\langle t_{ff} \rangle} \\ &= \Sigma_g \ f_{H_2} \frac{\langle f_{\star,ff} \rangle}{\langle t_{ff} \rangle}. \end{aligned} \tag{2.28}$$

where $f_{\star,ff}$ is the dimensionless star formation efficiency and which corresponds to the mass fraction of the molecular gas that is converted into stars per free-fall time $t_{ff,c}$ of the clumps. $\langle f_{\star,ff} \rangle$ and $\langle t_{ff} \rangle$ represent characteristic values of $f_{\star,ff}$ and $t_{ff,c}$ for the spectrum of clump masses found in the giant molecular for a given value of Σ_g. The quantity f_{H_2} is the mass fraction of the total gas that is in molecular form. In this work, we use the functional form of f_{H_2} obtained by Krumholz et al. [2009a] who derived f_{H_2} as a function of the gas surface density and metallicity (see their paper or Dib [2011] for the detailed formula). $\langle t_{ff,c} \rangle$ can be approximated by the free-fall time of the clump with the characteristic mass $t_{ff,c}(M_{char}) = 8\Sigma_{cl}^{'-3/4} M_{char,6}^{1/4}$ Myr where $M_{char,6} = M_{char}/10^6$ $M_\odot$. The characteristic mass M_{char} is given by :

$$M_{char} = \int_{M_{cl,min}}^{max(M_{cl,max}, M_{GMC})} M_{cl} N(M_{cl}) dM_{cl}, \tag{2.29}$$

where $N(M_{cl})$ is the mass function of protocluster-forming clumps which we take to be $N(M_{cl}) = A_{cl} M_{cl}^{-2}$, and A_{cl} is a normalisation coefficient given by $A_{cl} \int_{M_{cl,min}}^{max(M_{cl,max}, M_{GMC})} N(M_{cl}) dM_{cl} = \epsilon$, where $0 < \epsilon < 1$ is the mass fraction of the GMCs that is in protocluster clumps at any given time. In this work we use $\epsilon = 0.5$. The minimum clump mass $M_{cl,min}$ is taken to be 2.5×10^3 $M_\odot$ (this guarantees, for final SFEs in the range of 0.05 – 0.3 a minimum mass for the stellar cluster of ~ 50 $M_\odot$) and the maximum clump mass is 10^8 $M_\odot$. The characteristic GMC mass is determined by the local Jeans mass and is given by:

$$M_{GMC} = 37 \times 10^6 \left(\frac{\Sigma_g}{85 \ M_\odot \ pc^{-2}} \right) M_\odot. \tag{2.30}$$

Fig. 2.15 *Top*: displays M_{char} as a function of Σ_g. Fig. 2.13 displays the dependence of SFE_{exp} and t_{exp} on clump mass and metallicity for a series of models in which the $CFE_{ff} = 0.2$. The SFE_{exp} depends strongly on metallicity but weakly on mass whereas t_{exp} displays a clear dependence on both quantities. The quantity $f_{\star,ff} = SFE_{exp}/n_{exp}$ is displayed in Eq. 2.19 (left panel) as a function of mass and metallicity ($Z^{'} = Z/Z_\odot$). A fit to the $f_{\star,ff}$ $(M_{cl}, Z^{'})$ data points with a 2-variables second order polynomial yields the following relation (shown in Fig. 2.14, right panel):

$$\begin{aligned} f_{\star,ff}(M_{cl}, Z^{'}) = 11.31 &- 4.31 \log(\mathrm{M_{cl}}) + 0.41 [\log(\mathrm{M_{cl}})]^2 \\ &- 8.28 Z^{'} + 3.20 Z^{'} \log(\mathrm{M_{cl}}) - 0.32 Z^{'} [\log(\mathrm{M_{cl}})]^2 \\ &+ 2.30 Z^{'2} - 0.89 Z^{'2} \log(\mathrm{M_{cl}}) + 0.08 Z^{'2} [\log(\mathrm{M_{cl}})]^2. \end{aligned} \tag{2.31}$$

Using Eq. 2.31, it is then possible to calculate $\langle f_{\star,ff} \rangle$:

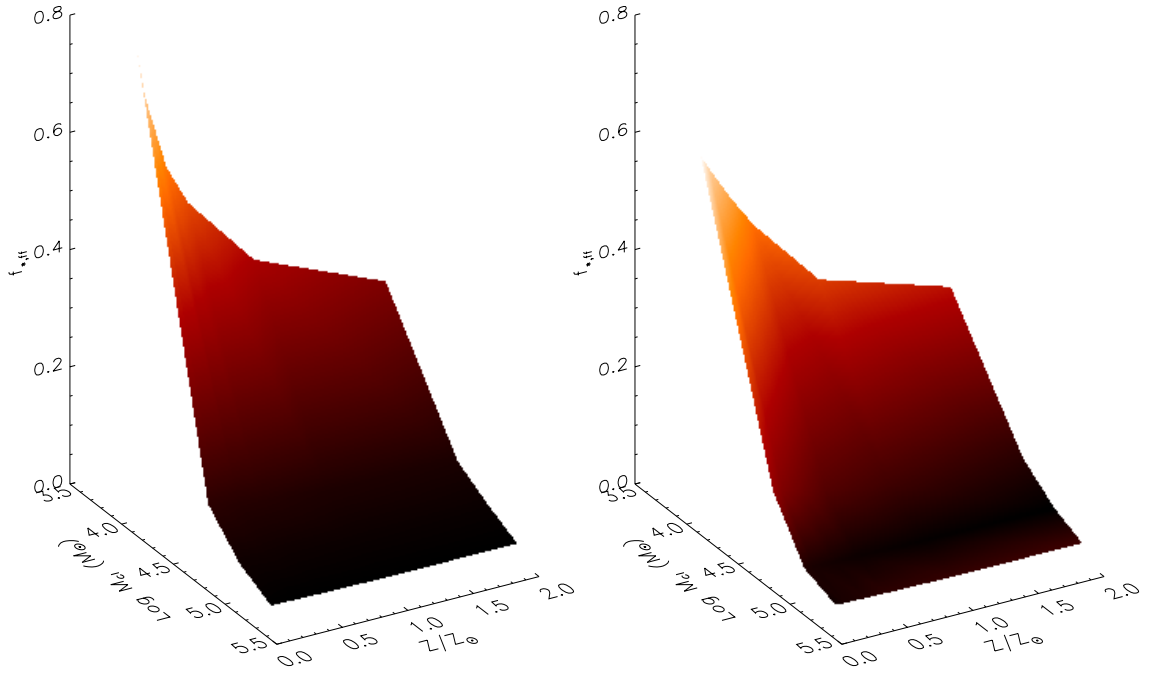

Figure 2.14: Star formation efficiency per unit free-fall time in the protocluster clump in the metallicity-dependent feedback model. The star formation efficiencies per free-fell use a core-to-star efficiency conversion factor of 1/3. The left panel displays $f_{\star,ff}$ as a function of both M_{cl} and $Z^{'} = Z/Z_{\odot}$ in the original data, while the right panel displays the analytical fit function to this data set given in Eq. 2.16. Adapted from Dib [2011].

$$\langle f_{\star,ff} \rangle \left(Z^{'}, \Sigma_g\right) = \int_{M_{cl,min}}^{max(M_{cl,max}, M_{GMC})} f_{\star,ff}(M_{cl}, Z^{'}) N(M_{cl}) dM_{cl}. \tag{2.32}$$

Fig. 2.15 *Bottom*: displays $\langle f_{\star,ff} \rangle \left(Z^{'}, \Sigma_g\right)$ for values of $Z^{'}$ in the range $[0.1 - 2]$. We assume that there is a critical value of $\Sigma_g = 85$ M$_\odot$ pc^{-2} below which clumps are pressurised by their internal stellar feedback, such that $\Sigma_{cl} = \Sigma_{g,crit}$ where $\Sigma_g < \Sigma_{g,crit}$ and $\Sigma_{cl} = \Sigma_{GMC} = \Sigma_g$ when $\Sigma_g \geq \Sigma_{g,crit}$. With the above elements, the star formation law can be re-written as:

$$\begin{aligned} \Sigma_{SFR} &= \frac{8}{10^6} f_{H_2}(\Sigma_g, c, Z^{'}) \Sigma_g \\ &\times \left\{ \begin{array}{ll} \frac{\langle f_{\star,ff} \rangle (Z^{'})}{M_{char,6}^{1/4}} & ; \frac{\Sigma_g}{85 \text{ M}_\odot \text{ pc}^{-2}} < 1 \\ \frac{\langle f_{\star,ff} \rangle (Z^{'})}{M_{char,6}^{1/4}} \left(\frac{\Sigma_g}{85 \text{ M}_\odot \text{pc}^{-2}}\right)^{3/4} & ; \frac{\Sigma_g}{85 \text{ M}_\odot \text{ pc}^{-2}} \geq 1 \end{array} \right\}, \end{aligned} \tag{2.33}$$

where Σ_{SFR} is in M$_\odot$ yr^{-1} kpc^{-2}, M_{char} is given by Eq. 2.29, and $\langle f_{\star,ff} \rangle$ by Eqs. 2.31 and 2.32. Fig. 2.16 (top panel) displays the results obtained using Eq. 2.33 for Σ_g values starting from low gas surface densities up to the starburst regime. The results are calculated for the metallicity values of $Z^{'} = [0.1, 0.3, 0.5, 1, 2]$. The results are compared to the sub-kpc data of Bigiel et al. [2008, 2010] and to the normal and starburst galaxies results of Kennicutt [1998] (Fig. 2.16, bottom panel displays the results of Krumholz et al. [2009] which is based on the regulation of star formation by turbulence in GMCs). Our models fits remarkably well the observational results over the entire range of surface densities. Furthermore, the segregation by metallicity extends beyond the low surface density regime up to the starburst regime where a segregation in metallicity of ~ 0.5 is observed, in contrast to the Krumholz et al. [2009b] models which do not contain a metallicity dependence in the intermediate to high surface density regimes. Furthermore the solar metallicity curve in our model overlaps with a significant fraction of the sub-regions in the data of Bigiel et al. [2008, 2010] in contrast to the Krumholz et al. model.

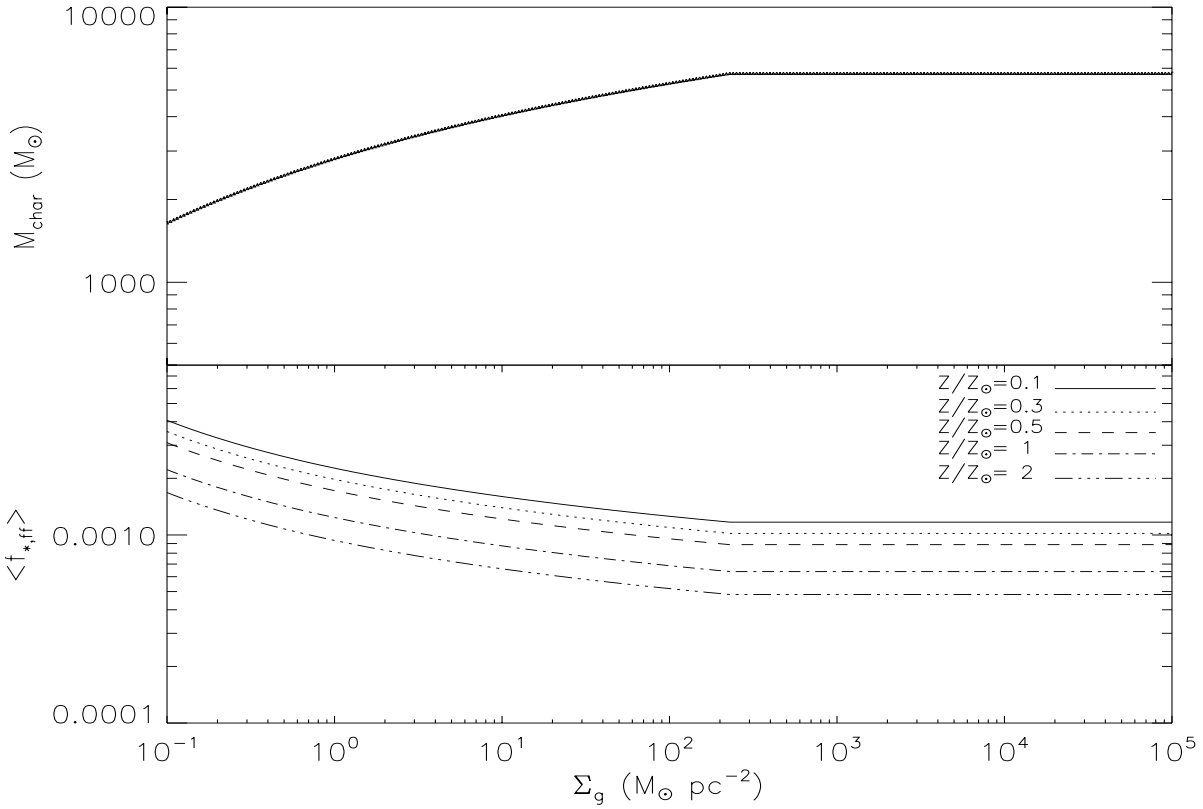

Figure 2.15: Characteristic clump mass as a function of the gas surface density (Eq. 2.12, top panel) and the star formation efficiency per unit free-fall time in this feedback regulated model of star formation. Adapted from Dib [2011].

Conclusions

We have described a model for star formation in protocluster clumps of difference metallicities. The model describes the co-evolution of the dense core mass function and of the IMF in the clumps. Cores form uniformly over time in the clumps following a prescribed core formation efficiency per unit time. Cores contract over timescales which are a few times their free fall time before they collapse to form stars. Feedback from the newly formed OB stars (> 5 $M_\odot$) is taken into account and when the ratio of the cumulated effective kinetic energy of the winds to the gravitational energy of the system (left over gas+stars) reaches unity, gas is expelled from the clump and further core and star formation are quenched. The radiation driven winds of OB stars are metallicity dependent. Metal rich OB stars inject larger amounts of energy into the clump than their low metallicity counterparts and thus help expel the gas on shorter timescales. This results in reduced final star formation efficiencies in metal rich clumps in comparison to their low metallicity counterparts. Both the final star formation efficiency and the gas expulsion timescales are combined for a grid of clump models with different masses and metallicities in order to calculate the star formation efficiency per unit time ($f_{\star,ff}$) in this feedback regulated model of star formation. We calculate the characteristic value of $f_{\star,ff}$ for a clump mass distribution associated with a gas surface density, Σ_g. This is combined with a description of the molecular mass fraction as a function of Σ_g and the assumption that there is a critical surface gas density ($\Sigma_g = 85$ $M_\odot$ pc^{-2}) above which the protocluster clumps and their parent giant molecular clouds switch from being pressurised from within by stellar feedback to being confined by the external interstellar medium pressure. The combination of these three elements allows us to construct the star formation laws in galaxies going from low gas surface densities up to the starburst regime. Our models exhibit a dependence on metallicity over the entire range of considered gas surface densities and fit remarkably well with the observational data of Bigiel et al. [2008, 2010] and Kennicutt [1998]. This dependence on metallicity of the KS relation may well explain the scatter (or part of it) that is seen in the observationally derived relations.

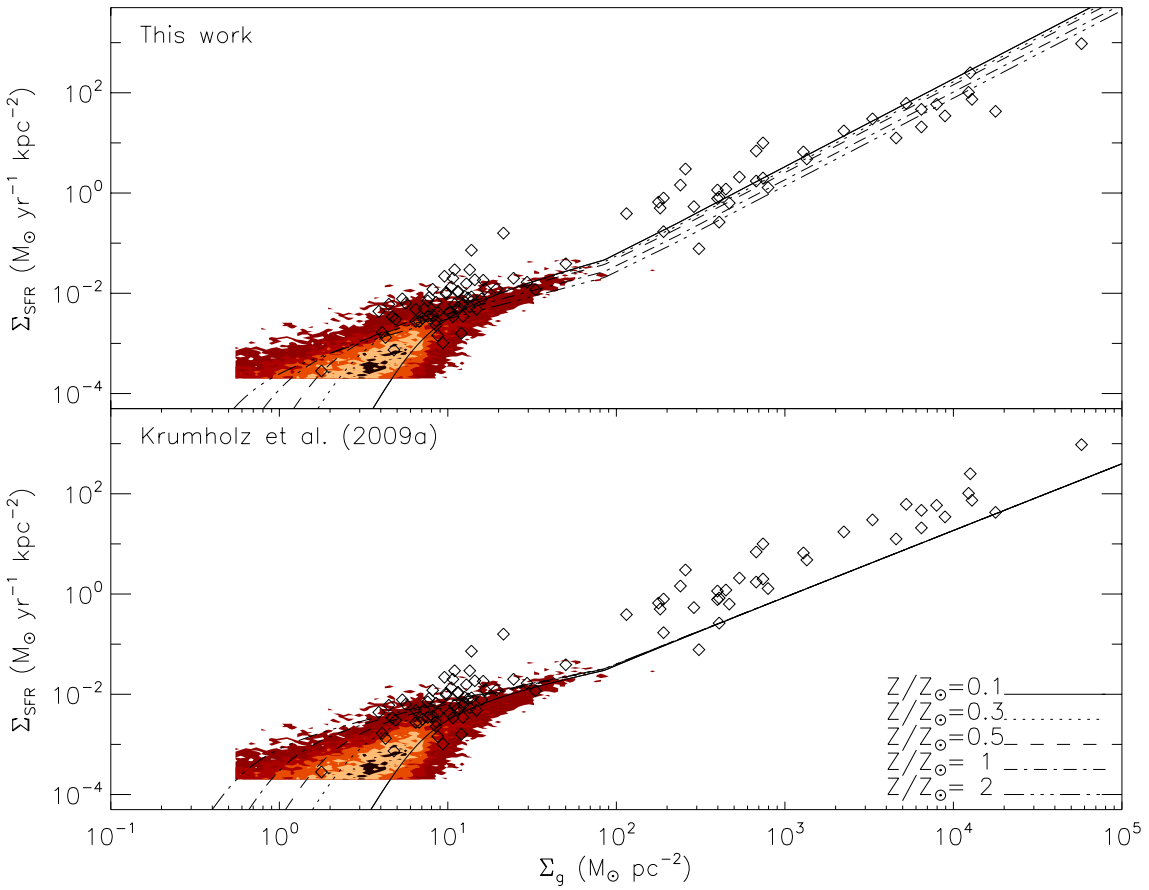

Figure 2.16: Star formation laws in the feedback-regulated star formation model (this work, top panel), and in the Krumholz et al. [2009a] model (bottom panel). Overplotted to the models are the normal and starburst galaxies data of Kennicutt [1998] and the combined sub-kpc data (4478 subregions in total) for 11 nearby galaxies from Bigiel et al. [2008, 2010]. The Bigiel et al. [2008, 2010] data is shown in the form of a 2D histogram with the colour coding corresponding, from the lighter to the darker colours to the 1,5,10,20, and 30 contour levels. The displayed theoretical models cover the metallicity range $Z^{'} = Z/Z_\odot = [0.1, 2]$. Adapted from Dib [2011].

Acknowledgments

I would like to thank the members of the organising committees for setting up a very inspiring conference and Subhanjoy Mohanty, Jonathan Braine, George Helou, Laurent Piau for useful discussions and collaboration on this work. Support for this work has been provided by STFC grant ST/H00307X/1.

Bibliography

Adams, F. C., & Fatuzzo, M. 1996, ApJ, 464, 256
Baumgardt, H., Kroupa, P., Parmentier, G. 2008, MNRAS, 384, 1231
Bigiel, F., Leroy, A. K., Walter, F., Brinks, E., de Blok, W. J. G., Madore, B., & Thornley, M. D. 2008, AJ, 136, 2846
Bigiel, F., Leroy, A. K., Walter, F., Blitz, L., Brinks, E., de Blok, W. J. G., & Madore, B. 2010, AJ, 140, 1194
Boissier, S., Boselli, A., Prantzos, N., & Gavazzi, G. 2001, MNRAS, 321, 733
Braine, J., Duc, P.-A., Lisenfeld, U., Charmandaris, V., Vallejo, O., Leon, S., & Brinks, E. 2001, A&A, 378, 51
Bresolin, F.,& Kudritzki, R. P. 2004, in Origin and Evolution of the Elements, ed. A. McWilliam & M. Rauch (Cambridge Univ. Press), 283
Csengeri, T., Bontemps, S., Schneider, N., Motte, F., & Dib, S. 2011, A&A, 527, 135

Dib, S., Bell, E., & Burkert, A. 2006, ApJ, 638, 797
Dib, S. 2007, JKAS, 40, 157
Dib, S., & Kim, J. 2007, in Small Ionized and Neutral Structures in the Diffuse Interstellar Medium, ed. M. Haverkorn, & M. Goss (ASP Conference Series), p. 166
Dib, S., Kim, J., Vázquez-Semadeni, E., Burkert, A., & Shadmehri, M. 2007a, ApJ, 661, 262
Dib, S., Kim, J., & Shadmehri, M. 2007b, MNRAS, 381, L40
Dib, S., Brandenburg, A., Kim, J., Maheswar, G., & André, P. 2008a, ApJ, 678, L105
Dib, S., Shadmehri, M., Maheswar, G., Kim, J., & Henning, Th. 2008b, in Massive Star Formation: Observations confront Theory, ASP Conf. Series, Ed. H. Beuther, H. Linz, T. Henning, 387, 282
Dib, S., Galván-Madrid, R., Kim, J., & Vázquez-Semadeni, E. 2008c, in the proceedings of the Annual meeting of the French Society of Astrobomy & Astrophysics, 309, Eds. C. Charbonnel, F. Combes, & R. Samadi, (arXiv:0808.3305)
Dib, S., Walcher, C. J., Heyer, M., Audit, E., & Loinard, L. 2009, MNRAS, 398, 1201
Dib, S., Hennebelle, P., Pineda, J. E., Csengeri, T., Bontemps, S., Audit, E., & Goodman, A. A. 2010a, ApJ, 723, 425
Dib, S., Shadmehri, M., Padoan, P., Maheswar, G., Ojha, D. K., & Khajenabi, F. 2010b, MNRAS, 405, 401
Dib, S., Piau, L., Mohanty, S., & Braine, J. 2011, MNRAS, accepted, (arXiv:1102.3839)
Dib, S., ApJ, submitted, (arXiv:1106.3282)
Elmegreen, B. G. 2011, preprint (arXiv:1101.3108)
Evans, N. J., Dunham, M. M., Jørgensen, J. K. et al. 2009, ApJS, 181, 321
Fukui, Y., & Mizuno, A. 1991, in IAU Symp. 147, Fragmentation of Molecular Clouds and Star Formation, eds. E. Falgarone, F. Boulanger, & G. Duvert, (Dordrecht: Kluwer), 275
Duerr, R., Imhoff, C. L., Lada, C. J. 1982, ApJ, 261, 135
Galván-Madrid, R., Vázquez-Semadeni, E., Kim, J., Ballesteros-Paredes, J. 2000, ApJ, 670, 480
Gong, H., & Ostriker, E. C. 2011, ApJ, 729, 120
Gratier, P., Braine, J., Rodriguez-Fernandez, N. J., Israel, F. P., Schuster, K. F., Brouillet, N., & Gardan, E. 2010a, A&A, 512, 68
Gratier, P., Braine, J., Rodriguez-Fernandez, N. J., Schuster, K. F., Kramer, C. et al. 2010b, A&A, 552, 3
Heitsch, F., Mac-Low, M.-M., Klessen, R. S. 2001, ApJ, 547, 280
Hernandez, A. K., Tan, J. C., Caselli, P., Butler, M. J., Jimenez-Serra, I., Fontani, F., Barnes, P. 2011, ApJ, accepted, (arXiv:1106.2499)
Jessop, N. E., & Ward-Thompson, D. 2000, MNRAS, 311, 63
Johnstone, D., & Bally, J. 2006, ApJ, 653, 383
Kauffmann, J., & Pillai, T. 2010, ApJ, 723, L7
Kennicutt, R. C. Jr. 1998, ApJ, 498, 541
Kennicutt, R. C. Jr. 2008, in Pathways through an Eclectic Universe, ASP Conf. Series, Eds J. H. Knapen, T. J. Mahoney, and A. Vazdekis , 390, 149
Klein, R., Posselt, B., Schreyer, K., Frobrich, J., & Henning, Th. 2005, ApJS, 161, 361
Krumholz, M. R., & McKee, C. F. 2005, ApJ, 630, 250
Krumholz, M. R., McKee, C. F., & Tumlinson, J. 2009a, ApJ, 699, 850
Krumholz, M. R., McKee, C. F., & Tumlinson, J. 2009b, ApJ, 693, 216
Lada, E. A., Bally, J., & Stark, A. A. 1991a, ApJ, 368, 432
Lada, E. A., DePoy, D. L., Evans, J. H., & Gatley, I. 1991b, ApJ, 371, 171
Lada, C. J., & Lada, E. A. 2003, ARA&A, 41, 57
Leitherer, C., Robert, C., Drissen, L. 1992, ApJ, 401, 596
Leroy, A. K., Bolatto, A., Walter, F., & Blitz, L. 2006, ApJ, 643, L825
Leroy, A. K., Walter, F., Brinks, E., Bigiel, F., de Blok, W. J. G., Madore, B., & Thornley, M. D. 2008, AJ, 136, 2728
Li, Z.-Y., Wang, P., Abel, T., & Nakamura, F. 2010, ApJ, 720, L26
Matzner, C. D., & McKee, C. F. 2000, ApJ, 545, 364
Morel, P., & Lebreton, Y. 2008, Ap&SS, 316, 61
Murgia, M., Craspi, A., Moscadelli, L., & Gregorini, L. 2002, A&A, 385, 412
Nakamura, F., & Li, Z.-Y. 2007, ApJ, 662, 395
Olmi, L., & Tesi, L. 2002, A&A, 392, 1053
Padoan, P. 1995, MNRAS, 277, 377
Padoan, P., & Nordlund, Å. 2002, ApJ, 576, 870
Pandey, A. K., Paliwal, D. C., & Mahra, H. S. 1990, ApJ, 362, 165

Parmentier, G., Goodwin, S. P., Kroupa, P., Baumgardt, H. 2008, ApJ, 678, 347
Piau, L., Kervella, P., Dib, S., & Hauschildt, P. 2011, A&A, 526, 100
Price, D. J., & Bate, M. R. 2008, MNRAS, 385, 1820
Rathborne, J. M., Jackson, J. M., & Simon, R. 2006, ApJ, 641, 389
Rathborne, J. M., Jackson, J. M., Chambers, E. T., Stojimirovic, I., Simon, R., Shipman, R., Frieswijk, W. 2010, ApJ, 715, 310
Rengarajan, T. N. 1984, ApJ, 287, 671
Saito, H., Saito, M., Sunada, K., & Yonekura, Y. 2007, ApJ, 659, 459
Schmidt, M. 1959, ApJ, 129, 243
Vázquez-Semadeni, E., & Passot, T. 1999, In interstellar Turbulence, eds., J. Franco and A Carramiñana, University Press (Cambridge), p. 223
Vázquez-Semadeni, E., Ballesteros-Paredes, J., & Klessen, R. S. 2003, ApJ, 585, L131
Vázquez-Semadeni, E., Kim, J., Shadmehri, M., & Ballesteros-Paredes, J. 2005a, ApJ, 618, 344
Vázquez-Semadeni, E., Kim, J., & Ballesteros-Paredes, J. 2005b, ApJ, 630, L49
Vink, J. S., de Koter, A., & Lamers, H. J. G. L. M. 2001, A&A, 369, 574
Ward-Thompson, D., André, P., Crutcher, R., Johnstone, D., Onishi, T., Wilson, C. 2007, in Protostars and Planets V., ed. B. Reipurth, D. Jewitt, & K., Keil (Tuscon:Univ. of Arizona Press), 33
Warin, S., Castets, A., Langer, W. D., Wislon, R. W., & Pagani, L. 1996, A&A 306, 935
Whitworth, A. P., & Ward-Thompson, D. 2001, ApJ, 547, 317
Wilking, B. A., & Lada, C. J. 1983, ApJ, 274, 698
Wolf, G., Lada, C. J., Bally, J. 1990, AJ, 100, 1892

2.4 Proper Motion Analysis of the Galactic Centre Quintuplet Cluster

Benjamin Hußmann[1], A. Stolte[1], W. Brandner[2] and M. Gennaro[2]

[1] Argelander Institut für Astronomie, Universität Bonn, Auf dem Hügel 71, 53121 Bonn, Germany
[2] Max-Planck-Institut für Astronomie, Königsstuhl 17, 69117 Heidelberg, Germany

Abstract

Individual proper motions of stars in the Galactic centre Quintuplet cluster were derived from two epochs of VLT/NACO observations. Cluster and field stars could be discerned based on their measured proper motions and a clean sample of cluster members was established after a subsequent colour-cut. From this sample the present-day mass function was derived for three different cluster ages and found to be top-heavy in all cases.

Introduction

The three young, massive star clusters found in the galactic centre region (Young Nuclear Cluster, Arches and Quintuplet cluster) are among the six most massive, open clusters in our galaxy. As the extreme conditions for star formation in the GC region are likely comparable to the ones found in the HII regions in starburst galaxies these clusters may serve as templates for extragalactic starburst clusters. Further they constitute unique laboratories for stellar evolution, as they contain large numbers of stars in the entire mass range and therefore sample the present-day mass function (PDMF) up to the most massive stars. The Quintuplet cluster with an age of 4 ± 1 Myr (Figer et al. [1999]) displays the lowest spatial density of the three Galactic centre clusters. In order to derive an unbiased sample of cluster stars and determine the mass function correctly, cluster and field stars have to be discerned out to radii where the member density drops below the field star density. The high spatial resolution archived by AO assisted NIR instruments enables to measure stellar proper motions even at Galactic centre distances and distinguish the cluster population from the field.

Observations

Two epochs of high precision astrometric observations of the Quintuplet cluster were obtained in 2003 and 2008 at the Very Large Telescope (VLT) with adaptive optics (AO) correction provided by the NAOS/CONICA (NACO) instrument. The first epoch cover a total field of view (FOV) about 40×40 arcsec^2 in the K_s- and H-band. The K_s-band observations of the second epoch in 2008 map the same area of the cluster. The time baseline between the two epochs is 5.0 yr. After basic data reduction the frames of each dataset were combined and the stellar fluxes and positions were derived with the *starfinder* algorithm (Diolaiti et al. [2000]). This code determines an empirical point spread function (PSF) from selected stars in the image, which is of special importance for AO data due to the complex PSF halo structures. As the *starfinder* code cannot account for a spatial PSF variation a constant PSF was used for each combined image. The usage of a uniform PSF led to an increase of the PSF fitting residuals towards the edges of the respective image and thus to increasing astrometric uncertainties. The analysis was therefore confined to stars within a radius of 13.6 arcsec $\hat{=}$ 0.5 pc from the centre of the observed FOV. Furthermore, stars fainter than $K_s = 19$ mag were excluded as the astrometric uncertainties increase towards the faint end. The photometric zeropoints were obtained from calibrated sources in the UKIRT Infrared Deep Sky Survey (UKIDSS) (Lawrence et al. [2007]; Lucas et al. [2008]), which could unambiguously be assigned to stars in the source catalogue of each combined image.

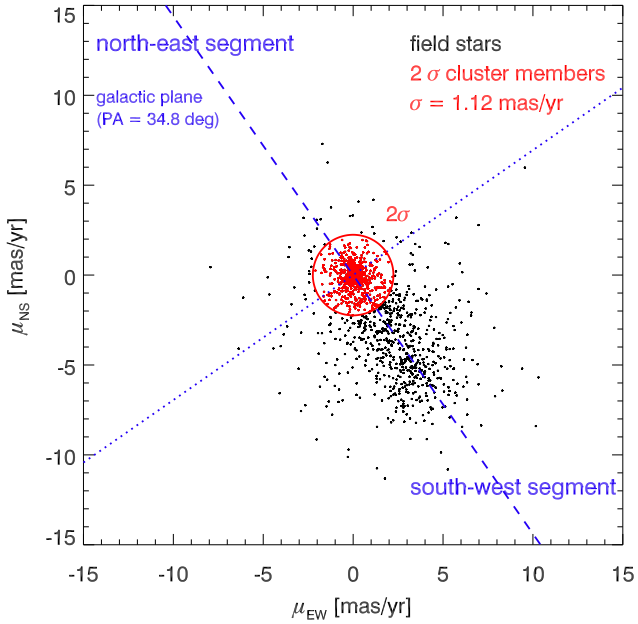

Figure 2.17: Proper motion diagram (taken from Hußmann et al. [2011]).

Member selection

Cluster stars were primarily distinguished based on their common proper motion with respect to the field population. The first epoch K_s-band data was mapped onto the K_s-band data from 2008 using a geometric transformation derived with the IRAF task *geomap*. Pre-selected cluster member candidates provided the reference positions for the transformation. In the proper motion diagram (PMD, Fig. 2.17) the distribution of cluster members is therefore centred around the origin. The orientation of the Galactic plane is indicated by the dashed line and the dotted line orientated vertically to it splits the PMD into the North-East and South-West segment. The field stars are mainly distributed within an elongated shape in the SW-segment and overlap with the cluster members. As the NE-segment is least affected by these contaminating field stars the membership criterion was derived by fitting the distribution of proper motions in this segment with a Gaussian function. A star with an absolute proper motion of less than $2\sigma = 2.24\,\mathrm{mas/yr}$ is designated as a proper motion member of the cluster.

Fig. 2.18 shows the colour-magnitude diagrams (CMDs) of the proper motion members and non-members. Although cluster and field stars separate well some blue foreground stars from the Galactic disc, with similar proper motions as the cluster, and a few very red objects likely located in the background, cannot be distinguished from the cluster on basis of their proper motions. These stars were removed by a two step colour-cut (for details see Hußmann et al. [2011]). Brighter stars in both CMDs were matched with the K-band spectral catalogue of Liermann et al. [2009]. All identified M, K giants were removed from the final cluster sample. All proper motion members, which were excluded based on their colour or spectral type are added to the non-member CMD (indicated by triangles).

Mass derivation and the present-day mass function

The age of the Quintuplet cluster was determined to be $4 \pm 1\,\mathrm{Myr}$ by Figer et al. [1999]. To cover this range of cluster ages the initial masses were derived from three isochrones with ages of 3, 4 and 5 Myr. The isochrones are a combination of Padova main sequence (MS) isochrones and Pisa-FRANEC pre-main sequence (PMS) isochrones (see Gennaro et al. [2011]; Marigo et al. [2008]; Degl'Innocenti et al. [2008]). We adopted solar metallicity and the distance to the Galactic centre of 8.0 kpc as the distance to the cluster (Ghez et al. [2008]). Each star in the final cluster sample was shifted along its line of reddening onto the isochrone using the extinction law of Nishiyama et al. [2009] to determine its initial mass at the intersection. The line of reddening of a stars may have several intersections caused by the local maximum of the PMS or the loop at the transition from the MS to the contraction phase. The regions with ambiguous mass assignments are shaded in grey in Fig. 2.18. The assigned mass of a star inside this region is the average of the masses at each intersection of its line of reddening with the isochrone. For the 11 Wolf-Rayet (WR) stars contained in our cluster sample the masses could not be inferred from the isochrones. These stars were therefore excluded from the mass function. Also stars within or

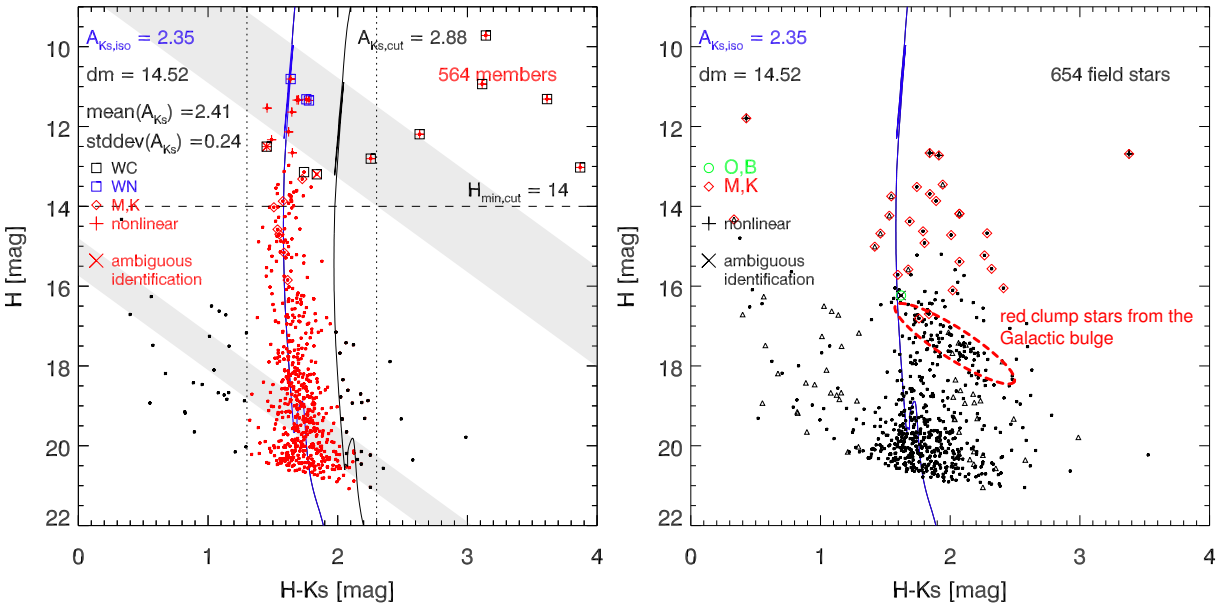

Figure 2.18: *Left panel*: Colour-magnitude diagram of proper motion cluster members. A 4 Myr isochrone is shown for reference. Stars rejected by the colour-cut are drawn in black, cluster members are plotted in red. *Right panel*: Colour-magnitude diagram of proper motion non-members (black dots) and of stars removed from the member sample based on their colour or known spectral type (triangles) (adapted from Hußmann et al. [2011]).

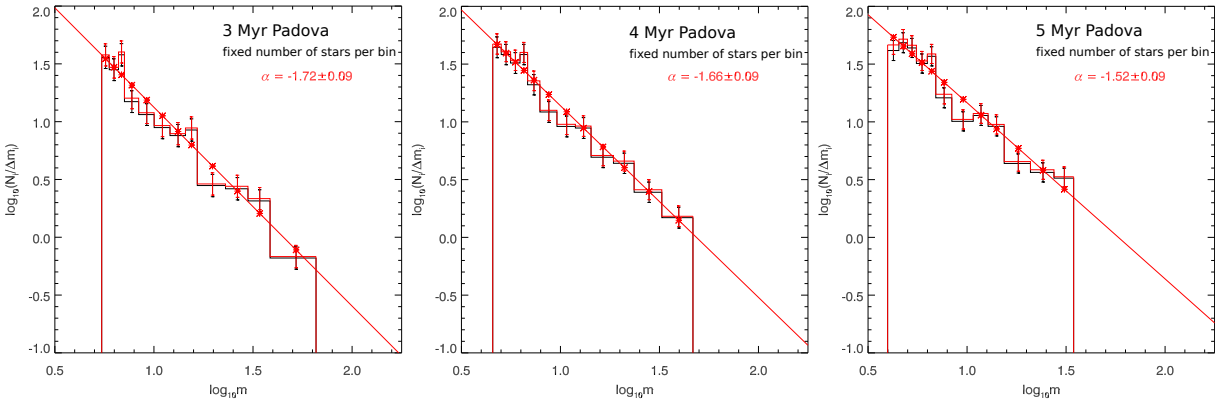

Figure 2.19: Mass functions with inital masses inferred from Padova MS-isochrone for a cluster age of 3, 4 or 5 Myr (adapted from Hußmann et al. [2011]).

below the ambiguity region caused by the PMS/MS transition were disregarded for the derivation of the mass function in order to avoid biases introduced by the large number of low-mass stars with averaged masses. The minimum mass of a star entering the mass function was then 5.5, 4.6 and 4.0 $M_\odot$ for the 3, 4 and 5 Myr isochrone, respectively. The data was distributed in bins with an approximately equal number of stars per bin following the method described in Maíz Apellániz & Úbeda [2005]. The mass functions for the three cluster ages dividing the data into 12 bins are shown in Fig. 2.19. The slopes of the mass function decrease with increasing age from $\alpha = (-1.72 \pm 0.09)$ to (-1.52 ± 0.09) (Salpeter slope: $\alpha = -2.35$; Salpeter [1955]). As the range of initial masses along the upper part of the MS ($M > 20\,M_\odot$) shrinks with age the same number of stars is squeezed into a smaller mass interval resulting in a flattening of the slopes with increasing cluster ages. The three derived slopes of the mass function above a mass of $\approx 5\,M_\odot$ are systematically flatter than the standard Salpeter slope. The PDMF of the Quintuplet cluster within a radius of 0.5 pc is therefore found to be top-heavy.

Outlook

So far the mass function was only derived for the central part of the cluster. It is therefore not clear if the whole cluster is depleted of lower mass stars or if the flat mass function is the result of mass segregation due to dynamical evolution in the tidal field of the inner Galaxy. The next step is therefore to apply the

proper motion analysis also to the outer part of the Quintuplet cluster and to determine if the slope of the mass function changes going to larger radii.

Acknowledgements

We acknowledge funding by the German Science Foundation Emmy Noether Programme under grant STO 496-3. Based on observations made with ESO Telescopes at the Paranal Observatories under Programme ID 081.D-0572 as well as observational data from the ESO science archive.

Bibliography

Degl'Innocenti, S., Prada Moroni, P. G., Marconi, M., & Ruoppo, A. 2008, Ap&SS, 316, 25
Diolaiti, E., Bendinelli, O., Bonaccini, D., et al. 2000, A&AS, 147, 335
Figer, D. F., McLean, I. S., & Morris, M. 1999, ApJ, 514, 202
Gennaro, M., Brandner, W., Stolte, A., & Henning, T. 2011, MNRAS, 412, 2469
Ghez, A. M., Salim, S., Weinberg, N. N., et al. 2008, ApJ, 689, 1044
Hußmann, B., Stolte, A., Brandner, W., & Gennaro, M. 2011, A&A, submitted
Lawrence, A., Warren, S. J., Almaini, O., et al. 2007, MNRAS, 379, 1599
Liermann, A., Hamann, W.-R., & Oskinova, L. M. 2009, A&A, 494, 1137
Lucas, P. W., Hoare, M. G., Longmore, A., et al. 2008, MNRAS, 391, 136
Maíz Apellániz, J. & Úbeda, L. 2005, ApJ, 873
Marigo, P., Girardi, L., Bressan, A., et al. 2008, A&A, 482, 883
Nishiyama, S., Tamura, M., Hatano, H., et al. 2009, ApJ, 1407
Salpeter, E. E. 1955, ApJ, 121, 161

2.5 Probing the Microscopic with the Macroscopic: from Properties of Star Cluster Systems to Properties of Cluster-Forming Regions

Geneviève Parmentier[1,2]

[1] Max-Planck-Institut für Radioastronomie, Bonn, Germany
[2] Argelander-Institut für Astronomie, Bonn, Germany

Abstract

To understand how systems of star clusters have reached their presently observed properties constitutes a powerful probe into the physics of cluster formation, without needing to resort to high spatial resolution observations of individual cluster-forming regions (CFRg) in distant galaxies. In this contribution I focus on the mass-radius relation of CFRgs, how it can be uncovered by studying the gas expulsion phase of forming star clusters, and what the implications are. I demonstrate that, through the tidal field impact upon exposed star clusters, the CFRg mass-radius relation rules cluster infant weight-loss in dependence of cluster mass. The observational constraint of a time-invariant slope for the power-law young cluster mass function is robustly satisfied by CFRgs with a constant mean volume density. In contrast, a constant mean surface density would be conducive to the preferential destruction of high-mass clusters. A purely dynamical line-of-reasoning leads therefore to a conclusion consistent with star formation a process driven by a volume density threshold. Developing this concept further, properties of molecular clumps and CFRgs naturally get dissociated. This allows to understand: (i) why the star cluster mass function is steeper than the molecular cloud/clump mass function; (ii) the presence of a massive star formation limit in the mass-size space of molecular structures.

Introduction

We are still a long way from observationally mapping active or future cluster-forming regions on a one-by-one basis in distant galaxies. Even at ALMA resolution (0.1 arcsec), to map clumps of cold dense molecular gas on a pc-scale is attainable only in galaxies less distant than $\simeq 2$ Mpc. In contrast, properties of *systems* of star clusters, such as the distribution functions of cluster ages, masses and radii, are retrievable out to distances of at least 20 Mpc. These distribution functions are shaped by both the dynamical evolution and the formation conditions of star clusters. Therefore, evolving model cluster systems for a wide range of initial conditions, and comparing their predicted distribution functions to their observed counterparts, constitutes a powerful tool to probe into the physics of cluster formation. That 'macroscopic' approach has the tremendous advantage to alleviate the need for a spatial resolution which is yet to be achieved in galaxies more distant than a few Mpc ('microscopic' approach).

Systems of young clusters are – obviously – those best suited to uncover cluster-forming region properties. At ages less than 100 Myr, a key-driver of cluster evolution is violent relaxation – namely the dynamical response of embedded clusters to the expulsion of their residual star-forming gas due to massive star activity (e.g. Geyer & Burkert [2001]). During violent relaxation, clusters expand and lose stars (infant weight-loss) as a result of the binding gaseous mass loss. Therefore, initial conditions of this phase leave signatures in the cluster age, mass and radius distribution functions (e.g. Parmentier et al. [2008]; Parmentier & Fritze [2009]). In this contribution, I highlight how the time-invariant shape of the *young* cluster mass function sheds light on the mass-radius relation of cluster-forming regions (hereafter CFRg). I show that this relation is one of constant mean volume density, that is, $r_{CFRg} \propto m_{CFRg}^{1/3}$ with r_{CFRg} and m_{CFRg} the CFRg radius and mass, respectively. Furthering this argument, I demonstrate: (i) why the young cluster mass function is steeper than the molecular cloud mass function, and (ii) why there is a massive star formation limit in the mass-size space of molecular structures.

CFRg Mass-Radius Relation: a Dynamical Perspective

Tidal field impact implies constant mean volume density for CFRgs

The amplitude of the cluster mass function is observed to steadily decrease with time over the first 100 Myr of cluster evolution due to infant weight-loss. Yet, its shape is reported to remain remarkably unchanged (e.g. Chandar et al. [2010]). That is, cluster infant weight-loss is mass-independent. When plotted as the number of clusters per linear mass interval, the cluster mass function is a featureless power-law of slope -2, $\mathrm{d}N \propto m_\star^{-2}\mathrm{d}m_\star$, irrespective of the cluster age bin (say, 1 – 10 or 10 – 100 Myr).

The mass fraction of stars remaining bound to a cluster by the end of its violent relaxation, F_{bound}, depends on the star formation efficiency of the parent CFRg, SFE, and on the gas expulsion time-scale, τ_{GExp}/τ_{cross}, expressed in units of the CFRg crossing-time: $F_{bound} = F_{bound}(SFE, \tau_{GExp}/\tau_{cross})$. That infant weight-loss, $1 - F_{bound}$, is mass-independent straightforwardly implies a mass-independent SFE (Fig. 1 in Parmentier & Gilmore [2007]; see also Section 3.1), and a mass-independent τ_{GExp}/τ_{cross} (Parmentier et al. [2008]), although the constraint on τ_{GExp}/τ_{cross} is looser than for the SFE (see Section 4.1 in Parmentier & Kroupa [2011] for a discussion).

A third, and so far overlooked, aspect is how the combination of an external tidal field with the mass-radius relation of CFRgs influences cluster infant weight-loss in dependence of cluster mass. Due to gas-expulsion-driven expansion, cluster stars – which, with no external tidal field, would remain bound – may be driven beyond the cluster tidal radius and turned into field stars. Therefore, infant weight-loss is partly governed by how deeply an embedded cluster sits within its limiting tidal radius, an effect quantified by the pre-expansion ratio of the cluster half-mass radius to tidal radius, r_h/r_t. Accordingly, $F_{bound} = F_{bound}(SFE, \tau_{GExp}/\tau_{cross}, r_h/r_t)$. The embedded cluster half-mass radius scales with the CFRg radius, i.e. $r_h \propto \kappa.r_{CFRg}$, with the factor κ depending on the assumed density profile. The tidal radius, r_t, depends on both the embedded cluster mass, m_{ecl}, and the strength of the external tidal field. Eq. 4 in Parmentier & Kroupa [2011] gives r_t for a cluster at a galactocentric distance D_{gal} in an isothermal galactic halo of circular velocity V_c:

$$r_t = \left(\frac{G.D_{gal}^2}{2V_c^2}.m_{ecl}\right)^{1/3} . \tag{2.34}$$

Baumgardt & Kroupa [2007] build on the r_h/r_t ratio to quantify how much an external tidal field enhances infant weight-loss compared to a tidal-field-free environment. I will refer r_h/r_t as the tidal field *impact*, to distinguish it from the tidal field strength. The tidal field strength depends solely on the external tidal field, say, V_c and D_{gal}. These parameters also define the galactic halo volume density at a galactocentric distance D_{gal}, $\rho_{gal}(D_{gal}) = V_c^2/(4\pi G D_{gal}^2)$, that is, in our example, the density of the CFRg environment. In contrast, the tidal field impact depends on *both* the tidal field (V_c, D_{gal}) *and* the embedded-cluster properties (m_{ecl}, r_h), where the stellar mass of the embedded cluster obeys $m_{ecl} = SFE \times m_{CFRg}$. In other words, the tidal field strength alone does not define the sensitivity of a cluster to the tidal field. It is the *contrast between the volume densities* of the CFRg and its environment which matters. For an isothermal galactic halo, using Eqs. 4 and 7 in Parmentier & Kroupa [2011], one can show that:

$$\frac{r_h}{r_t} = \kappa \left(\frac{2}{SFE}\right)^{1/3} \left(\frac{< \rho_{gal}(\leq D_{gal}) >}{\rho_{CFRg}}\right)^{1/3} , \tag{2.35}$$

where $< \rho_{gal}(\leq D_{gal}) >$ is the mean volume density of the galactic halo *within* D_{gal}.

When $r_h/r_t \lesssim 0.03$, the embedded cluster sits deeply within its limiting tidal radius, thereby giving rise to an expanded cluster 'shielded' against the external tidal field. In other words,

$$F_{bound}(SFE, \tau_{GExp}/\tau_{cross}, r_h/r_t) \simeq F_{bound}(SFE, \tau_{GExp}/\tau_{cross})$$

stars venturing beyond the tidal radius are lost because of velocities higher than the cluster escape velocity in the first place. In contrast, when $r_h/r_t \gtrsim 0.20$, clusters evade tidal disruption only if their spatial expansion is damped severely through either high SFE and/or long τ_{GExp}/τ_{cross}.

Fig. 3 of Parmentier & Kroupa [2011] shows F_{bound} in dependence of m_{CFRg}[1] for different CFRg mass-radius relations. For the sake of simplicity, the assumed environment is an isothermal galactic

[1]Note that what we refer to as 'cluster-forming region' is called 'cluster-forming core' in Parmentier & Kroupa [2011]

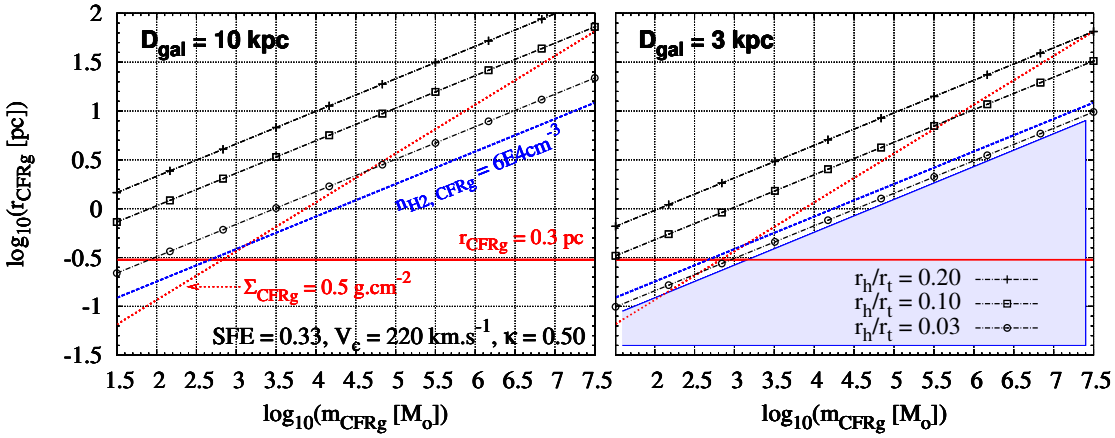

Figure 2.20: Mass-radius diagrams of cluster-forming regions (CFRg) as a tool to assess the tidal field impact r_h/r_t upon clusters expanding after residual star-forming gas expulsion. The parallelism between iso-r_h/r_t lines (black lines with symbols; see legend) and lines of given mean number density $n_{\mathrm{H}_2,CFRg}$ (e.g. $n_{H_2,CFRg} = 6 \times 10^4$ cm^{-3}, blue dashed line) demonstrates that $r_{CFRg} \propto m_{CFRg}^{1/3}$ is the most robust mass-radius relation to obtain mass-independent tidal field impact, hence an invariant shape of the cluster mass function through violent relaxation. In contrast, constant mean surface density and constant radius (e.g. $\Sigma_{CFRg} = 0.5$ gcm^{-2} and $r_{CFRg} = 0.3$ pc, red lines) lead to an increasing or decreasing, tidal field impact, respectively, with increasing CFRg masses. When $r_h/r_t \lesssim 0.03$ (shaded area in right panel), cluster evolution is not or only weakly affected by the external tidal field. Note that the iso-r_h/r_t lines' intercepts depend on the tidal field strength (here the galactocentric distance, D_{gal}).

halo. It should be noted, however, that CFRgs are embedded in molecular clumps, themselves embedded in Giant Molecular Clouds (GMC). The volume densities of these structures are higher than that of a galactic halo. For instance, the mean volume density of a $\simeq 10^5\,\mathrm{M}_\odot$ GMC is $\simeq 1\,\mathrm{M}_\odot\mathrm{pc}^{-3}$ (assuming spherical symmetry and $\Sigma_{GMC} \simeq 40\,\mathrm{M}_\odot pc^{-2}$, Heyer et al. [2009]). This is about 2 orders of magnitude denser than the density of an isothermal halo at $D_{gal} \simeq 8$ kpc. Therefore, the r_h/r_t and F_{bound} values estimated by Parmentier & Kroupa [2011] are lower and upper limits, respectively.

CFRgs of constant mean surface density ($r_{CFRg} \propto m_{CFRg}^{1/2}$) and constant radius ($r_{CFRg}$) are found to potentially lead to the preferential removal of high- and low-mass clusters, respectively. In contrast, CFRgs of constant mean volume density ($r_{CFRg} \propto m_{CFRg}^{1/3}$) satisfies the observational constraint of mass-independent cluster infant weight-loss. The physics driving these conclusions is best understood with a mass-radius diagram. Fig. 2.20 shows 3 CFRg mass-radius relations: one of constant radius $r_{CFRg} = 0.3$ pc (red solid line), one of constant mean surface density $\Sigma_{CFRg} = 0.5$ gcm^{-2} (red dotted line), and one of constant mean number density $n_{\mathrm{H}_2,CFRg} = 6.10^4$ cm^{-3} (blue dashed line). It also depicts 3 iso-r_h/r_t lines in the (m_{CFRg}, r_{CFRg}) space ($r_h/r_t = 0.03, 0.10$ and 0.20, black dash-dotted lines with symbols). Both panels of Fig. 2.20 differ by the tidal field strength (here the galactocentric distance). As Eq. 2.35 demonstrates, for a given environment, a given r_h/r_t value equates with a line of constant mean volume density (i.e. $r_{CFRg} \propto m_{CFRg}^{1/3}$, see also Eq. 10 in Parmentier & Kroupa [2011]). Note that iso-r_h/r_t lines shift downwards when the tidal field gets stronger, that is, higher ρ_{CFRg} are required to reproduce the same tidal field impact r_h/r_t.

For all CFRgs lying below the line $r_h/r_t = 0.03$ (shaded area in the right panel), the tidal field impact is negligible. In fact, for given SFE and τ_{GExp}/τ_{cross}, F_{bound} is mass-independent in that region of the plot, regardless of the mass-radius relation. This is because $r_h/r_t = 0.01$ or, say, $r_h/r_t = 0.001$ affects F_{bound} in the same way. If CFRgs have masses and radii above the line $r_h/r_t = 0.20$, cluster survival requires stringent conditions (high SFE, long τ_{GExp}/τ_{cross}). In the intermediate region bound by $r_h/r_t = 0.03$ and $r_h/r_t = 0.20$, infant weight-loss is higher than predicted for a tidal-field-free environment. Note that the respective extents of these 3 regions depend on the tidal field strength (compare left and right panels). Cluster-forming region mass-radius diagrams therefore constitute an exquisite tool to assess, in a glimpse, whether an external tidal field affects the early evolution of star clusters.

If the CFRg mass-radius relation were one of constant mean surface density, the tidal field impact would increase with the mass of CFRgs by virtue of their decreasing mean *volume* density. In other words,

high-mass CFRgs are more prone to tidal overflow than their low-mass counterparts and F_{bound} decreases with m_{CFRg}, thereby distorting the shape of the cluster mass function during violent relaxation (see Fig. 4 in Parmentier [2010]). The most robust way of reproducing mass-independent tidal field impact r_h/r_t is through constant mean *volume* density CFRgs (or, at least, mass-independent ρ_{CFRg}). This is conducive to mass-independent infant weight-loss $1 - F_{bound}$, and is in line with the observational constraint set by the invariant shape of the young cluster mass function. *We therefore conclude that the mean volume density of cluster-forming regions is constant.*

It may be worth stressing that the concepts 'constant *mean* volume density' ($r_{CFRg} \propto m_{CFRg}^{1/3}$) or 'constant *mean* surface density' ($r_{CFRg} \propto m_{CFRg}^{1/2}$), discussed in this contribution, are not to be misinterpreted as uniform (i.e. radially not varying) volume or surface density. On the contrary, structures in molecular clouds are nested (Kauffmann et al. [2010]), and molecular clumps have density gradients. This property will be the starting point of the two topics discussed in the next Section.

The above conclusion that the mass-radius relation of CFRgs must be one of constant mean *volume* density stems from a purely dynamical line-of-reasoning. This finding is independently confirmed by the tight linear correlation observed between the star formation rate and the *dense* molecular gas mass on galaxy scales (Gao & Solomon [2004]), molecular-cloud scales (Lada et al. [2010]), and molecular-clump scales (Wu et al. [2005]). Here, 'dense' means hydrogen molecule number densities $n_{\rm H2} \simeq 10^{4-5}\,cm^{-3}$. This implies the existence of a number density threshold for star formation, $n_{\rm H_2,\mathit{th}} \simeq 10^4\,cm^{-3}$. It also implies that the mean number density of CFRgs is a few times $n_{\rm H_2,\mathit{th}}$, the exact factor depending on the clump density profile (see Eq. 5 in Parmentier [2011]). Therefore, the observational mapping of star formation in dense molecular gas also leads to $r_{CFRg} \propto m_{CFRg}^{1/3}$ (see Section 2 in Parmentier [2011] for a brief summary).

Molecular Clumps versus CFRgs: Beware!

Observational mass-radius data sets of molecular clumps are to be handled with caution as they may be the imprint of the molecular tracer used to map them, rather than reflect cluster-formation conditions (see Section 3 in Parmentier & Kroupa [2011] for a discussion and enlightening examples). For instance, Figs. 9 and 21 in Wu et al. [2010] show the star-forming region W43S mapped in HCN 3−2 and CS 7−6 transitions, respectively. While the FWHM and its enclosed mass are lower in CS 7−6 than in HCN 3−2, the corresponding mean volume density is about 5 times higher. This is because CS 7−6 requires a higher volume density than HCN 3−2 to be excited. Since molecular clumps have density gradients (see below), the CS 7−6 transition probes deeper inner regions of molecular clumps than HCN 3−2, hence the smaller mass and FWHM size inferred in CS 7−6 than in HCN 3−2. Besides, molecular line emissions extend smoothly beyond the FWHM size down to the noise level. In other words, molecular clump FWHM sizes do *not* represent sharp physical boundaries (see Wu et al. [2010] and their Fig. 25). This illustrates that radii and masses of molecular clumps should *not* be interpreted as those of CFRgs. This is the very reason for the specific and clear-cut terminology "cluster-forming region" used throughout this contribution.

Molecular clumps have volume density profiles (e.g. Müller et al. [2002]):

$$\rho_{radial}(s) \propto s^{-p}\,, \tag{2.36}$$

where $\rho_{radial}(s)$ is the volume density at the distance s from the clump centre, and p is the density index.

With star formation driven by a volume density threshold $n_{\rm H_2,\mathit{th}} \simeq 10^4\,cm^{-3}$, one can distinguish two zones in a molecular clump: a central CFRg, actively forming stars by virtue of a local number density higher than $n_{\rm H2,\mathit{th}}$, and an outer envelope inert in terms of star formation (see left panel of Fig. 2.22)[2]. The mass of gas relevant to star formation is m_{CFRg}, rather than the overall clump mass m_{clump}, and the volume of star-forming gas does not coincide with the observed molecular clump. This concept constitutes the crux of the two topics developed below.

Consequence 1 - Mass Functions: from Clumps to CFRgs

It is puzzling that the young cluster mass function, $dN \propto m_\star^{-\beta_\star} dm_\star$, is steeper than the molecular cloud and clump mass functions, $dN \propto m_{clump}^{-\beta_0} dm_{clump}$, as their respective indices are $\beta_\star \simeq 2$ and $\beta_0 \simeq 1.7$.

[2]Another possible situation is that molecular clumps represent only a fraction of a CFRg because of a very high density molecular tracer

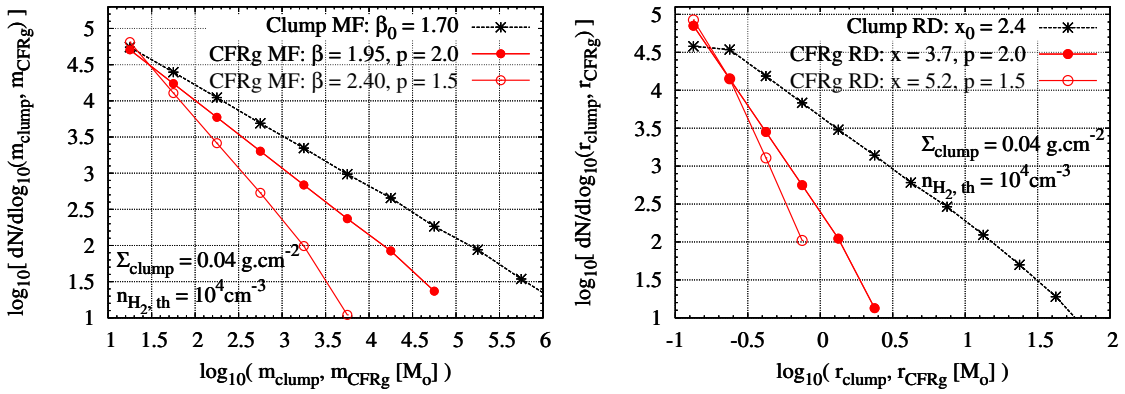

Figure 2.21: Explaining why the mass functions (MF, left panel) and radius distributions (RD, right panel) of star clusters are steeper than those of molecular clumps and clouds. In the model of relevance here, cluster-forming regions (CFRg) only occupy a limited volume of their host molecular clumps and are defined based on a number density threshold for star formation, $n_{H2,th}$ (see Fig. 2.22, left panel). The mean *volume* density of CFRgs is therefore constant. If, in contrast, the clump mean *surface* density is constant, the difference in the mass-radius relations of clumps ($r_{clump} \propto m_{clump}^{1/2}$) and CFRgs ($r_{CFRg} \propto m_{CFRg}^{1/3}$) steepens the MF and RD of CFRgs compared to those of their host clumps. The degree of steepening depends on the clump density index p. Note that Σ_{clump} is the clump *mean* surface density.

Since infant weight-loss is mass-independent, the mass function of young star clusters is also the mass function of embedded clusters, $dN \propto m_{ecl}^{-\beta_{ecl}} dm_{ecl}$ with $\beta_{ecl} = \beta_\star$. $\beta_0 \simeq 1.7$ and $\beta_{ecl} \simeq 2$ suggest that star formation is *less* efficient in high-mass clumps than in low-mass ones since the SFE averaged over a clump, SFE_{global}, obeys: $SFE_{global} = m_{ecl}/m_{clump} \propto m_{clump}^{-0.3}$. The slope -0.3 derives from $(\beta_0 - \beta_{ecl})/(\beta_{ecl} - 1)$. Accordingly, SFE_{global} varies by *an order of magnitude* over 3 decades in clump mass, a lower limit to the cluster mass range in star cluster systems. With the bound fraction F_{bound}, a very sensitive function of the SFE (Baumgardt & Kroupa [2007], their Fig. 1), a mass-varying SFE does not seem a viable solution. Assuming instantaneous gas expulsion and weak tidal field impact, F_{bound} can virtually vary from 0 to almost unity when the SFE varies by an order of magnitude (Fig. 1 in Parmentier & Gilmore [2007]). Such 0-to-1 variations in the bound fraction of stars at the end of the cluster violent relaxation are necessarily conducive to a severe reshaping of the cluster mass function through the first 100 Myr of dynamical evolution (see Fig. 2 in Parmentier et al. [2008]). This is in stark disagreement with observed young cluster mass functions. It would therefore be highly misleading to assume that the difference in slope between the mass functions of molecular clumps (or clouds) and young clusters is small enough ($\beta_\star - \beta_0 \simeq 0.3$) to lead to almost mass-independent SFE and infant weight-loss.

The issue we have to fix now is: how to reconcile mass-independent infant weight-loss with the difference in slope between the molecular clump and young star cluster mass functions. The line of reasoning detailed above hinges on the identification of molecular clumps as CFRgs – namely CFRg boundaries are those of molecular clumps. In contrast, if CFRgs constitute a fraction only of the volume of their host molecular clump (left panel of Fig. 2.22), star formation can be quantified by two distinct efficiencies *of different physical significances*. The *global* SFE, defined on a clump-scale, is relevant to understand the difference between the cloud (clump) and young cluster mass functions. We can also define an SFE on the CFRg-scale. This *local* SFE quantifies the ratio between the embedded-cluster stellar mass and the initial gas mass of the CFRg, m_{ecl}/m_{CFRg}. It is the local SFE – *not* the global one – which drives cluster violent relaxation. The early dynamical evolution of star clusters and the mass function slope difference $\beta_\star - \beta_0$ are now dissociated issues. Mass-independent infant weight-loss demonstrates that the local SFE at the onset of gas expulsion is CFRg-mass-*in*dependent. Consequently, the power-law mass functions of young star clusters, embedded clusters and CFRgs all have the same slopes (i.e. $\beta_\star = \beta_{ecl} = \beta_{CFRg}$), by virtue of mass-independent infant weight-loss and mass-independent local SFE, respectively. The mass function slope difference $\beta_\star - \beta_0$ tells us that the mass fraction of *dense star-forming gas* in molecular clumps, m_{CFRg}/m_{clump}, decreases with clump mass (see Fig. 1 in Parmentier [2011] for a summary plot). What can be the reason for such a behaviour?

The mean surface density of GMCs (the precursors of massive star clusters forming profusely in galaxy mergers) is observed to be about constant in our Galaxy and in the Magellanic Clouds (see Fig. 8 in Blitz et al. [2006]). This property may also characterize *star-forming* molecular clumps (see Fig. 10

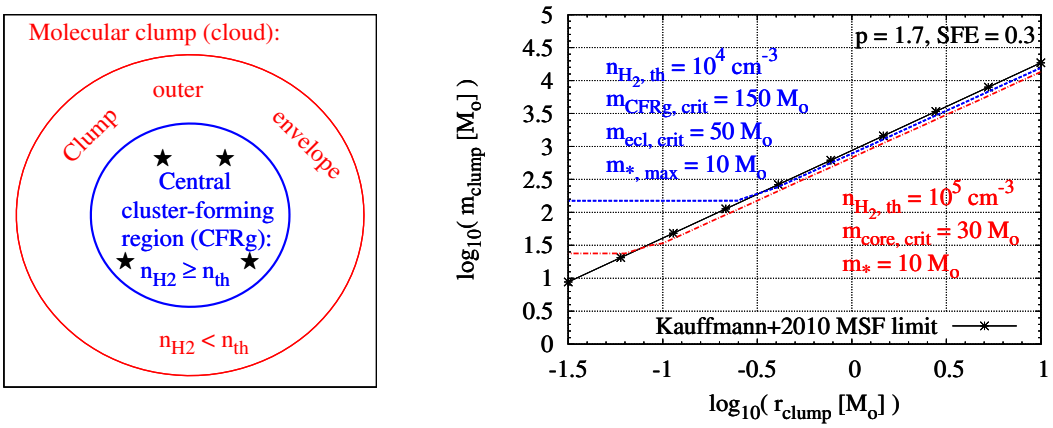

Figure 2.22: *Left*: Defining a cluster-forming region (CFRg) nested *within* a molecular clump. By virtue of the clump density gradient, the CFRg outer bound is defined by a volume (or number) density threshold for star formation, ρ_{th} (or $n_{H_2,th}$). *Right*: The observed massive star formation (MSF) limit (black solid line with asterisks). It equates with the mass-radius relation of molecular clumps containing the mass of star-forming gas (i.e. $n_{H_2} \geq n_{H_2,th}$) needed to form a 10 M$_\odot$-star, either on the small spatial scale ($r_{clump} < 0.2$ pc) of an individual pre-stellar core (red dash-dotted line and lower-right data set), or on the larger scale ($r_{clump} \geq 0.2$ pc) of a CFRg (blue dashed line and upper-left data set).

in Parmentier [2011]), where Galactic disc star clusters form. It therefore appears that the mass-radius relation of CFRgs on the one hand, and the mass-radius relations of molecular clumps and GMCs on the other, have different slopes with: $r_{CFRg} \propto m_{CFRg}^{1/3}$, while $r_{clump} \propto m_{clump}^{1/2}$. *This immediately implies a mass-dependent effect upon the ratio* m_{CFRg}/m_{clump}. As we already saw from Fig. 2.20, a constant mean surface density is conducive to a mean volume density decreasing towards higher masses. As a result, the clump mass fraction of gas denser than a given number density threshold is also a decreasing function of the clump mass. Considering the number density threshold for star formation, $n_{\rm H2,th}$, the desired trend follows logically: m_{CFRg}/m_{clump} decreases with m_{clump}, which steepens the CFRg mass function compared to the clump mass function.

The degree of steepening depends on the clump density index p: the shallower the clump density profile, the greater the difference in slope $\beta_{CFRg} - \beta_0$. The left panel of Fig. 2.21 illustrates this effect for $p = 2$ (isothermal sphere) and $p = 1.5$. The (black) dashed line with asterisks depicts the clump mass function, the (red) solid lines the resulting CFRg mass functions (full and open symbols: $p = 2.0$ and $p = 1.5$). The mean volume density of CFRgs is $\rho_{CFRg} = [3/(3-p)] \times \rho_{th}$, where ρ_{th} is the volume density threshold for star formation (Eq. 5 in Parmentier [2011]). The mean surface density of their host molecular clumps is assumed to be constant $\Sigma_{clump} = 0.04\,g.cm^{-2}$. Fig. 6 in Parmentier [2011] shows that to steepen the clump mass function $\beta_0 \simeq 1.7$ into that of CFRgs (hence of embedded clusters), $\beta_{CFRg} \simeq 2$, a density index $p \simeq 1.9$ is required. This is in excellent agreement with the mean density index inferred via dust-continuum mapping of star-forming regions by Müller et al. [2002]. Therefore, the model does a great job at explaining the observed slope difference $\beta_\star - \beta_0$. *We conclude that the difference in slope between the molecular clump and young star cluster mass functions can arise from different mass-radius relations for CFRgs and their host molecular clumps.*

Not only does this effect steepen the mass function, it also steepens the *radius* distribution, as illustrated in the right panel of Fig. 2.21 (same model parameters and same colour/symbol codings as in the left panel). x_0 and x are the spectral indices of the radius distributions of clumps and CFRgs, respectively: $dN \propto r_{clump}^{-x_0} dr_{clump}$ and $dN \propto r_{CFRg}^{-x} dr_{CFRg}$. This model has therefore the potential to explain why the observed GMC mass function *and* radius distribution are shallower than their young star cluster counterparts (see Section 5 in Parmentier [2011] for a full discussion of the radius distribution aspect).

Consequence 2 - The Massive Star Formation limit

Kauffmann & Pillai [2010] (top and middle panels of their Fig. 2) recently highlighted the presence of a limit for massive star formation (MSF) in the mass-size space of molecular structures. This MSF limit

Table 2.1: Density index p of molecular clumps (see Eq. 2.36)

p	Method	Source
$p = 1.9$	Mass function steepening	Section *Consequence 1*
$p = 1.7$	Massive star formation limit	Section *Consequence 2*
$< p >= 1.8 \pm 0.4$	Star-forming clump dust-continuum mapping	Müller et al. [2002]

obeys:

$$m(r) = 870 M_\odot (r/pc)^{1.3}\,, \tag{2.37}$$

where $m(r)$ is the gas mass enclosed within the effective radius, r. It is shown in the right panel of Fig. 2.22 as the (black) solid line with asterisks. Molecular structures lying below the MSF limit are void of massive stars, while those more massive than the MSF limit show HII regions and, therefore, contain stars more massive than 8-10 $M_\odot$. In other words, MSF demands a mass of molecular gas enclosed within any given projected radius higher than what Eq. 2.37 predicts.

Armed with the model presented in the previous Subsection, Parmentier et al. [2011] present an original solution for the origin of the MSF limit. The key-idea is to successively relate:
(1) the mass of a molecular clump, m_{clump}, to the mass of the CFRg, m_{CFRg}, it contains,
(2) the CFRg mass to the final mass of the embedded cluster it forms, m_{ecl}, and
(3) the mass of the embedded cluster m_{ecl} to the most probable mass of the most-massive star it contains, $m_{*,max}$. Fig. 3 of Weidner et al. [2010] illustrates the observed relation between the mass of young or embedded clusters, and the mass of their most massive star. As such, it provides us with a solution to Step 3: the formation of a star of mass $m_{*,max} \geq 8-10\,M_\odot$ requires $m_{ecl} \geq 50\,M_\odot$. Step 2 simply equates with the definition of the local SFE, that is, $m_{ecl} = SFE \times m_{CFRg}$, as seen in the previous Subsection. With the 'canonical' value, $SFE \simeq 0.3$, this gives a limit $m_{CFRg,crit} \simeq 150\ M_\odot$ of dense star-forming gas for the formation of a $10\,M_\odot$-star. Step 1 is implemented through Eq. 3 of Parmentier [2011], reproduced below for the sake of clarity. It relates the mass m_{clump} and radius r_{clump} of molecular clumps to the CFRg mass they contain[3]:

$$m_{CFRg} = \left(\frac{3-p}{4\pi\rho_{th}}\right)^{(3-p)/p} m_{clump}^{3/p}\, r_{clump}^{-3(3-p)/p}\,, \tag{2.38}$$

or:

$$m_{clump} = m_{CFRg}^{p/3} \left(\frac{4\pi\rho_{th}}{3-p}\right)^{(3-p)/3} r_{clump}^{3-p}\,. \tag{2.39}$$

For given density index p and star-formation density threshold ρ_{th}, Eq. 2.39 defines the mass-radius relation of molecular clumps containing a given CFRg mass, m_{CFRg}. (This mass-radius relation is of the same nature as the iso-m_{th} lines shown in top panel of Fig. 3 in Parmentier [2011] where r_{clump} is plotted against m_{clump} and $m_{th} \equiv m_{CFRg}$).

We can therefore identify the MSF limit, Eq. 2.37, to Eq. 2.39 with $m_{CFRg,crit} \simeq 150\,M_\odot$. This gives $p = 1.7$ and $n_{H_2,th} \simeq 10^4$ cm^{-3}. The inferred number density threshold is in remarkable agreement with values previously suggested in the literature (see end of Section: *CFRg Mass-Radius Relation: a Dynamical Perspective*). The density index p inferred from the MSF limit is also very similar to observed density indices of molecular clumps, and to the p-value needed to steepen the clump mass function index β_0 into that of young star clusters $\beta_\star$ (see the previous Subsection and Table 2.1). *We therefore conclude that the observationally inferred MSF limit equates with the mass-radius relation of molecular clumps containing the mass of dense star-forming gas needed for the formation of a* $8-10\,M_\odot$ *star.* Fig. 2.22 shows Eq. 2.39 with $m_{CFRg} = 150\,M_\odot$, $p = 1.7$ and $\rho_{th} = 700\,M_\odot$ ($\equiv n_{H_2,th} \simeq 10^4$ cm^{-3}) as the (blue) dashed line. Note that the result depends only weakly on the assumed local SFE since $m_{clump} \propto m_{CFRg}^{p/3} \propto (m_{ecl}/SFE)^{p/3}$ in Eq. 2.39.

The formation of massive stars as star cluster members allows us to explain the observed MSF limit down to a spatial scale of $\simeq 0.2$ pc. Below that limit, the entire clump gas is denser than the threshold $n_{H_2,th} \simeq 10^4\,cm^{-3}$ which causes the model to depart from the observed MSF limit. Over the range < 0.2 pc, a similar line of reasoning shows that the MSF limit is consistent with the mass a pre-stellar core[4] must have to form a $10\,M_\odot$ star. This 'individual star formation' picture is actually

[3]Note that in Parmentier [2011], the CFRg mass and radius are referred as m_{th} and r_{th}, respectively

[4]We adhere to the following nomenclature: the word 'core' refers to the gaseous precursor of an individual star or of a small group of stars, while the term 'clump' is designated for regions hosting cluster formation.

expected if observations look *into* a star-forming cluster, at the spatial scale of individual pre-stellar cores. Pre-stellar cores correspond to density peaks of at least $n_{\rm H_2,\it th} = 10^5$ cm^{-3} because stars form fastest where $n_{\rm H2} > 10^5\,cm^{-3}$ (see Elmegreen [2007], his Section 3.6). The comparison between the core mass function and the stellar IMF performed by Alves et al. [2007] for the Pipe dark cloud gives $SFE_{core} \simeq 0.3$. The formation of a $10\,{\rm M}_\odot$-star thus requires a mass of star-forming gas $m_{core,crit} = 30\,{\rm M}_\odot$. The (red) dash-dotted line in the right panel of Fig. 2.22 depicts Eq. 2.39 with $m_{core,crit} = 30\,{\rm M}_\odot$, $p = 1.7$ and $\rho_{th} = 7000\,{\rm M}_\odot$ ($\equiv n_{H_2,th} \simeq 10^5$ cm^{-3}). Obviously, the observed MSF limit is also consistent with the formation of a $10\,{\rm M}_\odot$-star out of its individual density peak with $n_{th} \simeq 10^5$ cm^{-3}. Note that the model does not allow to disentangle between individual star formation in the field, or individual star formation in clusters. *The observed MSF limit therefore embodies information about the formation of massive stars as star cluster members, and the formation of massive stars out of their individual pre-stellar cores. In this framework, the density threshold* $n_{\rm H_2,\it th} \simeq 10^4\,cm^{-3}$ *for clustered star formation probably represents the mean density above which the formation of local density peaks with* $n_{\rm H_2,\it th} \simeq 10^5\,cm^{-3}$ *is favoured in supersonically turbulent gas* (see Elmegreen [2011]).

Note that the slope of the MSF limit in the $r_{clump} - m_{clump}$ space is 1.3. Neither is the MSF limit a relation of constant mean surface density, nor is it a relation of constant mean volume density (although the model hinges on a volume density threshold for star formation). The one property common to all clumps along the MSF limit is the mass of star-forming gas, either on a star-cluster scale ($m_{CFRg} \simeq 150$ $M_\odot$, $n_{th} \simeq 10^4$ cm^{-3}), or on a pre-stellar core scale ($m_{core} \simeq 30$ $M_\odot$, $n_{H_2,th} \simeq 10^5$ cm^{-3}).

Conclusions

The analysis of the impact exerted by a tidal field upon star clusters which have expelled their residual star-forming gas has been carried out. It shows that the time-invariant shape of the young star cluster mass function is robustly reproduced if the mean *volume* density of cluster-forming regions (CFRgs) is constant. If the mass-radius relation of CFRgs were one of constant mean *surface* density, it would lead to the preferential removal of high-mass clusters, which contradicts observational results. These trends follow from how the CFRg volume density and the CFRg mass scale with each other. This stellar-dynamics-based finding is independently confirmed by studies mapping star formation activity in molecular clumps, molecular clouds and galaxies, which all show that star formation is driven by a volume (number) density threshold.

The fact that star formation takes place in gas denser than a given number density threshold, $n_{\rm H_2,\it th}$, and that molecular clumps are characterised by density gradients allows us to define two distinct regions in molecular clumps: a central dense CFRg, and an outer envelope inert in terms of star formation due to $n_{\rm H_2} < n_{\rm H_2,\it th}$. As a result, properties (e.g. mass, radius, mean volume densities) of CFRgs and molecular clumps get dissociated.

Building on that picture, I put forward an original explanation why the mass function of young star clusters is steeper than that of molecular clumps and clouds. The mass-radius relation of molecular clouds and, possibly, of star-forming clumps, is one of constant mean surface density. This contrasts with the constant mean volume density inferred for CFRgs. This difference in slope in their respective mass-radius relations steepens the mass function of CFRgs compared to that of their host clumps because clumps of higher mass have a lower mean volume density (hence a smaller fraction of star-forming gas) at constant mean surface density.

Finally, the same model is successfully applied to understand the origin of the massive star formation limit (MSF) in the mass-size space of molecular structures. This is shown to be consistent with a *threshold in star-forming gas mass* beyond which the star-forming gas reservoir is large enough to allow the formation of massive stars. Specifically, the MSF limit is consistent with the formation of a $10\,{\rm M}_\odot$-star out of its individual density peak with $n_{\rm H_2,\it th} \simeq 10^5$ cm^{-3}, or with the formation of a $10\,{\rm M}_\odot$-star as a CFRg member with $n_{\rm H_2,\it th} \simeq 10^4$ cm^{-3}.

Slides of oral presentations related to the topics discussed in this contribution are available at http://www.astro.uni-bonn.de/∼gparm/talks.html

Acknowledgments

This work has been supported by a Research Fellowship of the Humboldt Foundation and a Research Fellowship of the Max-Planck-Institut für Radioastronomie, Bonn, Germany.

Bibliography

Alves, J., Lombardi, M., Lada, C.J. 2007, A&A 462, 17
Baumgardt, H., & Kroupa, P. 2007, MNRAS, 380, 1589
Blitz, L., Fukui, Y., Kawamura, A., Leroy, A., Mizuno, N., & Rosolowsky, E. 2006, in Protostars and Planets V, B. Reipurth, D. Jewitt, and K. Keil (eds.), University of Arizona Press, Tucson, 951 pp., 2007, pp81-96
Chandar, R., Fall, S.M. & Whitmore, B.C. 2010, ApJ, 711, 1263
Elmegreen, B.G. 2007, ApJ, 668, 1064
Elmegreen, B.G. 2011, ApJ, 731, 61
Gao, Y., & Solomon, P.M. 2004, ApJ, 606, 271
Geyer, M.P., & Burkert, A. 2001, MNRAS, 323, 988
Heyer, M., Krawczyk, C., Duval, J., Jackson, J.M., 2009, ApJ, 699, 1092
Kauffmann, J., Pillai, T., Shetty, R., Myers, P. C., Goodman, A.A. 2010, ApJ, 712, 1137
Kauffmann, J. & Pillai, T. 2010, ApJ, 723, 7
Lada, C.J., Lombardi, M. & Alves, J. 2010, ApJ, 724, 687
Müller, K.E., Shirley, Y.L., Evans, N.J. II & Jacobson, H.R. 2002, ApJS, 143, 469
Parmentier, G., Gilmore, G. 2007, MNRAS, 377, 352
Parmentier, G., Goodwin, S., Kroupa, P. & Baumgardt, H. 2008, ApJ, 678, 347
Parmentier, G., Fritze, U. 2009, ApJ, 690, 1112
Parmentier, G. 2010, in: Star Clusters - Basic building blocks of galaxies through time and space, IAU Symp., Vol 266, pp 87-94
Parmentier, G., Kroupa, P. 2011, MNRAS, 411, 1258
Parmentier, G. 2011, MNRAS, 413, 1899
Parmentier, G., Kauffmann, J., Pillai, T. & Menten, K. 2011, MNRAS, in press [arXiv:1106.1173v1]
Weidner, C., Kroupa, P., Bonnell, I.A.D. 2010, MNRAS, 401, 275
Wu, J., Evans, N.J., Gao, Y., Solomon, P.M., Shirley, Y.L. & Vanden Bout, P.A. 2005, ApJ Lett., 635, 173
Wu, J., Evans, N.J., Shirley, Y.L. & Knez, C. 2010, ApJS, 188, 313

Chapter 3

Dynamical Evolution of Stellar Clusters

3.1 Searching for Initial Mass Function Variations in Resolved Stellar Populations

Kevin R. Covey[1], **N. Bastian**[2], **and M. R. Meyer**[3]

[1] Hubble Fellow; Department of Astronomy, Cornell University, 226 Space Sciences Building, Ithaca NY, 14853, USA
[2] Excellence Cluster Universe, Boltzmannstr. 2, 85748 Garching, Germany
[3] Institute of Astronomy, ETH Zürich, Wolfgang-Pauli-Str. 27, 8093 Zürich

Abstract

The initial mass function (IMF) succinctly characterizes a stellar population, provides a statistical measure of the end result of the star-formation process, and informs our understanding of the structure and dynamical evolution of stellar clusters, the Milky Way, and other galaxies. Detecting variations in the form of the IMF could provide powerful insights into the processes that govern the formation and evolution of stars, clusters, and galaxies. In this contribution, we review measurements of the IMF in resolved stellar populations, and critically assess the evidence for systematic IMF variations. Studies of the field, local young clusters and associations, and old globular clusters suggest that the vast majority were drawn from a "universal" IMF, suggesting no gross systematic variations in the IMF over a range of star formation environments, and much of cosmic time. We conclude by highlighting the complimentary roles that Gaia and the Large Synoptic Survey Telescope will play in future studies of the IMF in Galactic stellar populations.

Introduction

The Initial Mass Function (IMF) describes the number of stars formed in a stellar system as a function of stellar mass, and is a fundamental property of all stellar populations. As a statistical measure of the end result of the star formation process, the IMF is a key observable for testing theoretical models of star formation. As a succinct characterization of the fundamental components of a stellar population, the MF also serves to inform our understanding of the structure and dynamical evolution of stellar clusters, the Milky Way and other galaxies.

Numerous physical processes have been identified which may influence the shape of the IMF, such as: gravitational fragmentation of collapsing molecular cores (Klessen et al. [1998]); competitive accretion between multiple stars inhabiting the same mass reservoir (Larson [1992]); the truncation of

mass accretion due to radiative or dynamical feedback (Silk [1995]); dynamical interactions between stars in a clustered environment (Reipurth & Clarke [2001]); and the production of a clump mass spectrum by turbulent flows within molecular clouds (Padoan & Nordlund [2002]). The efficiency of each mechanism could also depend on other physical variables, such as the metallicity and magnetic field strength of the parent molecular cloud, the local stellar density, or the intensity of the surrounding radiation field. These effects may ultimately result in observable MF variations as a function of environment.

The effort to provide observational constraints on the form of the IMF can be traced back to the 'Luminosity Curve' measured by Kapteyn [1914], which determined the relative numbers of B type stars as a function of absolute magnitude. Salpeter [1955] subsequently produced a measurement of the IMF for high-mass stars which has remained essentially unchanged to the present day. Salpeter [1955] found that the shape of the IMF took the form of a power law, which can be expressed as:

$$\Phi(logm) = dN/d\log m \propto m^{-\Gamma}, \tag{3.1}$$

where m is the mass of a star and N is the number of stars in some logarithmic mass range $logm + dlogm$. Salpeter [1955] inferred a value of $\Gamma = 1.35$, which has come to be known as the 'Salpeter slope'.

While numerous observational studies have found the Salpeter slope to be a good description of the IMF in the super-solar mass regime, one of the first measurements of the low-mass IMF revealed that solar-mass and sub-solar mass stars are slightly less numerous than might be expected from an extrapolation of the Salpeter slope (Miller & Scalo [1979]). Changes in the slope of the IMF can be expressed within the power-law formalism by allowing different mass regimes to possess distinct power-law slopes, as in the seminal 'broken power-law' IMF derived by Kroupa et al. [1993]. Miller & Scalo [1979] adopted a different approach, describing the IMF over a large mass range with a single analytical expression, a Gaussian in $log(m)$, often known as a 'log-normal' function

$$\phi(m) \sim e^{-\frac{(\log\ m - \log\ m_c)^2}{2\sigma^2}} \tag{3.2}$$

where the variable m_c fixes the peak of the IMF (in $log(m)$ space), and σ characterizes the peak's width. Distinctions are often drawn between the power-law and log-normal characterizations of the IMF, but these differences are currently entirely in the realm of theory, not observation: Dabringhausen et al. [2008] have shown that the log-normal IMF advanced by Chabrier [2005] is extremely similar to a two-part power-law, hence distinguishing between a Kroupa-type broken power-law or Chabrier-type log-normal IMF is virtually impossible.

A great deal of observational work has been devoted to characterizing the IMF in a variety of astrophysical environments, across the full range of stellar masses, and extending into the brown dwarf regime. In a recent review (Bastian et al. [2010]), we provided a overview of recent empirical measurements of the IMF, and evaluated the evidence for systematic IMF variations. In this contribution we update that review, focusing on recent (2009 – 2011) IMF measurements in resolved stellar populations, which the upcoming Gaia mission will characterize in exquisite detail. Specifically, we review recent measurements of the mass function in the extended solar neighbourhood, in young star-forming regions, and Galactic open/globular clusters (see next Sections). We conclude in the last Section by examining the complimentary roles that Gaia and the Large Synoptic Survey Telescope will play in extending and improving IMF studies of resolved stellar populations.

The Mass Function of the extended solar neighbourhood & Galactic field

The IMF of field stars in the Galactic disk is a crucial reference for IMF measurements of any other stellar population. Resolving multiple systems in distant environments is sufficiently challenging that most IMF studies are only able to measure the 'system mass function', for example, which is unable to account for unseen companions. Inferring the single-star mass function from the system mass function, therefore, hinges on corrections inferred from intensive photometric and spectroscopic studies of the nearest stars, which are most favourable for detecting companions (e.g. Metchev & Hillenbrand [2009]; Raghavan et al. [2010]). The Galactic field also offers valuable opportunities to detect the coolest, lowest luminosity brown dwarfs within the local volume (e.g. Mainzer et al. [2011]) and/or assemble the largest possible samples to minimize statistical (though not systematic) uncertainties associated with mass function measurements (e.g. Covey et al. [2008b]).

Recent studies of the mass function in the extended solar neighbourhood have primarily been conducted with data from wide-field surveys, and with a particular focus towards the IMF near and below the stellar/sub-stellar boundary. Selecting a sample of $\sim$ 15 million low-mass (0.6 – 0.1 $M_\odot$) stars with reliable photometry in the Sloan Digital Sky Survey, Bochanski et al. [2010] jointly fit the structure of the thin and thick disks of the Milky Way, as well as the local MF: their inferred MF agrees well with that measured from the 8-pc volume complete sample of Reid & Gizis [1997], with a broad peak near log M $\sim$ -0.6. Burningham et al. [2010] identified nearly 50 nearby T dwarfs in data obtained by the UK Infrared Sky Survey. Using a Monte Carlo analysis to predict the number of T dwarfs expected for various combinations of the IMF, adopted Galactic star formation history (birth rate $\propto e^{\beta t}$, for -0.2 $< \beta <$ 0.2), and brown dwarf evolutionary models, Burningham et al. [2010] inferred an IMF that falls steeply[1] ($\Gamma < -1.0$) in the brown dwarf regime. Reylé et al. [2011] also inferred a similarly steep ($\Gamma < -1.0$) IMF from the space densities of $\sim$ 50 T and $\sim$ 170 L dwarfs confirmed in a 780 deg^2 survey with the Canada-France-Hawaii Telescope.

Photometric catalogues of low-mass stars and brown dwarfs from wide field surveys are now sufficiently large that uncertainties in IMF measurements are dominated by systematic errors in the analysis, such as biases due to the photometric distances estimates used to identify those stars lying within the sample volume. Several multi-epoch surveys are already underway, or will soon enter operation, and will provide astrometric precision sufficient to construct large, uniform samples of nearby stars with direct trigonometric distance estimates, eliminating the largest of these potential systematic errors. These surveys, such as Gaia (Perryman et al. [2001]), Pan-STARRS (Beaumont & Magnier [2010]), SkyMapper (Keller et al. [2007]), and the Large Synoptic Survey Telescope (Ivezic et al. [2008]), represent the next major advance in IMF measurements in the extended solar neighbourhood.

Open/Globular Clusters

The field star population provides unique leverage on the Galaxy-averaged IMF, but detecting IMF variations requires studies of discrete stellar populations with distinct properties and star-forming environments. The events that produce bound clusters are rare outliers along the spectrum of the Milky Way's star formation events, such that comparing cluster IMFs with that measured in the field provides an interesting test for the universality of the IMF. As high spatial density systems, clusters are also observationally convenient laboratories for efficient assembling of a statistically significant sample of stars. The 'cosmic scatter' introduced into colour-magnitude or magnitude-mass relations by stars with different metallicities or ages is also minimized for cluster studies: to the extent that clusters represent single stellar populations (an assumption with increasingly prominent counter-examples, e.g., ω Cen; Geisler, this volume; Lee et al. [1999]), each cluster's uniform age and metallicity minimizes uncertainties in the relative mass and magnitude determinations.

The advantages clusters provide for mass function measurements, however, come at the cost of additional complications. Strictly speaking, observations sample only a cluster's *present-day* mass function. To infer the form of the IMF, corrections must be applied to the present-day mass function to account for the loss of high-mass stars with $t_{life} < t_{cluster}$ and for spatial variations introduced into the cluster mass function due to dynamical effects (e.g. Portegies Zwart et al. [2010]). Care must also be taken to ensure that analyses of resolved clusters are based upon a robustly determined catalogue of cluster members [2], and for un- or marginally resolved clusters, that the effects of a stochastically sampled IMF are properly accounted for in modelling the cluster's colours and luminosity (Piskunov et al. [2011]).

As with studies of the field star IMF, the increased availability of deep, wide-field imaging has enabled significant progress in characterizing the IMFs of Galactic open clusters, as demonstrated by recent surveys of clusters such as IC 4665 (Lodieu et al. [2011]), the Pleiades (Casewell et al. [2011]), Hyades (Bouvier et al. [2008]), and Praesepe (Baker et al. [2010]; Boudreault et al. [2010]; Wang et al. [2011]). For brevity, we note that most of these surveys return mass functions that agree well with that measured in the solar neighbourhood, particularly after accounting for dynamical effects; we refer the reader to the contributions by Lodieu and Moraux for overviews of recent open cluster mass function measurements. The method presented by Bouy et al. for measuring accurate proper motions from

[1] strictly speaking, the 'steep decline' that Burningham et al. [2010] measure corresponds to a logarithmically binned MF, but the decline is sufficiently steep that the inferred IMF also declines in linear units.

[2] as an example of the impact different membership criteria can have on an IMF measurement, see the very different mass functions Baker et al. [2010] and Boudreault et al. [2010] obtained for the Praesepe open cluster, despite using quite similar observations and analysis techniques.

heterogenous archival data could also deliver significantly improved cluster membership catalogues for future open cluster mass function measurements.

With typical ages of a substantial fraction of a Hubble time, Galactic globular clusters provide an opportunity to probe the IMF in star-forming environments well-separated in space, time, and metallicity from star formation events that are currently ongoing in the Milky Way. The high space densities that have ensured the globular clusters' survival to the present epoch, however, also present observational challenges due to source crowding, which is exacerbated by their large distances, and challenges for analysis/interpretation, with even more severe dynamical evolution than in the open clusters discussed above. For these reasons, to fully sample the mass function to the faintest masses and characterize potential spatial variations in the cluster MF, reliable mass function measurements in globular clusters require high angular resolution observations at a range of cluster radii.

The most comprehensive and uniform analyses of the mass functions of Galactic globular clusters were performed by De Marchi et al. [2010] and Paust et al. [2010], respectively. Both studies analyzed ensembles of mass functions measured from Hubble Space Telescope observations of Galactic globular clusters, with care taken to account for the radial gradient in the present-day mass function due to dynamical evolution. While De Marchi et al. [2010] and Paust et al. [2010] reach differing conclusions in several areas (the optimal functional form to describe the MF in each cluster; the structural parameter that best correlates the clusters' dynamical states with the mass function shapes; etc.), the bottom line answers are the same – present-day mass functions of globular clusters, after correcting for the effects of dynamical evolution, are indistinguishable from that measured in the extended solar neighbourhood, with no evidence for trends with metallicity, age, or location in the Galaxy.

Young Star-Forming Regions

Studies seeking to understand the influence of the star formation environment on the resultant IMF often target young clusters or sites of ongoing star formation. Most active star-forming regions have ages $<$ 3 crossing times[3], so their current state likely closely reflects the initial conditions of the star-forming environment. As a result, star-forming regions represent the only environment in which one can attempt to directly trace the relationship between the stellar IMF and the mass function of pre- and protostellar molecular cores (e.g. André et al. [2010]; Michel et al. [2011]), though the core's subsequent evolution and potential fragmentation complicates efforts to provide a one-to-one mapping between cores and stars.

These observational and interpretational advantages carry with them certain burdens, such as the spatially structured extinction within star-forming molecular clouds, the variability inherent to young stars (e.g. Covey et al. [2011]), the presence of non-photospheric emission from stellar accretion and circumstellar disks, and the large uncertainties associated with pre-main sequence colour-magnitude and mass-magnitude relations. To minimize the impact of these affects, algorithms have been developed to interpret a star's observed colours and magnitudes with a model that includes photospheric emission as well as extinction and accretion/disk emission (for optical and NIR techniques, respectively, see Rio et al. [2010]; Covey et al. [2010]), or by obtaining spectroscopic data to help disentangle each star's properties. Nonetheless, care must be taken to construct extinction-limited samples in these regions to minimize biases related to source luminosity (and thus mass), and to measure the IMF as a function of position in the cluster to quantify any IMF variations due to intrinsic or dynamical mass segregation. Mass functions have recently been measured following these principles for several young, pre-main sequence populations: Upper Sco (Lodieu et al. [2011]), the Orion Nebular Cluster (Rio et al. [2010]), the ρ Oph surface population (Erickson, Wilking & Meyer, submitted), and even clusters in the Large Magellanic Cloud using HST imaging and STIS spectroscopy (Liu et al. [2009]). These studies, which are most sensitive to the shape of the mass function between 1.0 and 0.1 $M_\odot$, obtained IMFs which peak near 0.2 $M_\odot$ before declining toward the stellar-substellar boundary, consistent with the field star IMF.

By contrast with the regions noted above, studies of the Taurus star-forming region have identified an unusual abundance of stars with K7 – M0 spectral types, such that the (logarithmically binned) IMF peaks not at 0.2 – 0.3 $M_\odot$, but rather near 0.8 $M_\odot$ (Luhman et al. [2009]). This IMF thereby represents a strong, and statistically significant, counter-example to the more 'typical' stellar IMFs reported above: Luhman et al. [2009] find a $< 0.04\%$ probability that the Taurus IMF shares the same parent population as those measured in the Chameleon or IC 348 young clusters, whose IMFs are statistically indistinguishable from the field. Moreover, while Taurus' large angular size (> 20 deg^2) makes it a difficult target to

[3]though not necessarily all: see Covey et al. [2010] and references therein

survey in a uniform manner, it proximity and moderate extinction have made it a favoured region for observational work, such that it is arguably the best studied site of ongoing star formation (with the Orion Nebular Cluster as a close second). Homogeneous wide-field surveys of the Taurus star-forming region have now been performed over a wide range of wavelengths (Finkbeiner et al. [2004]; Güdel et al. [2007]; Rebull et al. [2010]; Takita et al. [2010]), and while there remain a number of candidate young stellar objects that require confirmation and characterization (e.g. Rebull et al. [2011]), unless the new candidates possess a markedly different distribution of spectral types & masses than previously identified members, it will be difficult to explain Taurus' anomalous IMF as a spurious observational result, and time to begin extracting physical insight from the discrepancy.

Recent observational surveys of star-forming regions have been increasingly focused on the sub-stellar IMF, as young brown dwarfs are significantly more luminous than they will be at ages greater than a few tens of Myrs. Recent surveys for extremely young brown dwarfs have been conducted in the ρ Oph (Alves de Oliveira et al. [2010]; Haisch et al. [2010]; Geers et al. [2011]), NGC 1333 (Scholz et al. [2009]), Chameleon I (Mužić et al. [2011]), and IC 348 (Burgess et al. [2009]) young clusters. These studies have begun to contribute sizable (n > 10) samples of brown dwarfs in each star-forming region; there is only modest statistical leverage for cluster to cluster comparisons, but clusters have been identified where the substellar IMF may show signs of mass segregation (e.g., the ONC: Andersen et al, this proceedings), or may not decline as steeply into the substellar regime as do the IMFs measured in other young clusters (Lodieu et al. [2011]). More generally, it has been difficult to reconcile the substellar IMFs measured in star-forming regions with those inferred from measurements of the field (Burningham et al. [2010]); these discrepancies may be at least partially due to inaccuracies in brown dwarf evolutionary models, however, as they are difficult to test given the small number of known binary brown dwarfs.

The surveys noted above provide considerable leverage on the shape of the IMF near and below its peak, but larger samples of high-mass stars are required to probe the shape of the super-solar IMF. Rich Galactic clusters, such as NGC 3603, Westerlund 1, and the Arches, and young clusters in the Large Magellanic Cloud, such as 30 Dor/R 136, have been useful laboratories for efficiently characterizing substantial populations of high-mass stars. The most recent generation of IMF measurements in these regions (e.g. Andersen et al. [2009]; Campbell et al. [2010]) have identified high-mass IMFs with Salpeter-type slopes, down to a characteristic mass of 1 – 2 $M_{\odot}$.

Recent attention has also turned to understanding how the relationship (or lack thereof) between the mass of a young cluster and of its most massive members may inform our understanding of the sampling mechanisms underlying the (high-mass) IMF. In brief, the question is to understand if a star forming in isolation is as likely to become a high-mass O star as a star forming in a rich, massive cluster: if so, the IMF is likely sampled in a completely random fashion; if not, some process (e.g., radiative feedback, dynamic interactions Dib et al. [2010]; Krumholz et al. [2010]) must allow the star-forming environment to influence the order in which the IMF is sampled. This means of probing the processes underlying the IMF was highlighted by Weidner & Kroupa [2006], and has inspired extensive scrutiny of the relationship between a cluster's mass and that of its most massive star [e.g., Lamb et al., 2010], and of the birthplace of apparently isolated massive stars (e.g. Selier et al. [2011]; Bressert et al. [2011]). Clearly a star of mass greater than the mass of the extant molecular cloud reservoir cannot form. Beyond that common-sense limit, however, there are multiple methods that can be adopted to set the upper mass limit of the IMF that will result from a given molecular cloud (i.e., the expectation mass of a perfectly sampled IMF with a total mass equal to that of the cloud, or the statistical upper mass limit that results from stochastically sampling an IMF truncated at the total cloud mass). These differing assumptions as to where to truncate a given cloud's IMF are simultaneously quite influential in determining the shape of the resultant IMF, but may also be quite difficult to test observationally (Elmegreen [2006]; Parker et al. [2011]). While a consensus view of the implications of these studies has yet to emerge, they have revived investigations into the relationship between the structure of molecular clouds, the dynamics of clusters, and the physics of star formation. Future insights may also be gleaned from linking these studies of the high-mass IMF with those investigating the dynamics and cluster-stellar mass relation in sparser star-forming groups (e.g. Kirk & Myers [2011]). For brevity, we direct the interested reader to the contributions by Weidner, Pflamm-Altenburg and Bressert elsewhere in this volume.

Future IMF Advances Enabled by the Gaia-LSST Synergy

As indicated by the summaries above, and the more extensive review by Bastian et al. [2010], despite decades of study and countless nights of observing time devoted to IMF measurements, we still lack

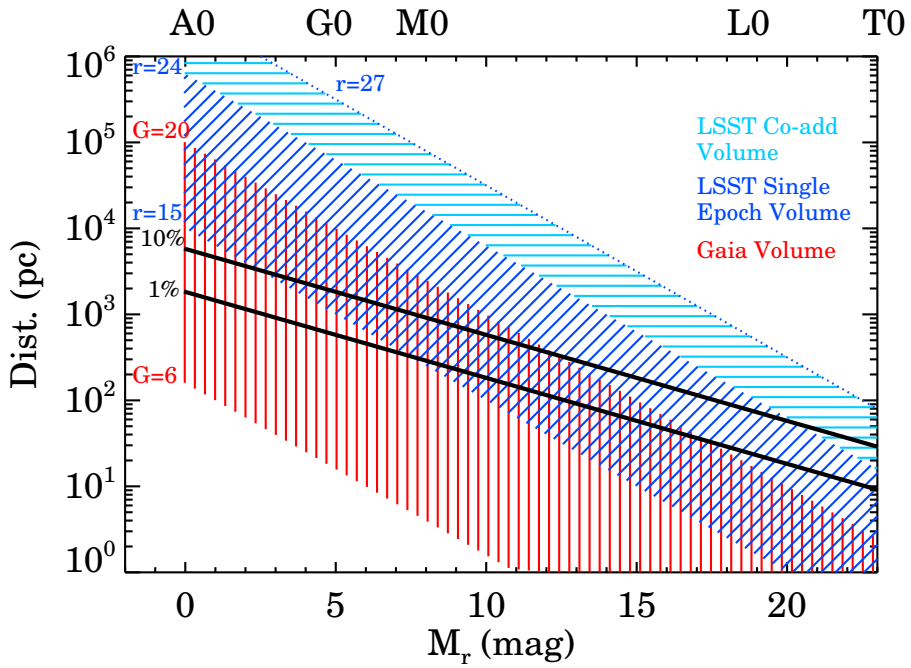

Figure 3.1: A visualization of the distances over which Gaia (red lines) and the Large Synoptic Survey Telescope (LSST; blue lines) will able to detect stars and brown dwarfs, as a function of r band absolute magnitude. Overplotted as solid black lines are the distances to which Gaia will obtain parallaxes accurate to 1% and 10%; LSST will achieve astrometric precision comparable to Gaia's faint end performance, consistent with the red/faintward extrapolation of Gaia's 10% precision limit.

confident detections of systematic IMF variations as function of environment and/or initial conditions. Instead, IMF measurements of resolved stellar populations return results that are broadly consistent, within the limits of their statistical precision, with an IMF that possesses a Salpeter slope above 1 $M_{\odot}$, flattens into a broad peak near 0.2 $M_{\odot}$, and then declines into the sub-stellar regime. Regions do exist that appear to possess anomalous IMFs (e.g., Taurus; Luhman et al. [2009]), but these exceptions are relatively rare, and no systematic link can be drawn from the region's current or initial state to its anomalous IMF, complicating attempts to attribute physical significance to these deviations.

As in the past, improved observational constraints on the presence or absence of IMF variations in resolved stellar populations require improved censuses of several key environments: the volume complete sample in the extended Solar neighbourhood, to provide the highest-fidelity template single-star mass function; nearby clusters, including both young star-forming regions and old open clusters, to provide sensitivity to environmental dependences; and distant star-forming regions, which probe environments with extreme metallicities and star formation rates, and provide the statistical leverage needed to probe the high-mass end of the IMF. The last environment is perhaps most amenable to study with the James Webb Space Telescope and/or the next generation of large aperture, AO-corrected facilities, which will enable studies of more distant and crowded regions than are currently feasible.

Studies of the volume complete sample and of nearby clusters, however, will benefit more from the next-generation of large area surveys with good astrometric performance; these capabilities will also contribute to studies of the high-mass IMF, by providing improved limits on the frequency and initial birth-places of apparently isolated young, high-mass stars. Moreover, with the imminent launch of the Gaia mission, operations now underway for the PanSTARRs and SkyMapper surveys, and first light expected for the Large Synoptic Survey Telescope (LSST) by the end of this decade, the community will soon see a significant increase in the depth, fidelity, and accuracy of large area surveys with good astrometric precision.

Fig. 3.1 illustrates the range of distances over which Gaia and LSST will produce reliable photometric catalogues, as a function of stellar absolute magnitude (and thus mass). We also include the distance limits to which Gaia is expected to provide distances accurate to 1% and 10%, calculated by adopting the model of Gaia's astrometric performance as a function of source magnitude summarized by Ivezic et al. [2008]. Ivezic et al. [2008] also demonstrate that Gaia's astrometric precision will be superior

to that of the LSST at all magnitudes brighter than Gaia's faint limit. At Gaia's faint limit, however, LSST will be able to achieve comparable astrometric precision, and LSST's large aperture will enable astrometric measurements for sources as faint as r $\sim$ 24, albeit with errors that increase as expected from photon noise.

Gaia and LSST will therefore produce highly complimentary photometric and astrometric catalogues, with Gaia providing unmatched precision for sources brighter than G $\sim$ 20, and LSST smoothly extending the error function faintward to r $\sim$ 24[4], and redward to y $\sim$ 22.1. These complimentary capabilities will advance IMF studies to a point significantly beyond where either survey could take us alone:

- **For stars at the peak of the IMF or blueward, Gaia will expand the volume complete sample by more than an order of magnitude.** Currently, the volume complete sample of solar-type stars extends reliably to a distance of 25 pc (e.g. Raghavan et al. [2010]). As Fig. 3.1 demonstrates, Gaia will provide distances accurate to 1% for solar-type stars as far 500 pc; this order of magnitude increase in the outer boundary of the volume complete sample corresponds to a *thousand-fold* increase in the volume of the volume complete sample!

  As Fig. 3.1 also shows, however, Gaia's astrometric precision does not decay as quickly with stellar absolute magnitude as its photon limit does: in other words, Gaia will run out of photons from the reddest stars more quickly than it will run out of baseline for measuring their parallaxes. As a result, Gaia's volume complete sample will be limited primarily by photometric limits for stars with $M_r \geq 12 - 15$, which lie near the peak of most IMF measurements and correspond to a mass of ~ 0.2 $M_\odot$. At these lowest masses, the distance limit of Gaia's volume complete sample will decline from $\sim$ 100 pc for M3/4 type stars to $\sim$ 10 pc at the M9/L0 stellar/substellar boundary, with typical T dwarfs only being detected within 2 – 3 pc.

- **With exquisite proper motions as well as parallaxes, Gaia will dramatically improve membership determinations for nearby open clusters, and dissect the kinematic subpopulations of the Galactic disk.** The volume complete sample described above will be sufficiently large that it will encompass numerous nearby clusters: α Per, the Pleiades, Hyades, Praesepe, and Rup 147 are a few notable benchmark clusters whose solar-type members will fall well within the horizon of Gaia's volume complete sample. Using Gaia's precise proper motion measurements to discriminate cluster members from the field, new studies of these clusters will improve our understanding of not only their IMFs, but also the dynamics of cluster dissolution and mass segregation. Gaia will similarly improve our membership lists for young moving groups like TW Hya, Beta Pic, and η Cha, combining kinematic criteria with multi-epoch photometry to diagnose the enhanced variability characteristic of pre-main sequence stars. Improving and extending the membership of these groups will enable important observational tests for our models of pre-main sequence stellar evolution, early cluster dynamics, and potential mechanisms for triggering star formation events. Finally, the kinematic properties of the remaining 'boring' Galactic field stars will provide remarkable traction for understanding the star formation history and dynamics of the Milky Way.

- **Gaia's photometric, astrometric and spectroscopic catalogue will provide considerable leverage for identifying stellar multiples, enabling new investigations of the IMF as a function of source multiplicity.** Currently, most investigations of the IMF are unable to fully diagnose the presence of stellar multiples, much less characterize their properties, and are thus only able to probe the IMF of stellar systems. The few investigations that have studied the IMF of companion stars directly, however, find evidence that single stars and stellar companions are drawn from distinct IMFs (e.g. Metchev & Hillenbrand [2009]; Reggiani & Meyer [2011]), suggesting new constraints for models of star formation and cluster dynamics. Gaia will be able to directly detect and characterize numerous multiples whose orbital motions can be resolved via astrometry and spectroscopy, and reveal countless more multiples via photometric offsets in the HR diagram. These photometrically detected binaries will provide useful statistical constraints on the IMF of multiple systems, but their true potential for IMF studies will not be achieved without spectroscopic follow-up to obtain orbital solutions and detailed mass ratios, highlighting the clear science case for a ground-based spectroscopic survey to complement and extend Gaia's spectroscopic coverage.

[4]at a single-epoch; co-added images will reach a depth of r $\sim$ 27

- **Gaia parallaxes will anchor LSST's colour-magnitude relations.** Compared to the major scientific advances outlined above, it may seem trite to note that Gaia's stellar catalogue will become the default source of calibrators for subsequent wide area surveys, but this will nonetheless be a major contribution to the astronomical community.

  To underscore the value of Gaia's catalogue for calibrating subsequent surveys, we can use the Sloan Digital Sky Survey (SDSS) as a case study. The SDSS's red sensitivity significantly advanced our ability to study the lowest mass members of the Galactic disk (e.g. Bochanski et al. [2007b]; Bochanski et al. [2007a]; Covey et al. [2008a]). The SDSS is sufficiently sensitive, however, that determining absolute luminosities, and thus masses, for these lowest mass stars has been surprisingly difficult; late-type stars with measured trigonometric parallaxes are nearly all sufficiently bright that they saturate the native SDSS photometry, and these stars are sufficiently red that they lie well outside the realm of the grid of SDSS' primary photometric standards, such that the large colour-terms required to convert existing colour-magnitude relations into the SDSS filterset are relatively uncertain [Davenport et al., 2006; Bilir et al., 2008]. These combined effects have complicated efforts to infer the colour-magnitude relation of low-mass stars on the native SDSS photometric system, with measurements of stellar spectral types (Covey et al. [2007]) often required to bootstrap internally consistent colour-spectral type relations to an externally calibrated spectral type-absolute magnitude relation (e.g. Hawley et al. [2002]).

  For these reasons, the sizable overlap in Fig. 3.1 between LSST's bright limit, and Gaia's 1 – 10% parallax limit is encouraging: LSST will obtain direct photometry for millions of stars with accurate Gaia parallaxes, enabling the construction of high fidelity colour-magnitude relations on LSST's native photometric system. Gaia's exquisite kinematic information will even allow these colour-magnitude relations to be derived for individual cluster populations, as well as for separate Galactic populations, providing ample opportunities to calibrate the impact that metallicity and age can have on these relations[5]. These data products will provide an incredibly robust foundation for nearly all studies of stellar astrophysics with LSST's photometric catalogue.

- **By smoothly extending Gaia's astrometric performance to fainter and redder sources, LSST will extend Gaia's IMF measurements to the lowest masses, and the youngest ages.** As Fig. 3.1 demonstrates, there are numerous sources for which Gaia's astrometric precision would be sufficient to provide accurate distances, if only the source would deign to emit enough photons to provide a confident photometric detection. By virtue of its significantly larger aperture, and enhanced red sensitivity, LSST will be able to smoothly extend Gaia's astrometric precision solidly to redder and fainter sources. Fig. 3.1 illustrates this complimentarity in the context of distance limits for unextincted main sequence stars and brown dwarfs in the solar neighbourhood; considering only r band sensitivity, LSST should be able to extend the limit for 10% distances by a factor of ~ 2 at the stellar-substellar boundary, and by a factor of ~ 3 for typical T-type brown dwarfs. These expanded distance limits correspond to a factor of $\sim 8 - 27$ increase in survey volume, and the availability of izy photometry will provide even greater increases in survey volume for the reddest sources.

  In addition to extending the outer boundary of the volume complete sample for the lowest mass objects, LSST's astrometric performance at red wavelengths will similarly improve IMF studies of open clusters and star-forming regions. LSST's accurate photometry and astrometry for red sources will enable the kinematic identification and characterization of low-mass stars and brown dwarfs in the nearest open clusters; the fiducial colour-magnitude diagrams defined by those kinematically defined samples will then enable statistical analyses of the memberships and IMFs of more distant open clusters, whose lower main sequences will only be detected in co-added LSST data products. LSST's red sensitivity will be of even more value for analyzing the memberships of regions with ongoing star formation activity. The stars in the youngest of these regions are often associated with significant extinction, making LSST's astrometric performance at red wavelengths all the more important for defining cluster membership, analyzing cluster dynamics, and enabling robust IMF determinations in extinction limited sub-samples of cluster members.

While we have yet to confidently detect robust signatures of IMF variations in resolved Galactic stellar populations, the above discussion demonstrates that we will soon experience a dramatic improvement

[5]Indeed, while these colour-magnitude relations for will be invaluable for interpreting LSST data, the leverage they will provide for investigating morphological changes in the structure of the main sequence across stellar populations will likely lead to significant advances in our understanding of stellar evolution.

in our ability to measure the mean IMF of the Milky Way, and contrast it with robust IMF measurements for distinct kinematic and cluster populations in our Galaxy. Whatever the results of these studies, they will have significant implications for our understanding of the astrophysics of star formation: the stringent limits these capabilities will be able to place on IMF variations will either demonstrate that star formation is a remarkably process, producing a consistent IMF across a range of star-forming environments, or reveal the manner in which the IMF does reflect the properties of the underlying star-forming environment.

Acknowledgments

We thank the organizers for hosting an enjoyable and productive meeting, and the countless scientists whose contributions to the Gaia mission will shortly enable us to re-write our understanding of star formation, stellar evolution, cluster dynamics, and the structure and history of the Milky Way.

Bibliography

Alves de Oliveira, C., Moraux, E., Bouvier, J., et al. 2010, A&A, 515, A75+
Andersen, M., Zinnecker, H., Moneti, A., et al. 2009, The Astrophysical Journal, 707, 1347
André, P., Men'shchikov, A., Bontemps, S., et al. 2010, A&A, 518, L102+
Baker, D., Jameson, R., Casewell, S., et al. 2010, Monthly Notices of the Royal Astronomical Society, 408, 2457
Bastian, N., Covey, K. R., & Meyer, M. R. 2010, ARA&A, 48, 339
Beaumont, C. & Magnier, E. 2010, Publications of the Astronomical Society of the Pacific, 122, 1389
Bilir, S., Ak, S., Karaali, S., et al. 2008, MNRAS, 384, 1178
Bochanski, J. J., Hawley, S. L., Covey, K. R., et al. 2010, AJ, 139, 2679
Bochanski, J. J., Munn, J. A., Hawley, S. L., et al. 2007a, AJ, 134, 2418
Bochanski, J. J., West, A. A., Hawley, S. L., & Covey, K. R. 2007b, AJ, 133, 531
Boudreault, S., Bailer-Jones, C. A. L., Goldman, B., Henning, T., & Caballero, J. A. 2010, A&A, 510, A27+
Bouvier, J., Kendall, T., Meeus, G., et al. 2008, Astronomy and Astrophysics, 481, 661
Bressert, E., , & and. 2011, A&A, submitted
Burgess, A., Moraux, E., Bouvier, J., et al. 2009, Astronomy and Astrophysics, 508, 823
Burningham, B., Pinfield, D., Lucas, P., et al. 2010, Monthly Notices of the Royal Astronomical Society, 406, 1885
Campbell, M., Evans, C., Mackey, A., et al. 2010, Monthly Notices of the Royal Astronomical Society, 405, 421
Casewell, S., Jameson, R., Burleigh, M., et al. 2011, Monthly Notices of the Royal Astronomical Society, 412, 2071
Chabrier, G. 2005, in Astrophysics and Space Science Library, Vol. 327, The Initial Mass Function 50 Years Later, ed. E. Corbelli, F. Palla, & H. Zinnecker, 41–+
Covey, K. R., Agüeros, M. A., Green, P. J., et al. 2008a, ApJS, 178, 339
Covey, K. R., Hawley, S. L., Bochanski, J. J., et al. 2008b, AJ, 136, 1778
Covey, K. R., Hillenbrand, L. A., Miller, A. A., et al. 2011, AJ, 141, 40
Covey, K. R., Ivezić, Ž., Schlegel, D., et al. 2007, AJ, 134, 2398
Covey, K. R., Lada, C. J., Román-Zúñiga, C., et al. 2010, ApJ, 722, 971
Dabringhausen, J., Hilker, M., & Kroupa, P. 2008, MNRAS, 386, 864
Davenport, J. R. A., West, A. A., Matthiesen, C. K., Schmieding, M., & Kobelski, A. 2006, PASP, 118, 1679
De Marchi, G., Paresce, F., & Portegies Zwart, S. 2010, ApJ, 718, 105
Dib, S., Shadmehri, M., Padoan, P., et al. 2010, Monthly Notices of the Royal Astronomical Society, 405, 401
Elmegreen, B. G. 2006, ApJ, 648, 572
Finkbeiner, D. P. et al. 2004, AJ, 128, 2577
Geers, V., Scholz, A., Jayawardhana, R., et al. 2011, ApJ, 726, 23
Güdel, M., Briggs, K. R., Arzner, K., et al. 2007, A&A, 468, 353
Haisch, K., Barsony, M., & Tinney, C. 2010, The Astrophysical Journal, 719, L90
Hawley, S. L., Covey, K. R., Knapp, G. R., et al. 2002, AJ, 123, 3409

Ivezic, Z., Tyson, J. A., Acosta, E., et al. 2008, ArXiv e-prints 0805.2366
Kapteyn, J. C. 1914, ApJ, 40, 43
Keller, S. C., Schmidt, B. P., Bessell, M. S., et al. 2007, PASA, 24, 1
Kirk, H. & Myers, P. 2011, The Astrophysical Journal, 727, 64
Klessen, R. S., Burkert, A., & Bate, M. R. 1998, ApJL, 501, L205+
Kroupa, P., Tout, C. A., & Gilmore, G. 1993, MNRAS, 262, 545
Krumholz, M., Cunningham, A., Klein, R., & Mckee, C. 2010, The Astrophysical Journal, 713, 1120
Lamb, J. B., Oey, M. S., Werk, J. K., & Ingleby, L. D. 2010, ApJ, 725, 1886
Larson, R. B. 1992, MNRAS, 256, 641
Lee, Y.-W., Joo, J.-M., Sohn, Y.-J., et al. 1999, Nature, 402, 55
Liu, Q., Grijs, R. D., Deng, L., et al. 2009, Monthly Notices of the Royal Astronomical Society, 396, 1665
Lodieu, N., de Wit, W. ., Carraro, G., et al. 2011, ArXiv e-prints
Lodieu, N., Dobbie, P., & Hambly, N. 2011, Astronomy and Astrophysics, 527, 24
Luhman, K. L., Mamajek, E. E., Allen, P. R., & Cruz, K. L. 2009, ApJ, 703, 399
Mainzer, A., Cushing, M., Skrutskie, M., et al. 2011, The Astrophysical Journal, 726, 30
Metchev, S. A. & Hillenbrand, L. A. 2009, The Astrophysical Journal Supplement, 181, 62
Michel, M., Kirk, H., & Myers, P. 2011, eprint arXiv:1104.4538
Miller, G. E. & Scalo, J. M. 1979, ApJS, 41, 513
Mužić, K., Scholz, A., Geers, V., Fissel, L., & Jayawardhana, R. 2011, The Astrophysical Journal, 732, 86
Padoan, P. & Nordlund, Å. 2002, ApJ, 576, 870
Parker, R., Bouvier, J., Goodwin, S., et al. 2011, Monthly Notices of the Royal Astronomical Society, 412, 2489
Paust, N., Reid, I., Piotto, G., et al. 2010, The Astronomical Journal, 139, 476
Perryman, M. A. C., de Boer, K. S., Gilmore, G., et al. 2001, A&A, 369, 339
Piskunov, A., Kharchenko, N., Schilbach, E., et al. 2011, Astronomy and Astrophysics, 525, 122
Portegies Zwart, S. F., McMillan, S. L. W., & Gieles, M. 2010, ARA&A, 48, 431
Raghavan, D., McAlister, H. A., Henry, T. J., et al. 2010, ApJS, 190, 1
Rebull, L. M., Koenig, X. P., Padgett, D. L., et al. 2011, ArXiv e-prints
Rebull, L. M., Padgett, D. L., McCabe, C.-E., et al. 2010, ApJS, 186, 259
Reggiani, M. M. & Meyer, M. R. 2011, ArXiv e-prints
Reid, I. N. & Gizis, J. E. 1997, AJ, 113, 2246
Reipurth, B. & Clarke, C. 2001, AJ, 122, 432
Reylé, C., Delorme, P., Willott, C., et al. 2011, A&A, 522, 112
Rio, N. D., Robberto, M., Soderblom, D., et al. 2010, The Astrophysical Journal, 722, 1092
Salpeter, E. E. 1955, ApJ, 121, 161
Scholz, A., Geers, V., Jayawardhana, R., et al. 2009, The Astrophysical Journal, 702, 805
Selier, R., Heydari-Malayeri, M., & Gouliermis, D. A. 2011, A&A, 529, A40+
Silk, J. 1995, ApJL, 438, L41
Takita, S., Kataza, H., Kitamura, Y., et al. 2010, A&A, 519, A83+
Wang, W., Boudreault, S., Goldman, B., et al. 2011, ArXiv e-prints
Weidner, C. & Kroupa, P. 2006, MNRAS, 365, 1333

3.2 Young Star Clusters in External Galaxies

Søren S. Larsen[1]

[1] Astronomical Institute, Utrecht University, The Netherlands

Abstract

I review the characteristics of cluster populations in other galaxies, with particular emphasis on young star clusters and a comparison with the (known) open cluster population of the Milky Way. Young globular cluster-like (compact, massive) objects can still form at the present epoch, even in relatively quiescent spiral discs, as well as starbursts. Comparison with other nearby spiral galaxies, like M 83 and NGC 6946, suggests that the Milky Way should host about 20 clusters with masses above 10^5 $M_\odot$ and ages younger than about 200 Myr. No such clusters have been found, however. I discuss the important roles of selection and evolutionary effects that may account for many of the apparent differences between cluster populations in different galaxies. One potentially important difference between ancient GCs and young star clusters is the presence of complex star formation / chemical enrichment histories in the GCs. Little is currently known about the presence or absence of such features in massive ($> 10^5$ $M_\odot$) young star clusters, but some tantalizing hints of extended star formation histories are now emerging also in young clusters.

Introduction

The classification of star clusters as either "open" or "globular" may first have been explicitly adopted by Shapley [1916]. However, it is clear that neither the "classical" globular nor open clusters constitute homogeneous classes of objects, and furthermore the boundary between the two classes is somewhat fuzzy. The Galactic globular clusters (GCs) can be grouped into at least two sub-populations, loosely associated with the Galactic halo and bulge/thick disc, that have distinct kinematics, spatial distributions and metallicities (Zinn [1985]; Minniti [1996]). Even in our Galaxy, the open clusters span large ranges in age, mass and concentration that overlap somewhat with the globular clusters, and making a clear-cut distinction between open and globular clusters becomes increasingly difficult as one moves to external galaxies (e.g. Hodge [1988]). This has become particularly true in the last few decades due to the discovery of young star clusters with masses in the range $10^5 - 10^7 M_\odot$, predominantly in interacting galaxies and starbursts (Whitmore [2003]; Portegies Zwart et al. [2010]), but also in some normal non-interacting spirals [Larsen & Richtler, 2000]. To accommodate these objects, terms such as young massive clusters (YMCs), super-star clusters (SSCs), etc., have been introduced.

Although classification is often a natural first step in the study of a new field, there is no generally accepted classification scheme for star clusters that has managed to gain foothold, and it is not clear to what extent the different labels that have been adopted by various authors correspond to physically different objects (see an excellent discussion of this point in Terlevich [2004]). It therefore appears more useful to discuss the differences and similarities among cluster systems in different environments in terms of quantifiable parameters. To this end, it is useful to distinguish between three different aspects of a cluster system: 1) The formation efficiency of (long-lived) star clusters relative to field stars, 2) the shape of the initial cluster mass function (ICMF), and 3) dynamical effects. Items (1) and (3) are dealt with extensively elsewhere in these proceedings (e.g. Bastian, Bressert, Gieles, Kruijssen). Here I will mainly concentrate on (2), the ICMF.

The initial cluster mass function (ICMF)

The ICMF is analogous to the stellar IMF, and constraining it is subject to many of the same difficulties. Like stars, clusters have finite lifetimes that must be taken into account when trying to infer the ICMF from the observed mass distribution of a cluster sample. It is straightforward to show that if clusters lose mass at a rate $\dot{M} \equiv -M/t_{\rm dis}$, with $t_{\rm dis} \propto M^\gamma$, then $dN/dM \sim M^{\gamma-1}$ independently of the ICMF

for $t \gg t_{\rm dis}$. Hence, memory of the initial shape of the MF is lost below some mass limit. This is consistent with observations showing that the present-day MF of ancient globular clusters is about flat at $M \lesssim 10^5 M_\odot$ if $t_{\rm dis}$ scales roughly linearly with cluster mass (Fall & Zhang [2001]; McLaughlin & Fall [2008]; Kruijssen & Portegies Zwart [2009]). At younger ages, only the low-mass end of the MF is expected to have been strongly affected by dynamical evolution, although the detailed relation between cluster mass and $t_{\rm dis}$ is more uncertain at younger ages (e.g. Bastian, these proceedings). At high masses, the main empirical difficulty is that the most massive clusters, like the most massive stars, are rare, and as a result there is still considerable uncertainty about the shape and degree of universality of the high-mass end of the ICMF. Care must be taken to separate statistical size-of-sample effects from real physical differences.

It is worth reflecting for a moment on the exact meaning of the term *initial* cluster mass function. The ICMF may be understood as the mass function "at birth" for a cluster population, but this is not a very useful definition in practice. The moment of birth is not well defined, and at young ages the identification of individual star clusters is often difficult (e.g. Bressert, these proceedings). In addition, since the most massive clusters are rare, a cluster sample spanning a very small range of ages will not be very suitable for constraining the behaviour of the ICMF at the high-mass end. A more practical approach is to view the ICMF as a *mean birthrate function*,

$$\Psi(M) \equiv \frac{d^2N}{dM\, d\tau} \tag{3.3}$$

i.e., $\Psi(M)$ is the average number of clusters born per unit mass per unit time interval. This may then be integrated over time and mass in order to yield, e.g., the expected number of clusters born with a given range of masses over a given time interval.

Several studies have constrained the shape of the ICMF over some mass interval. In the Milky Way, the shape of the ICMF is well approximated by a power-law $dN/dM \propto M^{-2}$ for $\lesssim 10^3$ M$_\odot$ (Elmegreen & Efremov [1997]; Lada & Lada [2003]; Selman & Melnick [2008]). At higher masses the ICMF in the Milky Way is poorly constrained, but the discovery of several young clusters with masses in the range $10^4 - 10^5$ M$_\odot$ shows that our Galaxy is certainly still capable of forming such objects (Clark et al. [2005]; Figer et al. [2006]; Davies et al. [2007]). The M^{-2} power-law behaviour has been found in other galaxies too, like the LMC (Hunter et al. [2003]; de Grijs & Anders [2006]; Chandar et al. [2010a]), M 51 (Bik et al. [2003]; Chandar et al. [2011]) and the Antennae (Zhang & Fall [1999]; Fall et al. [2009]), for higher masses than in the Milky Way.

Range of validity for the M^{-2} ICMF

While the M^{-2} power-law form seems relatively well established for masses up to $\sim 10^5 M_\odot$, the upper and lower limits remain less well constrained. This has to do with statistics in both cases, but of quite different nature. At the low-mass end, the discreteness of the *stellar* IMF becomes an important limiting factor especially when relying on the integrated properties of clusters to determine ages and masses, as is typically the case in extragalactic studies. The light from a 10^4 M$_\odot$ cluster is dominated by *on average* only 2 – 3 supergiants for ages up to several tens of Myr. Since this is an average, some clusters will have no supergiants at all, while others will have more than the average value. This leads to very large fluctuations in the integrated magnitude colours that are *not* symmetrically distributed around the values predicted for a continuously sampled IMF (Barbaro & Bertelli [1977]; Bruzual [2002]; Girardi et al. [1995]; Cerviño & Luridiana [2004]; Cerviño & Luridiana [2006]; Maíz Apellániz [2009]; Piskunov et al. [2009]; Fouesneau & Lançon [2010]; Popescu & Hanson [2010]). As an illustration of this, Fig. 3.2 shows the M_V magnitude vs. stellar mass for simulated star clusters with an age of $\log t/yr = 7.2$. At low masses there is a very large scatter in this relation, and it only starts to narrow down above $\sim 10^4$ M$_\odot$. This discreteness of the IMF also affects cluster detection itself; a low-mass cluster dominated by a single supergiant star is unlikely to be detected in any survey that uses size information to identify cluster candidates (Silva-Villa & Larsen [2011]).

At the high-mass end, the main difficulty is the low birthrates, resulting in poor statistics. Although a large galaxy like the Milky Way may have formed hundreds of clusters with $M > 10^5 M_\odot$ over its lifetime (see below), the numbers that are accessible to detailed study are generally much less than that. Ground-based imaging is generally restricted to ages $< 10^8 - 10^9$ yr, when the clusters are bright and blue enough to be separated from foreground stars (Larsen & Richtler [2000]; Dowell et al. [2008]). HST imaging can use size information to avoid confusion with individual stars, but typically covers only a small fraction of nearby galaxies.

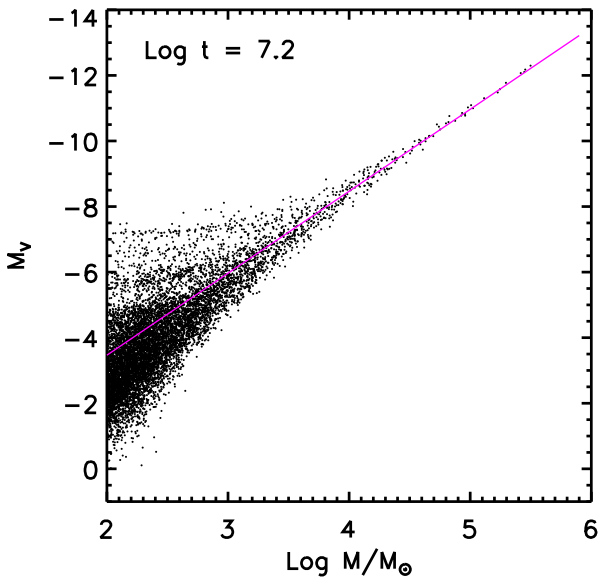

Figure 3.2: Absolute M_V magnitude as a function of mass for simulated star clusters with an age of $\log t/yr = 7.2$. Note that there is no unique mapping between M_V and masses less than $\log M/M_\odot \sim 4$, even for a fixed age.

Hidden massive clusters in the Milky Way?

If the total star formation rate in (long-lived) clusters and the shape of the ICMF are known, we can calculate how many clusters in a given mass range should have formed over some time interval. Observationally, it is challenging to constrain the current formation rate of star clusters in the Milky Way. To get an order-of-magnitude estimate, we assume a total star formation rate of the Milky Way of about 1 $M_\odot$ yr^{-1} (Robitaille & Whitney [2010]) and that about 10% of this is in the form of bound star clusters (Lada & Lada [2003]; Bastian [2008]; Silva-Villa & Larsen [2010]). In order to estimate the expected number of massive clusters for a pure M^{-2} ICMF, it is necessary to adopt upper and lower limits. Plausible values may be ~ 10 $M_\odot$ and $\sim 10^6$ $M_\odot$. In this case, a cluster formation rate of 0.1 $M_\odot$ yr^{-1} yields mean birthrates of ~ 0.9 Myr^{-1} for $M > 10^4$ $M_\odot$ and ~ 0.08 Myr^{-1} for $M > 10^5 M_\odot$. If the star formation rate was constant in the past, the total number of clusters formed over the past 10 Gyr would then be ~ 8000 and ~ 800 for $M > 10^4$ $M_\odot$ and $M > 10^5$ $M_\odot$, respectively. These are likely lower limits, as the SFR may well have been higher in the past, although many of these clusters will have dissolved. However, the fact that only $\sim$ one cluster with $M \sim 10^5$ $M_\odot$ is expected to form every 10 Myr may be consistent with the observation that even the most massive young clusters known in our Galaxy barely reach $10^5 M_\odot$ and all are only a few Myr old. Due to complicated and poorly quantified selection effects, the Milky Way may not be the best place for constraining the ICMF at high masses.

Constraints from other galaxies

As noted above, a number of studies have attempted to constrain the shape of the ICMF in several external galaxies, often finding it to be well represented by a $dN/dM \propto M^{-2}$ shape *over some mass range*. However, many of these studies have been based on HST pointings covering only a small fraction of the target galaxies, or have been targetting galaxies that are relatively small in the first place (like the LMC) and the behaviour of the ICMF is typically poorly constrained above $\sim 10^5$ $M_\odot$. In an attempt to obtain better statistics at high masses, Larsen [2009] used the ground-based imaging of Larsen & Richtler [1999] to study the MF of young star clusters in a sample of spiral galaxies. Fig. 3.3 shows the resulting combined mass function for the two spiral galaxies NGC 5236 and NGC 6946, both of which have high current star formation rates and rich populations of young star clusters. The figure includes objects younger than 200 Myr, where the data are still reasonably complete for $M > 10^5$ $M_\odot$. The MF is here sampled up to $\sim 10^6$ $M_\odot$, and is poorly fit by a pure $dN/dM \propto M^{-2}$ power-law over the range $10^5 - 10^6$ $M_\odot$ (dashed line). Instead, a Schechter mass function with a cut-off mass of 2×10^5 $M_\odot$, i.e., $dN/dM \propto \exp(-M/2 \times 10^5\ M_\odot) M^{-2}$, provides an excellent fit to the data (dotted-dashed line). There is no particular physical reason for choosing the Schechter function as a fitting formula, except

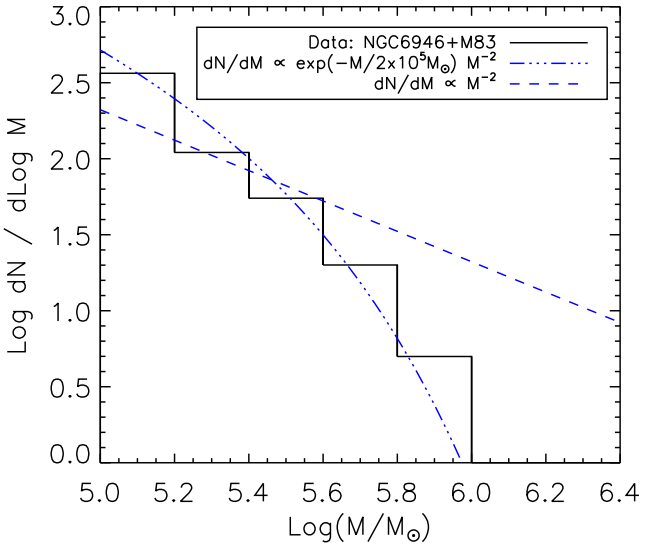

Figure 3.3: Observed mass function for the combined cluster populations of NGC 6946 and M 83 for clusters younger than 200 Myr. The dashed line shows an M^{-2} power-law while the dotted-dashed line is a Schechter function with a cut-off mass at 2×10^5 M$_\odot$.

that it preserves the M^{-2} shape found at lower masses, and provides a convenient way to parameterize a steepening or "cut-off" at higher masses.

The data in Fig. 3.3 allow us to make an independent estimate of the number of massive clusters expected in the Milky Way. The combined star formation rate of NGC 6946 and NGC 5236 is about 5 $M_\odot$ yr^{-1} and the sample contains 111 clusters with $M > 10^5$ M$_\odot$ and ages younger than 200 Myr. Scaling by the SFR, we would thus expect about 20 clusters in the same mass- and age range in the Milky Way. This is in surprisingly good agreement with the birthrate of about one cluster with $M > 10^5$ M$_\odot$ every 10 Myr estimated above (see previous Subsection).

Although an attractive attribute of the ground-based data is that they cover the full galaxies, there is clearly some risk that cluster samples may be contaminated by more extended groupings of stars. Although it appears unlikely that contamination would lead to what is essentially a *dearth* of high-mass objects compared to extrapolation of a pure M^{-2} power-law, the data shown in Fig. 3.3 should still be treated with a healthy dose of skepticism. Using HST imaging of NGC 5236, Chandar et al. [2010b] find the MF to be consistent with a cut-off above $10^5 M_\odot$, while Chandar et al. [2011] find cut-offs of $M_\star > 2 \times 10^5$ M$_\odot$ to be consistent with observations of NGC 5194. Hence, these studies are essentially consistent with a cut-off mass of several 10^5 M$_\odot$.

A more indirect way to constrain the ICMF is by means of the cluster *luminosity* function (LF). Although the LF is related to the ICMF, it is in general not possible to directly determine the ICMF from observations of the LF as this would require a detailed knowledge of the cluster formation history and dissolution. However, the LF can be predicted for various scenarios and then compared with observations. As an example, Fig. 3.4 shows the observed luminosity function for young clusters in NGC 5194, based on a large HST/ACS mosaic covering essentially the complete galaxy (Haas et al. [2008]). A very similar LF, based on the same data, has been shown by Hwang & Lee [2008]. Also shown in the figure are predicted LFs for various scenarios. The dashed line shows the LF for a pure power-law ICMF ($dN/dM_i \propto M_i^{-2}$) and no disruption. In this case, the LF itself will have a similar form, $dN/dL \propto L^{-2}$, which is not consistent with the data that instead show a considerably steeper slope at the bright end ($dN/dL \propto L^{-2.5}$ for $M_V < -8$; Haas et al. [2008]). Instead, a model LF based on a Schechter ICMF with cut-off mass $M_\star = 2 \times 10^5$ M$_\odot$ provides a good fit to the data, especially if some mass-dependent disruption is included. We have assumed here that cluster lifetimes depend on mass as $t_{\rm dis} = 5 \times 10^8 {\rm yr} (M/10^4 M_\odot)^{0.65}$.

Although luminosity functions are a somewhat indirect way to constrain the ICMF, they are observationally straightforward to determine and do not depend on model-dependent conversions from the observables to ages and masses. It is therefore not surprising that LFs are available for more cluster systems, compared to the relatively small number of systems where MFs have been derived. It is easy to show that a uniform M^{-2} MF will also yield an L^{-2} LF, if there is no disruption. Unless high-mass clusters are preferentially disrupted, an initial M^{-2} power-law ICMF should therefore always lead to a LF with the same -2 slope or shallower. Instead, most studies tend to find LFs that are *steeper* than

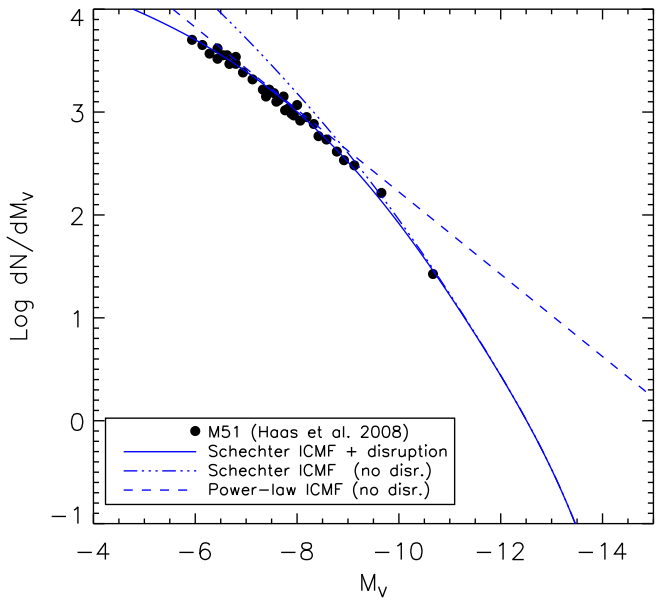

Figure 3.4: Dots: Observed luminosity function for clusters in M 51 = NGC 5194. The dotted line is an L^{-2} power-law, while the solid and dotted-dashed curves are LFs computed for an underlying Schechter ICMF with and without disruption.

this, with slopes getting increasingly steeper if they are measured at brighter magnitudes (Larsen [2002]; Gieles [2010]).

Both direct ICMF determinations and LF measurements appear to be consistent with a cut-off mass $\sim 2 \times 10^5 M_\odot$ in normal spiral discs (Portegies Zwart et al. [2010]), although there is a hint that the cut-off may be somewhat radially dependent in NGC 5236 (Bastian, these proceedings). The cut-off mass does *not* appear to be universal but must be significant higher in starburst galaxies, which often host large numbers of clusters with masses of 10^6 M$_\odot$ or above. For the best-studied on-going major merger, the Antennae, Zhang & Fall [1999] suggested a truncation near $10^6 M_\odot$ while a formal fit to their data yields $M_C \sim 8 \times 10^5 M_\odot$ (Jordan et al. [2007]). In old GC systems there also appears to be an upper cut-off mass near $\sim 10^6$ M$_\odot$, with a significant correlation with host galaxy luminosity (Jordan et al. [2007]). This may suggest that GCs formed under conditions that were more similar to those in present-day starbursts than quiescent discs.

The internal star formation histories of clusters

The preceding discussion does not suggest a natural division between globular and other clusters based on mass alone. Clusters are sampled from a continuous mass distribution that appears to be well approximated by a Schechter function. While the cut-off mass probably depends on environment, it is on the order of 10^5 M$_\odot$ even in present-day star-forming disc galaxies. Likewise, the sizes of young massive star clusters both in spiral galaxies and in starbursts/mergers appear similar to those of ancient globular clusters, with typical half-light radii of a few (2–4) pc (e.g. Whitmore et al. [1999]; Larsen [2004]).

Of course, there are potentially other parameters than size and mass to consider. In the Milky Way, most open clusters are (more or less per definition) associated with the disc, and tend to have roughly Solar metallicity (Friel et al. [2002]). Most globular clusters, by contrast, have metallicities well below solar and can be grouped into two populations with mean overall metallicities [Fe/H] ~ -1.5 and [Fe/H] ~ -0.5 (e.g. Zinn [1985]), although GCs in giant elliptical galaxies tend to reach near-solar metallicities (Peng et al. [2006]). GCs also differ from open clusters by typically having enhanced α-element abundances (relative to Fe). However, these differences mostly reflect the properties of the stellar populations with which the open and globular clusters are associated, and should not necessarily be taken as indications of fundamentally different formation mechanisms.

A perhaps more important clue comes from the degree of *internal* homogeneity of the clusters. Open clusters are generally very homogeneous, with no significant age spreads or star-to-star differences in chemical composition (e.g. Pancino et al. [2010]). Globular clusters, instead, are well known for

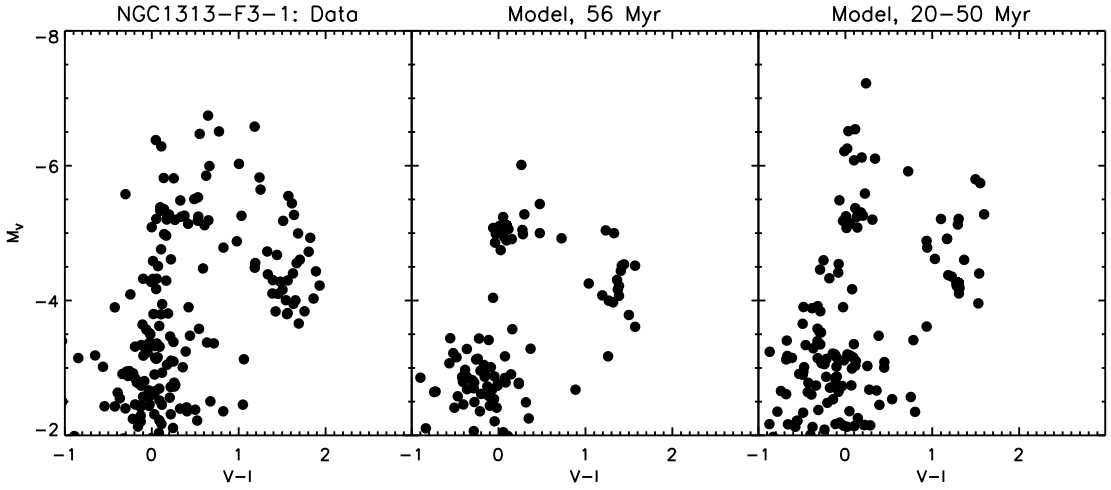

Figure 3.5: *Left*: Observed colour-magnitude diagram for the cluster NGC1313-F3-1. Middle: a model based on a single 56 Myr old isochrone. *Right*: A model including an age range from 20 – 50 Myr.

exhibiting internal variations in the abundances of some light elements (Kraft [1979]), in particular with anti-correlated abundances of O/Na and Mg/Al (Gratton et al. [2001]). This suggests that stars in these clusters formed from material that had been processed to different degrees via the CNO cycle, either in AGB or massive (single or binary) main sequence stars (D'Ercole et al. [2010]; Decressin et al. [2007]; de Mink et al. [2009]). In either case, star formation must then have been an extended process (tens to hundreds of Myr), in contrast to the conventional view that star clusters form very quickly (e.g. Elmegreen et al. [2000]) and data for Milky Way open clusters. Furthermore, high-quality colour-magnitude diagrams have now revealed the presence of multiple main sequences and/or sub-giant brances in several globular clusters, seemingly requiring strongly enhanced He abundances in some of the stars (e.g. Piotto [2009]; Milone et al. [2010]). In summary, globular clusters appear to have experienced complicated star formation- and chemical enrichment histories.

At this point, it is worth recalling that the ancient GCs and present-day open clusters in the galactic disc probe very different regimes of the ICMF. The GCs that have survived until the present day must all have had quite large initial masses, at least $\sim 10^5$ M$_\odot$. Open clusters, on the other hand, are typically low-mass objects with masses less than $10^3 - 10^4$ M$_\odot$. It is quite possible that the presence of internal abundance variations is linked to the initial cluster mass, with some scenarios predicting that complex internal star formation histories should mainly occur for initial masses greater than $10^5 - 10^6$ M$_\odot$ (Pflamm-Altenburg & Kroupa [2009]; Conroy & Spergel [2011]). The real test of whether GCs have a fundamentally different origin than star clusters in the local universe should thus involve objects of similar mass. Unfortunately, little is currently known about the detailed chemical composition of young massive star clusters in the regime $M > 10^5$ M$_\odot$, simply because most of them are too far away to study individual stars in detail.

While abundance anomalies have, so far, only been detected in ancient globular clusters, there is emerging evidence that complex star formation histories may not be unique to old GCs. In particular, age spreads of several 100 Myr have been claimed in some massive, intermediate-age ($\sim$ 2 Gyr) clusters in the Large Magellanic Cloud (Mackey et al. [2008]; Milone et al. [2009]; Girardi et al. [2009]), although it has also been suggested that the observed CMD features in these clusters might be at least partially explained by stellar evolutionary effects, e.g. due to stellar rotation (Bastian & de Mink [2009]). We have recently presented resolved photometry for a number of younger clusters in several nearby galaxies (Larsen et al. [2011]). Fig. 3.5 shows one example, for the cluster NGC 1313 – F3 – 1, with an estimated mass of $\sim 2 \times 10^5$ M$_\odot$. The left-hand panel shows the photometry, while the centre panel shows a model CMD based on a single isochrone that takes into account observational errors. This model CMD displays a smaller scatter in the luminosities of the supergiant stars, and also exhibits a distinct gap between the main sequence turn-off and the supergiants (the "blue Hertzsprung gap", BHG) that is far less clearly seen in the data. The right-hand panel shows a model CMD that includes an age spread between 20 and 50 Myr, which results in a better match to the data. While the multiple-age model is reasonably successful in reproducing the observed CMD for this particular cluster, there are other clusters in the sample of Larsen et al. [2011] for which an age spread cannot, by itself, reproduce the observed CMD features - in particular, the lack of a BHG seems to be a generic feature of the data, and may also be

the result of binary stellar evolution. Mass transfer or mergers in binary systems can produce stars that *appear* to be younger than the actual age of the cluster, and this can produce many of the same effects on the CMD as an age spread. Thus, the case for multiple stellar populations in younger star clusters remains somewhat ambiguous.

Summary

Comparison with other nearby spiral galaxies suggests that the Milky Way should contain a significant population of young star clusters with masses above 10^5 $M_\odot$. Scaling from the cluster systems of NGC 5236 and NGC 6946, about 20 clusters with $M > 10^5$ $M_\odot$ and ages younger than 200 Myr are expected. Are these objects young analogues of the ancient globular clusters that populate the halo and bulge of our own and other galaxies? In terms of masses and sizes, the young massive clusters in nearby spirals, as well as in on-going starbursts and mergers, certainly appear similar to their older counterparts. Differences in the "typical" masses may be largely due to a combination of selection effects and dynamical evolution – the "initial cluster mass function" (ICMF) appears to extend well above 10^5 $M_\odot$ whenever there are enough clusters to sample the high-mass end, although there appears to be an environmentally dependent truncation that occurs at a few times 10^5 $M_\odot$ in present-day, quiescent discs, but at $> 10^6$ $M_\odot$ in starbursts and ancient GC populations.

A more significant difference between ancient GCs and present-day cluster formation may be the presence of multiple stellar populations in the former. These are now revealed by direct colour-magnitude diagrams, although the presence of abundance anomalies have hinted at this for many decades. It remains unclear, however, whether these phenomena are uniquely related to ancient GCs. The surviving GCs must have had initial masses well above 10^5 $M_\odot$, and little is currently known about the detailed star formation histories of young clusters in this mass range, simply because they are generally too distant to observe individual stars in detail. However, there is evidence from CMDs that some young clusters in the Large Magellanic Cloud, as well as in more distant galaxies, may have extended star formation histories, although this is not entirely conclusive yet.

Bibliography

Barbaro, C. & Bertelli, G. 1977, A&A, 54, 243
Bastian, N. 2008, MNRAS, 390, 759
Bastian, N. & de Mink, S. E. 2009, MNRAS, 398, L11
Bik, A., Lamers, H. J. G. L. M., Bastian, N., Panagia, N., & Romaniello, M. 2003, A&A, 397, 473
Bruzual, G. 2002, in: Extragalactic Star Clusters, IAU Symp. 207, Eds. D. Geisler, E. K. Grebel and D. Minniti, ASP, p. 616
Cerviño, M. & Luridiana, V. 2004, A&A, 413, 145
Cerviño, M. & Luridiana, V. 2006, A&A, 451, 475
Chandar, R., Fall, S. M., & Whitmore, B. C. 2010a, ApJ, 711, 1263
Chandar, R., Whitmore, B. C., Calzetti, D., et al. 2011, ApJ, 727, 88
Chandar, R., Whitmore, B. C., Kim, H., et al. 2010b, ApJ, 719, 966
Clark, J. S., Negueruela, I., Crowther, P. A., & Goodwin, S. P. 2005, A&A, 434, 949
Conroy, C. & Spergel, D. N. 2011, ApJ, 726, 36
Davies, B., Figer, D. F., Kudritzki, R., et al. 2007, ApJ, 671, 781
de Grijs, R. & Anders, P. 2006, MNRAS, 366, 295
de Mink, S. E., Pols, O. R., Langer, N., & Izzard, R. G. 2009, A&A, 507, L1
Decressin, T., Meynet, G., Charbonnel, C., Prantzos, N., & Ekström, S. 2007, A&A, 464, 1029
D'Ercole, A., D'Antona, F., Ventura, P., Vesperini, E., & McMillan, S. L. W. 2010, MNRAS, 407, 854
Dowell, J. D., Buckalew, B. A., & Tan, J. C. 2008, AJ, 135, 823
Elmegreen, B. G. & Efremov, Y. N. 1997, ApJ, 480, 235
Elmegreen, B. G., Efremov, Y. N., & Larsen, S. 2000, ApJ, 535, 748
Fall, S. M., Chandar, R., & Whitmore, B. C. 2009, ApJ, 704, 453
Fall, S. M. & Zhang, Q. 2001, ApJ, 561, 751
Figer, D. F., MacKenty, J. W., Robberto, M., et al. 2006, ApJ, 643, 1166
Fouesneau, M. & Lançon, A. 2010, A&A, 521, A22
Friel, E. D., Janes, K. A., Tavarez, M., et al. 2002, AJ, 124, 2693

Gieles, M. 2010, in: Galaxy Wars: Stellar Populations and Star Formation in Interacting Galaxies ASP Conference Series Vol. 423, 423
Girardi, L., Chiosi, C., Bertelli, G., & Bressan, A. 1995, A&A, 298, 87
Girardi, L., Rubele, S., & Kerber, L. 2009, MNRAS, 394, L74
Gratton, R. G., Bonifacio, P., Bragaglia, A., et al. 2001, A&A, 369, 87
Haas, M. R., Gieles, M., Scheepmaker, R. A., Larsen, S. S., & Lamers, H. J. G. L. M. 2008, A&A, 487, 937
Hodge, P. 1988, PASP, 100, 568
Hunter, D. A., Elmegreen, B. G., Dupuy, T. J., & Mortonson, M. 2003, AJ, 126, 1836
Hwang, N. & Lee, M. G. 2008, AJ, 135, 1567
Jordan, A., McLaughlin, D. E., Cote, P., et al. 2007, ApJS, 171, 101
Kraft, R. P. 1979, ARA&A, 17, 309
Kruijssen, J. M. D. & Portegies Zwart, S. F. 2009, ApJ, 698, L158
Lada, C. J. & Lada, E. A. 2003, ARA&A, 41, 57
Larsen, S. r. S. 2002, AJ, 124, 1393
Larsen, S. S. 2004, A&A, 416, 537
Larsen, S. S. 2009, A&A, 494, 539
Larsen, S. S., de Mink, S. E., Eldridge, J. J., et al. 2011, A&A, in press (eprint arXiv:1106.4560)
Larsen, S. S. & Richtler, T. 1999, A&A, 345, 59
Larsen, S. S. & Richtler, T. 2000, A&A, 354, 836
Mackey, A. D., Broby Nielsen, P., Ferguson, A. M. N., & Richardson, J. C. 2008, ApJ, 681, L17
Maíz Apellániz, J. 2009, ApJ, 699, 1938
McLaughlin, D. E. & Fall, S. M. 2008, ApJ, 679, 1272
Milone, A. P., Bedin, L. R., Piotto, G., & Anderson, J. 2009, A&A, 497, 755
Milone, A. P., Piotto, G., Bedin, L. R., et al. 2010, in SF2A-2010: Proceedings of the Annual meeting of the French Society of Astronomy and Astrophysics. Eds.: S. Boissier, 319
Minniti, D. 1996, ApJ, 459, 175
Pancino, E., Carrera, R., Rossetti, E., & Gallart, C. 2010, A&A, 511, A56
Peng, E. W., Jordan, A., Cote, P., et al. 2006, ApJ, 639, 95
Pflamm-Altenburg, J. & Kroupa, P. 2009, MNRAS, 397, 488
Piotto, G. 2009, in: "The Ages of Stars", Proc. of the IAU, vol. 258, p. 233
Piskunov, A. E., Kharchenko, N. V., Schilbach, E., et al. 2009, A&A, 507, L5
Popescu, B. & Hanson, M. M. 2010, ApJ, 713, L21
Portegies Zwart, S. F., McMillan, S. L., & Gieles, M. 2010, ARA&A, 48, 431
Robitaille, T. P. & Whitney, B. A. 2010, ApJ, 710, L11
Selman, F. J. & Melnick, J. 2008, ApJ, 689, 816
Shapley, H. 1916, Contributions of the Mount Wilson Solar Observatory, 115, 201
Silva-Villa, E. & Larsen, S. S. 2010, A&A, 516, A10
Silva-Villa, E. & Larsen, S. S. 2011, A&A, 529, A25
Terlevich, R. 2004, in: The Formation and Evolution of Massive Young Star Clusters, ASP Conf. Ser. Vol. 322, ed. H. J. G. L. M. Lamers, L. J. Smith and A. Nota, p. 11
Whitmore, B. 2003, in: Extragalactic Globular Cluster Systems, ed. M. Kissler-Patig, ESO Astrophysics Symposia (Berlin/Heidelberg: Springer-Verlag), p. 336
Whitmore, B. C., Zhang, Q., Leitherer, C., et al. 1999, AJ, 118, 1551
Zhang, Q. & Fall, S. M. 1999, ApJ, 527, L81
Zinn, R. 1985, ApJ, 293, 424

3.3 What Gaia Could Tell Us about Star Formation

Simon P. Goodwin[1]

[1] Department of Physics & Astronomy, University of Sheffield, Hounsfield Road, Sheffield, S3 7RH, UK.

Abstract

Gaia will provide unprecedented information on the distribution, dynamics and binarity of stars within 1 – 2 kpc of the Sun. I discuss how this information could be used to test theories of star formation.

Star formation

Star formation is one of the key problems in astrophysics, and Gaia can provide huge amounts of new information on star formation which can be used to test different star formation theories.

At first sight, Gaia does not seem to be particularly useful in probing star formation. Gaia works with optical point sources but most young stars are either deeply embedded and invisible in the optical, or found in regions with strong diffuse emission from gas. But it is the accuracy of positional and distance information together with extremely good proper motions for dynamics that allow Gaia to be used to probe star formation in a new way.

After a few Myr the gas is removed from star-forming regions leaving them bare (see the contribution from Bastian in this volume). Once bare, Gaia can probe young regions, *and their surroundings*, in great detail. That Gaia surveys the whole sky is important, as it will be able to find escaping stars and look for larger structures around bare clusters that are currently impossible to find.

As a rough guide, Gaia will be able to detect most G-dwarfs to > 1 kpc, and M-dwarfs out to > 200 pc with a sub-km s^{-1} proper motion accuracy and around 10% distance error. That it is an all-sky survey means that it will not just probe the obvious young cluster, but also its environs and trace runaways.

There is currently a debate on the distributions of stars when they form (in particular see the contributions from Bastian and Kroupa in this proceedings). The two extremes of this view can be considered to be either distributed or clustered.

The more traditional view is that stars form in clusters with size scales of about a pc or less and memberships of tens to millions of members. Many of these clusters are destroyed after a few Myr creating the field population and explaining the lack of large numbers of old clusters (e.g. Lada & Lada [2003]). This destruction may be dynamical for small clusters, or due to gas expulsion (e.g. Goodwin & Bastian [2006]; Baumgardt & Kroupa [2007]). Thus the fundamental unit of star formation in this view is the cluster, many of which are later destroyed.

A more recent view is that star formation is hierarchical and that stars form with a filamentary and clumpy distribution (e.g. Bressert et al. [2010] and references therein). What we see as 'clusters' are sometimes just actively star-forming regions, or objects that have undergone collapse (e.g. Allison et al. [2009]). In this model there is no fundamental scale for star formation, rather it is hierarchical and in some 'lucky' places we might later see a cluster, whilst in others the stars that form just disperse into the field.

In some ways these models might appear fairly similar. In what way are the small-N clusters that rapidly disperse in the clustered model different to the low-density low-N regions in the hierarchical model? However, I would argue that these two models are fundamentally different.

In a clustered model of star formation there is a preferred scale for star formation (roughly a pc) and most star formation occurs in the fundamental unit that is the star cluster. Therefore most star formation occurs in a relatively dense environment. Encounters should be common (and thus the dynamical processing of binaries), and stars should be 'aware' of their environment. This model probably favours an origin for the IMF in a competitive accretion scenario (see Bonnell et al. [2007]), and provides a physical mechanism for a relationship between the maximum stellar mass and the cluster mass (e.g.

Weidner & Kroupa [2006]). It also requires a mechanism (gas expulsion?) for destroying the excess of young clusters over old clusters that it implies (Lada & Lada [2003]).

In a hierarchical model of star formation there is no preferred scale, and stars form with a wide (Gaussian?) range of surface densities (Bressert et al. [2010]). Many stars form in low density environments in relative isolation. In an extreme version of this model 'clusters' do not really exist at formation, rather they form later due to collapse in dynamically cold regions (Allison et al. [2009]). In particular, the hierarchical model suggests that stars should be unaware of their later environment and a IMF would be due to core masses rather than competitive accretion (see Bonnell et al. [2007]). This suggests a fundamental difference in the way stars collect their mass and how and why that mass is distributed in the apparently universal IMF. This has significant implications for the mechanisms of binary formation, and disc formation and evolution.

Of course, the truth may lie somewhere in between, or be completely different. However, with these models in mind we can consider ways in which they could be tested with Gaia data.

Spacial distribution. If star formation has a preferred scale, then do we see an imprint of that scale in the large scale distribution of young stars? Pockets of 1 pc scale clusters will presumably have a different spacial and kinematic signature than a hierarchical distribution. What is that signature? How rapidly does it disappear in the Galactic tidal field?

What is the wider distribution of young stars around known clusters? Does the dispersal of a cluster leave a distinct signature? In a dispersing group from a hierarchical origin do we retain information on the initial distribution?

Binarity. If we can isolate spacial and kinematic groups we can investigate their binary properties. Should even quite low-N clusters process some of their binaries? How are binaries processed in an initially hierarchical distribution? Is it different?

As an aside, Gaia will also be able to probe the binarities of different populations in the Galaxy, in particular thick disc, thin disc, and halo. Do these populations have different binary properties? If they do is it a signature of differences in their star formation?

Conclusion

This has been a rather short contribution with far more questions than answers. The Gaia data will contain a wealth of information that can be used to probe star formation. The next few years are the time for theorists to refine their models and investigate what signatures can be found in the Gaia data to prove or disprove them. The sorts of simulations required have not been done because we (theorists) never thought they could be tested, but thanks to Gaia we can.

Bibliography

Allison, R. J., Goodwin, S. P., Parker, R. J., et al. 2009, ApJ Lett., 700, L99
Baumgardt, H. & Kroupa, P. 2007, MNRAS, 380, 1589
Bonnell, I. A., Larson, R. B., & Zinnecker, H. 2007, 149–164
Bressert, E., Bastian, N., Gutermuth, R., et al. 2010, MNRAS, 409, L54
Goodwin, S. P. & Bastian, N. 2006, MNRAS, 373, 752
Lada, C. J. & Lada, E. A. 2003, ARA&A, 41, 57
Weidner, C. & Kroupa, P. 2006, MNRAS, 365, 1333

3.4 Cluster Disruption: From Infant Mortality to Long Term Survival

Nate Bastian[1]

[1] Excellence Cluster Universe, Boltzmannstr. 2, 85748 Garching, Germany

Abstract

How stellar clusters disrupt, and over what timescales, is intimately linked with how they form. Here, we review the theory and observations of cluster disruption, both the suggested initial rapid dissolution phase (infant mortality) and the longer timescale processes that affect clusters after they emerge from their progenitor GMCs. Over the past decade, the standard paradigm that has developed is that all/most stars are formed in clusters and that the vast majority of these groups are disrupted over short timescales (< 10 Myr). This is thought to be due to the removal of the left over gas from the star-formation process, known as infant mortality. However, recent results have suggested that the fraction of stars that form in clusters has been overestimated, with the majority being formed in unbound groups (i.e. associations) which expand and disrupt without the need of invoking gas removal. Dynamical measurements of young massive clusters in the Galaxy suggest that clusters reach a stable equilibrium at very young (< 3 Myr) ages, suggesting that gas expulsion has little effect on the cluster. After the early dynamical phase, clusters appear to be long lived and stable objects. We use the recent WFC 3 image of the cluster population in M 83 to test empirical disruption laws and find that the lifetime of clusters strongly depends on their ambient environment. While the role of cluster mass is less well constrained (due to the added parameter of the form of the cluster mass function), we find evidence suggesting that higher mass clusters survive longer, and that the cluster mass function (at least in M 83, outside the nuclear region) is truncated above $\sim 10^5$ $M_\odot$.

The Standard Paradigm of Early Cluster Evolution and Disruption

Star clusters form in the dense cores of giant molecular clouds. Assuming a non-100% star-formation efficiency (SFE; i.e., that only some fraction of the gas will turn into stars), at some point a natal cluster will be made of both gas and stars, and both will contribute to the total gravitational potential. Due to stellar feedback, thought to come mainly from the winds and photoionisation of massive stars (as clusters appear to be largely devoid of gas before the first supernovae occurs), the gas may be rapidly removed from the young cluster. If the system was in virial equilibrium the removal of the gas will leave the stellar part of the system out of equilibrium, in a super-virial state, and the stars will expand in order to find a new equilibrium (c.f., Tutukov [1978]; Hills [1980]). This will result in the loss of some stars from the system, and if the SFE is less than 33% the entire cluster may become unbound (assuming instantaneous gas removal), whereas above this critical threshold, some bound core may survive (e.g., Bastian & Goodwin [2006]).

This is a conceptually simple theory, with well defined initial conditions that can be easily parameterised. This allows for large systematic theoretical and numerical studies to be undertaken in order to find out how each parameter affects the final state of the remnant cluster (if such a remnant exists). For the 'classical' models (i.e. those that assume the system is in equilibrium at the beginning of the simulation - see Lada et al. [1984]), the main parameters are: 1) the SFE, i.e., the fraction of gas turned into stars (e.g., Hills [1980]); 2) the timescale over which the gas is removed (e.g., Goodwin [1997]; Baumgardt & Kroupa [2007]) and 3) how the gas and stars are distributed within the system, i.e. if they have the same profile shape/size (e.g., Chen & Ko [2009]). Generally, the system is modelled by adopting an analytic background potential for the gas and using N-body techniques for the stars.

Additionally, if full cluster populations are modelled, then one can also make assumptions on how each of the three above parameters vary with other cluster properties, such as mass (e.g, Kroupa & Boily

[2002]) or on the initial conditions of the population (e.g., any primordial mass-size relations; Parmentier & Kroupa [2011]). The response of the stellar system to gas removal is largely independent of the number of stars in the system (i.e. stellar mass) as it is driven by violent relaxation (e.g., Goodwin & Bastian [2006]).

A new flavour of models has recently been explored which relaxes the assumption of virialised starting conditions. In these models, like in the 'classical' case, the gas is modelled as a background potential, however the stars are either in a sub- or super-virial state with clumpy initial conditions (e.g., McMillan et al. [2007], Allison et al. [2009]). For the sub-virial case, i.e. the stars are moving slower than in the equilibrium case, the stars fall toward the center of the system, while the gas remains in the initial configuration. Such sub-virial motions have been found in turbulent hydrodynamical simulations (Offner et al. [2009]) and many young star forming regions appear to be highly sub-structured (see next Section), hence the initial conditions of young clusters may well be sub-virial and clumpy. Sub-virial motions result in an 'effective' SFE (eSFE; c.f., Goodwin [2009]) for the central regions that is significantly higher than the mean SFE (note that this is similar to assuming different profile shapes/sizes for the star and gas distributions). This contraction of the stellar system can largely offset the effects of gas expulsion (e.g., Smith et al. [2011]). For the super-virial case, the effect of gas expulsion is amplified.

The end result of the simulations presented to date is that a bound cluster is more likely to form if: 1) the (e)SFE is high; 2) the timescale of gas removal is long compared to a crossing time of the system; or 3) the system begins in a sub-virial state. In recent SPH simulations of star cluster formation, the sub-clumps that merge in order to form a cluster appear to have extremely high eSFE (Moeckel & Clarke [2011]; Kruijssen et al. [2011b]), which limits (or even negates) the effect of gas expulsion on the system.

In the next Section we discuss the observations that the infant mortality paradigm was designed to explain, and review ongoing studies to see if such a scenario is still necessary.

Initial Conditions

Do all stars form in clusters?

Star formation appears to be hierarchical within galaxies, meaning that there does not seem to be a preferred scale in the star-formation process, from $\sim$ 0.1 pc to hundred parsec scales (e.g. Elmegreen et al. [2006]; Bastian et al. [2007]; [2009]; Sánchez et al. [2010]). This is likely simply due to the fact that the ISM appears hierarchical (e.g. Elmegreen & Falgarone [1996]) and that star formation passively traces the gas. Because of this initial spatial distribution we would not expect to see all stars forming in clusters, but instead would expect a continuous distribution of surface densities ranging from the dense inner cores of massive clusters to extremely isolated stars. Pre-*Spitzer* studies that attempted to place constraints on the spatial distribution of young stellar objects (YSOs) used K-band excess techniques (i.e. looking for overdensities in K-band images) which were excellent in picking up the dense inner structures of clusters, but largely missed the lower density regions (e.g., Carpenter [2000]). This observational bias led to the notion that all stars form in clusters.

However, with the advent of the *Spitzer Space Telescope*, YSOs could be identified based on the mid-IR colours, i.e. independent of their surface density. In Fig. 3.6 we show the spatial distribution of YSOs in the star-forming region, NGC 1333 (Gutermuth et al. [2008]). Note their highly filamentary structure and the fact that they trace the gas distribution quite closely. This is a fairly typical example of a star-forming region, showing multiple sub-clumps which may or may not merge as the cluster evolves dynamically (e.g., Gutermuth et al. [2009]; Schmeja et al. [2009]). The hierarchical nature of star-forming regions becomes more clear when one zooms out an order of magnitude in spatial scale and looks at the structure of full clouds, with nested clumps from sub-parsec to tens of parsec scales (c.f. Elmegreen et al. [2000]; Allen et al. [2007]).

In Fig. 3.7 we show the surface density distribution of YSOs for a nearly complete sample of all star-forming regions within 500 pc as determined through *Spitzer* imaging (Bressert et al. [2010]). Note that there does not appear to be any preferred scale, i.e. no way to distinguish between clusters, associations, or distributed star formation. The vertical lines in the bottom panel refer to previous definitions that had been applied in the literature, resulting in a large range of estimates for the fraction of star formation in clusters, from 90% to $< 25\%$.

A similar conclusion was also reached by Gieles & Portegies Zwart [2011] (also see the contribution of M. Gieles in these proceedings) who found a continuous distribution, from loose associations to dense clusters, in the structures of star-forming to evolved stellar groups.

Implications for infant mortality

Lada & Lada [2003] compared the number of observed open clusters with that expected given their embedded cluster sample (see Fig. 3.7 for the definition that they applied to define an embedded cluster). They found that they would expect ~ 10 times more open clusters than observed if all embedded clusters evolve into open clusters. Due to this large difference, they postulated that $\sim$ 90% of clusters are disrupted as they pass from an embedded to an exposed state. The authors named this mass culling, "infant mortality". The suspected cause of this disruption was the removal of the left-over gas from the star-formation process, i.e. rapid gas removal (e.g. Geyer & Burkert [2001]; Kroupa & Boily [2002]; Bastian & Goodwin [2006]).

However, how much infant mortality is required depends strongly on how one defines an embedded cluster. If more conservative definitions are used (see Fig. 3.7) instead of 90% of all clusters being destroyed during this phase (or equivalently, due to the cluster mass function, each cluster losing 90% of its mass), less than 50% of clusters need to be destroyed in order to explain the observed open cluster numbers. Since it is difficult or impossible to define which stars are part of an embedded cluster, hence the embedded cluster's mass, other techniques are required to test the infant mortality scenario.

How important is gas expulsion? This is difficult to address using populations, due to the uncertainties outlined above. However, one can address this through detailed dynamical studies of individual clusters. Goodwin & Bastian [2006] showed that the observed dynamical mass (obtained through measuring the velocity dispersion and size of a cluster) of a cluster should be larger than the actual mass (obtained through comparing the observed light with M/L ratios from SSP models) if the cluster is undergoing expansion due to gas expulsion. The authors also presented a series of observations from the literature that showed that young clusters had systematically larger dynamical mass estimates, consistent with the idea of gas expulsion. However, Gieles et al. [2010] showed that this effect could be mimicked by the broadening of the velocity dispersion due to binary stars. Since O and B stars are more likely to be in tight binary systems than their lower mass counterparts, and that these massive stars dominate the light of young massive clusters, this broadening of the velocity dispersion will affect young clusters more than older clusters. This can also explain the observations without invoking infant mortality. Hence, studies of unresolved extragalactic clusters are not able to address the role of gas expulsion.

In order to make progress, multi-epoch high-resolution spectroscopy of individual cluster member stars is required, which is only possible in the Galaxy and SMC/LMC. The multi-epoch nature allows binaries to be detected and removed from the sample, resulting in a clean velocity dispersion estimate. Alternatively, proper motion studies of massive clusters are also not affected by binaries. While this is difficult and time consuming work, a handful of studies have been carried out to date. Studies of NGC 3603 (Rochau et al. [2010]), Westerlund 1 (Mengel & Tacconi-Garman [2007], Cottaar et al. in prep, Cottaar these proceedings) the Arches (Clarkson et al. [2011]; Clarkson et al. in prep) and R136 in the LMC (Hénault-Brunet et al. in prep) have all found low velocity dispersions for these young clusters. This is particularly surprising for NGC 3603 and the Arches, given their very young ages (≤ 2 Myr).

These results suggest that gas expulsion has not significantly affected these clusters and that once a cluster forms it is stable from a very young age. Hence, infant mortality may not be an important process in the early stages of cluster evolution. Whether the cluster stability comes from a high star-formation efficiency (e.g. Goodwin & Bastian [2006]), the merging of sub-virial sub-clumps (e.g. Allison et al. [2009]) or through a de-coupling of the gas and stars in a highly dynamical process (e.g. Moeckel & Clarke [2011]; Kruijssen et al. [2011b]; see also Kruijssen in these proceedings) is uncertain at present.

Why it matters

In addition to the question of whether infant mortality and gas expulsion are important phases in young cluster evolution, whether or not all stars form in clusters is important for a number of other studies. One issue that Gaia will make an important contribution to, is the question of whether associations are merely expanded clusters (due to gas removal), or if associations are merely part of the continuous hierarchical distribution of star-forming structures. Gaia will measure the proper motions of thousands of stars in young clusters and associations in the Galaxy. If all stars form in clusters, then the stars in associations should be traced back to a handful of specific points (i.e., the location of their parent clusters at the moment of gas expulsion). On the other hand, if associations are simply a level in a continuous hierarchy, the stars should have (largely) random motions.

If all stars form in clusters, then clusters can be viewed as a fundament unit in the star forming process. In this view, star formation can be broken up into discrete, or quantised events. Since the

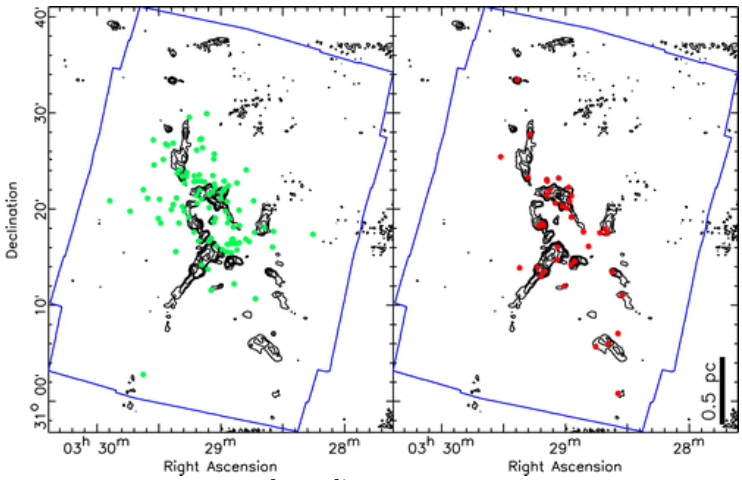

Figure 3.6: (from Gutermuth et al. [2008]) The spatial distribution of YSOs in the young embedded star-forming region NGC 1333. The contours show dense gas and the points represent Class Is (red, right panel) and Class IIs (green, left panel). Class Is are thought to be younger, on average, and their spatial distribution matches the gas distribution quite well, showing a very filamentary structure. The Class IIs also generally follow the gas, however, due to their older age they have dynamically evolved to some degree. This shows that stellar clusters do not form as a centrally concentrated system with the gas/stars in equilibrium, but rather as a filamentary/hierarchical structure where individual components may (or may not) merge to form the final stellar system.

difference in age between two stellar groups (i.e. two sub-clumps within a young cluster) is related to their separation distance, with spatially close groups having similar ages (Efremov & Elmegreen [1998]), young clusters (with radii less than a few parsecs) are single age populations to a good approximation. Alternatively, if many stars are born in associations, which span 10 s or 100 s of parsecs, then the individual sub-groups may have significantly different ages, hence star formation would not be made up of discrete events.

Whether or not star formation happens in a continuous/hierarchical way or is made up of discreet events has important implications for the integrated properties of stellar populations (see the contributions by E. Bressert and C. Weidner in these proceedings). For example, Weidner & Kroupa [2006] have suggested that the mass of the most massive star and the mass of the host cluster have a causal relation, meaning that a cluster *must* have a minimum mass before it forms massive stars. However, this only works if clusters are a basic unit in the star-formation process, as this relation can not hold for the individual sub-clumps that make a cluster *and* the final cluster at the same time. Nor could the relation hold for larger associations/complexes of clusters. Hence there would need to be a preferred scale in the process, i.e., a star must know about the final mass of the cluster that it will end up in. This type of behaviour has been seen in SPH simulations of cluster formation based on competitive accretion (Maschberger et al. [2010]), where the masses of stars are determined in large part by the environment from which they form.

Additionally, the spatial distribution of star formation can provide constraints on theories of star (and cluster) formation (e.g., Bressert et al. [2011]). Cluster disruption, specifically the infant mortality phase, is the largest uncertainty in addressing the role of environment in the cluster formation process, i.e., if the fraction of stars formed in clusters is related to the star-formation rate (or SFR surface density) of the host galaxies (e.g., Goddard et al. [2010]; Silva-Villa & Larsen [2011]; Adamo et al. [2011]).

Further Evolution

After a cluster transitions from an embedded to an exposed state, the surviving clusters are not expected to live indefinitely, but rather to disrupt due to internal (e.g., two-body relaxation, stellar evolution) and external (e.g., tidal fields and interactions with GMCs) processes. Fall, Chandar & Whitmore [2009] have suggested that these processes happen over different timescales, and hence can be treated independently, in addition to being largely independent of cluster mass. Alternatively, through an analytic approach, Gieles et al. [2011] find that all processes are acting concurrently and that the lifetime of a cluster

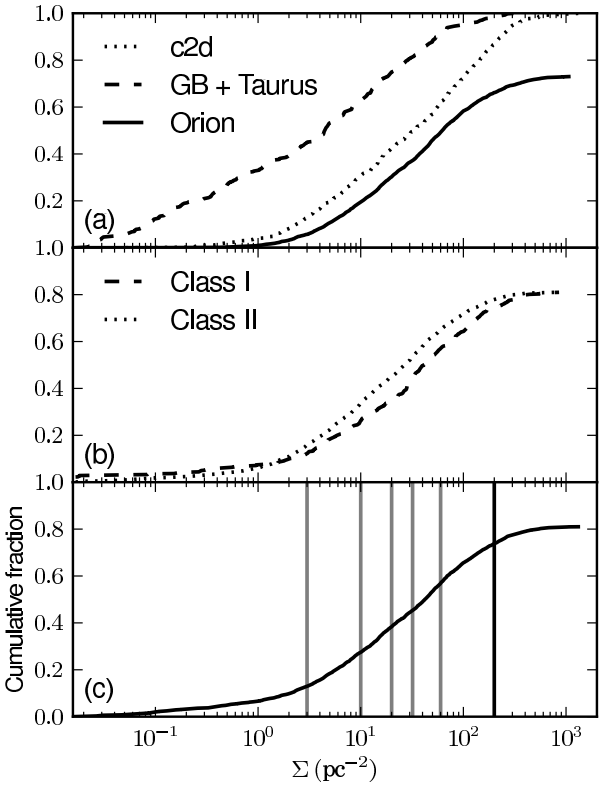

Figure 3.7: (from Bressert et al.[2010])(a) The cumulative fraction of surface densities for the Gould Belt and Taurus (GB+Taurus), Cores to Disks (c2d), and Orion surveys. Each SF region included in the distributions has N(YSOs) $\geq$ 10 and a sufficient field-of-view to properly calculate stellar surface densities. The Orion survey stops at 73% for the cumulative fraction since the ONC is excluded. A 65% disk fraction for all of the SF regions is adopted and each curve is normalised by the number of YSOs in each survey. (b) With the GB+Taurus, c2d, and Orion surveys combined we see Class I & II distributions having similar profiles with a small off- set in density, showing that we are likely seeing the primordial distribution of the YSOs. (c) With all of the Spitzer surveys combined we compare several cluster definitions. The vertical grey lines from left to right are Lada & Lada [2003], Megeath et al. (in prep.), Jørgensen et al. [2008], Carpenter [2000], and Gutermuth et al. [2009] stellar density requirements for clusters. These values correspond to 3, 10, 20, 32, and 60 YSOs pc^2 and intersect the corrected cumulative distribution profile, implying that 87%, 73%, 62%, 55%, and 43% of stars form in clusters, respectively. The percentages correlate to what fraction of stars form in clusters based on the various definitions. The black vertical line is for a dense environment where $\Sigma \geq 200$ YSOs/pc^2. The fraction of YSOs in a dense environment is $< 26\%$.

depends on the ambient environment and its mass, in agreement with other theoretical investigations (Spitzer [1958], Hénon [1961], etc).

Observationally, the situation is less clear, and the community has yet to reach a consensus regarding the amount of disruption observed in populations as well as the role of cluster mass and environment in the process. There have been two main empirical disruption laws put forward in the literature, based on different cluster samples in a variety of galaxies (explained in detail below). However, in only one case, the SMC, have the advocates for the different scenarios used the same dataset (Chandar, Fall & Whitmore [2006]; Gieles, Portegies Zwart & Lamers [2007]), and even here the authors come to different conclusions.

Below we summarise the two main empirical disruption laws and use the new WFC 3 imaging of the cluster population of the spiral galaxy M 83 to test the scenarios.

Empirical disruption laws

Mass dependent disruption (MDD)

The first empirical disruption law considered here is *Mass Dependent Disruption* (MDD). This was first presented, in the form used here, in Boutloukos & Lamers [2003], in order to explain the observed cluster population properties in the Galaxy, SMC, M 33 and M 51 (however, see Larsen [2008] for a thorough review of empirical mass dependent disruption laws). In this scenario, the lifetime of a cluster is dependent on the initial mass of the cluster as M^{γ} with $\gamma \sim 0.62$, and on the ambient environment with clusters surviving longer in galaxies with weak tidal forces and low numbers of GMCs. The empirical model was updated in Lamers et al. [2005], applied to a distance limited sample of open clusters in the Milky Way in Lamers & Gieles [2006], and was shown to agree with predictions from numerical N-body experiments in Gieles et al. [2004].

Mass independent disruption (MID)

The second empirical disruption law considered here is *Mass Independent Disruption* (MID). In this scenario, cluster disruption is independent of the cluster mass and the ambient environment. While the classic infant mortality falls in this category and is thought to last for ≤ 10 Myr (e.g. Lada & Lada [2003], the concept has been expanded up to ages of ~ 1 Gyr and has been invoked to explain cluster populations in the Antennae (Fall et al. [2005]), the LMC (Chandar et al. [2010a]), and M83 (Chandar et al. [2010b]). The model is described in detail in Whitmore et al. [2007]. The MID scenario suggests that 90% of clusters are disrupted every decade in age, independent of their mass or the environment that the cluster forms/evolves in. Hence, if 1000 clusters are formed at a given time, 100, 10 and 1 will be left after 10 Myr, 100 Myr and 1 Gyr, respectively. In this model, the sole parameter is $F_{\rm MID}$, the fraction of cluster disrupted after each decade in age, with $F_{\rm MID} = 0.9$ being the standard value.

A variant of this model has been put forward by Elmegreen & Hunter [2010] and Kruijssen et al. [2011a]), where clusters are destroyed through strong interactions with the hierarchical interstellar medium, a process which may be mass independent (if the shocks are strong enough, otherwise it will be mass dependent) but should depend strongly on the ambient density of the gas (i.e. environment).

M 83 as a test case

In order to differentiate between the two models discussed above, we have carried out a cluster population study in M 83, based on the early release science observations with WFC 3 on *HST*. The observations, source selection and fitting methods are discussed in detail in Bastian et al. [2011] and Bastian et al. (in prep). The main difference between the dataset used here, and previous studies of cluster disruption, is that an attempt was made in the present case to separate clusters from associations (i.e. only objects that satisfy the criteria that they are older than a current crossing time are considered; Gieles & Portegies Zwart [2011]). This was done through visual inspection of all detected candidates (carried out in the usual automated way) and only resolved, centrally concentrated and symmetric sources were considered. See Silva-Villa & Larsen [2010; 2011] for further discussions on the effects of visual inspection. Additionally, we have not included the inner 450pc of the galaxy, due to the significantly lower detection limit in this region, high and patchy extinction, and uncertain star-formation history (SFH). Outside this region, the SFH of M 83 appears to have been largely constant over the past 100 Myr (Silva-Villa & Larsen [2011]). Finally, we limit our analysis to clusters with masses in excess of 5×10^3 $M_{\odot}$, in order to limit stochastic sampling effects (e.g., Fouesneau & Lançon [2010]; Silva-Villa & Larsen [2011]).

Environmental dependence

The HST WFC 3 observations cover a wide range of galacticentric radii, extending from the nucleus to ~ 6 kpc. Hence, a wide range of environments are sampled by the data. We split our sample into an inner and outer region, and search for differences in the observed properties. Due to the lower surface density of GMCs and weaker tidal field in the outer regions of the galaxy, the MDD scenario predicts that clusters should live longer in the outer regions, hence that the average age should be older for increasing galactocentric radii. The MID scenario, on the other hand, predicts that cluster lifetimes are independent of location, resulting in a 'universal age/mass distribution', hence the inner/outer fields should show the same distribution.

We use two methods to distinguish between the theories. The first is (largely) independent of adopting specific simple stellar population (SSP) models. In Fig. 3.8 we show colour-colour diagrams of clusters in both of the fields. Filled circles represent individual clusters while the contours show the number density of clusters at that position. The red lines are SSP model tracks (see Adamo et al. [2010] and Zackrisson et al. [2011]), with the astericks labelling ages of 1, 10, 100 & 1000 Myr, from lower-left to upper-right. It is clear that the colour distribution of sources is different between the two fields, with the peak of the distribution happening at redder $F336W - F438W$ (essentially $U - B$) colours in the outer field. The redder $U - B$ colour (and similar $V - I$ colour) suggests an older average age of clusters in the outer field. Already here, it is clear that the distributions are different, inconsistent with the MID prediction. We note that extinction cannot explain the observed differences as 1) a lower average extinction in the outer field is expected and 2) the difference between the fields is mostly in the $U - B$ colour, whereas the $V - I$ colour distribution is largely the same.

As a second test between MID and MDD, we derived the age and mass of all the clusters in our sample by comparing the observed colours/magnitudes to SSP models (see Bastian et al. [2011] for details on the method and models used). We then look at the mass distribution of clusters in three separate age bins, normalised to the linear age range covered. This is the same method used by Chandar et al. [2010b] to study cluster disruption in the inner field of M 83. If cluster disruption (or cluster mass loss) was negligible, then the three bins would be expected to lie (nearly) on top of each other. If, on the other hand, cluster disruption was independent of mass and that 90% of clusters were disrupted (or each cluster lost 90% of its mass) then the mass function at each age should be a factor of 10 below the previous age.

In Fig. 3.9 we show the observed distributions. The first age bin (3 – 10 Myr) has the caveat that some clusters may have been missed due to the elimination of associations from the sample (discussed in detail in Bastian et al. in prep). The upper panel (ignoring the first age bin) agrees well with the results of Chandar et al. [2010b], who used the same data, but had different selection criteria[6]. In the inner field, the 10 – 100 Myr age bin is significantly higher than the 100 – 1000 Myr bin (roughly by a factor of 10), indicating a high level of disruption. In the outer field, however, the mass distributions (again focussing only on the last two age bins) lie nearly on top of each other, suggesting that little or no disruption has been acting on the population.

The observed differences in the age/mass distributions between the inner and outer field indicate that disruption has been much more significant in the inner regions of M 83 than in the outer regions. This is inconsistent with the MID scenario (where a universal distribution is expected, independent of environment) and in good agreement with predictions of the MDD paradigm. It is also qualitatively consistent with the environmentally dependent MID scenario of Elmegreen & Hunter [2010] and Kruijssen et al. [2011a]).

Mass dependence

The role of mass in the cluster disruption process is more difficult to discern than environmental influences. The reason is that the form of the cluster mass function plays a significant role. For example, Chandar et al. [2010] have shown that if the cluster mass function is a pure power-law with an index of -2, then the MDD scenario is not able to reproduce the observed distribution of clusters in the inner field of M 83. The reason is simple, in the MDD scenario, high-mass clusters, with masses above e.g., 10^6 $M_\odot$, are not expected to lose much mass. This means that the predicted models for mass distributions (such as that shown in Fig. 3.9) should all converge at high masses. However, if the mass function has a truncation at high masses, then the models no longer converge at the high-mass end.

Evidence for a truncation at the high-mass end has been seen in the luminosity function of clusters (Gieles et al. [2006]), the relation between the magnitude brightest cluster in a population and the host galaxies star-formation rate (Bastian [2008]), in the relation between the age and brightness of the brightest (and fifth brightest) clusters in a population (Larsen [2009]), as well as through direct fitting of the mass function clusters within a galaxy (Larsen [2009]; Bastian et al. in prep).

Hence, in order to see if there is a dependence on mass in the disruption process and distinguish between the MID and MDD scenarios, we must fit on the full age/mass distributions for three parameters. The parameters are: t_4 - the disruption timescale of a 10^4 $M_\odot$ clusters in the MDD scenario; $F_{\rm MID}$ - the fraction of cluster disrupted ever decade in age in the MID scenario; and M_c - the characteristic mass in

[6]This implies that after the first $\sim$ 10 Myr, clusters are fairly well defined objects and that different selection algorithms will generally do a good job in finding them. Before this age, the samples will be heavily influenced by the selection criteria used.

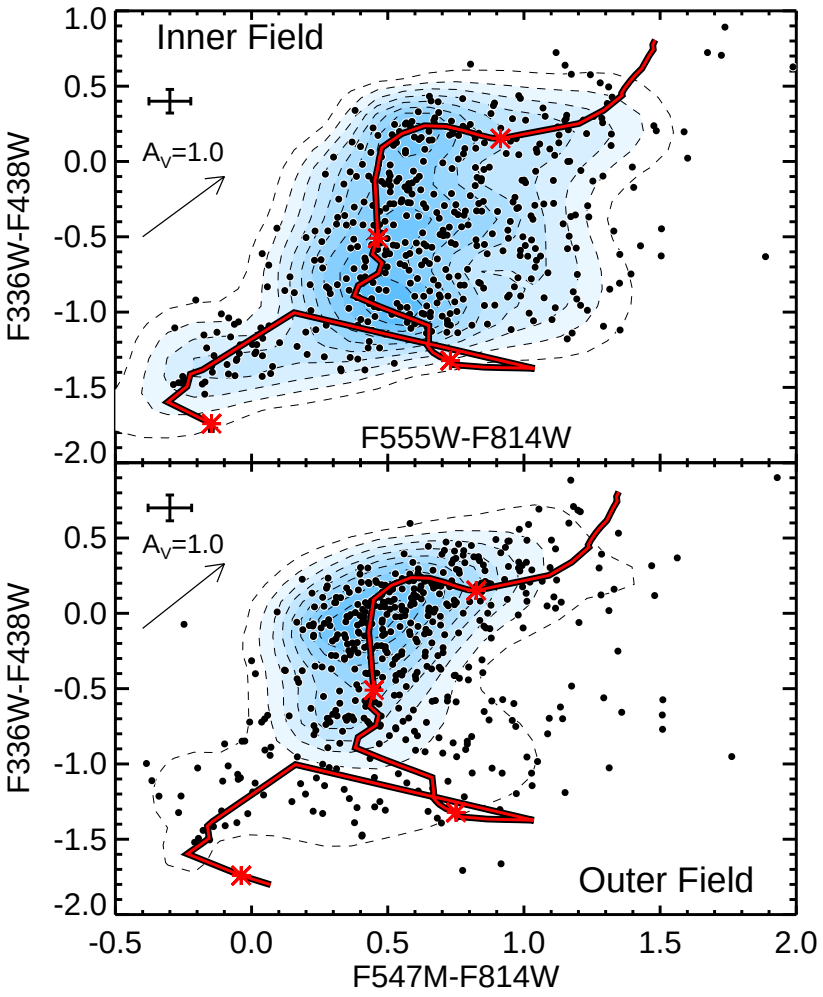

Figure 3.8: (from Bastian et al. [2011]) Colour-colour diagrams for the inner (upper panel) and outer (lower panel) fields. Each cluster is shown as a filled circle, while the contours denote the number density of points at that colour. The (red) solid lines are the SSP model tracks used in Adamo et al. [2010]. For reference the models are marked with asterisks at 1, 10, 100 & 1000 Myr, from lower-left to upper-right. Note the differences in the distributions, with a significantly higher fraction of clusters in the outer field having colours consistent with being older. The average error in colour for our cluster sample is shown in the upper left of each panel, and the extinction vector is also shown.

the cluster mass function, above which the distribution drops exponentially (we approximate the mass function as a Schechter function).

We adopt a value of $\gamma = 0.62$ (in the MDD scenario the disruption timescale is $t_{\rm dis} = t_4 M^{\gamma}$), which was found empirically by Boutloukos and Lamers [2003] and Lamers et al. [2005] and agrees with N-body simulations for clusters with an initial density distribution of a King profile of W_0=5 (Baumgardt & Makino [2003]; Gieles et al. [2004]). Models with W_0=7 have $\gamma = 0.70$ (Lamers et al. [2010]).

As a first step we apply the pure MID and MDD models to the same M 83 data shown in Fig. 3.9 and the best fitting models are shown in Fig. 3.10. The left panels show the results for the pure MDD case (i.e. $F_{\rm MID} = 0$) and the right panels show the best fit for the MID case (i.e. $t_4 = \infty$). We see that both the MID and MDD models can reproduce the observed distributions. However, in the MID case, different values of $F_{\rm MID}$ are needed for the inner and outer field, again suggesting non-universal age/mass distributions.

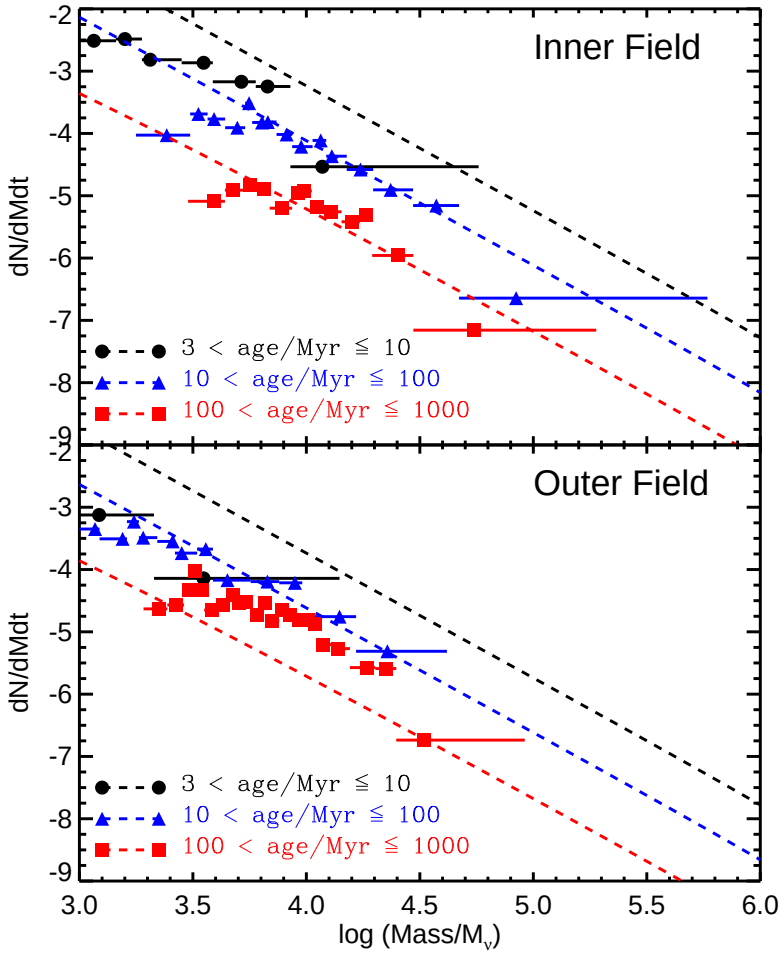

Figure 3.9: (from Bastian et al. [2011]) The mass distributions for three age bins (normalised to the linear age range considered) for the inner (top panel) and outer (bottom panel) fields. The points represent the median mass in each mass bin, while the horizontal lines show the mass range covered by the bin. The dashed lines show the predicted "universal" cluster distributions of the mass independent disruption scenario ($F_{MID} = 0.9$) normalised to fit the 10 – 100 Myr distributions. We have used bins with equal numbers of clusters (10 per bin). The distributions in the upper and lower panels are clearly different, suggesting that disruption has been much less pronounced in the outer field than in the inner field.

Finally, in order to avoid any artefacts of the binning from affecting the results, we have also carried out a maximum likelihood fitting analysis of the cluster population. Since the MID model advocated by Whitmore et al. [2007] and Fall et al. [2009] (that F_{MID} is universal) does not fit the data, we have limited the fit to only the MDD case. The results are shown in Fig. 3.11. The full details of the fitting will be presented in Bastian et al. (in prep), where MID will also be included as a free parameter.

The results indicate that cluster disruption has been much more rapid in the inner field ($t_4 \sim$ 130 Myr) than the outer field ($t_4 \sim 600$ Myr). The difference between the two fields is generally consistent with the predictions of the MDD theory (Lamers et al. [2010]). Additionally, we see that both fields require a truncation in the cluster mass function, with $M_c \sim 10^5$ M$_\odot$, being slightly larger in the inner field than the outer field. This is in good agreement with the estimated value of M_c, using independent methods, for spiral galaxies (Gieles et al. [2006]; Larsen [2009]) and for the LMC (Maschberger & Kroupa [2009]).

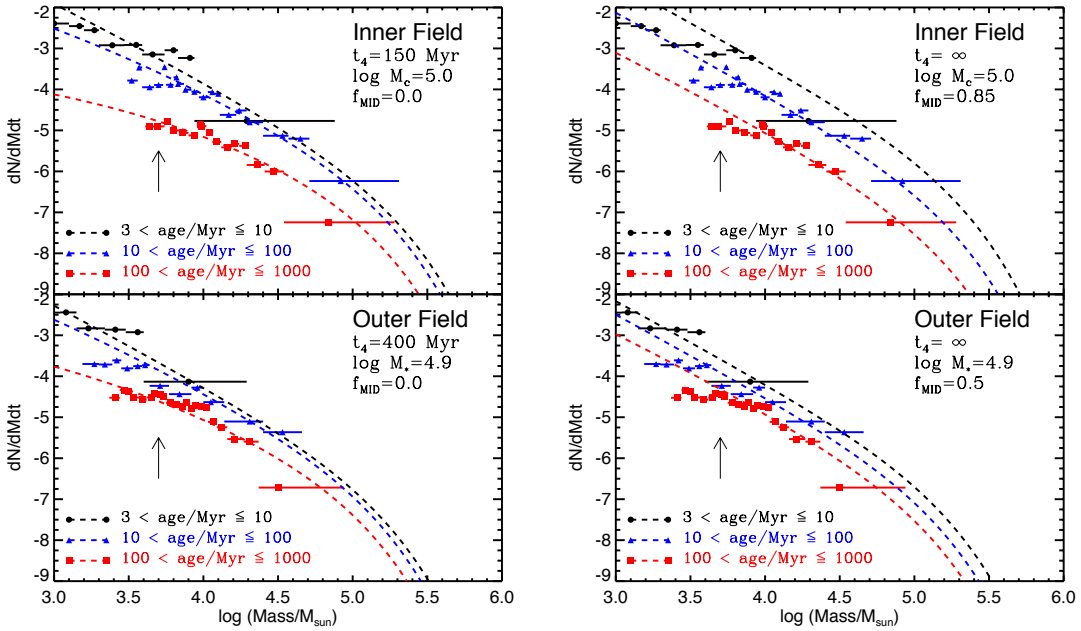

Figure 3.10: (from Bastian et al. in prep) The same as Fig. 3.9 except now the best fitting pure MDD (left panels) and MID (right panels) models are shown and a Schechter mass function is used. Note that both models can reproduce the data. However, in the MID case, different values of $F_{\rm MID}$ are needed, 0.85 in the inner field and 0.5 in the outer field. The arrows denote the lower mass limit adopted.

Conclusions

We have reviewed the standard paradigm of cluster formation and early dissolution. The role of gas expulsion in the disruption process is strongly dependent on the initial conditions of the system. Sub-virial and hierarchical stellar groups can evolve in such a way that gas expulsion has little or not effect on their evolution. Additionally, recent studies of the spatial distribution of YSOs in the solar neighbourhood suggest that only a small fraction of stars form in groups that would be associated with "clusters", with the majority formed in low density groups/associations that will disperse into the background without the need of gas expulsion. Studies of the dynamics of resolved massive clusters in the Galaxy and LMC have found low velocity dispersions, suggesting that previous studies of unresolved young clusters (that found high velocity dispersions) were affected by high-mass binaries. These resolved massive clusters appear to be in a stable (or even sub-virial) configuration, even at very young ages, meaning that gas expulsion has had little or no effect on their evolution. *Hence, it appears that the effect of gas expulsion on young clusters and the role of infant mortality in cluster populations has been overestimated.*

After a cluster passes from an embedded to an exposed phase, a variety of processes will act upon the cluster which may lead to its disruption. We have reviewed the two main empirical disruption laws of clusters, *mass dependent disruption* (MDD) and *mass independent disruption* (MID). In order to test the two models, we have used new *HST* observations of the cluster population in M 83. The properties of the cluster population clearly change as a function of galactocentric distance, with clusters in the outer portion of the galaxy having higher mean ages. This is in agreement with the MDD scenario, which predicts that cluster disruption should depend on the ambient environment. While the role of mass in the cluster disruption process is more difficult to assess, due to the added parameter of the shape of the cluster mass function in the fitting analysis, we find evidence that higher mass clusters live longer. However, both the MDD and MID models can fit the data if all three main parameters ($F_{\rm MID}$, t_4, and $M_{\rm c}$) are allowed to vary. Finally, the cluster population of M 83 requires a truncation in the mass function at $\sim 10^5$ M$_\odot$, which is similar to that found for other galaxies, using independent techniques.

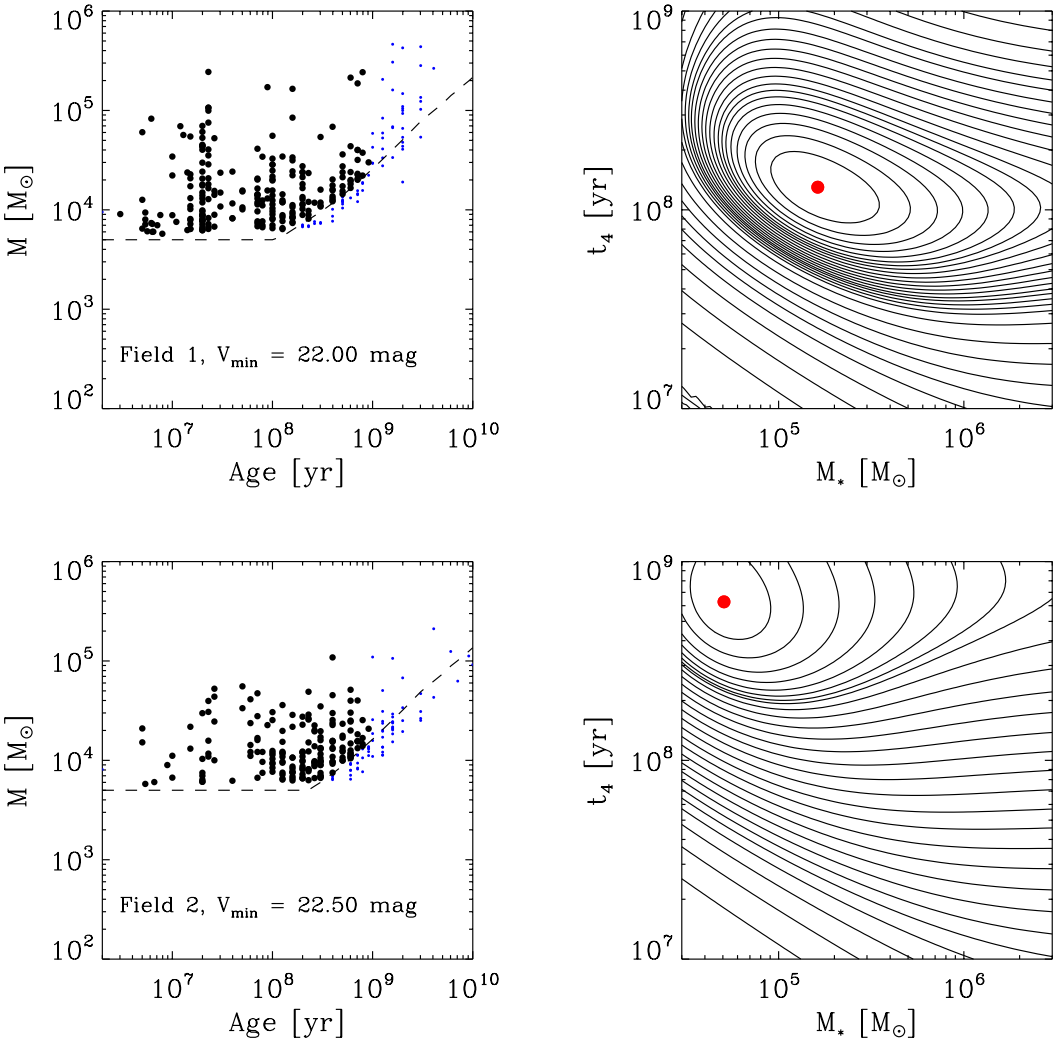

Figure 3.11: (from Bastian et al. [2011b]) *Left*: The age/mass diagrams for clusters in the inner (top) and outer (bottom) fields. Solid circles denote clusters that were used in the population fitting. The (blue) points represent clusters not used. The dashed line represents the surveys completeness limits, mass limited at young ages (5×10^3 $M_\odot$) and luminosity limited at older ages (the adopted limits are shown in the panels). *Right*: The results of a maximum likelihood fitting of each population, assuming only mass dependent disruption and a Schechter mass function. The solid (red) dotes shows the best fitting model.

Acknowledgments

We thank the organisers for a very lively and stimulating workshop. In additional, I am indebted to my collaborators, both for their insights and discussions as well as their help on the projects presented here. Namely, I would like to thank: Angela Adamo, Mark Gieles, Eli Bressert, Rob Gutermuth, Henny Lamers, Esteban Silva-Villa, Soeren Larsen, Simon Goodwin, Diederik Kruijssen, Linda Smith, Iraklis Konstantopoulos, and Erik Zackrisson.

Bibliography

Adamo, A., Zackrisson, E., Östlin, G., & Hayes, M. 2010, ApJ, 725, 1620
Adamo, A., Östlin, G., Zackrisson, E. 2011, MNRAS, in press (arXiv:1107.0725)
Allen, L., et al. 2007, Protostars and Planets V, 361
Allison, R. J., Goodwin, S. P., Parker, R. J., de Grijs, R., Portegies Zwart, S. F., & Kouwenhoven, M. B. N. 2009, ApJ, 700, L99

Bastian, N., & Goodwin, S. P. 2006, MNRAS, 369, L9
Bastian, N., Ercolano, B., Gieles, M., Rosolowsky, E., Scheepmaker, R. A., Gutermuth, R., & Efremov, Y. 2007, MNRAS, 379, 1302
Bastian, N. 2008, MNRAS, 390, 759
Bastian, N., Gieles, M., Ercolano, B., & Gutermuth, R. 2009, MNRAS, 392, 868
Bastian, N., et al. 2011, MNRAS, in press (arXiv:1106.2427)
Baumgardt, H., & Makino, J. 2003, MNRAS, 340, 227
Baumgardt, H., & Kroupa, P. 2007, MNRAS, 380, 1589
Boutloukos, S. G., & Lamers, H. J. G. L. M. 2003, MNRAS, 338, 717
Bressert et al. 2011, A&A, submitted
Carpenter, J. M. 2000, AJ, 120, 3139
Chandar, R., Fall, S. M., & Whitmore, B. C. 2006, ApJ, 650, L111
Chandar, R., Fall, S. M., & Whitmore, B. C. 2010a, ApJ, 711, 1263
Chandar, R., et al. 2010b, ApJ, 719, 966
Chen, H.-C., & Ko, C.-M. 2009, ApJ, 698, 1659
Clarkson, W., Lu, J. R., Ghez, A. M., Morris, M. R., McCrady, N., Stolte, A., & Yelda, S. 2011, Astronomical Society of the Pacific Conference Series, 439, 119
Efremov, Y. N., & Elmegreen, B. G. 1998, MNRAS, 299, 588
Elmegreen, B. G., & Falgarone, E. 1996, ApJ, 471, 816
Elmegreen, B. G., Efremov, Y., Pudritz, R. E., & Zinnecker, H. 2000, Protostars and Planets IV, 179
Elmegreen, B. G., Elmegreen, D. M., Chandar, R., Whitmore, B., & Regan, M. 2006, ApJ, 644, 879
Elmegreen, B. G., & Hunter, D. A. 2010, ApJ, 712, 604
Fall, S. M., Chandar, R., & Whitmore, B. C. 2005, ApJ, 631, L133
Fall, S. M., Chandar, R., & Whitmore, B. C. 2009, ApJ, 704, 453
Geyer, M. P., & Burkert, A. 2001, MNRAS, 323, 988
Gieles, M., Baumgardt, H., Bastian, N., & Lamers, H. J. G. L. M. 2004, The Formation and Evolution of Massive Young Star Clusters, 322, 481
Gieles, M., Larsen, S. S., Scheepmaker, R. A., Bastian, N., Haas, M. R., & Lamers, H. J. G. L. M. 2006, A&A, 446, L9
Gieles, M., Lamers, H. J. G. L. M., & Portegies Zwart, S. F. 2007, ApJ, 668, 268
Gieles, M., Sana, H., & Portegies Zwart, S. F. 2010, MNRAS, 402, 1750
Gieles, M., & Portegies Zwart, S. F. 2011, MNRAS, 410, L6
Gieles, M., Heggie, D. C., & Zhao, H. 2011, MNRAS, 413, 2509
Goddard, Q. E., Bastian, N., & Kennicutt, R. C. 2010, MNRAS, 405, 857
Goodwin, S. P. 1997, MNRAS, 284, 785
Goodwin, S. P., & Bastian, N. 2006, MNRAS, 373, 752
Goodwin, S. P. 2009, Ap&SS, 324, 259
Gutermuth, R. A., et al. 2008, ApJ, 674, 336
Gutermuth, R. A., Megeath, S. T., Myers, P. C., Allen, L. E., Pipher, J. L., & Fazio, G. G. 2009, ApJS, 184, 18
Hénon, M. 1961, Annales d'Astrophysique, 24, 369
Hills, J. G. 1980, ApJ, 235, 986
Jørgensen, J. K., Johnstone, D., Kirk, H., Myers, P. C., Allen, L. E., & Shirley, Y. L. 2008, ApJ, 683, 822
Kroupa, P., & Boily, C. M. 2002, MNRAS, 336, 1188
Kruijssen, J. M. D., Pelupessy, F. I., Lamers, H. J. G. L. M., Portegies Zwart, S. F., & Icke, V. 2011a, MNRAS, 414, 1339
Kruijssen et al. 2011b, MNRAS, submitted
Lada, C. J., Margulis, M., & Dearborn, D. 1984, ApJ, 285, 141
Lada, C. J., & Lada, E. A. 2003, ARA&A, 41, 57
Lamers, H. J. G. L. M., Gieles, M., Bastian, N., Baumgardt, H., Kharchenko, N. V., & Portegies Zwart, S. 2005, A&A, 441, 117
Lamers, H. J. G. L. M., & Gieles, M. 2006, A&A, 455, L17
Lamers, H. J. G. L. M., Baumgardt, H., & Gieles, M. 2010, MNRAS, 409, 305
Fouesneau, M., & Lançon, A. 2010, A&A, 521, A22
Larsen, S. S. 2008, Mass Loss from Stars and the Evolution of Stellar Clusters, 388, 279 (astro-ph/0609062)
Larsen, S. S. 2009, A&A, 494, 539
Maschberger, T., & Kroupa, P. 2009, MNRAS, 395, 931
Maschberger, T., Clarke, C. J., Bonnell, I. A., & Kroupa, P. 2010, MNRAS, 404, 1061
McMillan, S. L. W., Vesperini, E., & Portegies Zwart, S. F. 2007, ApJ, 655, L45

Mengel, S., & Tacconi-Garman, L. E. 2007, A&A, 466, 151
Moeckel, N., & Clarke, C. J. 2011, MNRAS, 410, 2799
Offner, S. S. R., Hansen, C. E., & Krumholz, M. R. 2009, ApJ, 704, L124
Parmentier, G., & Kroupa, P. 2011, MNRAS, 411, 1258
Rochau, B., Brandner, W., Stolte, A., Gennaro, M., Gouliermis, D., Da Rio, N., Dzyurkevich, N., & Henning, T. 2010, ApJ, 716, L90
Sánchez, N., Añez, N., Alfaro, E. J., & Crone Odekon, M. 2010, ApJ, 720, 541
Schmeja, S., Kumar, M. S. N., & Ferreira, B. 2008, MNRAS, 389, 1209
Silva-Villa, E., & Larsen, S. S. 2010, A&A, 516, A10
Silva-Villa, E., & Larsen, S. S. 2011, A&A, 529, A25
Smith, R., Fellhauer, M., Goodwin, S., & Assmann, P. 2011, MNRAS, 414, 3036
Spitzer, L., Jr. 1958, ApJ, 127, 17
Tutukov, A. V. 1978, A&A, 70, 57
Whitmore, B. C., Chandar, R., & Fall, S. M. 2007, AJ, 133, 1067
Weidner, C., & Kroupa, P. 2006, MNRAS, 365, 1333
Zackrisson, E., Rydberg, C. -., Schaerer, D., Ostlin, G., & Tuli, M. 2011, submitted (arXiv:1105.0921)

3.5 Early Dynamical Evolution of Eta Chamaeleontis

Christophe Becker[1] **and E. Moraux**[1]

[1] UJF-Grenoble 1 / CNRS-INSU, Institut de Planétologie et d'Astrophysique de Grenoble (IPAG) UMR 5274, Grenoble, F-38041, France

Abstract

The young association η Chamaeleontis displays some peculiar features: no low-mass stars or wide binaries were found in the central region. We investigate whether this is due to dynamical evolution from a very dense initial state with log-normal IMF, or if one needs to invoque a different IMF to reproduce these properties. The high density in the core suggests a very small time scale for gas expulsion, so we use a time-reversal method with a pure N-body code to find the initial conditions that lead to a state closest to the observed one. We test different values for initial density, virial ratio, as well as binary population. A set of 6 criteria is built in order to evaluate the degree of similarity between simulation results and observations. Results: We don't find any initial state that would evolve to fit the observations. We argue that η Chamaeleontis might have formed in a very peculiar environment, significantly changing the initial mass function and binary properties according to the very high initial density.

Introduction

Since its discovery by Mamajek et al. [1999], the stellar cluster η Chamaeleontis has been the target of many observational studies (Lyo et al. [2003]; Luhman [2004]; Brandeker et al. [2006]). It is a young (8 – 10 Myr), close (d $\sim$ 94 pc) and compact group of 18 systems showing unusual features: the system mass function, with range from 0.15 to 3.8 $M_\odot$, was found to be consistant with other young open clusters and field stars (Lyo et al. [2004]), predicting many more members below 0.15 $M_\odot$. But despite deep surveys, no low-mass systems were found as far as 2.6 pc from the center. The probability of having no such star from the predicted IMF is about 10^{-3}, so this lack of low-mass systems is statistically significant. Besides, among the binaries (representing 40% of the systems), there is a clear deficit of wide binaries: none has a separation larger than 30 AU. We will try to ascertain whether this feature, together with the lack of low-mass stars, arises from early dynamical evolution or from an intrinsic difference in the environment η Cha was born in, which could have yielded an abnormal IMF. This issue has been previously addressed by Moraux et al. [2007], where, at first order, binaries were considered as single objects. In the present study we tackle the same problem, but focusing on the initial binary population and its influence on the cluster dynamics.

Numerical simulations

The integration starts from an initial state where the cluster evolution is already purely dominated by gravity: stars have all formed, and gas has been removed. The time scale of gas evaporation is expected to be small (2 – 5 Myr) (Mamajek et al. [2000]), so we run our simulation for 4 – 8 Myr.
Regarding initial conditions, our main hypothesis concerns the initial mass function: thought to be invariant with stellar environment, we wish to verify that it represents η Cha well. The initial stellar population was chosen to follow a log-normal distribution (using the system IMF) (Chabrier [2003]) with a peak at m= 0.25 $M_\odot$ and standard deviation σ= 0.52. The range considered is 0.01 to 4 $M_\odot$, according to observations. The observed range of masses allowed for an estimation of the initial number of systems, N_{sys}= 50, looking for the normalisation that would produce 4 stars with more than 1 $M_\odot$. The inital cluster radius was first estimated to fit a constant surface density derived from observations (Adams et al. [2006]), giving 0.3 to 1.0 pc. A Plummer model is used to distribute systems spatially, and compute velocities, once a virial ratio is chosen.
As a follow-up work of Moraux et al. [2007], we took binary dynamics into account and started with 100% binaries (Duchêne [1999]). The binary population is characterized by its period distribution, as computed

by Kroupa [1995], a thermalized eccentricity distribution, and a way of pairing binaries, chosen at first to be random in the IMF.
We made use of the code NBODY3, written by Aarseth [1999], treating close encounters accurately thanks to a regularization method (Mikkola & Aarseth [1990]). The stellar systems evolve in a galactic potential with tidal radius defined by Oort's constants: a star is removed from the cluster when its distance to the cluster centre is more than twice the tidal radius.
The parameter space we considered is N_{sys}=20, 30, 40, 50, 60, 70, R_{Pl} = 0.3, 0.1, 0.05, 0.03, 0.01 and 0.005 pc., in order to span many orders of magnitude in initial density, and to check the influence of initial equilibrium, we took a virial ratio $Q = \frac{E_{kin}}{E_{pot}}$, from 0.3 to 0.7. For each configuration $\{N_{sys}, R_{Pl}, Q\}$ 200 simulations were generated, changing only random seed, for statistical purposes. In total, 180 configurations were tested.

Analysis

Observational criteria - qualitative analysis

We use a set of criteria to evaluate if, at a given time, a simulation is close to reproducing what is observed. In general, each criteria i is said to be satisfied if $N_i = O_i \pm \sqrt{O_i}$, where N_i is obtained by simulation and O_i given by observation.

Number of systems. First, to account for the membership and compactness of the core, we consider the number of systems in a 0.5 pc sphere. With 18 systems within the core radius, the range of our selection was 14 to 22 systems.
Each binary is considered as a system independently of its separation or its components' mass. During the analysis, binaries are identified on the basis of the nearest neighbour distance. This method was used to reproduce the way binaries are found observationally. Besides, since $NBODY3$ could retrieve the bound (double) systems, we could verify that the method based on distance was giving consistant results.

Number of massive stars. Since 3 stars were found in the central region with a mass $m > 1.5$ $M_\odot$, with a mass of 3.8 $M_\odot$ for the most massive one, we wanted to keep between 2 and 4 of them in the simulations. These stars tend to be less sensitive to two-body encounters and fall toward high density regions, whereas low-mass stars get ejected, producing mass segregation.

Number of low-mass stars. No stars with $m < 0.1\,M_\odot$ have been found up to 2.6 pc radius from the center. The associated criteria is to have 0 or 1 of such stars left. Many low-mass stars may be part of a binary system, so it appears important to establish a way to count them: given the observational limitation in separation and masses, we considered a binary to be resolved if the separation was higher that 20 AU.

Number of stars in the halo. Ejected stars form a halo around the central region, as studied by Murphy et al. [2010]. The supplementary members they provided seem to be consistant with early ejection, nevertheless this is checked by the following criteria: we want 2 to 6 members of $0.08 < m < 0.3$ $M_\odot$ between 2.7 and 10 pc. The halo starts appearing after the binary-breaking phase, and despite a large spread in the number of escapers, we can verify that this is consistant with these observations.

Binary proportion. Considering the binary population, we are interested in keeping a binary fraction in the core region around 30% and 50%. This is strongly correlated with the inital period distribution together with the inital density.

Separation limit. The lack of binaries with a separation larger than 30 AU was accounted for by having at most 1 binary with a separation larger than 50 AU. We choose a loose cut on separation to be more conservative.

Time constraint. With an age estimate around 8 – 10 Myr, the simulations are stopped at 10 Myr, and given that the gas was removed in a few Myr, we want the observational constraints to be fulfilled within the time range 5 – 8 Myr.

Quantitative analysis

The 7 criteria detailed above allow, when used simultaneoulsy, to determine the statistical likelyhood for a given set of initial conditions to reproduce the observation. In pratice, we only applied the first 6 criteria describing the stellar population: the time interval is studied as a last check. Considering each of the 200 simulations, we apply these criteria at each time snaphsot to see if they can be all satisfied. Fig. 3.12 shows a summary of this procedure for a specific value of virial ratio and number of systems. The time constraint is to be considered as a very last check.
It is interesting to notice that, even if 100% runs satisfy the first criteria (on the number of systems), this is valid for a particular time range, in which the next criteria will have to be fulfilled. The most important note is the percentage of runs passing the selection drops to zero as we apply the fourth condition (on the number of low-mass stars). This is also true for all other configurations tested, so no run presents an evolved state matching to the current state of η Cha.
The apparent divergence of these results with those in the previous study (Moraux et al. [2007]) is understood as a consequence of dealing with resolved binary dynamics : in the present case masses were initialized individually using a log-normal IMF, peaking at ~ 0.1 M$_\odot$, whereas a system IMF peaking at ~ 0.25 M$_\odot$ was used in the former study, where binaries were considered as single unbreakable objects. Then, while some binaries are destroyed dynamically, each of their two components evolve separatly and is accounted for. As many stars with mass $m < 0.1$ M$_\odot$ may be part of a binary system, we end up having more of these stars to eject than in the case where a system IMF was used.

Looking for tendencies

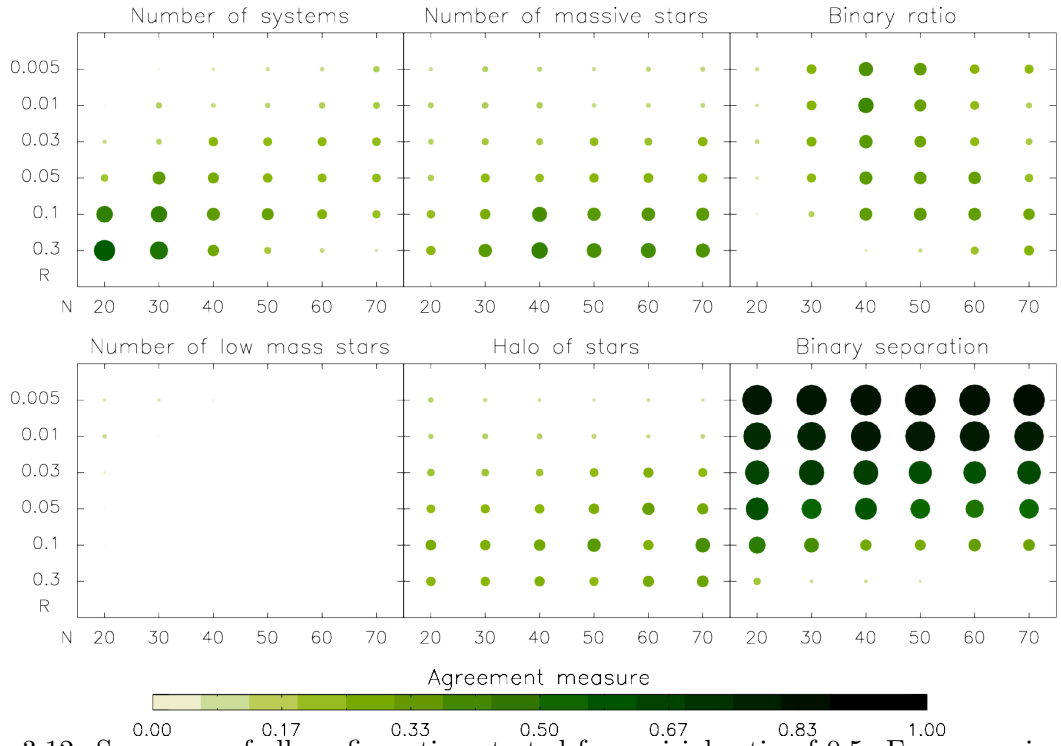

Figure 3.12: Summary of all configurations tested for a virial ratio of 0.5. For convenience the value for the quality measure is also indicated by the dot size, with a linear scale. The colour (and size) of the circles indicate a region where a criterion agrees best with the observation.

It is possible to individually check for every measurement if it is reproduced well in simulations within the time range considered. We compute an agreement measure using a Gaussian with mean value

m being the observational data, and deviation, σ chosen usually equal to $\sqrt{m}$.

$$a(t) = \frac{1}{N}\sum_{i}^{N} \exp\left(-\frac{(x_i - m)^2}{2\sigma^2}\right) \cdot P(t)$$

where $P(t) = 1$ if $t \in [5, 8]$ Myr and decreasing exponentially out of this interval. Varying from 0 to 1, $a(t)$ provides a rough estimate of the probability for a run to satisfy the considered criterion. Calculating $a(t)$ for every set of $\{N_{sys};R_{Pl};Q\}$ from the parameter grid pictures regions where the observational constraint might be best matched. Such an approach also aims at testing the parameter grid that was used.
From Fig. 3.12. it is clear that some observational conditions produce opposite constraints, considering for instance the number of systems together with the halo, or the number of low-mass stars together with the number of massive stars. Multiplying the six measures, we obtain a map taking into account all observational tests, for a given initial virial ratio. The main outcomes of this process are:

- The global agreement measure has a mean value of 10^{-9}, reflecting the fact that it is very unlikely to fit the observations.
- There is no tendency showing any improvement at the edge of the parameter grid, suggesting that the solution, if any, should lie in this area.
- The initial cold (Q=0.3) or hot (Q=0.7) states cannot be distinguished statistically from the state initially in equilibrium (Q=0.5).

Alternative initial conditions

So far we allowed only for the density and virial ratio to vary, so we will now discuss other parameters that might need to be corrected to be complete and to check more peculiar initial conditions.

Pairing of binaries. There is growing evidence (Kouwenhoven et al. [2009], Kraus et al. [2011]) that drawing binary companion mass from a random pairing from the individual IMF might not be realistic. An alternative is to consider a flat mass ratio distribution, in accordance with a fragmentation scenario (Bate [2000]). Using the individual IMF peaking at 0.08 $M_\odot$ to choose the primary mass, and drawing the secondary according to a flat mass ratio distribution, we ran simulations for $Q = 0.5$ only, $N_{sys} = 20$ and $N_{sys} = 40$, with the same range for R_{Pl} as before. The statistics did not improve in an appreciable way, neither qualitatively nor quantitatively. It seems that there were still too many low-mass stars being generated by binary decay to eject them all.

Separation distribution. Since the ejection of low-mass stars appears to be the most difficult effect to reproduce, and given the lack of wide binaries, we considered that no wide binaries might have formed at all initially. Indeed in a dense environment where the mean neighbour distance can be lower than 1000 AU, binaries wider than 300 AU, or lower, could not form. Then, using a cut-off in the initial separation distribution, also adjusting the binary ratio, we tried several cut-off values for $\{Q = 0.5, N_{sys} = 40, R_{pl} = 40\}$. In some cases where very few low-mass stars were present the agreement factor for the low-mass star criteria could increase by a factor of 7. Nevertheless, combining all criteria did not significantly improve the results.

Fractal initial conditions. Testing a more structured initial spatial/velocity arrangement, we created a clumpy, or fractal, configuration, using the method in Goodwin & Whitworth [2004]. Taking a fractal dimension of 1.6, we tried a sub-virial as well as virial set-up, for $N_{sys} = 20$ and $N_{sys} = 40$ and a scale radius of 0.3 and 0.1 pc. The results did not reveal any collapse phase (expected to be shorter than 0.5 Myr in most cases, given the inital density) nor important change in the setup of mass segregation. The low number of stars involved likely reduced the impact of the fractal structure on the dynamics.

Conclusion

We have conducted a significant set of simulations aiming at reproducing the observed properties of η Chamaeleontis, sweeping the parameter space in density, virial ratio, and testing different setups for the binary population. Since no initial state considered statistically match the observational constraints, we infer that this association might have formed in a special environment, from which the IMF drawn was not consistant with the log-normal system IMF.

Acknowledgments

This project is supported by ANR DESC 2010 JCJC 0501 1

Bibliography

Aarseth, S. J. 1999, PASP, 111, 1333
Adams, F. C., Proszkow, E. M., Fatuzzo, M., & Myers, P. C. 2006, ApJ, 641, 504
Bate, M. R. 2000, MNRAS, 314, 33
Brandeker, A., Jayawardhana, R., Khavari, P., Haisch, J. K. E., & Mardones, D. 2006, ApJ, 652, 1572
Chabrier, G. 2003, PASP, 115, 763
Duchêne, G. 1999, A&A, 341, 547
Goodwin, S. P. & Whitworth, A. P. 2004, A&A, 413, 929
Kouwenhoven, M. B. N., Brown, A. G. A., Goodwin, S. P., Portegies Zwart, S. F., & Kaper, L. 2009, A&A, 493, 979
Kraus, A. L., Ireland, M. J., Martinache, F., & Hillenbrand, L. A. 2011, ApJ, 731, 8
Kroupa, P. 1995, MNRAS, 277, 1507
Luhman, K. L. 2004, ApJ, 616, 1033
Lyo, A.-R., Lawson, W. A., Feigelson, E. D., & Crause, L. A. 2004, MNRAS, 347, 246
Lyo, A.-R., Lawson, W. A., Mamajek, E. E., et al. 2003, MNRAS, 338, 616
Mamajek, E. E., Lawson, W. A., & Feigelson, E. D. 1999, ApJ Lett., 516, L77
Mamajek, E. E., Lawson, W. A., & Feigelson, E. D. 2000, ApJ, 544, 356
Mikkola, S. & Aarseth, S. J. 1990, Celestial Mechanics and Dynamical Astronomy, 47, 375
Moraux, E., Lawson, W. A., & Clarke, C. 2007, A&A, 473, 163
Murphy, S. J., Lawson, W. A., & Bessell, M. S. 2010, MNRAS, 406, L50

3.6 The DANCE Project: Dynamical Analysis of Nearby Clusters

Hervé Bouy[1], **E. Bertin**[2], **J. C. Cuillandre,**[2,3] **E. Moraux,**[4] **J. Bouvier,**[4] **M. Arevalo Sanchez,**[1] **D. Barrado y Navascués**[1,5]

[1] Centro de Astrobiología, P.O. Box - Apdo. de correos 78, 28691 Villanueva de la Cañada, Spain
[2] Institut d'Astrophysique de Paris, 98 bd Arago, Paris, France
[3] CFHT Corporation, 65-1238 Mamalahoa Hwy, Kamuela, Hawaii 96743, USA
[4] Institut de Planétologie et d'Astrophysique de Grenoble, BP 53, F-38041 Grenoble, Cedex 9, France
[5] Calar Alto Observatory, Centro Astronómico Hispano Alemán, Calle Jesús Durbán Remón, 2-2, 04004 Almería, Spain

Abstract

We present the results of the DANCE project, a ground-based survey meant to prepare and complement Gaia i) down to the planetary mass regime; ii) in regions of high extinction. The DANCE project takes advantage of archival wide-field surveys to derive precise astrometry, and in particular proper motions, for millions of stars in young nearby associations. We present the first preliminary results obtained for the Pleiades cluster, as well as our immediate objectives for other associations.

Introduction: Motivations

Gaia will provide precision astrometry for all sources up to V $\approx$ 20 mag. While it represents a tremendous improvement with respect to Hipparcos, this V $\approx$ 20 mag limit will nevertheless be a serious limitation for the specific study of stellar formation in young associations.

Over the past two decades, a great number of studies have discovered very low-mass objects, extending the mass function down to the planetary mass regime (see contributions by Petr-Gotzens, Lodieu, Moraux, Caballero, Barrado in these proceedings). Gaia's sensitivity limit of V $\approx$ 20 mag corresponds to $\approx$ 25 M_{Jup} at 100 pc and for an age of 1 Myr, when we know that the mass function extends at least down to 3 $\sim$ 4 M_{Jup}. These very low-mass brown dwarfs and planetary mass objects seem to be numerous, and are considered an important product of stellar formation. Any study of stellar formation must therefore account for them.

Additionally, young stellar clusters and young associations are very often deeply embedded. Because it will be operating in the V-band, Gaia will be heavily affected by extinction. Unfortunately the most embedded regions are very often the place where most of the stellar formation is occuring. Deeper astrometric surveys at longer wavelengths are therefore highly required to complement Gaia in these very important regions.

Objectives

The main objective of the DANCE project is to provide very deep and high precision astrometry over entire young associations. More specifically, the DANCE project focuses on two areas of interest: i) deriving a complete census of various associations based on kinematics; ii) studying the internal dynamics and dynamical evolution of various associations as a function of various parameters (age, mass, environment, density,...). These scientific goals define our requirements in turns. In particular, an accuracy better than 1 km/s and a spatial coverage of the entire associations are required to perform meaningful comparisons with numerical simulations and study mass dependent mechanisms.

An accuracy of 1 km/s at the typical distance of 200 pc corresponds roughly to 1 mas/yr. To reach such an accuracy using ground based data, one usually needs high quality images, and a long time baseline between several epochs. The DANCE project was originally motivated by the availability of wide field surveys performed more than a decade ago, and targeting many of the nearest young associations. These

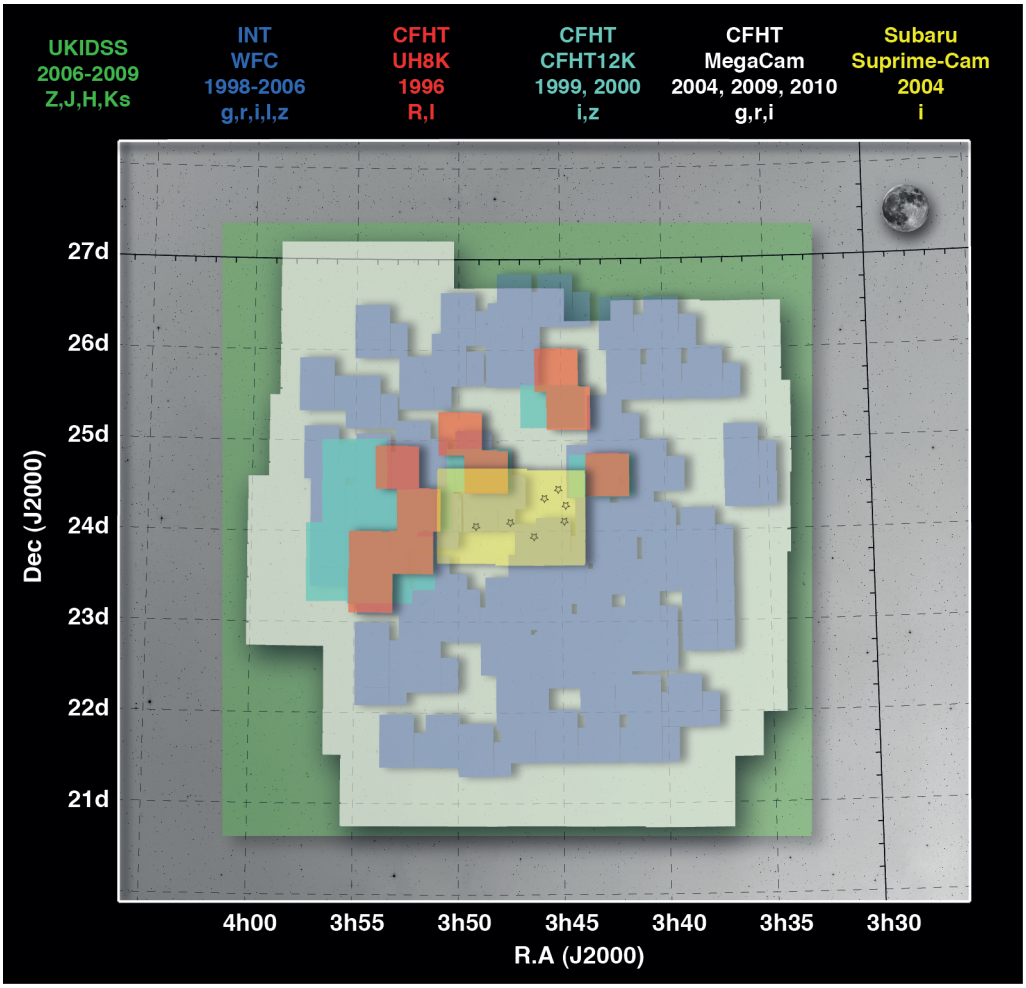

Figure 3.13: Coverage of the Pleiades. The various colours correspond to different datasets, as described in the legend. The Seven Sisters are indicated in the center, and the full moon is represented to illustrate the scale.

surveys covered several hundreds of square degrees in various associations. Processing and analyzing these data with precision astrometry in mind required first to develop an advanced pipeline for automatic processing of the vast amount of data, and second the development of robust algorithms to derive accurate astrometry and proper motions.

Dancefloor: The Pleiades

The Pleiades cluster was the perfect test bench fo developing such tools: its fast projected motion and the vast amount of data available in various archives made it the ideal place to test and develop the methods. The diversity of the data used in our project, originating from 9 different observatories, and 17 instruments, each in various filters, was one of the biggest challenge that we had to overcome. Fig. 3.13 shows the coverage of the various datasets compiled for the Pleiades. The total area covered by our survey encompasses more than 30 deg^2. The final database includes a total of 5469 individual images (not counting calibration files), filling more than 1 Tb. The source extraction and astrometric registration and analysis was performed using Astr*O*matic[7] software on the super-computing facilities at ESAC and IAP.

[7] `www.astromatic.net`

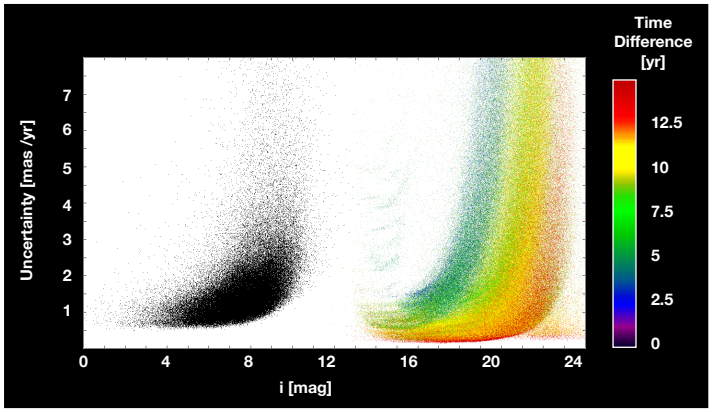

Figure 3.14: Measurement uncertainty as a function of i-band magnitude, and maximum time difference (colour scale).

Preliminary results

Special care was taken to derive realistic and conservative uncertainty estimates. Fig. 3.14 shows the accuracy that we obtain as a function of magnitude and time difference between epochs. The entire Hipparcos catalogue is also represented for comparison. We routinely reach an accuracy of 0.15 mas/yr up to i $\approx$ 21 mag, which is comparable to Gaia's expected performances on the faintest sources. The colour scale shows that there is a clear dependance on the time baseline.

A similarly good accuracy has been achieved in the past by many other groups (see for example contributions by Balaguer-Núñez and Hußman in these proceedings). The originality and novelty of the DANCE project resides in the scale of the survey. While previous studies covered a few square arcminutes or a couple of square degrees at most, the data processing pipelines and Astr*O*matic softwares together allow us to efficiently cover hundreds of square degrees, making it 2 orders of magnitude larger than any previous ground-based astrometric survey.

Analysis

When the association has a sufficiently large mean transverse motion, one can use proper motion to identify co-moving members. Fig. 3.15 shows the proper motion diagrams obtained for the Pleiades. The field star distribution is centred around (0, 0) and the co-moving cluster members are concentrated in a small clump around (20, -30). We can thus select sources based on their location in this diagram. Selecting members based on their kinematics offers several advantages: it does not rely on mostly untested theoretical tracks; it rejects the majority of unrelated foreground and background sources; it is insensitive to variability or flux excess/deficiency related to e.g circumstellar material; it can disentangle 2 coincident or neighbouring associations, provided that they have differing mean motions. Contamination of kinematically selected samples is thus negligible, and allows to derive robust stellar census and mass functions. Once a clean sample of co-moving members has been identified, one can perform detailed studies of their properties, such as their spatial distribution and internal dynamics.

Immediate objectives

We have identified a number of young nearby associations and clusters for which archival data are available (Table 3.1). They cover a broad range of age, total mass, density and dynamical states. Most of the data is downloaded and processed. In many cases we need second epoch images to increase the time baseline. For some regions we already have enough data, and will perform the analysis in the coming months. Data should keep flowing, as a growing number of facilities are being equiped with wide field instruments, and as new generations of deep, multi-epoch all sky surveys will start in the coming years.

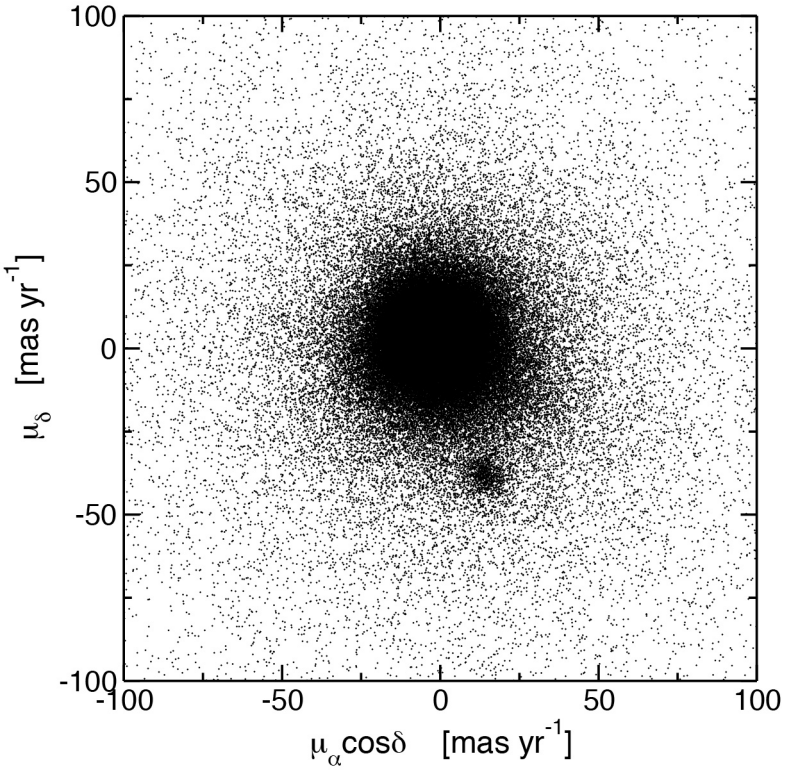

Figure 3.15: Vector point diagram of the Pleiades.

Limitations

The DANCE survey suffers from several limitations. Because the data sets are inhomogeneous in depth, spatial resolution, and ambient conditions, it is sometimes difficult to interpret the data, in particular estimate the limit of sensitivity of the entire survey, both in term of luminosity or astrometric accuracy. Additionally, DANCE is currently limited to the study of proper motions only. Radial velocities would be needed to have a 3D knowledge of the velocities, and parallax to have a full 6D knowledge of the kinematics.

Table 3.1: Associations targeted by the DANCE project

Assoc.	Age [Myr]	Dist. [pc]	$\mu_{\rm RA}$ [mas/yr]	$\mu_{\rm Dec}$ [mas/yr]
Pleiades	120	120	-35	-15
CrA	1	130	-35	51
ηCha	9	100	-30	28
Upper Sco	5	125	-9	-24
α Per	50	180	24	-26
IC2391	55	155	-25	23
IC2602	50	145	-22	10
Lupus	3	140	-17	-27
IC348	3	350	7	-9
NGC1333	1	350	7	-9
Serpens	3	450	...	...
Praesepe	650	180	-36	-13
Ophiuchus	1	145	-10	-25
Taurus	3	140	-8	-25
Blanco 1	100	210	19	4
Hyades	625	40	$\approx$100	
Orion	1-10	400	...	...

DANCIN': DANCE over the INternet:

We nevertheless believe that the DANCE database is novel and very rich. For this reason, and since we see the large catalogues including several tens of millions of sources as an important contribution to the community, we are going to make all the catalogues and processed images available publicly online via a web interface currently developed by the Spanish VO Team and hosted at the Center for Astrobiology. Users will be able to query by position, browse all the overlapping images and catalogues and retrieve the corresponding data. The catalogues will also be converted to VO standard format and be accessible via your favourite VO tools.

3.7 Gaia and σ Orionis from 20 $M_\odot$ to 3 M_{Jup}: the Most Complete and Precise Initial Mass Function with a Parallax Determination?

José Antonio Caballero[1]

[1] Centro de Astrobiología (CSIC-INTA), PO Box 78, E-28691 Villanueva de la Cañada, Madrid, Spain

Abstract

The σ Orionis cluster is to date the star-forming region with the largest number of confirmed brown dwarfs and substellar objects below the deuterium burning mass limit. The most massive star, σ Ori Aa, just in the cluster centre, is the $\sim$20 $M_\odot$-mass O9.5V star that illuminates the Horsehead Nebula, while the least massive object yet reported, S Ori 70, is only around 3 M_{Jup}. In the middle, there is a continuum of stars and substellar objects of all types (including magnetically active B2Vp stars, Herbig-Haro objects, FU Ori stars or T Tauri brown dwarfs) that makes the cluster a cornerstone in the study of the initial mass function, disc presence, X-ray emission or accretion at all mass domains. However, the derived masses strongly depend on the actual heliocentric distance to the cluster. Gaia will solve the dilemma.

σ Orionis: significance

The σ Orionis cluster ($\tau \sim 3$ Myr, $d \sim 385$ pc, $A_V < 0.3$ mag) is located in the easternmost part of the Ori OB1b association and is one of the most attractive and visited regions for night sky observers (Garrison [1967]; Wolk [1996]; Walter et al. [2008]; Caballero [2008b]). The cluster gets the name from the homonymous massive star system in its centre, which is the fourth brightest star in the Orion Belt. The σ Orionis cluster is important for several reasons:

- Its stars illuminate the Horsehead Nebula photodissociation region (Pound et al. [2003]; Pety et al. [2005]; Goicoechea et al. [2006]).
- It contains an abundant X-ray emitter population (Franciosini et al. [2006]; Skinner et al. [2008]; Caballero et al. [2010]).
- It is a cornerstone for studying disc frequency at $\tau \sim 3$ Myr at all mass domains (Oliveira et al. [2004]; Caballero et al. [2007]; Zapatero Osorio et al. [2007]; Luhman et al. [2008]).
- The helium-rich, magnetically active, B2Vp star σ Ori E is in its centre (Walborn [1974]; Groote & Hunger [1982]; Townsend et al. [2005]).
- It holds four Herbig-Haro objects and dozens Herbig Ae/Be, T Tauri and FU Ori stars (Haro & Moreno [1953]; Reipurth et al. [1998]; Andrews et al. [2004]).
- The central star system is the most massive "binary" with an astrometric orbit (Hartkopf et al. [1996]; Mason et al. [1998]; Caballero [2008a]).
- Its proximity, youth and low extinction facilitate studies of accretion rates and frequency at low masses (Scholz & Eislöffel [2004]; Kenyon et al. [2005]; Gatti et al. [2008]).
- It is the star-forming region with the largest number of confirmed brown dwarfs ($M < 70$ M_{Jup}) and objects below the deuterium burning mass limit (i.e., isolated planetary-mass objects; $M < 13$ M_{Jup}) with spectroscopy and youth features, e.g., Li I absorption, Hα and X-rays emission, infrared excess, radial velocity (Béjar et al. [1999]; Zapatero Osorio et al. [2000]; Barrado y Navascués et al. [2001]; Rigliaco et al. [2011]).

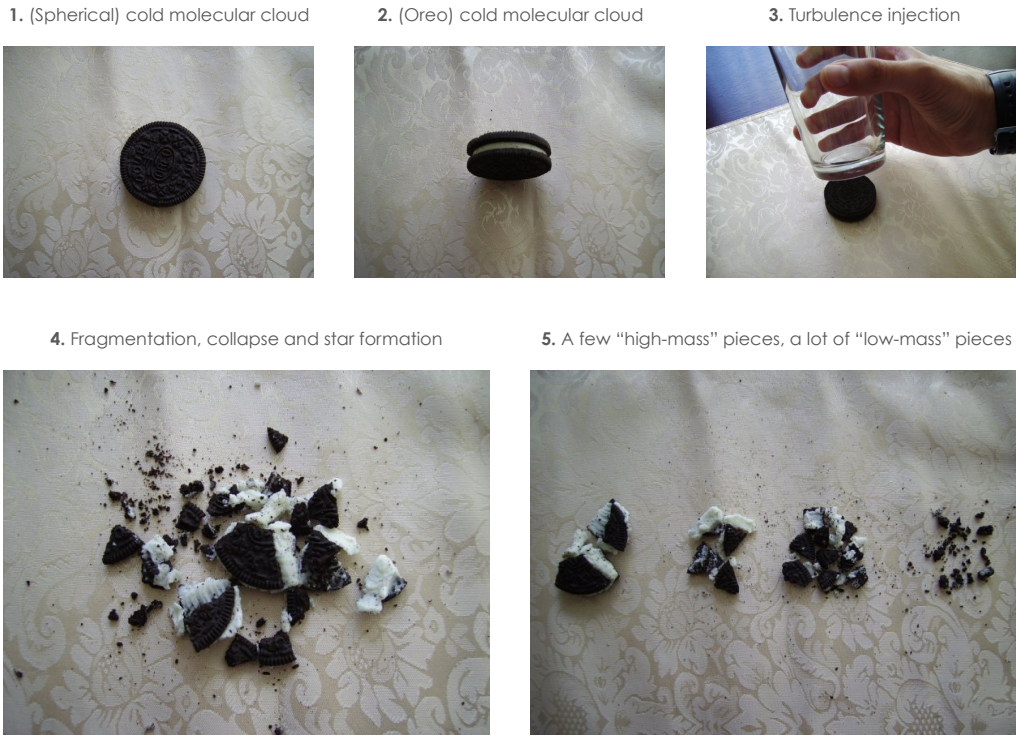

Figure 3.16: Pictorical sketch of the star formation process and cluster IMF determination (the original idea of breaking into pieces, "fragmenting", a cookie and counting the pieces was first stated by V. J. S. Béjar; all pieces were eaten after the making of this figure).

σ Orionis: previous IMF works

The abundance of known substellar objects has led σ Orionis to become a key region all over the sky to study the initial mass function (IMF), especially at *very* low masses. The IMF is the empirical function that describes the mass distribution (the histogram of stellar masses) of a population of recently-born stars, and its determination in a cluster is illustrated in Fig. 3.16.

The behaviour of the IMF has been described repeatedly (e.g., Kroupa [2002]), but σ Orionis is probably the cluster where the IMF studies have gone lowest in mass with completeness and confidence, perhaps in more detail than in the Pleiades or the Orion Nebula Cluster. In Table 3.2, I summarise all IMF works on σ Orionis. I tabulate the mass interval and the corresponding α index in the mass spectrum, $\Delta N/\Delta N = AM^{-\alpha}$ ($\alpha \equiv -\gamma \equiv 1 - \Gamma$). The general trend indicates a Salpeter-like slope between 20 and $1\,M_\odot$ ($\alpha \sim +2.35$), a rather flat mass spectrum ($\alpha \sim +0.3$) between 0.3 and $0.006\,M_\odot$ ($6\,M_{Jup}$) and a soft elbow in between, at $1 - 0.3\,M_\odot$. The mass spectrum may go *down* at a few Jupiter masses after the results exposed by Peña Ramírez et al. [2011]. See Fig. 3.17.

σ Orionis: what to do next?

There are some caveats in the IMF determination in σ Orionis:

- The IMF relies on cluster parameters and on the used theoretical models. But which models to use? How to handle uncertainties at young ages? Which band or combination of bands to use? Are colour-dependent bolometric corrections better than apparent magnitudes only? How to match different isochrones of different authors valid at different mass and effective temperature intervals?
- How old is σ Orionis? There have been reports of ages from 1 to 10 Myr, with a general consensus towards the 2 – 4 Myr interval, being 3 Myr the canonical value. But what if it is slightly older or younger? Is there any age spread? How do we account for the different accretion history?

Table 3.2: IMF works in the σ Orionis cluster.

Work	Mass interval $[M_\odot]$	α	Colour in Fig. 3.17
Béjar et al. 2001	0.1 – 0.015	+0.6	Red
Tej et al. 2002	0.45 – 0.025	+1.2	Orange (dashed)
Sherry et al. 2004	0.2 – 1.0	+2.7	Not drawn
Caballero 2006, 2010a	3 – 0.6	+1.4	Yellow
	0.4 – 0.006	+0.4	Yellow
González-García et al. 2006	0.072 – 0.007	+0.6	Not drawn
Caballero 2007	18 – 1.5	+2.0	Green
Caballero et al. 2007	0.11 – 0.006	+0.6	Not drawn
	0.072 – 0.006	+0.4	Light blue
Lodieu et al. 2009	0.49 – 0.010	+0.5	Blue (dashed)
Bihain et al. 2009	0.012 – 0.0035	+0.0:	Dark blue
Caballero 2009	20 – 1	+2.3	Magenta
	0.3 – 0.035	+0.3	Magenta

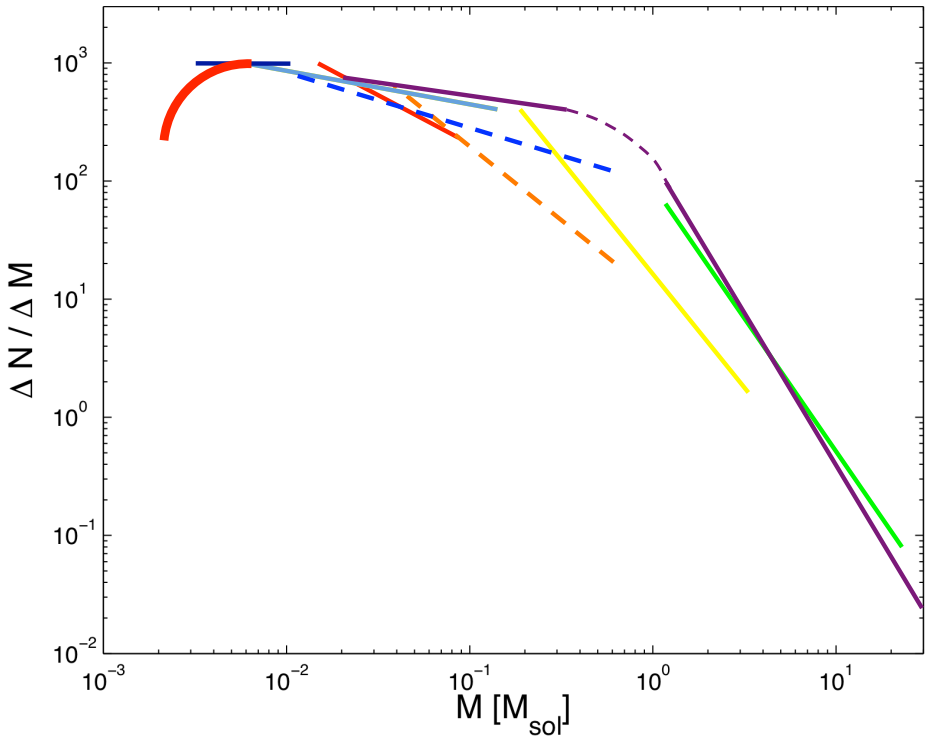

Figure 3.17: Some mass spectra reported in the σ Orionis cluster (see Table 3.2 for the references and colour code).

- What is the contamination rate in the cluster? In σ Orionis, there is contamination by B stars in nearby star-forming regions in Ori OB1b, foreground low proper-motion AFG dwarfs, background giants, field late-M-, L- and T-type stars and brown dwarfs, red quasars... Spectroscopy, astrometry and methane imaging help disentangling actual cluster members from interlopers (Sacco et al. [2008]; Caballero et al. [2008]; Caballero [2010b]; Peña Ramírez et al. [2011]).
- What is the "system IMF"? Further binarity studies at all mass and separation domains are required. Some surprises await us, such as the confirmation that the σ Ori star itself is not only an astrometric binary, but also a *massive spectroscopic triple* containing an O9.5V, a B0.5V and and early B dwarf (Simón-Díaz et al., these proceedings).
- Is there a cut-off of the IMF below 0.006 $M_\odot$? To ascertain it, there is no other way than performing

ultradeep imaging ($I > 26$ mag, $J > 22$ mag, $H > 22$ mag) in an area wider than 1000 arcmin^2 with methane, astrometric and spectroscopic follow-up of T-type candidates, which requires a strong observational effort.

- What is the distance to σ Orionis? Is it 350 pc (*Hipparcos*, with large error bars), 450 pc (Sherry et al. [2008]), or something in between at around 400 pc (Caballero [2008a]; Mayne & Naylor [2008])? Solution: Gaia!

Gaia will likely not detect cluster brown dwarfs ($J > 14.5$ mag), and some cluster dynamical studies (radial velocities, proper motions) will arrive earlier than the ESA mission, but Gaia will measure the parameter with the largest error contribution to the IMF, *distance*, from accurate parallax determination. A list of dozens of confirmed cluster members with $V < 20$ mag is easy to accomplish; we only need to wait a couple of years.

Acknowledgments

This work was supported by the Spanish Ministerio de Ciencia e Innovación and the Comunidad de Madrid under under grants AYA2008-00695, AYA2008-06423-C03-03 and S2009/ESP-1496.

Bibliography

Andrews, S. M., Reipurth, B., Bally, J., & Heathcote, S. R. 2004, ApJ, 606, 353
Barrado y Navascués, D., Zapatero Osorio, M. R., Béjar, V. J. S., et al. 2001, A&A, 377, L9
Béjar, V. J. S., Martín, E. L., Zapatero Osorio, M. R., et al. 2001, ApJ, 556, 830
Béjar, V. J. S., Zapatero Osorio, M. R., & Rebolo, R. 1999, ApJ, 521, 671
Bihain, G., Rebolo, R., Zapatero Osorio, M. R., et al. 2009, A&A, 506, 1169
Caballero, J. A. 2007, A&A, 466, 917
Caballero, J. A. 2008a, MNRAS, 383, 750
Caballero, J. A. 2008b, A&A, 478, 667
Caballero, J. A. 2009, in American Institute of Physics Conference Series, Vol. 1094, American Institute of Physics Conference Series, ed. E. Stempels, 912–915
Caballero, J. A. 2010a, in Highlights of Spanish Astrophysics V, ed. J. M. Diego, L. J. Goicoechea, J. I. González-Serrano, & J. Gorgas, 79
Caballero, J. A. 2010b, A&A, 514, A18
Caballero, J. A., Albacete-Colombo, J. F., & López-Santiago, J. 2010, A&A, 521, A45
Caballero, J. A., Béjar, V. J. S., Rebolo, R., et al. 2007, A&A, 470, 903
Caballero, J. A., Valdivielso, L., Martín, E. L., et al. 2008, A&A, 491, 515
Franciosini, E., Pallavicini, R., & Sanz-Forcada, J. 2006, A&A, 446, 501
Garrison, R. F. 1967, PASP, 79, 433
Gatti, T., Natta, A., Randich, S., Testi, L., & Sacco, G. 2008, A&A, 481, 423
Goicoechea, J. R., Pety, J., Gerin, M., et al. 2006, A&A, 456, 565
González-García, B. M., Zapatero Osorio, M. R., Béjar, V. J. S., et al. 2006, A&A, 460, 799
Groote, D. & Hunger, K. 1982, A&A, 116, 64
Haro, G. & Moreno, A. 1953, Boletín de los Observatorios Tonantzintla y Tacubaya, 1, 11
Hartkopf, W. I., Mason, B. D., & McAlister, H. A. 1996, AJ, 111, 370
Kenyon, M. J., Jeffries, R. D., Naylor, T., Oliveira, J. M., & Maxted, P. F. L. 2005, MNRAS, 356, 89
Kroupa, P. 2002, Sci, 295, 82
Lodieu, N., Zapatero Osorio, M. R., Rebolo, R., Martín, E. L., & Hambly, N. C. 2009, A&A, 505, 1115
Luhman, K. L., Hernández, J., Downes, J. J., Hartmann, L., & Briceño, C. 2008, ApJ, 688, 362
Mason, B. D., Gies, D. R., Hartkopf, W. I., et al. 1998, AJ, 115, 821
Mayne, N. J. & Naylor, T. 2008, MNRAS, 386, 261
Oliveira, J. M., Jeffries, R. D., & van Loon, J. T. 2004, MNRAS, 347, 1327
Peña Ramírez, K., Zapatero Osorio, M. R., Béjar, V. J. S., Rebolo, R., & Bihain, G. 2011, ArXiv e-prints
Pety, J., Teyssier, D., Fossé, D., et al. 2005, A&A, 435, 885
Pound, M. W., Reipurth, B., & Bally, J. 2003, AJ, 125, 2108
Reipurth, B., Bally, J., Fesen, R. A., & Devine, D. 1998, Nat, 396, 343
Rigliaco, E., Natta, A., Randich, S., et al. 2011, A&A, 526, L6
Sacco, G. G., Franciosini, E., Randich, S., & Pallavicini, R. 2008, A&A, 488, 167

Scholz, A. & Eislöffel, J. 2004, A&A, 419, 249
Sherry, W. H., Walter, F. M., & Wolk, S. J. 2004, AJ, 128, 2316
Sherry, W. H., Walter, F. M., Wolk, S. J., & Adams, N. R. 2008, AJ, 135, 1616
Skinner, S. L., Sokal, K. R., Cohen, D. H., et al. 2008, ApJ, 683, 796
Tej, A., Sahu, K. C., Chandrasekhar, T., & Ashok, N. M. 2002, ApJ, 578, 523
Townsend, R. H. D., Owocki, S. P., & Groote, D. 2005, ApJ Lett., 630, L81
Walborn, N. R. 1974, ApJ Lett., 191, L95
Walter, F. M., Sherry, W. H., Wolk, S. J., & Adams, N. R. 2008, in Handbook of Star Forming Regions, Volume I, ed. Reipurth, B. (ASP Monograph Publications), 732–+
Wolk, S. J. 1996, PhD thesis, Harvard–Smithsonian Center for Astrophysics Cambridge, Massachusetts, USA
Zapatero Osorio, M. R., Béjar, V. J. S., Martín, E. L., et al. 2000, Sci, 290, 103
Zapatero Osorio, M. R., Caballero, J. A., Béjar, V. J. S., et al. 2007, A&A, 472, L9

3.8 Dynamical state of Westerlund 1

Michiel Cottaar[1], M. R. Meyer[1], M. Andersen[2], and P. Espinoza[3]

[1] Institute for Astronomy, ETH Zurich
[2] European Space Agency, RSSD, ESTEC
[3] Steward Observatory, University of Arizona

Abstract

Using high resolution optical spectroscopy (R = 53.000) we constrain the dynamical state of Westerlund 1, perhaps the most massive Population I cluster in the Milky Way. Our goal is to understand whether massive clusters such as Westerlund 1 emerge bound or whether they will disperse and contribute significantly to the field star population. The cluster also serves as a template for young extragalactic star clusters. We have obtained 64 optical spectra of a sample of 22 stars in Westerlund 1 using the MIKE spectrograph on the Magellan Clay telescope. All of the stars were observed for two or three epochs to allow us to check for the presence of short period equal mass binaries which can substantially affect the observed single epoch velocity dispersion. We are left with a sample of ten stars, after removing stars showing large variability and early-type stars for which we do not obtain the necessary precision in the radial velocity. We find that these stars are consistent with being drawn from a velocity distribution characterized by a sigma of $3.5^{+1.8}_{-0.5}$ km/s. After correcting for possible mass segregation and the effect of undetected binaries this corresponds to a dynamic mass of Westerlund I of $3^{+5}_{-3} \times 10^4$ $M_\odot$, compared to a NIR photometric mass estimate of $4.9^{+1.8}_{-0.5} \times 10^4$ $M_\odot$. This dynamic mass implies that Westerlund 1 is not strongly supervirial and is thus not expanding into the field.

Introduction

In the first few Myr of the lifetime of a star cluster the winds of the massive stars or the first supernova can remove the gas out of which the cluster formed. This weakens the potential well in which the stars reside, causing the cluster to expand or even become unbound, if the stars were initially in virial equilibrium with their surroundings (Hills [1980]; Goodwin & Bastian [2006]). The efficiency of gas expulsion to disrupt clusters depends on several variables, including the star formation efficiency, the distribution of the remaining gas with respect to the stars and whether the stars have achieved virial equilibrium with the potential of the surrounding gas before the gas is ejected. Kruijssen (these proceedings) argues that effective accretion in the subclusters in which star clusters may form might cause very little gas to be left locally, even while the star formation efficiency over the total cluster is much lower. In such a scenario the gas expulsion would have little effect on the evolution of the star cluster, but clusters could still dissolve due to external perturbation, stellar evolution mass loss, and two-body interactions. This is supported observationally by Bastian (these proceedings), who points out the difficulty of distinguishing clusters and associations in extragalactic clusters. Using a conservative definition of a cluster, they found little evidence of "infant mortality" in the first 10 Myr of a star cluster, with which the gas expulsion discussed above is often associated. However, different methods to identify extra-galactic clusters lead to different conclusions (see Chandar et al. [2010]).

An excellent target to test the importance of gas expulsion is the young, massive Galactic cluster Westerlund 1. Photometric observations with the NTT/SOFI in the JHKs bands (Brandner et al. [2008]; Gennaro et al. [2011]; Gennaro, these proceedings) show an elongated cluster with a mass of $4.9^{+1.8}_{-0.5} \times 10^4$ $M_\odot$, a half mass radius $r_{\rm hm} = 1.1$ pc, a distance of 4 ± 0.2 kpc (also see Kothes & Dougherty [2007]), and an age of $4.5 - 5$ Myr (also see Crowther et al. [2006]). This makes it perhaps the most massive young cluster known in the Milky Way. Westerlund 1 has only recently expelled the remnants of the molecular cloud out of which it formed, so by determining the dynamical state of Westerlund 1, we can hope to constrain the effect of the gas expulsion on this young, massive cluster.

Here we present multi-epoch high-resolution spectroscopy to find the velocity dispersion of Westerlund 1. By measuring the velocities over 2-3 epochs over a baseline of one year, we are able to correct

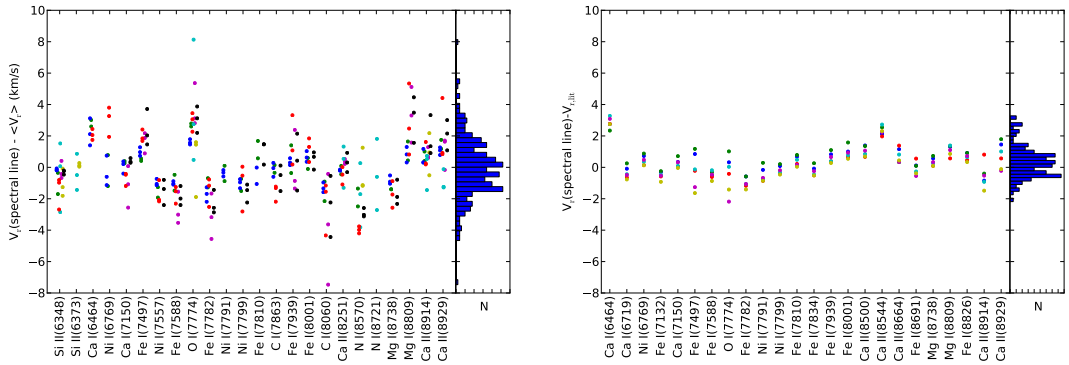

Figure 3.18: *Left*: The offsets from the radial velocities measured for individual spectral features to the averaged velocity for every epoch of every yellow hypergiant and the LBV, namely Wd1 8a (blue) Wd1 32 (green), Wd1 4 (red), Wd1 16a (cyan), Wd1 12a (magenta), Wd1 243 (yellow), Wd1 265 (black). *Right*: The offsets from the measured radial velocities to the literature value of the standard stars HD 120223 (blue), HD 193231 (green), HD 196983 (red), HD203638 (cyan), and two epochs of HD 223311 (magenta and yellow). In both figures the x-axis gives the ion and the rest wavelength in Å of the spectral line. In the case of a multiplet only the first spectral line is given.

for the presence of binaries.

Observations

Observations were made using the MIKE spectrograph located on the Magellan Clay telescope at the Las Campanas Observatory in June 2009, August 2009 and July 2010. At a resolution of 53.000 in the red we observed 22 targets of the brightest spectroscopically confirmed members ($I < 14.7$ mag), which were selected from Clark et al. [2005]. These stars include two of the four red supergiants, all six supergiants, a sgB[e] star, a LBV in its cool phase and 12 OB-supergiants. All targets were observed for 2 or 3 epochs.

The spectra were reduced with the MIKE Redux pipeline[8] with some minor adjustments. The wavelength calibration was tested by measuring the shift of telluric lines with respect to the NSO telluric spectrum. We find that the wavelength calibration is accurate to a level of at least 230 m/s.

Results

We measure the radial velocities of the stars by fitting Gaussians to spectral lines and comparing the measured line centres with the rest wavelengths in the NIST-database (Ralchenko et al. [2010]). The fitted spectral lines do not show up as close blends in synthetic spectra. If the spectral lines lie in a multiplet, where the line centres are still separated, we fit the lines simultaneously, enforcing the same velocity for all lines (e.g. the O I triplet at 7774 Å). Average radial velocities using all measurable lines and the respective standard deviation of the mean were calculated for the individual epochs.

When comparing the radial velocities measured for individual spectral lines with the average radial velocity for a total spectrum, we find that the offsets are of a systematic, rather than random nature. This is visible in Fig. 3.18(left), where the offsets of the measured radial velocity to the mean radial velocity are plotted for all epochs of the six yellow hypergiants and the luminous blue variable Wd1 243, which is currently in its cool phase. This figure shows that radial velocity measured for some spectral features (e.g. the O I triplet at 7774 Å) are consistently redshifted, while other features consistently give a lower radial velocity than average. These systematic offsets could have several origins, such as undetected close blends, or stratification in the atmospheres (Verschueren et al. [1999]; Griffin et al. [2000]).

[8]The MIKE Redux pipeline was written by S. M. Burles, J. X. Prochaska and R. Bernstein in IDL (http://web.mit.edu/ burles/www/).

We find similar systematic offsets for the radial velocity standards in Fig. 3.18(right) when we compare the radial velocities measured from individual spectral lines to the literature value (Udry et al. [1999]). However, we find that for the radial velocity standards the averaged radial velocities are close to the literature values of Udry et al. [1999] within 0.5 km/s. This gives us confidence that the averaged radial velocities are a good representation of the true radial velocities for the super- and hypergiants.

The measured velocities of these yellow hypergiants and the other post-main sequence stars have been summarized in Table 3.3. The last column gives the largest velocity difference for a star between two epochs, calculated as an average of velocity differences computed on a line-by-line basis. This velocity difference can be measured to a higher accuracy than the absolute velocity, because the systematic effects discussed above remain the same between epochs and thus cancel out. As we can see in this last column nearly all stars show radial velocity variations at the 3 sigma level, either due to binarity or due to atmospheric instabilities.

Table 3.3: The observed stars with the id of the star from Clark et al. [2005], its spectral type (Negueruela et al. [2010]; Clark et al. [2010]), the average velocities over all epochs with the internal and external velocity dispersion and finally the largest velocity difference between epochs with uncertainty.

id	spec. type	velocity	σ_i	σ_e	$\Delta \mathrm{v}_\mathrm{max}$
56	B0 Ia	Insufficient lines			
13	B0.5 Ia	Spectroscopic binary			
238	B1 Iab	Insufficient lines			
23a	B2 Ia	Insufficient lines			
2a	B2 Ia	Insufficient lines			
11	B2 Ia	Insufficient lines			
28	B2 Ia	Insufficient lines			
71	B2.5 Ia	-49.7	1.6	8.7	11.8 ± 0.9
70	B3 Ia	-53.5	1.0	8.9	13.0 ± 1.4
57a	B4 Ia	-53.7	1.8	2.1	5.2 ± 0.8
33	B5 Ia+	-48.2	1.8	7.3	14.5 ± 0.9
7	B5 Ia+	-46.3	1.8	4.0	6.7 ± 1.4
16a	A5 Ia+	-37.7	1.0	4.5	8.1 ± 0.5
243	LBV	-43.5	0.8	1.2	1.5 ± 0.4
9	sgB[e]	-31.8	1.7	2.1	1.2 ± 0.7
12a	F1 Ia+	-43.6	1.0	0.8	1.9 ± 0.5
4	F3 Ia+	-46.5	0.6	2.6	4.6 ± 0.4
265	F1-5 Ia+	-47.3	0.6	1.7	2.6 ± 0.5
32	F5 Ia+	-48.2	0.4	2.1	3.3 ± 0.2
8a	F8 Ia+	-44.9	0.3	0.9	1.8 ± 0.2
237	M3 Ia	No consistent velocity between lines			
26	M5-6 Ia	-45.2	4.5	5.0	2.0 ± 0.5

For ten of these stars the radial velocity variations are small enough that we can expect them to not significantly influence the measured velocity dispersion ($\sigma \leq 5$ km/s, excluding the four sigma outlier Wd1 9). Due to the small number of stars in our sample we will have a large statistical uncertainty in the measured velocity dispersion. To calculate this statistical uncertainty we calculate the likelihood that the observed distribution would have been drawn from a cluster with a Gaussian radial velocity distribution with standard deviation σ_v and mean μ:

$$P(\sigma_\mathrm{v}, \mu) = \prod_j \frac{1}{\sqrt{2\pi(\sigma_\mathrm{v}^2 + \sigma_i^2)}} \exp\left(-\frac{(v_j - \mu)^2}{2(\sigma_\mathrm{v}^2 + \sigma_j^2)}\right), \tag{3.4}$$

where v_i is the observed velocity of the star and σ_j is the maximum of the internal and external standard deviation. The likelihood that a distribution with a given velocity dispersion would give the observed velocities is calculated by integrating over μ, while for the chance for a given average velocity we integrate

over σ_v. Assuming that the velocities were indeed drawn from a Gaussian distribution, maximum likelihood estimation then gives $\sigma = 3.5^{+1.8}_{-0.5}$ km/s and $\mu = -46.2 \pm 1.3$ km/s for the massive stellar population in Westerlund 1. Note that this velocity dispersion is very similar to the value we would have gotten by taking the variance of the measured velocities and subtracting the variance expected due to the uncertainties in the measured velocity, which gives $\sigma = 3.6$ km/s. These two methods would give the exact same velocity dispersion, if the uncertainties in the measured radial velocities were all the same. This velocity dispersion is much lower than the one previously found from NIR radial velocity measurements from Mengel & Tacconi-Garman [2009], perhaps because they did not consider the presence of binaries.

Undetected binaries with a period of a few years can inflate our estimate of the velocity dispersion as well. So our value should be considered an upper bound. Due to the possible presence of mass segregation (Gennaro et al. [2011]) the velocity dispersion for the massive stars measured above might not be representative of the velocity dispersion of the cluster as a whole (Fleck et al. [2006]). When we compare the distribution of massive stars from which our sample was drawn (Clark et al. [2005]) to that of the total cluster, we find that in virial equilibrium the velocity dispersion of the total population is 6% larger than for the subset of massive star using a two-fluid approximation ([Eq. 7.158 in Binney & Tremaine, 2008]). So for the total population of Westerlund 1 we find a velocity dispersion of $\sigma = 3.7^{+1.9}_{-3.7}$ km/s.

Discussion

To identify whether Westerlund 1 is in virial equilibrium we will still need the radius of the cluster. NIR photometry of Westerlund 1 (Gennaro et al. [2011]) shows that the cluster is significantly elongated with the effective radius along the Galactic plane 1.5 times larger than perpendicular to the Galactic plane. The half-mass radius is roughly 1.1 pc (Brandner et al. [2008]). If we make the assumption that the cluster is not much more elongated along the line of sight, the effective half-mass radius could vary between 0.9 and 1.3 pc. With this we can finally calculate the dynamical mass of Westerlund 1 to be

$$M_{\rm dyn} = \eta \frac{\sigma_{\rm 1D}^2 r_{\rm hm}}{G} = 3^{+5}_{-3} \times 10^4 M_\odot, \tag{3.5}$$

where G is the graviational constant, $\eta = 32/\pi$ for a Plummer sphere, $\sigma_{\rm 1D}$ is the 1-dimensional (e.g. radial) velocity dispersion and $0.9 < r_{\rm hm} < 1.3$ pc. is the half-mass radius of the cluster (Portegies Zwart et al. [2010]). For the higher mass estimate of 1.5×10^5 $M_\odot$ from Negueruela et al. [2010], we find that the cluster is subvirial or virial even at the 95% confidence limit ($M_{\rm dyn} < 1.3 \times 10^5$ $M_\odot$). For the lower mass estimate of Gennaro et al. [2011] of $M_{\rm Wd1} = 4.9^{+1.8}_{-0.5} \times 10^4$ $M_\odot$, the cluster might be slightly supervirial, although a subvirial or virial solution is more likely.

This nearly virial (or even subvirial) state of Westerlund 1 implies that the cluster is not currently expanding and that the cluster has survived any recent gas expulsion. A caution is that the uncertainties are quite severe, especially in the measured velocity dispersion, which enters quadratically in Eq. 3.5. Since the uncertainty in the measured radial velocity is dominated by a statistical error, this can be reduced in the future by increasing the sample size with other single stars, or determine the system velocity of the binaries by long-term many-epoch surveys (see Ritchie et al. [2009, 2010]; Clark et al. [2011]; Negueruela, these proceedings; for such a long-term survey).

Bibliography

Binney, J. & Tremaine, S. 2008, Galactic Dynamics: Second Edition, ed. Binney, J. & Tremaine, S. (Princeton University Press)
Brandner, W., Clark, J. S., Stolte, A., et al. 2008, A&A, 478, 137
Chandar, R., Whitmore, B. C., & Fall, S. M. 2010, ApJ, 713, 1343
Clark, J. S., Negueruela, I., Crowther, P. A., & Goodwin, S. P. 2005, A&A, 434, 949
Clark, J. S., Ritchie, B. W., & Negueruela, I. 2010, A&A, 514, A87+
Clark, J. S., Ritchie, B. W., Negueruela, I., et al. 2011, A&A, 531, A28+
Crowther, P. A., Hadfield, L. J., Clark, J. S., Negueruela, I., & Vacca, W. D. 2006, MNRAS, 372, 1407
Fleck, J., Boily, C. M., Lançon, A., & Deiters, S. 2006, MNRAS, 369, 1392
Gennaro, M., Brandner, W., Stolte, A., & Henning, T. 2011, MNRAS, 412, 2469
Goodwin, S. P. & Bastian, N. 2006, MNRAS, 373, 752
Griffin, R. E. M., David, M., & Verschueren, W. 2000, A&AS, 147, 299

Hills, J. G. 1980, ApJ, 235, 986
Kothes, R. & Dougherty, S. M. 2007, A&A, 468, 993
Mengel, S. & Tacconi-Garman, L. E. 2009, Ap&SS, 324, 321
Negueruela, I., Clark, J. S., & Ritchie, B. W. 2010, A&A, 516, A78+
Portegies Zwart, S. F., McMillan, S. L. W., & Gieles, M. 2010, ARA&A, 48, 431
Ralchenko, Y., Kramida, A. E., Reader, J., & NIST ASD Team. 2010, NIST Atomic Spectra Database (ver. 4.0.1), online, http:/physics.nist.gov/asd. National Institute of Standards and Technology, Gaithersburg, MD.
Ritchie, B. W., Clark, J. S., Negueruela, I., & Crowther, P. A. 2009, A&A, 507, 1585
Ritchie, B. W., Clark, J. S., Negueruela, I., & Langer, N. 2010, A&A, 520, A48+
Udry, S., Mayor, M., Maurice, E., et al. 1999, in Astronomical Society of the Pacific Conference Series, Vol. 185, IAU Colloq. 170: Precise Stellar Radial Velocities, ed. J. B. Hearnshaw & C. D. Scarfe, 383–+
Verschueren, W., David, M., & Griffin, R. E. M. 1999, A&AS, 140, 107

3.9 Dynamical Evolution of Stellar Clusters

Mark Gieles[1]

[1] Institute of Astronomy, University of Cambridge, Madingley Road, Cambridge, CB3 0HA, UK

Abstract

The evolution of star clusters is determined by several internal and external processes. Here we focus on two dominant internal effects, namely energy exchange between stars through close encounters (two-body relaxation) and mass-loss of the member stars through stellar winds and supernovae explosions. Despite the fact that the former operates on the relaxation timescale of the cluster and the latter on a stellar evolution timescale, these processes work together in driving a nearly self-similar expansion, without forming (hard) binaries. Low-mass clusters expand more, such that after some time the radii of clusters depend very little on their masses, even if all clusters have the same (surface) density initially. Throughout it is assumed that star clusters are in virial equilibrium and well within their tidal boundary shortly after formation, motivated by observations of young ($\sim$ few Myr) clusters. We start with a discussion on how star clusters can be distinguished from (unbound) associations at these young ages.

Introduction

Ambartsumian [1947] introduced the term association in reference to loose agglomerates and he pointed out in subsequent studies that it is unlikely that they are bound by their own gravity (see also Blaauw [1964]). It is often stated that the majority of stars form in star clusters and that there is a high rate of early cluster disruption (e.g. Lada & Lada [2003]). In this view associations are clusters that have expanded. But if the star formation process is hierarchical then only a small fraction of the newborn stars reside in agglomerates that satisfy the conditions necessary to be bound by self-gravity at formation (e.g. Kravtsov & Gnedin [2005]; Elmegreen [2008]; Bressert et al. [2010]). When observational samples of star clusters are used to support either one of the above scenarios it is vital to know how star clusters are separated from associations (Bastian et al. [2011]). Here we provide a definition of the distinction between these two classes of stellar agglomerates (see next Section). In Section *N-body simulations of star clusters* we present results of N-body simulations of star clusters including the effect of stellar evolution.

The distinction between star clusters and associations

To illustrate our case we use the recent literature compilation of young massive clusters and associations of Portegies Zwart et al. [2010, hereafter PZMG10]. This sample consists of stellar agglomerates for which a value of the half-light radius $r_{\rm eff}$, mass M, and age t are available in literature. The sample contains 105 agglomerates with $M \gtrsim 10^4\,{\rm M}_\odot$ and $t \lesssim 100\,{\rm Myr}$ in nearby ($\lesssim 10\,{\rm Mpc}$) galaxies, including the Milky Way. The ratio of the age over the crossing time, $\Pi = t/t_{\rm cr}$, can be used to separate star clusters from associations [PZMG10; Gieles & Portegies Zwart, 2011]. Objects that are older than their crossing time ($\Pi > 1$) are most likely bound star clusters, whereas objects with $\Pi < 1$ are expected to be unbound associations. The crossing time is defined in terms of empirical cluster parameters

$$t_{\rm cr} \equiv 10 \left(\frac{r_{\rm eff}^3}{GM} \right)^{1/2}, \tag{3.6}$$

where $G \simeq 4.5 \times 10^{-3}\,{\rm pc^3\,M_\odot}^{-1}\,{\rm Myr}^{-2}$ is the gravitational constant. Eq. 3.6 is valid for systems in virial equilibrium, because the formal definition includes the root-mean square velocity dispersion: $t_{\rm cr} \propto r_{\rm eff}/\sigma$ and in virial equilibrium $\sigma \propto \sqrt{M/r_{\rm eff}}$. However, σ values are available for fewer agglomerates and at young ages the empirically determined σ can be higher because of orbital motions of multiples (Gieles et al. [2010b]). Surprisingly, the more convenient Eq. 3.6 fascilites in making the distinction between bound and unbound objects. Because super-virial associations expand with a (roughly) constant velocity,

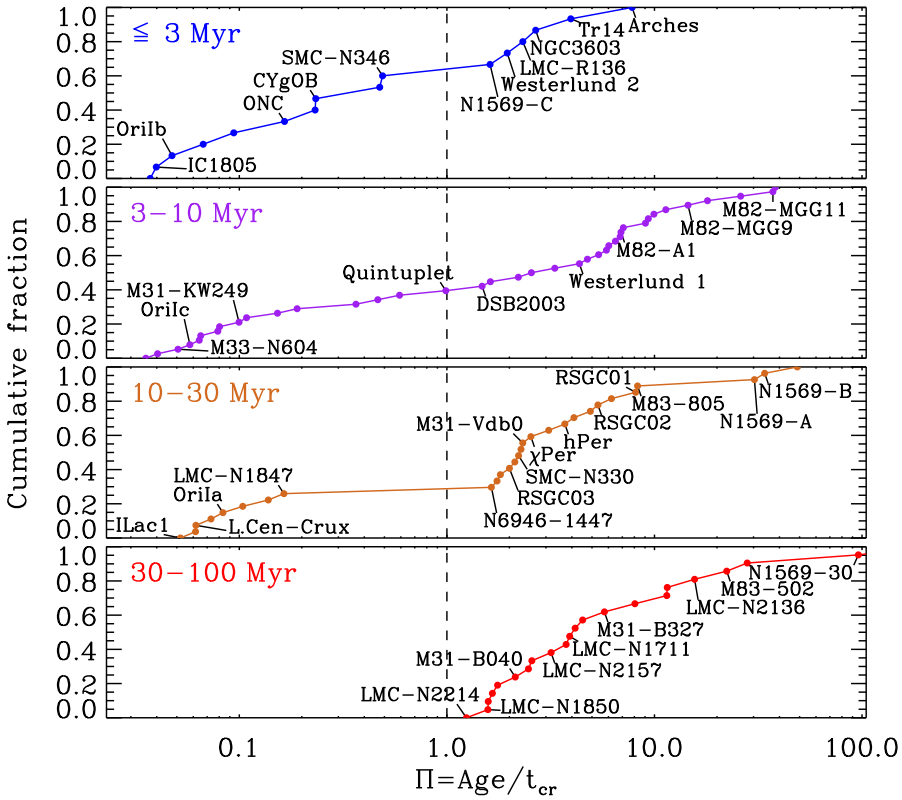

Figure 3.19: Cumulative distribution of Π values for nearby ($\lesssim 10$ Mpc) agglomerates in different age bins. The vertical dashed line indicates the value $\Pi = 1$ that separates star clusters from associations. From Gieles & Portegies Zwart [2011].

their crossing evolves as $t_{\rm cr} \propto r_{\rm eff} \propto t$. Using Eq. 3.6 for super-virial objects, therefore, overestimates $t_{\rm cr}$ and underestimates Π, thereby pushing them more into the unbound regime.

In Fig. 3.19 we show the cumulative distribution of Π values of all objects in different age bins. The top panel shows that the youngest age bin is a continuous distribution from associations with $\Pi \sim 0.03$ to star clusters with $\Pi \sim 10$. There seems not to be a distinct mode of star cluster formation, but rather a smooth transition from star clusters to associations. Bressert et al. [2010] come to a similar conclusion based on the surface density distribution of young stellar objects in the solar neighbourhood.

The bottom panel shows that the oldest agglomerates all have $\Pi \gtrsim 1$ and these are, therefore, star clusters. The intermediate age curves contain both associations and star clusters. If we interpret the curves for the different age bins as an evolutionary sequence then a distinct gap develops between star clusters and associations around ~ 10 Myr at a value of $\Pi \simeq 1$. At older ages an observer should be able to make an unambiguous distinction between an (unbound) association and a (bound) star cluster using this straight-forward method.

For the youngest (continuous) distribution a useful first order separation can still be made at a value of $\Pi = 1$, as can be noted from the labels of several well known star clusters and associations. Independent confirmation comes from recent determinations of velocity dispersions of (resolved) young ($\sim 1 - 2$ Myr) star clusters. For NGC 3603 (Rochau et al. [2010]), Westerlund 1 (Mengel & Tacconi-Garman [2007]; and M. Cottaar in these proceedings) and R136 in 30 Doradus (Bosch et al. [2009]; Hénault-Brunet in prep.) it was found that the dynamical mass estimates agree very well with the photometric masses, suggesting that these clusters are in virial equilibrium and stable (i.e. bound). This is also what their Π values suggest (see Fig. 3.19). In the next section we consider the dynamical evolution of such star clusters.

N-body simulations of star clusters

We want to understand the evolution of a stellar cluster with a realistic stellar mass function in which the stars evolve and lose mass in time (Gieles et al. [2010a]; hereafter G10). Because most young star clusters

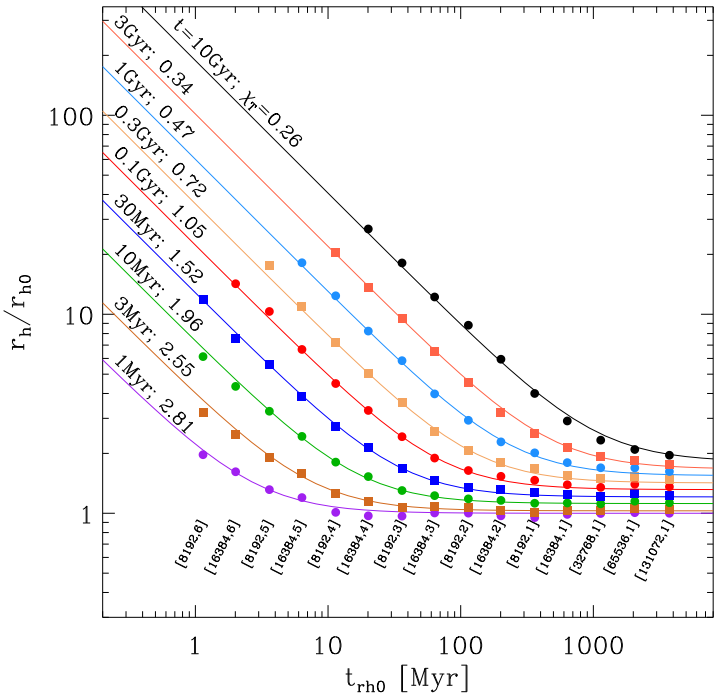

Figure 3.20: Expansion from the N-body runs including the effect of stellar evolution. The full lines show a functional description that is used to evolve the inital mass-radius relation in Figs. 3.21 and 3.22 (see G10 for more details).

are very deeply embedded in their tidal limit (see e.g. Harayama et al. [2008] and Gennaro et al. [2011] for the cases of NGC 3603 and Westerlund 1, respectively) we ignore the effect of a tidal cut-off. The transition from expansion-dominated evolution to tidally limited evolution is considered in more detail elsewhere (Gieles et al. [2011]).

We model clusters with initial half-mass relaxation timescales ranging from $t_{\rm rh0} \simeq 1\,$Myr to $t_{\rm rh0} \simeq 4\,$Gyr by considering different combinations of $[N, \log \rho_{\rm h}]$ at the start of the simulation. The stars follow a Kroupa [2001] initial mass function between $0.1\,{\rm M}_\odot$ and $100\,{\rm M}_\odot$. We use the `kira` integrator and the stellar evolution package `SeBa` for solar metallicity (Portegies Zwart et al. [2001]). The retention fraction of black holes and neutron stars was set to zero.

In Fig. 3.20 we show how $r_{\rm h}/r_{\rm h0}$ increases with time as a function of $t_{\rm rh0}$. The asymptotic behaviour of these results can easily be understood by considering the extremes. Clusters that are dynamically young (low $t/t_{\rm rh0}$) expand adiabatically in order to retain virial equilibrium after stellar mass loss. This adiabatic expansion is slow in time and gives a maximum increase of $r_{\rm h}/r_{\rm h0} \simeq 2$ after a Hubble time. At the other extreme we have clusters that are dynamically old (high $t/t_{\rm rh0}$) and they expand in a way that is comparable to what is found for equal-mass clusters in the sense that all clusters evolve towards the same $t_{\rm rh}$.

We conclude that the energy that is released to the core of the cluster as a result of stellar mass-loss acts as a central energy source that is in 'balance' with the energy that is driven outwards by 2-body relaxation, without the need of forming binaries in the core. One of the consequences of this interplay between stellar evolution and dynamical relaxation is that there is no sharp transition between a stellar evolution dominated phase and a relaxation dominated phase.

Comparing the theory to observations

With the expression for the evolution of the radius as a function of $t_{\rm rh0}$ at hand (equation 6 in G10) we can easily calculate the evolution of any initial mass-radius relation. We first apply the results to the sample of young objects discussed in the previous section.

In Fig. 3.21 we show mass-radius diagrams for all objects for two age ranges: $< 10\,$Myr (left panel) and $10 - 100\,$Myr (right panel). The dashed lines in the left panel are lines of constant (arbitrary) $\rho_{\rm h}$. In the right panel we have evolved these lines to an age of 100 Myr. These lines are lower limits to the radius

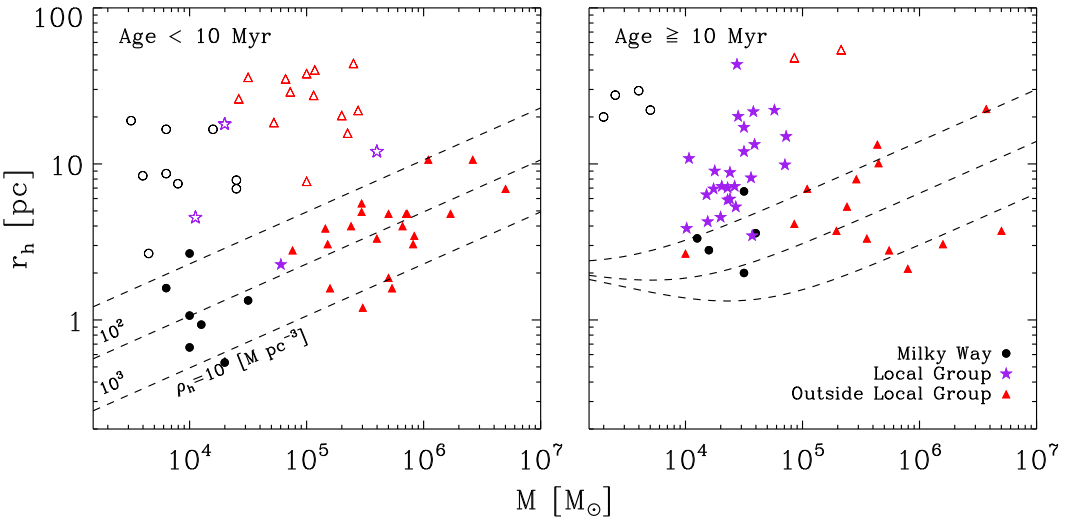

Figure 3.21: Mass-radius relation for all clusters (filled symbols) and associations (open symbols) from PZMG10, using $r_{\rm h} = (4/3)r_{\rm eff}$. Lines of constant half-mass density, $\rho_{\rm h} \equiv 3M/(8\pi r_{\rm h}^3)$, are over-plotted. The clusters are subdivided into two groups: younger than 10 Myr (left) and between 10 Myr and 100 Myr (right). There is a lack of compact ($\lesssim 2$ pc) and low-mass ($\lesssim 10^4\,{\rm M}_\odot$) clusters in the older bin due to dynamical expansion.

at the left-side of this diagram. There are indeed no compact ($\lesssim 2$ pc) low-mass ($\lesssim 10^4\,{\rm M}_\odot$) clusters in this age bin.

Next we apply our result to the mass-radius relation of old stellar systems in the mass range $\sim 10^4 - 10^8\,{\rm M}_\odot$. In Fig. 3.22 we show how a Faber-Jackson type initial mass-radius relation (Haşegan et al. [2005]) evolves in time together with data points of (old) globular clusters and ultra-compact dwarfs (UCDs) in different galaxies that cover the mass regime we are interested in. For high $t/t_{\rm rh0}$ the radius is

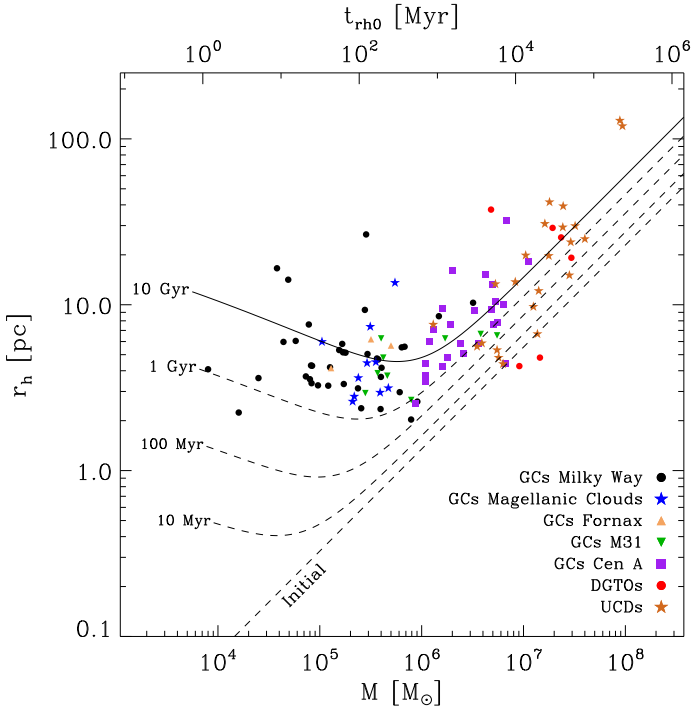

Figure 3.22: Mass-radius values for hot stellar systems (see G10 for more details on the data). The lines show the evolution of the mass-radius relation. The break at $\sim 10^6\,{\rm M}_\odot$ at 10 Gyr is because lower mass objects have expanded.

set by M_0, independent of $r_{\rm h0}$, while for low $t/t_{\rm rh0}$ we are seeing roughly the initial mass-radius relation. At an age of 10 Gyr the break between the two regimes occurs at $M_0 \simeq 10^6\,{\rm M}_\odot$ and at that age systems with this mass have $t_{\rm rh}/t \simeq 0.8$. Mieske et al. [2008] noticed already that the break occurs at systems with $t_{\rm rh}$ roughly equal to a Hubble time. Here we give a quantitative explanation for it.

We conclude that the evolution of almost all (old) globular clusters is 'balanced', in the sense that the rate of central energy production equals the flow of energy due to 2-body relaxation[9]. An important property of this 'balanced' evolution is that the half-mass radius is independent of its initial value and is a function of the number of stars and the age only. It is therefore not possible to infer the initial mass-radius relation of globular clusters, and we can only conclude that the present day properties are consistent with the hypothesis that all hot stellar systems formed with the same mass-radius relation and that globular clusters have moved away from this relation because of a Hubble time of stellar and dynamical evolution.

Bibliography

Ambartsumian, V. A. 1947, Stellar Evolution and Astrophysics (Armenian Acad. of Sci.); German translation, Abhandl. Sowjetischen Astron. Ser. 1, 33, (1951)
Bastian, N., Adamo, A., Gieles, M., et al. 2011, MNRAS, in press (ArXiv:1106.2427)
Blaauw, A. 1964, ARA&A, 2, 213
Bosch, G., Terlevich, E., & Terlevich, R. 2009, AJ, 137, 3437
Bressert, E., Bastian, N., Gutermuth, R., et al. 2010, MNRAS, 409, L54
Elmegreen, B. G. 2008, ApJ, 672, 1006
Gennaro, M., Brandner, W., Stolte, A., & Henning, T. 2011, MNRAS, 412, 2469
Gieles, M., Baumgardt, H., Heggie, D. C., & Lamers, H. J. G. L. M. 2010a, MNRAS, 408, L16 (G10)
Gieles, M., Heggie, D. C., & Zhao, H. 2011, MNRAS, 413, 2509
Gieles, M. & Portegies Zwart, S. F. 2011, MNRAS, 410, L6
Gieles, M., Sana, H., & Portegies Zwart, S. F. 2010b, MNRAS, 402, 1750
Haşegan, M., Jordán, A., Côté, P., et al. 2005, ApJ, 627, 203
Harayama, Y., Eisenhauer, F., & Martins, F. 2008, ApJ, 675, 1319
Kravtsov, A. V. & Gnedin, O. Y. 2005, ApJ, 623, 650
Lada, C. J. & Lada, E. A. 2003, ARA&A, 41, 57
Mengel, S. & Tacconi-Garman, L. E. 2007, A&A, 466, 151
Mieske, S., Hilker, M., Jordán, A., et al. 2008, A&A, 487, 921
Portegies Zwart, S., McMillan, S. L. W., Hut, P., & Makino, J. 2001, MNRAS, 321, 199
Portegies Zwart, S. F., McMillan, S. L. W., & Gieles, M. 2010, ARA&A, 48, 431 (PZGM10)
Rochau, B., Brandner, W., Stolte, A., et al. 2010, ApJ, 716, L90

[9]We deliberately avoid the term 'post-collapse' evolution because core-collapse is not required for the evolution to be 'balanced', see the discussion in Gieles et al. [2011]

3.10 NIR View on Young Stellar Clusters in Nearby Spirals

Preben Grosbøl[1] **and H. Dottori**[2]

[1] European Southern Observatory, Garching, Germany
[2] Instituto de Física, Univ. Federal do Rio Grande do Sul, Porto Alegre, RS, Brazil

Abstract

Observations in the near-infrared (NIR) allow a detailed study of young stellar clusters in grand-design spiral galaxies which in visual bands are often highly obscured by dust lanes along the arms. Deep JHK-maps of 10 spirals were obtained with HAWK-I/VLT. Data for NGC 2997 are presented here to illustrate the general results for the sample.
The (H-K)–(J-H) diagrams suggest that most stellar clusters younger than 7 Myr are significantly attenuated by dust with visual extinctions reaching 7 mag. A gap between younger and older cluster complexes in the (J-K)–M_K diagram indicates a rapid reduction of extinction around 7 Myr possibly due to expulsion of dust and gas after supernovae explosions. The cluster luminosity function is consistent with a power law with an exponent $\alpha \approx 2$. Cluster luminosities of $M_K = -15$ mag are reached, corresponding to masses close to $10^6\,M_\odot$, with no indication of a cut-off. Their azimuthal angles relative to the main spiral arms show that the most massive clusters are formed in the arm regions while fainter ones also are seen between the arms. Older clusters are more uniformly distributed with a weaker modulation relative to the arms.

Introduction

Many grand-design spirals have strings of knots along their arms on NIR maps. Such knots have been identified as complexes of very young stellar clusters (Grosbøl et al. [2006]) which may have been triggered by a star-formation front associated with a spiral density wave (Lin & Shu [1964]; Roberts [1969]). The usage of NIR bands for the analysis of clusters provides two main advantages: a much more complete census of young clusters, often embedded in dust lanes, and age estimates for clusters younger than 7 Myr.

A sample of 10 grand-design, spiral galaxies with a range of Hubble types were selected from the study by Grosbøl & Dottori [2008] and observed in the NIR to study possible relations between spiral perturbations and star formation. In this paper, we will only present results for NGC 2997 as a representative for the full sample.

Data

Deep maps of the galaxies were obtained in JHK-bands with the HAWK-I/VLT instrument which provides a 7 arcmin field with 0.1 arcsec pixels. NGC 2997 is classified as Sc(s)I.3 and has an oval distortion in its central parts outside which a grand-design, two-armed spiral structure with a pitch angle of 21 deg is seen. Its distance was assumed to be 19.2 Mpc derived from its velocity relative to the 3K-CMB and a Hubble constant of 73 km/s/Mpc. The reduced, stacked images had a seeing of 0.4 arcsec which translates to a linear resolution of ≈ 40 pc at the distance of NGC 2997.

More than 5300 sources were identified on the K-band image of NGC 2997 using *SExtractor* (Bertin & Arnouts [1996]). The photometric zero points were established through the 2MASS photometry (Skrutskie et al. [2006]) of foreground stars in the field. The limiting magnitude was estimated to $K_l = 20.1$ mag (i.e. M_K = -11.3 mag) for 90% completeness depending on the local crowding. Individual stellar clusters cannot be resolved with the resolution of 40 pc making it likely that many non-stellar sources are complexes of clusters or star-forming regions.

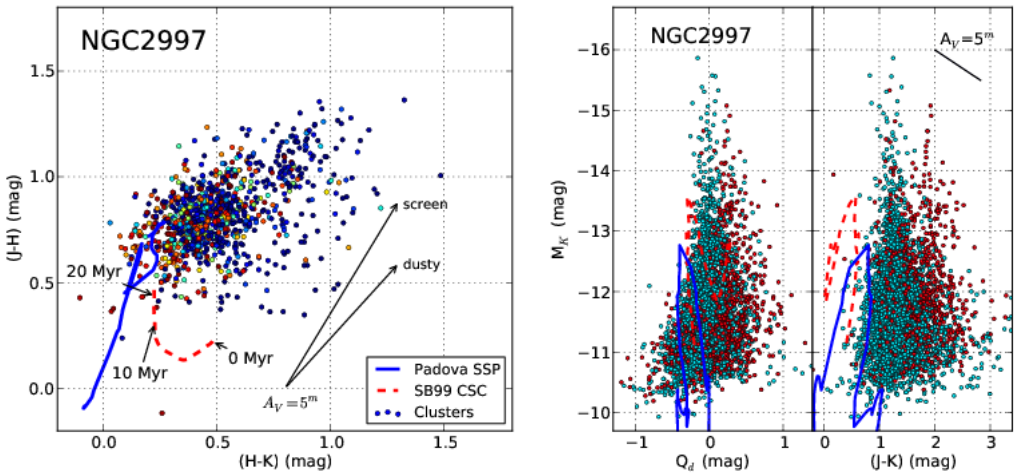

Figure 3.23: Colour-colour and colour-magnitude diagrams for non-stellar sources in NGC 2997.

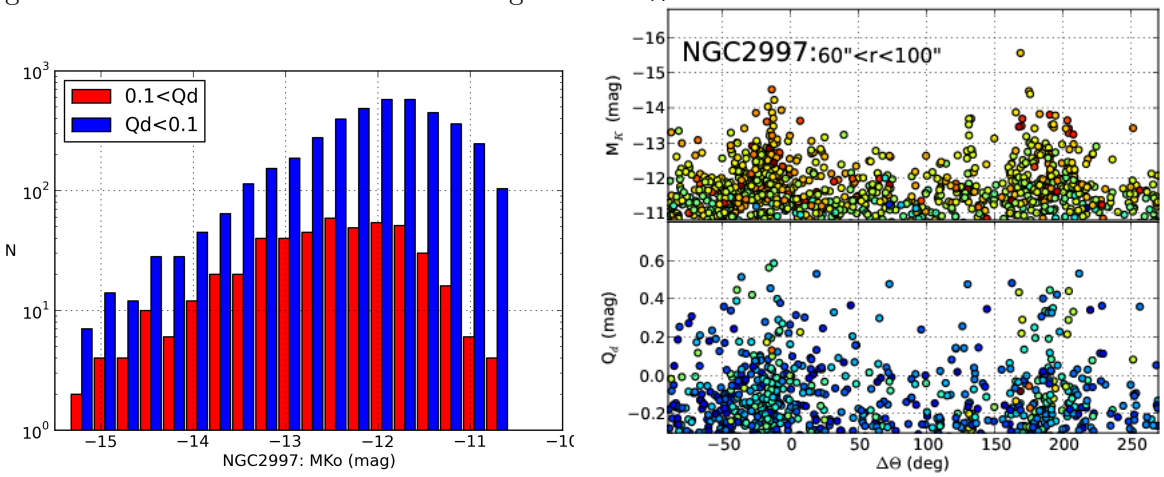

Figure 3.24: Luminosity function (left) and azimuthal distribution relative to the main two-armed spiral in the radial region 60 – 100 arcsec (right) of cluster complexes in NGC 2997.

Colour and magnitude diagrams

The general properties of the sources can be deduced from the colour-colour and colour-magnitude diagrams as given in Fig. 3.23. The (H-K)–(J-H) diagram for sources with photometric errors < 0.05 mag shows a main group centered around (0.4, 0.8) being consistent with colours of somewhat reddened, stellar clusters with ages > 50 Myr. Evolutionary tracks for a single-burst stellar population (SSP) using the Padova isochrones (Marigo et al. [2008]) and a continuous star-forming cluster (CSC) from Starburst99 (Leitherer et al. [1999]; hereafter SB99) are indicated on the figure. The reddening vectors for a screen model (Indebetouw et al. [2005]) and a dusty environment (Witt et al. [1992]; Israel et al. [1998]) are also plotted for a visual extinction of 5^m. A second, smaller group is located close to (0.8, 1.1) which is likely to contain highly reddened, dusty young clusters. Finally, there is a scatter of sources to redder (H-K) values which may be caused by emission from hot dust. Whereas many older clusters have a small extinction, most young complexes have several magnitudes of visual extinction.

A reddening correction colour index Q_d = (H-K) - 0.84 × (J-H) can be constructed using the dusty models of Witt et al. [1992]. The colour-magnitude diagrams for the absolute magnitude M_K is shown on the right in Fig. 3.23 as functions of Q_d and (J-K) indexes. Tracks of evolutionary SSP models are indicated on the figures together with a dusty reddening vector. The Q_d-M_K diagram is consistent with the tracks with some (H-K) excess due to hot dust and absolute magnitudes up to $M_K \approx -15$ mag corresponding to masses of the order of $10^6\,M_\odot$ with a Salpeter IMF and an upper mass limit of $100\,M_\odot$. The (J-K) plot shows a double branch structure where the redder one with (J-K) = 1.9 mag consists of the young, dusty clusters in the colour-colour diagram while the older clusters are located around 1.2 mag. From the evolutionary tracks, it is expected that intrinsic (J-K) colours of clusters become redder with age. The gap between the two branches suggests a rapid reduction of extinction in the clusters which may be caused by expulsion of dust and gas due to supernovae explosions.

Luminosity and spatial distribution

The attenuation by dust can be estimated from the (H-K)–(J-H) diagram using the SB99 model track for the intrinsic colours. Applying this correction, the distribution of the 'reddening free' absolute magnitude M_{Ko} is shown in Fig. 3.24 where the sources are separated in young complexes with 0.1 mag $< Q_d$ (i.e. age $<$ 7 Myr) and older ones. Incompleteness starts to be important at -12 mag $< M_{Ko}$ for the older population while the young one is affected already around -13^m due to their higher average extinction. The high luminosity part of both samples follows a power law with almost the same exponent $\alpha = 2.1$ and no significant indication of a cut-off at brightest magnitudes. The ratio between the two populations varies significantly from galaxy to galaxy in the sample and reflects the current star-formation rate relative to the average.

The main symmetric part of the spiral pattern in NGC 2997 starts around 60 arcsec, just outside the oval distortion, and breaks up close to 100 arcsec. The phase of the arms in this region was determined from the m = 2 Fourier component of the azimuthal K-band intensity variation in 1 arcsec radial bins. Absolute magnitude M_K and colour index Q_d of complexes are plotted as function of their azimuthal angle $\Delta\Theta$ relative to the main arms in the right panel of Fig. 3.24. The M_K values are clearly peaked in the arm regions (i.e. around 0 deg and 180 deg) with very few sources brighter than -13 mag between the arms. A similar picture is seen for the $\Delta\Theta$-Q_d diagram where young complexes with 0.1 mag $< Q_d$ are more frequent in the arms although some fainter clusters are formed in between the arms. Older, fainter complexes are more uniformly distributed with only a moderate increase in density in the arm regions.

Conclusions

In a sample of 10 nearby grand-design, spiral galaxies, NGC 2997 was selected to illustrate the general properties of their stellar cluster populations as observed in the NIR. The cluster complexes form two distinct groups in the (H-K) – (J-H) diagram where the larger one is consistent with an older stellar population with low extinction while the smaller one mainly contains of young complexes with ages $<$ 7 Myr and visual extinctions in the range 2 – 7 mag. No young cluster with $A_V < 1$ mag was found while some are scattered to redder (H-K) colours possibly by emission from hot dust. A gap between older and younger complexes in (J-K) – M_K diagram suggests a rapid expulsion of dust at an age around 7 Myr which could be triggered by supernovae explosions.

The upper part of the cluster luminosity function is well fitted by a power law with an index $\alpha \approx 2$ with no indication of a cut-off at the bright end. The most luminous complexes with M_{Ko} around -15 mag may have masses close to $10^6\,M_\odot$ assuming a Salpeter IMF. The distribution of sources relative to the spiral arms indicates that the most massive clusters are predominantly formed in the arm regions while fainter and older clusters show a more uniform azimuthal distribution with a weaker modulation relative to the arms.

Bibliography

Bertin, E. & Arnouts, S. 1996, A&AS, 117, 393
Grosbøl, P. & Dottori, H. 2008, A&A, 490, 87
Grosbøl, P., Dottori, H., & Gredel, R. 2006, A&A, 453, L25
Indebetouw, R., Mathis, J. S., Babler, B. L., et al. 2005, ApJ, 619, 931
Israel, F. P., van der Werf, P. P., Hawarden, T. G., & Aspin, C. 1998, A&A, 336, 433
Leitherer, C., Schaerer, D., Goldader, J. D., et al. 1999, ApJS, 123, 3
Lin, C. C. & Shu, F. H. 1964, ApJ, 140, 646
Marigo, P., Girardi, L., Bressan, A., et al. 2008, A&A, 482, 883
Roberts, W. W. 1969, ApJ, 158, 123
Skrutskie, M. F., Cutri, R. M., Stiening, R., et al. 2006, AJ, 131, 1163
Witt, A. N., Thronson, H. A., & Capuano, Jr., J. M. 1992, ApJ, 393, 611

3.11 Speckle Photometry of Close Stellar Systems in Galactic Open Star Clusters

Carlos Alberto Guerrero Peña[1], **V. Orlov**[1]

[1] Instituto de Astronomía, UNAM, Apdo. Postal 70-264, Cd. Universitaria, 04510 México D.F., México

Abstract

The study of the binary and multiple star population in open clusters represents an important field of research in stellar astrophysics, however, the HR diagram is affected if these stars are not taken into account, since the colour dispersion among the stars in the CMD along the Main Sequence is due in part to a large population of unresolved binary stars. But this problem cannot be solved by classical photometry because photometry does not have enough spatial resolution. This problem can be solved with space telescopes like the Hubble Space Telescope or the Gaia ESA space mission, but it is difficult to get time for this purpose. Another solution to this problem can be based on speckle photometry. In this presentation, I will discuss how we can resolve this issue and confirm whether the suspected binary stars actually are binaries, with the telescopes of the OAN Mexico.

Introduction

The study of the binary and multiple star population in open clusters represents an important field of research, however, the HR diagram is affected if these stars are not resolved. This problem cannot be solved by classical photometry because photometry does not have enough spatial resolution. AO and telescopes like the Hubble Space Telescope or the Gaia ESA space mission can address on this problem, but it is difficult to get time for this purpose. Another solution to this problem can be based on speckle interferometry.

Galactic open clusters are ensembles of stars with low concentration and irregular shape, gravitationally-bound systems formed at the same time from the same original cloud. They represent examples of stars of comparable age and intrinsic chemical composition and are important in the study of stellar evolution and star formation. Classical photometry helps us determine the general physical characteristics of clusters, however, there is an observational problem by the presence of stars in binary or multiple systems that are not resolved (Reid [1986]).

Colour Magnitude Diagram (CMD)

The theoretical colour magnitude diagram shows a well defined line for the MS, however, the observational CMD shows that the MS is a line with a finite width and there are many stars that are less than a magnitude above the SP. The colour dispersion among the stars in the CMD along the MS is due in part to a large population of unresolved binary stars (Daniel et al. [1994]). This observational bias affects the determination of the parameters of the stars in two ways (Stobie et al. [1987]): firstly, the star's luminosity is enhanced, and secondly, the colour index of the system is redder. These effects affect the determination of physical parameters. Fig. 3.25 shows the CMD of Praesepe (NGC 2632), containing all the photometric data published to date (WEBDA, 2011). We can see the main sequence but also a large number of stars above the MS.

To identify binary systems in the cluster we went to the astronomical data bases, but there were no reported binary stars. So we needed a criterion to determine possible binary star candidates. The first and most obvious is their location in the CDM, one magnitude above the MS. There are previous publications on this matter (Sollima et al. [2009]; Bica & Bonato [2005]), refering to the minimum fraction of binary stars required to reproduce the morphologies we see in the CMD. They conclude that the global fraction of binaries in OC's should range from 35% to 75% of the total content of stars.

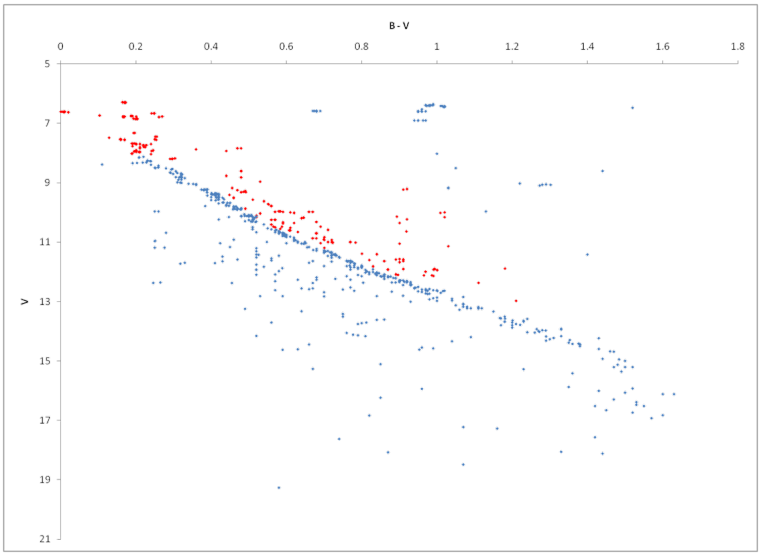

Figure 3.25: Colour Magnitude Diagram of Praesepe (NGC 2632), WEBDA 2011.

Figure 3.26: *Left*: Pattern of speckles of a binary star. *Right*: WDS 00279+234, $\rho = 0.6$ arcsec, $\Delta m = 0.49$.

Once we have the set of stars, we seek all the related information available: photometric data, spectral class, cross identificators, etc., and we started our observational program, using speckle interferometry and speckle photometry in three colours VRI (see the poster of Valeri Orlov).

Speckle Interferometry

Speckle Interferometry is a technique introduced by Labeyrie [1970]. The traditional long-exposure images consist of a large number of snapshots, "speckles", which together form the seeing disk. Speckle interferometry allows us to reach a resolution of up to 0.053 arcsec in the V band (Orlov et al. [2010]; Orlov et al. [2011]) for the 2.1 m telescope (OAN, México), and gives us information about the difference in magnitude of the components of the system.

Fig. 3.26 shows a specklegram of a binary star; we can see that the distance between the speckles is preserved. If we take multiple images of the star, we can momentarily freeze the atmosphere, and then use all the images to retrieve a diffraction limited image of the star.

The final result of speckle interferometry is the Auto Correlation Function (ACF), which gives us the information about the position angle and angular separation between the stars, modulo 180 deg. To obtain the magnitude difference between the stars, we analyse the power spectrum of the system, which is the Fourier transform of the convolution between the PSF and the brightness distribution of the object.

Fig. 3.27 (left) shows the power spectrum of a binary star, with the typical interference fringes; the magnitude difference is related to the contrast of the fringes. Fig. 3.27 (right) shows the ACF of a binary star.

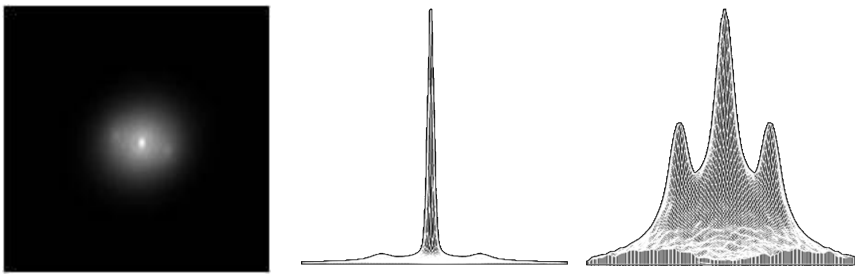

Figure 3.27: *Left*: Power Spectrum of the star DF Tau. *Right*: ACF of DF Tau $\rho = 0.1$ arcsec, $\Delta m = 0.23$.

The power spectrum $P(\nu)$ can be described by the following formula:

$P(\nu) = P_0(\nu)[A + Bcos(2\pi\nu r)]$,

where coefficients A and B define the relative scaling and the magnitude difference, $P_0(\nu)$ is the power spectrum of the reference star:

$P_0(\nu) \approx exp\{-3.44(\nu/\nu_c)^{5/3}(D/r_0)^{5/3}\} + 0.435(D/r_0)^{-2}T_0(\nu)$,

Where $\nu = |\nu|$, $T_0(\nu)$ is the diffraction-limited transfer function:

$T_0(\nu) = 2/\pi[arccos(\nu = \nu_c) - (\nu/\nu_c)\sqrt{1 - (\nu/\nu_c)^2}$.

Finally, we find the magnitude difference using the following expression:

$\Delta m = m_A - m_B = -2.5log(A/B)$.

Speckle Interferometry of Open Clusters

Using the available data in the literature, in a combination with an observational technique that requires small telescopes, we can address a problem that can not be solved by classical photometry. We are developing a new method of differential photometry using 3 colours to identify the spectral class of the components of the binary systems. We are conducting an observational program which aims to look at some nearby open clusters, to assess the potential binary or multiple stars candidates.

The data for the first campaigns were recorded during the two observation sessions carried out in February and April 2011. Observations of more than 500 binary stars were performed at the OAN-SPM 1.5 m telescope. The atmospheric conditions (seeing and transparency) during both sets were moderate. For five nights in February 2011 we observed 290 stars. For five nights in April 2011 we observed 260 stars. All stars were observed through three filters: V(540/90 nm), R(640/130 nm) and I(800/160 nm). In these speckle observations we measured 36 binary candidates in the Praesepe open cluster.

Acknowledgments

The speckle interferometry program at the OAN telescopes is supported by the Direccion General de Asuntos del Personal Académico (UNAM, México) under the projects IN104910 and IN113308 (PAPIIT).

Bibliography

Bica, E. & Bonato, C. 2005, 431, 943
Daniel, S., Latham, D., Mathieu, R., & Twarog, B. 1994, PASP, 106, 281
Orlov, V., Voitsekhovich, V., Guerrero, C., et al. 2011, 47, 12
Orlov, V., Voitsekhovich, V., Guerrero, C., & Ortiz, F. 2010, 46, 245
Reid, N. 1986, MNRAS, 225, 873
Sollima, A., Carballo-Bello, J., Beccari, G., et al. 2009, MNRAS, 000, 1
Stobie, R., Ishida, K., & Peacock, J. 1987, MNRAS, 208, 709

3.12 Stellar Clusters in M 31 from PHAT: Survey Overview and First Results

L. Clifton Johnson[1], A. C. Seth[2], J. J. Dalcanton[1], N. Caldwell[2], D. A. Gouliermis[3], P. W. Hodge[1], S. S. Larsen[4], K. A. G. Olsen[5], I. San Roman[6], A. Sarajedini[6], D. R. Weisz[1], and the PHAT Collaboration

[1] Department of Astronomy, University of Washington, Box 351580, Seattle, WA 98195, USA
[2] Harvard-Smithsonian Center for Astrophysics, 60 Garden Street Cambridge, MA 02138, USA
[3] Max Planck Institute for Astronomy, Königstuhl 17, 69117 Heidelberg, Germany
[4] Astronomical Institute, University of Utrecht, Princetonplein 5, NL-3584 CC, Utrecht, The Netherlands
[5] National Optical Astronomy Observatory, 950 North Cherry Ave., Tucson, AZ 85719, USA
[6] Department of Astronomy, University of Florida, 211 Bryant Space Science Center, Gainesville, FL 32611-2055, USA

Abstract

The Panchromatic Hubble Andromeda Treasury (PHAT) is an on-going Hubble Space Telescope (HST) multi-cycle program that will image one-third of the M 31 disk at high resolution, with wavelength coverage from the ultraviolet through the near-infrared. This dataset will allow for the construction of the most complete catalogue of stellar clusters obtained for a spiral galaxy. Here, we provide an overview of the PHAT survey, a progress report on the status of observations and analysis, and preliminary results from the PHAT cluster program. Although only $\sim 20\%$ of the survey is complete, the superior resolution of HST has allowed us to identify hundreds of new intermediate and low-mass clusters. As a result, the size of the cluster sample within the Year 1 survey footprint has grown by a factor of three relative to previous catalogues.

Introduction

The Andromeda galaxy (M 31) is an exquisite laboratory for studying stellar clusters. Its proximity (785 kpc; McConnachie et al. [2005]) allows for the detailed study of individual stars in clusters, while simultaneously providing a large, galaxy-wide sample of objects. Studies of M 31's stellar cluster system have been on-going since the work of Hubble [1932]. The Panchromatic Hubble Andromeda Treasury (PHAT) survey, described in next Section, represents a significant step forward in the study of Andromeda's cluster system, extending the sample of known clusters well into the intermediate and low-mass regimes. This dataset will inform our understanding of cluster evolution as a whole, through its wide sampling of age, mass, and galactic environment parameter space. The survey's cluster science goals include placing constraints on cluster disruption behaviour, assessing environmental dependencies of cluster formation and destruction, and measuring the star cluster initial mass function, among many others. The first step to achieving these goals lies in the accurate identification and characterization of M 31's cluster system. We describe our current progress on this task in Section *Stellar Cluster Survey*, and direct the reader to our forthcoming paper (Johnson et al., in prep.) for complete details.

The PHAT Survey

The PHAT survey[10] (PI: Dalcanton) is a Hubble Space Telescope (HST) multi-cycle treasury program that will image one-third of M 31's stellar disk. The survey region extends across the northeast half of M 31, resulting in areal coverage stretching from the galactic nucleus out to the edge of the star-forming disk at galactocentric radii of ~ 20 kpc. The full survey footprint is shown in Fig. 3.28. Imaging across $\sim$

[10] Project Website: http://www.astro.washington.edu/groups/phat

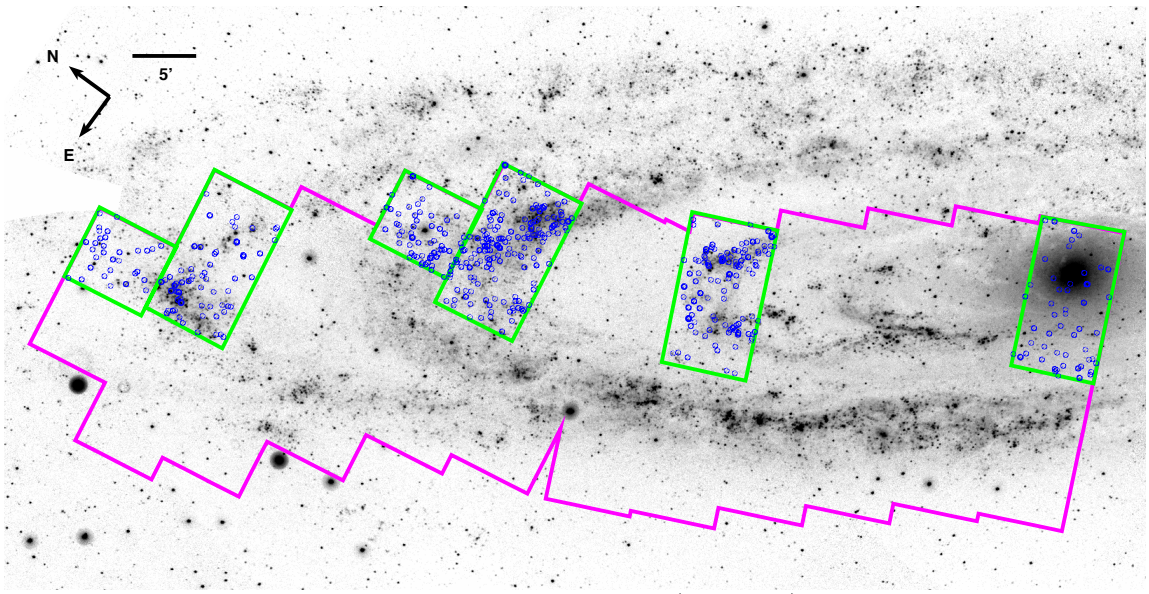

Figure 3.28: The footprint of the PHAT survey region (magenta) displayed on a GALEX NUV image of the northeast half of M 31. Green rectangles represent the "bricks" that make up the Year 1 imaging data. Blue circles show the spatial distribution of cluster identifications resulting from our Year 1 by-eye search.

0.5 deg^2 of contiguous spatial coverage will be obtained using three different HST instruments (WFC3-UVIS, ACS-WFC, WFC3-IR) in six filters ranging from the ultraviolet to the near-infrared (UV to NIR; F275W, F336W, F475W, F814W, F110W, F160W). Observations are grouped into 23 units known as "bricks", each of which is made up of 18 tiled fields-of-view arranged in two side-by-side, 3×3 half-brick arrays. Bricks are observed over two epochs, separated by six months, in which the optical imaging is collected for one of the half-brick arrays, and the UV and NIR images in the other. Six months later, these wavelength assignments are reversed in accordance with a 180-degree difference in HST roll angle, and six-filter imaging coverage for the brick is completed. For a complete survey and data reduction description, please see Dalcanton et al. (in prep.).

The PHAT survey has been allocated more than 800 HST orbits, which will be executed over the course of four years. As of May 2011, four full bricks and two additional half-bricks have been observed, representing $\sim$ 20% of the total expected survey data. The spatial positions of these Year 1 bricks are shown in Fig. 3.28, and we discuss the cluster analysis results from these data in next Section.

In addition to the HST data, there is a remarkable amount of ancillary imaging and spectroscopy of M 31 that is already available or will be obtained as part of the PHAT survey. Imaging datasets from GALEX, Swift/UVOT, Spitzer, and Herschel extend wavelength coverage further into the UV and IR, while observations from CARMA and the EVLA will provide important gas-phase diagnostics. Finally, red-sensitive spectroscopy of RGB stars from Keck/DEIMOS will improve constraints on galactic kinematics, while MMT/Hectospec observations will provide critical follow-up cluster spectroscopy.

The stellar cluster results will also contribute to other science goals of the PHAT survey, which include placing constraints on the high-mass (> 5 M$_\odot$) stellar initial mass function and the calibration of stellar evolution models. Additionally, the survey goal to derive a spatially-resolved star formation history of the field population of M 31 will allow for an interesting comparison between field and cluster age distributions and formation history.

Stellar Cluster Survey

Our study of M 31 stellar clusters is currently underway, with early work focusing on cluster identification and characterization. For PHAT, we chose to begin the cluster identification process with a systematic by-eye image search, and are currently implementing two automated search techniques to complement the by-eye work. This approach allows for the careful construction of a well-vetted cluster catalogue (following comparable work in M 31 by Krienke & Hodge [2007]; Krienke & Hodge [2008]; Hodge et al. [2009]; Hodge et al. [2010]), while simultaneously providing an optimal training set to help refine the automated identification techniques. Proper calibration of the automated cluster finding routines is

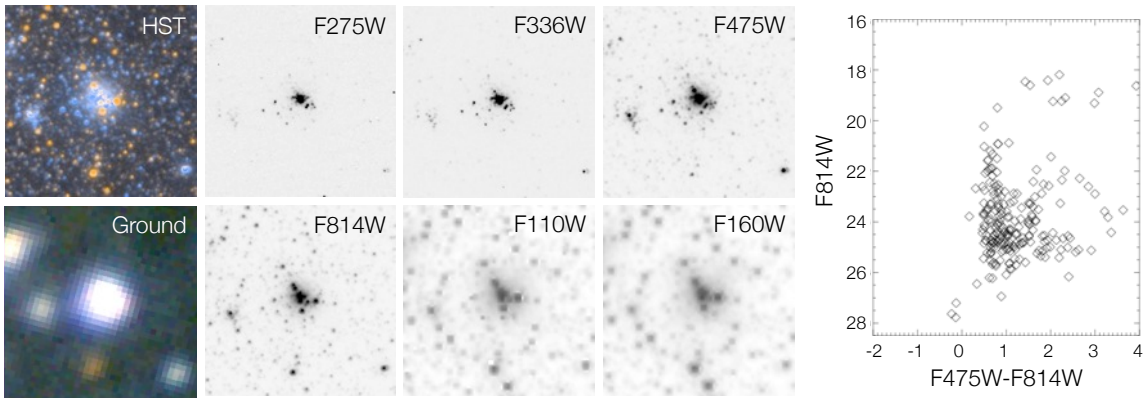

Figure 3.29: Image cutouts and optical CMD of cluster B256D showing the data quality available from the PHAT survey imaging. Image cutouts are 10×10 arcsec^2. We also include an optical colour composite of ground-based imaging from the Local Group Survey (Massey et al. [2006]) for comparison.

required, because unlike most automated extragalactic cluster searches, our clusters are resolved into individual stars (as faint as $M_{F814W} \sim +0$). For an example of the cluster images provided by PHAT, see Fig. 3.29. Instead of searching for slightly extended point sources, our search routines must account for both cluster components: the resolved stars and the underlying unresolved light. Our automated identification routines will take advantage of both the resolved and unresolved light components to obtain the best possible identification results.

The first results of our PHAT by-eye search show the great potential of this dataset. From the Year 1 imaging, we have preliminarily identified ~ 500 likely clusters, whose spatial distribution is shown in Fig. 3.28. Our current cluster catalogue represents a factor of ~ 3 increase in the number of known clusters for the same area (previously 139 clusters; Caldwell et al. [2009]; and references therein). As illustrated in Fig. 3.30, we find that previous ground-based catalogues were generally complete for bright clusters ($M_{F475W} < -6$), whereas HST imaging allows us to identify clusters more than ~ 3 mag fainter. In terms of the faint end of the cluster distribution, we have greatly increased the number of catalogued faint clusters as a result of the marked increase in HST imaging coverage available through PHAT, compared to the limited number of objects discovered through previous, targeted HST observations. Extrapolating from these results, we estimate the final PHAT stellar cluster sample will include ~ 2000 clusters, sampling a mass range down to < 1000 $M_{\odot}$.

Understanding the completeness characteristics of our cluster sample is a high priority considering the population-wide questions we plan to address. Sample completeness will be easier to quantify once we have incorporated automated cluster-finding routines, but even as part of the by-eye search, we employ artificial cluster tests to make completeness measurements. Following the philosophy of completeness testing developed for stellar photometry, we insert samples of artificial clusters into the same reduction and analysis pipeline we use for the by-eye search. This allows us to make an assessment of sample completeness as a function of cluster age, mass, and galactic environment (due to the effects of crowding and extinction).

In addition to understanding sample completeness, our survey has placed great importance on deriving robust age and mass measurements. One advantage of the PHAT dataset is that it provides us the opportunity to determine cluster characteristics using multiple techniques, and to test for potential systematic differences in the results. Specifically, we plan to compare age and mass determinations obtained by fitting integrated light measurements to stochastically sampled models (e.g. Fouesneau & Lançon [2010]), through fitting cluster spectroscopy (e.g. Caldwell et al. [2009]; Caldwell et al. [2011]), and using colour-magnitude diagram (CMD) analysis of individual resolved stars (e.g. Dolphin [2002]). Using this multi-method approach, we will test for consistency between the different techniques, and determine the best methods to derive accurate ages and masses for these clusters, especially in the low to intermediate mass regime.

We expect to publish the first PHAT cluster results in the coming months. Our Year 1 cluster catalogue and accompanying six-band integrated photometry will be included in Johnson et al. (in prep.), while first age and mass assessments will appear in a subsequent paper (Fouesneau et al., in prep.). After these publications, we plan to periodically expand and update the cluster catalogue as additional data arrives over the next three years. Our team looks forward to reporting the results of our work studying

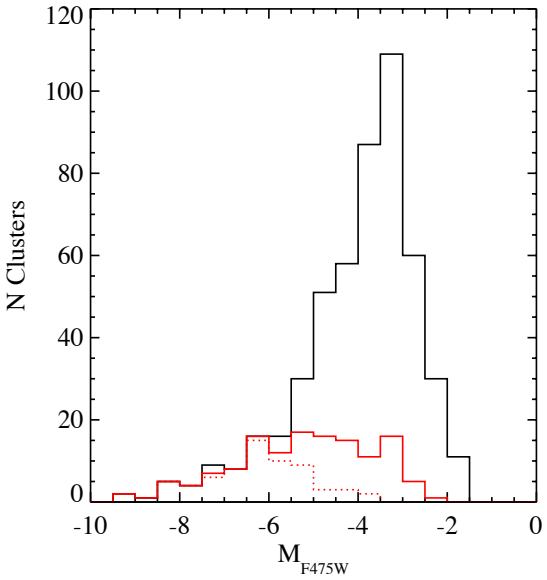

Figure 3.30: A histogram showing the F475W absolute magnitude distributions of our PHAT by-eye clusters (black) and previously catalogued clusters (red) that lie within the Year 1 imaging. The subset of previously known clusters that were discovered using ground-based data are represented by the dotted histogram, while the remaining, fainter known clusters were discovered using limited HST imaging available before PHAT.

the cluster initial mass function, cluster disruption processes, and the environmental dependencies of cluster formation and destruction, among many other studies made possible by the PHAT survey data.

Acknowledgments

Support for this work was provided by NASA through grant number HST-GO-12055 from the Space Telescope Science Institute, which is operated by AURA, Inc., under NASA contract NAS5-26555.

Bibliography

Caldwell, N., Harding, P., Morrison, H., et al. 2009, AJ, 137, 94
Caldwell, N., Schiavon, R., Morrison, H., Rose, J. A., & Harding, P. 2011, AJ, 141, 61
Dolphin, A. E. 2002, MNRAS, 332, 91
Fouesneau, M. & Lançon, A. 2010, A&A, 521, A22+
Hodge, P., Krienke, O. K., Bianchi, L., Massey, P., & Olsen, K. 2010, PASP, 122, 745
Hodge, P. W., Krienke, O. K., Bellazzini, M., et al. 2009, AJ, 138, 770
Hubble, E. 1932, ApJ, 76, 44
Krienke, O. K. & Hodge, P. W. 2007, PASP, 119, 7
Krienke, O. K. & Hodge, P. W. 2008, PASP, 120, 1
Massey, P., Olsen, K. A. G., Hodge, P. W., et al. 2006, AJ, 131, 2478
McConnachie, A. W., Irwin, M. J., Ferguson, A. M. N., et al. 2005, MNRAS, 356, 979

3.13 The Star Cluster Populations of Compact Galaxy Groups

Iraklis S. Konstantopoulos[1], K. Fedotov[2], S. C. Gallagher[2], A. Maybhate[3], P. R. Durrell[4], J. C. Charlton[1]

[1] The Pennsylvania State University, 525 Davey Lab, University Park, PA 16802, USA
[2] The University of Western Ontario, London, ON, N6A 3K7, Canada
[3] Space Telescope Science Institute, Baltimore, MD
[4] Youngstown State University, Youngstown, OH 44555

Abstract

Star clusters are ideal tracers of star formation activity in systems outside the volume that can be studied using individual, resolved stars. These unresolved clusters span orders of magnitude in brightness and mass, and their formation is linked to the overall star formation in their host galaxy. In that sense, the age distribution of a cluster population is a good proxy of the overall star formation history of the host.
This talk presents a comparative study of clusters in seven compact galaxy groups. The aim is to use the cluster age distributions to infer the star formation history of these groups and link these to a proposed evolutionary sequence for compact galaxy groups.

Introduction

Compact galaxy groups (CGs) occupy an interesting part of the parameter space that pertains to the clumping of matter in the universe. On the one hand, they lie at the low end tail of the distribution of membership size, as they contain few galaxies – typically three or four (Hickson [1982]). On the other hand, their compactness places them on the high end of the number density distribution, similar to that in the centres of galaxy clusters (Dressler [1980]; Whitmore [1990]).

In addition, CGs display low velocity dispersions of $\sigma_{\rm CG} \sim 250$ km/s (Tago et al. [2008]; Cox [2000]), compared to galaxy cluster dispersions of $\sigma_{\rm cluster} \sim 750$ km/s (Binggeli et al. [1987]; The & White [1986]; Cox [2000]). This dynamical situation lengthens interactions, when such events occur, or forces galaxies to a state of quasi-secular evolution: while they may not interact physically with their neighbours, they are always affected by them dynamically (Martig & Bournaud [2008]; Konstantopoulos et al. [2010]). In terms of galaxy evolution, they present potential precursors of isolated ellipticals. Furthermore, they allow for close studies of galaxy evolution and morphological transformation, given their relatively few degrees of freedom (as compared with galaxy clusters and their hundreds of members).

The work presented here relates qualitative age dating of thousands of star clusters in seven Hickson compact groups (HCGs) to the CG evolutionary diagram proposed by Konstantopoulos et al. [2010, Fig. 3.31]. This draws upon results presented in an ongoing series of papers on individual groups (Gallagher et al. [2010]; Konstantopoulos et al. [2010]; Fedotov et al. [2011]), and on the collective properties of HCGs (Johnson et al. [2007]; Gallagher et al. [2008]; Walker et al. [2010]; Tzanavaris et al. [2010]). In brief, the diagram classifies galaxy groups according to a gas richness criterion. With the basic assumption that H I represents the reservoir of gas available for further star formation (star formation potential), Johnson et al. [2007] uses the ratio of gas mass to dynamical mass (total mass) to split CGs into three types: I, II, and III, for gas-rich, intermediate and gas-poor. This is then filtered through the spatial distribution of the H I gas (Verdes-Montenegro et al. [2001]; cf.), to give rise to a two-pronged diagram, shown in Fig. 3.31. One sequence maps CGs where the gas in contained wholly within the galaxies; the other includes groups that have started to build an intra-group medium through the release of gas during interactions.

Methodology

We study star clusters in seven Hickson CGs (HCGs) following the methodology presented in Gallagher et al. [2010]. This is refined by using more recent simple stellar population (SSP) models by Marigo

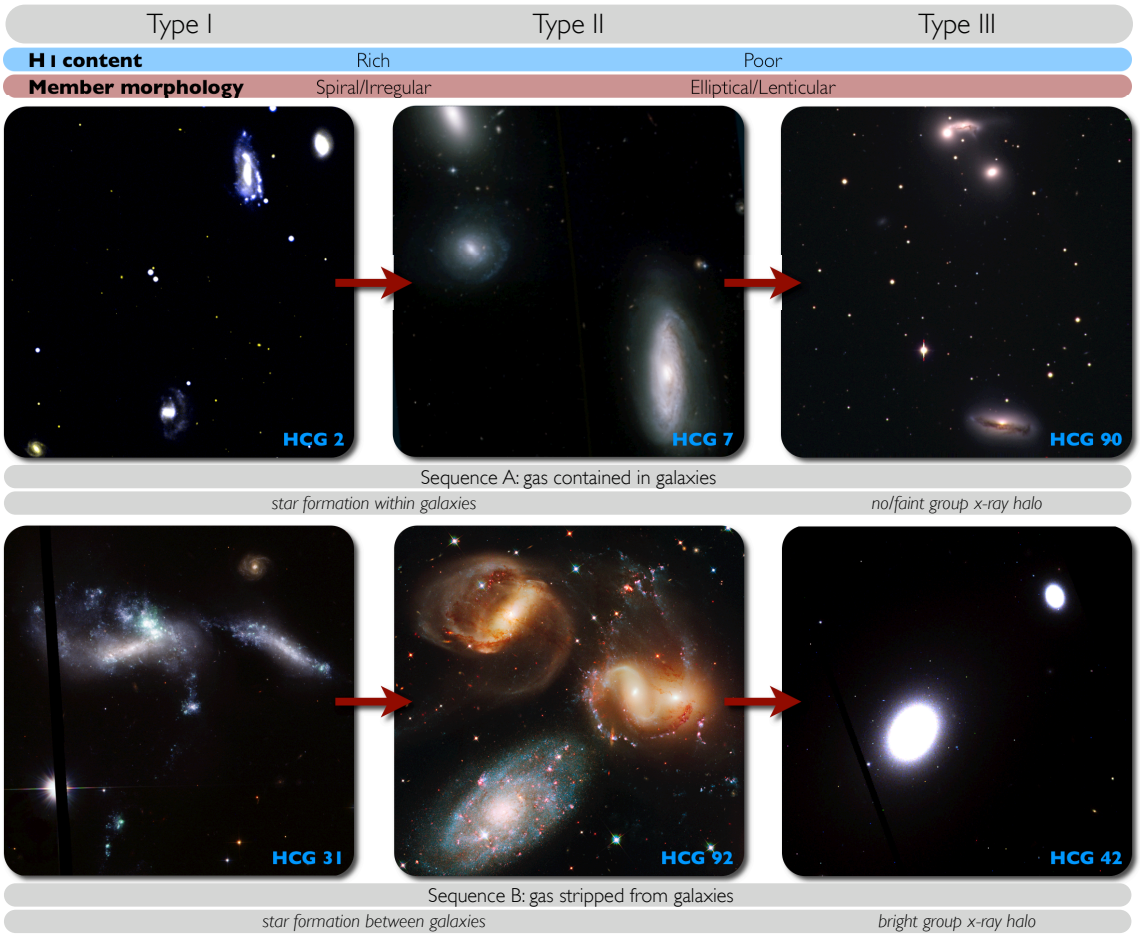

Figure 3.31: The evolutionary diagram proposed by Konstantopoulos et al. [2010]. Gas content decreases from left to right, according to the definition of Johnson et al. [2007]. The top sequence includes groups that hold the H I gas within the member galaxies, while the CGs of the bottom sequence have developed a gaseous (and stellar) intra-group medium through physical interactions. The top sequence includes the possible precursors of dry mergers, as galaxies within these groups evolve separately and are likely to have a very low, or no gas content when they eventually merge.

et al. [2008]. We compare the *HST*-ACS $B-V$ (F435W–F606W) and $V-I$ (F606W–F814W) colours of the clusters to these SSP models and infer their ages. Lacking photometric coverage in the U-band, we cannot break the age-extinction degeneracy inherent in the BVI baseline. We therefore compare CG cluster ages qualitatively.

We are largely aided by the fact that CGs are deficient in H I gas (Haynes & Giovanelli [1984]): since neutral gas is related to dust (e.g. Pohlen et al. [2010]), this implies an overall low dust content for HCGs, thus allowing for a 'clearer', relatively unextinguished view of their cluster populations. In addition, we take advantage of the long bandpass of the F606W filter, which covers the Hα line, by synthesising a Starburst99 (Leitherer et al. [1999]) SSP model that includes emission lines (i. e. from Hβ, [OIII], Hα and [NII]). In the observations, an excess in V-band light is interpreted as nebular emission arising from the ionisation of residual gas from star formation around a young cluster. Sources with such an excess are considered to be no older than 10 Myr, a timescale appropriate for the dispersal of gas from the maturing generation of supernovæ.

Results

The colour plots of Fig. 3.32 summarise our results. Groups of different evolutionary stage feature strikingly different cluster populations (left). Selecting according to the proposed evolutionary diagram

of Konstantopoulos et al. [2010] reveals a pattern (right panel): the median cluster age relates well to the Johnson et al. [2007] type, therefore echoing the evolutionary sequence among those three types, as described in Konstantopoulos et al. [2010].

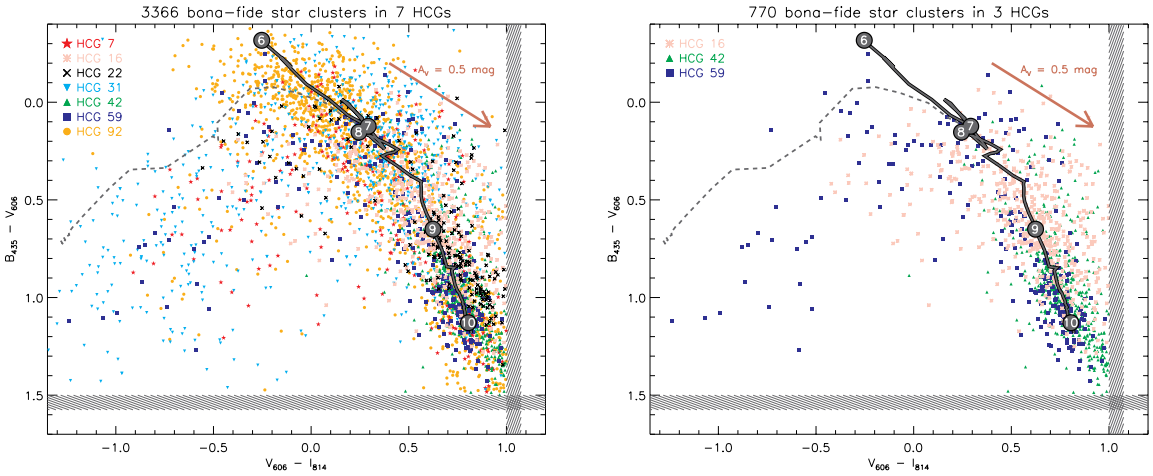

Figure 3.32: *Left*: The star cluster populations of seven compact galaxy groups. We only consider clusters brighter than $M_V = -9$ mag, in order to eliminate contamination from giant stars local to the host galaxies. Furthermore, a selection based on PSF-photometry ensures little or no contamination from foreground stars and background galaxies. The solid line plots a Marigo et al. [2008] SSP model, while the dashed line represents a Starburst99 model (Leitherer et al. [1999]) that includes the emission lines transmitted in the V (F606W) band. Thus, any source shifted to 'greener' values is considered to be younger than 10 Myr old, a timescale appropriate for the clearing of the natal gas of clusters from supernovæ.
The evolutionary state of a group is closely linked with the cluster age distribution: star-forming groups show a large concentration of 'nebular' sources (those bracketed by the dashed line) and many bright, blue clusters (ages less than a few hundred Myr); groups containing both star-forming and evolved/quiescent galaxies show an even spread of nebular, young and old (red) sources; while evolved groups, those containing mostly or entirely quiescent galaxies, show few clusters outside the tight, red globular cluster clump – centred around $(V-I, B-V) \simeq (0.8, 1.1)$.
Continuing along that line, the right panel selects groups along the proposed evolutionary sequence of Konstantopoulos et al. [2010], where HCGs 16, 59, and 42 represent classes I, II, and III, as defined in Johnson et al. [2007]. The correlations between the mentioned sequence and the cluster populations are discussed in detail in Section *Results*.

More specifically: the 'early-type' HCG 16 shows an even star formation history (as evidenced by the cluster formation history) from the present, all the way to 12 or so Gyr. It has a small population of globular clusters, perhaps owing to the apparent lack of major mergers in its past (it contains only disk galaxies).

Next in the sequence, the intermediate type HCG 59 shows increased star formation in the current era, as compared to HCG 16. This is likely due to recent interactions between its member galaxies, which have led to bursts of star formation across the group. This is supported by a plethora of observational evidence, to be presented in Konstantopoulos et al. (submitted).

Finally, the 'late-type' HCG 42 contains only bulge-dominated, evolved galaxies. Its cluster population mirrors that state, as it is heavily skewed toward old ages. We find no evidence of massive cluster formation over the past few Gyr in this system and no nebular sources – i. e. no ongoing formation.

Summary

We have used the optical colours, and therefore ages, of thousands of *HST*-selected star clusters to infer the properties of their host galaxies, members of compact groups. We have linked the distribution of

cluster colours to the evolutionary state of their hosts and provide evidence in favour of the evolutionary sequence for CGs proposed by Konstantopoulos et al. [2010]. While the lack of U-band coverage prohibits precision age-dating, the dust deficiency of the CG environment facilitates the qualitative age-dating of clusters with BVI only. The full study, including modelling of the cluster populations with inferences on star cluster evolution, will be presented in a future work.

Acknowledgments

This work was undertaken as part of the HCG collaboration. In addition to the authors, credit is due to the following scientists: P. Tzanavaris, A. E. Zabludoff, D. M. Elmegreen, K. E. Johnson, C. Gronwall, J. English, A. E. Hornschemeier, R. Chandar, J. S. Mulchaey, as well as others who have participated in several works mentioned in this paper.

Bibliography

Binggeli, B., Tammann, G. A., & Sandage, A. 1987, AJ, 94, 251
Cox, A. N. 2000, Allen's astrophysical quantities, ed. Cox, A. N.
Dressler, A. 1980, ApJ, 236, 351
Fedotov, K., Gallagher, S. C., Konstantopoulos, I. S., et al. 2011, ArXiv e-prints
Gallagher, S. C., Durrell, P. R., Elmegreen, D. M., et al. 2010, AJ, 139, 545
Gallagher, S. C., Johnson, K. E., Hornschemeier, A. E., Charlton, J. C., & Hibbard, J. E. 2008, ApJ, 673, 730
Haynes, M. P. & Giovanelli, R. 1984, AJ, 89, 758
Hickson, P. 1982, ApJ, 255, 382
Johnson, K. E., Hibbard, J. E., Gallagher, S. C., et al. 2007, AJ, 134, 1522
Konstantopoulos, I. S., Gallagher, S. C., Fedotov, K., et al. 2010, ApJ, 723, 197
Leitherer, C., Schaerer, D., Goldader, J. D., et al. 1999, ApJS, 123, 3
Marigo, P., Girardi, L., Bressan, A., et al. 2008, A&A, 482, 883
Martig, M. & Bournaud, F. 2008, MNRAS, 385, L38
Pohlen, M., Cortese, L., Smith, M. W. L., et al. 2010, A&A, 518, L72+
Tago, E., Einasto, J., Saar, E., et al. 2008, A&A, 479, 927
The, L. S. & White, S. D. M. 1986, AJ, 92, 1248
Tzanavaris, P., Hornschemeier, A. E., Gallagher, S. C., et al. 2010, ApJ, 716, 556
Verdes-Montenegro, L., Yun, M. S., Williams, B. A., et al. 2001, A&A, 377, 812
Walker, L. M., Johnson, K. E., Gallagher, S. C., et al. 2010, AJ, 140, 1254
Whitmore, B. C. 1990, in Clusters of Galaxies, ed. W. R. Oegerle, J. Fitchett, & L. Danly, 139–+

3.14 The Dynamics of Star-Forming Regions – Which Mechanisms Set the Cluster Formation Efficiency?

J. M. Diederik Kruijssen[1,2,3]

[1]Astronomical Institute, Utrecht University, PO Box 80000, 3508 TA Utrecht, The Netherlands, kruijssen@astro.uu.nl;
[2]Leiden Observatory, Leiden University, PO Box 9513, 2300 RA Leiden, The Netherlands;
[3]Current address: Max-Planck Institut für Astrophysik, Karl-Schwarzschild Straße 1, 85748 Garching, Germany

Abstract

The fraction of star formation that results in bound stellar clusters (cluster formation efficiency or CFE) is a central quantity in many studies of star formation, star clusters and galaxies. Recent results suggest that contrary to popular assumption, the CFE is not (solely) set by gas expulsion, but is also influenced by the primordial environment, although its precise behaviour remains unknown. Here it is discussed which mechanisms set the CFE, which recent advancements have been made to disentangle their contributions, and which studies are needed in the near future to achieve a quantitative understanding of the CFE.

Introduction

Star clusters are popular tracers of the star formation process, both on stellar and galactic scales (e.g. Smith et al. [2007]; Pflamm-Altenburg et al. [2007]; Bastian et al. [2010]). This approach assumes a certain fraction of star formation that produces bound stellar clusters, also dubbed the *cluster formation efficiency* (CFE). It has recently become clear that the CFE is not the product of two different 'modes' of dispersed and clustered star formation. Instead, star formation proceeds according to a continuous density spectrum, of which the high-density end yields bound star clusters and the low-density end consists of unbound associations (Bressert et al. [2010]; Gieles & Portegies Zwart [2011]). This suggests the existence of a (possibly varying) critical density that allows for the formation of bound structure. If the density spectrum of star formation would vary with environment, this would also imply that the CFE is environmentally dependent – dense star-forming regions should then yield a high CFE (see e.g. Adamo et al. [2011] for a discussion).

It was originally thought that *infant mortality* (disruption by gas expulsion) would be the key mechanism behind a CFE lower than 100% (Lada & Lada [2003]). The question thus arises how this new picture, in which stars do not form in clusters but in a hierarchical setting, connects to the concept of infant mortality, and also which other (environmental) processes may determine whether stellar structure ends up being bound. The following sections address the different mechanisms at play, and the question how Gaia can be used to estimate their relative contributions to the CFE.

Infant mortality: internal disruption by gas expulsion

In the classical picture of cluster formation, the removal of gas from the star-forming environment by stellar winds and supernovae leads to a perturbation of the gravitational potential. If the gas fraction is large enough, this unbinds the cluster – the aforementioned 'infant mortality' (e.g. Bastian & Goodwin [2006]; Goodwin & Bastian [2006]). The indications for infant mortality are largely empirical. Surveys of young stellar clusters show that some 90% of all gas-embedded clusters does not survive the transition to the exposed phase (Lada & Lada [2003]). However, this need not imply that the decrease of the number of clusters is causally related to gas expulsion.

As is shown by Bressert et al. [2010] and Gieles & Portegies Zwart [2011], not all stars form in clusters. At least a certain fraction of gas-embedded stellar structure is gravitationally unbound from the onset. While these unbound associations disperse on a crossing time, the bound part of the embedded

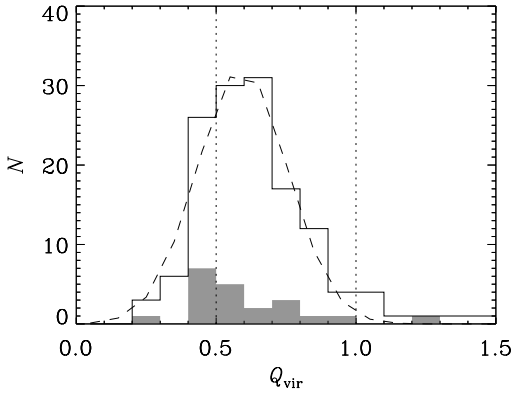

Figure 3.33: Histogram of the virial ratios $Q_{\rm vir}$ of the subclusters from all snapshots of the simulation (solid line). The shaded histogram represents the set of subclusters from the last snapshot at $t = 0.641$ Myr (after approximately one free-fall time). The dashed line is a Gaussian fit to the data for all snapshots, with mean value $Q_{\rm vir} = 0.59$ and standard deviation $\sigma_Q = 0.16$. The vertical dotted lines again indicate the marginally gravitationally bound case ($Q_{\rm vir} < 1$) and the virialised case ($Q_{\rm vir} = 0.5$).

structure could still be subject to infant mortality. The disruption of a cluster by gas expulsion requires a sufficiently massive central concentration of gas. The theoretical evidence for infant mortality is largely based on analytical estimates (e.g. Tutukov [1978]; Hills [1980]) or numerical experiments that obey such conditions – either by assuming a static gas potential[11] or dynamical equilibrium between the gas and stars (e.g. Boily & Kroupa [2003]; Baumgardt & Kroupa [2007]).

It was recently found by Offner et al. [2009] that the velocity dispersion of stars in simulations of star formation are about a factor of five smaller than that of the gas. This result has recently been investigated further by Kruijssen et al. [2011a], where we analysed the dynamics of the stellar structure in the simulation by Bonnell et al. [2008]. They identify subclusters using a minimum spanning tree [see Maschberger et al., 2010] and compute the virial ratios of the stellar component *only*, by ignoring the gravitational potential of the gas. This is equivalent to observing the system at the moment of instantaneous gas expulsion. The virial ratios are also corrected for binaries and higher-order multiple systems. The resulting distribution of virial ratios is shown in Fig. 3.33 for the ensemble population of subclusters from all snapshots. On average, the subclusters are very close to virial equilibrium when neglecting the gas, particularly after one free-fall time has passed.

The virialised state of the subclusters is traced to the fact that they are generally gas-poor, with typical gas fractions below 10% within their half-mass radii. Since the simulation by Bonnell et al. [2008] does not include feedback by radiation or stellar winds, the low gas fractions must have a dynamical origin. About half of the gas depletion can be attributed to the accretion of gas onto the sink particles, while the other half is due to the accretion-induced shrinkage of the subclusters, which is the dynamical response of the subcluster to the mass increase of the sink particles (see Moeckel & Clarke [2011]). This indicates that the accretion of gas onto the sinks is sufficient to balance the overall gas inflow. The subclusters only become gas-rich (with gas fractions above 20%) beyond about three half-mass radii, and are thus embedded in an evacuated cocoon of gas. The lack of a central concentration of gas implies that the subclusters are relatively unperturbed by gas expulsion – a simple analytical estimate yields an $\sim 8\%$ expansion after the gas has been removed.

The degree to which the subclusters are able to evacuate the surrounding gas dynamically depends on the free-fall time. For a certain density spectrum of star formation, a gas-poor state is more easily achieved in the high-density regions, which complete the largest number of free-fall times before the onset of gas expulsion. In low-density regions, the free-fall time is longer and the evacuation would be less efficient, implying that the disruptive effect of infant mortality could be more important. It is worth noting that the densities at which the effect of infant mortality is strongest thus coincide with the range where stars are predominantly formed in unbound associations.

[11] Except for a normalisation of the gas potential that decreases with time when the gas is expelled.

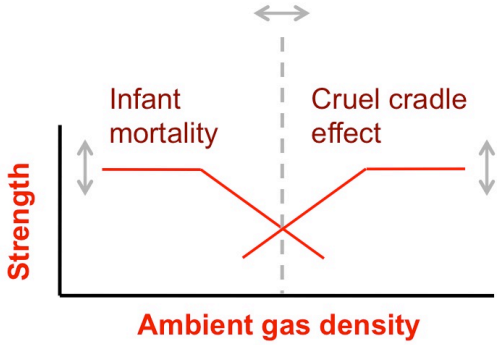

Figure 3.34: Schematic representation of the relative importance of the mechanisms that set the cluster formation efficiency (CFE). Shown are the disruptive strengths of infant mortality and the cruel cradle effect as a function of ambient gas density. The slopes, normalisations, and the location of the cross-over point of the curves are all unknown.

The cruel cradle effect: external disruption by the primordial environment

The transition of young star clusters from the gas-embedded to the exposed phase is also accompanied by an environmental effect that decreases the number of clusters more strongly before and during gas expulsion than after it. Star clusters are tidally disrupted by passing giant molecular clouds (GMCs), particularly in dense environments, where the frequency and strength of the tidal shocks is high (Gieles et al. [2006]). In recent work, it has been indicated that star-forming regions affect their offspring in this way: the GMCs in these regions are capable of efficiently disrupting the new-born stellar clusters (Elmegreen & Hunter [2010]; Kruijssen et al. [2011b]). In those cases where the ambient density is high enough, the tidal shocks would be capable of disrupting young clusters in a single encounter, independently of their mass (also see Gieles et al. [2006]). This form of enhanced disruption is most prevalent in star-forming regions because the mean disruption rate decreases as a cluster population ages. We identified the two responsible mechanisms for a decreasing disruption rate in Kruijssen et al. [2011b, see their Fig. 10]: *cluster migration*, i.e. the motion of clusters away from dense star-forming regions into the field, and *natural selection*, i.e. the preferential survival of those clusters residing in less disruptive environments. Because the enhanced disruption terminates when the gas has been expelled, it influences the cluster population in a way that is very similar to infant mortality. However, rather than being an internal effect like infant mortality is, the primordial disruption by tidal shocks is external. In Kruijssen et al. [2011a], we therefore named it the *cruel cradle effect*.

Contrary to infant mortality, which should peak in low-density regions, the cruel cradle effect decreases the CFE in high-density regions. This implies that in different environments, the CFE may well be determined by different physical mechanisms. In order to understand the relation between the CFE and the gas or star formation rate density (e.g. Goddard et al. [2010]; Silva-Villa & Larsen [2011]; Adamo et al. [2011]), the relative contributions of these mechanisms need to be accounted for. The 'importance' of infant mortality and the cruel cradle effect is shown schematically in Fig. 3.34 as a function of the ambient gas density $\rho_{\rm amb}$. While the precise form of these relations is unknown, the evidence outlined above leads to the trends sketched in the diagram. Infant mortality becomes more effective as the ambient density decreases, with the curve flattening at very low densities to reflect the saturation that occurs when star formation is so dispersed that virtually all structure would be disrupted by gas expulsion. The efficiency of the cruel cradle effect increases with ambient density, with the curve potentially flattening at very high densities where (nearly) all newly formed clusters are immediately disrupted by the strong and numerous tidal shocks. The relation between the CFE and $\rho_{\rm amb}$ is then given by the product of the curves due to infant mortality and the cruel cradle effect.

The relations in Fig. 3.34 apply to the fraction of star formation that takes place in initially bound (sub)clusters, meaning that star formation in unbound associations is not included. If the fraction of star formation taking place in unbound associations also exhibits a trend with ambient gas density, it should be multiplied with the result of Fig. 3.34 to obtain the actual CFE–$\rho_{\rm amb}$ relation. In the coming years, combined theoretical and observational efforts should enable the quantification of the relative contributions of star formation in unbound associations, infant mortality, and the cruel cradle effect.

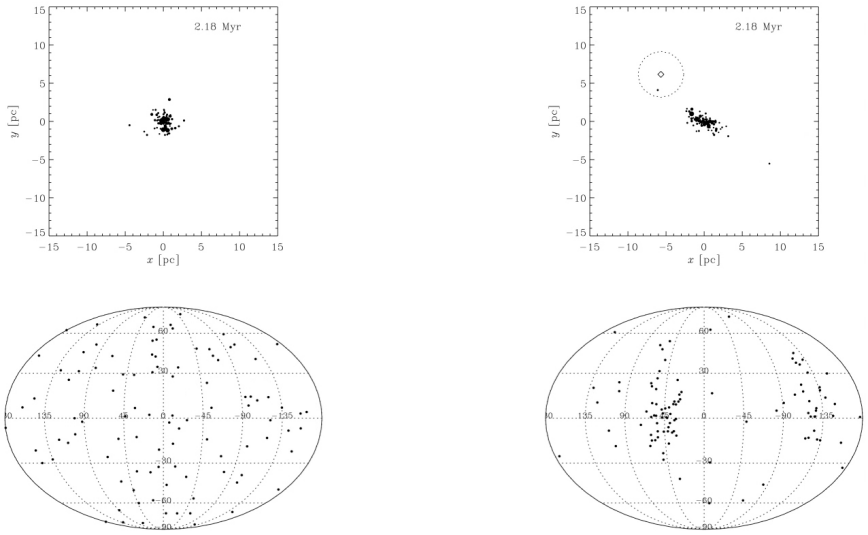

Figure 3.35: Movie of two toy N-body simulations to illustrate the kinematic difference between the disruption of a ~ 25 $M_\odot$(sub)cluster by infant mortality (left) and the cruel cradle effect (right). Infant mortality is modelled by removing a static background potential with the same properties as the (sub)cluster at $t = 3$ Myr, while the cruel cradle effect is characterised by the passage of a GMC with mass $1.25\times$ 10^4 $M_\odot$. The top panels show the projected spatial configuration of the stars in their centre of mass frame. In the top-right panel, the GMC is indicated with a diamond and a dotted circle, which denotes its Plummer radius. In the bottom panels, the directions of the velocity vectors of the stars are projected onto a sphere, with angles in degrees. Infant mortality retains the random orientation of the velocities, but the cruel cradle effect induces structure in velocity space. Click on the figure to start the movie. If your PDF reader does not support embedded movies, you can also access it here.

Using Gaia to distinguish between the mechanisms that determine the cluster formation efficiency

Because the early disruption of stellar structure due to infant mortality and the cruel cradle effect should occur on similar time scales, it is hard to distinguish between both mechanisms observationally. However, the kinematic properties of disrupted cluster remnants will depend on the process that destroyed them. When gas expulsion leads to the disruption of a young cluster, the orientations of the velocity vectors of the stars remain random – after all, there are no external torques acting on the cluster. However, the cruel cradle effect has a different impact, since disruption by an external perturbation does lead to a preferential orientation of the stellar velocities. This is illustrated in Fig. 3.35, which shows a movie of two toy N-body simulations in which a low-mass (sub)cluster is being disrupted. The striking difference in velocity space implies that it should be possible to distinguish between infant mortality and the cruel cradle effect. While Fig. 3.35 shows two highly idealised scenarios, it also indicates the key characteristics that can be used to observe in which environments infant mortality and the cruel cradle effect play a role. An additional advantage of considering the kinematics of young cluster *remnants* is that they need not be caught in the act of being disrupted. Depending on the local strength of the Galactic tidal field, the imprint of the disruption mechanism will remain visible for some time after the actual dispersal took place.

The combination of radial velocities from spectroscopy with proper motion measurements and membership identification by Gaia will provide the 3D positions and space velocities that are needed to reconstruct the processes shown in Fig. 3.35. Until these data become available, a theoretical effort should be made to consider the kinematics of star formation in unbound associations, infant mortality and the cruel cradle effect in more detail. This will expand the current qualitative understanding of the mechanisms that set the CFE to a quantitative census, which in turn will be essential for the predictive potential of star clusters as tracers of galaxy-scale star formation.

Acknowledgments

The Leids Kerkhoven-Bosscha Fonds is acknowledged for supporting attendance to the meeting. I am very grateful to my collaborators for inspiring discussions and help. In particular, Thomas Maschberger, Cathie Clarke, Nick Moeckel, Nate Bastian, Ian Bonnell, and Henny Lamers have contributed greatly to the work summarised here.

Bibliography

Adamo, A., Ostlin, G., & Zackrisson, E. 2011, `ArXiv:1107.0725`
Bastian, N., Covey, K. R., & Meyer, M. R. 2010, ARA&A, 48, 339
Bastian, N. & Goodwin, S. P. 2006, MNRAS, 369, L9
Baumgardt, H. & Kroupa, P. 2007, MNRAS, 380, 1589
Boily, C. M. & Kroupa, P. 2003, MNRAS, 338, 673
Bonnell, I. A., Clark, P., & Bate, M. R. 2008, MNRAS, 389, 1556
Bressert, E., Bastian, N., Gutermuth, R., et al. 2010, MNRAS, 409, L54
Elmegreen, B. G. & Hunter, D. A. 2010, ApJ, 712, 604
Gieles, M. & Portegies Zwart, S. F. 2011, MNRAS, 410, L6
Gieles, M., Portegies Zwart, S. F., Baumgardt, H., et al. 2006, MNRAS, 371, 793
Goddard, Q. E., Bastian, N., & Kennicutt, R. C. 2010, MNRAS, 405, 857
Goodwin, S. P. & Bastian, N. 2006, MNRAS, 373, 752
Hills, J. G. 1980, ApJ, 235, 986
Kruijssen, J. M. D., Maschberger, T., Moeckel, N., et al. 2011a, MNRAS submitted
Kruijssen, J. M. D., Pelupessy, F. I., Lamers, H. J. G. L. M., Portegies Zwart, S. F., & Icke, V. 2011b, MNRAS, 414, 1339
Lada, C. J. & Lada, E. A. 2003, ARA&A, 41, 57
Maschberger, T., Clarke, C. J., Bonnell, I. A., & Kroupa, P. 2010, MNRAS, 404, 1061
Moeckel, N. & Clarke, C. J. 2011, MNRAS, 410, 2799
Offner, S. S. R., Hansen, C. E., & Krumholz, M. R. 2009, ApJ, 704, L124
Pflamm-Altenburg, J., Weidner, C., & Kroupa, P. 2007, ApJ, 671, 1550
Silva-Villa, E. & Larsen, S. S. 2011, A&A, 529, A25+
Smith, L. J., Bastian, N., Konstantopoulos, I. S., et al. 2007, ApJ, 667, L145
Tutukov, A. V. 1978, A&A, 70, 57

3.15 Dynamics in Young Star Clusters: From Planets to Massive Stars

Christoph Olczak[1,2,3], R. Spurzem[3,1], Th. Henning[2], T. Kaczmarek[4], S. Pfalzner[4], S. Harfst[5], and S. Portegies Zwart[6]

[1] Astronomisches Rechen-Institut (ARI), Zentrum für Astronomie Universität Heidelberg, Mönchhofstrasse 12-14, 69120 Heidelberg, Germany
[2] Max-Planck-Institut für Astronomie (MPIA), Königstuhl 17, 69117 Heidelberg, Germany
[3] National Astronomical Observatories of China, Chinese Academy of Sciences (NAOC/CAS), 20A Datun Lu, Chaoyang District, Beijing 100012, China
[4] Max-Planck-Institut für Radioastronomie, Auf dem Hügel 7, 53121 Bonn, Germany
[5] Technische Universität Berlin, Zentrum für Astronomie und Astrophysik, Hardenbergstraße 36, 10623 Berlin, Germany
[6] Sterrewacht Leiden, Leiden University, Postbus 9513, 2300 RA Leiden, The Netherlands

Abstract

The young star clusters we observe today are the building blocks of a new generation of stars and planets in our Galaxy and beyond. Despite their fundamental role we still lack knowledge about the conditions under which star clusters form and the impact of these often harsh environments on the evolution of their stellar and substellar members.
We demonstrate the vital role numerical simulations play to uncover both key issues. Using dynamical models of different star cluster environments we show the variety of effects stellar interactions potentially have. Moreover, our significantly improved measure of mass segregation reveals that it can occur rapidly even for star clusters without substructure. This finding is a critical step to resolve the controversial debate on mass segregation in young star clusters and provides strong constraints on their initial conditions.

Introduction

According to current knowledge, planetary systems form from the accretion discs around young stars. These young stars are in most cases not isolated, but are part of a cluster (e.g. Lada & Lada [2003]; Evans et al. [2009]). Densities in these cluster environments vary considerably, spanning a range of $10\,\mathrm{pc}^{-3}$ (e.g. η Chameleontis) to $10^6\,\mathrm{pc}^{-3}$ (e.g. Arches Cluster). Though it is known that discs disperse on a time-scale of 1-10 Myr (Haisch et al. [2001]; Hillenbrand [2002]; Sicilia-Aguilar et al. [2006]; Currie et al. [2008]) and that in dense clusters ($n \geq 10^3\,\mathrm{pc}^{-3}$) the disc frequency seems to be lower in the core (e.g. Balog et al. [2007]), it is an open question as to how far interactions with the surrounding stars influence the planet formation in clusters of different densities. An encounter between a circumstellar disc and a nearby passing star can lead to a significant loss of mass and angular momentum from the disc. While such isolated encounters have been studied in a large variety (Heller [1993]; Clarke & Pringle [1993]; Ostriker [1994]; Heller [1995]; Hall et al. [1996]; Hall [1997]; Pfalzner [2004]; Pfalzner et al. [2005]; Moeckel & Bally [2006, 2007]; Kley et al. [2008]), only a few numerical studies have directly investigated the effect of stellar encounters on circumstellar discs in a dense cluster environment (Scally & Clarke [2001]; Adams et al. [2006]).

The dynamical evolution of a star cluster leaves a variety of imprints in the phase space of its stellar population which are good tracers of the *dynamical* age of the cluster. One of the most widely discussed aspects is that of mass segregation. Due to energy equipartition – hence via two-body encounters – the more massive particles tend to settle towards the cluster centre over time while the lower-mass particles are preferentially pushed to the outer parts (Spitzer [1969]; Farouki et al. [1983]; Spurzem & Takahashi [1995]; Khalisi et al. [2007]). However, it is a much more challenging task to identify mass segregation observationally in real objects than theoretically from 'clean' numerical simulations. The investigation of mass segregation in young stellar systems is of particular interest for a deeper understanding of the star formation process.

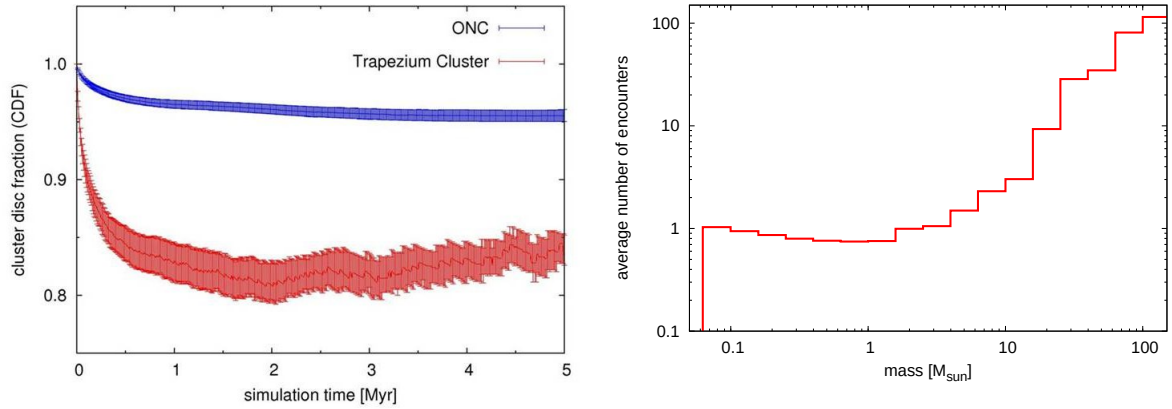

Figure 3.36: *Left:* Fraction of star-disc system over time in the entire ONC ($R = 2.5\,\mathrm{pc}$) and its dense core, the Trapezium cluster ($R = 0.3\,\mathrm{pc}$). *Right:* Average cumulative number of encounters vs. stellar mass after 1 Myr of dynamical evolution.

Star-Disc Encounters in Young Star Clusters

Method

We follow the idea of Scally & Clarke [2001], combining a simulation of the dynamics of a cluster to determine the interaction parameters of close encounters between stars in the cluster with results from studies of isolated star-disc encounter simulations. Throughout this work we assume that initially all stars are surrounded by protoplanetary discs. This is justified by observations that reveal disc fractions of nearly 100 % in very young star clusters (e.g. Haisch et al. [2000]; Lada et al. [2000]; Haisch et al. [2001]; Hillenbrand [2005]).

The dynamical cluster models contain only single stellar components without considering embedded gas. The simulations were performed with NBODY6^{++}, NBODY6-GPU (Spurzem [1999]; Aarseth [2003, 2008]), and `starlab` (McMillan [1996]; Portegies Zwart et al. [2001]; Hut [2003]). The details of the numerics can be found in [Olczak et al., 2006, 2011, in prep].

The encounter-induced transport of mass and angular momentum in protoplanetary discs is calculated via fit formulae based on simulations of star-disc encounters (Olczak et al. [2006]; Pfalzner et al. [2006]; Pfalzner & Olczak [2007]). These quantify upper limits due to the restriction to low-mass discs and co-planar, prograde, and parabolic orbits, which are the most perturbing. A simplified prescription terms stars that have lost more than 90 % of their initial disc mass as "discless". The results presented here apply to a scenario where all stars have initially a disc size of 150 AU. A lerger range of models has been investigated in the cited publications.

Results

From a numerical model of the Orion Nebula Cluster (ONC) we demonstrate that the encounter-induced disc-mass loss becomes significant in its dense core, known as the "Trapezium Cluster" (Fig. 3.36, left). Up to 20 % of the discs can be destroyed by gravitational interactions within a radius of 0.3 pc (compared to ~ 5 % in the entire cluster of 2.5 pc radius).

The massive stars in the centre of such a stellar cluster act as gravitational foci for the lower mass stars (Pfalzner et al. [2006]). This becomes evident from the average number of encounters as a function of stellar mass (Fig. 3.36, right): the number of disc-perturbing interactions is nearly constant for low- and intermediate-mass stars but increases largely for high-mass stars. Because discs are most affected when the masses of the interacting stars are unequal (Olczak et al. [2006]; Moeckel & Bally [2007]) massive stars dominate the encounter-induced disc-mass loss in star clusters like the ONC. For low-mass stars the mass-loss occurs through few strong encounter events, whereas the disc of high-mass stars is removed via a steady nibbling by many encounters with stars of lower mass.

The dynamically outstanding role of high-mass stars does also affect the stellar multiplicity in the ONC. It turns out that the most massive star ($M_1^* = 50\,\mathrm{M}_\odot$) has on average of the order of 200 so-called "capturing encounters" – encounter events with an eccentricity $\epsilon < 1$ – in the first 5 Myr while a star with $M_1^* = 1\,\mathrm{M}_\odot$ has less than one. These interactions lead to the formation of relatively stable configurations

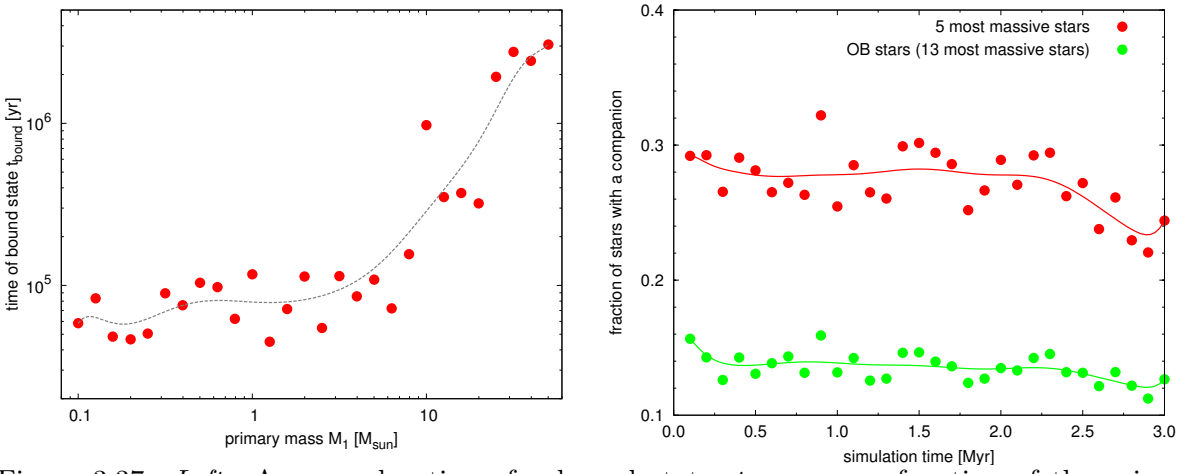

Figure 3.37: *Left:* Average duration of a bound state, t_{bound}, as a function of the primary mass M_1. *Right:* Fraction of the 5 (red) and 13 (green) most massive stars that are part of an encounter-induced binary as a function of cluster age. The lines are Bezier curves of the data.

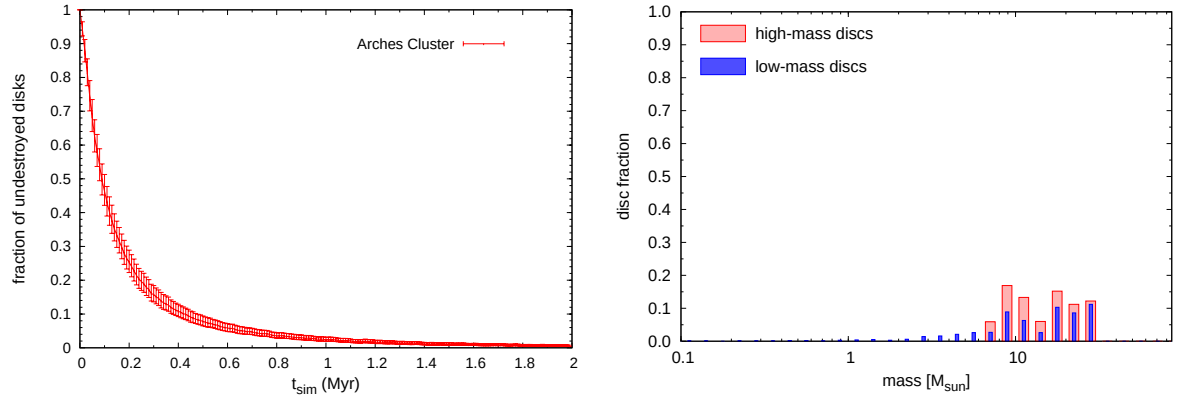

Figure 3.38: *Left:* Fraction of star-disc system over time in the entire Arches cluster. *Right*: Average disc fraction vs. stellar mass after 2 Myr of dynamical evolution.

termed as "transient bound systems" (TBS). The left plot in Fig. 3.37 shows a striking increase of t_{bound} towards more massive stars by more than one order of magnitude. These TBS translate directly into an observed apparent binarity (Fig. 3.37, right): of the five most massive stars in the ONC on average 30 % would appear to be in a binary system at the cluster's current age of $\sim$ 1 Myr. The average for all 13 OB stars in the ONC would be more than 10 %.

The encounter-induced disc-mass loss becomes much more apparent in more extreme environments. Using a numerical model of the Arches cluster, one of the densest and most massive clusters in our Milky Way (Figer et al. [2002]; Stolte et al. [2005]), we find that at its current age of $\sim$ 2.5 Myr (Najarro et al. [2004]; Martins et al. [2008]) nearly all circumstellar discs could have been destroyed just due to gravitational interactions (Fig. 3.38, left). A striking result is that the low fraction of members that could retain their discs to some degree at an age of 2 Myr is populated by stars with masses between 2 $M_\odot$ and 30 $M_\odot$ (Fig. 3.38, right).

Mass Segregation in Young Star Clusters

Method

As a proxy for mass segregation we extend the method $\mathcal{M}^{\Lambda}_{\rm MST}$ developed by Allison et al. [2009] (see also Cartwright & Whitworth [2004]; Schmeja & Klessen [2006]). In summary, the authors use the minimum spanning tree (MST), the graph which connects all vertices within a given sample with the lowest possible sum of edges and no closed loops (Gower & Ross [1969]). The length of the MST, $l_{\rm MST}$, is a measure of the concentration or compactness of a given sample of vertices. Mass segregation of a stellar system of size N is quantified by comparing $l_{\rm MST}$ of the n most massive stars, $l^{\rm mass}_{\rm MST}$, with the average $l_{\rm MST}$ of k sets of n random cluster stars, $< l^{\rm ref}_{\rm MST} >$, and its standard deviation, $\Delta l^{\rm ref}_{\rm MST}$.

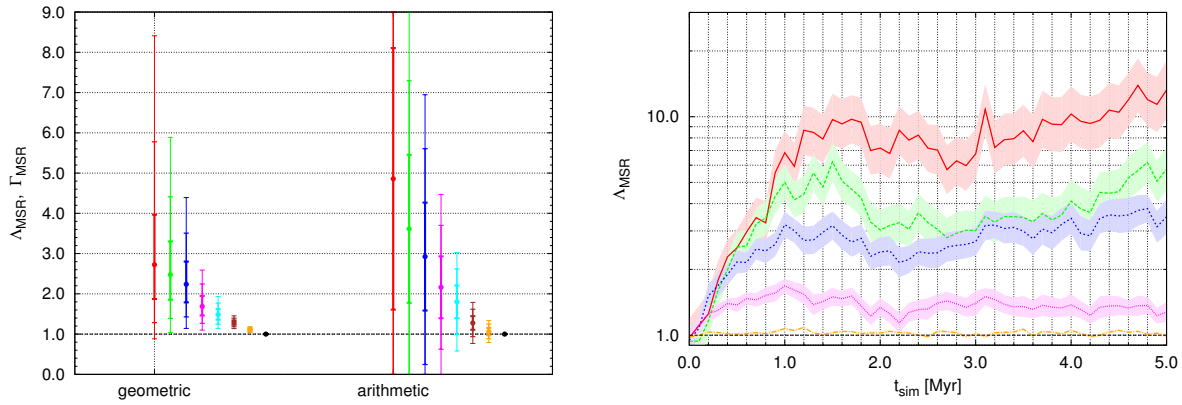

Figure 3.39: *Left:* $\Gamma_{\rm MST}$ and $\Lambda_{\rm MST}$ for the 5, 10, 20, 50, 100, 200, 500, 1000 most massive stars of an initially mass segregated cluster of 1k stars and $S = 0.3$. The error bars and line thickness mark the 1 σ, 2 σ, and 3 σ uncertainties. *Right:* $\Gamma_{\rm MST}$ of the 5, 10, 20, 50, and 500 most massive stars over time for a cluster with 1k members and cold initial conditions ($Q = 0.1$). The filled regions indicate 1 σ uncertainties.

Our method $\mathcal{M}^{\Gamma}_{\rm MST}$ involves a crucial modification of $\mathcal{M}^{\Lambda}_{\rm MST}$ that boosts its sensitivity: we do not use directly the *sum* of the edges $l_{\rm MST}$ as a measure yet their *geometric mean* $\gamma_{\rm MST}$,

$$\gamma_{\rm MST} = \left(\prod_{i=1}^{n} e_i \right)^{1/n} = \exp\left[\frac{1}{n} \sum_{i=1}^{n} \ln e_i \right], \tag{3.7}$$

and its associated geometric standard deviation $\Delta\gamma_{\rm MST}$, where e_i are the n MST edges. We obtain the new measure $\Gamma_{\rm MST}$ via a proper normalisation:

$$\Gamma_{\rm MST} = \frac{\gamma^{\rm ref}_{\rm MST}}{\gamma^{\rm mass}_{\rm MST}}, \quad \Delta\Gamma_{\rm MST} = \Delta\gamma^{\rm ref}_{\rm MST}. \tag{3.8}$$

The geometrical mean acts as an intermediate-pass that damps contributions from extreme edge lengths very effectively, hence significantly reduces the contribution of any "outlier".

Results

Using the method of Šubr et al. [2008] we have created initially mass-segregated star clusters to verify our algorithm. In the left plot of Fig. 3.39 we compare our improved measure $\Gamma_{\rm MST}$ ("geometric") with $\Lambda_{\rm MST}$ ("arithmetic"). We find that our measure of mass segregation, $\Gamma_{\rm MST}$, detects an intermediate degree of mass segregation, $S = 0.3$, with at least 3 σ significance while $\Lambda_{\rm MST}$ provides only a very weak 1 σ significance.

We have used this highly improved sensitivity to follow the dynamical mass segregation of a numerical star cluster model. The initial configuration is based on our ONC model as described in previous publications (e.g. Olczak et al. [2010]). Note that we use a spherically symmetric model with a smooth density distribution without any substructure. However, our stellar system is initially collapsing, starting from a virial ratio $Q = 0.1$. The simulations were carried out until a physical age of 5 Myr, corresponding to 13.5 N-body time units. On the right-hand side of Fig. 3.39 we see that $\Gamma_{\rm MST}$ increases rapidly within the first 2 Myr (or 5.5 N-body time units) and then saturates. The different mass groups are clearly separated, inversely correlated with the sample size.

Discussion and Conclusions

From numerical simulations of star cluster dynamics and star-disc encounters we find that pure gravitational interactions of disc-surrounded stars can lead to a significant depletion of their circumstellar matter. The disc-mass loss increases with cluster density but remains unaffected by the size of the stellar population. In moderately dense clusters like the ONC it is the massive stars that dominate the encounter-induced disc-mass loss by gravitational focusing of low-mass stars.

Massive stars have a much higher probability to be involved in a capturing encounter in such a cluster environment than solar-mass stars. In the ONC at least 10 % of the OB stars form a (transient) bound state due to dynamical capture that would be observed as a binary. The properties of these systems strongly depend on the cluster age with a development towards smaller periastra, higher mass ratios and longer duration of the bound states.

In extreme environments like the Arches cluster the pairwise interaction of all stars leads nearly to a complete destruction of the entire disc population. The preferential survivability of discs around B-type stars in the Arches cluster implies that these could be the best candidates for detecting planetary systems in Galactic starburst clusters.

We have developed a significantly improved method to measure mass segregation based on the minimum spanning tree (MST). In general, using only the ten to twenty most massive stars $\Gamma_{\rm MST}$ provides a robust and sensitive measure of mass segregation for the entire population of star clusters in our Galaxy. In particular, very low degrees of mass segregation can be detected in massive clusters like NGC 3603 that consist of 10k or more stars.

We note that mass segregation in a collapsing, intermediate-size stellar cluster of 1k stars can occur very quickly, i.e. within only a few crossing times. This finding demonstrates that rapid mass segregation (in terms of dynamical time scale) does *not* require substructure.

Acknowledgments

CO and RS acknowledge support by NAOC CAS through the Silk Road Project, and by Global Networks and Mobility Program of the University of Heidelberg (ZUK 49/1 TP14.8 Spurzem). CO appreciates funding by the German Research Foundation (DFG), grant OL 350/1-1. RS is funded by the Chinese Academy of Sciences Visiting Professorship for Senior International Scientists, Grant Number 2009S1-5. We have partly used the special supercomputers at the Center of Information and Computing at National Astronomical Observatories, Chinese Academy of Sciences, funded by Ministry of Finance of People's Republic of China under the grant ZDY Z2008–2.

We thank S. Aarseth for providing the highly sophisticated N-body code NBODY6 (and its GPU extension) and greatly appreciate his support.

Bibliography

Aarseth, S. 2003, Gravitational N-body Simulations (Cambridge, Cambridge University Press, 2003, 430 p.)

Aarseth, S. J. 2008, in Lecture Notes in Physics, Berlin Springer Verlag, Vol. 760, Lecture Notes in Physics, Berlin Springer Verlag, ed. S. J. Aarseth, C. A. Tout, & R. A. Mardling, 1–4020

Adams, F. C., Proszkow, E. M., Fatuzzo, M., & Myers, P. C. 2006, ApJ, 641, 504

Allison, R. J., Goodwin, S. P., Parker, R. J., et al. 2009, MNRAS, 395, 1449

Balog, Z., Muzerolle, J., Rieke, G. H., et al. 2007, ApJ, 660, 1532

Cartwright, A. & Whitworth, A. P. 2004, MNRAS, 348, 589

Clarke, C. J. & Pringle, J. E. 1993, MNRAS, 261, 190

Currie, T., Kenyon, S. J., Balog, Z., et al. 2008, ApJ, 672, 558

Evans, N. J., Dunham, M. M., Jørgensen, J. K., et al. 2009, ApJS, 181, 321

Farouki, R. T., Hoffman, G. L., & Salpeter, E. E. 1983, ApJ, 271, 11

Figer, D. F., Najarro, F., Gilmore, D., et al. 2002, ApJ, 581, 258

Gower, J. C. & Ross, G. J. S. 1969, Journal of the Royal Statistical Society. Series C (Applied Statistics), 18, pp. 54

Haisch, K. E., Lada, E. A., & Lada, C. J. 2000, AJ, 120, 1396

Haisch, Jr., K. E., Lada, E. A., & Lada, C. J. 2001, ApJ Lett., 553, L153

Hall, S. M. 1997, MNRAS, 287, 148

Hall, S. M., Clarke, C. J., & Pringle, J. E. 1996, MNRAS, 278, 303

Heller, C. H. 1993, ApJ, 408, 337

Heller, C. H. 1995, ApJ, 455, 252

Hillenbrand, L. A. 2002, ArXiv Astrophysics e-prints

Hillenbrand, L. A. 2005, ArXiv Astrophysics e-prints

Hut, P. 2003, in IAU Symposium, Vol. 208, Astrophysical Supercomputing using Particle Simulations, ed. J. Makino & P. Hut, 331–+
Khalisi, E., Amaro-Seoane, P., & Spurzem, R. 2007, MNRAS, 374, 703
Kley, W., Papaloizou, J. C. B., & Ogilvie, G. I. 2008, A&A, 487, 671
Lada, C. J. & Lada, E. A. 2003, ARA&A, 41, 57
Lada, C. J., Muench, A. A., Haisch, Jr., K. E., et al. 2000, AJ, 120, 3162
Martins, F., Hillier, D. J., Paumard, T., et al. 2008, A&A, 478, 219
McMillan, S. L. W. 1996, in Astronomical Society of the Pacific Conference Series, Vol. 90, The Origins, Evolution, and Destinies of Binary Stars in Clusters, ed. E. F. Milone & J.-C. Mermilliod, 413–+
Moeckel, N. & Bally, J. 2006, ApJ, 653, 437
Moeckel, N. & Bally, J. 2007, ApJ, 656, 275
Najarro, F., Figer, D. F., Hillier, D. J., & Kudritzki, R. P. 2004, ApJ Lett., 611, L105
Olczak, C., Pfalzner, S., & Eckart, A. 2010, A&A, 509, A260000+
Olczak, C., Pfalzner, S., & Spurzem, R. 2006, ApJ, 642, 1140
Ostriker, E. C. 1994, ApJ, 424, 292
Pfalzner, S. 2004, ApJ, 602, 356
Pfalzner, S. & Olczak, C. 2007, A&A, 462, 193
Pfalzner, S., Olczak, C., & Eckart, A. 2006, A&A, 454, 811
Pfalzner, S., Umbreit, S., & Henning, T. 2005, ApJ, 629, 526
Portegies Zwart, S. F., McMillan, S. L. W., Hut, P., & Makino, J. 2001, MNRAS, 321, 199
Scally, A. & Clarke, C. 2001, MNRAS, 325, 449
Schmeja, S. & Klessen, R. S. 2006, A&A, 449, 151
Sicilia-Aguilar, A., Hartmann, L., Calvet, N., et al. 2006, ApJ, 638, 897
Spitzer, L. J. 1969, ApJ Lett., 158, L139+
Spurzem, R. 1999, Journal of Computational and Applied Mathematics, 109, 407
Spurzem, R. & Takahashi, K. 1995, MNRAS, 272, 772
Stolte, A., Brandner, W., Grebel, E. K., Lenzen, R., & Lagrange, A.-M. 2005, ApJ Lett., 628, L113
Šubr, L., Kroupa, P., & Baumgardt, H. 2008, MNRAS, 385, 1673

3.16 A Possible Distributed Population Near the Cluster-Forming Region W3(OH)

Carlos G. Román-Zúñiga[1], G. Megías Vázquez[2], J. F. Alves[3], and E. A. Lada[4]

[1] Instituto de Astronomía (Sede Ensenada), Universidad Nacional Autónoma de Mexico
[2] Departamento de Física Atómica y Molecular, Universidad de Sevilla, Spain
[3] Astronomy Department, University of Wien, Austria
[4] Astronomy Department, University of Florida, USA

Abstract

We describe some of our preliminary results from a near-infrared imaging study of the W3(OH) region. We compare the brightness distribution of young embedded clusters and the stars spread to the East with cluster models of different ages. Our analysis suggests that stars outside the clusters may belong to a spread population from a previous episode of formation.

Introduction

The current picture of star formation is changing rapidly. Some definitions are perhaps too rigid as observations show that as a result of the heterogeneity of star-forming environments there is a consequent diversity among the stellar aggregations they produce. This is evident even at the level of their most basic properties (e.g. sizes, numbers and density structures).

Embedded clusters in a molecular cloud or complex may trace the current or more recent episode of formation. As stellar systems, they can be dynamically bound or not, thus they may remain together or disperse rapidly. In simple terms, a cluster requires to have at least a high volume density, a high forming efficiency, a large relaxation timescale and a minimum number of members to survive as a system once it disperses its prenatal gas. One simple scenario contemplates two "modes" of formation: clusters and small or "distributed" groups (e.g. Meurer et al. [1995]). The former usually involves the presence of massive members –which also serve as detection beacons–, while in the second case, with massive stars not necessarily present[12], they are small and feeble, and thus difficult to spot. Failing to detect a small group near its formation stage (when it may still be traced by a large infrared excess fraction, bright infrared sources or associated nebulosities) will make it difficult to trace back its origin. Moreover, not being able to detect sparse populations does not mean they are not crucial for the reconstruction of the star-forming history of clouds. Surveys of molecular clouds show that small groups and so called distributed populations may account for a significant percentage of the total young star population in star-forming clouds (10 to 30%; e.g Carpenter [2000], Román-Zúñiga et al. [2008]). Also, distributed populations may have important implications for the global efficiency of formation in clouds (Bonnell et al. [2011]). Observations suggest that sparse members also help to account for age spreads (Nakajima et al. [1998]; Feigelson & Townsley [2008]) and may be present in any environment, from relatively low yield clouds like Taurus (Slesnick et al. [2006]) to massive complexes like the Carina Nebula (Preibisch et al. [2011]).

We chose W3, a very prominent cluster-forming region in the Heart and Soul molecular complex, as part of a study of the influence of the local environment in the modes of star formation. One of our main goals is to trace a distributed or low-density population near or at the same regions where we observe clusters, and to estimate its relative importance in terms of the star-forming history of the cloud. W3, located at a distance of 2 kpc, hosts three major episodes of recent cluster formation, with IC 1795 marking the start line at 3 – 5 Myr (Oey et al. [2005]), followed by the "main" W3 to its West side and W3(OH) to the East. It has been suggested that IC 1795 triggered the other two episodes (Oey et al. [2005]). The Chandra study by Feigelson et al. [2008] suggested that the clusters are well extended and highly structured, with sources located at relatively large distances from the dynamical centers, including a relatively isolated O star that might have escaped from the main cluster.

[12] for instance, O stars *forming* in isolation would be extremely rare, see paper by in these same proceedings

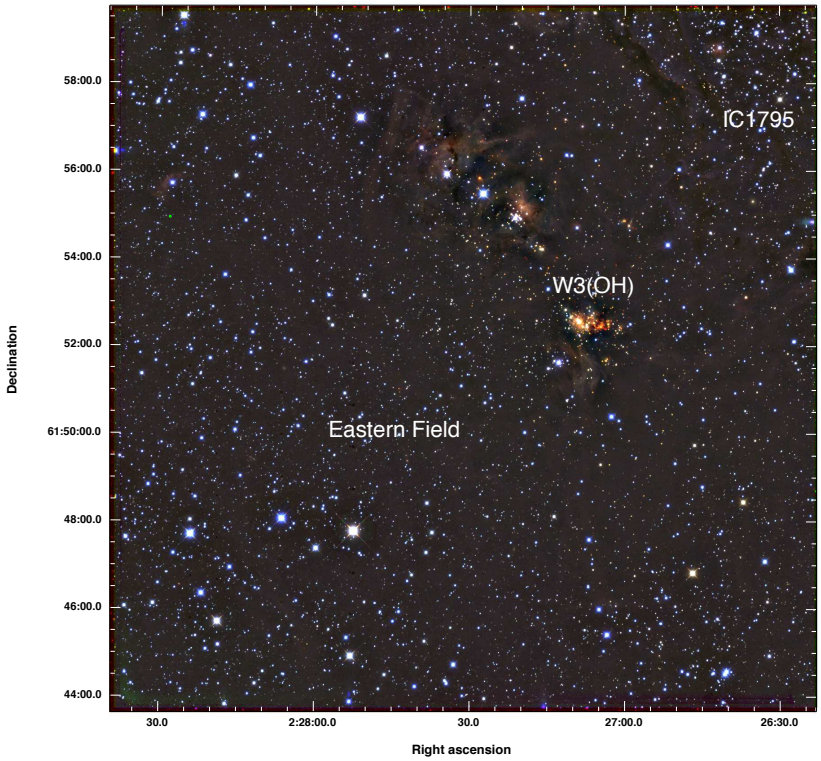

Figure 3.40: The panel shows our Calar Alto image of the W3(OH) region. Labels indicate the location of IC 1795 (nor complete in this field) and the main cluster-forming region in W3(OH), as well as the Eastern field where we attempted to search for a distributed population.

Near Infrared Data

We imaged W3(OH) within a relatively large area to its Eastern side using the 15×15 arcmin^2 FOV of the Omega 2000 camera at the 3.5 m telescope in Calar Alto. We obtained deep ($K < 19.0$ mag) images in J, H and K which resolved in great detail the cluster episode at W3(OH). Our catalogues probe well into the mass distribution of the cluster population, possibly resolving stars near the Deuterium burning limit.

From our sample we determined which stars presented a significant infrared excess, above a brightness of K=16.5 mag to avoid contamination by quasars and high redshift dusty galaxies, which can mimic colours of embedded T-Tauri stars (Foster et al. [2008]). When comparing the spatial distribution of near-infrared infrared excess sources with that of mid-infrared excess sources in IRAC-Spitzer catalogues (Ruch et al. [2007]) and embedded sources from the Chandra catalogue, we confirmed that most, but not all of the young members present in our field belong to the IC 1795 and W3(OH) clusters. It is worth mentioning that the largest cluster in W3(OH) is very prominent and lies on one edge of a dark filament that roughly delimitates the boundaries of IC 1795. Following this filament to the north, another two small clusters are clearly distinguished, each with a decreasing number of members. In addition to these, our spatial distribution maps show excess sources located at distances up to 8 pc (near the edge of the field). Some of these spread over excess sources, especially those lying near W3(OH) also appear to belong to small groups.

We divided the region into three sections marked by circles at 5 and 10 pc from the center of IC 1795 (located off our field): the first circle separates out sources from the young open cluster, another one encloses the band where the bright W3(OH) clusters are located, and the third one comprises the rest of the field to the East (see Fig. 3.40). We constructed K band luminosity functions for each field section and carefully subtracted the luminosity function from a nearby control field with minimum extinction. The brightness function in the East or "bottom" region is comparable in significance to that of the clusters. The three clean functions were then compared with models of embedded clusters using the Monte Carlo engine by Muench et al. [2000]. In Fig. 3.40 we show the luminosity functions compared to those from the cluster models. For each section we made sets of 500 artificial embedded cluster realizations, each with an age between 0.5 and 12 Myr, an IMF similar to the Trapezium cluster, a 20% fraction of binaries and

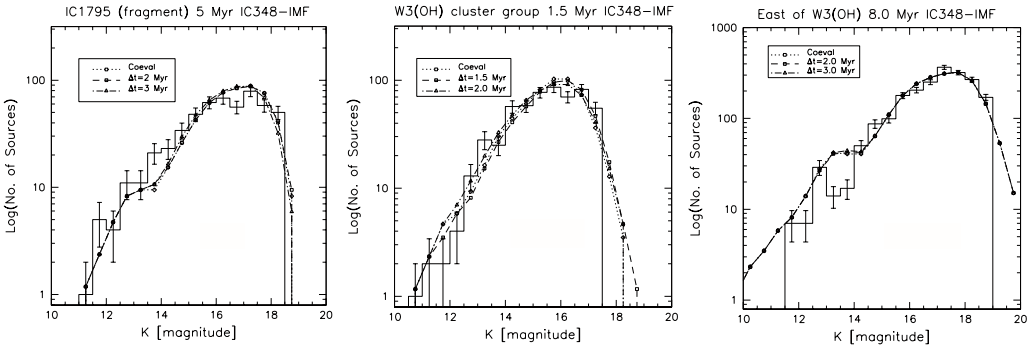

Figure 3.41: *Panels from left to right*: K luminosity functions and their best-fitting artificial cluster models for IC 1795, W3(OH), and the Eastern region, respectively. Notice that coeval and age spread criteria yield similar results. As expected,W3(OH) is very young with a best age fit of 1.5 Myr. For IC 1795, we obtained a best fit age of 5 Myr. For the bottom region, the KLF adjusts well to a population similar to an embedded cluster of 8 Myr.

similar excess fractions and extinction distributions as those in each field section. We found that the IC 1795 section compares well with a cluster model with an age of 5 Myr, and the W3(OH) clusters compare well with a cluster model with an age of 1.5 Myr, both in excellent agreement with literature values. For the East section, the best model fit corresponds to an embedded cluster with an age of 8 Myr.

Discussion

We considered the possibility that the population at the Eastern side could belongs to some other cluster located in the foreground or background of the cloud. We actually found that the cluster Tombaugh 4 is located just a few pc to the East of our field, but after comparing its brightness distribution from 2MASS with that of the East section we see that Tombaugh 4 is significantly more luminous. It is located at a distance of 4 kpc and has an age of 8.5 Gyr. Also, a radial profile constructed from IPHAS data shows that it is very unlikely that Tombaugh 4 reaches into our field, or at least not with enough surface density. Our data could suggest that we may be observing a distributed population to the East of W3(OH), which may belong to an older episode of formation. One hypothetical scenario would implicate a previous stage in the cloud where small groups formed from small gas clumps and dispersed quickly during the contraction of the cloud, then IC 1795, W3-main and W3(OH) formed once larger, denser clumps of material piled up at the north edge of the W4/IC 1805 super bubble.

Acknowledgments

GMV wants to acknowledge CSIC, Spain for support from a JAE-Intro summer scholarship at the Instituto de Astrofísica de Andalucía. CRZ wants to acknowledge CONACYT, México for support from a repatriation grant at the Instituto de Astronomía, UNAM.

Bibliography

Bonnell, I. A., Smith, R. J., Clark, P. C., & Bate, M. R. 2011, MNRAS, 410, 2339
Carpenter, J. M. 2000, AJ, 120, 3139
Feigelson, E. D. & Townsley, L. K. 2008, ApJ, 673, 354
Foster, J. B., Román-Zúñiga, C. G., Goodman, A. A., Lada, E. A., & Alves, J. 2008, ApJ, 674, 831
Meurer, G. R., Heckman, T. M., Leitherer, C., et al. 1995, AJ, 110, 2665
Muench, A. A., Lada, E. A., & Lada, C. J. 2000, ApJ, 533, 358
Nakajima, Y., Tachihara, K., Hanawa, T., & Nakano, M. 1998, ApJ, 497, 721
Oey, M. S., Watson, A. M., Kern, K., & Walth, G. L. 2005, AJ, 129, 393
Preibisch, T., Ratzka, T., Kuderna, B., et al. 2011, A&A, 530, A34+
Román-Zúñiga, C. G., Elston, R., Ferreira, B., & Lada, E. A. 2008, ApJ, 672, 861
Ruch, G. T., Jones, T. J., Woodward, C. E., et al. 2007, ApJ, 654, 338
Slesnick, C. L., Carpenter, J. M., Hillenbrand, L. A., & Mamajek, E. E. 2006, AJ, 132, 2665

3.17 Unlocking the Formation History of M 33 as Revealed by its Star Clusters

Izaskun San Roman

Department of Astronomy, University of Florida, 211 Bryant Space Science Center, Gainesville, FL 32611-2055, USA. E-mail: izaskun@astro.ufl.edu

Abstract

Star clusters provide a unique and powerful probe useful for studying the star formation histories of galaxies. In particular, the ages and metallicities of star clusters bear the imprint of the galaxy formation process. M 33 is the only nearby late-type spiral galaxy and it provides a notable connection between the cluster populations of earlier-type spirals and the numerous, nearby later-type dwarf galaxies. However, it is only recently that the entire body of M 33 has been searched for star clusters using wide-field CCD images. We discuss here photometric properties as well as structural parameters of the star cluster system in M 33 based on the largest sample to-date. We examine colour-colour diagrams of 599 new candidate stellar clusters and 204 confirmed clusters, and analyze their spatial distribution. In addition, we determine structural parameters, using King model fits, in a sample of 161 confirmed star clusters. Through the properties of the star clusters in M 33, we will provide relevant information of the star formation history and evolution of the galaxy.

Introduction

It is widely accepted that galaxy evolution occurs in the framework of the Lambda-Cold Dark Matter (Λ-CDM) model. Within this hierarchical clustering theory, large disk galaxies, like the Milky Way (MW) and M 31, derive from the merger and accretion of many smaller subsystems. It is less clear how accurate the Λ-CMD framework is at lower galaxy masses and if we should expect disrupted dwarf galaxies of tidal tails in the vicinity of a dwarf spiral galaxy. The best way to answer these questions is to study the nearest examples of dwarf spiral galaxies. M 33 is the only nearby late-type spiral galaxy, and it provides us with the essential piece between the populations of massive spiral galaxies and the numerous dwarf galaxies.

The ages, metallicities and kinematics of star clusters (SCs) are directly affected by the galaxy formation history. This makes them powerful tracers of the halo, disk and bulge populations. Therefore, the SC system in M 33 is an ideal laboratory for studying the formation and evolution of galaxies as well as SC themselves. We will make use of the SCs properties of M 33 to study its formation and evolution.

Photometric Properties

As pointed out by several authors (e.g. Sarajedini & Mancone [2007]; San Roman et al. [2009]), the sample of clusters in M33 suffers from significant incompleteness. For this reason, we have undertaken a photometric study of M 33 (San Roman et al. [2010]) using the MegaCam/CFHT instrument that offers nearly a full 1 x 1 deg^2 field of view with a high angular resolution of 0.187 arcsec/pixel. After subtracting the stellar PSF from all of the sources in our frames, extended objects leave a doughnut-shaped appearance, as they are under-subtracted in the wings and over-subtracted in the center. After visual inspection of the residual images, this technique leaves us 599 new candidate stellar clusters and 204 previously confirmed clusters.

We have performed *ugriz* integrated photometry of the candidate and confirmed. Fig. 3.42 shows colour-colour diagrams of the candidate and confirmed SCs as compared with simple stellar population (SSP) models. It is important to note that Galev models include contributions from nebular emission, considering the continuum nebular and also emission lines.

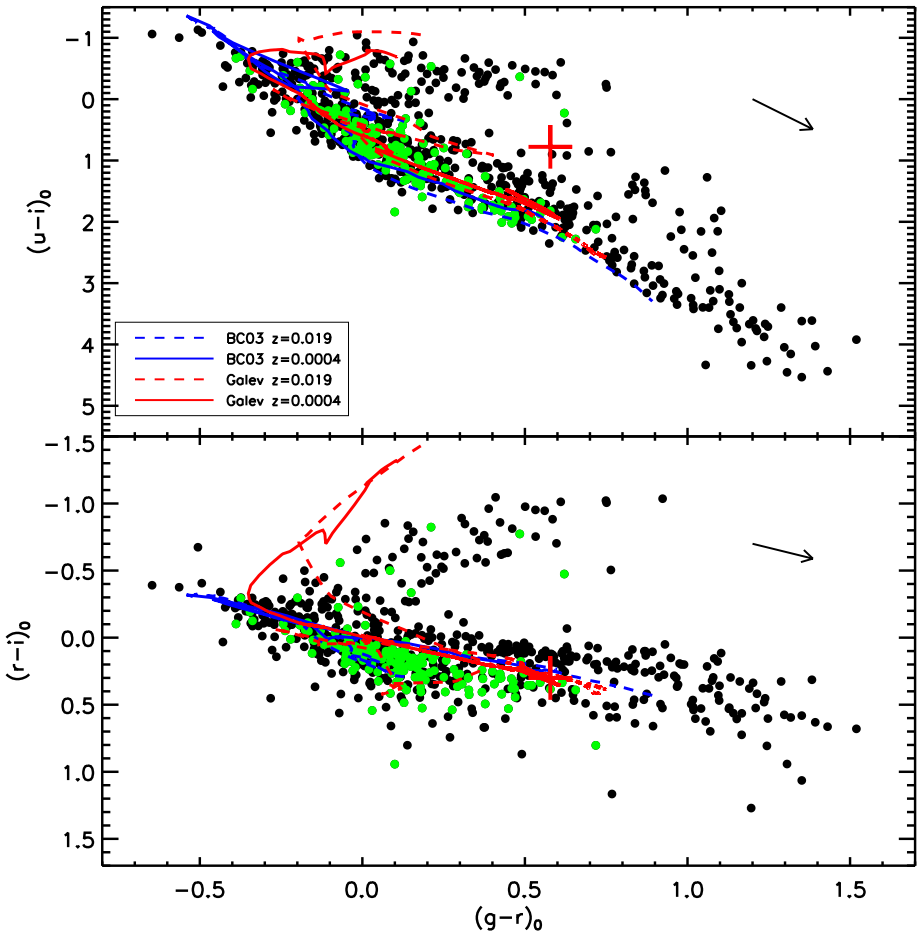

Figure 3.42: Colour-colour diagrams of the candidate SCs (black circles) and confirmed SC (green circles). The solid lines correspond with SSP models of Bruzual & Charlot [2003, BC03] and Kotulla et al. [2009, Galev] for two different metallicities. From San Roman et al. [2010]

A significant fraction of "bluish" clusters, that occupy a unique location in the diagram, appear in both panels. These clusters represent a finger-like feature that deviates from the expected direction of evolution. Based on the different sets of models, this feature could be associated with the presence of a significant population of very young clusters ($< 10^7$ yr) exhibiting nebular emission. The colour-colour diagram reveals a wide age range of 1 Myr – 10 Gyr with at least 50% of objects corresponding to young clusters ($<$ 100 Myr) and 10% of the total corresponding to very young clusters with nebular emission. The broad range of colours implies a large range of ages, suggesting a prolonged epoch of formation.

When comparing M 33 with similar morphological-type galaxies such as NGC 300 or M 101, M 33 seems to posses a unique very young SC population. Environmental factors may play a key role in the star formation history of M 33 as compared to NGC 300, which is isolated from other galaxies. Close encounters with M 31 could have triggered an epoch of star formation in M 33.

Spatial Distribution

We have divided our sample into two groups based on comparisons with SSP models, older than 100 Myr and younger. The left panel in Fig. 3.43 shows the cumulative radial distributions of the young and old cluster populations as compared to the field-star population from Hartman et al. [2006]. Young clusters follow a spatial distribution similar to the young field stars. The older clusters are more dispersed over a wider region than the younger ones, indicating that the majority of the older clusters likely belong to the halo while the younger SCs generally belong to the disk of M 33.

The right panel in Fig. 3.43 shows the radial density distribution of the sample. The star and cluster distributions have been scaled to match in the region between R = 0.6 – 2 kpc where the completeness levels are likely similar. Inside $\sim$ 0.8 kpc, the cluster profile presents some level of incompleteness. For

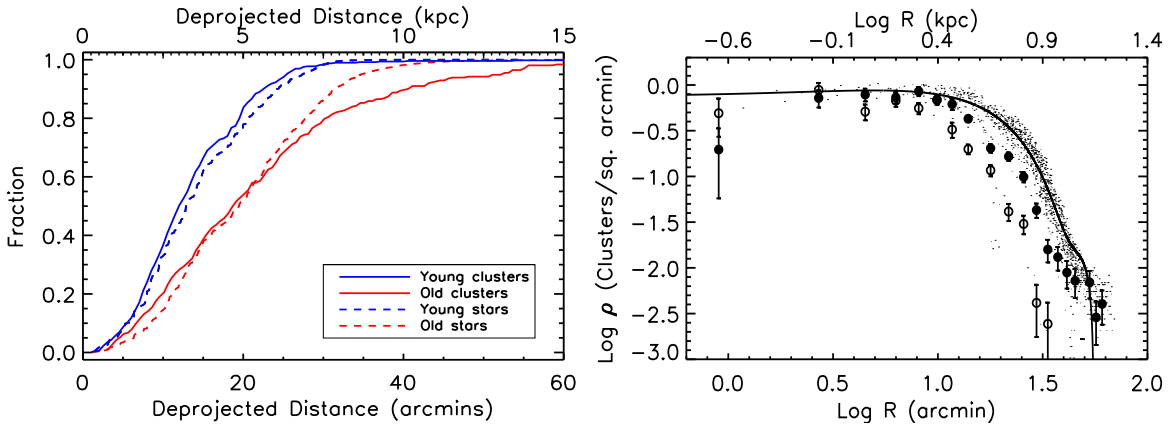

Figure 3.43: *Right*: Cumulative radial distribution for the SCs and field stars. *Left*: Radial density distribution of SCs (filled circles: candidates and open circles: confirmed) and fields stars (small dots) versus deprojected radius. The solid line corresponds with the best fit to the field stars. From San Roman et al. [2010].

a given radial bin in the outer region of the galaxy, the density of clusters is significantly lower than the density of stars, suggesting that the cluster system in M 33 has suffered from destruction or depletion of clusters. Environment effects, such as interactions between M 33 and M 31, can play a role in the depletion or disruption of clusters. Regardless of the source of this anomaly, we would need an additional $\sim$ 350 clusters between R = 3 – 9 kpc in order to match the stellar density in the same region.

Structural Parameters

We have analyzed the surface brightness profiles of the 161 confirmed SCs from San Roman et al. [2009]. We have fitted elliptical isophotes to the cluster images to obtain cluster shapes. With a mean ellipticity of e = 0.2, M 33 clusters are, on average, more flattened than those of the MW or M 31 and more similar

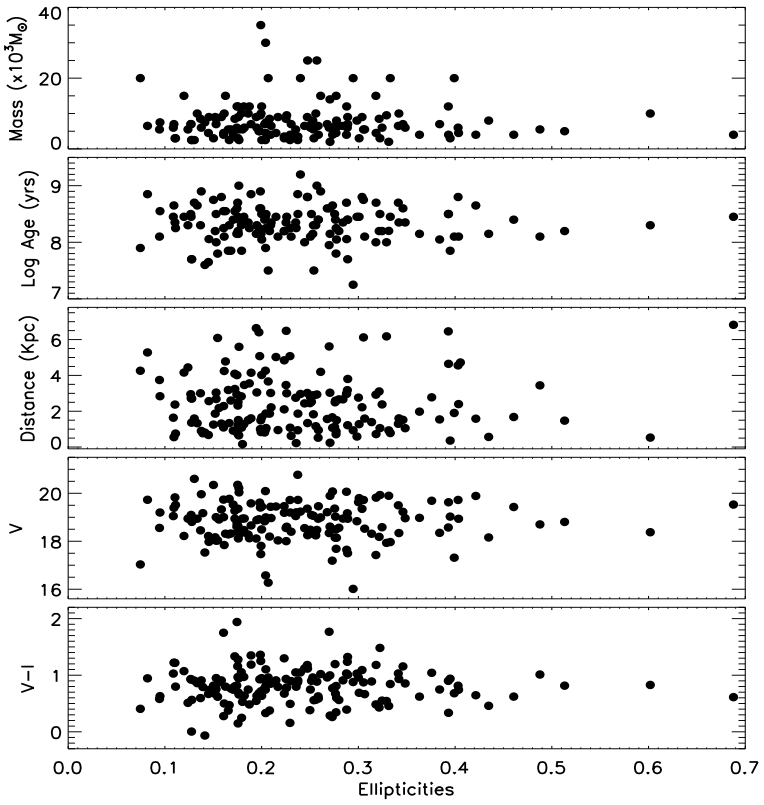

Figure 3.44: Ellipticity versus different cluster properties.

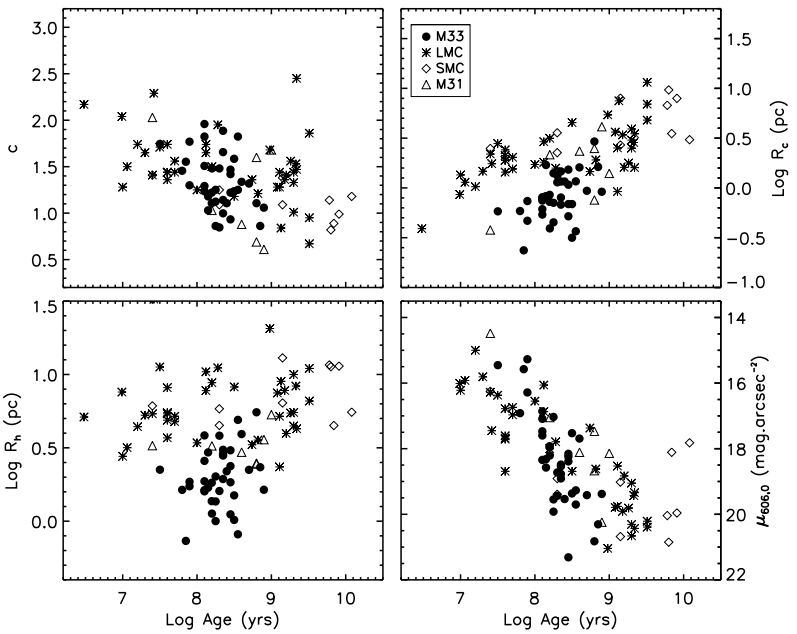

Figure 3.45: Structural parameters as a function of age.

to clusters in the SMC. Fig. 3.44 shows no correlations between the ellipticity and any of the explored properties. If ellipticities in M 33 clusters are not mainly driven by any cluster property, tidal forces may have significant effects on the elongation of these clusters.

Additional structural parameters for the clusters were derived by fitting King models [King, 1962] to the surface brightness profiles. Fig. 3.45 shows different structural parameters versus age and compares them with M 31 (Barmby et al. [2007]), LMC and SMC (McLaughlin & van der Marel [2005]). Although all of the galaxies follow essentially the same trends, M 33 clusters cover a slightly smaller range of concentration (c = log [R_c/R_t]) and central surface brightness ($\mu_{606,0}$) than M 31. With an average of 1.3, the concentration is slightly smaller than the 1.4 for MW, M 31 and LMC. The core radius (R_c) increases significantly with increasing clusters age. This trend has been suggested to be a real evolution in the structure of clusters as they grow older since significant mass loss from stellar evolution could cause the cluster to expand.

Following Barmby et al. [2007], we use the renormalized galactocentric distance as a better indicator

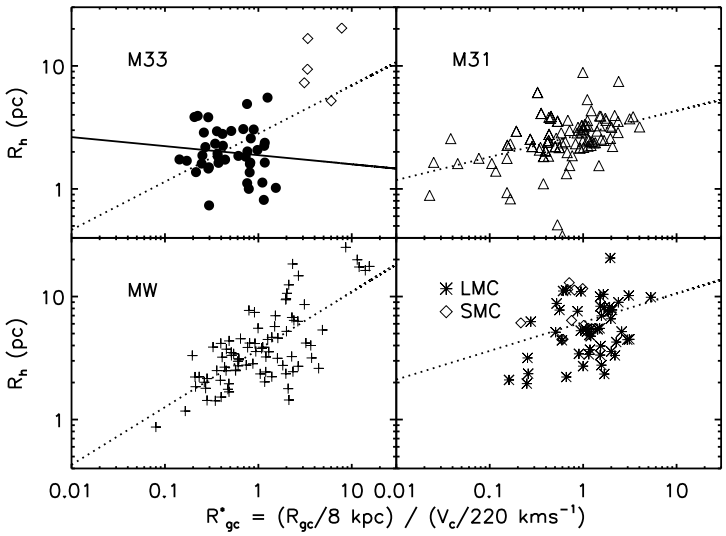

Figure 3.46: Projected half-light radius as a function of renormalized galactocentric distance. Dashed lines are the least-squares fits for each sample. Solid line corresponds to the least-squares fits of our sample (filled symbols).

of galactic potential than galactocentric distance alone. Fig. 3.46 presents the half-light radius (R_h) as a function of renormalized galactocentric distance for nearby galaxies. The lines correspond to least-squares fits for each sample. No correlation has been found in our M 33 sample. If we combine our sample with the 5 known clusters in the outskirt of M 33 (open symbols in top left panel), the data suggest a similar tendency.

Summary

Analysis of multi-colour photometry of the M 33 star cluster system reveals a wide range of colours implying a large range of ages. Colour-colour diagrams present a finger-like feature that deviates from the expected direction of evolution and suggests a very young cluster population with significant nebular emission. Comparison of the radial density distribution between the field stars and cluster sample indicates a deficit of clusters. M 33 SCs are more flattened, on average, than MW or M 31. No correlation has been found between the ellipticities and cluster properties as a function of age or luminosity. Environmental factors, such as interactions between M 33 and M 31, may play a key role in the star formation history of M 33.

Bibliography

Barmby, P., McLaughlin, D. E., Harris, W. E., Harris, G. L. H., & Forbes, D. A. 2007, AJ, 133, 2764
Bruzual, G. & Charlot, S. 2003, MNRAS, 344, 1000
Hartman, J. D., Bersier, D., Stanek, K. Z., et al. 2006, MNRAS, 371, 1405
King, I. 1962, AJ, 67, 471
Kotulla, R., Fritze, U., Weilbacher, P., & Anders, P. 2009, MNRAS, 396, 462
McLaughlin, D. E. & van der Marel, R. P. 2005, ApJS, 161, 304
San Roman, I., Sarajedini, A., & Aparicio, A. 2010, ApJ, 720, 1674
San Roman, I., Sarajedini, A., Garnett, D. R., & Holtzman, J. A. 2009, ApJ, 699, 839
Sarajedini, A. & Mancone, C. L. 2007, AJ, 134, 447

3.18 Properties of the Young Embedded Cluster G287.47-0.54 = Tr14-N4 in NGC 3372

Mauricio Tapia[1], M. Roth[2], J. Bohigas[1] and P. Persi[3]

[1] Instituto de Astronomía, Universidad Nacional Autónoma de México, Apdo. Postal 877, 22800 Ensenada, BC, Mexico
[2] Las Campanas Observatory, Carnegie Institution of Washington, Casilla 601, La Serena, Chile
[3] Istituto Nazionale di Astrofisica - IASF, Via del Foso del Cavaliere, I-00133, Roma, Italy

Abstract

New deep broad- and narrow-band (JHK and Br γ at 2.17 μm and H_2 at 2.12 μm) images of the mid-infrared source G287.47-0.54 (Tr14-N4) are presented and analysed along with archive 3.6 to 8 μm *Spitzer* images. We demonstrate the presence of a compact (0.3 pc) embedded infrared cluster with at least 72 young members. The age of the cluster is around 10^5 years and $\geq 32\%$ of the sources show significant infrared excess emission. The SEDS of the two most luminous sources indicate that these are Class I young stellar objects. We found a 0.05 pc-long disk with $i \sim 40-70$ deg around source #902, which is seen directly through the dust disk only at $\lambda \geq 2.2$. Most of its near-IR radiation is scattered light from lobes on both sides of the disk. A second YSO, #438, displays symmetrically elongated features that seem to be caused by scattering, also suggesting the presence of a disk. The young cluster G287.47-0.54 is embedded at the head of a dust pillar where the interaction of a very massive cluster, in this case Tr 16, with a dense molecular core has triggered a new star formation episode. We suggest that the dense cloudlet is sticking out of the remnant giant molecular cloud located at the far side of the northern Carina nebula. Also, five small molecular hydrogen 2.12 μm emission knots with no Brγ counterpart are found in the vicinity of a nearby CO emission peak. These shock excited knots evince the presence of mass outflows in the region. At present, it is unclear whether the engine of this outflow is a member of the cluster or rather a yet undetected, younger YSO deeply embedded in the molecular core.

Introduction

G287.47-0.54 is a mid-infrared MSX source in the northern part of the Carina nebula named Tr 14-N4 by Rathborne et al. [2002]). These autors provided evidence of its very young age. This suggestion has been further supported by infrared observations by Tapia et al. [2003], Rathborne et al. [2004], Sanchawala et al. [2007] and others. Based on the integrated flux at 870 μm, Preibisch et al. [2011] estimated a mass of 1,000 to 2,000 $M_\odot$ for the cloud associated with this source. In this contribution we present new deeper and higher-resolution near-infrared images of the area around G287.47-0.54 supplemented by archive *Spitzer*-IRAC images. The properties of an embedded cluster with at least 72 members found to be associated with a photodissociation region (PDR) powered by Tr 16 are described. The details and full discussion can be found in Tapia et al. [2011].

Observations and results

We have obtained deep narrow- and broad-band near-infrared 130×130 arcsec^2 images of the region containing G287.47-0.54 with PANIC, a near-infrared camera equipped with a Rockwell 1024×1024 Hawaii array that provides a 2×2 arcmin^2 field of view with 0.125 arcsec/pix (Martini et al. [2004]) attached to the 6.5 m Baade Magellan telescope at Las Campanas Observatory. The JHK_s images were obtained on 10 April 2007 and were supplemented with images taken on 10 June 2009 through narrow-band filters centred in the H_2, and Brγ lines at 2.12 and 2.17 μm and bandwidths of 0.024 and 0.022 μm, respectively.

Eight hundred and twenty six sources in the field were measured photometrically in the K_s band,

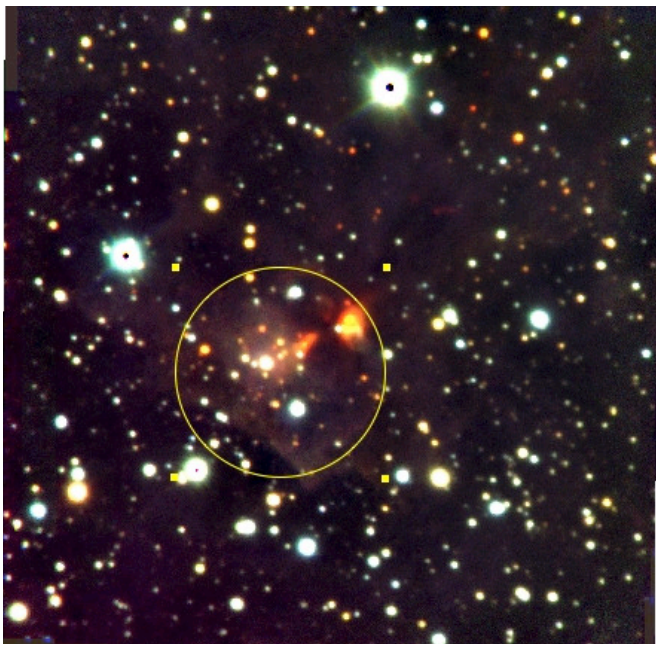

Figure 3.47: Colour-coded JHK_s image of G287.47-0.54 (Tr 14-N4) taken with PANIC on the Baade/Magellan telescope. The centre is at $\alpha = 10^{\rm h}\ 44^{\rm m}\ 32.6^{\rm s}$; $\delta = -59^o\ 33'\ 19''$ (J2000). The 47 arcsec-diameter circle marks the formal boundaries of the embedded young stellar cluster.

600 in both H and K_s and 485 in the three bands. The limiting magnitudes are estimated to be 19.0, 18.6, 18.2, in JHK_s respectively. Radial star counts proved the presence of a small cluster of very red sources of approximate diameter 47 arcsec centred close to the nominal position of G287.47-0.54. The K_s-band frame is displayed in Fig. 3.47 showing the formal boundaries of the cluster, and the $J-H$ vs $H-K_s$ diagrams of all sources within and outside these limits are shown in Fig. 3.48, where the different photometric characteristics of the sources belonging to the cluster and those in the surroundings are evident. Fig. 3.49 shows a K_s vs $H-K_s$ diagram of all probable cluster members, most lying on or to the right of the 10^5-year isochrone.

Archive images of the same region taken with IRAC on the *Spitzer* infrared space telescope were also analysed. The strong diffuse PAH emission dominating the 8 μm frame delineates a PDR with a "head-tail" structure reminiscent of other "dust pillars" seen in the souther part of the Carina nebula (eg. Rathborne et al. [2004]). The centre of the embedded cluster is found at the "head" of the pillar, where the two most luminous and youngest sources, #902 and #438, are located. Both these sources have SEDs of Class I YSO and extended morphology in the H and K_s bands that show the presence of associated dust disks, though at different inclination angles. Fig. 3.50 shows, at 2.2 μm, the nucleus of the cluster with a gray scale to clearly illustrate the disks. In all IRAC frames, both sources are bright and unresolved.

The westernmost of these sources, #902, is dominated by two lobes of emission separated by a dark lane. The asymmetry of the emission and the different IR colours of both lobes suggest that the inclination angle of the disk is 40 to 70 deg and that the lobes are scattered light from the central YSO barely seen in K_s near the centre of the dark band. Source #438, shows elongated emission that could be interpreted as sections of the projected disk being illuminated by the central YSO. Fits of Robitaille et al.'s [2007] to the SEDs of these objects with inclination angles compatible to the their observed projected morphology, suggest stellar masses of $6-9M_\odot$ and luminosities of $400-500L_\odot$

Some 30 arcsec (0.39 pc) to the northwest of source #902, a series of five small 2.12 μm molecular hydrogen line emission knots, with no Brγ counterpart, was detected. The brightness of the five small H_2 knots, their compactness and grouping suggest that these are shock-excited regions resembling Herbig-Haro objects (HHOs), thus strongly suggesting the presence of outflows in the region. Any one of the YSOs in the cluster nucleus may be producing a sizable outflow, with the most likely candidates being sources #902 and #438. It is also possible that the outflow engine is an undetected (at $\lambda \leq 10.4\,\mu$m) deeply embedded Class 0 object. This possibility is supported by the occurrence of a nearby CO emission peak. With the available data, no firm conclusion on this can be drawn.

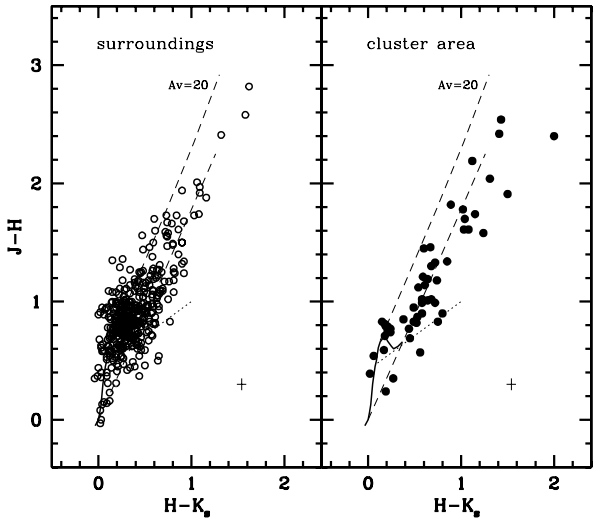

Figure 3.48: *Left*: $J-H$ *vs.* $H-K_s$ diagram for all the sources outside the cluster circle (see text) that were measured in JHK_s. *Right*: Same plot but for sources within the cluster. In both panels, the solid line marks the locus of main sequence stars (Koornneef [1983]). The dotted line marks the region occupied by unreddened T Tauri stars. The parallel dashed lines represent the standard reddening for late and early-type stars for $A_V = 20$. The small cross to the lower right represents the typical photometric errors.

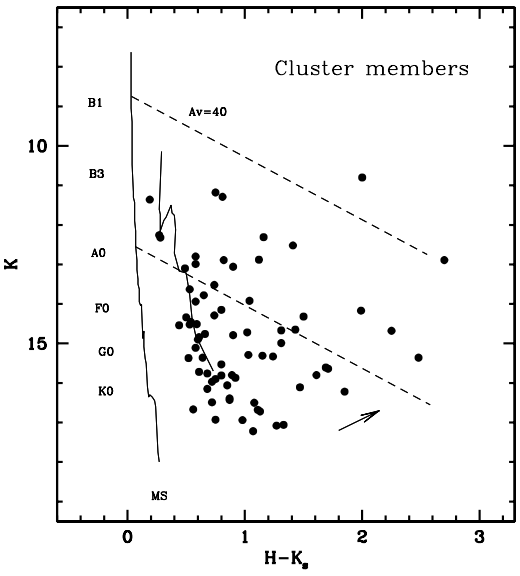

Figure 3.49: K_s versus $H-K_s$ diagram of all sources with HK_s colours of all probable cluster members. The ZAMS for $d = 2.35$ kpc and $A_V = 1.4$ and a 10^5 year isochrone (Pahla & Stahler [1999]) at $d = 2.4$ kpc and $A_V = 5.8$ are shown as continuous lines. The broken lines are the reddening vectors (Rieke & Lebofsky [1985]) for B0 and A0 stars, and the arrow marks the average slope of near-infrared excesses caused by discs around young stellar objects, as determined by López-Chico & Salas [2007].

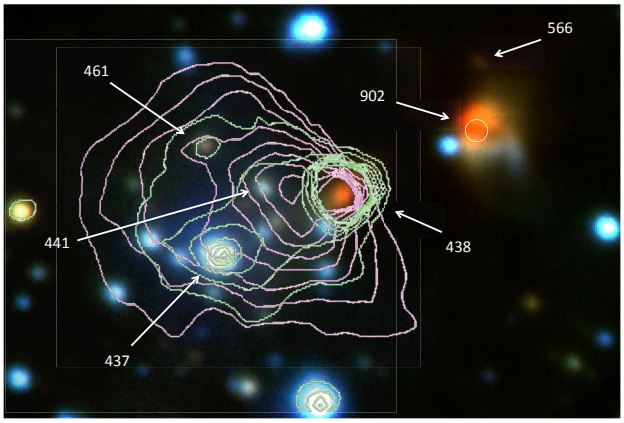

Figure 3.50: Colour-coded enlargement of the nuclear region of N4 through the JHK_s filters with the intensity scale chosen so to illustrate the morphology of the brightest sources. The individual sources discussed in the text are labeled. The contours represent the IRAC 8 μm (magenta) and the 4.5 μm (green) image. The diffuse emission in the former is dominated by the 7.8 μm PAHs line, and the latter by scattered continuum and warm dust emission. For clarity, the brightest contours from the point-like source #438 have been suppressed; likewise, all contours corresponding to source #902 are omitted and only a small white circle is drawn to indicate the location of the unresolved source in the four IRAC bands.

Conclusions

The following are the main conclusions of the present work.

1. The presence of a photodissociation (PDR) front as a consequence of the interaction of strong UV radiation and stellar winds from external main sequence massive stars, most probably members of Tr 16, with a dense molecular clump. This PDR is clearly delineated by strong emission of PAHs that dominates the IRAC 5.8 and 8 μm bands. The morphology of this structure is similar to that found in other dust pillars, particularly in the southern half of NGC 3372 (eg. Rathborne et al. [2004]).

2. The presence of a compact (diameter $\sim$ 0.5 pc) embedded cluster with its core located just behind the PDR front. We identified 72 probable members, a third of which show significant excess emission at $\lambda > 2\,\mu$m . The infrared colour-magnitude diagram shows a concentration of sources around a 10^5 year isochrone, suffering a minimum extinction of $A_V \simeq 6$, that is some 3 to 4 magnitudes higher than the stars in Tr 16. The two most luminous sources ($L \sim 400 - 500 L_\odot$), #902 and #438, have complex morphology in the near-IR, with resolved disks either in reflection or in absorption. These seem to be significantly younger than the bulk of the cluster.

3. A set of five small molecular hydrogen emission knots at 2.12 μm with no Brγ counterpart are found some 0.4 pc to the northwest of the core of the embedded cluster and very close to the molecular core corresponding to a CO emission peak (Brooks et al. [1998]). These emission nebulae are probably shock excited, suggesting the presence of mass outflows in the region. At present, it is unclear whether the engine of this outflow is a member of the cluster or rather a yet undetected, younger (Class 0) YSO deeply embedded in the molecular core.

4. In spite of TR 14-N4 being at a projected distance of only 4.6 arcmin from the core of Tr 14, a compact open cluster rich in main sequence massive stars (eg. Ascenso et al. [2007]), the "head-tail" configuration of the PDR characteristic structure suggests that most of the interacting energy comes from the direction of the nucleus of the more distant (in projection, 8 arcmin), more dispersed massive cluster, Tr 16 (of which η Carinae is its most famous member).

Acknowledgments

Part of this work was financially supported (MT) by DGAPA-UNAM grant IN-100210. This paper makes use of archival data obtained with the *Spitzer Space Telescope*, which is operated by the Jet Propulsion Laboratory, California Institute of Technology (CIT) under National Aeronautics and Space

Administration (NASA) contract 1407.

Bibliography

Ascenso, J., Alves, J., Vicente, S., Lago, M. T. V. T. 2007, A&A, 476, 199
Koornneef, J. 1983, A&A, 128, 84
López-Chico, T. A., Salas, L. 2007, Rev. Mex. Astr. Astrofis., 43, 155
Martini, P., Persson, S. E., Murphy, D. C., Birk, C., Schectman, S. A., Gunnels, S. M., Koch, E. 2004, In Proc. SPIE 5492, Ground-based instrumentation for Astronomy, ed. F. M. A. Moorwood, M. Iye (Bellingham WA:SPIE), 1653
Palla, F., Stahler, S. W. 1999, ApJ, 525, 771
Preibisch, T., Schuller, F., Ohlendorf, H., Pekruhl, S., Menten, K. M., Zinnecker, H. 2011, A&A, 252, A92
Rathborne, J. M., Burton, M. G., Brooks, K. J., Cohen, M., Ashley, M.C.B., Storey, J. W. V. 2002, MNRAS, 331, 85
Rathborne, J.M., Brooks, K. J, Burton, M. G., Cohen, M., Bontemps, S. 2004, A&A, 418, 563
Rieke, G. H., Lebofsky, M. J. 1985, ApJ, 288, 618
Robitaille, T. P., Whitney, B. A., Indebetouw, R., Wood, K. 2007, ApJS, 169, 328
Sanchawala, K., Chen, W.-P., Oiha, D., Ghosh, S. K., Nakajima, Y., Tamura, M., Baba, D., Sato, S., Tsujimoto, M. 2007, ApJ, 667, 963
Tapia, M., Roth, M., Vázquez, R.A., Feinstein, A. 2003, MNRAS, 339, 44
Tapia, M., Roth, M., Bohigas, J, Persi, P. 2011, MNRAS (in press)

3.19 Clusters within Clusters: Spitzer & Chandra Observations of Subclusters in RCW 38

Elaine Winston[1], S. Wolk[2], T. Bourke[2], S. Thomas Megeath[3], R. Gutermuth[4,5], and B. Spitzbart[2]

[1] European Space Agency, ESTEC
[2] Harvard-Smithsonian Center for Astrophysics
[3] Ritter Observatory, Dept. of Physics & Astrophysics, University of Toledo
[4] Five Colleges Astronomy Dept., Smith College
[5] Dept. of Astronomy, University of Massachusetts

Abstract

The majority of young stars are believed to form in star clusters. The effect this has on their circumstellar environments will depend on the star formation history and structure of the cluster itself. At a distance of 1.7 kpc, RCW 38 contains an estimated 20 – 40 OB stars and an estimated total of $\sim 10^3$ members. Here we use the mid-IR *Spitzer* IRAC observations to identify young stellar objects with circumstellar emission in an extended region around RCW 38. Elevated X-ray emission from young stars enables us to also locate diskless young members using the *Chandra* ACIS X-ray observation. We identify 624 young stellar objects in RCW 38. Of these, 226 were detected in X-rays. The YSOs have the following evolutionary classes: 23 class I, 90 flat spectrum, 437 class II, and 74 class III. Of the YSOs, 9 class I, 18 flat spectrum, 125 class II, and 74 class III were also detected in the *Chandra* X-ray observation. Through a study of the spatial distribution of the YSOs we find strong evidence of subclustering in the region, particularly among the most massive and variable stars. Four subclusters are identified; the central region of star formation in RCW 38 is surrounded by three subclusters and distributed young stars. This indicates that star formation is ongoing over a much larger area of the region than previously realised.

Introduction

The RCW 38 cluster is a region of high-mass star formation, which lies at a distance of 1.7 kpc from the Sun, centred on coordinates $08^{hr}59^{m}00^{s}$, $-47^{d}33^{m}40^{s}$ ($J2000$). The region is one of the closest high-mass star-forming regions known to contain approximately a thousand members, after Orion and Cep OB3b (Wolk et al. [2006]) and was first identified in the Hα survey of Rodgers et al. [1960] and the HII survey of Gum et al. [1955]. An extensive overview of the previous studies of RCW 38 is to be found in the Handbook of Star Formation article on the cluster (Wolk, Bourke & Vigil [2008]).

We obtained observations of the RCW 38 region with the *Spitzer* InfraRed Array Camera (IRAC; Fazio et al. [2004]) in four wavelength bands: 3.6, 4.5, 5.8, and 8.0 μm and with the Multiband Imaging Photometer for *Spitzer* (MIPS; Rieke et al. [2004]). This photometry was supplemented by J, H and K-band photometry from the 2MASS point source catalogue (Skrutskie et al. [2006]). The infrared observations were further combined with *Chandra* Advanced CCD Imaging Spectrometer (ACIS) X-ray data. A full discussion of this work is presented in Winston et al. [2011].

Identifying the YSOs in RCW 38

Young stellar objects can be identified by their excess emission at IR wavelengths. This emission arises from reprocessed stellar radiation in the dusty material of their natal envelopes or circumstellar disks. Four colour-colour diagrams were used to determine the colour excess of the sources: two IRAC diagrams: [3.6] - [4.5] vs. [5.8] - [8.0] and [3.6] - [4.5] vs. [4.5] - [5.8], and two IRAC-2MASS diagrams: $J - H$ vs. $H - [4.5]$ and $H - K$ vs. $K - [4.5]$. Fig. 3.51 shows the four diagrams. We required photometry to have uncertainties < 0.2 mag in all bands used for a *particular* colour-colour diagram.

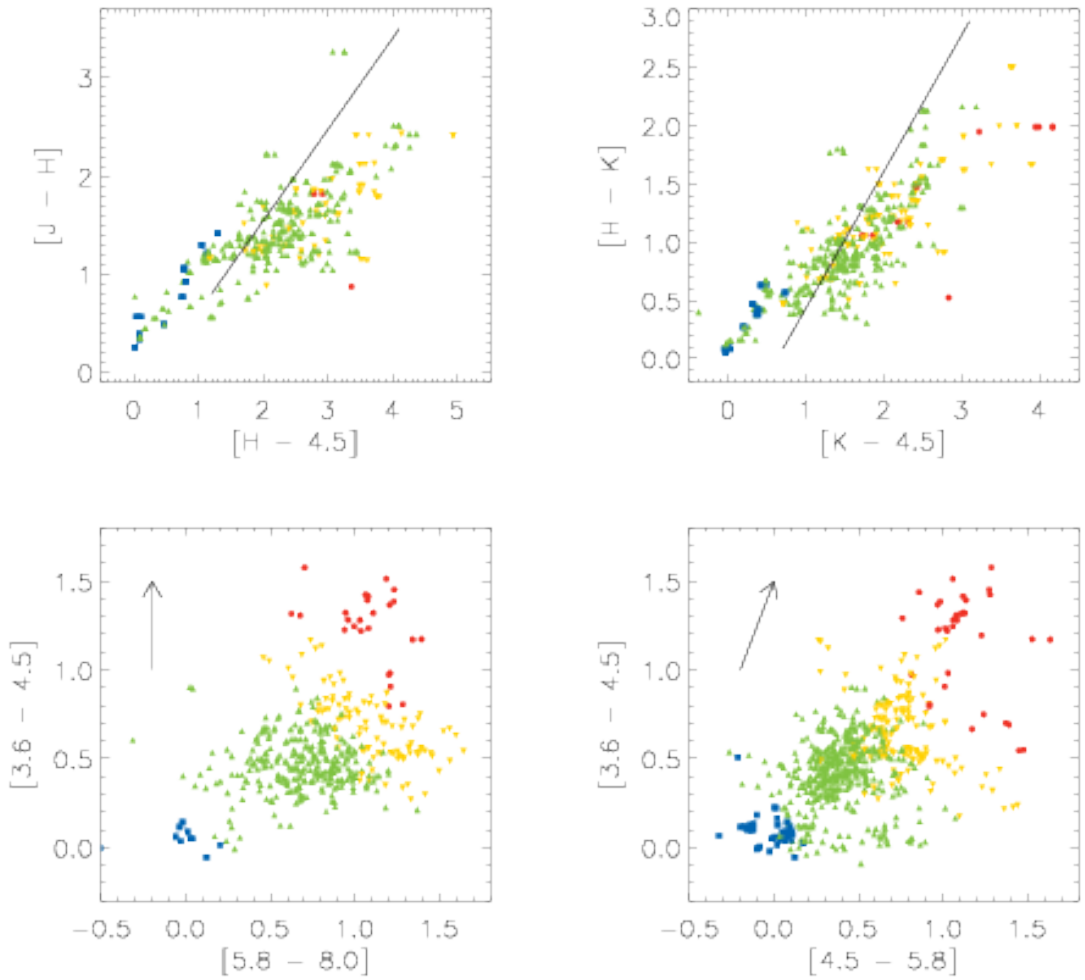

Figure 3.51: *Upper Left*: $J-H$ vs. $H-[4.5]$ diagram. The solid line shows the reddening vector for these wavelengths; objects with $H-[4.5]$ greater than 1σ below the reddening vector are considered to have an excess. *Upper Right*: $H-K$ vs. $K-[4.5]$ diagram. Similar to upper left, for those sources with excess in their $K-[4.5]$ colours. *Lower Left*: IRAC colour-colour diagram, $[3.6]-[4.5]$ vs. $[5.8]-[8.0]$. The locus for field stars lies on the origin. A reddening vector of $A_K = 5$ is shown. *Lower Right*: IRAC colour-colour diagram, $[3.6]-[4.5]$ vs. $[4.5]-[5.8]$. A reddening vector of $A_K = 5$ is shown. The Class 0/I objects are marked by red circles, inverted yellow triangles mark the flat spectrum sources, green triangles mark the Class II objects. The X-ray identified Class III are shown by blue squares.

Further to their excess emission in the IR, young stellar objects are also extremely bright X-ray emitters - typically producing X-ray luminosities, L_X, of $\frac{L_X}{L_{sol}} \sim 10^{3.5}$ that can be used to distinguish them from foreground or background field stars (Feigelson & Montmerle [1999]). This method is particularly useful in identifying bona fide class III members of a cluster - those young stars where the circumstellar material has been processed and no longer emits in the IR - providing both another, less contaminated, measure of the stellar disk fraction as well as presenting a more complete understanding of the spatial distribution of the cluster members.

The evolutionary classification of a YSO can be determined from its position on the colour-colour diagram and the slope of its SED (Spectral Energy Distribution); the sources are classified as class 0/I, flat spectrum, class II, and class III (Winston et al. [2007]). The different classes are identified by differently coloured symbols in Fig. 3.51. A total of 624 young stellar objects were identified in the IRAC field of view. Of the 624 YSOs, 226 were also detected in X-rays with *Chandra*. The YSOs were of the following evolutionary classes: 23 class 0/I, 90 flat spectrum, 437 class II, and 74 class III. Of the YSOs, 9 class I, 18 flat spectrum, 125 class II, and 74 class III were also identified in the *Chandra* X-ray observation.

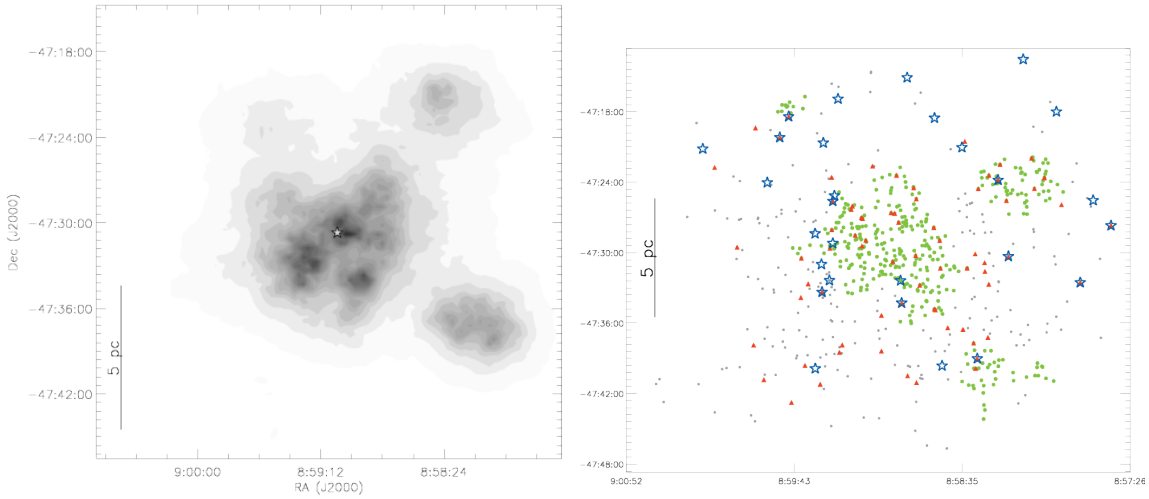

Figure 3.52: *Left*: Surface density map of the YSOs in the RCW 38 cluster. The stellar surface density was calculated with a grid size of 100×100 using $N = 20$, the distance to the 20th nearest neighbour, to smooth out smaller scale structure. The density contours range linearly from $0/pc^2$ (white) to $30/pc^2$ (black). The surface density map also indicates the presence of two subclusters to the NW and SW, and a possible third subcluster to the NE, of the central core, which itself shows three density peaks. The position of IRS 2 is marked by a star. *Right*: Spatial distribution of the identified YSOs in RCW 38 showing the positions of the O star and variable candidates. The dots indicate the young stars identified via IR excess emission and X-ray detection; clustered YSOs are shown by green dots, distributed YSOs in gray. The triangles show the positions of the variable objects, while the open stars show the positions of the candidate O stars in the field. Both the variable and O star candidates are distributed throughout the extended cluster, with candidates of both types appearing in the subclusters.

Subclustering in RCW 38

The spatial distribution of the young stars in a cluster traces the history of star formation in the region and the underlying structure of the molecular cloud from which the stars have formed. By mapping the stellar spatial distribution and surface density it is possible to locate any overdensities which are present and which indicate the location of subclusters. The stellar surface density of the newly identified YSOs was calculated to determine the underlying structure of the cluster; the resulting density map is shown in Fig. 3.52 (left). The density at each point on the grid is found by calculating the distance, D, to the N^{th} nearest neighbour at that point and calculating $(N-1)/\pi D^2$ at that point. In this case, the stellar surface density was calculated with a grid size of 100×100 using $N = 18$, the distance to the 18th nearest neighbour, to smooth out smaller scale structure. Four regions can be identified on the plot: the previously known central cluster is surrounded by three others in a sea of distributed young stars.

Fig. 3.52 (right) shows the spatial distribution of all the identified YSOs (small circles) with those young stars identified as having variable IR magnitudes shown by triangles, and the O-star candidates marked by asterisks. From these data we infer the existence of four subclusters - the previously known centre of RCW 38 is surrounded by three other subclusters where star formation appears to have been initiated independently. The similar properties of the distributed population linking the subclusters indicates that the subclusters are related and form part of a larger structure in the molecular cloud where star formation is ongoing over an extended region.

Conclusion

Combining *Spitzer* mid-IR and *Chandra* X-ray observations, we have undertaken an extensive survey of the RCW 38 massive star-forming region. These data enable us to identify the young stellar population of the region and to determine its overall clustering properties.

We identify 624 young stellar objects in RCW 38 in the IRAC field of view. Of these, 226 were detected in X-rays with *Chandra*. The YSOs were of the following evolutionary classes: 23 class I, 90 flat spectrum, 437 class II, and 74 class III. Of the YSOs, 9 class I, 18 flat spectrum, 125 class II, and 74

class III were also detected in the *Chandra* X-ray observation. We identify four subclusters in RCW 38; the central region of star formation in RCW 38 is surrounded by three subclusters and distributed young stars. Variables sources were identified in each of the four subclusters.

Acknowledgments

This work is based on observations made with the *Spitzer* Space Telescope (PID 20127), which is operated by the Jet Propulsion Laboratory, California Institute of Technology under NASA contract 1407. Support for this work was provided by NASA through contract 1256790 issued by JPL/Caltech. Support for the IRAC instrument was provided by NASA through contract 960541 issued by JPL. This publication makes use of data products from the Two Micron All Sky Survey, which is a joint project of the University of Massachusetts and the Infrared Processing and Analysis Center/California Institute of Technology, funded by the National Aeronautics and Space Administration and the National Science Foundation. This research has made use of the NASA/IPAC Infrared Science Archive, which is operated by the Jet Propulsion Laboratory, California Institute of Technology, under contract with the National Aeronautics and Space Administration. TLB acknowledges support from NASA through a grant for HST program 11123 from the Space Telescope Science Institute, which is operated by the Association of Universities for Research in Astronomy, Incorporated, under NASA contract NAS5-26555.

Bibliography

Fazio, G.G., et al., 2004, ApJS, 154, 10.
Feigelson, E. D., Montmerle, T., 1999, ARA&A, 37, 363-408.
Gum, C.S., 1955, MmRAS, 67, 155.
Rieke, et al., 2004, ApJS, 154, 25-29.
Rodgers, A.W., Campbell, C.T., Whiteoak, J.B., 1960, MNRAS, 121, 103.
Skrutskie, M.F., Cutri R.M., Stiening R., et al., 2006, AJ, 131, 1163.
Winston, E., et al., 2007, ApJ, 669, 493.
Winston, E., et al., 2011, ApJ, submitted.
Wolk, S. J., Spitzbart, B. D., Bourke, T. L., Alves, J., 2006, AJ, 132, 1100-1125.
Wolk, S. J., Bourke, T. L., Vigil, M., 2008, in "Handbook of Star Forming Regions Vol.II", ASP, editor: Reipurth, B.

Chapter 4

Stellar Populations in Clusters

4.1 High-Mass Stars in Clusters and Associations

Ignacio Negueruela[1]

[1] Departamento de Física, Ingeniería de Sistemas y Teoría de la Señal, Universidad de Alicante, Apdo. 99, E03080 Alicante, Spain

Abstract

High-mass stars are major players in the chemical and dynamical evolution of galaxies. Open clusters and associations represent the natural laboratories to study their evolution. In this review, I will present a personal selection of current research topics that highlight the use of open clusters to constrain different properties of high-mass stars, such as the possible existence of an upper limit for the mass of a star, the evolutionary stage of blue supergiants or the characterisation of supernova progenitors.

Introduction

The study of high-mass stars (also, though not quite correctly, known as massive stars) is intimately linked to, and difficult to disentangle from, the study of young open clusters. This is not only because most high-mass stars are found within young open clusters and associations, but also because clusters are the natural laboratories for investigating the evolution of high-mass stars. At the most basic level, determining the fundamental parameters of a massive star requires knowledge of its distance (e.g. Herrero et al. [1992]). Since very few high-mass stars have accurate parallaxes (Maíz Apellániz et al. [2008]), membership in a cluster or association is required for calibration. In view of such a close connection, this short review can only cover a very small fraction of the many topics subject to active study that I could have considered for inclusion. I will concentrate on a few issues of current research that highlight the importance of open clusters as laboratories for understanding massive star evolution. The selection of these topics is undoubtedly biased by my personal preferences, but is representative of the areas currently generating the highest interest among researchers in the field.

Definition of high-mass stars

There are several possible definitions for high-mass stars, all of them indirect. We can define high-mass stars as those initiating C burning non-explosively in their cores. Modern theoretical models including overshooting indicate that this will happen for $M_* \gtrsim 8\mathrm{M}_\odot$ (e.g. Eldridge & Tout [2004]). We can also define high-mass stars as those ending their lives in supernova explosions. These two definitions are

almost identical, though the latter implies a slightly higher mass (e.g. Poelarends et al. [2008], for a description of the physics involved). The limit for a star to produce a supernova explosion has recently been set from observations of supernova progenitors at $\gtrsim 8.5^{+1}_{-1.5}$ $M_\odot$ (Smartt et al. [2009], and see also Section *Cool massive stars*). A third possible definition of high-mass stars is those stars with self-initiating radiation-driven winds (Kudritzki & Puls [2000]). Radiative winds become detectable for main-sequence stars with spectral type earlier than B2 V, which again roughly corresponds to $M_* \gtrsim 8\,M_\odot$.

Observationally, high-mass stars comprise the OB stars (approximately, O2–B2 V, O2-B5 III and O2-B9 I; Reed [2009]; Walborn & Fitzpatrick [1990]) and some later type supergiants (the most luminous supergiants of spectral types A, F, G, and K, and the M-type supergiants). For an observational review, see Massey [2003].

Formation of high-mass stars

The formation of high-mass stars is a major research topic in modern astrophysics, and will not be discussed here. See Zinnecker & Yorke [2007] for a recent review. High-mass stars may have an effect on the formation of low-mass stars, and thus on the Initial Mass Function (IMF). In addition, high-mass stars may play a role in triggering further star formation. This issue has been controversial since the emergence of the classical theory (Elmegreen & Lada [1977]), because a causal relationship is difficult to assess, even if indications of sequential formation are widespread and strong indirect evidence for triggering has been found (e.g. Walborn [2002]; Zavagno et al. [2005]). I will not discuss star formation here, but simply note that sequential star formation within a cluster or association may give rise to populations with different ages, which might be difficult to disentangle, meaning that accurate ageing is not always possible for young open clusters.

The most massive stars

The possible existence of an upper limit to the IMF has been a hotly debated issue in recent times. Several stars believed to be extremely luminous, and thus extremely massive, have been resolved into two or more components (e.g. Maíz Apellániz et al. [2007]). Based on an analysis of the stellar population in the compact young Arches open cluster, Figer [2005] concluded that there was clear evidence for an upper limit to stellar masses around 150 $M_\odot$. This result is dependent on several factors, such as the extinction law to the Galactic Centre, but has also been reproduced for the Large Magellanic Cloud (Koen [2006]).

Recent modelling advances have revealed that hydrogen-rich Wolf-Rayet (WR) stars of the nitrogen sequence (WN) are really main-sequence objects with heavy mass loss. These are candidates to be the most massive stars in their hydrogen core burning phase (Langer et al. [1994]; de Koter et al. [1997]; Crowther & Dessart [1998]). The fact that they are commonly found heavily packed at the core of the densest young open clusters supports this view. Searches for very massive stars have thus concentrated on possible binaries amongst this population, as close binaries may provide accurate masses via dynamical studies.

One of the best examples is found in the obscured starburst cluster Westerlund 2. Located in the Sagittarius Arm (likely at ~ 8 kpc, though distances as short as 3 kpc have been given), this cluster contains at least 14 early O or WR stars (Rauw et al. [2007]). Its total mass is also open to discussion, but may approach $M_{\rm cl} = 10^4\,M_\odot$ (Ascenso et al. [2007]), a result supported by the recent discovery of two very massive stars likely ejected from the cluster core (Roman-Lopes et al. [2011]). One of the most luminous members of Westerlund 2, the WN6h star WR20a, was identified as a massive binary by Rauw et al. [2004] and as an eclipsing binary by Bonanos et al. [2004]. Combination of the radial velocity curve and the lightcurve provides an accurate solution with $P_{\rm orb} = 3.69 \pm 0.01$ d. The components have masses $M_1 = 83 \pm 5\,M_\odot$ and $M_2 = 82 \pm 5\,M_\odot$. They have the same spectral type and the same mass, which is the highest stellar mass measured with high accuracy.

Even more massive than Westerlund 2, the cluster at the core of the giant H II region NGC 3603, also located in the Sagittarius arm (at ~ 7 kpc), is extraordinarily compact. It contains ≈ 35 early O or WR stars (Moffat et al. [1994]) and likely has a mass $M_{\rm cl} = 1.5 \times 10^4\,M_\odot$ (Rochau et al. [2010] and references therein). Its central concentration contains 3 WN6ha stars, the brightest of which is an eclipsing binary with $P_{\rm orb} = 3.7724$ d. The orbit has been solved using K-band spectroscopy (Schnurr et al. [2008]). The radial velocity curve of the secondary has large uncertainties and therefore the masses are not very tightly constrained. The solution implies $M_1 = 116 \pm 31\,M_\odot$ and $M_2 = 89 \pm 16\,M_\odot$. Component 1 is thus the most massive star with a dynamically determined mass (Schnurr et al. [2008]).

Outside the Milky Way, the 30 Dor complex in the Large Magellanic Cloud is likely the most massive starburst in the Local Group. Its nuclear cluster, Radcliffe 136, is 2.7 pc across and contains hundreds of OB stars. Its mass has been estimated to be, at least, $M_{\rm cl} = 1 \times 10^5\,{\rm M}_\odot$ (Andersen et al. [2009]). Using updated stellar models, Crowther et al. [2010] found that the dynamical masses of the WN6ha stars in NGC 3603 could be well reproduced by evolutionary tracks. If these models are then extrapolated to the even brighter WN5h stars at the core of 30 Dor, they indicate enormous masses. Three of the WN5h stars are fitted with models implying current masses $\geq 150\,{\rm M}_\odot$, with Star a1 having $265^{+80}_{-35}\,{\rm M}_\odot$ (Crowther et al. [2010]). This would be the most massive star known, well above the proposed upper mass limit. Unfortunately, none of the stars at the core of 30 Dor appears to be a spectroscopic binary to confirm this determination with a dynamical measurement.

Stellar evolution

High-mass stars play a decisive role in driving the chemical evolution of galaxies. Heavy mass loss through all their life stages and in the final supernova explosion provides an important fraction of the heavy elements in the interstellar medium. In order to understand the chemical enrichment of the medium, we need to constrain how and when mass is lost by high-mass stars, and this means being able to map observed phases on to theoretical evolutionary tracks.

Open clusters and associations allow us to explore the evolutionary context of massive stars in different evolutionary stages (e.g. Walborn [2010]). This process starts with the youngest stellar systems. For example, the Carina nebula provides many of the MK standards for the earliest O subtypes (Walborn et al. [2002]). The fact that O3–4 stars are still on the main sequence indicates that the complex is very young, while this very youth constrains its only evolved star, η Car, to be extremely massive.

At a slightly older age, Cyg OB2 represents an important laboratory for the study of O-type stars. Considered a very promising target since its discovery (Johnson & Morgan [1954]), it could only be studied in detail after the advent of CCD detectors because of the high obscuration, in spite of its relative low distance (see Fig. 4.1). Massey & Thompson [1994] identified ~ 60 stars more massive than 15 ${\rm M}_\odot$, finding that Cyg OB2 is very compact for an OB association and seems to occupy a more or less unique position somewhat intermediate between an open cluster and a normal OB association (Knödlseder [2000], cf.). The central region contains two cluster-like stellar concentrations (Bica et al. [2003]). They form an elongated figure $\sim 4' \times 10'$ ($\sim 2 \times 5$ pc at the distance of Cyg OB2) and contain 18 O-type stars (assuming that all systems are single; given the observed multiplicity – see below –, the actual number is likely to be a factor of two higher).

After analysis of the 2MASS data in this region suggested a much richer population of early type stars (Knödlseder [2000]), several recent studies (e.g. Comerón et al. [2002]; Hanson [2003]) have shown that the association contains > 50 (and likely $\sim$ 70–80) O-type stars (e.g. Kiminki et al. [2007]; Negueruela et al. [2008]). The main sequence is very well defined, showing a clear turn-off at O6 V. A number of giants and supergiants follow the 2.5 Myr isochrone from this turnoff. However, there is also a population of O3–O5 supergiants, which seems incompatible with this age (see Negueruela et al. [2008] and Fig 4.1). With the data available, it is impossible to rule out the possibility that these stars represent a younger population. However, the similarity of the HR diagram for Cyg OB2 to theoretical plots in which very fast rotation generates blue stragglers (de Mink et al. [2009]) is striking.

The presence of blue supergiants with spectral types too early for the main-sequence turnoff is very frequent in young open clusters, but these objects have not generally been classified as blue stragglers, even if they are located to the left of the cluster isochrone, the classical definition of a blue straggler. A paradigmatic case is h Persei (NGC 869), one of the most well-studied clusters in the Northern sky, and a rather massive cluster – recent mass estimates indicate $\sim 4\,500$ ${\rm M}_\odot$ in the core region (Currie et al. [2010]). Most recent works seem to converge on an age $\sim$ 14 Myr, in good agreement with an apparent main-sequence turn-off at B1 V. The luminous supergiants in the cluster, however, have spectral types too early for this age (Marco & Bernabeu [2001]), at B2 Ia (HD 14143) and B3 Ia (HD 14134), and evolutionary masses approaching $40\,M_\odot$ (McErlean et al. [1999]; Crowther et al. [2006a]). A similar situation is found in many other clusters (Marco et al. [2007]). In most cases, there are no observational reasons to suggest that these supergiants are members of a younger (second-generation) population. This clearly shows that we are still very far from understanding exactly which evolutionary phase blue supergiants represent.

Because of the huge size of its stellar population, the young cluster Westerlund 1 (Wd 1) is currently our best laboratory for studying the evolution of high-mass stars. Located at ~ 5 kpc, its mass exceeds 5×10^4 ${\rm M}_\odot$ (Gennaro et al. [2011]) and may approach 10^5 ${\rm M}_\odot$. With more than twenty WR stars

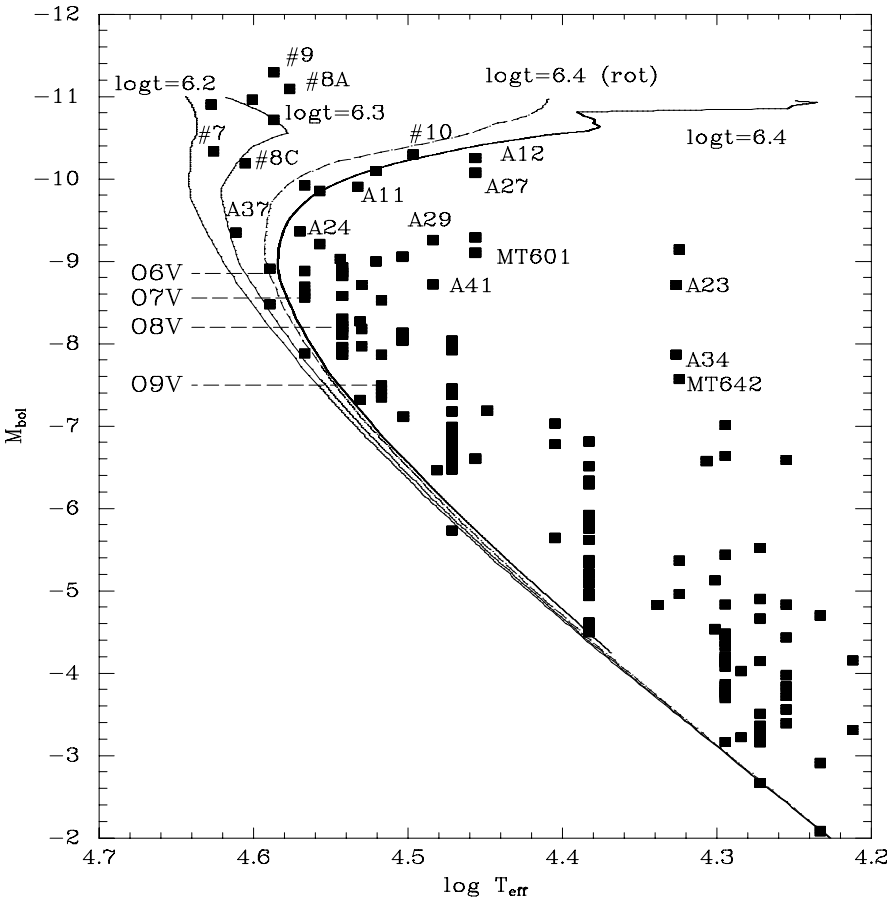

Figure 4.1: Semi-empirical HR diagram for Cyg OB2, after Negueruela et al. [2008]. Note that, in the original paper, the $(V-K)_0$ term was added twice, because of a mistake with the spreadsheet. When this is taken into account, the distance modulus $DM = 10.8$ proposed by Hanson [2003] is no longer favoured. A better fit is now obtained with the classical value $DM = 11.3$, as displayed. Continuous lines are non-rotating isochrones for $\log t = 6.2$, 6.3 and 6.4 from Schaller et al. [1992]. The dashed line is the $\log t = 6.4$ isochrone in the high-rotation models (Meynet & Maeder [2003]).
The main-sequence turn-off at O6 V seems to be followed by a number of evolved stars tracing the $\log t = 6.4$ isochrone. A number of O3–5 supergiants, though, fall well to the left of the isochrone.

(Crowther et al. [2006b]) and several dozen OB supergiants (Negueruela et al. [2010]), Wd 1 provides stringent tests on current theoretical models. The population observed is consistent with a single burst of star formation. There may be some mild blue stragglers, but the blue supergiants in the cluster (including some very luminous late-B hypergiants with $M_V \sim -9$) fit rather well the theoretical isochrones for ages between 5 and 6 Myr (Negueruela et al. [2010]). Moreover, the dynamical determination of the mass for the two components of the eclipsing binary Wd1-W13 shows good agreement with the expected theoretical masses, with the B1 I component having a mass $M_* = 35 \pm 5$ M$_\odot$ (Ritchie et al. [2010]). This good agreement is comforting in view of the difficulties in understanding blue supergiants in other clusters and provides strong support for the basic assumptions underlying current evolutionary tracks (e.g. Meynet & Maeder [2000]).

Binarity

The large number of high-mass stars present in Wd 1 offers an ideal opportunity to study their binary fraction. The population of WR stars offers strong indirect evidence for a very high binary fraction (Crowther et al. [2006b]). Targeted observations of the blue supergiant population revealed that at least 40% of the stars observed are binaries (Ritchie et al. [2009]). Observations of a larger sample, including

stars closer to the main sequence, are in progress.

Searches for binaries in Cyg OB2 are, to date, more complete. A radial velocity survey carried out over several years (Kiminki et al. [2007]; Kobulnicky & Kiminki [2011]) should be able to reveal, except for very unfavourable inclinations, all massive companions and a substantial fraction of low-mass companions. The survey has so far detected 20 spectroscopic binaries, while 20 other objects show radial velocity variations, and might be binaries. Comparison to theoretical expectations suggests a very high binary fraction, perhaps approaching unity. The masses of the companions seem to follow a flat distribution (Kiminki et al. [2009]; Kobulnicky & Kiminki [2011]).

The binary fraction and companion mass distribution do not seem to be universal, though. Variability in both observables is high among the few clusters with dedicated studies. In NGC 6231, the complete sample of O-type stars (16 objects) presents $f_{\rm bin} > 0.63$, with companions having consistently $M_* > 5$ M$_\odot$ (Sana et al. [2008]). In contrast, the smaller cluster NGC 2244, with 6 O-type stars, has a much smaller binary fraction, $f_{\rm bin} > 0.17$, while in IC 1805 (10 O-type stars) $f_{\rm bin} > 0.20$, with the possibility of massive companions almost ruled out (Mahy et al. [2009]; de Becker et al. [2006]).

Meanwhile, spectroscopic monitoring of a large sample of O and WN stars has revealed a very high fraction of spectroscopic binaries (Barbá et al. [2010]). Interferometric observations, which sample a different range of orbital sizes, have also demonstrated a very high degree of multiplicity amongst high-mass stars. O-type stars in clusters display a much higher binary fraction than field O stars (Mason et al. [2009]). This can be naturally explained if many (most) field stars have been ejected from open clusters (in accordance with theoretical predictions presented in several contributions to these proceedings).

Cool massive stars

After the blue supergiant phase, the evolutionary tracks of massive stars become more uncertain. An important fraction of high-mass stars (perhaps all with $M_* \gtrsim 25$ M$_\odot$) become WR stars. Before reaching this hydrogen-depleted phase, the stars must lose their envelopes, but the evolutionary phase when this mass loss takes place is unclear. Wd 1 contains a high number of yellow hypergiants (with spectral types A and F), which seem to be subject to heavy pulsations (Clark et al. [2010]). Current evolutionary tracks would predict these objects to become Luminous Blue Variables (LBV) and then reach the WR stage. Nevertheless, the cluster also contains a number of red supergiants, which are not predicted to exist at such high luminosities (Clark et al. [2010]).

Stars less massive than ~ 25 M$_\odot$ are expected to end their lives as red supergiants (RSGs). Modelling of RSGs is very complex due to a number of factors, among which we can cite their huge size, poorly determined molecular opacities and the expected heavy mass loss. Because of these difficulties, their fundamental properties are not very well known, though important advances have been obtained with new model fits to a sample of RSGs in open clusters and associations (Levesque et al. [2005]). Spectroscopic monitoring of RSGs in clusters has allowed the detection of irregular radial velocity variations, which may be the signature of pulsation, the most likely source of mass loss (Mermilliod et al. [2008]).

In recent years, RSGs have shown their usefulness as signposts of massive clusters. As they are very bright in the infrared, they can be seen through heavy absorption. Several clusters rich in RSGs have been discovered towards the inner Galaxy (e.g. Figer et al. [2006]; Clark et al. [2009a]). Determination of their chemical composition has provided extremely valuable clues to the Galactic chemical distribution (Davies et al. [2009]). These studies are allowing the discovery of an increasing number of massive young open clusters in the Galaxy (see Portegies Zwart et al. [2010] for a review). Unfortunately, the actual masses of these obscured clusters are not known, as we can only see the RSGs and not the associated main sequence (see Fig. 4.2). The most extreme case is the open cluster Stephenson 2, which contains at least 26 RSGs (Davies et al. [2007]), and might have a mass approaching 10^5 $M_\odot$, if current predictions for the duration of the RSG phase are correct. Unfortunately, this is not certain, as the case of the open cluster NGC 7419 (Marco & Negueruela [2011] and Fig. 4.2) highlights.

One important test for stellar evolution models is the ratio of blue to red supergiants in a population. This ratio is very sensitive to input physics, such as treatment of mass loss, convection and mixing processes. Unfortunately, in most Galactic clusters, the number of supergiants is so small that the ratio is not statistically significant. Studies so far have considered average values over a number of open clusters, finding an apparent dependence on Galactocentric radius. When observations of the Magellanic Clouds are also included, there is strong evidence for an increase in the blue to red supergiant ratio with increasing metallicity (Eggenberger et al. [2002]). This is exactly the opposite behaviour to what current

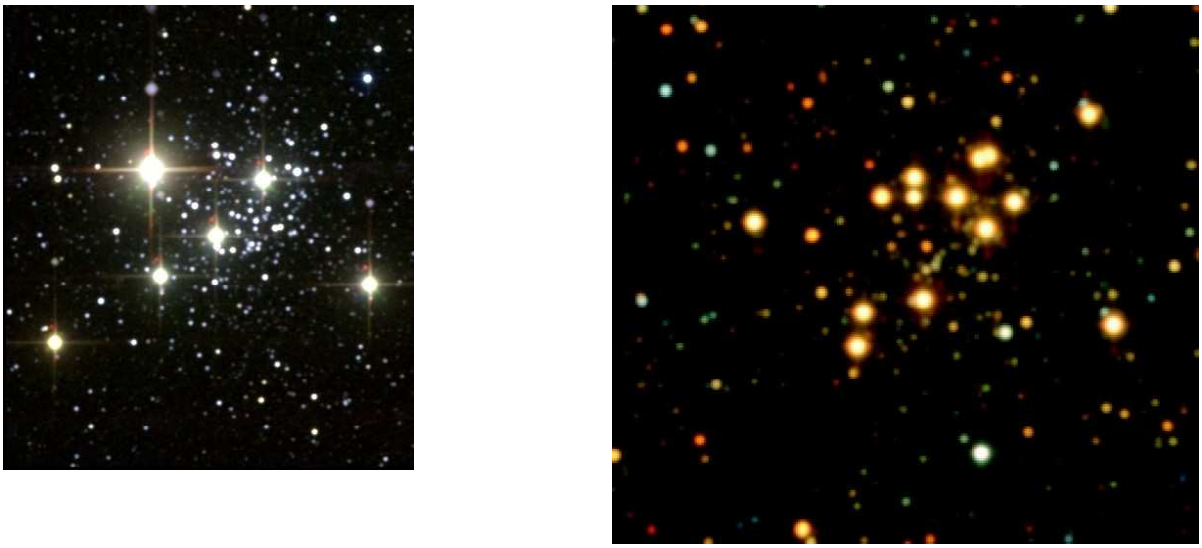

Figure 4.2: *Left*: 2MASS image of the open cluster NGC 7419. This obscured cluster in the Perseus Arm contains 5 red supergiants for no blue supergiants and presents the highest fraction of Be stars among Galactic clusters (Marco & Negueruela [2011]). Current theoretical models predict that this cluster should have a mass approaching 10^4 $M_\odot$ to contain 5 RSGs (Clark et al. [2009b]), but its mass is unlikely to exceed 3×10^3 $M_\odot$. *Right*: 2MASS image of RSGC1, a cluster of red supergiants at $d \sim 6$ kpc, in the Inner Galaxy (Figer et al. [2006]). This cluster has an age ~ 10 Myr and may have $\gtrsim 3 \times 10^4$ $M_\odot$ (Davies et al. [2008]). Comparison of this image to the one in the left panel highlights the brightness of RSGs in the near infrared and their role as signposts of recent star formation. The population of blue stars easily seen in NGC 7419 fades out in RSGC1 due to the higher distance, much higher extinction, and confusion.

evolutionary tracks would predict (Meynet et al. [2011]).

However, simply counting all red and blue supergiants may provide a distorted picture, as not all "supergiants" sample the same population. As an example, the open cluster NGC 6649, located at ~ 2 kpc in the Sagittarius arm, has an age ~ 50 Myr (Turner [1981]) and contains at least three low-luminosity RSGs (with spectral types around K1 Ib) and one supergiant Cepheid variable. According to modern evolutionary tracks (e.g. Marigo et al. [2008]), the progenitors of these supergiants had initial masses ~ 8 $M_\odot$. Stars of such low masses should never appear as blue supergiants (according to the same tracks), and so including them in counts to determine the red to blue ratio may be misleading.

Nevertheless, these low-mass RSGs are very interesting objects in themselves, as they must be the progenitors of most Type II supernovae. This is a simple consequence of the shape of the IMF, as there must be many more stars with $M_* \sim 8$ $M_\odot$ than with $M_* \sim 20$ $M_\odot$. As Type II supernovae are very important contributors to the dynamical and chemical evolution of galaxies, determining the lower mass for a supernova explosion becomes a fundamental issue to understand the history of the Universe. In recent years, an important observational effort has been dedicated to identifying supernova progenitors and deriving their properties (see Smartt [2009]). In some cases, it has been possible to identify the actual star in pre-explosion images. Sometimes, the supernova seems to have taken place within an open cluster or association and properties can be inferred from the parent population.

Based on these observations, the minimum mass for an exploding star has been estimated at $\approx 8.5^{+1}_{-1.5}$ $M_\odot$ (Smartt et al. [2009]). Efforts are also being dedicated to determining whether there is a direct relation between the initial mass of a star and the class of supernova explosion it will undergo. Of course, the final fate of a massive star depends on several factors, such as mass loss rates during the different evolutionary phases, initial rotational velocity and its evolution, and, perhaps most decisively,

binary interaction (e.g. Meynet et al. [2011]). In spite of this, attempts have been made to the develop "typical" scenarios (e.g. Smith et al. [2011]).

Another interesting fact is the apparent correlation between the fraction of Be stars among B-type stars and the number of RSGs. Both seem to increase in a similar way with decreasing metallicity (Meynet et al. [2007]), suggesting a possible evolutionary connection with fast rotation. In this sense, the open cluster NGC 7419 (Fig. 4.2), which has the highest fraction of Be stars amongst Milky Way clusters, presents a blue to red supergiant ratio of 0/5 (Marco & Negueruela [2011]), atypical for Milky Way clusters. In contrast, NGC 663, which also has a very high Be-star fraction and is located at approximately the same Galactocentric distance, presents a ratio 5/0 for the core region (6/2 when the halo is also considered), showing that correlations are not always direct or simply that statistical fluctuations may dominate the observables even in moderately massive clusters.

Outlook

In the near future, Gaia is bound to play a decisive role in furthering our knowledge of high-mass stars. Accurate parallaxes will result in much better distances to open clusters, implying improved luminosity determinations. In addition, confirmation of membership for individual peculiar objects will give them an evolutionary context, providing strong constraints for evolutionary tracks. Gaia may also contribute strongly to the study of binarity amongst high-mass stars, as it will obtain accurate lightcurves for huge samples and may detect orbital motions in wide binary systems.

Of course, Gaia cannot solve every problem. We will need other data and also new theoretical developments. High-resolution spectroscopy coupled with accurate stellar atmosphere models will be needed to determine stellar parameters beyond luminosity (see, e.g., Simón-Díaz et al., in these proceedings). Improved evolutionary tracks will result from deeper interaction between theory and observations. Radial velocity curve solutions for spectroscopic binaries will sample the intermediate range of binary separations.

But, above all, we have to be conscious of one main limitation: Gaia will not be able to sample the inner Galaxy, where high extinction and crowding will impede the acquisition of high-quality data. Almost all the massive young clusters known will be beyond its reach. Fortunately, a full complement of new instruments will help us to study star formation in the inner Galaxy. Among them, the first generation of infrared spectrographs with high multiplexing capabilities, such as KMOS at the VLT or MIRADAS at GTC, will play a fundamental role in studying obscured clusters and massive star-forming regions. Meanwhile, new space telescopes will provide the tools to resolve clusters in the galaxies of the Local Group. JWST may be an ideal tool for detecting RSGs in distant galaxies (and hence identifying supernova progenitors), while WSO/UV will be used to study low-extinction populations of massive hot stars. In all, with this formidable set of new missions and instruments, the next few years are likely to see important developments in this field.

Acknowledgments

This research is partially supported by the Spanish Ministerio de Ciencia e Innovación (MICINN) under grants AYA2010-21697-C05-05 and CSD2006-70. I thank Jesús Maíz Apellániz and Sergio Simón Díaz for comments on the manuscript.

The Two Micron All Sky Survey (2MASS) is a joint project of the University of Massachusetts and the Infrared Processing and Analysis Center/California Institute of Technology, funded by the National Aeronautics and Space Administration and the National Science Foundation.

Bibliography

Andersen, M., Zinnecker, H., Moneti, A., et al. 2009, ApJ, 707, 1347
Ascenso, J., Alves, J., Beletsky, Y., & Lago, M.T.V.T. 2007, A&A, 466, 137
Barbá, R.H., Gamen, R., Arias, J.I., et al. 2010, RMxAC, 38, 30
de Becker, M., Rauw, G., Manfroid, J., & Eenens, P. 2006, A&A, 456, 1121
Bica, E., Bonatto, Ch., & Dutra, C. M. 2003, A&A, 405, 991
Bonanos, A.Z., Stanek, K.Z., Udalski, A., et al. 2004, ApJ, 611, L33

Clark, J.S., Negueruela, I., Davies, B., et al. 2009a, A&A, 498, 109
Clark, J. S., Davies, B., Najarro, F., et al. 2009b, A&A, 504, 429
Clark, J.S., Ritchie, B.W., & Negueruela, I. 2010, A&A, 514, A87
Comerón, F., Pasquali, A., Rodighiero, G., et al. 2002, A&A, 389, 874
Crowther, P.A., & Dessart, L. 1998, MNRAS, 296, 662
Crowther, P.A., Lennon, D.J., & Walborn, N.R. 2006a, A&A, 446, 279
Crowther, P.A., Hadfield, L.J., Clark, J.S., et al. 2006b, MNRAS, 372, 1407
Crowther, P.A., Schnurr, O., Hirschi, R., et al. 2010, MNRAS, 408, 731
Currie, T., Hernandez, J., Irwin, J., et al. 2010, ApJS, 186, 191
Davies, B., Figer, D.F., Kudritzki, R.-P., et al. 2007, ApJ, 671, 781
Davies, B., Figer, D.F., Law, C.J., et al. 2008, ApJ, 676, 1016
Davies, B., Origlia, L., Kudritzki, R.-P., et al. 2009, ApJ, 696, 2014
Eggenberger, P., Meynet, G., & Maeder, A. 2002, A&A, 386, 576
Eldridge, J.J., & Tout, C.A. 2004, MNRAS, 353, 87
Elmegreen, B.G., & Lada, C.J. 1977, ApJ, 214, 725
Figer, D.F. 2005, Nature, 434, 192
Figer, D.F., MacKenty, J.W., Robberto, M., et al. 2006, ApJ, 643, 1166
Gennaro, M., Brandner, W., Stolte, A., & Henning, Th. 2011, MNRAS, 412, 2469
Hanson, M.M. 2003, ApJ 597, 957
Herrero, A., Kudritzki, R.-P., Vilchez, J.M., et al. 1992, A&A, 261, 209
Johnson, H.L., & Morgan, W. W. 1954, ApJ, 119, 344
Kiminki, D.C., Kobulnicky, H. A., Kinemuchi, K., et al. 2007, ApJ, 664, 1102
Kiminki, D.C., Kobulnicky, H.A., Gilbert, I., et al. 2009, AJ, 137, 4608
Knödlseder, J. 2000, A&A, 360, 539
Kobulnicky, H.A., & Kiminki, D.C. 2011, BSRSL, 80, 616
Koen, C. 2006, MNRAS, 365, 489
de Koter, A., Heap, S.R., & Hubeny, I. 1997, ApJ, 477, 792
Kudritzki, R.-P., & Puls, J. 2000, ARA&A, 38, 613
Langer, N., Hammann, W.-R., Lennon, M., et al. 1994, A&A, 290, 819
Levesque, E.M., Massey, P., Olsen, K.A.G., et al. 2005, ApJ, 628, 973
Mahy, L., Nazé, Y., Rauw, G., et al. 2009, A&A, 502, 937
Maíz Apellániz, J., Walborn, N.R., Morrell, N.I., et al. 2007, ApJ, 660, 1480
Maíz Apellániz, J., Alfaro, E., & Sota, A. 2008, `arXiv:0804.2553`
Marco, A., & Bernabeu, G. 2001, A&A, 372, 477
Marco, A., & Negueruela, I. 2011, BSRSL, 80, 396
Marco, A., Negueruela, I., & Motch, C. 2007, ASPC, 361, 388
Marigo, P., Girardi, L., Bressan, A., et al. 2008, A&A, 482, 883
Mason, B.D., Hartkopf, W.I., Gies, D.R., et al. 2009, AJ, 137, 3358
Massey, P. 2003, ARA&A, 41, 15
Massey, P., & Thompson, A.B. 1991, AJ, 101, 1408
McErlean, N.D., Lennon, D.J., & Dufton, P.L. 1999, A&A, 349, 553
Mermilliod, J.C., Mayor, M., & Udry S. 2008, A&A, 485, 303
Meynet, G., & Maeder, A. 2000, A&A, 361, 101
Meynet, G., & Maeder, A. 2003, A&A, 404, 975
Meynet, G., Eggenberger, P., & Maeder, A. 2007, IAUS, 241, 13
Meynet, G., Georgy, C., Hirschi, R., et al. 2011, BSRSL, 80, 266
de Mink, S.E., Pols, O.R., Langer, N., & Izzard, R.G. 2009, A&A, 497, 243
Moffat, A.F.J., Drissen, L., & Shara, M.M. 1994, ApJ, 436, 183
Negueruela, I., Marco, A., Herrero, A., & Clark, J.S. 2008, A&A, 487, 575
Negueruela, I., Clark, J.S., & Ritchie, B.W. 2010, A&A, 516, A78
Poelarends, A.J.T., Herwig, F., Langer, N., & Heger, A. 2008, ApJ, 675, 614
Portegies Zwart, S.F., McMillan, S.L.W., & Gieles, M. 2010, ARA&A, 48, 431
Rauw, G., de Becker, M., Nazé, Y., et al. 2004, A&A, 420, L9
Rauw, G., Manfroid, J., Gosset, E., et al. 2007, A&A, 463, 981
Reed, B.C. 2003, AJ, 125, 2531
Ritchie, B.W., Clark, J.S., Negueruela, I., & Crowther P.A. 2009, A&A, 507, 1585
Ritchie, B.W., Clark, J.S., Negueruela, I., & Langer, N. 2010, A&A, 520, A48
Rochau, B., Brandner, W., Stolte, A., et al. 2010, ApJ, 716, L90
Roman-Lopes, A., Barba, R.H., & Morrell, N.I. 2011, MNRAS, in press

Sana, H., Gosset, E., Nazé, Y., et al. 2008, MNRAS, 386, 447
Schaller, G., Schaerer, D., Meynet, G. & Maeder, A. 1992, A&AS, 96, 269
Schnurr, O., Casoli, J., Chené, A.-N., et al. 2008, MNRAS 389, L38
Smartt, S.J. 2009, ARA&A, 47, 63
Smartt, S.J., Eldridge, J.J., Crockett, R.M., & Maund, J.R. 2009, MNRAS, 395, 1409
Smith, N., Li, W., Filippenko, A.V., & Chornock, R. 2011, MNRAS, 412, 1522
Turner, D.G. 1981, AJ, 86, 231
Walborn, N.R. 2002, ASPC, 267, 111
Walborn, N.R. 2010, ASPC, 425, 45
Walborn, N.R. & Fitzpatrick, E.L. 1990, PASP, 102, 379
Walborn, N.R., Howarth, I.D., Lennon, D.J., et al. 2002, AJ, 123, 2754
Zavagno, A., Deharveng, L., Brand, J., et al. 2005, IAUS, 227, 346
Zinnecker, H., & Yorke, H.W. 2007, ARA&A, 45, 481

4.2 Low-mass Stars, Brown Dwarfs and Isolated Planetary Mass Objects in Stellar Associations: Lithium Ages

David Barrado y Navascués[1,2], A. Bayo[3], M. Morales-Calderón[4], and L. M. Sarro[5]

[1] Calar Alto Observatory, German-Spanish Astronomical Center, Almería, Spain
[2] Astronomy Department, Center of Astrobiology (INTA-CSIC), Madrid, Spain
[3] ESO, European Southern Observatory, Alonso de Córdova 3107, Vitacura, Santiago, Chile
[4] IPAC, Spitzer Science Center, California Institute of Technology, Pasadena, CA 91125, USA
[5] Depto. de Inteligencia Artificial, UNED, Juan del Rosal, 16, 28040 Madrid, Spain

Abstract

The formation mechanism/s, properties and evolution of low-mass objects are not well understood. Stellar associations provide a chance to solve this, by providing homogeneous samples of very low-mass stars and brown dwarfs. A clear shortcoming is the lack of high-quality spectroscopy, specially in the case of mid- and high resolution spectroscopy, which allow accurate determination of ages, radial velocities or chemical abundances, among other properties. We will review the observational results collected during the last years, focusing on ages derived using the Lithium Depletion Boundary technique, and briefly discuss the role that Gaia might have in this field.

Introduction

Although bright, massive stars dominate stellar associations, swarms of low-mass objects can be found inside them. Our aim is to provide a summary of what we know about cluster very low-mass stars and substellar members, and how the European Space Agency mission Gaia can be used to enlarge our understanding of these objects. In particular, what Gaia will and will not provide –high-quality, deep spectra, specifically for members of stellar associations. We will focus on several examples (Initial Mass Function, disk ratios, ages) in order to emphasize the need of massive and very deep spectroscopic cartography.

Table 4.1: An overview of a collection of brown dwarfs searches in stellar associations.

Association	Age* (Myr)	References
Trapezium	1	Lucas & Roche [2000]; Lada et al. [2000]
Rho Oph	1	Alves de Oliveira et al. [2010]; Marsh et al. [2010b]; Luhman et al. [2007]
“		Luhman & Rieke [1999];Shirono et al. [2011]
Cha I-II-III	1	Barrado y Navascués & Jayawardhana [2004]; Luhman [2004]; Mužić et al. [2011]
Lupus	1-2	Allen et al. [2007];Comerón et al. [2009]; López Martí et al. [2010, 2011]
Taurus	1-3	Tamura et al. [1998]; Luhman et al. [2009, 2006]
Serpens	2	Lodieu et al. [2002]; Shirono et al. [2011]
NGC 6611	2-3	Oliveira et al. [2009]
IC 348	3	Najita et al. [2000]; Luhman et al. [2003, 2005]; Mainzer & McLean [2003]
Sigma Ori	3-5	Zapatero Osorio et al. [1999, 2000]; Béjar et al. [1999, 2001];
“		Caballero et al. [2007]; Caballero [2010], Lodieu et al. [2009]; Bouy et al. [2009b]
Collinder 69	5	Barrado y Navascués et al. [2004b, 2007]; Barrado Y Navascués et al. [2007];
“		Morales-Calderón [2008]; Bouy et al. [2009a]; Bayo [2009]; Bayo [2011]
Upper SCo	5	Ardila et al. [2000]; Slesnick et al. [2006]; Bouy & Martín [2009]; Lodieu et al. [2008, 2011]
TW Hya Association	10	Webb et al. [1999]; Gizis [2002]
IC 4665	36	Jeffries et al. [2009]
IC 2391	36	Barrado y Navascués et al. [1999, 2001b, 2004c]; Boudreault & Bailer-Jones [2009]
Alpha Per	51	Stauffer et al. [1999]; Barrado y Navascués et al. [2002, 2004c]; Lodieu et al. [2005]
NGC 2547	55	Oliveira et al. [2003]
The Pleiades	70	Rebolo et al. [1995]; Stauffer et al. [1998a,b]; Bouvier et al. [1998]; Pinfield et al. [2000]; Moraux et al. [2003]
Blanco	90	Moraux et al. [2007]
The Hyades	500-600	Bouvier et al. [2008]
Praesepe	590	Baker et al. [2010]; Boudreault et al. [2010]

* The age for each association corresponds to the common values quoted in the literature, either from the nuclear or the contacting age scales.

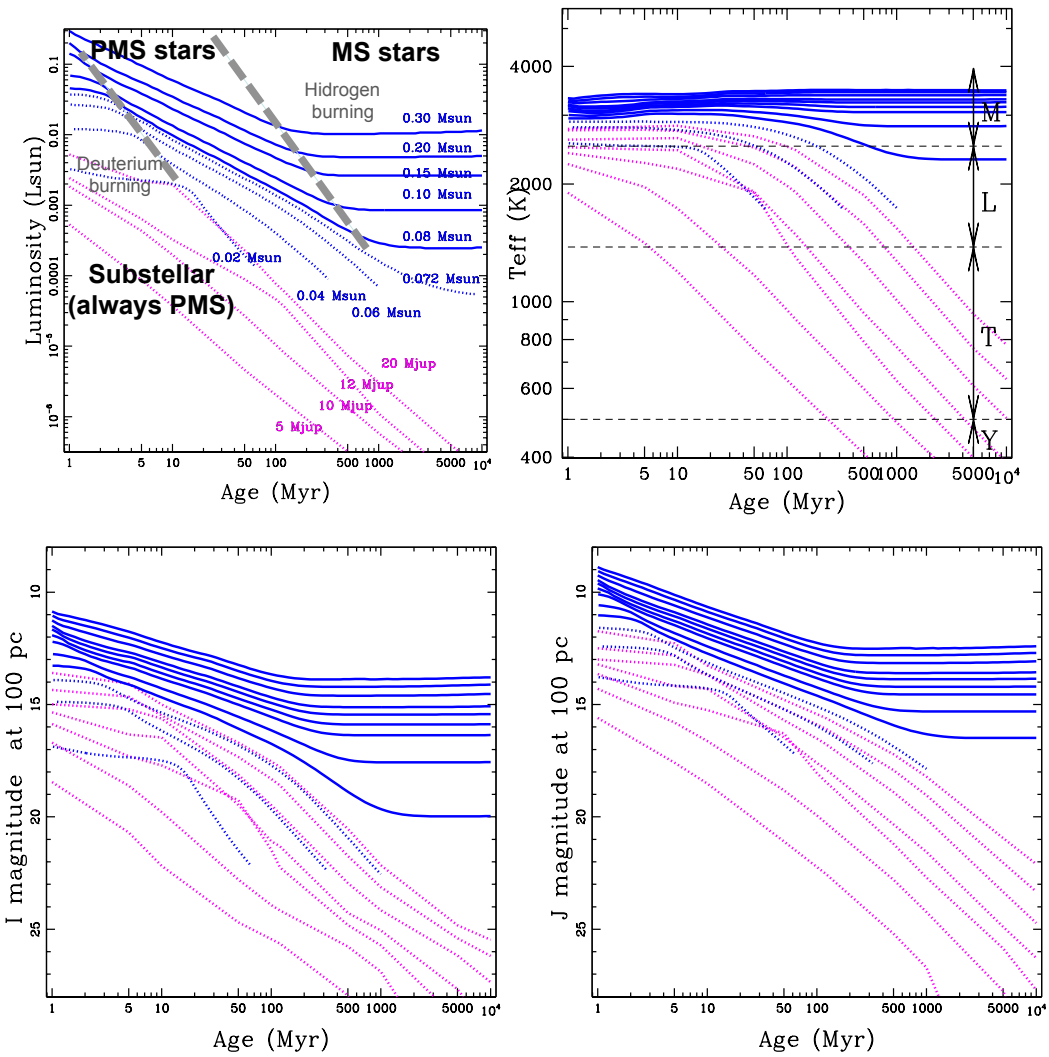

Figure 4.3: The different panels display the luminosity, the effective temperature and the apparent magnitudes in two filters, as a function of age, for different evolutionary tracks from the Lyon group: blue for NextGen and magenta for COND models (Baraffe et al. [1998], Chabrier et al. [2000]). Solid and dotted lines represent stars and substellar objects, respectively. The age ranges when deuterium and hydrogen burning happens are easily identified as plateaus in each track. Masses are labelled in panel a; in the other panels we represent isochrones of 0.35, 0.30, 0.25, 0.20, 0.175, 0.15, 0.13, 0.10, 0.080, 0.06, 0.04, 0.03, 0.02 $M_{\odot}$ -NextGen, in blue, and 50, 40, 30, 20, 15, 10, 5 M_{Jup} - COND, in magenta.

What are they? Are they really important?

Substellar objects share a number of properties with those typical of stars. In addition, they can be understood as stepping stones in our understanding of the properties of exoplanets, since brown dwarfs (BDs) have very cool temperatures, akin to the hot jupiters discovered so far, and can be studied directly. Brown dwarfs have masses below 0.072 $M_{\odot}$, whereas isolated planetary mass objects (IPMOs) are below 0.013 $M_{\odot}$ (about 14 M_{Jup}). Thus, they are unable to fuse hydrogen in order to sustain the weight of the external layers, and they slowly contract and emit electromagnetic radiation (essentially in the infrared) at the expenses of their gravitational potential. This fact is illustrated in Fig. 4.3, where we display models by the Lyon Group (NextGen and COND tracks by Baraffe et al. [1998] and Chabrier et al. [2000]). In a sense, we can assume that substellar objects are always Pre-Main Sequence objects (PMS), decreasing their luminosity steadily, whereas *bona fide* stars eventually arrive at the Main Sequence (MS), once they ignite their nuclear furnaces after several million years. As a matter of fact, the length of the PMS phase is mass-dependant. As an example, stars of spectral type late K and cooler have not reach

the MS for the Pleiades, a 125 Myr cluster (Stauffer et al. [1998b]). It is true, however, that for a brief interval when they are very young, BDs can fuse deuterium, and stop the contraction for a brief episode. During short phase, they might show pulsations (Palla & Baraffe [2005], Moya et al. [2011]) similar to those observed in their more massive counterparts, such as cepheids. Since they cool down with age, the spectral type is also age-dependant, as shown in Fig. 4.3b, and they can have spectral types later than M6 (young, very massive BDs), L (dominated by alkali features in the optical spectrum, Kirkpatrick et al. [1997]) or T (with a prominent methane absorption band in the near-IR, Kirkpatrick et al. [1999]; Burgasser et al. [2002]). Cooler objects would show an ammonia band, and a hypothetical spectral type Y has been postulated.

The formation mechanism of the lowest mass objects remain controversial. There are currently four main camps - (1) these objects form like stars, from protostellar core collapse and subsequent accretion, including turbulent fragmentation (Padoan & Nordlund [2004]); or (2) they form as low-mass members of small groups, with the lowest mass members of the groups being preferentially ejected and/or starved (Reipurth & Clarke [2001]; Bate et al. [2002]); or (3) they form like planets within circumstellar disks of higher-mass objects, but are ejected either due to internal-dynamics or external interactions (Rice et al. [2003], Stamatellos & Whitworth [2008]); or (4) they can form via photoevaporation by massive pre- stellar cores (Whitworth & Zinnecker [2004]). Perhaps several of these mechanisms operate simultaneously. Resolving this issue requires careful observational programs to vette cluster membership lists, to determine their properties (e.g. kinematics, presence and frequency of circumstellar disks, multiplicity, etc.) and detect the end of the IMF, the so called mass cut-off (if it exists). Since we do not have laboratories to test our theories, we have to rely on very well designed observations, especially in stellar associations. A well tested strategy in the search for lowest-mass objects combines photometry from red (optical) and near-infrared filters, since they appear very red and clearly detached from the fore- or background population from the field.

What do we know inside the substellar domain?

Since the discovery and confirmation of the first brown dwarfs in a cluster (Rebolo et al. [1995]), a big deal of work has been done, and multiple surveys have been executed, essentially in young associations, since BDs are easier to spot due to their brightness and colours (they are more luminous and bluer compared with older objects of the same mass, see Fig. 4.3). Table 4.1 presents a compilation, not complete, of different works.

To the best of our knowledge, the least massive substellar object discovered so far in a stellar association, confirmed by spectroscopy, is SOri70, a T4-T7 isolated planetary mass object (IPMO) associated –including proper motions- to the 3 Myr Sigma Orionis cluster. Models indicated a mass of 3^{+5}_{-1} M_{Jup} (Zapatero Osorio et al. [2002, 2008]). This object might be at the IMF cut-off, which seems to be at about 5 M_{Jup}, as found by Morales-Calderón [2008] and Bayo [2009], based on very deep optical and near-IR imaging in the 5 Myr Collinder 69 cluster.

Other IPMOs have been identified and/or confirmed in Sigma Orionis (Zapatero Osorio et al. [2000]; Barrado y Navascués et al. [2001c]; Caballero et al. [2007], Peña Ramírez et al. [2011]) and other associations: Trapezium (Lucas & Roche [2000]; Weights et al. [2009]); Taurus (Quanz et al. [2010], but some debate remains), Collinder 69 (Barrado y Navascués et al. [2004b, 2007]; Morales-Calderón [2008]; Bayo [2009]; Bayo [2011]), Upper Sco (Lafrenière et al. [2008]), TW Hydrae Association (Chauvin et al. [2004]; Mohanty et al. [2007]), and Rho Oph (Marsh et al. [2010a]).

In the following subsections, we will discuss three properties which provide important hints in order to understand the formation mechanism (or mechanisms) within the substellar domain: the presence of circumstellar disks, the Initial Mass Function (IMF) and the so called Lithium Detection Boundary (LDB). In the last two cases, Gaia and high quality spectroscopy will play an essential role. Other properties, such as proper motions, will not be considered here, but Gaia will have an important say on this (the expulsion of very low-mass members due to dynamical interactions within the cluster or a planetary system). We refer to the talk by Herve Bouy for a modern view on proper motions.

The Initial Mass Function

The universality of the IMF has been an object of active debate for quite a long time. While in most cases the IMF slopes built from observations agree with the standard Salpeter's value (within the uncertainties) for the range of masses from solar-type stars to high mass, some cases have been presented where heavy

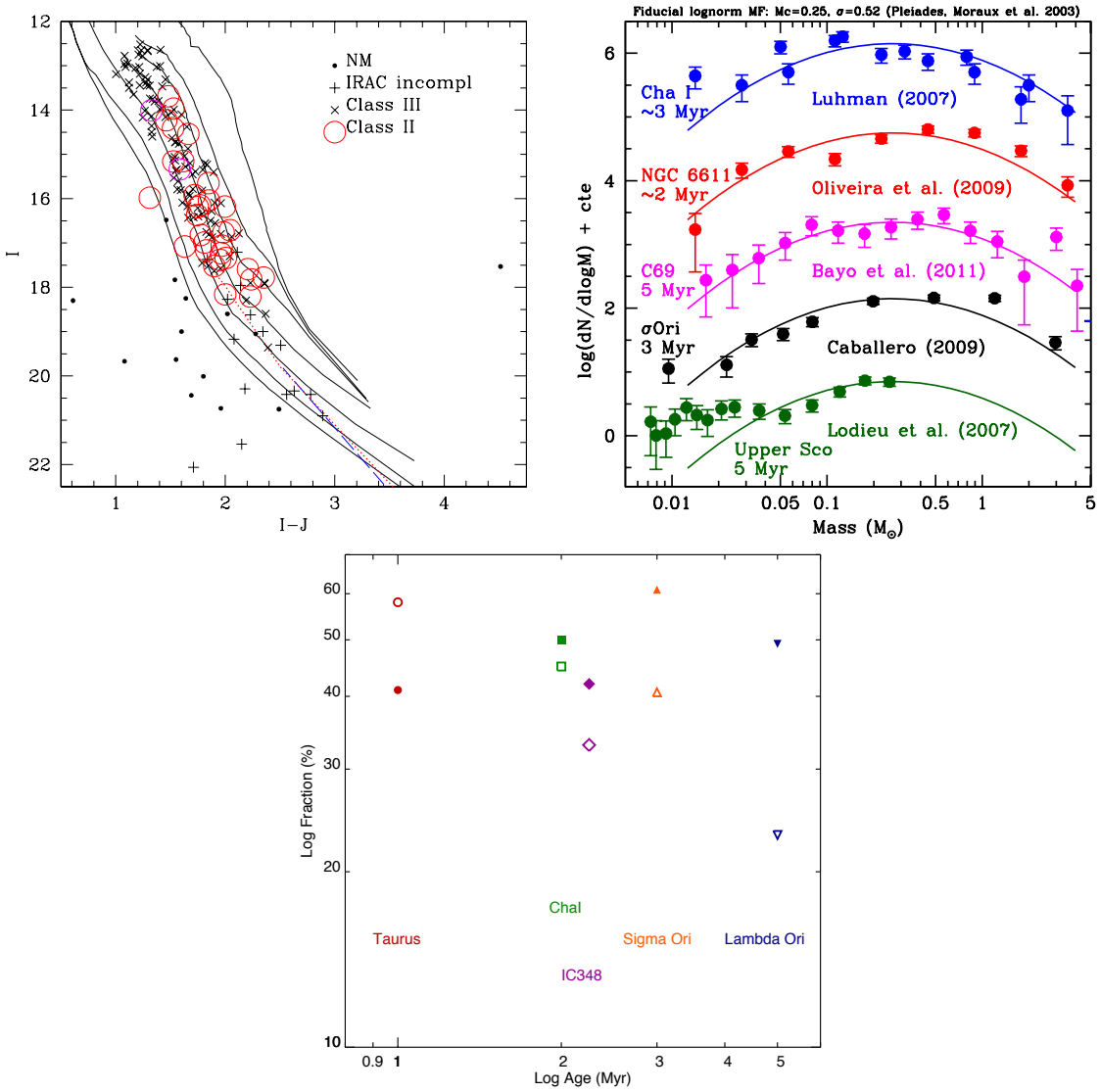

Figure 4.4: *a* Optical/IR Colour-Magnitude Diagram for Collinder 69, a 5 Myr cluster located inside Orion's Head. Class II sources (Classical TTauri stars and substellar analogs) have been included as big (red) circles, whereas Class III (Weak-line TTauri) objects appear as crosses, and other Lambda Orionis members lacking the complete set of IRAC photometry are displayed with the plus symbol. Non-members appear as dots. The figure includes 1, 3, 5, 10, 20, 50, and 100 Myr isochrones from Baraffe et al. [1998] as solid lines, as well as 5 Myr isochrones corresponding to dusty and COND models (Baraffe et al. [1998]; Chabrier et al. [2000]), as dotted and dashed lines. After Barrado y Navascués et al. [2007]. *b* Log-log representation of the IMF for different young associations. We compare our very complete spectroscopically confirmed IMF (in magenta) with photometric ones derived for associations with similar ages (2 – 5 Myr). The compilation of the data corresponding to clusters other than Collinder 69 are courtesy of J. Bouvier and E. Moraux. *c* Disk fraction for a set of studies that yield values for both very low-mass stars (open symbols) and brown dwarfs (filled symbols). The data come from: Monin et al. [2010], Luhman et al. [2005], Luhman et al. [2008], Barrado y Navascués et al. [2007], Morales-Calderón [2008]. Note that the errors in the disk fraction are between 4 and 20%.

top IMF or deficit of massive stars is claimed (Bartko et al. [2010], Park et al. [2000]). In the lower mass end of the IMF, some excess of brown dwarfs and planetary mass objects have been reported (Luhman [2007]; Caballero [2009] and Lodieu et al. [2007]). On the contrary field, Taurus might show a scarcity of very low-mass members, although the debate is still open (Guieu et al. [2006]). Some of these IMFs have been represented in Fig. 4.4b.

As stated before, the IMF cut-off (the minimum mass) might be located close to 5 M_{Jup}, as suggested by very deep optical and near-IR imaging in the 5 Myr Collinder 69 cluster (Morales-Calderón [2008]; Bayo [2009]).

In any case these over-representations (or low numbers, if any) have to be further investigated since the IMFs have been built based on photometric surveys (see Fig. 4.4a as an example). Therefore, contamination (especially by background stars and galaxies) can be an issue in the very low-mass domain. Further effort in spectroscopic and/or proper motion confirmation of the candidates has to be pursued before any strong result can be claimed. In this direction, Bayo [2011] built the IMF of Collinder 69 (a well-defined, compact open cluster, $\sim$ 5 Myr old being the central association of the Lambda Orionis Star-Forming Region) out of spectroscopically confirmed members down to 0.017 $M_{\odot}$ (i.e., the bottom of the BD domain) without finding this excess of low-mass members (Fig. 4.4b). We must note, of course, that this result does not rule out the possibility that the IMFs from different regions will still show this excess once the membership of the photometric candidates is confirmed/rejected. This would be a strong indication that several mechanism are at work (such as the effect of the environment: strong winds from massive stars, supernova, initial conditions of the molecular cloud, and so on).

Disks in the Substellar Domain

A variety of observational diagnostics –infrared excess, mm observations, signs of material accreted from disk onto the central object, evidence of outflows/winds– has been used to establish that, like their more massive counterparts, BDs experience a T Tauri-like phase (Barrado y Navascués & Martín [2003]).

A large fraction of young sub-stellar objects harbour $(K-L)$ excess consistent with optically thick dusty disks. In the last years rapid progress has been made in this field thanks to the Spitzer Space Telescope's unique sensitivity to faint IR sources which has enabled measurements of disk fractions well into the substellar regime in nearby star-forming regions (e.g. 37.5% for the 5 Myr old C69 –Barrado y Navascués et al. [2007], 50% in the 5 Myr old Upper Sco –Bouy et al. [2007], 48% in the 1 – 2 Myr old Taurus –Guieu et al. [2007]). Fig. 4.4c illustrates this point, and suggests that the time scale for BD disk evolution might be longer than in the case of disks around stars (Barrado y Navascués & Martín [2003]).

These kinds of observations allow not only to derive a disk fraction but also to characterize the geometry of the disks around brown dwarfs (see, for instance, a comprehensive analysis in Bouy et al. [2008]) and look for evidence of evolution. Mid-IR and mm observations suggest a range of disk geometries and dust properties similar to those of TTS: a large fraction of Taurus disks are strongly flared while most Upper Sco disks are "flatter" indicating a possible evolution of the dust, settling to the disk mid-plane. Several of the Upper Sco BD disks show evidence of big inner holes. In principle, this evidence is against formation by ejection due to dynamical interactions or by photoevaporation, either if they have formed as stellar embryos, or in circumstellar disks.

Thanks to spectroscopic studies, signs of accretion such as broad asymmetric Hα emission profiles have been discovered in many brown dwarfs (e.g. Barrado y Navascués et al. [2004a]; Muzerolle et al. [2005]). Some extremely low-mass substellar objects have very intense Hα equivalent widths, a clear signpost of very active accretion (Barrado y Navascués et al. [2003]).

Apai et al. [2005]) presented for the first time possible signs of grain processing in some BD disks, in that some fraction of the grains appear to be crystalline, whereas ISM grains tend to be amorphous. Finally, Phan-Bao et al. [2008] reported the first detection of a bipolar molecular outflow from the young BD ISO-Oph 102 (60 M_{Jup}) in the Rho Ophiuchi dark cloud demonstrating that the molecular outflow process occurs in BDs as a scaled-down version of that seen in low-mass stars.

As a summary, at least most BDs seem to be formed by a mechanism analogous to star formation, but we cannot rule out that some massive "planets", even with masses above the planetary mass threshold, might have been formed in circumstellar disks and expelled later on.

Table 4.2: Data for the seven clusters with LDB ages.

Cluster	Age scale			Mass	$(m\text{-}M)_0$	E(B-V)	Mag LDB		
	LDB* (Myr)	Nuclear (Myr)	contracting (Myr)	LDB			M(Ic)	MKs	Mbol
IC 4665	28 ± 4	36 ± 10[1]	22 ± 5[4]	0.24	7.93 ± 0.22	0.00 ± 0.18	8.47 ± 0.33	6.05 ± 0.34	8.65 ± 0.33
NG C2547	35 ± 3	55 ± 25[2]	14 ± 4[2]	0.12	8.10 ± 0.10	0.02 ± 0.06	9.33 ± 0.14	6.74 ± 0.12	10.36 ± 0.14
IC 2602	46 ± 6	36 ± 10[1]	22 ± 5[5]	0.00	5.86 ± 0.10	0.01 ± 0.035	9.65	7.37 ± 0.20	$--$
IC 2391	50 ± 5	36 ± 10[1]	22 ± 5[5]	0.12	5.95 ± 0.00	0.00 ± 0.06	10.15 ± 0.14	7.52	10.24
APer	85 ± 10	51 ± 10[1]	100 ± 20[6]	0.085	6.23 ± 0.10	0.00 ± 0.04	11.42 ± 0.15	8.31	11.31
Pleiades	130 ± 20	78 ± 10[1]	70 ± 10[7]	0.075	5.60 ± 0.00	0.00 ± 0.03	12.18 ± 0.15	8.94	12.14
Blanco 1	132 ± 24	90 ± 25[3]	80 ± 20[8]	0.074	6.58 ± 0.12	0.01 ± 0.02	12.17 ± 0.24	8.97 ± 0.25	11.99 ± 0.30

[1] Mermilliod [1981b] gives a nuclear age of 36.3 Myr for the complex composed by IC 4665, IC 2602 and IC 2391 (and NGC 2451 and NGC 4609), 51.3 Myr for Alpha Per (including NGC 5281, NGC 6242, and NGC 6405), and 77.6 Myr for the Pleiades (including NGC 2323, NGC 2422, NGC 6067, NGC 6709, NGC 7790 and Tr 2). No errors are provided, and we have estimated them as 10 Myr.
[2] From Jeffries et al. [1998]
[3] No turn-off. Age based on Hα (Panagi & O'dell [1997])
[4] Isochrone fitting by Manzi et al. [2008]
[5] Isochrone fitting by Stauffer et al. [1997]
[6] From the colour-magnitude diagrams made with the UKIDSS GCS photometry (Lodieu priv.comm.)
[7] Isochrone fitting by Stauffer et al. [1995], the error is an estimate from their Fig. 5cd
[8] Isochrone fitting by Cargile & James [2010]
* References for the LDB ages: IC 4665.- Manzi et al. [2008]; NGC 2547.- Jeffries & Oliveira [2005]; IC 2602.- Dobbie et al. [2010]; IC 2391.- Barrado y Navascués et al. [2004c]; APer.- Stauffer et al. [1999]; Pleiades.- Stauffer et al. [1998b]; Blanco 1.- Cargile et al. [2010].

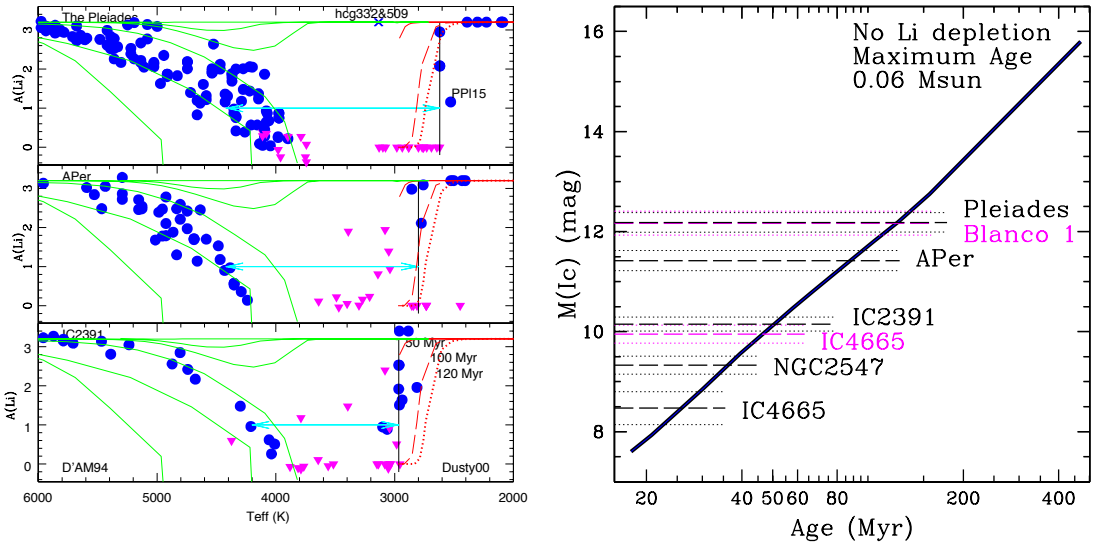

Figure 4.5: The lithium depletion boundary. *a* Lithium abundance versus the effective temperature for three well known clusters: the Pleiades, Alpha Per and IC 2391 (see Barrado y Navascués et al. [2004c]). *b* Location of the LDB boundary and its relation with the cluster age. We have represented the absolute I magnitude for the LDB -dashed lines– and the associated errors –dotted lines.

The Lithium Depletion Boundary and a New Age Scale

The Lithium Depletion Boundary (LDB) is a powerful technique which allows an accurate, independent determination of the cluster age (Basri et al. [1996]). It was first successfully applied to the Pleiades (Stauffer et al. [1998b]), Alpha Persei (Stauffer et al. [1999]) and IC2391 (Barrado y Navascués et al. [1999]). Since then, the technique has been applied to a small number of clusters (see Table 4.2).

Lithium is a very fragile element which is easily destroyed at very low temperatures (2.5×10^6 K, Dantona & Mazzitelli [1984]; D'Antona et al. [1998]) inside the stellar nucleus. Due to convection, the surface abundance decreases with age and for low-mass objects the decay is very rapid, to the point of no detection within few million years. For masses below 0.06 $M_\odot$ the core temperature is never hot enough to cause its destruction, and its abundance (both internal or in the stellar/substellar atmosphere) remains the same. Therefore, lithium is an excellent witness of the nature of a low-mass object, since its detection might reveal its substellar nature (Rebolo et al. [1992, 1995]). Moreover, the process is so fast and depends so strongly on mass that there is a sharp edge between cluster members with and without lithium (see Fig. 4.5a). The most conspicuous spectral feature (less than 1 Å equivalent width) is located at 6707.8 Å, and for M spectral types a resolution about R = 2000 and moderate SNR are enough for its detection Bayo [2011]. Note, however, that warmer stars requite a better resolution with a good SNR.

Fig. 4.5a displays the lithium abundance versus the effective temperature for IC 2391, APer and the Pleiades (after Barrado y Navascués et al. [2004c]). The lithium gap widens with age, but it is difficult

to use it since for G and K stars there is a significant lithium spread, probably related to rotation and activity (although other effects cannot be ruled out, see Soderblom et al. [1993]; Barrado y Navascués et al. [2001a]; Stauffer et al. [2003]). However, the LDB is very clearly marked and corresponds to very narrow ranges of effective temperatures or magnitudes (in a colour-magnitude diagram, CMD). Note that this method can only be used for clusters with ages in the range $\sim 15 - 500$ Myr, either because lithium depletion has not started yet, or because stars and BDs with masses above 0.06 $M_{\odot}$ older than 500 Myr have completely depleted their lithium (and those with lower masses cannot destroy it since their interior never reaches temperatures hot enough to ignite the conversion into helium).

In combination with theoretical models (for instance, Baraffe et al. [1998]), the LDB can be used to derive a cluster age with very small error-bars (mostly coming from uncertainties in the cluster distance). We have done this exercise for the seven clusters having appropriate data from the literature, listed in Table 4.2. Fig. 4.5b illustrates the method and the results for these seven associations, in this case based on the location of the LDB in a CMD using the I magnitude as a basic reference.

As first noted by Basri et al. [1996] and Stauffer et al. [1998b], the LDB age can be significantly larger (up to 50%) than values derived from other methodologies. Note, however, that other methods present problems. We will discuss two of these methods: Upper Main Sequence Turn Off (a nuclear age) and low-mass isochrone fitting (a contracting age).

Nuclear ages as derived by Upper Main Sequence Turn Off (when the massive components depart from the MS) are based on very low numbers, since massive stars, if present, are few. This is a consequence of the IMF and the Salpeter's shape ($\psi(M)$=$k\times\ M^{-\alpha}$, where $\alpha = 2.35$). As a matter of fact, the method should work better for well populated clusters, and for more evolved ones. This is due to two facts: the cluster Mass Function implies a larger fraction of low-mass members, and more stars should have evolved off the MS, more and more detached from it for more evolved associations. Thus, a larger number of cluster members in the giant branch should result in a more accurate fit of the cluster isochrone. As an example, the well-known Hyades cluster (about 600 Myr) has only four stars outside the MS, whereas the M 67 cluster (about 5 Myr) has a much larger number of subgiants and giants, and therefore its nuclear age should be more accurate (providing that the distance is not introducing an additional source of uncertainty, which is not the case).

Low-mass isochrone fitting relies on the properties (effective temperature and luminosity) of PMS cluster members. It corresponds, essentially, to a contraction age, since the star luminosity comes from its thermal energy, which ultimately is derived from the contraction of the star (or BD) and the gravitational potential. Since the distance between isochrones in a HR diagram depends on mass and age, being larger for lower masses and decreasing with age (making it difficult to differentiate between a several hundred million years isochrone and the Zero Age MS, when the hydrogen starts its conversion into helium), the method works best for the bottom of the PMS and for very young clusters.

Fig. 4.6a displays a comparison between nuclear and contracting ages. The diagram clearly shows the obvious differences, and a clear trend: clusters below 50 Myr have older nuclei than their contracting ages. A similar result has been obtained by Naylor [2009]. In this case, he computed ages a factor 1.5 to 2 longer than commonly used values. Since the contracting ages should be more accurate for this mass range (see, for instance, the error-bars in the figure), we will use preferentially the contracting ages below 50 Myr and nuclear values above this amount.

The LDB age scale is compared with other values in Fig. 4.6b. We have emphasized the values selected as described in the paragraph above (in black), but for convenience other values are reproduced (in red, with error-bars in light grey). Also represented are 1:1 and 1:1.5 ratio lines. All clusters are below the 1:1 line, and most are even below the 1:50 line, a clear indication of a substantially larger age for the LDB method. Thus, it seems like some physics are not being taken into account in the theoretical models (opacities, overshooting, etc): either the cluster sequence is adjusted by too young an isochrone (see Naylor [2009]), or the rate of lithium depletion is too slow in the current computations. Note that we have not taken into account the possibility of having non-solar metallicities for the clusters (and differences from each other).

Independently from the question which age scale is valid (perhaps none of them is), the LDB cleanly provides a clear shorting for the age, a sequence of ages more sharply delineated than other methodologies. Ultimately it depends on: i) our ability of determine the cluster distance (which would be greatly improved by Gaia, hopefully ending the debate about the Hipparcos results for nearby clusters), ii) to identify a significant number of low-mass cluster members within a small magnitude range and iii) to obtain quality medium-resolution spectra of them. In any event, a sanity check of cluster ages.

As shown in Fig. 4.7, where we represent the location in an age-distance diagram for the clusters

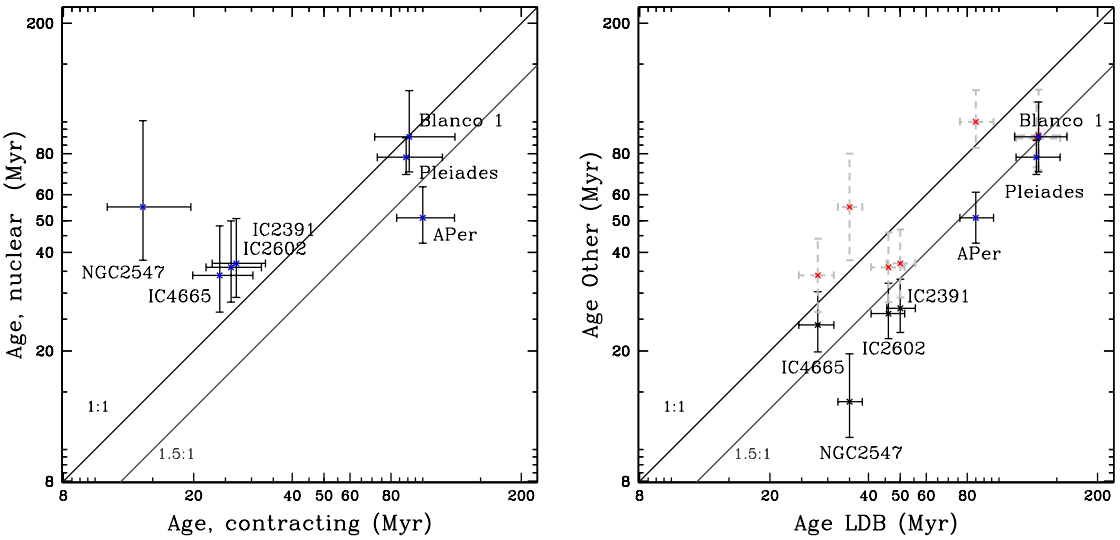

Figure 4.6: Comparison of different age scales. *a* Ages derived from Upper Main-Sequence Turn Off (nuclear, using the more massive members) versus low-mass isochrone fitting (contracting age in the PMS). *b* LDB ages versus other values. We have selected the optimal method for different mass ranges: isochrone fitting for very young and nuclear ages for older clusters (blue crosses -actual values- and solid, black lines -for the errors). Other values are represented by red crosses and dashed, grey lines.

listed in Dias et al. [2002], and the location of the LDB in the same diagram, expressed as a relation between the distance and the age curves corresponding to different apparent magnitudes (in the R and I bands), following Baraffe et al. [1998]. In the figure we have also included the position of the seven clusters with derived ages based on the LDB technique.

Two conclusions can be extracted from Fig. 4.7: i) First, there is a significant number of clusters to which the LDB chronology can be successfully applied, especially for ages younger than 100 Myr, in order to verify whether the trend seen between LDB and other age scales still holds (in the sense that the former are about a 50% larger). ii) Although extremely challenging, it is possible to apply the LDB technique to several clusters older than 150 Myr, and extent the LDB age up to 600 Myr (approximately the ages of the Hyades and Praesepe).

Some discussion about the data for the clusters

We would like to remark that all ages are model dependent, since they ultimately rely on stellar evolution theory and theoretical computations for the stellar interiors and atmospheres, including specific mixtures of chemical compositions -hydrogen, helium and other elements. In addition, other parameters, such as the cluster distance and the interstellar reddening play a significant role (and they are important error sources). Metallicity might also contribute to the results and the error budget, but we have not taken them into account. Moreover, as discussed in Mermilliod [2000], the nuclear and contracting methods might have an uncertainty factor of up to two in age. Finally, there is a significant number of age estimates for the most famous clusters, such as the Pleiades, which are in some cases quite far apart, and we will only discuss the most widely used.

IC 4665

Mermilliod [1981a] gives a nuclear age of 36.3 Myr for the complex composed by the clusters IC 4665, IC 2602, IC 2391, NGC 2451 and NGC 4609, whereas a significantly younger age of 22 ± 5 has been derived by Manzi et al. [2008] using isochrone fitting (contracting age). No errors are provided for the nuclear age, so arbitrarily we have estimated the uncertainty as 10 Myr (see Naylor [2009] for several examples of PMS ages), in order to plot them in Fig. 4.6. The LDB age estimate comes from Manzi et al. [2008], who derived $27.7^{+4.2}_{-3.5}$ Myr. Other works have produced ages in the range 30 – 40 Myr (Lynga [1995]; Dambis [1999]; Kharchenko et al. [2005]).

The distances range from 324 pc up to 430 pc: 324 pc by Abt & Chaffee [1967], 320 pc by Crawford & Barnes [1972], 350 pc by Mermilliod [1981a], 430 pc by Lynga [1995], 370 ± 100 pc by Dambis [1999], 385 ± 40 pc by Hoogerwerf et al. [2001], 352 pc by Kharchenko et al. [2005]. The last three values

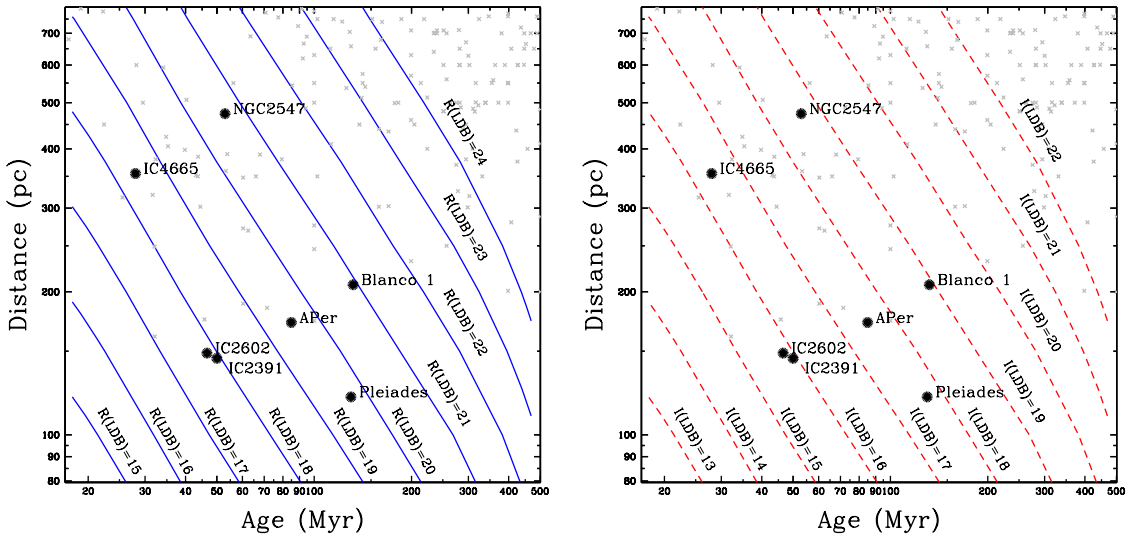

Figure 4.7: Relation between the distance and the age for the Lithium Depletion Boundary. We have included the clusters listed in Dias et al. [2002] as small grey crosses, whereas the seven clusters with derived lithium ages appear as big symbols. The lines correspond to the apparent magnitudes when lithium is 99% depleted, from models from Baraffe et al. [1998]. Magnitudes in the R and I bands are represented in the panels a –blue lines– and b –red, dashed lines. Note that the LiI6707.8 Å doublet is located in the R band.

correspond to different analyses based on Hipparcos data. A more recent analysis by van Leeuwen [2009] –also Hipparcos data, see these proceedings– produces a distance modulus of 7.75 ± 0.21 mag, equivalent to $354.8^{+36.0}_{-32.7}$ pc, assuming $E(B-V) = 0.04$.

Finally, the interstellar extinction has been evaluated by Hogg & Kron [1955], $E(B-V) = 0.18$ mag.

NGC 2547

Jeffries & Tolley [1998] provided age estimates of 55 ± 25 –nuclear– and 14 ± 4 Myr –contracting, whereas Jeffries & Oliveira [2005] derived the LDB age: 53 ± 3 Myr (see also Jeffries et al. [2003]). Naylor et al. [2002] provides a contracting age of 20 – 35 Myr and an intrinsic distance modulus of 8.10 ± 0.10 –$416.9^{+19.6}_{-18.8}$ pc. More recently, Naylor [2009] derived a nuclear age (MS) of 48^{+14}_{-21} Myr, assuming a distance modulus of 8.03 mag –404 pc– and a excess of $E(B-V) = 0.04$ mag.

The distance and the interstellar extinction have been measured by Clariá (1982): $E(B-V) = 0.06$ ± 0.02 and 450 ± 45 pc. A more recent value appears in van Leeuwen [2009], with a distance modulus of 8.38 ± 0.17 mag, equivalent to $474.2^{+38.7}_{-35.7}$ pc, assuming $E(B-V) = 0.05$ mag.

IC 2602

Mermilliod [1981a] published a nuclear age of 36.3 Myr for the complex composed by IC 4665, IC 2602 and IC 2391 (and NGC 2451 and NGC 4609). No errors are provided, and we have estimated them as 10 Myr (see Naylor [2009] for examples and uncertainties based on this technique). Naylor [2009] derived a nuclear age (MS) of 44^{+18}_{-16} Myr, assuming a distance modulus of 5.88 mag and an excess of $E(B-V) = 0.02$ mag. The isochrone fitting age (22 ± 5 Myr) has been taken from Stauffer et al. [1997], assuming $(m-M)_0 = 5.95$ and $E(V-I)_c = 0.04$ for IC 2602. Finally, Dobbie et al. [2010] has computed the LDB age, 46 ± 6 Myr, very similar to the value derived by Barrado y Navascués et al. [1999, 2004c] for the twin cluster IC 2391.

The Hipparcos distance modules is $(m-M)_0 = 5.84 \pm 0.07$ –147.2 pc– and the interstellar excess –$E(B-V) = 0.04$ comes from Pinsonneault et al. [1998]. Using Hipparcos data, a recent analysis by van Leeuwen [2009] produced a distance of 148.6 ± 2.0 pc, assuming $E(B-V) = 0.03$ mag.

IC 2391

The nuclear age of this cluster is 36.3 Myr (as in the case of IC 2602, for the complex composed by IC 4665, IC 2602, IC 2391, a NGC 2451 and NGC 4609, Mermilliod [1981a]). Based on similar data and technique, although no errors are provided in the previous study, we assume them as 10 Myr. The isochrone fitting age (22 ± 5 Myr), which assumed $(m-M)_0 = 6.05$ –162.2 pc– and $E(V-I)_c = 0.01$ mag, has been taken from Stauffer et al. [1997].

The LDB age was initially estimated by Barrado y Navascués et al. [1999] with a further refinement in Barrado y Navascués et al. [2004c], producing a value of 50 ± 5 Myr. Other distances are $146.5^{+5.5}_{-5.3}$ pc –from $(m-M)_0 = 5.83 \pm 0.08$ as estimated by Hipparcos– or van Leeuwen [2009], 144.9 ± 2.5 pc, assuming $E(B-V) = 0.01$, also using Hipparcos data. Pinsonneault et al. [1998] quotes a reddening of $E(B-V) = 0.01$ mag.

Alpha Per

Mermilliod [1981a] derived a nuclear age of the group which includes Alpha Per, NGC 5281, NGC 6242, and NGC 6405, 51.3 Myr. Later on, Meynet et al. [1993] also computed a nuclear age of 52.5 Myr –including α Per itself– using $E(B-V) = 0.09$ and a distance of 350 pc. Again, our own error estimate is 10 Myr. The best age estimate from the colour-magnitude diagrams made with the UKIDSS GCS photometry and a 180 pc distance is 100 Myr (Lodieu priv.comm.)
A fine LDB age –85 ± 10 Myr– was derived in Stauffer et al. [1999]. See also Barrado y Navascués et al. [2004c] for a recomputation, which yielded 85 ± 10 Myr. Stauffer et al. 1999 assumed 176 pc and A_I = 0.17, $E(R-I)_C = 0.07$ mag. A previous value of the average reddening is $E(V-I)_K = 0.16$ mag, by Stauffer et al. [1985]. Finally, van Leeuwen [2009] obtained a distance 172.4 ± 2.7 pc with Hipparcos data, assuming $E(B-V) = 0.09$ mag.

The Pleiades

Mermilliod [1981a] gives a nuclear age of 77.6 Myr for the Pleiades (including NGC 2323, NGC 2422, NGC 6067, NGC 6709, NGC 7790 and Tr 2). No errors are provided, and we have estimated them as 10 Myr. As in the case of APer, Meynet et al. [1993] derived a nuclear age of 100 Myr using $E(B-V)$ = 0.04 and a distance of 131.8 pc. The contracting of 70 Myr has been taken from Stauffer et al. [1995]. However, Mazzei & Pigatto [1989] obtained 150 Myr with a particular set of metallicity and overshooting. Finally, Naylor [2009] derived a nuclear age (MS) of 115^{+3}_{-11} Myr, assuming a distance modulus of 5.35 mag –117.5 pc– and an excess of $E(B-V) = 0.02$ mag. An initial LDB age was obtained by Basri et al. [1996] – ∼ 115 Myr, and an accurate value of 125 ± 8 Myr was derived by Stauffer et al. [1998b], with a re-estimate –130 ± 20 Myr– using the same methodology as in the case of IC 2391 and APer in Barrado y Navascués et al. [2004c].

Stauffer & Hartmann [1987] obtained $A_I = 0.06$ and $E(R-I) = 0.03$ mag, and used in a consistent manner the set: $(m-M)_0 = 5.53$ and $E(V-I) = 0.06$ mag (see, for instance, Stauffer et al. [1998a]). Another reddening is $E(B-V) = 0.04$ mag, from Pinsonneault et al. [1998], together with $(m-M)_0$ = 5.60 ± 0.01. On the contrary, the Hipparcos value is $(m-M)_0 = 5.40 \pm 0.03$ also from Hipparcos data, van Leeuwen [2009] derived 120.2 ± 1.9 pc, assuming $E(B-V) = 0.04$ mag. This last work also summarizes the derived distance for the Pleiades by different groups for the last 30 years.

Blanco 1

This cluster has no obvious turn-off, as commented by Panagi & O'dell [1997]. They estimated the age based on the Hα emission of late-type stars (i.e., by direct comparison with other clusters). The isochrone fitting age –contracting– comes from Cargile & James [2010]. On the other hand, Moraux et al. [2007] used 100 and 150 Myr isochrones, although the 100 Myr model seemed to be slightly better but the difference was very small. LDB age, 132 Myr, was derived by Cargile et al. [2010]. Finally, a recent analysis of Hipparcos data yields 207.0 ± 12.0 pc, assuming $E(B-V) = 0.01$ –van Leeuwen [2009].

What can be known?

We will discuss the availability of clusters and their substellar population with current instrumentation, and some aspects about what can be known.

Figure 4.8a displays the apparent magnitude (R filter, centered at ∼6500 Å) for the frontier between stars and BDs, as a function of the cluster age. Different lines correspond to various distances (from bottom to top: 10, 50, 100, 500 and 1000 pc). For convenience, we have plotted a cross representing the Pleiades. As expected, the stellar/substellar borderline appear dimmer for older and/or further away associations. For example, the 600 Myr Hyades, located about 50 pc, has a frontier at about $R \sim 21$, whereas for the Pleiades, much younger but further away, it is located at about $R \sim 20$. Current instrumentation allows to go much fainter than these magnitudes but, of course, it depends on the resolution used for spectroscopic studies.

Fig. 4.8b has been created by using the Exposure Time Calculator for the Flames multifibre spectrograph at the VLT. The upper panel includes three sets of calculations, all of them using a resolution of R = 250 and a SNR = 20: i) In magenta, for the stellar/substellar borderline at 0.072 $M_\odot$ and an

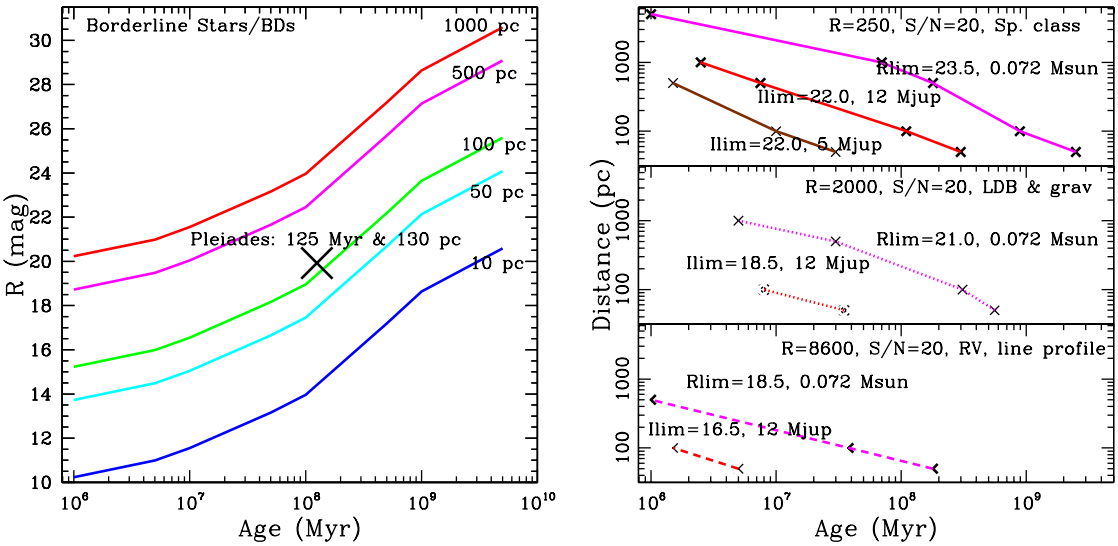

Figure 4.8: *a* Location of the borderline between stars and brown dwarfs for clusters with different ages, assuming different distances (using models by Baraffe et al. [1998]). *b* Spectroscopic "accessibility" for a signal-to-noise of 20 and different spectral resolutions. We have used the VLT/Flames exposure Time Calculator in order to estimate the conditions under which spectroscopic data can be acquired. See text.

apparent magnitude of $R = 23.5$ mag. ii) In red, for the isolate planetary mass frontier at 0.013 $M_\odot$ (about 12 M_{Jup} and an apparent magnitude of $I = 22.0$ mag. iii) In brown, IPMOs with 5 M_{Jup}, a possible cut-off for the IMF, and an apparent magnitude of $I = 22.0$ mag. This setup is very adequate for spectral typing and to measure the Hα equivalent width (and other strong lines, if present), i.e., for membership confirmation. From the graph, it is clear that it is possible to obtain low-resolution spectra of very young clusters (less 1 Myr within 5,000 pc), or young clusters (less than 100 Myr) within about 800 pc or so.

In the same manner, the middle panel of Fig. 4.8b represents the computation using a resolution of about R = 2000, and a SNR = 20, useful to derive the location of the Lithium Depletion Boundary via the detection of the LiI6708 Å doublet and other alkali features such as KI7699 Å or NaI8200 Å. In this case, two lines have been represented: one corresponding to $R = 21$ mag and 0.072 $M_\odot$ and another for $I = 18.5$ mag and 12 M_{Jup}.

Finally, the panel at the bottom of Fig. 4.8b corresponds to estimates with a resolution of about R=8600, which is adequate for line profiles and radial velocity measurements, for instance. In this case, the borderlines for stars/BDs and BDs/IPMOs are represented, equivalent to $R = 18.5$ mag and $I = 16.5$ mag, respectively.

A query at the WEBDA database[1] produces a large number of clusters: seventy seven with ages less than 10 Myr, 258 with ages between 10 and 100 Myr, 307 with ages in the range 100 and 1000 Myr, and another 42 clusters older than 1000 Myr. These samples are represented in Fig. 4.9ab, where we show the cluster distance versus its galactic longitude. A question lingers: how many of these clusters can be reached with spectroscopy, with a 8m class telescope?

Figure 4.9 displays the open clusters listed in WEBDA, discriminating by ages: blue for clusters with 1 – 10 Myr, cyan for 10 – 100 Myr, magenta for 100 – 1000 Myr, and red for associations older than 1000 Myr. The cluster distance appears in the y-axis, whereas the galactic longitude is represented in the x-axis.

Figure 4.9a also includes the limit for low-resolution spectroscopy, following the estimates represented in Fig. 4.8b, for the entire stellar population (essentially all clusters with ages below approx. 5 Myr can be observed), the bottom of the substellar population at 12 M_{Jup} (all young clusters within 1000 – 2000 pc), and IPMOs with a mass of about 5 M_{Jup} (there are few clusters in 500 pc fulfilling this criterion). Note, however, that we have not taken into account star-forming regions, and there is a significant number of them. The effect of intrinsic reddening or interstellar absorption have not been contemplated in all these considerations, which would reduce the number of accessible associations.

[1] http://www.univie.ac.at/webda/

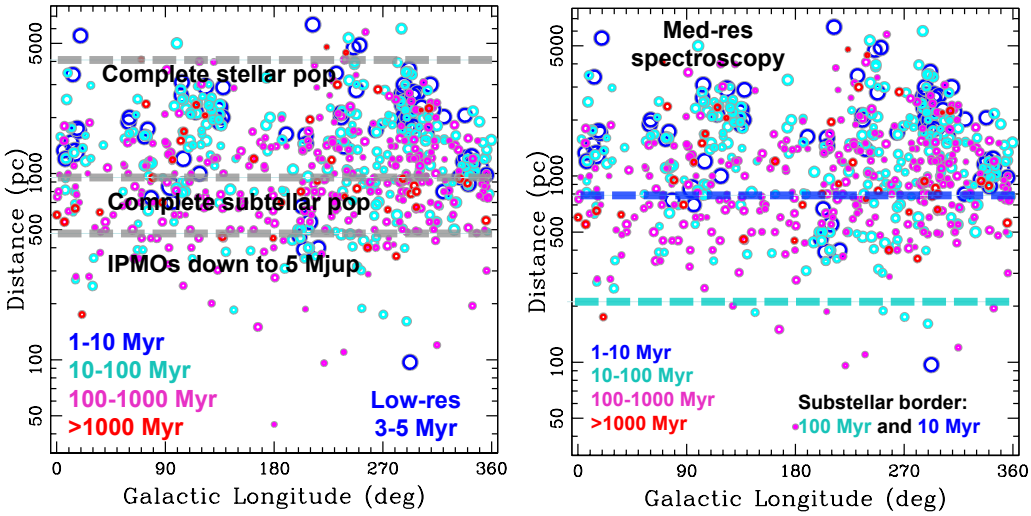

Figure 4.9: Clusters from the WEBDA database, displayed using different colours for several age groups: blue for 1 – 10 Myr, cyan for 10 – 100 Myr, magenta for 100 – 1000 Myr and red for older than 1000 Myr. The symbol size is related to age (larger for younger ones) *a* The dashed lines correspond to the "accessibility" using the estimates represented in Fig. 4.8b, top panel (low-resolution spectroscopy), assuming cluster ages in the range 3 – 5 Myr. *b* Location of the stellar/substellar borderline for clusters with ages of 10 and 100 Myr, assuming the estimates represented in Fig. 4.8b, middle panel.

Regarding studies requiring med-resolution spectroscopy, we have represented the location of the stellar/substellar frontier in Fig. 4.9b. Only a handful of 100 Myr clusters can be observed, but younger counterparts, with 10 Myr, can be reached at much further distances at about 700 pc.

Role of Gaia

Accurate ages from Gaia

Without doubt, Gaia will play a definitive role in order to improve our knowledge of the life (and death) of stars and stellar associations. One key point will be to improve the age determination, independently of the technique.

On one hand, the extremely precise individual distance for members of stellar associations, and the ability to weed out false members using proper motions and radial velocities (at least for the most massive members) will allow the built up of accurate HR diagrams. The comparison with theoretical isochrones will yield much more accurate ages (and will be key to solve the problem with the Pleiades distance, among other clusters). The confrontation of the measured parameters of eclipsing binaries in clusters (masses, radii, Teff, luminosity) with the values obtained with the same isochrones (and the complementary evolutionary tracks) will be essential in this exercise.

On the other hand, the lithium age scale will greatly benefit from Gaia, since distances are the major source of uncertainty when deriving ages with this method.

Therefore, a comprehensive analysis can be done, and a "definitive" age scale will be settled down.

Detectability with Gaia

The estimates represented in Fig. 4.8b (i.e., the necessary conditions to collect low-, medium and high-resolution spectroscopy with an 8m class telescope), allow us to have a look at the number of clusters we can, indeed, observe. The complementary information will come from Gaia data. Indeed, Fig. 4.10 represents evolutionary tracks (Baraffe et al. [1998]; Chabrier et al. [2000]) for low-mass stars and sub-stellar objects: flux at the I band as a function of the age, assuming two different distances: 100 and 500 pc. Essentially, Gaia will measure positions and proper motions for brown dwarfs up to about several hundred Myr (depending on the mass of the BD) and in fact it has the capability of detecting objects with masses around the planetary mass frontier, if they are young and close enough. Unfortunately, few

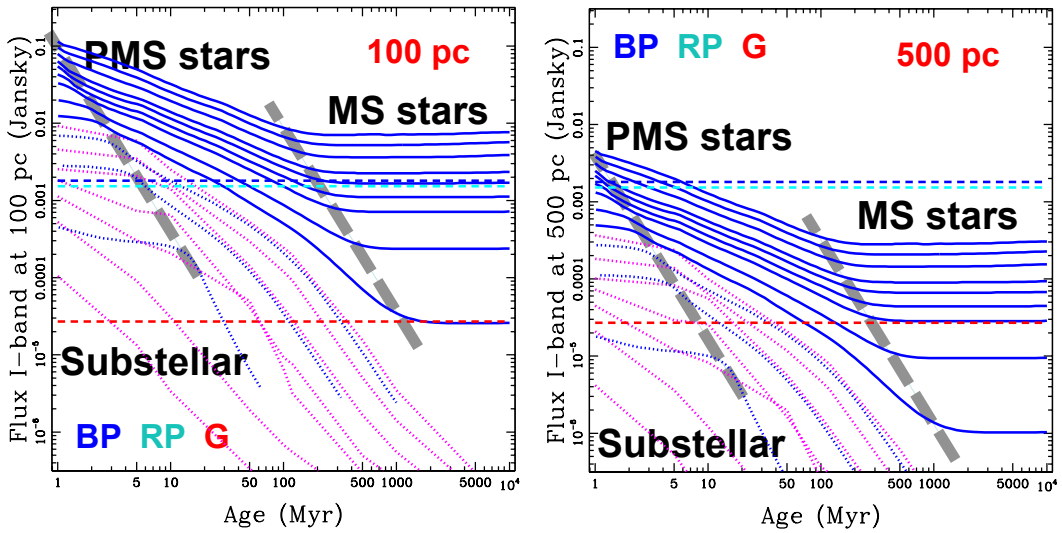

Figure 4.10: The diagram is similar to Fig. 4.3c, but we have plotted the flux instead of the magnitude in the I band, for easier comparison with the Gaia detection limits: blue for BP, cyan for RB, and red for G –much deeper. We have plotted models by the Lyon group for a distance of 100 pc (panel a) or 500 pc (panel b). Gaia will detect a huge amount of young, low-mass cluster members even up to several hundred parsec, providing accurate proper motions and, in come cases, radial velocities. The isochrones correspond to 0.35, 0.30, 0.25, 0.20, 0.175, 0.15, 0.13, 0.10, 0.080, 0.06, 0.04, 0.03, 0.02 $M_{\odot}$ -NextGen, in blue, and 50, 40, 30, 20, 15, 10, 5 M_{Jup} - COND, in magenta.

associations fulfill both criteria simultaneously.

Figure 4.11 corresponds to an approximation to what Gaia can detect assuming $G_{lim} = 20$ mag. The diagram includes several spectra: observed in the case of the upper three panels, theoretical in the panel at the bottom (see Allard & Freytag [2010] and references therein). The spectra correspond to substellar or very cool objects located at different distances or have been scaled at different distances. The Gaia detection limits have been represented with dashed lines: blue for BP, cyan for RP, and red for G band.

The RP photospectrometer will be able to obtain some interesting measurements for some young, nearby brown dwarfs (such as massive brown dwarfs in Taurus), whereas proper motions for isolated Planetary Mass Objects will be derived for associations up to 400 pc (such as in Sigma Ori). However, it is probable that neither their less massive siblings nor the older counterparts will be detected in stellar associations, since they are significantly dimmer and cooler, and we will have to rely on comparisons with field objects with L and T spectral type (see the two panels at the bottom of Fig. 4.11) or even Y, not yet discovered and characterized by the presence of ammonia in the near IR spectrum.

Final remarks

During the past 15 years, a lot of work has been done in the brown dwarfs domain. Mostly, involving photometry and low-res spectroscopy. The exploitation of Gaia data will require a massive investment in high-resolution spectroscopy.

- For BDs, med- and high spectral resolution data are needed, in order to produce complete censuses of stellar and substellar members in different stellar associations and to be able to derive unbiased IMFs.
- We only know a handful of isolated planetary mass objects, mostly young. Detailed spectroscopic characterization is awaiting.
- Current telescopes can be used to derive a more complete LDB chronology covering the whole range of ages where this method is valid (15 – 600 Myr, approx).
- Gaia will be key in several important problems related to star formation, such as the shape and origin of the IMF, disk evolution and the age scale. In particular, when combined with med-res

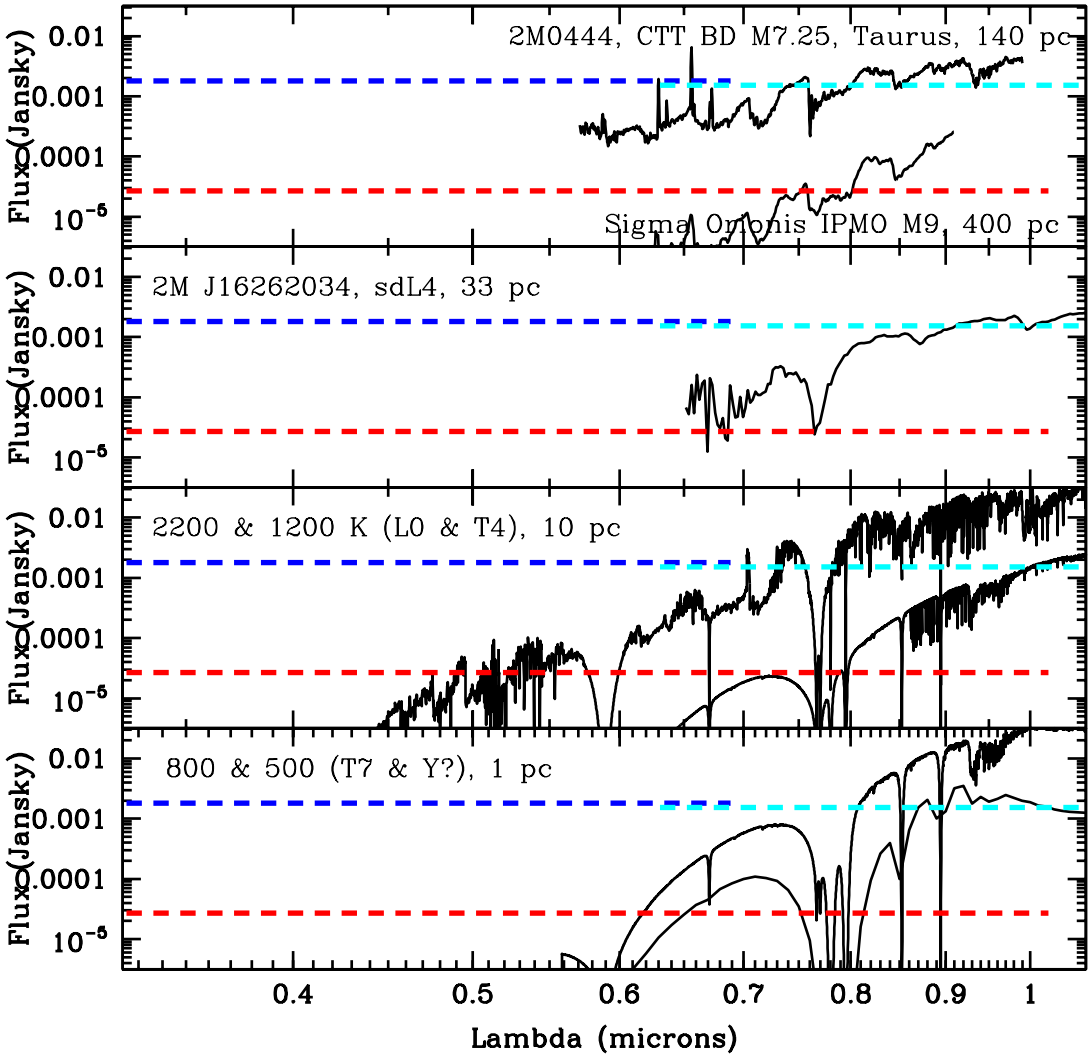

Figure 4.11: Several spectra of late spectral type objects and, for comparison, the detectability with Gaia, represented as blue and cyan dashed lines for the BP and RB spectrometer and a red, dashed line for the G magnitude. The top panel includes observed spectra for a brown dwarf, a M7.25 from Taurus and an isolated planetary mass object with M9 from Sigma Orionis. Inmediately below we display another observed spectrum, corresponding to a nearby subdwarf. The other two panels display theoretical data (Allard & Freytag [2010]) with different temperatures, at different distances.

spectroscopy of quality, it should settle down this issue.

- Gaia will give us access to very important information, especially for nearby, young associations. But spectroscopy is a must. The scientific community should be ready to obtain and analyze a huge amount of data, including spectroscopy.
- The full exploitation of the immense wealth Gaia will deliver to the community will require comprehensive spectroscopic cartography, and the collection of tens of million of spectra.
- This observational effort can only be achieved with dedicated telescopes with big apertures and large multiplexing capabilities.

Acknowledgments

We would like to thank the organizers of the workshop for their kind invitation and support. This research has been funded by Spanish grants AYA 2010-21161-C02-02, CDS2006-00070 and PRICIT-S2009/ESP-

1496. We do appreciated the comments and data by N. Lodieu, E. Moraux and J. Bouvier.

Bibliography

Abt, H. A. & Chaffee, F. H. 1967, ApJ, 148, 459
Allard, F. & Freytag, B. 2010, Highlights of Astronomy, 15, 756
Allen, P. R., Luhman, K. L., Myers, P. C., et al. 2007, ApJ, 655, 1095
Alves de Oliveira, C., Moraux, E., Bouvier, J., et al. 2010, A&A, 515, A75+
Apai, D., Pascucci, I., Bouwman, J., et al. 2005, Science, 310, 834
Ardila, D., Martín, E., & Basri, G. 2000, AJ, 120, 479
Baker, D. E. A., Jameson, R. F., Casewell, S. L., et al. 2010, MNRAS, 408, 2457
Baraffe, I., Chabrier, G., Allard, F., & Hauschildt, P. H. 1998, A&A, 337, 403
Barrado Y Navascués, D., Bayo, A., Morales-Calderón, M., et al. 2007, A&A, 468, L5
Barrado y Navascués, D., Béjar, V. J. S., Mundt, R., et al. 2003, A&A, 404, 171
Barrado y Navascués, D., Bouvier, J., Stauffer, J. R., Lodieu, N., & McCaughrean, M. J. 2002, A&A, 395, 813
Barrado y Navascués, D., García López, R. J., Severino, G., & Gomez, M. T. 2001a, A&A, 371, 652
Barrado y Navascués, D. & Jayawardhana, R. 2004, ApJ, 615, 840
Barrado y Navascués, D. & Martín, E. L. 2003, AJ, 126, 2997
Barrado y Navascués, D., Mohanty, S., & Jayawardhana, R. 2004a, ApJ, 604, 284
Barrado y Navascués, D., Stauffer, J. R., Bouvier, J., Jayawardhana, R., & Cuillandre, J.-C. 2004b, ApJ, 610, 1064
Barrado y Navascués, D., Stauffer, J. R., Briceño, C., et al. 2001b, ApJS, 134, 103
Barrado y Navascués, D., Stauffer, J. R., & Jayawardhana, R. 2004c, ApJ, 614, 386
Barrado y Navascués, D., Stauffer, J. R., Morales-Calderón, M., et al. 2007, ApJ, 664, 481
Barrado y Navascués, D., Stauffer, J. R., & Patten, B. M. 1999, ApJ, 522, L53
Barrado y Navascués, D., Zapatero Osorio, M. R., Béjar, V. J. S., et al. 2001c, A&A, 377, L9
Bartko, H., Martins, F., Trippe, S., et al. 2010, ApJ, 708, 834
Basri, G., Marcy, G. W., & Graham, J. R. 1996, ApJ, 458, 600
Bate, M. R., Bonnell, I. A., & Bromm, V. 2002, MNRAS, 332, L65
Bayo, A. 2009, PhD dissertations, Universidad Autónoma de Madrid
Bayo, A., e. 2011, A&A, submitted
Béjar, V. J. S., Martín, E. L., Zapatero Osorio, M. R., et al. 2001, ApJ, 556, 830
Béjar, V. J. S., Zapatero Osorio, M. R., & Rebolo, R. 1999, ApJ, 521, 671
Boudreault, S. & Bailer-Jones, C. A. L. 2009, ApJ, 706, 1484
Boudreault, S., Bailer-Jones, C. A. L., Goldman, B., Henning, T., & Caballero, J. A. 2010, A&A, 510, A27+
Bouvier, J., Kendall, T., Meeus, G., et al. 2008, A&A, 481, 661
Bouvier, J., Stauffer, J. R., Martin, E. L., et al. 1998, A&A, 336, 490
Bouy, H., Huélamo, N., Barrado Y Navascués, D., et al. 2009a, A&A, 504, 199
Bouy, H., Huélamo, N., Martín, E. L., et al. 2007, A&A, 463, 641
Bouy, H., Huélamo, N., Martín, E. L., et al. 2009b, A&A, 493, 931
Bouy, H., Huélamo, N., Pinte, C., et al. 2008, A&A, 486, 877
Bouy, H. & Martín, E. L. 2009, A&A, 504, 981
Burgasser, A. J., Kirkpatrick, J. D., Brown, M. E., et al. 2002, ApJ, 564, 421
Caballero, J. A. 2009, in American Institute of Physics Conference Series, Vol. 1094, American Institute of Physics Conference Series, ed. E. Stempels, 912–915
Caballero, J. A. 2010, A&A, 514, A18+
Caballero, J. A., Béjar, V. J. S., Rebolo, R., et al. 2007, A&A, 470, 903
Cargile, P. A. & James, D. J. 2010, AJ, 140, 677
Cargile, P. A., James, D. J., & Jeffries, R. D. 2010, ApJ, 725, L111
Chabrier, G., Baraffe, I., Allard, F., & Hauschildt, P. 2000, ApJ, 542, 464
Chauvin, G., Lagrange, A.-M., Dumas, C., et al. 2004, A&A, 425, L29
Comerón, F., Spezzi, L., & López Martí, B. 2009, A&A, 500, 1045
Crawford, D. L. & Barnes, J. V. 1972, AJ, 77, 862
Dambis, A. K. 1999, Astronomy Letters, 25, 10
Dantona, F. & Mazzitelli, I. 1984, A&A, 138, 431
D'Antona, F., Ventura, P., Mazzitelli, I., & Zeppieri, A. 1998, Mem. Soc. Astron. Ital., 69, 575

Dias, W. S., Alessi, B. S., Moitinho, A., & Lépine, J. R. D. 2002, A&A, 389, 871
Dobbie, P. D., Lodieu, N., & Sharp, R. G. 2010, MNRAS, 409, 1002
Gizis, J. E. 2002, ApJ, 575, 484
Guieu, S., Dougados, C., Monin, J.-L., Magnier, E., & Martín, E. L. 2006, A&A, 446, 485
Guieu, S., Pinte, C., Monin, J.-L., et al. 2007, A&A, 465, 855
Hogg, A. R. & Kron, G. E. 1955, AJ, 60, 365
Hoogerwerf, R., de Bruijne, J. H. J., & de Zeeuw, P. T. 2001, A&A, 365, 49
Jeffries, R. D., Jackson, R. J., James, D. J., & Cargile, P. A. 2009, MNRAS, 400, 317
Jeffries, R. D., James, D. J., & Thurston, M. R. 1998, MNRAS, 300, 550
Jeffries, R. D. & Oliveira, J. M. 2005, MNRAS, 358, 13
Jeffries, R. D., Oliveira, J. M., Barrado y Navascués, D., & Stauffer, J. R. 2003, MNRAS, 343, 1271
Jeffries, R. D. & Tolley, A. J. 1998, MNRAS, 300, 331
Kharchenko, N. V., Piskunov, A. E., Röser, S., Schilbach, E., & Scholz, R.-D. 2005, A&A, 438, 1163
Kirkpatrick, J. D., Beichman, C. A., & Skrutskie, M. F. 1997, ApJ, 476, 311
Kirkpatrick, J. D., Reid, I. N., Liebert, J., et al. 1999, ApJ, 519, 802
Lada, C. J., Muench, A. A., Haisch, Jr., K. E., et al. 2000, AJ, 120, 3162
Lafrenière, D., Jayawardhana, R., & van Kerkwijk, M. H. 2008, ApJ, 689, L153
Lodieu, N., Caux, E., Monin, J.-L., & Klotz, A. 2002, A&A, 383, L15
Lodieu, N., Dobbie, P. D., Deacon, N. R., et al. 2007, MNRAS, 380, 712
Lodieu, N., Dobbie, P. D., & Hambly, N. C. 2011, A&A, 527, A24+
Lodieu, N., Hambly, N. C., Jameson, R. F., & Hodgkin, S. T. 2008, MNRAS, 383, 1385
Lodieu, N., McCaughrean, M. J., Barrado Y Navascués, D., Bouvier, J., & Stauffer, J. R. 2005, A&A, 436, 853
Lodieu, N., Zapatero Osorio, M. R., Rebolo, R., Martín, E. L., & Hambly, N. C. 2009, A&A, 505, 1115
López Martí, B., Jiménez-Esteban, F., & Solano, E. 2011, A&A, 529, A108+
López Martí, B., Spezzi, L., Merín, B., et al. 2010, A&A, 515, A31+
Lucas, P. W. & Roche, P. F. 2000, MNRAS, 314, 858
Luhman, K. L. 2004, ApJ, 602, 816
Luhman, K. L. 2007, ApJS, 173, 104
Luhman, K. L., Allers, K. N., Jaffe, D. T., et al. 2007, ApJ, 659, 1629
Luhman, K. L., Hernández, J., Downes, J. J., Hartmann, L., & Briceño, C. 2008, ApJ, 688, 362
Luhman, K. L., Lada, C. J., Hartmann, L., et al. 2005, ApJ, 631, L69
Luhman, K. L., Mamajek, E. E., Allen, P. R., & Cruz, K. L. 2009, ApJ, 703, 399
Luhman, K. L. & Rieke, G. H. 1999, ApJ, 525, 440
Luhman, K. L., Stauffer, J. R., Muench, A. A., et al. 2003, ApJ, 593, 1093
Luhman, K. L., Whitney, B. A., Meade, M. R., et al. 2006, ApJ, 647, 1180
Lynga, G. 1995, VizieR Online Data Catalog, 7092, 0
Mainzer, A. K. & McLean, I. S. 2003, ApJ, 597, 555
Manzi, S., Randich, S., de Wit, W. J., & Palla, F. 2008, A&A, 479, 141
Marsh, K. A., Kirkpatrick, J. D., & Plavchan, P. 2010a, ApJ, 709, L158
Marsh, K. A., Plavchan, P., Kirkpatrick, J. D., et al. 2010b, ApJ, 719, 550
Mazzei, P. & Pigatto, L. 1989, A&A, 213, L1
Mermilliod, J. C. 1981a, A&AS, 44, 467
Mermilliod, J. C. 1981b, A&A, 97, 235
Mermilliod, J.-C. 2000, in Astronomical Society of the Pacific Conference Series, Vol. 198, Stellar Clusters and Associations: Convection, Rotation, and Dynamos, ed. R. Pallavicini, G. Micela, & S. Sciortino, 105–+
Meynet, G., Mermilliod, J.-C., & Maeder, A. 1993, A&AS, 98, 477
Mohanty, S., Jayawardhana, R., Huélamo, N., & Mamajek, E. 2007, ApJ, 657, 1064
Monin, J.-L., Guieu, S., Pinte, C., et al. 2010, A&A, 515, A91+
Morales-Calderón, M. 2008, PhD dissertations, Universidad Autónoma de Madrid
Moraux, E., Bouvier, J., Stauffer, J. R., Barrado y Navascués, D., & Cuillandre, J.-C. 2007, A&A, 471, 499
Moraux, E., Bouvier, J., Stauffer, J. R., & Cuillandre, J.-C. 2003, A&A, 400, 891
Moya, A., Baraffe, I., & Barrado, D. 2011, A&A, submitted
Mužić, K., Scholz, A., Geers, V., Fissel, L., & Jayawardhana, R. 2011, ApJ, 732, 86
Muzerolle, J., Luhman, K. L., Briceño, C., Hartmann, L., & Calvet, N. 2005, ApJ, 625, 906
Najita, J. R., Tiede, G. P., & Carr, J. S. 2000, ApJ, 541, 977
Naylor, T. 2009, MNRAS, 399, 432

Naylor, T., Totten, E. J., Jeffries, R. D., et al. 2002, MNRAS, 335, 291
Oliveira, J. M., Jeffries, R. D., Devey, C. R., et al. 2003, MNRAS, 342, 651
Oliveira, J. M., Jeffries, R. D., & van Loon, J. T. 2009, MNRAS, 392, 1034
Padoan, P. & Nordlund, Å. 2004, ApJ, 617, 559
Palla, F. & Baraffe, I. 2005, A&A, 432, L57
Panagi, P. M. & O'dell, M. A. 1997, A&AS, 121, 213
Park, B.-G., Sung, H., Bessell, M. S., & Kang, Y. H. 2000, AJ, 120, 894
Peña Ramírez, K., Zapatero Osorio, M. R., Béjar, V. J. S., Rebolo, R., & Bihain, G. 2011, ArXiv e-prints
Phan-Bao, N., Riaz, B., Lee, C.-F., et al. 2008, ApJ, 689, L141
Pinfield, D. J., Hodgkin, S. T., Jameson, R. F., et al. 2000, MNRAS, 313, 347
Pinsonneault, M. H., Stauffer, J., Soderblom, D. R., King, J. R., & Hanson, R. B. 1998, ApJ, 504, 170
Quanz, S. P., Goldman, B., Henning, T., et al. 2010, ApJ, 708, 770
Rebolo, R., Martin, E. L., & Magazzu, A. 1992, ApJ, 389, L83
Rebolo, R., Zapatero Osorio, M. R., & Martín, E. L. 1995, Nature, 377, 129
Reipurth, B. & Clarke, C. 2001, AJ, 122, 432
Rice, W. K. M., Armitage, P. J., Bonnell, I. A., et al. 2003, MNRAS, 346, L36
Shirono, C., Itoh, Y., & Oasa, Y. 2011, ArXiv e-prints
Slesnick, C. L., Carpenter, J. M., & Hillenbrand, L. A. 2006, AJ, 131, 3016
Soderblom, D. R., Jones, B. F., Balachandran, S., et al. 1993, AJ, 106, 1059
Stamatellos, D. & Whitworth, A. P. 2008, A&A, 480, 879
Stauffer, J. R., Barrado y Navascués, D., Bouvier, J., et al. 1999, ApJ, 527, 219
Stauffer, J. R. & Hartmann, L. W. 1987, ApJ, 318, 337
Stauffer, J. R., Hartmann, L. W., & Barrado y Navascues, D. 1995, ApJ, 454, 910
Stauffer, J. R., Hartmann, L. W., Burnham, J. N., & Jones, B. F. 1985, ApJ, 289, 247
Stauffer, J. R., Hartmann, L. W., Prosser, C. F., et al. 1997, ApJ, 479, 776
Stauffer, J. R., Jones, B. F., Backman, D., et al. 2003, AJ, 126, 833
Stauffer, J. R., Schild, R., Barrado y Navascues, D., et al. 1998a, ApJ, 504, 805
Stauffer, J. R., Schultz, G., & Kirkpatrick, J. D. 1998b, ApJ, 499, L199+
Tamura, M., Itoh, Y., Oasa, Y., & Nakajima, T. 1998, Science, 282, 1095
van Leeuwen, F. 2009, A&A, 497, 209
Webb, R. A., Zuckerman, B., Platais, I., et al. 1999, ApJ, 512, L63
Weights, D. J., Lucas, P. W., Roche, P. F., Pinfield, D. J., & Riddick, F. 2009, MNRAS, 392, 817
Whitworth, A. P. & Zinnecker, H. 2004, A&A, 427, 299
Zapatero Osorio, M. R., Béjar, V. J. S., Bihain, G., et al. 2008, A&A, 477, 895
Zapatero Osorio, M. R., Béjar, V. J. S., Martín, E. L., et al. 2000, Science, 290, 103
Zapatero Osorio, M. R., Béjar, V. J. S., Martín, E. L., et al. 2002, ApJ, 578, 536
Zapatero Osorio, M. R., Béjar, V. J. S., Rebolo, R., Martín, E. L., & Basri, G. 1999, ApJ, 524, L115

4.3 Towards Observational Isochrones from Star Cluster Data

Floor van Leeuwen[1]

[1] Institute of Astronomy, Cambridge, UK

Abstract

Data from the Gaia mission will provide a solid basis for deriving a set of fully calibrated observational isochrones. It will allow for cluster parallaxes and proper motion membership to be measured with unprecedented accuracy. When complemented with high-definition photometry and spectroscopy, this gives access to observational isochrones which are detailed for chemical composition and differential ages. Gaia will provide accurate identifications and distances for a few hundred open clusters, as well as a few of the nearby globular clusters. A first glimpse at what we may be able to discover is already provided through the Hipparcos results for open cluster distances.

Introduction

Although the use of isochrones is a fundamental tool in astronomy, the details of those isochrones still remain largely uncalibrated. This is due to the limited possibilities for calibration, for which currently either the Sun as a single point, or the Hyades main sequence are used. For the resolution of the isochrones with age and chemical composition the interpretations rely almost entirely on the models involved: stellar structure, stellar evolution and stellar atmospheres. In order to improve this situation and provide a more reliable backing to the models underlying the isochrones, detailed information is required on star clusters, most crucially information on cluster membership and distance is needed that has been derived in a way completely independent from the photometric and spectroscopic data later used for the tracking of the isochrones. A still very limited amount of such data is currently only provided by the Hipparcos mission (ESA [1997]; van Leeuwen [2007b]; van Leeuwen [2009]). The Gaia mission can improve on this situation very significantly, with at least one order of magnitude more clusters with accurate membership and distances available, and a much wider coverage of membership than obtained by Hipparcos. To take full advantage of these data, they will need to be complemented with photometric and spectroscopic data of sufficient accuracy and detail.

Despite the limitations of the Hipparcos data, they do already provide the first clear age-sequence in the HR diagram, by combining the parallax-based cluster distances with homogeneous and accurate photometric data. An examination of those data also shows the first hints that small adjustments may be needed to the current sets of isochrones.

In this paper I will review briefly the potential of astrometric cluster data we can expect from Gaia (Section *The Gaia potential for cluster data*). This is followed in Section *Supplementary data needed* by a description of supplementary information that would be needed to fully interpret those data. Section *Independent and absolute distance determinations* describes briefly why only direct and independent distance determinations like those obtained with Hipparcos or Gaia can be used in this context. Section *A first experiment with Hipparcos parallax data* shows the results from a recent study using the new Hipparcos reduction together with Geneva photometric data. Section *A comparison with field star data* shows how information from field stars can further help understanding the cluster data. Finally, Section *Conclusions* presents the main conclusions.

The Gaia potential for cluster data

The Gaia potential for open clusters in the context of isochrone definition is set by criteria on magnitude coverage, proper motion accuracies (reliability of membership determination) and relative parallax accuracy (distance modulus uncertainty). The typical parallax accuracy for a cluster with about 200 to 500 identified members will be of order 1 μas, equivalent to a distance modulus error of 2 millimag at 1 kpc. At 1 kpc the variation in parallax within the cluster is still of order $\pm$ 5 μas, though the sigma is

already a factor 3 to 5 smaller. A distance of 1 kpc therefore seems a reasonable first guess as to how far out it is worthwhile considering clusters as significant contributors for the isochrone studies. Within that distance, the WEBDA[2] gives some 350 clusters, many of which have had so far little or no confirmation. On the other hand, it could be expected that some of the in particular older clusters have so far avoided detection, and will be first noticed by Gaia. A number of 300 to 400 clusters seems a reasonable starting point. The age range covered by those clusters is:

$$6.0 < \log(T) < 9.6, \tag{4.1}$$

and there is also some spread in chemical composition. In principle, this selection can be supplemented by the nearest OB associations (with individual member-star parallaxes) and a few of the nearest globular clusters, for which Gaia can derive parallaxes based on the large numbers of halo stars. This would further widen the age and chemical composition ranges. For the younger open clusters and OB associations the data will include significant coverage of pre-main sequence stars.

A very important advantage Gaia data will have with respect to most ground-based surveys is the completeness of the coverage on the sky. This ensures that the wider mass range is properly covered. Ground-based surveys mostly cover cluster cores and tend to be biased towards the more massive cluster members as a result of mass segregation in the cluster. Typically, a relatively young cluster like the Pleiades extends over more than four times the diameter of the immediately visible cluster core.

Supplementary data needed

The task of the supplementary data is to provide a connection to the physical parameters that are considered to be of influence on the brightness of the stars: temperature, surface gravity, chemical composition, age as the main dependencies, reddening, rotational velocity, duplicity, atmospheric activity etc as the secondary (indirect) dependencies.

The photometric system

For the photometric data to be effective it needs to fulfil a broad range of requirements. The photometric system, i.e. the collection of passbands, needs to be capable of distinguishing between the main immediate influences on luminosities and colours: temperature, surface gravity, reddening and chemical composition. An example of such a system design is presented by Jordi et al. [2006]. The passbands need to be very accurately defined and reproduced if used on different instruments. The exact shape of the passbands will be input to the interpretation of stellar atmosphere models, while passband transformations between instruments should be avoided as much as possible, as any such transformation will lead to loss of accuracy. A problem here will be the variable QE of CCDs and the stability of filter passbands as well as the difficulty of measuring simultaneously in different passbands.

Photometric accuracies

The most accurate photometric data for star clusters show very narrow main sequence tracks, with clearly visible duplicity sub-tracks. The intrinsic width of each cluster main sequence may be less than 0.01 mag, reflecting the homogeneity of the cluster stars in chemical composition and age. The parallax information from Gaia will be of similar accuracy, equivalent to 1 to 2 millimag uncertainty at most. To take full advantage of these data, the photometric data should add as little measurement noise as possible, and therefore aim at accuracies of order 1 millimag in both colour indices and magnitudes. Repeated observations, at a good coverage of epochs, are needed to cover variability, although a lot of information on variable stars will already be extracted from the Gaia data.

Spectroscopic data

The spectroscopic data will be used to obtain radial velocities (for final membership determination, duplicity detection and internal velocities), rotational velocities (because of their influence on luminosities and as indicator of luminosity class), and chemical composition. Repeated observations will be needed for the detection of binaries and as supplementary information for pulsating variables.

[2]http://www.univie.ac.at/webda/

Independent and absolute distance determinations

It will be crucially important to use only distance modulus determinations that are completely independent of the photometric and spectroscopic data obtained for the clusters. A so-called main-sequence fitting for the distance modulus will by definition have lost any information on the position of the main sequence. Main-sequence fitting will become useful again after the full calibration of the theoretical isochrones with age, luminosity and chemical composition. Differential parallax measurements are also not suitable, as they are incapable of providing the accuracy and coverage required. The accuracy limitations of differential parallax determinations show clearly when comparing pre-Hipparcos determinations with the Hipparcos data, exposing an absolute calibration error with an average sigma value of about 2.4 mas (van Leeuwen [2009]).

A first experiment with Hipparcos parallax data

The new Hipparcos reduction

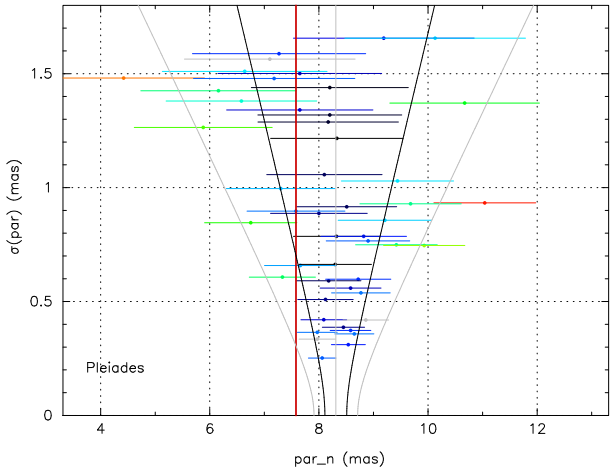

Figure 4.12: Distribution of parallaxes against formal errors for 53 Pleiades cluster members, spread over an area of more than 8 degrees in diameter on the sky. The central line represents the mean cluster parallax. The black lines on either side represent the 1 σ error levels, including the effects of the depth of the cluster. The outer grey lines represent similarly the 2 σ error levels. Finally, the vertical red line represents the parallax as predicted by main-sequence fitting (An et al. [2007]).

The new reduction of the Hipparcos data (van Leeuwen [2007a]; van Leeuwen [2007b]) has allowed for significant improvements in both the accuracies and reliability level of the cluster parallaxes. Error correlations that still existed in the original catalogue (ESA [1997]; van Leeuwen & Evans [1998]) have been reduced to an insignificant level, and through the same process, which eliminated a major source of systematic errors in the data reductions, the accuracies of the bright stars have been improved by up to a factor four. For the cluster parallaxes this meant a much simplified reduction procedure and an improvement in accuracies by on average a factor 2.5. The improvements also affect the proper motions and thus the membership selections, which were reviewed for all clusters involved. It should be noted here that for the more distant clusters membership was not always certain, and inclusion of a star as a cluster member could noticeably affect the derived parallax.

Cluster parallaxes

Four methods were used for determining the parallaxes. For the nearest cluster, the Ursa Major group, individual stellar parallaxes were used. For the Hyades an inverse of the convergent point method was used (Madsen [1999]; Madsen et al. [2001]), in which the observed proper motion gives an accurate reflection of the position of the star in the cluster. For clusters up to 250 pc the mean astrometric parameters were determined while taking into account the small effects of the projection on the sky. For clusters between 250 and 400 pc the astrometric parameters of the cluster were derived directly from the abscissa

measurements of the member stars, creating a single common solution for proper motion and parallax. Close to 250 pc two clusters were treated with both methods to ensure that no systematic differences would result from the use of different methods.

Fig. 4.12 shows the most marked difference found this way for the Pleiades cluster between the distance determination as based on the absolute parallax and as based on main sequence fitting. For the astrometric data it can be stated that error correlations are effectively non-existent, and never existed over an area as large as the Pleiades cluster. The individual parallax determinations for the 53 stars used here are therefore essentially independent. The overall statistics of the parallax and error distributions over the cluster stars is fully satisfactory. The difference with the main-sequence fitting based distance (An et al. [2007]) is very significant and needs to be found in the criteria used in the main-sequence fitting methods, most importantly that one can calibrate theoretical isochrones on just one cluster, and fully rely on the age and metallicity effects as these are predicted by the models.

Cluster-age groups

The position of the Pleiades main sequence is confirmed by two clusters, NGC 2516 and Blanco 1, both of which have been described in the past as very similar to the Pleiades (Snowden [1975]). Consistency in the HR diagrams of very similar clusters is a requirement for being able to reconstruct observational isochrones, and this level of consistency is not only observed for this small Pleiades group, but also for the Hyades and Praesepe, and for Coma Ber, UMa and NGC 7092. The HR diagrams for these clusters, using Geneva photometric data as extracted from WEBDA, are shown in two age groups in Fig. 4.13. The

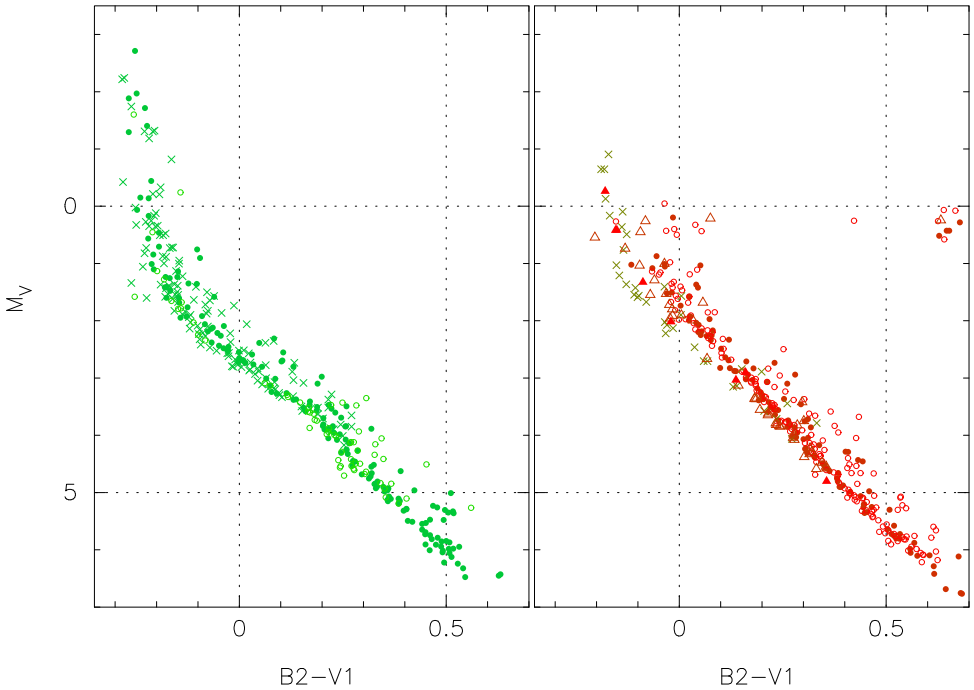

Figure 4.13: *Left*: The HR diagram in the Geneva photometry for the Pleiades (dots), NGC 2516 (crosses) and Blanco 1 (open circles), showing the closely coinciding sequences of these three clusters. *Right*: similarly for the Hyades (dots), Praesepe (open circles), UMa (closed triangles), Coma Ber (open triangles) and NGC 7092 (crosses).

overall agreement between each set of sequences is clear, as are the differences between the groups. If the difference as observed for the Pleiades cluster, between the Hipparcos parallax-based and main-sequence fitting-based distance modulus estimates, would be due to systematic, correlated errors in the Hipparcos catalogue, as has been suggested on numerous occasions in the past (Soderblom et al. [2005]), then those errors would have to extend far beyond any natural correlation level in the Hipparcos data, and would also for some peculiar reason repeat themselves for clusters of very similar age in entirely different parts of the sky. Similarly, such errors would be completely absent when considering the Hyades and Praesepe clusters. Considering the global nature of the Hipparcos astrometric reductions, this seems to be a more than unlikely scenario.

The Hyades anomaly

The relative offset in position of the Pleiades-group main sequence and that of the Hyades group is not the only difference between those two groups. It has been known for nearly 50 years that there is also a systematic difference observed in the (B − V) versus (U − B) diagram (van Altena [1966]), known as the "Hyades anomaly". This offset, shown here for the Geneva photometry in Fig. 4.14, when interpreted as due to a difference in chemical composition, has given rise in the past to discrepant metallicity estimates as obtained through spectroscopy and photometry (Nissen [1970]). The difference is present not only

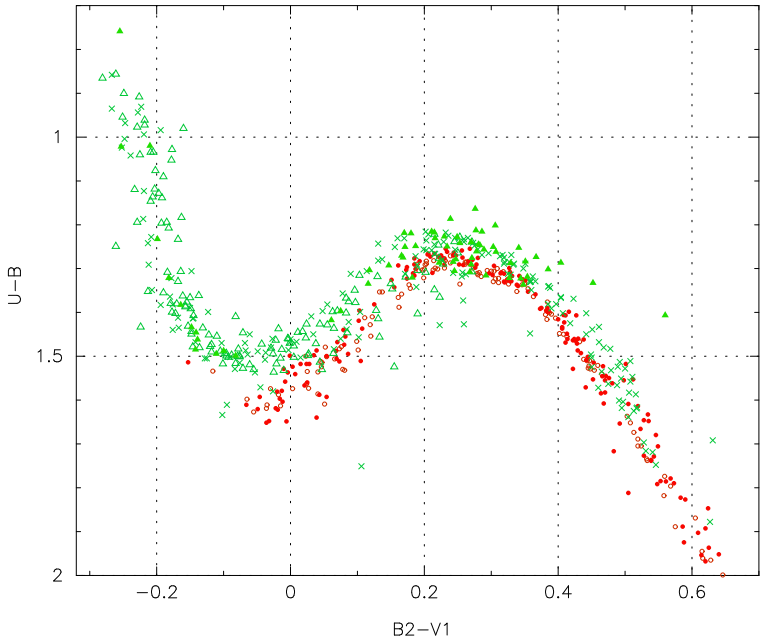

Figure 4.14: The Hyades anomaly as shown through the Geneva photometric data. The anomaly exists between the clusters in the same two groups that show the difference in main sequence positions. Red dot and circles represent the Hyades and Praesepe clusters. Green crosses, open and closed triangles the Pleiades, Coma Ber and NGC 2516 clusters. Note that due to differential reddening in the Pleiades some data points are shifted.

between the Pleiades and Hyades, but between all clusters in the two groups. Spectroscopic data on those clusters seems to exclude that this difference is the result of differences in chemical composition. However, there are many nearby field stars showing similar variations in their position in the same two-colour diagram, so it would be interesting to see if similar differences between field stars are also reflected in luminosity differences.

A comparison with field star data

The focus here is on the F-type stars, for which the differences in the two-colour diagram referred to above are most clear. Details of the calibrations briefly described here can be found in van Leeuwen [2009]. The equivalent parameter in the Strömgren system is referred to as 'c1', and has been investigated in the past by Crawford [1975]. That study was based on a very small number of ground-based parallaxes with relatively poor accuracies. A systematic difference between the c1 index for Pleiades and Hyades stars was recorded by Nissen [1988] as between 0.033 and 0.04. Using data extracted from Hauck & Mermilliod [1997, 1998], a very clear relation between offsets in c1 and M_V is observed for 3748 nearby F stars (nearly all with parallax errors well below 10 per cent) (Fig. 4.15), while for a smaller sub-sample where spectroscopic data is available (Cayrel de Strobel et al. [2001]), a clear relation is observed between surface gravity and offsets in c1. Translated to the observed differences in c1 between the Pleiades and the Hyades, the relation observed for the field stars would translate in an absolute magnitude difference of around 0.3. The relation between $\log g$ and c1 indicates that the observed difference is equivalent to about 0.1 in surface gravity, where the older Hyades stars are larger. A possible source for this difference could be evolution in the depth of the convection layer (C. Tout, priv.comm). The correction for the absolute magnitudes is equivalent to shifting the distance of the cluster by 18 pc away from the current parallax-

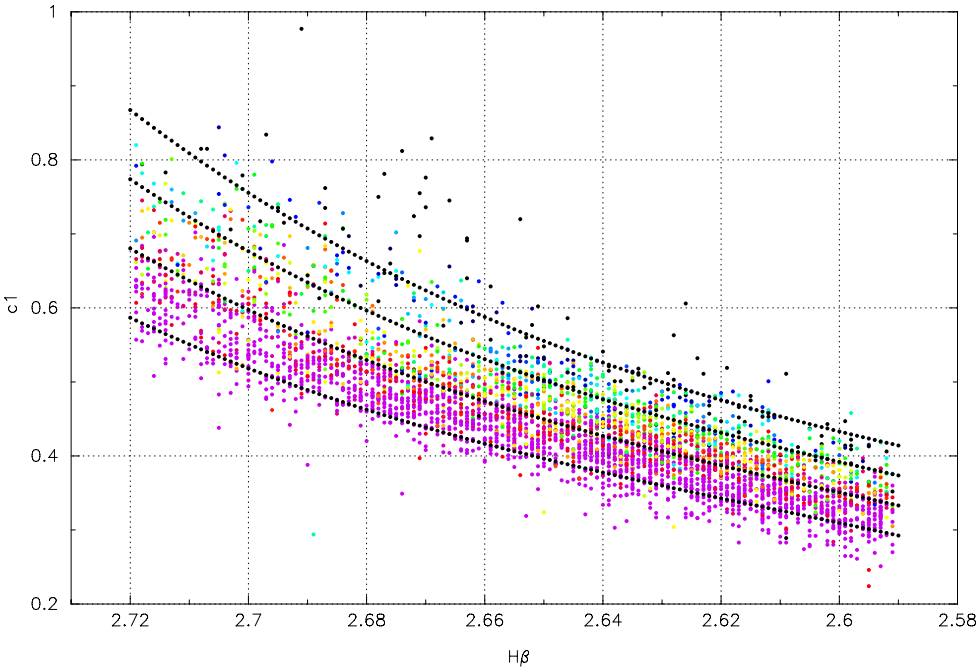

Figure 4.15: The relation between Hβ and c1 in the Strömgren system for nearby F-type stars. The curved lines represent the calibrated offsets in absolute magnitudes, also indicated by the colour gradient in the dots.

based distance, close to what is observed when main-sequence fitting is used to determine the cluster distance. But these models don't include the possibility of an adjustment in surface gravity and can only adjust according to chemical composition. Variations in absolute magnitude as a result of metallicity variations are observed to be very small for nearby F-type stars, where the luminosity variations are dominated by surface gravity variations. It is in fact from a purely observational point of view far more difficult to explain the more generally favoured Pleiades distance modulus of around 5.6 to 5.7, as this would create a discrepancy in the behaviour of the c1 index between cluster and field stars. The only real discrepancy that remains is between the parallax-based main sequence positions of cluster such as the Pleiades, Coma Ber and NGC 2516, and as predicted for those clusters by the current isochrones as calibrated on the Hyades main sequence. This is exactly the kind of information we need for the empirical calibration of those isochrones through groups of clusters of different ages and compositions. It is also the kind of information that can never be extracted when distance moduli are calibrated using the established set of isochrones. The internal consistency of the data and confirmation from different clusters as shown here are important aspects in such study.

Conclusions

Fig. 4.16 shows the composite diagram of cluster data and field stars. Clearly visible is how clusters within the same age groups coincide, as well as the systematic shifts in the cluster HR diagrams with age. This diagram is only a very primitive reflection of what will be possible with the support of the Gaia astrometric data, when complemented by accurate photometric and spectroscopic measurements. This diagram is not about interpreting distances for individual clusters, it is about the consistency between clusters of roughly the same age and chemical composition, and the systematics shown when comparing clusters of different ages. Consistency with observational aspects of field stars as were shown to be clearly present in previous Section is also crucially important. The cluster and field-star data together provide a picture of internally consistent observational data. Any discrepancies with what is expected to be observed on the basis of current isochrone models is what needs to feed into the further developments of the models on which the isochrones are based: stellar structure, stellar evolution and stellar atmospheres.

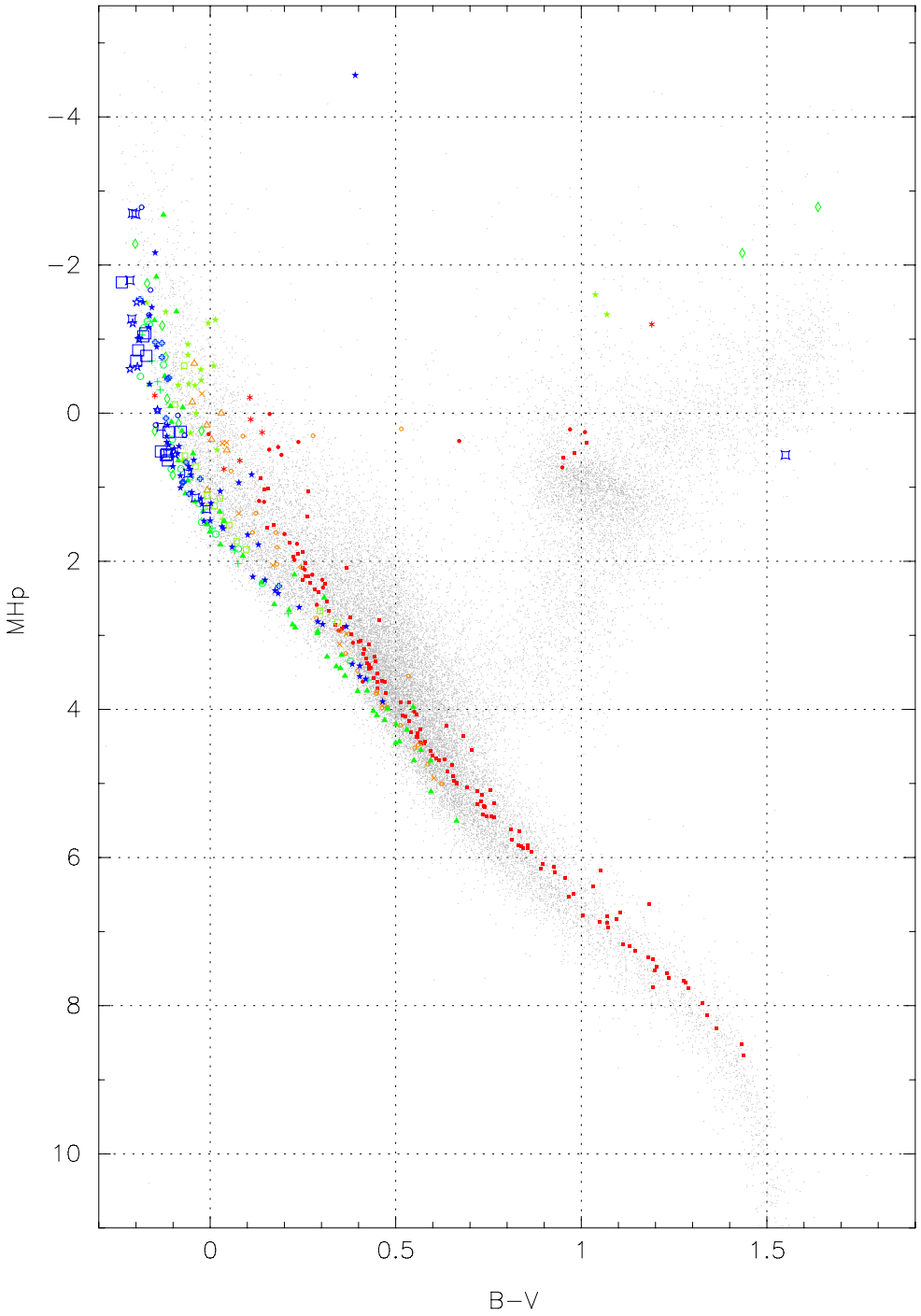

Figure 4.16: The composite HR diagram for about 30 000 stars with relative parallax errors below 10 per cent (grey) and the data for 14 open clusters. The cluster data are colour-coded according to their age estimate, from blue (youngest) to red (oldest).

Photometrically determined cluster distances don't contribute information to this discussion as their calibration method is already based on assumptions for the isochrones. Differential parallaxes don't contribute information due to the large uncertainties in their calibration to absolute. Distance determinations for double stars can only make a very limited contribution to the discussion, as the position of a single double star within a cluster remains an uncertain quantity.

Assuming that one can calibrate a set of isochrones using the data for one cluster only, and relying for all differential effects (age, composition) on their definition by the models, will not provide a sound basis for photometric distance calibrations. Isochrones need also to be calibration as a function of age and chemical composition and various other secondary effects (for example rotation). This may show, as seems to be the case with the Hipparcos results, some interesting discrepancies between the models and the observational data. It is only with an open mind and using reliable astrometrically determined absolute parallaxes, supported by good photometric and spectroscopic data, that we can progress on the empirical definition of the isochrones, which in turn will help further with the underlying models: stellar structure, stellar evolution and stellar atmospheres, and distance calibrations for cluster that are outside the reach of accurate parallax determination. Clusters, both open and globular, will play a crucial and defining role in this.

Acknowledgments

I would like to thank the organizers of the workshop for their kind invitation and support.

Bibliography

An, D., Terndrup, D. M., Pinsonneault, M. H., et al. 2007, ApJ, 655, 233
Cayrel de Strobel, G., Soubiran, C., & Ralite, N. 2001, A&A, 373, 159
Crawford, D. L. 1975, AJ, 80, 955
ESA, ed. 1997, The Hipparcos and Tycho Catalogues, SP No. 1200 (ESA)
Hauck, B. & Mermilliod, M. 1997, VizieR Online Data Catalog, 2215, 0
Hauck, B. & Mermilliod, M. 1998, A&AS, 129, 431
Jordi, C., Høg, E., Brown, A. G. A., et al. 2006, MNRAS, 367, 290
Madsen, S. 1999, in Astronomical Society of the Pacific Conference Series, Vol. 167, Harmonizing Cosmic Distance Scales in a Post-HIPPARCOS Era, ed. D. Egret & A. Heck, 78–83
Madsen, S., Lindegren, L., & Dravins, D. 2001, in ASP Conf. Ser. 228: Dynamics of Star Clusters and the Milky Way, ed. S. Deiters, B. Fuchs, A. Just, R. Spurzem, & R. Wielen, 506–508
Nissen, P. E. 1970, A&A, 8, 476
Nissen, P. E. 1988, A&A, 199, 146
Snowden, M. S. 1975, PASP, 87, 721
Soderblom, D. R., Nelan, E., Benedict, G. F., et al. 2005, AJ, 129, 1616
van Altena, W. F. 1966, AJ, 71, 482
van Leeuwen, F. 2007a, Hipparcos, the new reduction of the raw data (Dordrecht: Springer)
van Leeuwen, F. 2007b, A&A, 474, 653
van Leeuwen, F. 2009, A&A, 497, 209
van Leeuwen, F. & Evans, D. W. 1998, A&A, 323, 157

4.4 Probing the Near-IR Flux Excess in Young Star Clusters

Angela Adamo[1], G. Östlin[1], and E. Zackrisson[1]

[1] Department of Astronomy, Stockholm University, Oscar Klein Center, AlbaNova, Stockholm SE-106 91, Sweden

Abstract

We report the results of a recent study of young star clusters (YSCs) in luminous blue compact galaxies (BCGs). The age distributions of the YSCs suggest that the starburst episode in Haro 11, ESO 185 – IG13, and Mrk 930 started not more than 30-40 Myr ago. A peak of cluster formation only 3 – 4 Myr old is observed, unveiling a unique sample of clusters still partially embedded. A considerable fraction of clusters (30 - 50 %), mainly younger than 10 Myr, shows an observed flux excess between 0.8 and 2.2 μm. This so-called near-infrared (NIR) excess is impossible to reproduce even with the most recent spectral synthesis models (that include a self-consistent treatment of the photoionized gas). We have used these YSCs to probe the very early evolution phase of star clusters. In all the three host galaxies, the analysis is limited to the optically brightest objects, i.e., systems that are only partially embedded by their natal cocoons (since deeply embedded clusters are probably too faint to be detected). We discuss possible explanations for this NIR excess, in the context of IR studies of both extragalactic young star clusters and resolved massive star-forming regions in the Milky Way and in the nearby Magellanic Clouds.

Introduction

Young star clusters (YSCs) are considered a powerful tool to study the star formation history of their hosts. However, many assumptions and constraints on the evolutionary properties are needed in order to compare YSCs properties and the bulk of the host stellar population. In nearby galaxies, it is possible to study both the resolved stellar population and cluster population (e.g. Silva-Villa & Larsen [2011]). In farther galaxies, however, the study of YSCs is conducted with an analysis of their integrated light at different wavelengths under the assumption of an instantaneous burst, i.e. single stellar population.

The luminous ($M_B < -17.0$, corresponding to total stellar masses of $\sim 10^{9-10}$ $M_\odot$) blue compact galaxies (BCGs) show clear signatures of interactions and/or mergers, and the numerous observed massive YSCs are likely the result of these encounters (Östlin et al. [2003]; Adamo et al. [2010a]; Adamo et al. [2011a]; Adamo et al. [2011b]). The very bright ultraviolet and optical luminosities of these systems suggest rather low dust and metallicity content. Spectra dominated by emission lines clearly demonstrate that BCGs are undergoing a starburst episode. The youth of the burst episode is also observed in the recovered age distribution of the star clusters, which shows a peak of cluster formation younger than 5 Myr.

The analysis of the young cluster populations in BCGs is quite challenging due to the rapid evolution a cluster experiences during the first 10 Myr (still partly in an embedded phase). Moreover, this analysis is based on the integrated luminosities of the clusters, which appear unresolved at the distance of the targets. Observations of resolved newly born star clusters in the Milky Way and in the Magellanic Clouds reveal that these are quite complex systems. A cluster forms in a hierarchical medium, from the fragmentation and collapse of giant molecular cloud complexes (Elmegreen [2010]). This implies that stars form in a fractal distribution and only in some cloud cores are their number densities high enough to eventually form a bound cluster (Bressert et al. [2010]). This picture is confirmed also by dynamical studies. Gieles & Portegies Zwart [2011] observed a continuous distribution between associations (unbound) and clusters (bound) at very young ages, and a clear distinction at older stages, when the crossing time of unbound systems exceeds their stellar age.

In a newly born cluster, the massive and short-lived stars rapidly reach the main sequence and produce strong winds and UV radiation, which ionize the intracluster gas and create bubbles and shells. These HII regions surround the optically bright core of stars and significantly contribute to the integrated

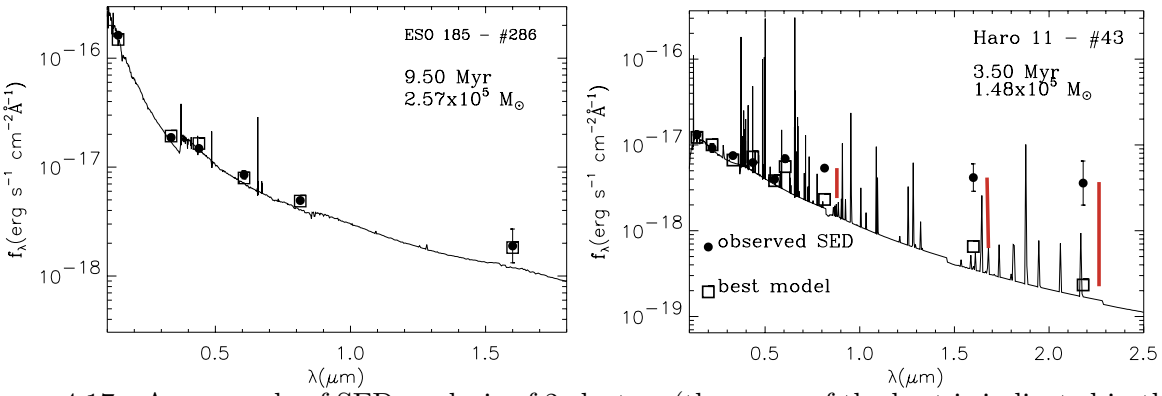

Figure 4.17: An example of SED analysis of 2 clusters (the name of the host is indicated in the inset). The two objects are representative of different cases: on the left a young cluster with a good fit, i.e. regular SED; on the right, a cluster affected by an excess in flux at wavelengths longer than 8000 Å. The filled black points indicated the observed fluxes for each cluster. The integrated model fluxes are labelled with open squares. They sit above the best fitting spectrum overplotted with a solid line. Red vertical lines indicate which data points have been excluded from the fit. The age and mass of the cluster are shown.

fluxes. However, a large fraction of the stars is still accreting material from their dusty disks (young stellar objects, YSOs) or contracting (in the pre-main sequence phase, PMS). Moreover, the edges of the clusters are places for triggered (Elmegreen [2011]) and progressive star formation (e.g. Carlson et al. [2007]), which can explain the observed age spread in the star-forming regions /e.g. Bik et al. [2010]).

Evidence for the NIR excess

A significant fraction of young star clusters in Haro 11 (Adamo et al. [2010a]), ESO 185-IG13 (Adamo et al. [2011a]), and Mrk 930 (Adamo et al. [2011b]) shows a clear signature of a flux excess at near-IR wavebands. The models used (Zackrisson et al. [2001]; Adamo et al. [2010b]) include a self-consistent treatment of the photoionized gas, important during the first few Myrs of the cluster evolution. However, these models are not able to reproduce the NIR observed fluxes of the clusters. In Fig. 4.17, we show two representative cases of cluster spectral energy distributions (SEDs). A large fraction of analyzed clusters in the 3 galaxies have regular SEDs, easily fitted by our models (see left panel, Fig. 4.17). However, a considerable number of clusters have SEDs similar to cluster # 43 in the right panel of Fig. 4.17. Three different sets of fits have been performed for each cluster (see Adamo et al. [2010a]; Adamo et al. [2011a]; for details) and depending on the outcomes, clusters have been divided into 3 samples: 1) regular SEDs have been fitted from UV to IR; 2) if the source presented an excess at $\lambda > 1.0$ μm, the fit was performed excluding the IR data (so called IR excess); 3) if the excess affected also I band ($\sim$ 8000 Å), then only the data from UV to optical ($\lambda <$ 8000 Å) were included in the fit (referred to as NIR excess). The exclusion of the data points with an excess was necessary in order to reproduce the observed UV and optical SEDs of the clusters. The two observed fluxes at 0.5 and 0.6 μm of cluster # 43 are produced, respectively, by a narrow filter (F550M) centred on the continuum and a filter (F606W) which transmits Hα. A jump between these two filters can be used as an age indicator (only clusters younger than 10 Myr have Hα in emission). Clearly, # 43 is a very young cluster. However, if the NIR data points (including I band) are included in the fit, the age obtained for this cluster is 45 Myr (see Adamo et al. [2010a], for details). In Table 4.3, we give the fractions of clusters with a regular SED or NIR excess.

Table 4.3: Fraction of clusters in each SED sample, of the three galaxies.

targets	regular SEDs	IR excess	NIR excess
	%	%	%
Haro 11	44	14	42
ESO 185	68	10	22
Mrk 930	62	12	26

Colour-colour diagrams of the whole Mrk 930 cluster population (see Adamo et al. [2011b] for s complete

analysis) are shown in Fig. 4.18. The $R-I$ colour is used as reference. Generally, a negative $R-I<0$ colour indicates ages younger than 10 Myr and is produced by a strong nebular contribution to the R filter, which includes the bright Hα line. However, this assumption is not always valid due to the flux excess in the I band. The clusters in the diagrams have different symbols depending of their observed SEDs: black dots indicate normal SEDs, red triangles clusters with an excess at $\lambda \geq 1.0$ μm (hereafter, IR excess), and blue diamonds SEDs which deviate at $\lambda \geq 0.8$ μm (hereafter, NIR excess). We notice that clusters with a NIR excess have a $R-I$ colour between 0.2 and 1.2 mag redder than the prediction made by the best-fitting SED model. The $R-I$ colour of the "blue" cluster-diamonds is such that, if overlooked, causes age (and mass) overestimates, affecting the results of the optical based cluster analysis. The $UV-R$ (left panel) colour shows that the clusters detected in the FUV are young, at least younger than 30 – 40 Myr. Many of the clusters with an NIR excess are located in an area where $R-I>0$, e.g., corresponding to ages older than 10 Myr. However, their UV colour is compatible with being a few Myrs old. The FUV band is sensitive to the reddening. Looking at the colour-colour diagram, one can see that clusters detected in the FUV have extinctions $A_V \leq 1.0$ (e.g., the arrow in the plot). Therefore, we consider these very young FUV bright clusters as systems which have already gone through the deeply embedded phase. The inclusion of the IR colour (right panel), clearly shows that clusters with a flux excess (clearly young) at the redder wavelengths are mainly located in an area of the diagram where the $R-I>0$ and $H-R>1.0$ mag, e.g. apparently older than 1 Gyr. The IR colour of the clusters with a red excess suggests that the extinction in these objects should be much higher than the one predicted by the optical and UV colours. In other words, at the NIR wavelengths it is possible that we are probing a different, more deeply embedded stellar population, indicating that these are very young clusters.

Possible origin of the NIR excess

The I band excess

The I band excess has been found only in very young clusters (usually <6 Myr). A viable explanation for this feature is the extended red emission (ERE, see for a review Witt & Vijh [2004]). The ERE is observed as a soft rising continuum between $0.6-0.9$ μm. It is observed around galactic and extragalactic HII regions and caused by a photoluminescence reaction on dust grains heated by hard UV radiation. Such energetic photons are mainly produced in short-lived massive stars. This could explain why the I band excess in our clusters is over after 6 Myr.

The IR excess

Several mechanisms can concur to make the flux at $\lambda > 1.0$ μm higher than predicted by models. The distance of the galaxy and the resolution achieved - the best with the current accessible facilities - limit our studies to the integrated properties of these YSCs. However, observations of close-by resolved clusters and numerical predictions of stellar populations in clusters can give us an hint of the mechanisms which are likely producing the observed excess.

Among the youngest and massive resolved star clusters, 30 Doradus (hereafter 30 Dor) in the Large Magellanic Cloud (LMC), represents the best reference to understand what a recently born star cluster looks like. 30 Dor is the central region of the extended Tarantula nebula. Multiwavelength studies of this regions have dissected the different components of the complex 30 Dor environment. Walborn & Blades [1997] identified five different stellar populations in the region: the bright core early O-type stars which are part of the compact star cluster R 136; in the north and west region embedded massive YSOs; 3 more evolved stellar population groups in the southern and 1.0' away in the western region. The R 136 cluster has a mass of $\sim 10^5$ $M_\odot$ and is 3 Myr old. This nuclear region (≤ 3 pc) is dust and gas-free. However, the aperture radius we are using in our analysis is much larger (radius of ≈ 36 pc) than the size of R136. Our apertures are comparable to the size of the image of 30 Dor showed in Fig. 1 of Campbell et al. [2010]. This suggests that while the optical range is dominated by the stellar and gas emission, the IR transmits also flux from the diffuse dust, heated by the hard UV radiation field, the embedded YSOs formed in triggered star formation events at the edge of the nucleus, where most of the dense gas and dust filaments are located, and the low-mass stars still in the PMS phase.

In the literature, studied cases of IR excess in young embedded or partially embedded unresolved extragalactic clusters have explained the red excess as due to an important contribution by YSOs (Fernández-Ontiveros et al. [2009]), or hot dust (Cresci et al. [2005]). Likely, the same mechanism is

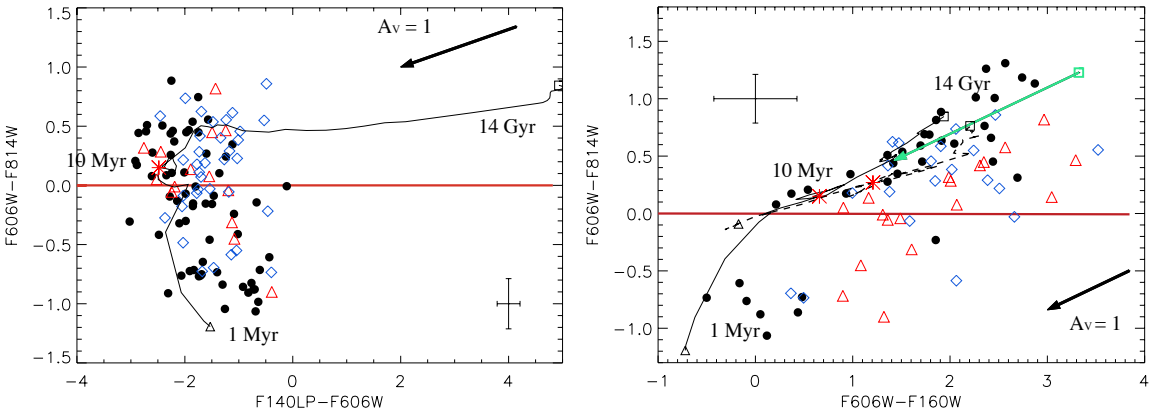

Figure 4.18: Color-colour diagrams of the cluster population in Mrk 930 (Adamo et al. [2011b]). Different filter combinations are compared to the $R-I$ colour (F606W-F814W). *Left*: $UV-R$ (F140LP-F606W); *Right*: $R-H$ (F606W-F160W). In each panel, the Z01 evolutionary tracks are plotted as a solid black line. Where predictions for the used filters were available we included the M08 tracks (dashed lines) as well. Ages are labelled along the tracks. The black dots are clusters with regular SEDs (from UV to IR). The red triangles are clusters with an excess at $\lambda > 1.0$ μm. The blue diamonds show objects with an excess starting longword $\lambda \geq 0.8$ μm. The black arrows indicate a visual extinction of $A_V = 1$. Mean errors are included. A solid red line divides the plots in two regions: $R-I > 0$ (older than 10 Myr) and $R-I < 0$ (younger than 10 Myr).

causing the excess in young star clusters in BCGs.

After several Myr this complex phase is over, so it cannot explain why we still observe objects with an IR excess at older ages. For these evolved clusters a possible source of excess can be an important contribution from red super giants (RSGs). Models usually predict the number of RSGs, assuming that the stars in a cluster fully populate the underlying initial mass function (IMF). However, this assumption is not valid if the cluster is less massive than 10^4 $M_\odot$ and causes important variations for cluster masses below 5×10^3 $M_\odot$ (Silva-Villa & Larsen [2011]). Moreover, it has been observed that in metal-poor environments the number of observed RSGs tends to be higher than the predicted one from the ratio of blue versus RSGs. Therefore, both effects would be observed as a rise in the NIR integrated flux of an unresolved cluster which our current models cannot fully account for. It is not clear, however, why we do not see any mass dependence between the excess in H band and the mass of the cluster, which could support the stochasticity scenario, or why our models cannot predict the correct number of RSGs only for some of the clusters. NIR spectroscopy is needed to test these scenarios.

Another possible explanation is that a second stellar population is forming in the clusters. If a second population is forming now then we expect to detect it mainly in the NIR. Multiple stellar populations have been detected in globular clusters and, recently, even in young star clusters (Larsen et al. [2011]). Are we observing the formation of a new stellar population in these massive YSCs?

Finally, a bottom heavy IMF, i.e. a much steeper slope at low-mass ranges (higher number of low-mass stars), could also explain the excess. However, studies of IMF variations in massive star clusters (see Bastian et al. [2010]) have not found any confirmed case of such type of cluster. Moreover, it is not clear how, in the same galaxy, a fraction of clusters could form with a different IMF.

Bibliography

Adamo, A., Östlin, G., Zackrisson, E., & Hayes, M. 2011a, MNRAS, 414, 1793
Adamo, A., Östlin, G., Zackrisson, E., et al. 2010a, MNRAS, 407, 870
Adamo, A., Östlin, G., Zackrisson, E., et al. 2011b, MNRAS, 739
Adamo, A., Zackrisson, E., Östlin, G., & Hayes, M. 2010b, ApJ, 725, 1620
Bastian, N., Covey, K. R., & Meyer, M. R. 2010, ARA&A, 48, 339
Bik, A., Puga, E., Waters, L. B. F. M., et al. 2010, ApJ, 713, 883
Bressert, E., Bastian, N., Gutermuth, R., et al. 2010, MNRAS, 409, L54
Campbell, M. A., Evans, C. J., Mackey, A. D., et al. 2010, MNRAS, 405, 421

Carlson, L. R., Sabbi, E., Sirianni, M., et al. 2007, ApJ Lett., 665, L109
Cresci, G., Vanzi, L., & Sauvage, M. 2005, A&A, 433, 447
Elmegreen, B. G. 2010, in IAU Symposium, Vol. 266, IAU Symposium, ed. R. de Grijs & J. R. D. Lépine, 3–13
Elmegreen, B. G. 2011, ArXiv e-prints
Fernández-Ontiveros, J. A., Prieto, M. A., & Acosta-Pulido, J. A. 2009, MNRAS, 392, L16
Gieles, M. & Portegies Zwart, S. F. 2011, MNRAS, 410, L6
Larsen, S. S., de Mink, S. E., Eldridge, J. J., et al. 2011, ArXiv e-prints
Östlin, G., Zackrisson, E., Bergvall, N., & Rönnback, J. 2003, A&A, 408, 887
Silva-Villa, E. & Larsen, S. S. 2011, A&A, 529, A25+
Walborn, N. R. & Blades, J. C. 1997, ApJS, 112, 457
Witt, A. N. & Vijh, U. P. 2004, in Astronomical Society of the Pacific Conference Series, Vol. 309, Astrophysics of Dust, ed. A. N. Witt, G. C. Clayton, & B. T. Draine, 115–+
Zackrisson, E., Bergvall, N., Olofsson, K., & Siebert, A. 2001, A&A, 375, 814

4.5 Uncovering the Substellar Population of Nearby Young Clusters

Catarina Alves de Oliveira[1], E. Moraux[1], J. Bouvier[1], H. Bouy[2], G. Duchêne[1,3]

[1] Institut de Planétologie et d'Astrophysique de Grenoble (UMR 5274), BP 53, F-38041 Grenoble Cédex 9, France
[2] Centro de Astrobiología (INTA-CSIC); LAEFF, P.O. Box 78, 28691 Villanueva de la Cañada, Spain
[3] Astronomy Department, University of California Berkeley, Berkeley CA 94720-3411, USA

Abstract

The origin of the initial mass function is an important problem in star formation theories. In particular, at the substellar regime the formation processes of brown dwarfs are still debated and no agreed paradigm has yet been reached. Numerical simulations of different formation scenarios are now able to predict observable properties of clusters. The new observational frontier is therefore the detection and characterization of very low-mass objects and the lower limit of the initial mass function (IMF) in star-forming regions, which can be confronted with the model predictions. This is the aim of the WIRCam/CFHT survey, from which I will present the results on the study of the young clusters ρ Ophiuchi and IC 348. Deep near-IR imaging surveys of both clusters were used to uncover their low-mass population, after which a major spectroscopic follow-up was conducted (using TNG, GTC, NTT, VLT, Gemini) to ascertain their spectral types and masses, and ultimately, to construct the low-mass end of their IMFs.

Introduction

Although there is a generally accepted theory on how a star forms through the collapse of a molecular cloud core and contracts to the main-sequence (Shu et al. [1987]; Larson [1973]), two major breakthroughs in the mid-90s have added a new complexity to the star formation field: the discovery of exoplanets (Oppenheimer et al. [1995]; Mayor & Queloz [1995]) and brown dwarfs (BDs, M $<$ 75 M_{Jup}, (Rebolo et al. [1995]; Nakajima et al. [1995]; Chabrier & Baraffe [1997]). BDs are a key element in understanding the origin of stellar masses and their distribution, the Initial Mass Function (IMF), and in identifying the plethora of hospitable hosts where planetary systems can form. There is however not an accepted explanation on how they form and several scenarios are currently proposed. These defend either a star-like formation, i.e. fragmentation of molecular clouds into low mass cores driven by turbulence (Padoan & Nordlund [2002]; Bonnell et al. [2001]) or gravity (Bate et al. [2003]; Hennebelle & Chabrier [2008]); or distinct formation processes such as gravitational instabilities in discs (Stamatellos & Whitworth [2009]), premature ejection from pre-stellar cores (Reipurth & Clarke [2001]), or photo-erosion of cores (Kroupa & Bouvier [2003]). The observational properties of BDs in young clusters show so far a global scaling down trend from those of stars, arguing in favour of a common formation scenario (Luhman et al. [2007]). However, up to date, most studies in young star-forming regions suffer from incompleteness both at lower masses (below $\sim$ 40 M_{Jup}) and in the spatial content, frequently focusing on the cluster inner regions. It is therefore unknown if, as one moves to lower masses, other formation mechanisms start to dominate (Whitworth et al. [2010]). At the same time, the increasing capacity of numerical simulations to reproduce the collapse of entire molecular clouds, means the comparison between simulations and observations starts to be hampered by limited statistics on the properties of the low-mass end of the brown dwarf regime. Extensive studies of the lowest mass populations in different environments and stages of evolution are therefore required to address these pressing questions. This problematic is the main driver behind an on-going large program using the Wide Field IR Camera (WIRCam) at the Canada−France− Hawaii Telescope (CFHT), originally designed to fully characterize a series of young stellar clusters chosen to represent different environments, and detect brown dwarfs down to a few Jupiter masses.

The WIRCam/CFHT survey of nearby star-forming regions

Using the WIRCam at the CFHT telescope, we conducted a deep near-IR survey of the following nearby star-forming regions: ρ Ophiuchi, IC 348, NGC 1333, Serpens, NGC 2264, and λ Ori. The WIRCam is a wide-field camera operating in the near-IR, consisting of four 2048 x 2048 array detectors, and with a pixel scale of 0.3 arcsec. The four detectors make a total field of view of approximately 21 arcmin in one pointing. All clusters mentioned above were observed in the *Y*, *J*, *H*, and K_s filters. Furthermore, IC 348, NGC 1333, Serpens, and λ Ori were also observed with two narrowband methane filters, CH_4-*off* and CH_4-*on*. Depending on the area each cluster occupies on sky, between one and seven pointings were needed to map the entire region. All images were reduced in an analogous way. First, the individual images are processed by the 'I'iwi reductions pipeline at the CFHT, which includes detrending (e.g. bias subtraction, flat-fielding, non-linearity correction, cross-talk removal), sky subtraction, and astrometric calibration. The more detailed reduction is then handled by Terapix (Marmo [2007]), the data reduction centre at the *Institut d'Astrophysique de Paris* (France) responsible for carrying out the final quality assessment of the individual images, determining precise astrometric and photometric calibrations, and the final stacked images are produced by combining the dither and individual exposures. The photometric calibration of the WIRCam data is done with 2MASS stars in the observed frames as part of the nominal pipeline reduction. To extract the photometric catalogues we used PSFEx (PSF Extractor), a software tool that computes a PSF model from well-defined stellar profiles in the image, and the SExtractor programme (Bertin & Arnouts [1996]) to compute the photometry for each detected object. Brown dwarfs candidates are then chosen by comparing their colours to those predicted by the evolutionary models from the Lyon group (Baraffe et al. [1998]; Chabrier et al. [2000]), and to previously confirmed members of each cluster. We also make extensive use of multi-wavelength archive data for characterization of the candidates, from the optical (using, for example, Subaru archival images) to the mid-IR using the various public surveys from the *Spitzer* Space Telescope.

Selection of results

In this section, we will present a selection of results for the young clusters which were firstly studied, the ρ Ophiuchi cluster and IC 348 (Burgess et al. [2009]; Alves de Oliveira et al. [2010]; Alves de Oliveira et al. [2011]a, b, *in prep*).

The ρ Ophiuchi cluster

The ρ Ophiuchi cluster is one of the youngest ($\sim$ 1 Myr) and closest star-forming regions (120 to 145 pc), with an estimated population of $\sim$ 300 members (Wilking et al. [2008]). The high visual extinction in the cloud's core, with A_V up to 50 – 100 mag, make it one of the most challenging regions to study low-mass young stellar objects and before our survey only 15 brown dwarfs were known in this cluster. With the WIRCam survey, we covered the entire core of the cluster in a total area of ~ 0.7 deg^2 down to a completeness limit of J $\sim$ 20.5 and H $\sim$ K $\sim$ 19.0. According to models, this allows us to detect young objects down to 3 M_{Jup} through 10 mag of A_V. The final photometric catalogue contains approximately 57,000 objects.

Using the Lyon group models (Baraffe et al. [1998]; Chabrier et al. [2000]), we select candidate members if their colours fell redward from the model isochrones in the *J* vs. *J*-*H*, *J* vs. *J*-K_s, and K_s vs. *H*-K_s colour-magnitude diagrams. From these, only objects that had colours consistent with them being young and substellar in the *J*-*H* vs. *H*-K_s colour-colour diagram were kept. After removing previously known members from the list we find 110 substellar candidates, 80 of each had not previously been associated with the cloud. By extensive use of archive multi-wavelength data we find evidence of mid-IR excess for 27% of the candidates and a variability behaviour consistent with that of YSOs for 15%. To confirm their youth and hence membership, we carried out a large spectroscopic follow-up in the near-IR using SofI/NTT, NICS/TNG, and ISAAC/VLT, and in the optical using OSIRIS/GTC. We identify 21 new brown dwarfs with spectral types down to the L-dwarf regime (5 – 9 M_{Jup}). In an unrelated study, two candidate brown dwarfs from our study have also been confirmed as substellar members (McClure et al. [2010]). In total, $\sim$ 23 new brown dwarfs are uncovered and confirmed in this cluster with the WIRCam survey, more than doubling the number of previously known substellar members. When comparing the number of brown dwarfs to stars in the region, we derive a preliminary value which is in accordance with other star-forming regions (Luhman et al. [2007]).

IC 348

The IC 348 young cluster ($\sim$ 3 Myr) is located at a distance of 300 pc and about 360 stellar members are known to date (Herbst [2008]). Assuming a log-normal IMF (Chabrier [2003]), we thus estimate that this young stellar cluster should host at least 60 members in the substellar regime, double the number of BDs identified so far in this cluster. In fact, a scarcity of brown dwarfs has been claimed to exist in IC 348 in comparison to other star-forming regions (e.g. Orion). However, there are several indications that the census of the cluster substellar population is far from complete.
One of the most exciting results from the WIRCam survey, is indeed the discovery of 3 T-dwarf candidates in this cluster, using the deep methane images. After thoroughly analysis of all colour/colour and colour/magnitude diagram analysis, including available optical deep images, two candidates have been rejected for being too bright at optical wavelengths. One good candidate remains though, with an estimated spectral type of T6. Theoretical models suggest a mass of a few M_{Jup} for this object at 3 Myr. Its methane colours, luminosity, significant extinction and spatial location are consistent with it being a member of IC 348. With just a few Jupiter masses, this young T-dwarf candidate is one of the youngest, lowest mass objects found so far in a star-forming region. Furthermore, we find that its frequency is consistent with the extrapolation of current lognormal IMF estimates down to the planetary mass domain.
Using the near-IR imaging data for this cluster, we try to uncover the remaining substellar population. The WIRCam study improves upon previous surveys by probing a larger area at an increased sensitivity which we hope will allow us to derive a complete census of the BD population down to $\sim$ 7 M_{Jup} over a cluster halo with a radius of 17 arcmin, corresponding to the largest unclipped radius permitted by our survey. We identified 25 substellar candidates, some of which have already been followed-up spectroscopically with OSIRIS/GTC in the optical, and GNIRS/Gemini in the near-IR. Another spectroscopic run using GNIRS/Gemini is scheduled to take place in Fall 2011. Preliminary analysis of the spectroscopic follow-up confirms the youth and membership of 6 new brown dwarfs. We also report on the discovery of two L0 young brown dwarf members of the cluster. According to evolutionary models, both objects have masses of $\sim$ 10 M_{Jup}, making them the least massive brown dwarfs spectroscopically confirmed in IC 348. Using Spitzer data, we confirm the presence of a disc around one of the candidates, making it one of the few brown dwarfs in this mass regime known to harbour a circumstellar disk. This result provides observational evidence to the fact that the IMF extends below the deuterium burning limit and that free-floating brown dwarfs with masses as small as $\sim$ 10 M_{Jup} possess the circumstellar material required for planet formation.

Final remarks

The first results from our WIRCam/CFHT survey of nearby star-forming regions, demonstrate the success of deep near-IR surveys in uncovering young brown dwarfs down to the planetary regime. The confirmation of the photometric candidates relies, however, on extensive spectroscopic follow-up runs on 8-meter class telescopes. These studies reflect a clear need for a multi-object near-IR spectrograph to the European community. The discovery of new substellar members in the two highlighted star-forming regions with masses down to the deuterium burning limit are an important step towards achieving a complete census of their population and understanding the brown dwarf formation mechanism.

Acknowledgments

We thank Loic Albert, Chiara Marmo, Patrick Hudelot and Emmanuel Bertin, for their help with the observations and data reduction of the data for this WIRCam survey. Research partly supported by the Marie Curie Research Training Network CONSTELLATION under grant no. MRTN-CT-2006-035890.

Bibliography

Alves de Oliveira, C., Moraux, E., Bouvier, J., et al. 2010, A&A, 515, A75+
Baraffe, I., Chabrier, G., Allard, F., & Hauschildt, P. H. 1998, A&A, 337, 403
Bate, M. R., Bonnell, I. A., & Bromm, V. 2003, MNRAS, 339, 577
Bertin, E. & Arnouts, S. 1996, A&AS, 117, 393

Bonnell, I. A., Bate, M. R., Clarke, C. J., & Pringle, J. E. 2001, MNRAS, 323, 785
Burgess, A. S. M., Moraux, E., Bouvier, J., et al. 2009, A&A, 508, 823
Chabrier, G. 2003, PASP, 115, 763
Chabrier, G. & Baraffe, I. 1997, A&A, 327, 1039
Chabrier, G., Baraffe, I., Allard, F., & Hauschildt, P. 2000, ApJ, 542, 464
Hennebelle, P. & Chabrier, G. 2008, ApJ, 684, 395
Herbst, W. 2008, Star Formation in IC 348, ed. Reipurth, B., 372–+
Kroupa, P. & Bouvier, J. 2003, MNRAS, 346, 369
Larson, R. B. 1973, MNRAS, 161, 133
Luhman, K. L., Joergens, V., Lada, C., et al. 2007, in Protostars and Planets V, 443–457
Marmo, C. 2007, in Astronomical Society of the Pacific Conference Series, Vol. 376, Astronomical Data Analysis Software and Systems XVI, ed. R. A. Shaw, F. Hill, & D. J. Bell, 285–+
Mayor, M. & Queloz, D. 1995, Nat, 378, 355
McClure, M. K., Furlan, E., Manoj, P., et al. 2010, ApJS, 188, 75
Nakajima, T., Oppenheimer, B. R., Kulkarni, S. R., et al. 1995, Nat, 378, 463
Oppenheimer, B. R., Kulkarni, S. R., Matthews, K., & Nakajima, T. 1995, Sci, 270, 1478
Padoan, P. & Nordlund, Å. 2002, ApJ, 576, 870
Rebolo, R., Zapatero Osorio, M. R., & Martín, E. L. 1995, Nat, 377, 129
Reipurth, B. & Clarke, C. 2001, AJ, 122, 432
Shu, F. H., Adams, F. C., & Lizano, S. 1987, ARA&A, 25, 23
Stamatellos, D. & Whitworth, A. P. 2009, MNRAS, 392, 413
Whitworth, A., Stamatellos, D., Walch, S., et al. 2010, in IAU Symposium, ed. R. de Grijs & J. R. D. Lépine, Vol. 266, 264–271
Wilking, B. A., Gagné, M., & Allen, L. E. 2008, Star Formation in the ρ Ophiuchi Molecular Cloud, ed. Reipurth, B., 351–+

4.6 Dissecting High-Mass Star-Forming Regions; Tracing Back Their Complex Formation History

Arjan Bik[1], T. Henning[1], A. Stolte[2], W. Brandner[1], D. Gouliermis[1], M. Gennaro[1], A. Pasquali[3], B. Rochau[1], H. Beuther[1], and Y. Wang[4]

[1] Max-Planck-Institut für Astronomie, Königstuhl 17, 69117 Heidelberg, Germany
[2] Argelander Institut für Astronomie, Auf dem Hügel 71, 53121 Bonn, Germany
[3] Astronomisches Rechen Institut, Mönchhofstrasse 12 - 14, 69120 Heidelberg, Germany
[4] Purple Mountain Observatory, Chinese Academy of Sciences, 210008, Nanjing, PR China

Abstract

We present near-infrared JHKs imaging as well as K-band multi-object spectroscopy of the massive stellar content of W3 Main using LUCI at the LBT. We confirm 13 OB stars by their absorption line spectra in W3 Main and spectral types between O5V and B4V have been found. Three massive Young Stellar Objects are identified by their emission line spectra and near-infrared excess. From our spectrophotometric analysis of the massive stars and the nature of their surrounding HII regions we derive the evolutionary sequence of W3 Main and we find evidence of an age spread of at least 2 – 3 Myr. While the most massive star (IRS2) is already evolved, indications for high-mass pre-main-sequence evolution is found for another star (IRS N1), deeply embedded in an ultra compact HII region, in line with the different evolutionary phases observed in the corresponding HII regions. We have detected the photospheres of OB stars from the more evolved diffuse HII region to the much younger UCHII regions, suggesting that the OB stars have finished their formation and cleared away their possible circumstellar disks very fast. Only in the hyper-compact HII region (IRS5) are the early type stars still surrounded by circumstellar material.

Introduction

Despite the impact on their surroundings, the formation and early evolution of massive stars is poorly constrained, primarily because of their scarcity and short lifetimes. Most OB stars form in stellar clusters and associations, and are still partly hidden in their natal molecular cloud. To detect the stellar content of these regions directly, near-infrared observations, especially spectroscopy, have proven to be a powerful method to find and characterize the newborn OB stars. A pure photometric characterization of young stellar clusters is strongly hampered by highly varying extinction, unknown distances and infrared excess of the young cluster members.

A spectroscopic identification, however, results in a unambiguous identification of the (massive) stellar content. Stellar properties, like effective temperature and luminosity, are derived based on the spectral features and extinction, distance and infrared excess can be determined reliably (e.g. Blum et al. [2000]; Hanson et al. [2002]; Bik et al. [2005]; Puga et al. [2006]; Bik et al. [2010]; Puga et al. [2010]). By comparing the effective temperature and luminosity to main sequence and pre-main-sequence isochrones, the age of a stellar cluster can be derived more reliably than from photometry alone [Bik et al., 2010]. When studying larger samples of massive stars in the same star cluster, estimates of an age spread in the cluster can be obtained. Based on the massive stars, Clark et al. [2005] finds very little age spread (less than 1 Myr) in starburst clusters. However, in Orion an age spread has been found based on the PMS stars (Da Rio et al. [2010]). Additional evidence for an age spread has been found in S255 where the most massive star is still deeply embedded and driving an outflow, while the PMS population has an age of 1 – 3 Myr (Wang et al. [2011]).

We present deep LUCI near-infrared JHKs imaging as well as K-band multi-object-spectroscopy of the massive stellar content of W3 Main. This allows for the first time a spectral classification of the massive stellar content. Using their derived spectral type we discuss the evolutionary status of the massive stars as well as the HII regions in detail. The different evolutionary phases of the HII regions make W3 Main an ideal target to study age spread and the evolution of circumstellar disks around massive stars.

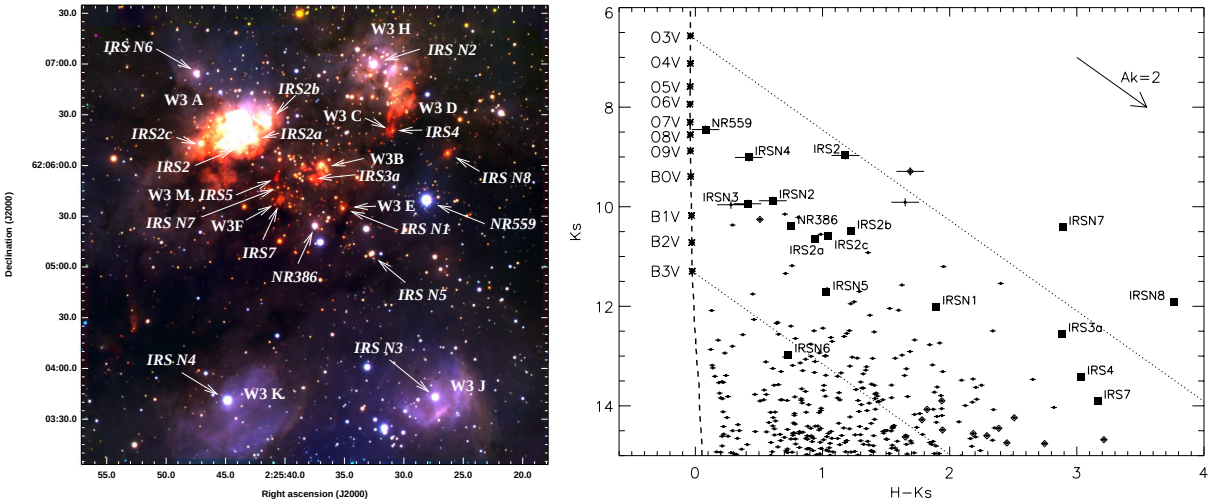

Figure 4.19: *Left*: JHKs colour composite of W3 Main taken with LUCI at the LBT. The HII regions as well as the massive stars are annotated. *Right*: Overplotted as a dashed line is the main sequence isochrone with an age of 1 Myr from Lejeune & Schaerer [2001]; the location of the spectral types between O3V and B3V are indicated as well. The two diagonal dotted lines show the reddening lines for an O3V and a B3V star using the extinction law of Indebetouw et al. [2005]. Additionally, the reddening vector for $A_{Ks} = 2$ mag is indicated.

Near-infrared imaging and spectroscopy

JHKs imaging of W3 Main has been obtained with LUCI at the Large Binocular Telescope (LBT) on Mount Graham, Arizona. Fig. 4.19 shows the resulting three colour image of a 4×4 arcmin^2 field centered on W3 Main. Photometry on the JHKs images was performed using the *starfinder* software (Diolaiti et al. [2000]). The photometry as well as the astrometry is calibrated with 2MASS. The resulting Ks vs H-Ks colour-magnitude diagram (Fig. 4.19) shows the enormous spread in colour of the massive stars caused by large extinction variations.

K-band spectra of 16 candidate massive stars inside W3 Main were obtained with the multi-object spectroscopic mode of LUCI. We classified 13 stars as OB stars from their absorption lines (Fig. 4.20) compared with K-band spectra of optically visible OB stars (Hanson et al. [2005]; Bik et al. [2005]). Three objects are classified as massive Young Stellar Objects, massive stars surrounded by a circumstellar disk. See Bik et al. (to be submitted) for a detailed description of the obtained data and reduction process.

HR-diagram

After their spectral classification, the bolometric luminosities of the massive stars are calculated and the stars are placed in the Hertzsprung Russell diagram (HRD, Fig. 4.20) and compared with stellar evolution isochrones. Overplotted in the HRD are the main sequence isochrones from the zero age main sequence (ZAMS) to 3 Myr from Lejeune & Schaerer [2001], the PMS isochrones for intermediate mass stars ($M < 5$ M$_\odot$; Siess et al. [2000]) as well as the theoretical birth-line (Palla & Stahler [1990]). Also overplotted are the high-mass protostellar evolutionary tracks from Hosokawa & Omukai [2009] for 10^{-5} and 10^{-4} M$_\odot$ yr^{-1} accretion rates.

In the upper regions of the HRD ($\log L/L_\odot \geq 5$), the main sequence isochrones indicate that the most massive stars already show significant evolution after a few Myr. Two stars are located in the upper regions of the HRD, IRS2 and IRS3a. IRS2 is located to the right of the ZAMS and its location is more consistent with the 2 – 3 Myr isochrones. The foreground extinction is not very extreme, therefore the location of IRS2 in the HRD does not vary a lot by changing the extinction law. IRS3a (O5V – O7V), however, is very reddened ($A_{Ks} = 5.42 \pm 0.79$ mag) and its location in the HRD depends very strongly on the adopted extinction law. Additionally, the presence of a near infrared excess makes its luminosity more uncertain. However, the effective temperature determination is more reliable and independent of extinction and excess. This allows us to place an upper limit on the age of 3 Myr, as stars on older isochrones will be of later spectral type than IRS3a.

In the middle area of the HRD ($3.5 \leq \log L/L_\odot \leq 5$), most of the sources are within 3 σ of the

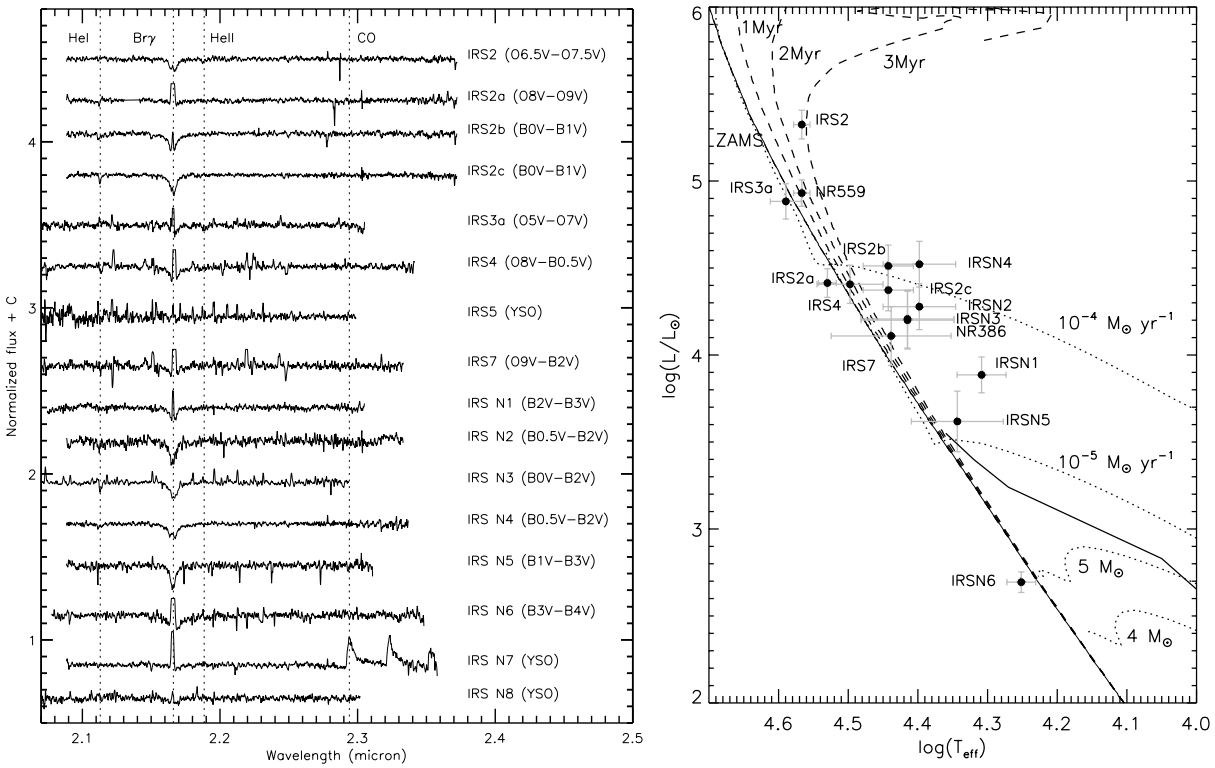

Figure 4.20: *Left*: Normalized K-band spectra of the massive stars in W3 Main as taken with the multi-object-mode of LUCI. Annotated with dashed lines are the spectral features which are important for the classification of their stellar spectra. *Right*: Hertzsprung Russell diagram of the massive stars in W3 Main. The dashed lines represent the main-sequence isochrones from Lejeune & Schaerer [2001] for 1, 2 and 3 Myr. The dotted lines show the pre-main-sequence evolutionary tracks for a 4 and 5 $M_\odot$ star (Siess et al. [2000]) as well as high-mass protostellar evolution tracks for 10^{-4} and 10^{-5} $M_\odot$ yr^{-1} from Hosokawa & Omukai [2009]. The solid line represents the theoretical birth-line, above which an optically visible pre-main-sequence star is not detectable (Palla & Stahler [1990]).

main sequence. For spectral types between O9V and B1V, where most of the objects are found, the change in effective temperature as well as K-band magnitude is very large, while the change in spectral features is not that dramatic. This is reflected in the large error bars of e.g. IRS N5 and IRS7. However IRS N1 and also IRS N4 are significantly away from the main sequence. As their extinction is relatively low, their position does not change much with extinction. Below we discuss possible scenarios explaining this offset.

Most of the massive stars are observed to be binary stars (e.g. Apai et al. [2007]). An equal mass binary would result in a mismatch in the observed luminosity of a factor of 2 (log L/L_⊙ = 0.3), with a multiple star system, increasing the offset even more. Both sources would have to be a system of 5 – 6 equal mass stars to explain their location above the main sequence.

Stellar evolution in main sequence or pre-main-sequence could be the reason why these objects are located away from the main sequence. The location of IRS N4 would be compatible with a 10 Myr main sequence track, while IRS N1 would require an even older isochrone. This is highly unlikely for IRS N1, as the star is located inside an ultra-compact HII region, still very young (10^5 years, Wood & Churchwell [1989]). IRS N4 is the central star of a diffuse and more evolved HII region, however, as shown by Lada & Lada [2003], a time span of 10 Myrs would be enough to disperse the surrounding gas.

Above the "birth-line" in the HRD, no optically visible PMS stars are expected (Palla & Stahler [1990]). However, using deep near-infrared observations we might start to probe the pre-main-sequence phase of the massive stars. Theoretical modelling of high-mass proto-stellar evolution predicts that massive proto-stars might have a similar evolution to intermediate PMS stars towards the main sequence (Hosokawa & Omukai [2009]). The exact path of the proto-stars in the HRD depends on their accretion rate. Overplotted in Fig. 4.20 are two Hosokawa tracks for 10^{-4} $M_\odot$ yr^{-1} and 10^{-5} $M_\odot$ yr^{-1}. The location of IRS N1 would be consistent with an accretion rate in between 10^{-5} and 10^{-4} $M_\odot$ yr^{-1}.

Discussion and Conclusions

W3 Main harbours several different evolutionary stages of HII regions, ranging from very young hyper-compact HII (HCHII) regions (few 10^3 years), ultra-compact HII (UCHII) regions ($\sim 10^5$ yr, Wood & Churchwell [1989]) to evolved, diffuse HII regions (few 10^6 years). All these regions are most likely formed out of the same molecular cloud. This provides the possibility to study the evolution of young HII regions and their stellar content in great detail. Tieftrunk et al. [1997] derived an evolutionary sequence for the HII regions in W3 Main, based on the morphology of the radio sources. The youngest are the HCHII regions W3 M and W3 Ca, with the UCHII regions W3 F, W3 C and W3 E, slightly older, the compact HII regions W3 B and W3 A even more evolved, and the diffuse HII regions, W3 K and W3 J being the oldest HII regions in W3 Main. This classification can be compared to the ages of the massive stars deduced from their position in the HRD.

We have detected OB stars in three diffuse HII regions, two compact HII regions and three UCHII regions. The HCHII region W3 M harbours the high-mass protostar IRS5 (see first Section). Additionally three stars have no detectable HII region associated with them (IRS N5 and the massive YSOs IRS N7 and IRS N8). The position of IRS2 in the HRD suggests an age of 2 – 3 Myr, consistent with its location in a relatively evolved compact HII region (W3 A) with a similar or younger age derived for IRS3a, harboured in a younger UCHII region. For the lower-mass stars (late O, early B) the isochrones are too close to each other to derive any age information. For IRS N1, located inside the UCHII region W3 E, the offset from the main sequence could be explained by high-mass pre-main-sequence evolution (Hosokawa & Omukai [2009]), consistent with the expected young age of the UCHII region.

A similar sequence can be seen in the extinction towards the different HII regions. The extinction varies from $A_{Ks} = 0.9$ mag for the diffuse HII regions W3 J and W3 K to very high extinction ($A_{Ks} = 5.9$ mag) towards W3 F. Such a sequence in extinction indicates that the stars in the diffuse HII regions have already cleared out their surroundings and destroyed the molecular cloud, while those in UCHII regions are still embedded in their parental molecular cloud.

The evolutionary sequence of the HII regions seen in the radio morphology, is consistent with an increase in extinction from the older (diffuse HII) regions to the younger (UCHII) regions. We have detected the photospheres of OB stars from the more evolved diffuse HII region to the much younger UCHII regions, suggesting that the OB stars have finished their formation and cleared away their possible circumstellar disks very fast. Only in the HCHII phase (IRS 5), the massive star is still surrounded by circumstellar material.

Based on the presence of different evolutionary stages of HII regions as well as the location of the most massive stars in the HRD, we can conclude that an age spread of 2 – 3 Myr is most likely present for the massive stars in W3 Main. A growing number of young stellar clusters show evidence for an age spread, usually based on the analysis of their PMS population in the HRD. In Orion an age spread of a few Myr has been found [Palla & Stahler, 1999; Da Rio et al., 2010]. In starburst clusters, however, upper limits on the age spread of less than 1 Myr have been found for Westerlund 1 (Clark et al. [2005]) based on its massive stars. This suggests that W3 Main is not formed in one star formation burst as expected for starburst cluster, but, more likely, through a temporal sequence of star formation events.

Bibliography

Apai, D., Bik, A., Kaper, L., Henning, T., & Zinnecker, H. 2007, ApJ, 655, 484
Bik, A., Kaper, L., Hanson, M. M., & Smits, M. 2005, A&A, 440, 121
Bik, A., Puga, E., Waters, L. B. F. M., et al. 2010, ApJ, 713, 883
Blum, R. D., Conti, P. S., & Damineli, A. 2000, AJ, 119, 1860
Clark, J. S., Negueruela, I., Crowther, P. A., & Goodwin, S. P. 2005, A&A, 434, 949
Da Rio, N., Robberto, M., Soderblom, D. R., et al. 2010, ApJ, 722, 1092
Diolaiti, E., Bendinelli, O., Bonaccini, D., et al. 2000, A&A, 147, 335
Hanson, M. M., Kudritzki, R.-P., Kenworthy, M. A., Puls, J., & Tokunaga, A. T. 2005, ApJS, 161, 154
Hanson, M. M., Luhman, K., & Rieke, G. H. 2002, ApJS, 138, 35
Hosokawa, T. & Omukai, K. 2009, ApJ, 691, 823
Indebetouw, R., Mathis, J. S., Babler, B. L., et al. 2005, ApJ, 619, 931
Lada, C. J. & Lada, E. A. 2003, ARA&A, 41, 57
Lejeune, T. & Schaerer, D. 2001, A&A, 366, 538
Palla, F. & Stahler, S. W. 1990, ApJ, 360, L47

Palla, F. & Stahler, S. W. 1999, ApJ, 525, 772
Puga, E., Feldt, M., Alvarez, C., et al. 2006, ApJ, 641, 373
Puga, E., Marín-Franch, A., Najarro, F., et al. 2010, A&A, 517, 2
Siess, L., Dufour, E., & Forestini, M. 2000, A&A, 358, 593
Tieftrunk, A. R., Gaume, R. A., Claussen, M. J., Wilson, T. L., & Johnston, K. J. 1997, A&A, 318, 931
Wang, Y., Beuther, H., Bik, A., et al. 2011, A&A, 527, 32
Wood, D. O. S. & Churchwell, E. B. 1989, ApJ, 340, 265

4.7 Massive Stellar Content of Stellar Clusters in M 31's Giant HII Region Pellet 550

Wolfgang Brandner[1], A. Bik[1], B. Rochau[1], M. Gennaro[1], N. Kudryavtseva[1], A. Stolte[2], B. Hußmann[2], and H. Zinnecker[3]

[1] Max Planck Institute for Astronomy, Heidelberg, Germany
[2] Argelander Institut, University of Bonn, Germany
[3] Deutsches SOFIA Institut, University of Stuttgart, Germany

Abstract

We report on the first set of LBT/LUCIFER near infrared observations of Pellet 550, one of the most massive star-forming regions in the disk of M 31. Compared to the Milky Way, M 31 offers a complete census of star-forming regions and starburst clusters, all located at virtually the same distance. The regions under study have been selected to include the most luminous HII regions as well as still partially embedded star-forming regions recently revealed by Spitzer. For the first time we are able to establish the massive stellar content, identify young, massive clusters, and study the nature of still partially embedded luminous infrared sources. The M 31 study is a first application of our previous studies to establish the properties of Milky Way starburst clusters as templates for extragalactic massive star-forming regions.

Introduction

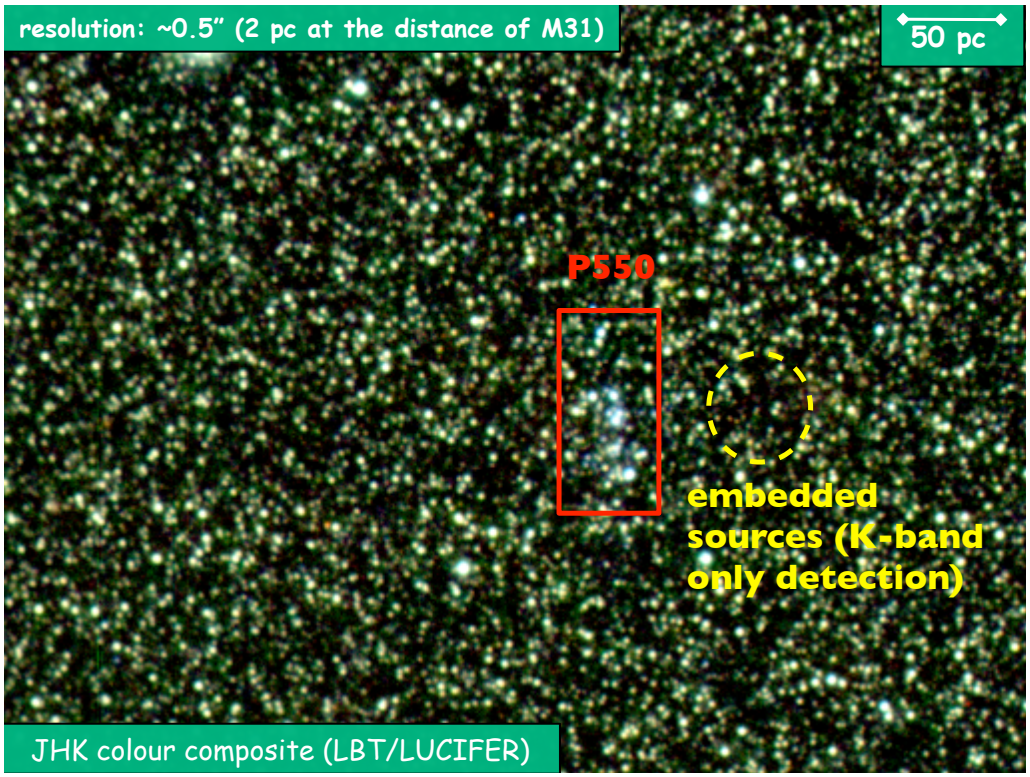

Figure 4.21: Composite colour JHKs image of the region around Pellet 550 obtained with LBT/LUCIFER. The field of view is $\approx 2.9 \times 1.5$ arcmin^2, i.e. a subset of the full 4×4 arcmin^2 LUCIFER frame. The red box marks an area of $\approx 50\,\mathrm{pc} \times 100\,\mathrm{pc}$ in size. North is up, and east is to the left.

Why study star formation in M 31?

Studies of massive star-forming environments in the Milky Way are severely hampered by high foreground extinction as well as source confusion due to other objects along the line of sight. Uncertainties in the distance estimates to individual star-forming regions further complicate the determination of basic astrophysical quantities like source luminosities and physical size scales.

Star-forming regions in M 31, on the other hand, are all at virtually the same distance from us. From our vantage point of view, M 31 is located outside the Galactic plane, and M 31's disk is seen from above. Hence both foreground extinction and confusion by Galactic foreground stars is small. Pellet 281 and 550, two of the most luminous Giant HII regions (GHRs) in M 31s' 10 kpc ring have luminosities comparable to NGC 3603 and W 49. The latter have $L_{H\alpha} \approx 10^{39}$ erg/s, $N_c \approx 10^{51}$ s^{-1} (i.e. 100× Orion Nebula), and hence are among the most luminous GHRs in the Milky Way (Kennicutt [1984]). Thus M 31 is also the ideal place to extend our studies of Milky Way starburst clusters (Stolte et al. [2005]; Brandner et al. [2008]; Rochau et al. [2010]; Gennaro et al. [2011]; Hußmann et al. [2011]) to extragalactic environments. Furthermore, with modern ground-based telescopes and instruments routinely achieving sub-arcsecond resolution, studies of M 31 star-forming region on parsec-scales are quite feasible (at a distance of d = 780 kpc, 0.5 arcsec correspond to ≈ 2 pc).

M 31 & Gaia

Young, massive, and compact star clusters in M 31 are seen by Gaia as bright (V ≤ 19 mag) "point sources". As such, they are ideal test particles for Gaia to probe M31 space motions. By measuring the proper motions and obtaining spectra of the brightest young star clusters in M 31, Gaia will probe the rotation curve of M 31 as well as its 3D space motion within the Local Group of galaxies. The transversal motion of M 31 within the Local Group is currently estimated to 100 km/s, which corresponds to ≈ 30 μarcsec/yr. For the flat portion of M 31's rotation curve, a velocity of ± 250 km/s has been estimated, corresponding to a maximum proper motion of ≈ ± 75 μarcsec/yr. This compares well with the astrometric accuracy of 10 to 25 μarcsec, and radial velocity accuracy ≤ 15 km/s predicted for Gaia on individual objects with V ≈ 15 mag (Prusti [2011]). The average of the Gaia measurements for several tens of bright clusters should thus improve our knowledge of M31 kinematics and dynamics considerably.

Observations with LBT/LUCIFER

In 2008 we initiated a study of the stellar content of GHRS in M31 in preparation of the commissioning and science verification programmes of LUCIFER 1 (Seifert et al. [2010]) at the Large Binocular Telescope (LBT). The scientific reasons for choosing infrared observations were that we wanted to probe for infrared excess as well as being able to detect deeply embedded regions. The technical reasons were that infrared observations are less sensitive to variations of (moderate) foreground extinction than observations in the visual. Even more important was the better seeing in the near infrared compared to the visual, making observations less affected by crowding.

The first JHKs imaging data set of the area around the Giant HII region Pellet 550 (Pellet et al. [1978]) was obtained in November 2010. We used LUCIFER with the N3.75 camera, resulting in an image scale of 0.12 arcsec per pixel, and a field of view of 4 × 4 arcmin^2. Individual exposure times were 10 s, and six exposures were coadded for each of the eight dither positions, resulting in a total exposure time of 8 min in each filter. In addition, a nearby field off the 10 kpc ring was observed with the same set-up to facilitate for better sky-subtraction and in order to characterise the general (older) M 31 disk population. Seeing as measured on the images was in the range of 0.4 to 0.6 arcsec. Photometric calibration was based on sources in common with the 2MASS Point Source Catalog.

Results

Starburst clusters in Pellet 550

The observations nicely resolve the star formation environment in Pellet 550 at a physical resolution of ≈ 2 pc, and reveal numerous bright and compact sources (Fig. 4.21). The brightest of the blue sources in Pellet 550 has an apparent magnitude of J ≈ 15.8 mag (Fig. 4.22, left), which for a near infrared extinction

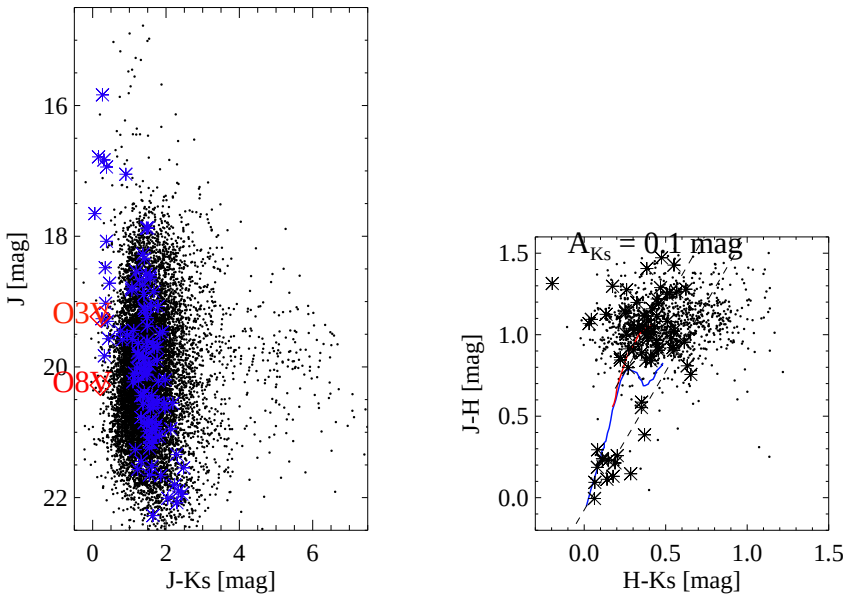

Figure 4.22: The NIR colour magnitude diagram of the LUCIFER field shows a sequence of blue, compact O-star clusters significantly brighter than individual O-stars at the distance of M 31. The colour-colour diagram reveals that the brightest O-star clusters show a moderate amount of extinction, and little IR excess. Sources located in the box depicted in Fig. 4.21, which is centered on Pellet 550, are marked by an asterisk.

close to ≈0 mag (see Fig. 4.22, right) corresponds to an absolute magnitude of $M_J = -8.7$ mag, i.e. about 3.5 mag *brighter* than an individual O3V star.

Our (simplistic) population synthesis modelling based on Monte Carlo simulations of a Kroupa initial mass function (Kroupa [2002]), and assuming our own compilation of zero age main sequence magnitudes and colours for all the stars, reproduces observed source magnitudes and near-infrared colours. The brightest cluster is modeled as a starburst cluster containing ≈ 35 O-type stars, and ≈ 10,000 stars in total (but see also Table 2 in Zinnecker & Yorke [2007] for the expected ratio between lower mass stars and O-type stars for a range of mass function exponents). The sequence of blue sources depicted in the colour magnitude diagram indicates that Pellet 550 is composed of ≈ 10 young, massive clusters with individual stellar masses in the range of several 1,000 to 10,000 solar masses. The most massive cluster in Pellet 550 is comparable to the NGC 3603 Young Cluster, which houses several O2V stars in its center.

The GHR Pellet 550 seems to be powered by an association of clusters. This string of blue compact clusters, which extends roughly in the North-South direction, might trace the shape of the giant molecular cloud which gave birth to Pellet 550.

Cluster sizes

The majority of the blue, compact clusters is unresolved on our ≈ 0.5 arcsec resolution imaging, hence they have NIR half-light radii ≤ 1 pc. These clusters are comparable to the compact Arches and NGC 3603 young clusters in the Milky Way (Stolte et al. [2005]; Stolte et al. [2006]). The brightest of the Pellet 550 clusters ("Cluster 46" in the notation of Hodge et al. [2010]) is clearly resolved, and has a (seeing-corrected) half-light radius of ≈ 2 pc in the K-band. This puts Cluster 46 on the same spatial scale as the Westerlund 1 and Quintuplet clusters in the Milky Way.

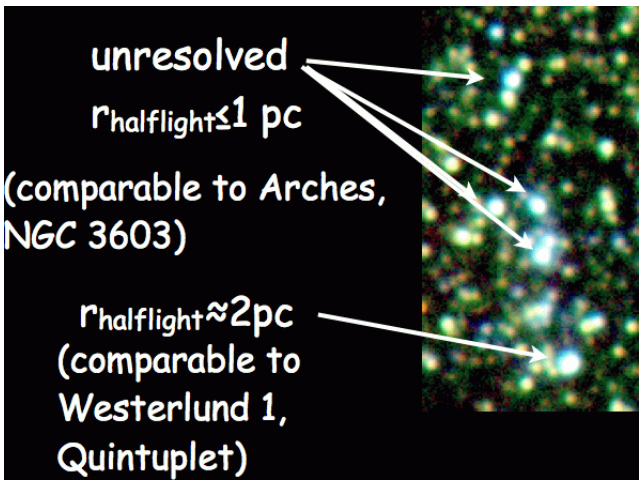

Figure 4.23: Close-up of Pellet 550, with resolved and unresolved ($r_{halflight} \leq 1\,pc$) clusters marked.

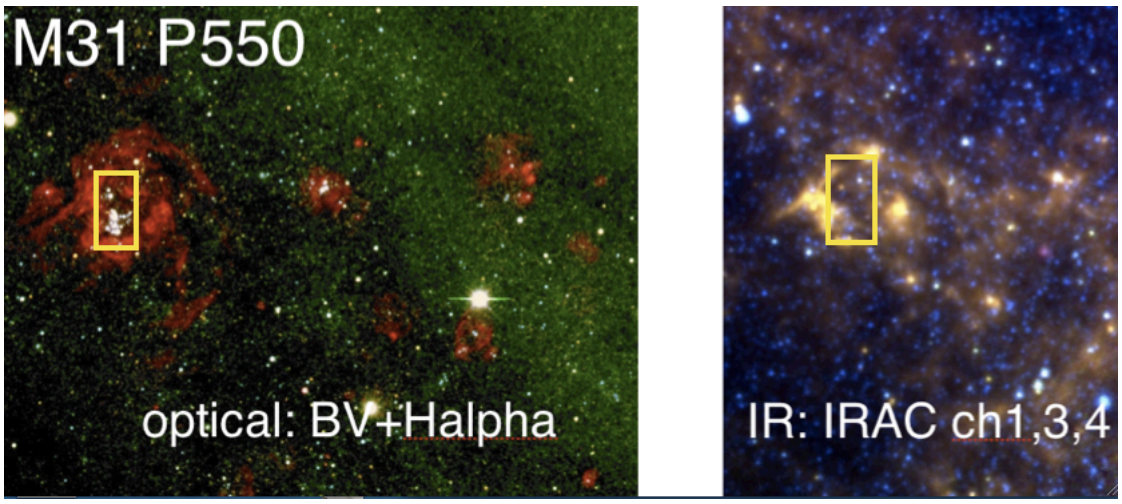

Figure 4.24: Comparison of optical (constructed from the images of the NOAO Local Group Galaxies Survey (Massey et al. [2007])) and SPITZER/IRAC infrared observations of Pellet 550. The boxes mark the same area as indicated on the LBT/LUCIFER images (Fig. 4.21), displayed in more detail in Fig. 4.23. IRAC traces Polycyclic Aromatic Hydrogen emission originating at the interfaces between the HII regions and the molecular clouds, as well as deeply embedded compact sources not detectable in the visual. Some of the deeply embedded sources are for the first time revealed in the near infrared with LBT/LUCIFER.

Embedded sources

The deep LUCIFER imaging data for the first time reveal some deeply embedded compact sources in the K-band, which were not detectable in the optical. These sources seem to coincide with SPITZER/IRAC detections, and might be massive young clusters in the process of forming stars (see Figs. 4.21, 4.24).

Outlook

The next steps are to extend our NIR imaging survey to other GHRs in M 31, and to quantify the stellar content by optical and near infrared spectroscopy. This will then facilitate more detailed population synthesis modeling. Spectral features of the embedded sources should reveal their nature. In addition, higher angular resolution imaging observations should resolve the clusters into the individual bright stars, which would allow us to test and verify the population synthesis models.

Acknowledgments

We would like to thank Ric Davies and Jochen Heidt for obtaining high quality data during the service observing run, the LUCIFER team, in particular Nancy Ageorges, Walter Seifert and Holger Mandel for their great effort in building and commissioning such a powerful instrument, and the LBT team for running and fine tuning the telescope to provide such a high image quality.

Bibliography

Brandner, W., Clark, J. S., Stolte, A., et al. 2008, A&A, 478, 137
Gennaro, M., Brandner, W., Stolte, A., & Henning, T. 2011, MNRAS, 412, 2469
Hodge, P., Krienke, O. K., Bianchi, L., Massey, P., & Olsen, K. 2010, PASP, 122, 745
Hußmann, B., Stolte, A., Brandner, W., Gennaro, M., & Liermann, A. 2011, A&A
Kennicutt, R. C. 1984, ApJ, 287, 116
Kroupa, P. 2002, Sci, 295, 82
Massey, P., McNeill, R. T., Olsen, K. A. G., et al. 2007, AJ, 134, 2474
Pellet, A., Astier, N., Viale, A., et al. 1978, A&AS, 31, 439, a&AA ID. AAA021.132.016
Prusti, T. 2011, EAS Publications Series, 45, 9
Rochau, B., Brandner, W., Stolte, A., et al. 2010, ApJ Lett., 716, L90
Seifert, W., Ageorges, N., Lehmitz, M., et al. 2010, Ground-based and Airborne Instrumentation for Astronomy III. Edited by McLean, 7735, 256, (c) 2010: American Institute of Physics
Stolte, A., Brandner, W., Brandl, B., & Zinnecker, H. 2006, AJ, 132, 253
Stolte, A., Brandner, W., Grebel, E. K., Lenzen, R., & Lagrange, A.-M. 2005, ApJ, 628, L113
Zinnecker, H. & Yorke, H. W. 2007, ARA&A, 45, 481

4.8 The Rotational Evolution of Solar-like Stars Close to the Zero Age Main Sequence

Alessandro C. Lanzafame[1,3], F. Spada[2], A. Lanza[3], S. Messina[3], and A. Collier-Cameron[4]

[1] Sezione Astrofisica, Dipartimento di Fisica e Astronomia, Università degli Studi di Catania, Via S. Sofia, 78, 95123, Catania, Italy
[2] Department of Astronomy, Yale University, 260 Whitney Avenue, New Haven, CT 06511, USA
[3] INAF - Osservatorio Astrofisico di Catania, Via S. Sofia, 78, 95123, Catania, Italy
[4] SUPA, School of Physics and Astronomy, University of St Andrews, North Haugh, St Andrews, Fife KY16 9SS, Scotland

Abstract

We investigate the rotational evolution of solar-like stars approaching and evolving from the zero age main sequence (ZAMS). Most of the observed period distributions in open clusters and young associations available to date are considered. The double zone model, in which the star's radiative core and convective envelope are assumed to rotate as solid bodies, is used to test simple relationships between the core-envelope coupling timescale and rotational properties like the envelope angular velocity or the differential rotation at the core-envelope interface. The trial relationships are tested by fitting the model parameters to available observations via a Monte Carlo Markov Chain method. The synthetic distributions are tested for compatibility with their observational counterparts by means of the Kolmogorov-Smirnov test. A general satisfactory agreement with the observed evolution of rotational periods is found. However, we find it impossible to reconcile the high fraction of fast rotators in α Persei with the rotation period distributions in stellar systems at earlier and later evolutionary stages. Furthermore, the evolution of the rotational period cumulative distribution function of two clusters slightely older than the Pleiades and for which a good number of rotation periods is available, viz. M 50 (130 Myr) and M 35 (150 Myrs), does not follow the evolutionary trend expected from the model. We discuss possible local environmental effects (e.g. early removal of circumstellar discs due to UV radiation and winds from nearby high-mass stars), basic parameters uncertainties (e.g. ages), model oversimplified assumptions, and likely observational biases.

Introduction

Rotation period measurements in open clusters and young associations represent one of the most stringent information on the angular momentum evolution of late-type stars. In recent years, photometric measurements of the stellar rotation period ($P_{\rm rot}$), based on the rotational modulation of the light curve induced by photospheric inhomogeneities, have supplemented the $v \sin i$ measurements, considerably improving both the number and the precision of available rotation periods.

The currently accepted scenario identifies a few dominant processes. During the pre-main sequence (PMS) phase, solar-mass stars undergo a global contraction. However, for the first few Myr, the interaction with a circumstellar disc drains angular momentum from the star, thus delaying its spin up for the (variable) duration of the disc lifetime. This process is not understood in detail yet (see, e.g., Collier Cameron & Campbell [1993]; Shu et al. [1994]; Matt et al. [2010]) and is usually modelled by means of very simplified assumptions, e.g., the disc-locking hypothesis (Königl [1991]). Once on the main sequence (MS), the rotational evolution is driven by the loss of angular momentum through a magnetised stellar wind (Weber & Davis [1967]; Kawaler [1988]; Chaboyer et al. [1995a]; Chaboyer et al. [1995b]).

Surface period measurements are an indirect probe of the internal rotation profile. Phenomenological modelling of MS angular momentum evolution, the so-called double zone model (DZM) (MacGregor & Brenner [1991]; Keppens et al. [1995]; Allain [1998]; Bouvier [2008b]), assuming that the radiative core and the convective envelope rotate rigidly at all ages, has reproduced the general trend of the observations provided a certain amount of differential rotation between the core and the envelope is allowed. This is parameterised through a coupling timescale $\tau_{\rm c}$, which determines the rate of angular momentum

exchange between the two regions. From the comparison of synthetic rotational tracks and the upper and lower percentiles of the observed period distributions, Bouvier [2008b] concluded that τ_c is of the order of 10 Myr for the stars that begun their evolution on the ZAMS as fast rotators (i.e., with an initial rotation period of $\sim$ 1 d), while it is remarkably longer ($\tau_c \sim 100$ Myr) for initially slow rotators (i.e., with initial periods $\sim$ 10 d). An understanding of the physical processes that give rise to such a behaviour and eventually establish a nearly solid-body rotation within the age of the Sun (as observed through helioseismology, see e.g. Thompson et al. [2003]) is still lacking. Note also that rotation is closely linked to the dynamo process, which in turn powers magnetic activity, and it can influence the surface abundance of light elements through rotationally-induced mixing.

In Spada et al. [2011] we exploited the information currently available on the observed period distribution comparing them with synthetic ones, constructed by evolving the Orion Nebula Cluster (hereafter ONC) distribution by means of the DZM. On the basis of intuitive physical arguments, we formulated some hypotheses on the scaling of τ_c. The set of parameters in the DZM that produces the best fit of the synthetic distributions to the observed ones is determined by means of an iterative procedure based on a Markov Chain Monte Carlo (MCMC) sampling. We used rotation period distributions extracted from photometric surveys of stellar open clusters and young associations, as available in the literature. Only stars in the mass range $0.9 \leq M_*/M_\odot \leq 1.1$ were considered. Notably, the dataset used includes recent measurements of rotational periods of all young associations known to date (Messina et al. [2010]; Messina et al. [2011]) which fill an age gap previously present between Tau-Aur ($\sim$ 6 Myr old) and α Persei ($\sim$ 70 Myr) in the mass range $0.9 \leq M_*/M_\odot \leq 1.1$.

Here we focus on the discrepancies found for α Persei, M 50, and M 35, which may reveal local environmental effects (e.g. early removal of circumstellar discs due to UV radiation and winds from nearby high-mass stars), basic parameters uncertainties (e.g. ages), oversimplified model assumptions, and likely observational biases.

Method

The method used is described in detail in Spada et al. [2011]. Here we briefly summarise only the main points. We construct a series of synthetic rotation period distributions at the ages reported in Table 1 of Spada et al. [2011]. Each period in the ONC solar analogue subsample is evolved forwards in time with the DZM, calculated for a 1 $M_\odot$ star. The synthetic distributions are tested for compatibility with their observational counterparts by means of the standard Kolmogorov-Smirnov (KS) test. The input to our numerical procedure is an initial guess for the parameters of the DZM. The parameter space is then sampled by means of the MCMC method, which performs random jumps in each parameter, guided by a probabilistic acceptance rule. The best-fitting set of model parameters is obtained in output.

Based on intuitive physical arguments, we consider and tested two prescriptions on the dependence of τ_c on stellar rotation.

The first is a two-valued function of the form:

$$\tau_c = \begin{cases} 10 \text{ Myr} & \text{if } \Omega_e(t_0) \geq \Omega_{\rm crit} \\ \tau_0 & \text{otherwise} \end{cases} . \tag{4.2}$$

This is the simplest implementation of the early empirical finding (e.g. Krishnamurthi et al. [1997]; see also Bouvier [2008b]) that fast rotators are well described by a nearly solid-body inner profile, while a sizeable decoupling is necessary for slow rotators. The value of 10 Myr used for initially fast rotators is so short as to ensure nearly instantaneous coupling at all ages. The timescale for slow rotators, τ_0, and the initial angular velocity threshold, $\Omega_{\rm crit}$, are treated as free parameters to be determined by means of the MCMC procedure.

The second is a power law dependence on the instantaneous amount of differential rotation:

$$\tau_c(t) = \tau_0 \left[\frac{\Delta\Omega_\odot}{\Delta\Omega(t)} \right]^\alpha , \tag{4.3}$$

where $\Delta\Omega(t) = \Omega_c(t) - \Omega_e(t)$ and $\Delta\Omega_\odot$ is the inner differential rotation of the present Sun, assumed as a reference value (we used $\Delta\Omega_\odot = 0.2\ \Omega_\odot$).

Other simple prescriptions, e.g. a dependence of τ_c on the surface angular velocity $\Omega_e(t)$, failed to give suitable results.

For the best fitting parameters see Table 2 of Spada et al. [2011].

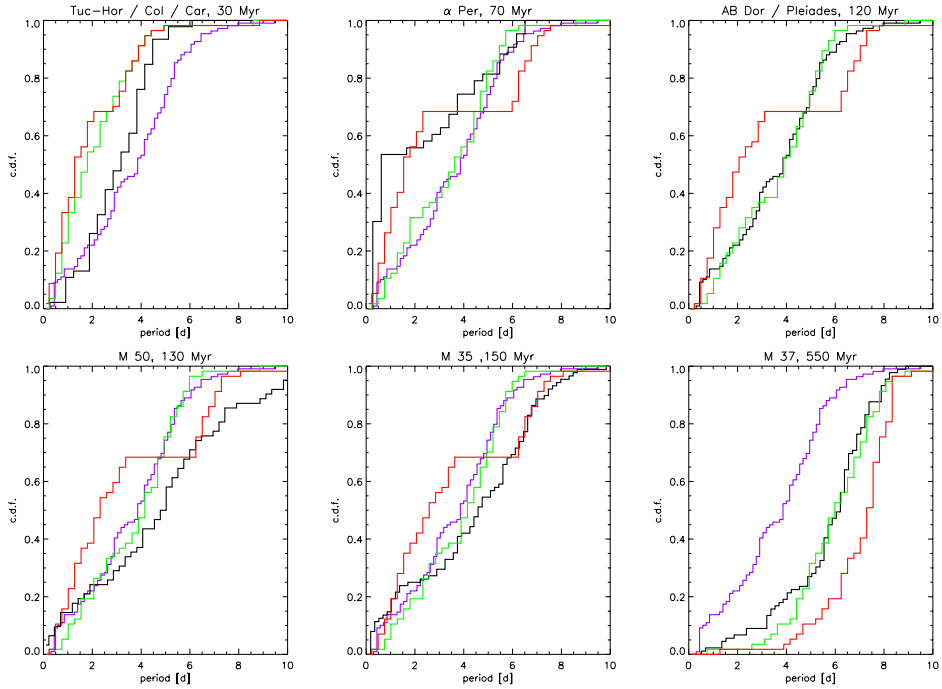

Figure 4.25: Synthetic (green power-law, red two-value τ_c, respectively) and observed (black line) rotation period cumulative distributions for clusters and associations close to the ZAMS and at approximately the age of the Pleiades in our analysis. For comparison, the observed CDF of the Pleiades is reported in blue in all panels.

Discussion

In Fig. 4.25 the synthetic and observed cumulative distribution functions (CDF) for clusters and associations close to the ZAMS and with age close to the Pleiades are reported. The probabilities that the observed and synthetic distributions are not incompatible are reported and discussed in Spada et al. [2011]. Here we focus only on the behaviour of the clusters and associations in Fig. 4.25.

For ages older than approximately 30 Myr, the agreement is strongly dependent on the angular momentum loss via the magnetised wind and on the model assumed for τ_c. We note, however, that the CDFs derived from the observations do not follow an evolution as regular as expected from the models. The α Persei CDF, in particular, displays a sharp rise at short rotation periods due to an excess of fast and ultra-fast rotators. The two-value τ_c model can account for this sharp rise, but then fails to reproduce the smooth CDF shape of AB Dor/Pleiades, M 50, etc. The power-law τ_c model, on the other hand, cannot reproduce any sharp rise in the CDF and therefore fails to reproduce the α Persei CDF. In the DZM framework, such a behaviour cannot be reproduced unless, for the fast and ultra-fast rotators, a remarkable amount of angular momentum is transferred from the core to the envelope within a very short timescale ($\sim 30-40$ Myr). In this case, however, very little angular momentum would be left in the core for the later evolution (see Figs. 5 and 6 in Spada et al. [2011]).

At ages slightly older than the Pleiades, we note that the slow rotator part of the observed CDF for M 50 (130 Myr) is lower than predicted by the DZM (both with the two-value and the power-law prescription for τ_c) and indeed even lower than the observed CDF for the older M 35 (150 Myr). The slower rotator part of the observed M 35 CDF is itself lower than the τ_c power-law CDF. This part is satisfactorily reproduced by the two-value CDF, which however fails to reproduce the fast rotators part because of the discontinuity imposed by α Per. Regardless the detailed fitting, this behaviour is counterintuitive under the DZM assumptions.

The reasons for such a discrepancy could be: a) the DZM is inadequate or contains oversimplified assumptions; b) the stellar rotation period distributions in open clusters and young associations may be affected by characteristics of the (parent) cluster as a whole, particularly those leading to the evaporation of circumstellar discs by UV radiation and wind from neighbour high-mass stars (e.g. Hernández et al. [2008]); c) the observed period distributions are incomplete and/or biased. The dispersal of clusters' stars into the field may add other selection effects.

Other possible sources of uncertainties in the period distribution include cluster contamination by

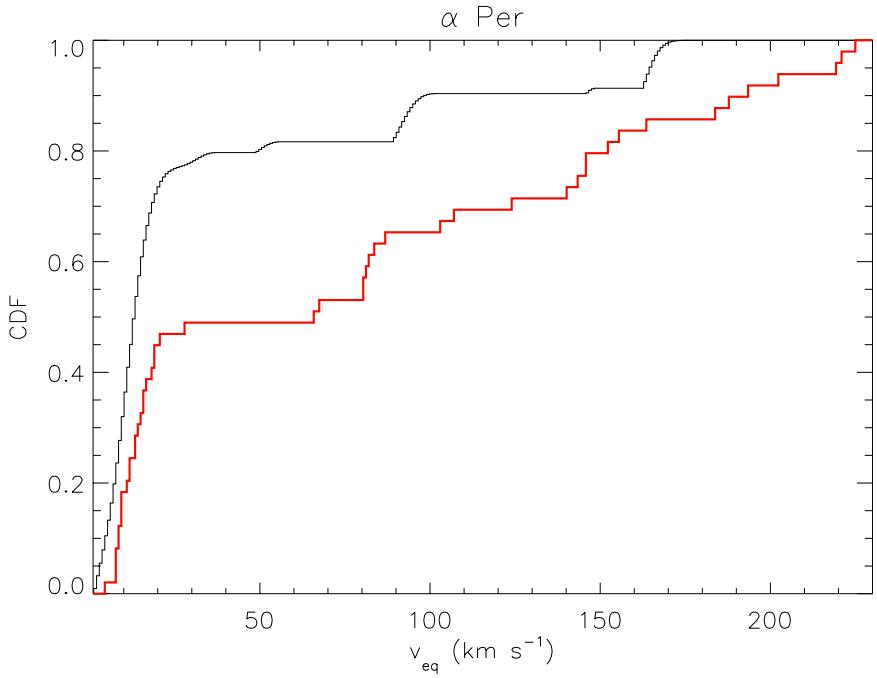

Figure 4.26: Cumulative distributions for the equatorial rotational velocities derived from the $v \sin i$ data (red line) and from the rotation period data (black line) in α Per.

field stars, the presence of close binaries whose high rotation rate is maintained by the tidal synchronisation between the components, and observational biases. Concerning these latter, photometric monitoring with a limited temporal extension (generally of 10 – 15 d) prevents us from detecting the slow rotation periods, making the derived distributions incomplete. Moreover, for MS stars with $P_{\rm rot} > 10$ d the amplitude of the optical light curve is very small ($< 0.001 - 0.01$ mag), so their rotational modulation cannot be measured by ground-based photometry. The absence of rotators with periods longer than ~ 10 d in the observed distributions can therefore be due to such limitations.

Some indication of possible observational biases can be derived from a comparison between the CDF of the equatorial velocities derived from the period and the $v \sin i$ measurements (Fig. 4.26; see Spada et al. [2011] for details). The two distributions are very different, with a KS probability of only 0.008, and a mean equatorial velocity of 35.5 km/s from $v \sin i$ and 63.9 km/s from rotation periods, respectively. This points to the presence of a bias in the measured period distribution in α Per towards an excessive number of fast rotators.

Although the completeness and accuracy of observational data have considerably improved in recent years, possible selection effects as well as the uncertainties in clusters ages, are therefore still severe limitations for the use of the period distributions to study stellar rotational evolution. More observations of clusters and associations in the age range 30 – 200 Myr are therefore required, together with an improvement of the model, e.g., by including correlations with the global properties of each cluster and association.

Bibliography

Allain, S. 1998, A&A, 333, 629
Bouvier, J. 2007, in Star-disk Interaction in Young Stars, Proceedings IAU Symp. 243 eds. J. Bouvier & I. Appenzeller, p. 231
Bouvier, J. 2008, in Proceedings of the Annual meeting of the French Society of Astronomy and Astrophysics Eds.: C. Charbonnel, F. Combes and R. Samadi
Bouvier, J. 2008, A&A, 489, L53
Chaboyer, B., Demarque, P., Pinsonneault, M. H. 1995a, ApJ, 441, 865
Chaboyer, B., Demarque, P., Pinsonneault, M. H. 1995b, ApJ, 441, 876
Collier Cameron, A., & Campbell, C. G. 1993, A&A, 274, 309
Hernández, J., Hartmann, L., Calvet, N., Jeffries, R. D., Gutermuth, R., Muzerolle, J., Stauffer, J. 2008, ApJ, 686, 1195

Kawaler, S. D. 1988, ApJ, 333, 236
Keppens, R., MacGregor, K. B., Charbonneau, P. 1995, A&A, 294, 469
Königl, A. 1991, ApJL, 370, L39
Krishnamurthi, A., Pinsonneault, M. H., Barnes, S., & Sofia, S. 1997, ApJ, 480, 303
Lanza, A. F. 2010, A&A, 512, A77
MacGregor, K. B., & Brenner, M. 1991, ApJ, 376, 204
Matt, S. P., Pinzón, G., de la Reza, R., & Greene, T. P. 2010, ApJ, 714, 989
Messina, S., Desidera, S., Turatto, M., Lanzafame, A. C., Guinan, E. F. 2010, A&A 520, 15
Messina, S., Desidera, S., Lanzafame, A. C., Turatto, M., Guinan, E. F. 2011, A&A, *in press*
Pont, F. 2009, MNRAS, 396, 1789
Shu, F., Najita, J., Ostriker, E., Wilkin, F., Ruden, S., & Lizano S. 1994, ApJ, 429, 781
Spada, F., Lanzafame, A. C., Lanza, A. F., Messina, S., Collier Cameron, A. 2011, MNRAS, *in press*
Thompson, M. J., Christensen-Dalsgaard, J., Miesch, M. S., Toomre, J. 2003, ARA&A, 41, 599
Weber, E. J., Davis, L. J. 1967, ApJ, 148, 217

4.9 On the Equivalent Effective Temperatures of Massive Young Star Clusters: The Case of NGC 595

Enrique Pérez-Montero[1], J. M. Vílchez[1], M. Relaño[2], and A. Monreal-Ibero[1]

[1] Instituto de Astrofísica de Andalucía - CSIC. Apdo. de correos 3004, Granada, Spain
[2] Universidad de Granada, Campus Fuentenueva, Granada, Spain

Abstract

The softness parameter is based on the relative intensity of several optical emission lines emitted by the gas ionized by young massive star clusters and can be used to derive the equivalent effective temperature (T_*) in those objects whose stellar population cannot be resolved. This method has several uncertainties due to the disagreement between different synthesis model atmospheres but it is robust to study the relative variations between objects.
Following the 2D photoionization models of the giant HII region NGC 595 (Pérez-Montero et al. 2011) we show that the determination of T_* with the η parameter is also robust in different regions of a same object with large variations in the geometry of the gas and in the dust-to-gas ratio.

Introduction

The study of the properties of young massive star clusters in our Local Group can be done by means of the census of the stars that belong to the corresponding object and the analysis of their properties using a colour-magnitude diagram. In the case of those objects whose stellar population cannot be resolved with the facilities that are nowadays available, it is necessary to appeal to other tecniques. A possible approach is to study the massive stars by inspecting their effects on the surrounding interstellar medium (ISM), including the supply of mechanical energy from stellar winds and supernovae explosions, the ejection of new metals produced in the interiors of the stars, or the excitation and ionization of the atoms in the ISM by the energetic photons emitted by the stars. These factors make the optical spectrum of an HII region frequently characterized by the presence of bright prominent recombination lines emitted by hydrogen and helium, and of collisional lines emitted by the metals. Although the shape of the stellar continuum and some stellar features are sometimes detectable (*e.g.* the Wolf-Rayet features), the most important source of information about the properties of the ionizing stellar clusters can only be the relative intensities of these lines.

These intensities are mainly dominated by the so-called functional parameters, including the metallicity (Z), the ionization parameter (U, *i.e.* the ratio between ionizing photons and the density of particles), and the equivalent effective temperature (T_*). This last is the unique parameter that only depends on the spectral energy distribution (SED) of the ionizing star or cluster.

The *softness* parameter

This parameter, denoted by the greek letter η, was introduced by Vílchez & Pagel [1988] to derive T_* using only the information from emission-line intensities in the optical spectrum. It is defined as:

$$\eta = \frac{O^+/O^{2+}}{S^+/S^{2+}} = \frac{[OII]3727\text{ÅÅ}/[OIII]4959,5007\text{ÅÅ}}{[SII]6717,6731\text{ÅÅ}/[SIII]9069,9532\text{ÅÅ}} + o(Z) \tag{4.4}$$

depending mainly on the ionic abundances of oxygen and sulphur ions. This ratio is basically a function of the ratio between the number of ionizing photons of O^+ (I.P. = 35.1 eV) and S^+ (I.P. = 23.3 eV) and has also a certain dependence on the overall metallicity [$o(Z)$] when it is derived directly from the emission-line intensities.

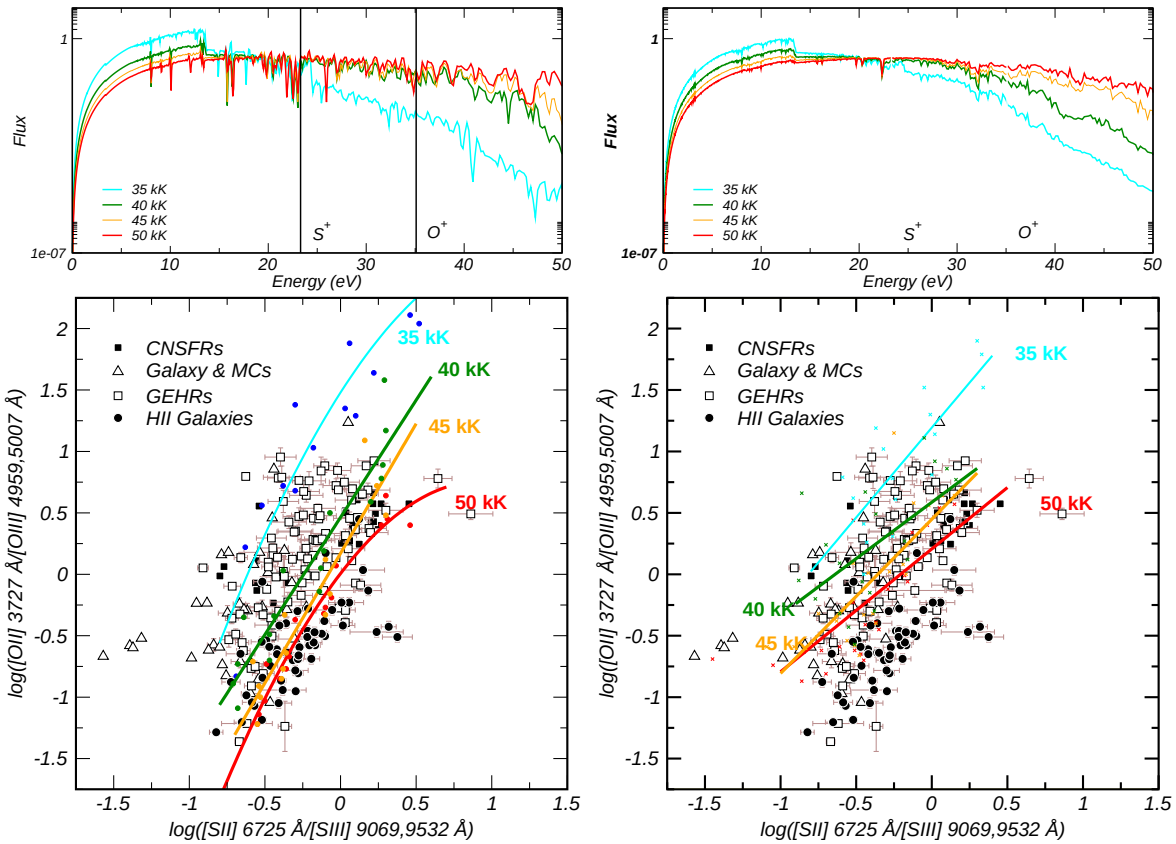

Figure 4.27: *Upper panels*: SEDs of synthesis model atmospheres from WM-Basic (left) and Tlusty (right) for different values of the metallicity and $T_* = 40$ kK. The vertical solid lines represent the ionization potentials of S^+ and O^+. In the lower panels we show the relation between the ratios of optical emission line-intensities [OII]/[OIII] and [SII]/[SIII] for different objects. The solid lines show the quadratical fits to sets of photoionization models with stars of different equivalent effective temperatures from WM-Basic (left) and Tlusty (right).

In the ideal case of a blackbody it only has a linear relation with the slope of the SED, but for young massive star atmospheres it noticeably changes for different model atmospheres. In upper panels of Fig. 4.27 we show the SEDs of WM-Basic (Pauldrach et al. [2001] with an expanding spherical geometry) at left and Tlusty (Hubeny & Lanz [1995], with a plane-parallel geometry) at right for the same value of T_* (40000 K) and different values of the metallicity. The slope and the shape of the SEDs can be very different in the energetic range covered by the optical η parameter (Simón-Díaz & Stasińska [2008]). An alternative to the optical η parameter was proposed for the mid-infrared spectral range with emission lines of [NeII] (12.8 μm), [NeIII] (15.6 μm), [SIII] (18.7 μm), and [SIV] (10.5 μm) (Martín-Hernández et al. [2002]; Morisset et al. [2004]), but this involves an even more energetic range between the ionization potentials of S^{2+} (I.P. = 34.8 eV) and Ne^+ (I.P. = 40.5 eV), where discrepancies between the different synthesis model atmospheres are larger (see Pérez-Montero & Vílchez [2009], for a more detailed discussion).

In the lower panels of Fig. 4.27 we show the relation between the optical emission-line ratios of oxygen ([OII]/[OIII]) and sulphur ([SII]/[SIII]) for a sample of objects with emission-line-like spectra compiled by Pérez-Montero & Vílchez [2009]. The solid lines are quadratical fits to different sets of Cloudy (Ferland et al. [1998]) photoionization models with different values of T_* (from 35 kK to 50 kK). At left, these models are calculated using WM-Basic stellar atmospheres and, at right, Tlusty (see Pérez-Montero & Vílchez to see a deeper descripion of these models). As can be seen, there are substantial differences between the two studied synthesis model atmospheres. These differences prevent an accurate determination of the absolute value of T_* in HII regions but, apparently, allow a good relative characterization for different families of objects. In both panels, Circumnuclear Star-Forming Regions (CNSFRs) and HII galaxies have the higher temperatures and, in contrast, smaller regions in our Galaxy and the Magellanic Clouds have lower temperatures.

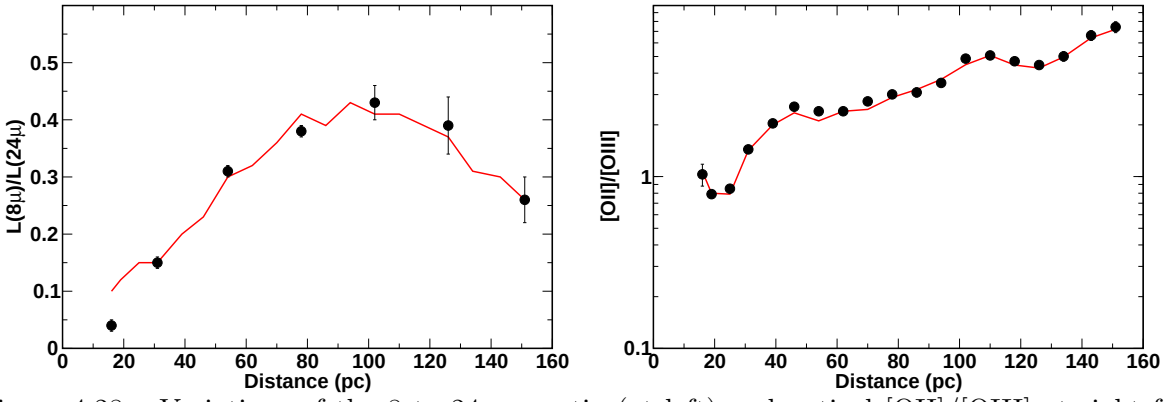

Figure 4.28: Variations of the 8 to 24 μm ratio (at left) and optical [OII]/[OIII] at right for different elliptical apertures around the central ionizing cluster in the giant HII region NGC 595. Black points represent the observed properties and the red solid line the results from tailored photoionization models for each of these apertures (from Pérez-Montero et al. [2011]).

The case of NGC 595

One of the possible caveats when using the η parameter to find out T_* in massive star clusters is that the information comes from the ionized gas. This implies that possible variations in the properties of the gas other than the functional parameters, such as gas geometry or density, or dust structure could also affect to the η parameter.

As a test to check to what extent these variations can affect the determination of T_* we use the Cloudy photoionization models of the 2D structure of the giant HII region NGC 595 (Pérez-Montero et al. [2011]). The observational input for these models comes from integral field spectroscopy taken with the PMAS instrument at the CAHA 3.5m telescope in the optical range between 3700 Å - 6800 Å (Relaño et al. [2010]) and photometric information from Spitzer space observatory at 8 and 24 μm filters. In these models a single ionizing source for all the HII region according to the properties of the CMD diagram derived by Malumuth et al. [1996] was assumed. These models reproduce the variations in the optical and mid-IR properties for different elliptical aperture regions with similar observational properties by assuming different matter-bounded geometries combined with different dust-to-gas ratios, in good agreement with the dust-to-gas ratio derived in the integrated region (Pérez-Montero et al. [2011]). In Fig. 4.28, we show the comparison between the models and the observations in each elliptical aperture.

In Fig. 4.29 we show the relation between the two optical emission-line ratios [OII]/[OIII] and [SII]/[SIII] involved in the η parameter with the fits to the photoionization models with Tlusty atmospheres shown in the lower right panel of Fig. 4.27. The black circles represent the values derived from the tailored models for each region in NGC 595. As can be seen, with the exception of some models, the most part of the elliptical apertures lie in regions consistent with a single value of T_* across the nebula, independently from the inner variations in the geometry of the gas and in the dust-to-gas ratio. The value of T_* (between 35 kK and 40 kK) is consistent to the value associated with the properties of the cluster derived by Malumuth using a CMD diagram, which is around 40 kK. It must be noted, however, that neither the slope of the grid of models for NGC 595 nor the slopes of the grids of models for different T_* are equal to 1, which is the value of the slope for the lines with different η across the diagram, so this implies that this parameter must not be used one-dimensionally. On the contrary, its analysis must be undertaken using a 2D approach as in this case. For instance, in the models of NGC 595, there is a variation in η of a factor 2 which is not contradictory with an homogeneous value of T_* in the models.

Conclusions

The determination of properties of a massive young stellar cluster can be obtained by using information from the emission line spectrum from the ionized gas in those cases where the stellar population of the cluster cannot be resolved. The η parameter as analyzed in 2 dimensions is a robust method to derive the equivalent effective temperature of a cluster, even in those cases where there are variations in the geometry of the gas or in the dust-to-gas ratio. The most important caveat appears as a consequence of the disagreements in the involved energetic ranges between different synthesis model atmospheres, but it

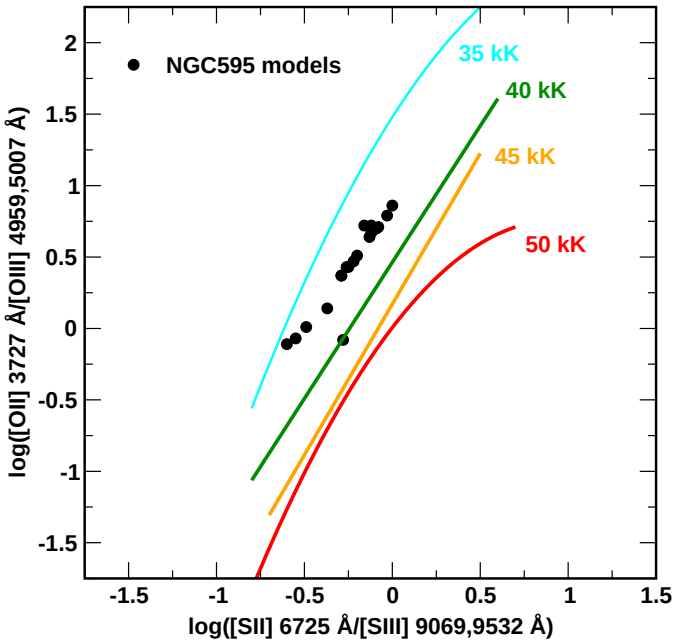

Figure 4.29: Relation between the optical emission-line ratios [OII]/[OIII] and [SII]/[SIII]. Solid lines represent the same fits to grids of photoionization models of different T_* for Tlusty atmospheres represented in Fig. 4.27. Black circles represent the models for NGC 595 derived by Pérez-Montero et al. [2011].

is possible to use this to study the relative variations of T_* in homogeneous samples of objects. This is the case of the variation of T_* across spiral disks found by Pérez-Montero & Vílchez [2009], which points to a hardening of the ionizing radiation above all in spiral galaxies of low dynamical mass and luminosity with late morphological type.

Acknowledgments

This work has been supported by the projects AYA2007- 67965-C03-02 of the Spanish National Plan for Astronomy and Astrophysics and CSD2006 00070 "1st Science with GTC" of the Spanish Ministry of Science and Innovation (MICINN).

Bibliography

Ferland, G.J., Korista, K.T., Verner, D.A., Ferguson, J.W., Kingdom, J.B., & Verner, E.M., 1998, PASP, 110, 761
Hubeny, I., & Lanz, T., 1995, ApJ, 439, 875
Martín-Hernández, N. L:, Vermeij, R., Tielens, A.G.G.M., van der Hulst, J.M., & Peeters, E., 2002, A&A, 389, 286
Malumuth, E.M., Waller, W.H., & Parker, J.W., 1996, AJ, 111, 1128
Morisset, C., Schaerer, D., Bouret, J.-C., & Martins, F., 2004, A&A, 415, 577
Pauldrach, A.W.A., Hoffmann, T.L., & Lennon, M., 2001, A&A, 425, 849
Pérez-Montero, E., Relaño, M., Vílchez, J.M., Monreal-Ibero, A., 2011, MNRAS, 412, 675
Pérez-Montero, E. & Vílchez, J.M., 2009, MNRAS, 400, 1721
Relaño, M., Monreal-Ibero, Vílchez, J.M., & Kennicutt, R.C., 2010, MNRAS, 402, 1635
Simón-Díaz, S., & Stasińska, G., 2008, MNRAS, 389, 1009
Vílchez, J.M., Pagel, B.E.J., 1988, MNRAS, 231, 257

4.10 Radiative Feedback in Massive Star and Cluster Formation

Thomas Peters[1], R. S. Klessen[1], M.-M. Mac Low[2], and R. Banerjee[1,3]

[1] Zentrum für Astronomie der Universität Heidelberg, Institut für Theoretische Astrophysik, Albert-Ueberle-Str. 2, D-69120 Heidelberg, Germany
[2] Department of Astrophysics, American Museum of Natural History, 79th Street at Central Park West, New York, New York 10024-5192, USA
[3] Hamburger Sternwarte, Gojenbergsweg 112, D-21029 Hamburg, Germany

Abstract

Understanding the origin of high-mass stars is central to modern astrophysics. We shed light on this problem with simulations using a novel, adaptive-mesh, ray-tracing algorithm. These simulations consistently follow the gravitational collapse of a massive molecular cloud core, the subsequent build-up and fragmentation of the accretion disk surrounding the nascent star, and, for the first time, the interaction between its intense UV radiation field and the infalling material. We show that ionization feedback can neither stop protostellar mass growth nor suppress fragmentation. We discuss the effects of feedback by ionizing and non-ionizing radiation on the evolution of the stellar cluster. The accretion is not limited by radiative feedback but by the formation of low-mass companions in a process we call "fragmentation-induced starvation". This behaviour consistently reproduces the observed relation between the most massive star and the total mass of stars in a cluster. We show that magnetic fields reduce the star formation rate and lead to the formation of more massive stars.

Introduction

High-mass stars form in denser and more massive cloud cores (Motte et al. [2008]) than their low-mass counterparts (Myers et al. [1986]). High densities also result in local gravitational instabilities in the accretion flow, resulting in the formation of multiple additional stars (Klessen & Burkert [2000]; Kratter & Matzner [2006]). Young massive stars are almost always observed to have companions (Ho & Haschick [1981]), and the number of their companions significantly exceeds those of low-mass stars (Zinnecker & Yorke [2007]). Such companions influence subsequent accretion onto the initial star (Krumholz et al. [2009]). Observations show an upper mass limit of about $100\,\mathrm{M}_\odot$. It remains unclear whether limits on internal stability or termination of accretion by stellar feedback determines the value of the upper mass limit (Zinnecker & Yorke [2007]).

The most significant differences between massive star formation and low-mass star formation seem to be the clustered nature of star formation in dense accretion flows and the ionization of these flows. We present the first three-dimensional simulations of the collapse of a molecular cloud to form a cluster of massive stars that include ionization feedback by Peters et al. [2010a,c,b, 2011], allowing us to study these effects simultaneously.

Numerical Method and Initial Conditions

We present the first three-dimensional, radiation-(magneto-)hydrodynamical simulations of massive star formation, taking into account heating by both ionizing and non-ionizing radiation, using the adaptive-mesh code FLASH (Fryxell et al. [2000]). We propagate the radiation on the adaptive mesh with our extended version of the hybrid characteristics raytracing method (Rijkhorst et al. [2006]; Peters et al. [2010a]). We use sink particles (Federrath et al. [2010]) to model young stars. Sink particles are inserted when the Jeans length of collapsing gas can no longer be resolved on the adaptive mesh. They continue to accrete any high-density gas lying within their accretion radius. We use the sink particle mass and accretion rate to determine the radiation feedback with a prestellar model (Peters et al. [2010a]). A

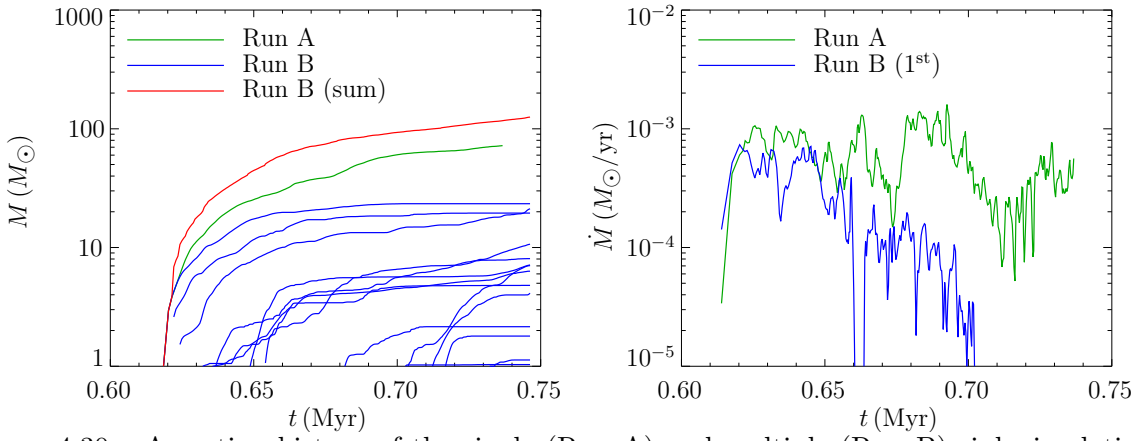

Figure 4.30: Accretion history of the single (Run A) and multiple (Run B) sink simulations. Run A was stopped at 72 $M_\odot$, while no sink particle in Run B exceeds 25 $M_\odot$ over the simulation runtime. The left hand plot shows the sink particle masses for Run A (green), the individual sink masses of Run B (blue) as well as the total mass in sink particles in Run B (red). The right hand plot shows the accretion rates of the sink particle in Run A (green) and the sink particle which forms first in Run B (blue), which also turns out to end up as the most massive at the end of the simulation. While the accretion rate in Run A never drops below $10^{-5}\,M_\odot\,\mathrm{yr}^{-1}$, accretion onto the most massive sink can drop significantly below this value and even be stopped totally in Run B.

detailed description of our numerical method and the underlying assumptions can be found in Peters et al. [2010a].

We start our simulations with a 1000 $M_\odot$ molecular cloud having a constant density core with $\rho = 1.27 \times 10^{-20}$ g cm^{-3} within a radius of $r = 0.5$ pc, surrounded by an $r^{-3/2}$ density fall-off out to $r = 1.6$ pc. The cloud rotates as a solid body with an angular velocity $\omega = 1.5 \times 10^{-14}\,\mathrm{s}^{-1}$. The initial temperature is $T = 30$ K. The highest resolution cells on our adaptive mesh have a size of 98 AU. Sink particles are inserted at a cut-off density of $\rho_{\mathrm{crit}} = 7 \times 10^{-16}\,\mathrm{g\,cm}^{-3}$ and have an accretion radius of $r_{\mathrm{sink}} = 590$ AU.

We compare the results of four different simulations. In the first simulation (Run A), a dynamical temperature floor is introduced to suppress secondary fragmentation. Only one sink particle (representing a massive protostar) is allowed to form. In the second simulation (Run B), secondary fragmentation is allowed, and many sink particles form, representing a group of stars, each contributing to the radiative feedback. The third simulation (Run D) is a control run in which secondary fragmentation is still allowed, but no radiation feedback is included. The fourth simulation (Run E) is a magnetized version of Run B, the full stellar group simulation with radiation feedback from all stars. Run E includes an initially homogeneous magnetic field along the rotation axis of the cloud with a magnitude of 10 μG, corresponding to a mass-to-flux ratio $(M/\Phi) = 14(M/\Phi)_{\mathrm{cr}}$ in the central core at the beginning of the simulation. See Peters et al. [2010b] and Peters et al. [2011] for a thorough discussion of these initial conditions.

Fragmentation-Induced Starvation

We first examine the accretion histories of our different models. Fig. 4.30 shows that in Run A, with only one sink particle allowed to form, nothing halts accretion onto the central protostar. It continues to grow at an average rate of $\dot{M} \approx 5.9 \times 10^{-4}\,M_\odot\,\mathrm{yr}^{-1}$ until we stop the calculation when the star has reached 72 $M_\odot$. The increasingly massive star ionizes the surrounding gas, raising it to high pressure. This gas breaks out above and below the disk plane, but it cannot halt mass growth through the disk[3] mid-plane.

In contrast, in Run B, where multiple sink particles are allowed to form, two subsequent sink particles form and begin accreting soon after the first one, and many more follow within the next 10^5 yr (see Fig. 4.30). By that time the first sink has accreted 8 $M_\odot$. Within another 3×10^5 yr seven further fragments have formed, with masses ranging from 0.3 $M_\odot$ to 4.4 $M_\odot$ while the first three sink particles

[3]We will hereafter refer to the flattened, dense, accretion flow that forms in the midplane of our rotating core as a disk. However, it is not necessarily a true Keplerian, viscous, accretion disk, which probably only forms within the central few hundred astronomical units, unresolved by our models.

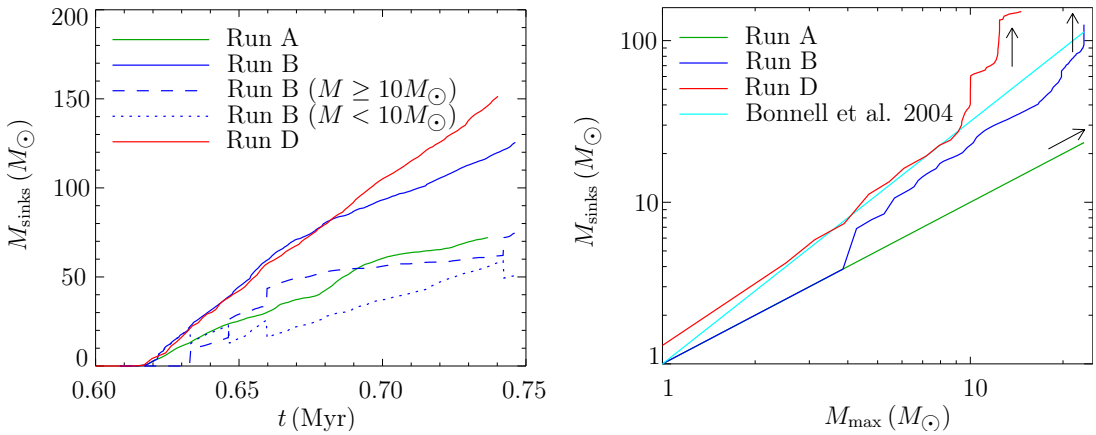

Figure 4.31: *Left*: Total accretion history of all sink particles combined forming in Runs A, B, and D. While the heating by non-ionizing radiation does not affect the total star formation rate, the ionizing radiation appreciably reduces the total rate at which gas converts into stars once the most massive object has stopped accreting and its H II region can freely expand. The slope of the total accretion history in Run B goes down because the massive stars (dashed line) accrete at a decreased rate, while the low-mass stars (dotted line) keep accreting at the same rate. *Right*: The total mass in sink particles $M_{\rm sinks}$ as a function of the most massive star in the cluster $M_{\rm max}$. We plot the curves for Run A, Run B and Run D as well as the fit from the competitive accretion simulations by Bonnell et al. [2004]. The turn-off away from the scaling relation (indicated by arrows) is shifted towards higher masses by radiative feedback.

have masses between $10\,\mathrm{M}_\odot$ and $20\,\mathrm{M}_\odot$, all within a radius of 0.1 pc from the most massive object. Accretion by the secondary sinks terminates the mass growth of the central massive sinks. Material that moves inwards through the disk driven by gravitational torques accretes preferentially onto the sinks at larger radii (Bate [2002]). Eventually, hardly any gas makes it all the way to the center to fall onto the most massive objects. This fragmentation-induced starvation prevents any star from reaching a mass $> 25\,\mathrm{M}_\odot$ in this case.

Fig. 4.30 also reveals that the most massive stars in the cluster are those which form first and then keep accreting at a high rate. The most massive stars in Run B are the same for all times, but their mass keeps increasing during the formation of the stellar cluster.

The accretion behaviour in Run B contrasts sharply with competitive accretion models (Bonnell et al. [2001]; Bonnell et al. [2004]), which have no mechanism to turn off accretion onto the most massive stars. In these models, material falls all the way down to the massive stars sitting in the center of the gravitational potential which thereby take away the gas from the surrounding low-mass stars. In our fragmentation-induced starvation scenario, exactly the opposite happens. Fig. 4.31 illustrates that, although the accretion rates of the most massive stars ($M \geq 10\,\mathrm{M}_\odot$) steadily decrease, the low-mass stars ($M < 10\,\mathrm{M}_\odot$), keep accreting at the same rate.

Competitive accretion models show a correlation between the mass of the most massive star $M_{\rm max}$ and the total cluster mass $M_{\rm sinks}$ during the whole cluster evolution that is roughly $M_{\rm max} \propto M_{\rm sinks}^{2/3}$ (Bonnell et al. [2004]). This correlation has been argued to represent a way to observationally confirm competitive accretion (Krumholz & Bonnell [2009]) and is in fact in good agreement with observations (Weidner & Kroupa [2006]; Weidner et al. [2010]). However, we find that our simulations also reproduce the observed relation between $M_{\rm max}$ and $M_{\rm sinks}$.

Fig. 4.31 shows $M_{\rm sinks}$ as function of $M_{\rm max}$ for Run A, Run B and Run D, and the relation $M_{\rm max} = 0.39 M_{\rm sinks}^{2/3}$, which was found by Bonnell et al. [2004] as a fit to their simulation data. Over the whole cluster evolution, the curve for Run D lies above this fit, while the curve for Run B always lies below it. The fit agrees with our simulation data as well as it does to that of Bonnell et al. [2004]. This indicates that the scaling is not unique to competitive accretion, but can also be found with the fragmentation-induced starvation scenario and hence cannot be used as an observational confirmation of competitive accretion models.

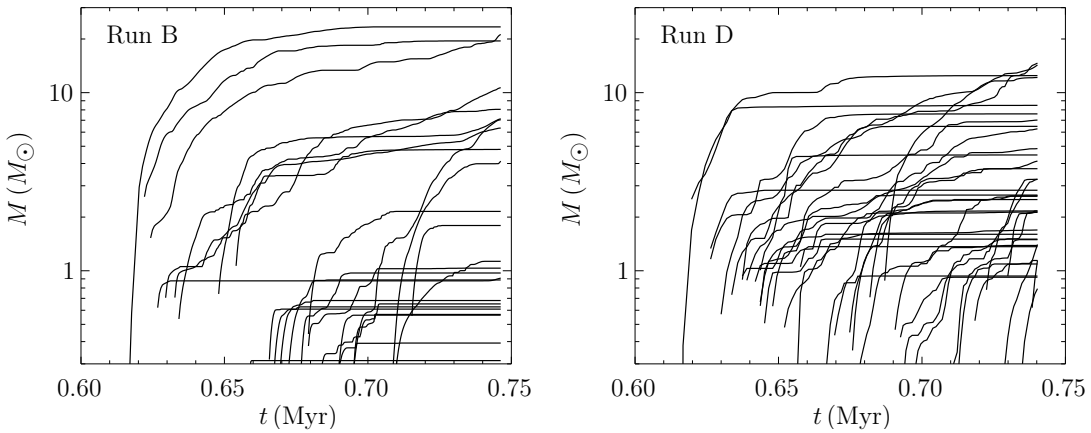

Figure 4.32: Individual accretion histories for Run B and Run D. The figure shows the stellar masses as function of time for all sink particles that form in Run B (left) and Run D (right). Because the Jeans mass is lower without radiative feedback (Run D), many more sink particles form in Run D than in Run B, and the mass of the most massive stars is also lower.

Effects of Radiative Feedback and Magnetic Fields

Fig. 4.32 shows the individual accretion histories of each of the sink particles in Run B and Run D. Radiative heating cannot prevent disk fragmentation but raises the local Jeans mass. Hence, many fewer stars form in Run B than in Run D, and the mass of the most massive stars in Run B is higher. It is also evident from the figure that star formation is much more intermittent in the case with radiation feedback (Run B). The reason for this behavior is that the star formation process is controlled by the local Jeans mass, which depends to a large degree on how the filaments in the disk shield the radiation. Shielding can lower the Jeans mass temporarily and thereby allow gravitational collapse that would not have occurred otherwise.

Since the accretion heating raises the Jeans mass and length in Run B, the total number of sink particles is higher in Run D than in Run B, and the stars in Run D generally reach a lower mass than in Run B. These two effects cancel out to lead to the same overall star formation rate for some time (see Fig. 4.31). At one point in the evolution, however, also the total accretion rate of Run B drops below that of Run D. At time $t \approx 0.68\,\mathrm{Myr}$ the accretion flow around the most massive star has attenuated below the value required to trap the H II region. It is able to break out and affect a significant fraction of the disk area. A comparison with the mass growth of Run D clearly shows that there is still enough gas available to continue constant cluster growth for another 50 kyr or longer, but the gas can no longer collapse in Run B. Instead, it is swept up in a shell surrounding the expanding H II region.

It is also notable that the expanding ionization front around the most massive stars does not trigger any secondary star formation, which suggests that triggered star formation (Elmegreen & Lada [1977]) may not be as efficient as expected, at least on the scales considered here.

The total accretion histories of all sink particles combined in each of the four simulations are contrasted in Fig. 4.33. For the first 20 kyr, the total accretion rate of Run B, Run D and Run E is nearly identical. The accretion rate in these multiple sink simulations is generally higher than in the single sink Run A since the large group of sinks accretes from a large volume, without needing to rely on outward angular momentum transport to deliver material to the direct feeding zone of the central sink. In the magnetized Run E, no secondary sink particles form during the first 20 kyr, so that the increased accretion rate in this phase is due to the additional angular momentum transport performed by the magnetic field. After the initial 20 kyr, the total accretion rate in Run E falls below Run B and the control Run D, deviating increasingly with time, but always staying above the accretion rate in Run A. The accretion histories of Run B and Run D only start to separate at relatively late time when the ionizing radiation begins to terminate accretion onto the most massive sinks in Run B (see the discussion in Peters et al. [2010b]), but the magnetic field additionally reduces the rate at which gas collapses in Run E. Thus, the total accretion rate with magnetic fields is lower than without magnetic fields.

The central star in Run E can grow to larger masses because in the initial phase fragmentation is delayed by magnetic support. This allows the central object to maintain a high accretion rate for a longer time. Nevertheless, the accretion rate of the massive star in Run E drops significantly when secondary

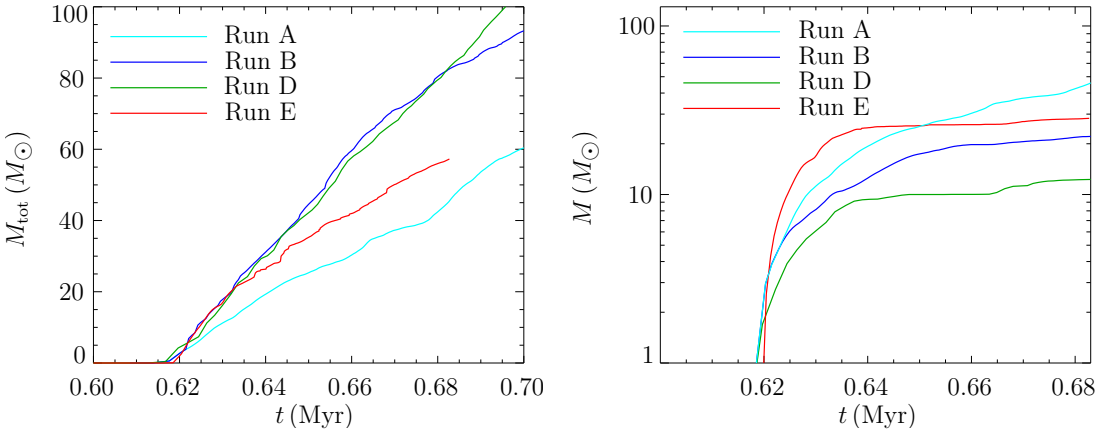

Figure 4.33: *Left*: Total accretion history of Run A, Run B, Run D and Run E. While the total accretion rates of Run B and Run D agree until ionization feedback stops massive star formation in Run B, the total accretion rate in Run E already starts to decline after 20 kyr. The magnetic field in Run E additionally supports the gas against collapse, reducing the total accretion rate. *Right*: Protostellar masses of the first sink particles in Run A, Run B, Run D and Run E. Radiative heating (Run B) and presence of magnetic fields (Run E) increase the final masses of the massive stars. The largest part of the additional mass accretion in Run E compared to Run B is due to the stronger initial accretion phase.

sink particles form, since they form in a dense ring around the central massive sink and to some extent starve it of material, even though they never cut off accretion entirely.

The stronger initial accretion phase in Run E compared to Run B yields the main contribution to the larger final mass of the massive sink. The magnetic field very efficiently redistributes angular momentum, resulting in an increased radial mass flux through the high-density equatorial plane. Consequently, the initial accretion rate in the magnetized simulation (Run E) even lies considerably above the non-magnetized single sink calculation (Run A).

Conclusions

We have reviewed some of the results of our recent radiation-(magneto-)hydrodynamical simulations of massive star formation (Peters et al. [2010a]; Peters et al. [2010c]; Peters et al. [2010b]; Peters et al. [2011]), which for the first time simultaneously include the effect of heating by both ionizing and non-ionizing radiation. We find that ionization feedback is unable to stop protostellar mass growth. Instead, the mass of the most massive stars is limited by the formation of lower-mass companions in their gravitationally unstable accretion flow in a process we call fragmentation-induced starvation. Our numerical model reproduces the observed relation between the most massive star in a cluster and the total cluster mass. We find that heating by non-ionizing radiation decreases the total number of stars formed and increases the mass of the most massive stars, but does not change the total star formation rate. The star formation rate is reduced by ionizing radiation once the H II regions can steadily expand. Even initially very weak magnetic fields can markedly reduce the star formation rate by providing additional support against gravitational collapse and lead to the formation of more massive stars via magnetic braking of the accretion flow.

Bibliography

Bate, M. R. 2002, MNRAS, 314, 33
Bonnell, I. A., Bate, M. R., Clarke, C. J., & Pringle, J. E. 2001, MNRAS, 323, 785
Bonnell, I. A., Vine, S. G., & Bate, M. R. 2004, MNRAS, 349, 735
Elmegreen, B. G. & Lada, C. J. 1977, ApJ, 214, 725
Federrath, C., Banerjee, R., Clark, P. C., & Klessen, R. S. 2010, ApJ, 713, 269

Fryxell, B., Olson, K., Ricker, P., Timmes, F. X., Zingale, M., Lamb, D. Q., MacNeice, P., Rosner, R., Truran, J. W., & Tufo, H. 2000, ApJS, 131, 273
Ho, P. T. P. & Haschick, A. D. 1981, ApJ, 248, 622
Klessen, R. S. & Burkert, A. 2000, ApJS, 128, 287
Kratter, K. M. & Matzner, C. D. 2006, MNRAS, 373, 1563
Krumholz, M. R. & Bonnell, I. A. 2009, in Structure Formation in Astrophysics, ed. G. Chabrier (Cambridge: Cambridge Univ. Press), 288
Krumholz, M. R., Klein, R. I., McKee, C. F., Offner, S. S. R., & Cunningham, A. J. 2009, Science, 323, 754
Motte, F., Bontemps, S., Schneider, N., Schilke, P., & Menten, K. M. 2008, in Astronomical Society of the Pacific Conference Series, Vol. 387, Massive Star Formation: Observations Confront Theory, ed. H. Beuther, H. Linz, & T. Henning, 22–29
Myers, P. C., Dame, T. M., Thaddeus, P., Cohen, R. S., Silverberg, R. F., Dwek, E., & Hauser, M. G. 1986, ApJ, 301, 398
Peters, T., Banerjee, R., Klessen, R. S., & Mac Low, M.-M. 2011, ApJ, 729, 72
Peters, T., Banerjee, R., Klessen, R. S., Mac Low, M.-M., Galván-Madrid, R., & Keto, E. R. 2010a, ApJ, 711, 1017
Peters, T., Klessen, R. S., Mac Low, M.-M., & Banerjee, R. 2010b, ApJ, 725, 134
Peters, T., Mac Low, M.-M., Banerjee, R., Klessen, R. S., & Dullemond, C. P. 2010c, ApJ, 719, 831
Rijkhorst, E.-J., Plewa, T., Dubey, A., & Mellema, G. 2006, A&A, 452, 907
Weidner, C. & Kroupa, P. 2006, MNRAS, 365, 1333
Weidner, C., Kroupa, P., & Bonnell, I. A. D. 2010, MNRAS, 401, 275
Zinnecker, H. & Yorke, H. W. 2007, ARAA, 45, 481

4.11 On the Large-Scale Distribution of Massive Stars

Jan Pflamm-Altenburg[1] **and S. Oh**[1]

[1] Argelander-Institut für Astronomie, Auf dem Hügel 71, D-53121 Bonn, Germany

Abstract

Massive stars are believed to form in star clusters but are also found in the Galactic field. Ejections of massive stars from their birth sites due to close encounters between and due to supernova-disruption of multiple-high-mass star systems are thought to be responsible for the presence of high-mass field stars. So far only individual massive stars have been traced back to their parent star cluster. But it has not been clarified whether the dynamical processes in star clusters can account for both the spatial large-scale distribution and the number frequency of massive field-stars. Here we present first results of dynamical population synthesis models of massive stars on Galaxy-wide scales. These models will serve as a theoretical basis for the upcoming Gaia space mission in order to derive constraints on the birth places of high-mass stars.

Introduction

High-mass stars are found in compact young star clusters as well as in the Galactic field. There are no doubts that massive stars which are observed in star clusters have formed there. But in the case of massive stars in the Galactic field it is debated whether they have formed there or they have been ejected from stars clusters. Ejections of massive stars are possible due to two processes: i) The explosion of a component of a massive binary as a supernova releases the companion with nearly orbital velocity. ii) Close encounters between massive star binaries lead to ejections of massive stars.

Once they have left the star cluster they move in the Galactic potential and basically all stars ejected by these processes can be traced back to their parent star cluster. But very few Galactic field high-mass stars can currently not be traced back to any star cluster (Schilbach & Röser [2008]). Combining both ejection scenarios, i.e. the dynamical ejection of a massive binary from a star cluster with a subsequent supernova ejection, which is called two-step ejection, produces massive runaways which cannot be traced back to their parent star clusters (Pflamm-Altenburg & Kroupa [2010]). At the moment no convincing evidence exists that massive stars can form in isolation (see conference contribution by Carsten Weidner, Weidner et al. submitted).

So far, the issue of massive runaway stars has only been considered for individual cases, i.e. whether or not a particular massive field star can have its origin in a star cluster. E.g. in the case of the runaways AE Aurigae and μ Columbae, and the massive binary ι Orionis, a possible common dynamical origin 2.5 Myr ago was demonstrated (Gualandris et al. [2004]).

On the other hand, the quantitative aspect of massive runaways has been addressed only in a few studies: Clarke & Pringle [1992] deduced using an analytical approach that massive stars must form in compact small-N groups in order to explain the number of massive runaway. Pflamm-Altenburg & Kroupa [2006] show that very compact cores of O and B stars can loose up to 50 per cent of their massive stars within 2 Myr. But a detailed study to determine if ejection processes in star clusters are in general able to also account quantitatively for the observed number of massive runaways still remains to be performed.

Ejection fraction of massive stars

In order to address the question if standard dynamical processes in young star clusters are capable to account quantitatively for the observed Galactic massive runaways, the ejection probability of high-mass stars from young star clusters has to be quantified first for the whole observed parameter range of star cluster properties.

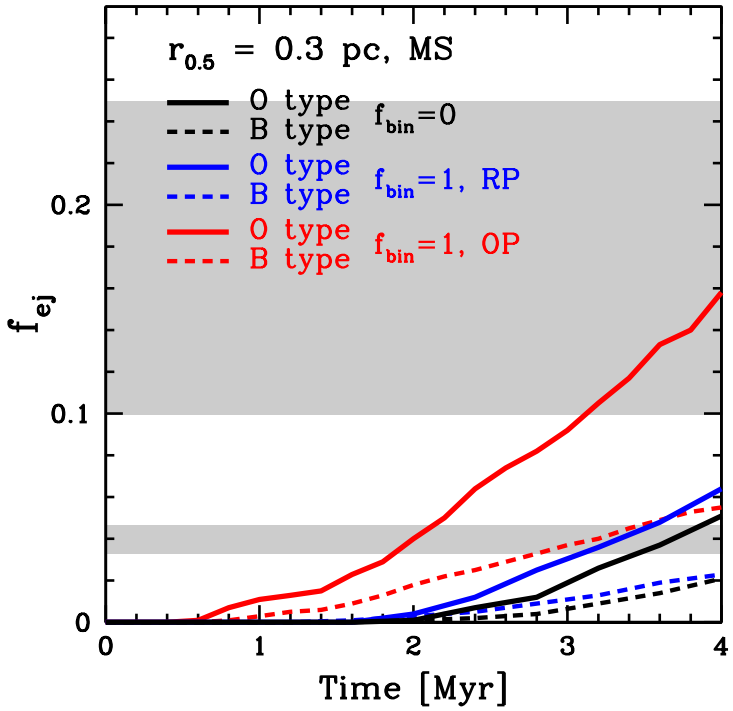

Figure 4.34: Shown is the fraction of O (solid lines) and B-type (dashed lines) stars which are ejected from a primordially mass segregated star cluster with a total stellar mass of $10^{3.5}$ $M_\odot$, an initial half-mass radius of 0.3 pc, as a function of time. For this type of star cluster models with different massive star binary populations the following are compared: with no initial binaries (black), with an initial binary fraction of $f_{\rm bin}$=1 and random pairing (RP) of the binaries (blue), and with $f_{\rm bin}$=1 and ordered pairing (OP) of the binaries (red). Each curve is the average over 100 N-body simulations. (See text for details).

The ejection probability of a massive star from young star clusters is expected to depend on several properties of both the whole star cluster and the population of massive-star binaries, as for example the IMF, the star cluster mass, star cluster initial half-mass radius, the star formation efficiency, the gas expulsion time scale, and mass ratio and period distributions of massive-star binaries.

The full set of dynamical data will be made publicly available as the Bonn-Star-Cluster-Library, which is growing continuously. First results will be published soon (Oh. et al – in prep.). The data bank will list the ejection fractions and the ejection velocity spectra of high-mass stars as a function of their mass and evolutionary time.

Fig. 4.34 shows the example of the ejection fraction of O (solid lines) and B stars (dashed lines) as a function of time of an initially mass-segregated star cluster with a total stellar mass of $10^{3.5}$ $M_\odot$ and a half-mass radius of 0.3 pc and for three different initial binary populations: no primordial binaries (black), a primordial binary frequency of 100 per cent with random pairing (RP, blue), and a primordial binary frequency of 100 per cent with ordered pairing (OP, red).

In the case of random pairing (RP) stars are drawn randomly from the IMF with an upper mass limit determined by the star cluster mass (Weidner et al. [2010]) and paired randomly. In the case of ordered pairing (RP) stars are drawn randomly from the IMF and ordered with respect to their mass. Then the most-massive and the second massive star are paired, the third-massive star and the fourth-massive star are paired .... Below 5 $M_\odot$ the stars are paired randomly. This type of paring produces a massive-binary population with nearly unity mass-ratios.

The ejection fractions are lowest for the case of no primordial binaries (black curves). In this case the binaries required for dynamical ejections have to be produced dynamically first taking a few crossing times.

If the star cluster contains primordial binaries than close encounters between them can immediately lead to ejection of stars. But surprisingly, an initial binary population which has been created with random sampling does not accelerate the ejection process of massive stars significantly compared with models with no primordial binaries.

The reason is that binaries created with random pairing consist of massive stars with low-mass companions as low-mass stars are much more frequent than high-mass stars. Therefore, it is most-likely that a massive star is paired with a low-mass star. Scattering events between such binaries typically lead to the ejection of the lightest stars leaving massive binaries behind, i.e. a massive star with a massive companion. Thus, in both cases (no primordial binaries and 100 per cent primordial binary fraction and random pairing) massive binaries have to be produced first dynamically, which takes nearly the same time.

In models with 100 per cent initial binary fraction and ordered pairing (red curves) massive stars are ejected immediately as massive binaries do not have to be produced dynamically first.

A general result is that, independent of the initial binary properties, the ejection fractions of O stars are always higher than the ejection fractions of B stars. On first sight, it would be expected that lower mass stars are ejected preferentially and the fraction of ejected B stars should be higher than the ejection fraction of O stars. But as a result of mass-segregation, O stars are more concentrated than less-massive B stars. Thus, the close encounter probability among O stars is higher than among B stars.

The upper (lower) gray shaded area marks the 10 – 25 per cent ($\approx$ 4 per cent) runaway fraction of O stars (B stars) as given in Clarke & Pringle [1992]. For this type of star clusters only models with a primordial binary fraction of 100 per cent and ordered pairing are in quantitative agreement with the observations.

Although a realistic modelling of the Galactic runaway population needs the full star cluster spectrum to be taken into account, it is not expected that the required binary properties will be too different.

Large-scale distribution of massive stars

The calculation of the large-scale distribution of massive stars requires to embed the resulting star cluster library in a Galactic orbit integration code. As the star-cluster library is still not complete first results are applied to all star clusters.

This is modelled as follows: The Milky Way is represented by a radially symmetric gas distribution and a constant star formation rate (SFR) of 1 $M_\odot$/pc. Star clusters are drawn from the embedded cluster mass function with an upper mass limit determined by the SFR (Weidner et al. [2004]). A birth time, an initial position and velocity vector are assigned to each star cluster. They are populated with stars drawn from a canonical IMF (Kroupa [2001]). In order to reduce the enormous number of stars only those with masses larger than 8 $M_\odot$ are considered in the model. An ejection direction, an ejection velocity, and the moment of ejection is assigned to each star. The orbits of all stars are integrated in the Milky Way potential by Allen & Santillan [1991].

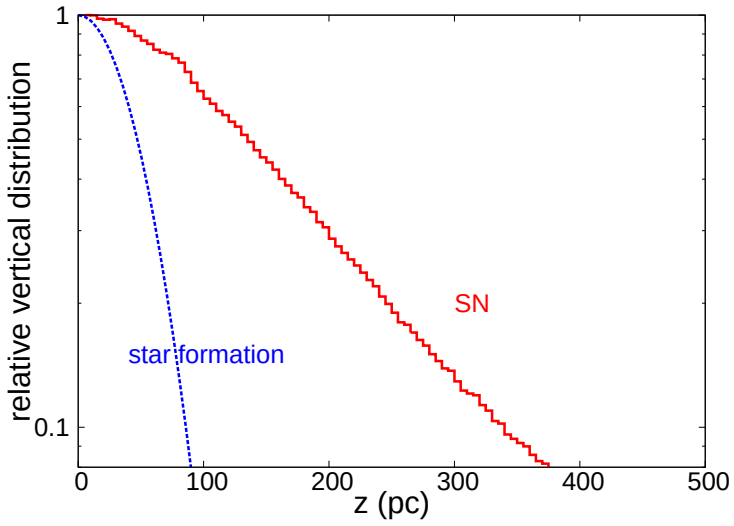

Figure 4.35: Shown are the vertical distribution of massive star supernovae and the vertical distribution of the underlying star formation. Single supernovae occur up to $\sim$ 3.5 kpc above the plane (Pflamm-Altenburg, in prep.).

As a first result the vertical supernova distribution is plotted in Fig. 4.35. The star formation layer (blue dashed line), described by a Gaussian distribution with a dispersion of 40 pc, reaches one tenth of the central value at a vertical distance of ≈ 90 pc. Due to ejections of massive stars the vertical supernovae layer (red curve) is much thicker than the star formation layer. Single supernovae occur up to ~ 3.5 kpc.

The dynamical modelling of the large-scale distribution of massive stars will not only provide a theoretical basis for constraining the properties of the birth places of massive stars but will very likely also lead to new insights on the chemical evolution of large disk and dwarf galaxies.

Bibliography

Allen, C. & Santillan, A. 1991, Revista Mexicana de Astronomia y Astrofisica, 22, 255
Clarke, C. J. & Pringle, J. E. 1992, mnras, 255, 423
Gualandris, A., Portegies Zwart, S., & Eggleton, P. P. 2004, mnras, 350, 615
Kroupa, P. 2001, mnras, 322, 231
Pflamm-Altenburg, J. & Kroupa, P. 2006, mnras, 373, 295
Pflamm-Altenburg, J. & Kroupa, P. 2010, mnras, 404, 1564
Schilbach, E. & Röser, S. 2008, aap, 489, 105
Weidner, C., Kroupa, P., & Bonnell, I. A. D. 2010, mnras, 401, 275
Weidner, C., Kroupa, P., & Larsen, S. S. 2004, mnras, 350, 1503

4.12 VLT–MAD Observations of Trumpler 14

Boyke Rochau[1], W. Brandner[1], A. Stolte[2], T. Henning[1], N. Da Rio[1,3], M. Gennaro[1], F. Hormuth[1], E. Marchetti[4] and P. Amico[4]

[1]Max-Planck-Institut für Astronomy, Königstuhl 17, 69115 D-Heidelberg
[2]Argelander Institut für Astronomie, Universität Bonn, Auf dem Hügel 71, 53121 D-Bonn
[3]Space Telescope Science Institute, 3700 San Martin Drive, Baltimore, MD 21218
[4]European Southern Observatory, Karl-Schwarzschild-Straße 2, 85748 D-Garching

Abstract

We present H and K_S observations of the young massive cluster Trumpler 14 obtained with the MCAO system VLT–MAD which provides homogeneous Strehl ratios over a large field of view. We derived maximum Strehl ratios of 9.8% and 12.6% with mean Strehl ratios of 6.0% and 5.9% with in H and K_S, respectively, revealing significant improvement of the spatial PSF stability compared to SCAO systems. We detected 2 – 3 times more sources than comparable seeing-limited observations, and comparison of the colour-magnitude diagram with isochrones reveals a very young cluster that originated in a starburst-like event 1 ± 0.5 Myr ago. We also tentatively detect hints for an older population of 3 Myr. The mass function between 0.25 $M_\odot$ and 3.2 $M_\odot$ appears as a broken power law with a change of the power law slope at $m_c \sim 0.53^{+0.12}_{-0.10}$ $M_\odot$. Shallow power law slopes are found to be $\Gamma_{\rm PD,PMS1} = -0.48 \pm 0.11$ above m_c and $\Gamma_{\rm PD,PMS2} = 0.68 \pm 0.30$ below m_c.

Introduction

Adaptive optics (AO) systems are outstanding in compensating atmospheric seeing. However, with single conjugated AO (SCAO) systems the AO correction is restricted to small field of views (FoV). In order to provide a more spatially stable performance over a larger field, multi-conjugate AO (MCAO) systems are required which use several guide stars (GS) to correct the blurring due to Earths atmosphere. The Multi-conjugate Adaptive optics Demonstrator (MAD) was developed in 2007 in the framework of 2nd generation instruments for the VLT and the E–ELT, and as the first MCAO system at the VLT to demonstrate the feasibility of MCAO systems (e.g. Marchetti et al. [2007]).

The proximity of NGC 3372, or Carina Nebula, provides an ideal testbed to assess the capability of VLT–MAD and its combination of high spatial resolution and the wide-field. NGC 3372, a Galactic giant molecular cloud, includes a population of young and massive clusters. The youngest cluster of the region is Trumpler 14 (hereafter Tr 14) incldluding a few 10^3 $M_\odot$ (Sana et al. [2010]) and several O-type stars, such as the O2If* star HD93129Aa (Walborn et al. [2002]). This puts it close to the regime of the Galactic starburst clusters like NGC 3603 YC or the Arches Cluster (e.g. Rochau et al. [2010]; Stolte et al. [2002]; resp.). Recent distance estimates place Tr 14 between $\sim$ 2 and 3 kpc (e.g. Tapia et al. [2003]; Carraro et al. [2004]; Ascenso et al. [2007]) and the age of the high-mass content is estimated to be around 1 – 2 Myr (Vazquez et al. [1996]). The formation of intermediate-mass stars probably started earlier. We were able to obtain MCAO assisted observations with VLT–MAD to investigate the young massive star cluster Tr 14 (PIs: H. Sana, B. Rochau). For further details I refer the reader to Rochau et al. [2011].

MAD

MAD is the first prototype MCAO system and has been developed for the VLT to demonstrate the feasibility of MCAO systems. With Natural Guide Stars (NGS) it corrects the blurring due to atmospheric turbulence over 2' on the sky. The MCAO correction uses two Deformable Mirrors (DM) and in the star-oriented mode, in which our observations have been processed using 3 NGS, it is supported by a Multi Shack–Hartmann wavefront sensor. CAMCAO (CAmera for MCAO) is the IR camera of MAD offering near-infrared broad- and narrow-band imaging and an image scale is 0.028 arcsec/pixel such that the

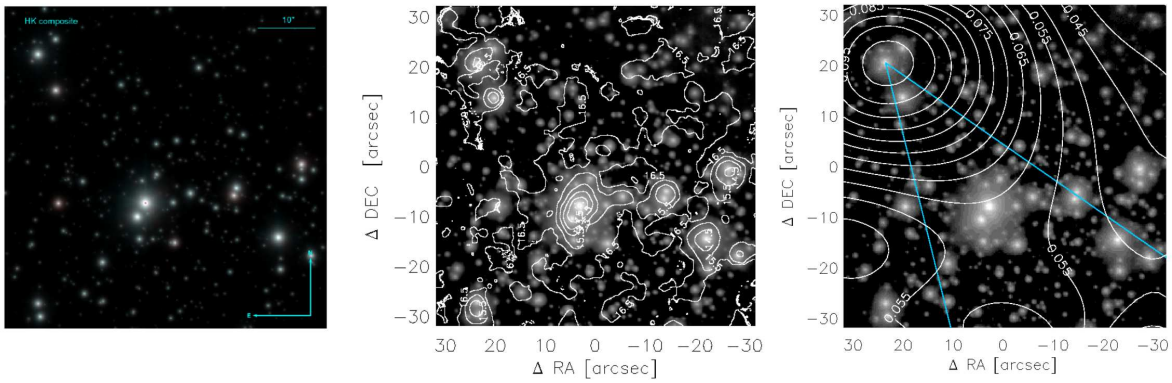

Figure 4.36: *Left*: HK_S colour composite of centre region of Tr 14 with HD93129Aa at $\alpha = 10^{\rm h}43^{\rm m}57.5^{\rm s}$, $\delta = -59°32'52.3"$. *Middle*: K_S-band image with contours showing the level of equal Strehl ratios. Blue lines show part of the triangle encircled by the GSs. *Right*: K_S-band completeness map. Contours correspond to the K_S-band magnitude at which a completeness of 70% is achieved. In each image North is up and east to the left.

camera covers a 59 ×59 arcsec^2 FoV (Amorim et al. [2006]). The 2 × 2 arcmin^2 FoV is covered by moving the camera with a closed AO loop while the telescope is tracking.

Observations and Photometry

The innermost region of Tr 14 was observed in H and K_S with a total integration time of 28 min. The final FoV covers an area of 68"×68" shown as a HK_S colour composite of Fig. 4.36 (left panel). We perform PSF photometry using IRAF/DAOPHOT (Stetson [1990]) with a 2nd order variable Penny-PSF. Comparison of our MAD photometry with seeing-limited NTT–SofI of Ascenso et al. [2007] reveals no trend of the zeropoint (ZP) with position, magnitude or colour and shows a scatter of 0.11 mag in H and 0.12 mag in K_S. This agrees very well with Sana et al. [2010] and, thus, we obtain high precision photometry across the entire FoV combining a 2nd order variable PSF with star-oriented MAD observations. The final catalogue of 972 stars (1347 if stars with $\sigma_{DAO} > 0.1$ mag are considered) includes 2 – 3 times as many sources when compared to the NTT–SofI observations (453 sources).

Intending to derive the present-day mass function (PDMF) of Tr 14, we require accurate knowledge of the photometric catalogue completeness. We carry out artificial star tests and apply the same technique as described in Gennaro et al. [2011]. This delivers the completeness $C(x, y, \mu) = \frac{\alpha(x,y)}{\exp(\frac{\mu-\beta(x,y)}{\gamma(x,y)})+1.}$ as a function of position (x,y) and magnitude (μ) of the star. The middle panel of Fig. 4.36 shows the 70% completeness limits at different magnitudes as contours superimposed to the K_S-band image. The absence of large scale structures shows that crowding effects are not severe. Together with the largely increased number of detections, this illustrates the improved performance of MAD.

Technical analysis

To assess the MCAO performance, we measure the Strehl ratio of the combined image across the field. Their distributions are shown in the right panel of Fig. 4.36 superimposed as contours and revealing a shallow decrease of the Strehl ratio over the FoV, indicated by mean Strehl ratios 6.0% for H and 5.9% for K_S. We simulated SCAO observations with the spatial variation of the Strehl ratio following $\mathrm{SR} = \mathrm{S_0}\exp(-[\frac{\Delta\Theta}{\Theta_{\rm iso}}]^{5/3})$ (Cresci et al. [2005]); $\mathrm{S_0}$ as the maximum Strehl ratio and an isoplanatic angle $\Theta_{\rm iso} = 15$ arcsec as a typical value of SCAO observations. Simulated mean Strehl values are only 1.6% and 2.0% in H- and K_S-band, respectively. SCAO observations usually provide higher peak Strehl ratios (9.8% (H-band) and 12.6% (K_S-band) in our observation), but a good characterization of the PSF at larger distances from the GS is difficult due to the decreasing performance with distance to the GS. Especially in crowding-limited regions, such as dense stellar clusters, this hampers the census of the stellar population. The good characterisation of the PSF of our MCAO observations allows, therefore, to cover larger AO corrected areas on the sky, which is crucial for photometric and astrometric studies of extended stellar populations.

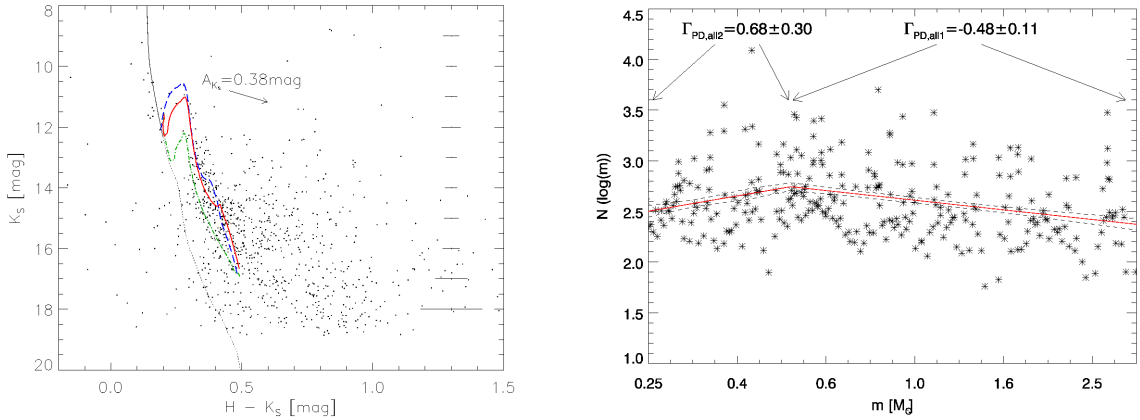

Figure 4.37: *Left*: The K_S vs. H-K_S CMD with a populated PMS which is well represented by a Siess isochrone of 1 Myr in age (red solid line); The 0.5 Myr and 3 Myr Siess isochrones are overplotted as the blue dashed and green dash-dotted line, respectively. The MS isochrone is shown by the thin and the dotted black line. *Right*: PDMF of Tr 14 composed of PMS stars. The best fit to the PDMF is shown as straight red lines while dashed lines display the 1σ interval. Above $m_c \sim 0.53$ M$_\odot$ it is well represented by a slope of $\Gamma_{\rm PD,all1} = -0.48 \pm 0.11$ and below $m_c \sim 0.53$ M$_\odot$ by a slope of $\Gamma_{\rm PD,all2} = 0.68 \pm 0.30$.

K_S vs. H-K_S colour–magnitude diagram

The colour–magnitude diagram (CMD, left panel of Fig. 4.37) allows the clear identification of the cluster pre-main sequence (PMS) population. Stars redder than the PMS ($H - K_S > 0.5$ mag) suffer either from differential extinction, are background objects or belong to the cluster as PMS stars with K_S-band excess. The identification of different features of the cluster in the CMD (PMS, PMS/MS transition region) allows the comparison with stellar evolutionary models. For the PMS, we use Siess tracks (Siess et al. [2000]), computed as in Da Rio et al. [2009], using the BT–Settl Grid of Allard & Freytag [2010]. MS isochrones are from Marigo et al. [2008]. Superimposed isochrones onto the CMD in the left panel of Fig. 4.37 resemble the observed features. We find the cluster PMS best represented by the 1 Myr isochrone, with an uncertainty of 0.5 Myr on the age. From the distance modulus of $DM = 11.8 \pm 0.4$ mag we obtain a distance of $\sim 2.3 \pm 0.4$ kpc and the extinction is measured to $A_{K_S} = 0.38 \pm 0.03$ mag. With a different combination of distance and extinction (distance $= 2.6 \pm 0.4$ kpc, $\rm A_{K_S} = 0.36 \pm 0.03$ mag), a slightly younger isochrone (0.5 Myr) represents the PMS-MS colour difference well, but the PMS shape is not reproduced equally well. A sequence of stars which exhibit bluer colours when compared to the 1 Myr isochrone might be caused by differential extinction and photometric errors. However, by superposition, we observe that a 3 Myr isochrone nicely follows the observed sequence.

Mass function

To assign a mass to each PMS star (with and without K_S-band excess), we use the mass-luminosity-relation of the 1 Myr Siess isochrone considering the distance and extinction as derived in previous Section. To obtain the PDMF of Tr 14, we use the method suggested by Maíz Apellániz & Úbeda [2005] (see also Maíz Apellániz [2009]). We have chosen to derive the PDMF in single star bins, such that bias introduced by the binning remains low. The PDMF is corrected for incompleteness and divided by the width of the bin (mean of the mass of the star and the preceding and following star, respectively). As the resulting PDMF turns over at $log(m) \sim -0.25$ (right panel of Fig. 4.37), we fit a two-component power law with a variable characteristic mass in the mass range $0.25 < \rm M < 3.2 M_\odot$. We find a characteristic mass of $m_c = 0.53^{+0.12}_{-0.10}$ M$_\odot$ and power law slopes of $\Gamma_{\rm PD,all1} = -0.48 \pm 0.11$ above m_c and $\Gamma_{\rm PD,all2} = 0.68 \pm 0.30$ below m_c (Salpeter slope $\Gamma = -1.35$). The turnover mass agrees very well with the mass at which the flattening of the Kroupa–IMF occurs (Kroupa [2001]) and is not an unique feature of Tr 14, but observed in other clusters, e.g. the Orion Nebular Cluster (Hillenbrand [1997]; Da Rio et al. [2010]; see also Fig. 3 of Bastian et al. [2010]) Unresolved binaries can significantly alter the observed slope by up to $\Delta\Gamma \sim +0.5$ (Kroupa [2001]), but even with such a large correction our PDMF would appear flatter than

a Kroupa–IMF. However, comparable to the central PDMFs in other young and massive clusters such as NGC 3603 YC (e.g. Sung & Bessell [2004]; Stolte et al. [2006]; Harayama et al. [2008]) or Westerlund 1, (Brandner et al. [2008]; Gennaro et al. [2011]).

Summary

i) MAD (MCAO) in crowded regions:
We derived maps of Strehl ratios over the 68 $\times$68 arcsec^2 FoV revealing an impressive performance of the AO system. We found larger mean Strehl values of 6.0% in H and 5.9% in K_S in our observations when compared to simulated SCAO observations (1.6% in H and 2.0% in K_S). Although lower maximum Strehl ratios have been measured (9.8% in H, 12.6% in K_S), this shows a significantly improved spatial stability of an AO performance. The photometric catalogue includes 972 (1347) sources which is 2 – 3 times the number of detections when compared to seeing-limited observations.

ii) K_S vs. H-K_S CMD of Tr 14:
The CMD of Tr 14 reveals a sequence of PMS stars, tens of sources with 'excess' as well as a sparsely populated MS. Through comparison with PMS isochrones, we find the CMD as best resembled by an isochrone of 1 ± 0.5 Myr which places Tr 14 at a distance of 2.3 ± 0.4 kpc with an extinction of $A_{K_S} = 0.38 \pm 0.03$ mag. Tentative hints for a somewhat older PMS population are observable and star formation over the last 3 Myr would support earlier studies that found a continuous star formation in the region (e.g. Ascenso et al. [2007]).

iii) The PMS stellar PDMF:

The PDMF between 0.25 and 3.2 $M_\odot$ is well represented by a broken power law. The change of the slope is found at $m_c = 0.53^{+0.12}_{-0.10}$ $M_\odot$ comparable to that of a Kroupa–IMF and as observed in other clusters. Derived power law slopes are shallower than the Kroupa–IMF (Salpeter slope $\Gamma = -1.35$) with $\Gamma_{\mathrm{PD,all}_1} = -0.48 \pm 0.11$ above m_c and $\Gamma_{\mathrm{PD,all}_2} = 0.68 \pm 0.30$ below m_c. However, similar slopes of the PDMF have been found in the central regions of other young massive clusters.

This study could show the great improvement of AO corrections provided by MCAO systems. MCAO systems offer an ideal combination of high spatial resolution instruments as well as a large FoV and VLT–MAD gives a very promising idea of observations with upcoming new telescopes and instruments.

Bibliography

Allard, F. & Freytag, B. 2010, Highlights of Astronomy, 15, 756
Amorim, A., Lima, J., Alves, J., et al. 2006, in Society of Photo-Optical Instrumentation Engineers (SPIE) Conference, Vol. 6269, Society of Photo-Optical Instrumentation Engineers (SPIE) Conference Series
Ascenso, J., Alves, J., Vicente, S., & Lago, M. T. V. T. 2007, A&A, 476, 199
Bastian, N., Covey, K. R., & Meyer, M. R. 2010, ARA&A, 48, 339
Brandner, W., Clark, J. S., Stolte, A., et al. 2008, A&A, 478, 137
Carraro, G., Romaniello, M., Ventura, P., & Patat, F. 2004, A&A, 418, 525
Cresci, G., Davies, R. I., Baker, A. J., & Lehnert, M. D. 2005, A&A, 438, 757
Da Rio, N., Gouliermis, D. A., & Henning, T. 2009, ApJ, 696, 528
Da Rio, N., Robberto, M., Soderblom, D. R., et al. 2010, ApJ, 722, 1092
Gennaro, M., Brandner, W., Stolte, A., & Henning, T. 2011, MNRAS, 412, 2469
Harayama, Y., Eisenhauer, F., & Martins, F. 2008, ApJ, 675, 1319
Hillenbrand, L. A. 1997, AJ, 113, 1733
Kroupa, P. 2001, MNRAS, 322, 231
Maíz Apellániz, J. 2009, Ap&SS, 324, 95
Maíz Apellániz, J. & Úbeda, L. 2005, ApJ, 629, 873
Marchetti, E., Brast, R., Delabre, B., et al. 2007, Messenger, 129, 8
Marigo, P., Girardi, L., Bressan, A., et al. 2008, A&A, 482, 883
Rochau, B., Brandner, W., Stolte, A., et al. 2010, ApJ Lett., 716, L90
Rochau, B., Brandner, W., Stolte, A., et al. 2011, MNRAS, submitted
Sana, H., Momany, Y., Gieles, M., et al. 2010, A&A, 515, A26+
Siess, L., Dufour, E., & Forestini, M. 2000, A&A, 358, 593
Stetson, P. B. 1990, PASP, 102, 932

Stolte, A., Brandner, W., Brandl, B., & Zinnecker, H. 2006, AJ, 132, 253
Stolte, A., Grebel, E. K., Brandner, W., & Figer, D. F. 2002, A&A, 394, 459
Sung, H. & Bessell, M. S. 2004, AJ, 127, 1014
Tapia, M., Roth, M., Vázquez, R. A., & Feinstein, A. 2003, MNRAS, 339, 44
Vazquez, R. A., Baume, G., Feinstein, A., & Prado, P. 1996, A&AS, 116, 75
Walborn, N. R., Howarth, I. D., Lennon, D. J., et al. 2002, AJ, 123, 2754

4.13 NGC 346: Tracing the Evolution of a Super Star Cluster*

Elena Sabbi[1], A. Nota[1,2], M. Cignoni[3,4], S. Degl'Innocenti[5,6], G. De Marchi[7], J. S. Gallagher[8], N. Panagia[1,9,10], P. G. Prada Moroni[5,6], M. Romaniello[11], L. J. Smith[1,2], M. Sirianni[7], M. Tosi[4]

[1] Space Telescope Science Institute, 3700 San Martin Drive, Baltimore, MD 21218, USA
[2] European Space Agency, Research and Scientific Support Department, Baltimore, MD 21218, USA
[3] Dipartimento di Astronomia, Univeristà degli Studi di Bologna, via Ranzani 1, 40127 Bologna, Italy
[4] Istituto Nazionale di Astrofisica, Osservatorio Astronomico di Bologna, via Ranzani 1, 40127 Bologna, Italy
[5] Dipartimento di Fisica "Enrico Fermi", Univerità di Pisa, Largo Pontecorvo 3, 56127 Pisa, Italy
[6] INFN - Sezione di Pisa, Largo Pontecorvo 3, 56127 Pisa, Italy
[7] European Space Agency, Space Science Department, Keplerlaan 1, 2200 AG Noordwijk, Netherlands
[8] Department of Astronomy, 457 North Charter Street, Madison, WI 53706, USA
[9] Istituto Nazionale di Astrofisica, Osservatorio Astrofisico di Catania, via S. Sofia 78, 95123 Catania, Italy
[10] Supernova Limited, OYV #131, Northsound Rd., Virgin Gorda, British Virgin Islands
[11] European Southern Observatory, Karl-Schwarzshild-Str. 2, 85748 Garching, Germany
* Based on observations with the NASA/ESA *Hubble Space Telescope*, obtained at the Space Telescope Science Institute, which is operated by Aura, Inc., under Nasa Contract NAS5-26555

Abstract

We discuss how star formation (SF) has been progressing - in space and time - in NGC 346, the site of most intense SF in the Small Magellanic Cloud (SMC), as derived from the analysis of optical broad ($\sim V$ and $\sim I$) and narrow band ($\sim H\alpha$) *Hubble Space Telescope* (HST) images. Our analysis reveals that NGC 346 experienced different regimes of SF, in a number of compact sub-clusters. In the youngest ones, we find a puzzling and intriguing deficiency of massive stars, either suggestive of an evolution of the initial mass function with time, with the youngest sub-clusters not having had sufficient time to build the more massive stars yet, or that high and low-mass stars may form through different mechanisms. The combination of the broad and narrow-band data allowed us to identify bona fide pre-main sequence (PMS) stars that are actively accreting material from their circumstellar disks. Interestingly, the identified PMS stars show a bimodal age distribution - peaked respectively at ~ 1 and ~ 20 Myr - with the two generations of stars that appear to be spatially independent.

Introduction

Young super star clusters are rare in the Local Group (LG), and yet they provide important insights on the process of SF in nearby starburst and high-redshift interacting galaxies, formation and disruption of globular clusters, and formation of massive stars.

With more than 30 O-type stars (Massey et al. [1989]; Evand et al. [2006]), the young (~ 3 Myr) cluster NGC 346 is the site of the most intense SF in the SMC, as well as one of the most active regions in the LG. Mid-IR and sub-millimeter observations revealed the presence of several embedded sources in the body of NGC 346, confirming the presence of very recent and/or still ongoing SF (Contursi et al. [2000]; Rubio et al. [2000]).

More recent HST optical observations revealed that the structure of NGC 346 is complex, with its stars being organized in a multitude of almost coeval sub-clusters (Sabbi et al. [2007]; Hennekemper et al. [2008]; Gouliermis et al. [2008]; Fig.4.38 – Left Panel), each of which is hosting massive young stellar obgects (YSOs Bollatto et al. [2007]; Simon et al. [2007]; Fig.4.38 – Right Panel).

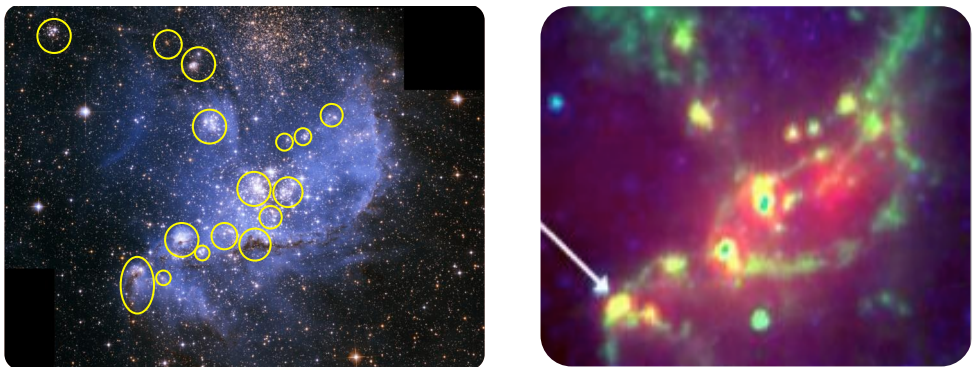

Figure 4.38: *Left Panel*: HST/ACS colour composite image of NGC 346. North is up and East is to the left. Yellow circles mark the position of the 16 sub-clusters identified in Sabbi et al. [2007]. *Right Panel*: Spitzer/IRAC colour composite image of NGC 346.

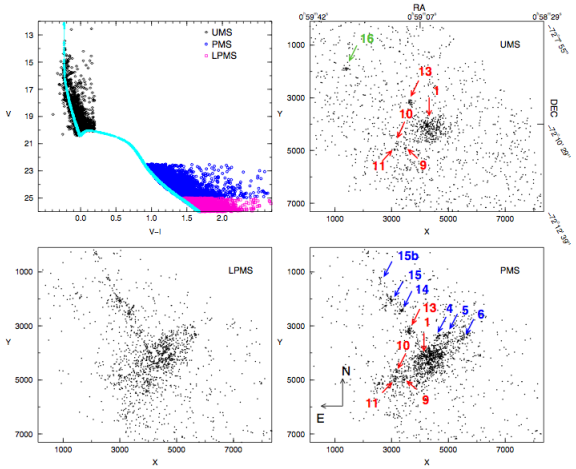

Figure 4.39: *Top left panel*: CMD for the region NGC 346. The cyan line corresponds to a 3 Myr isochrone that includes the PMS phase. UMS stars are indicated by open black diamonds, PMS stars are in blue and LPMS stars in magenta. The top right panel shows the spatial distribution of the UMS stars, PMS stars spatial distribution is shown in the bottom right panel, and LPMS stars in the bottom left panel. The number labelling of each sub-cluster follows the nomenclature provided by Sabbi et al. [2007].

NGC 346 Star Formation History

We used deep ACS/WFC optical broad-(F555W and F814W) and narrow-band (F658N) HST images to infer how star formation occurred and developed in NGC 346. Photometric studies (i.e. Sabbi et al. [2007]; Hennekemper et al. [2008]; Gouliermis et al. [2008]) of this dataset indicate that SF has taken place in a variety of sub-clusters at different local conditions.

To better constrain the star formation history (SFH) and the evolution of this complex region we used a standard application of the synthetic colour-magnitude diagram (CMD) method (see, e.g., Tosi, et al. [1991]; Cignoni et al. [2006]; Cignoni & Tosi [2010]) and a novel technique based on the identification of bona fide pre-main-sequence (PMS) stars with active accretion (De Marchi, Panagia & Romaniello [2010]).

History and modes of star formation from synthetic CMDs

To trace how SF occurred and evolved in NGC 346 itself we used objects on the upper main-sequence (UMS) and objects still on the PMS. We considered as UMS stars all objects above the Turn-On (TOn) of a 3 Myr isochrone and bluer than $V - I = 0.2$ (black open diamonds in Fig. 4.39 – Top Left Panel). In doing this we sampled the intermediate and high-mass stars. To trace the distribution of PMS stars we considered objects redder than the 3 Myr isochrone with magnitude in the range $22.5 < V < 25$

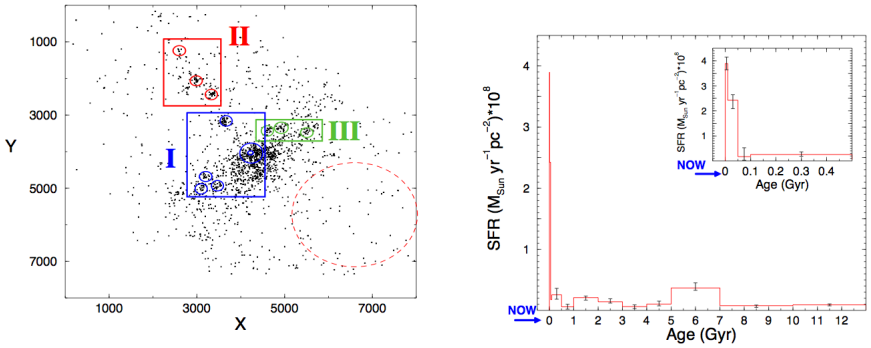

Figure 4.40: *Left Panel*: Position of the three groups of sub-clusters in NGC 346. *Right Panel*: SFH of the SMC field around NGC 346. For sake of clarity the most recent 500 Myr are zoomedin in the upper right onset. The uncertainty on the SFR is also shown for each age bin. The two episodes of SF associated to BS90 and NGC 346 are not included.

(blue open circles) and fainter than $V = 25$ (magenta open squares, hereafter LPMS). According to this selection, PMS stars trace a population younger than ~ 3 Myr, the UMS sample include MS stars as old as 600 Myr. Moreover, while there is no doubt that the PMS and LPMS samples are free from any contamination, the UMS sample can include a minor fraction of PMS stars starting to approach the MS.

The top right, bottom right, and bottom left panels of Fig. 4.39 show the location of the selected stellar populations. These distributions provide a clue to the evolution of NGC 346. In particular we find that half of the UMS stars are clumped into the most massive sub-clusters SC-1, SC-13, and SC-16, while the remaining half are more evenly distributed and are probably foreground and background stars. PMS and LPMS stars are found almost exclusively either clumped or irregularly arranged along filaments. A further intriguing aspect of the star spatial distribution is that not all the sub-clusters visible in the UMS map are detected in the PMS maps and vice versa.

We divided the sub-clusters in three groups, based on the fraction of PMS stars with the respect of UMS (Fig. 4.40 - Left Panel). The bulk of the stars in Group I sub-clusters are well consistent with a major star-forming episode started about 6 Myr ago and lasted about 3 Myr. After that, their star formation activity has proceeded at a lower rate (Cignoni et al. [2011]). As already noted by Hennekemper et al. [2008], models do not fully reproduce the large colour spread shown by PMS stars. Since our PMS evolutionary tracks do not include circumstellar reddening, a more likely explanation is that the redward broadening of the PMS stars is caused by variable reddening affecting individual PMS stars. Moreover, our models seem to underestimate the observed PMS counts by about 40%. We speculate that a very young generation of stars, so young not to have had time to assemble more massive stars, could account both for the observed excess of PMS stars and for the intrinsic redness of such stars (Cignoni et al. [2011]).

As we already pointed out in Sabbi et al. [2008], in NGC 346 massive stars are underrepresented. In particular we find that Group II sub-clusters are dominated by low-mass PMS stars, with the PMS/UMS ratio being at least three times higher than in Group I. Such a population should have a MS counterpart, which is not visible, however. Furthermore, the PMS stars are redder than in Group I. We speculate that in Group II SF is occurring only now, and that PMS stars are redder because they still retain some/more circumstellar material. The lack of massive stars in this regions can be ascribed, as suggested by Panagia et al. [2000], either to the fact that for different stellar masses SF requires different initial conditions, or that more massive stars may form later than low-mass stars (e.g. because they need more time to collect enough material to form). In this case the Group II sub- clusters are simply too young to have produced massive stars (Cignoni et al. [2011]). Finally, Group III sub-clusters have characteristics intermediate between Group I and II.

From the comparison of the observed V versus $V - I$ CMD to the synthetic ones and the analysis of the spatial distribution of the stellar component in the NGC 346 region we concluded that in the field of the SMC 60% of the mass astration occurred earlier than 5 Gyr ago (Fig. 4.40 - Right Panel), with a peak between 5 and 7 Gyr ago (Cignoni et al. [2011]), in agreement with the SFH of other regions of the SMC derived by other authors (e.g. Dolphin et al. [2001]; McCumber et al. [2005]; Cignoni et al. [2009]; Noël et al. [2009]; Sabbi et al. [2009]).

The average star formation rate density in the field surrounding NGC 346 is 1.5×10^{-9} M$_{\odot}$ yr^{-1} pc^{-2}. This value is in agreement with those derived by Noël et al. [2009] for several SMC regions. However, the rate of star formation in the NGC 346 region appears to have increased in the last tens

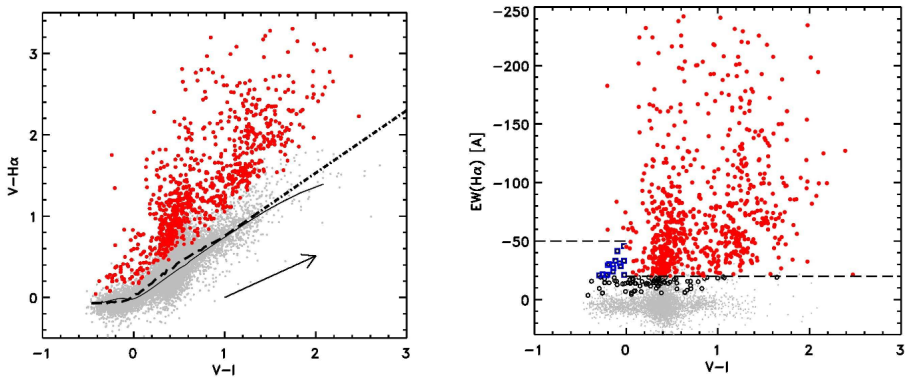

Figure 4.41: *Left Panel*: Colour-colour diagram of the 18,764 stars with error $\sigma_3 \leq 0.1$ mag. The dashed line represents the running median $V - H\alpha$ colour, obtained with a box-car size of 100 points, whereas the thin solid line shows the model atmospheres of Bessell et al. [1998]. The arrow in the figure corresponds to the reddening vector for $A_V = 2.7$ or $E(V - I) = 1$. The red dots mark the 791 objects with a $V - H\alpha$ excess larger than 4σ. *Right Panel*: $H\alpha$ equivalent width of the stars in the field of NGC 346, as a function of their $V - I$ colour. Red circles indicate the 694 sources with $W_{eq}(H\alpha) < -20$ Å (or < -50 Å for stars hotter than $10,000K$). As customary, we use negative equivalent widths for emission lines.

of Myr from a relatively lower and steady regime. In the last 100 Myr the average star formation rate density in the field is about 1.4×10^{-8} $M_\odot$ yr^{-1} pc^{-2}, two orders of magnitude higher than in nearby late-type dwarfs, and similar to the quietest cases of Blue Compact Dwarfs (see Tolstoy et al. [2009] and references therein).

NGC 346 SFH as derived from bona fide PMS with active accretion

We used the self-consistent method recently developed by De Marchi, Panagia & Romaniello [2010] that combine broad-band V and I photometry and narrow-band $H\alpha$ imaging to identify all stars with excess $H\alpha$ emission in the region around NGC 346. This technique allows us to derive for all of these stars the accretion luminosity L_{acc} and mass accretion rate $\dot{M}_{acc}$.

Following the method developed in De Marchi, Panagia & Romaniello [2010], we identified 791 PMS candidates with $H\alpha$ excess above the 4σ level with respect to the reference provided by normal stars (Fig 4.41 – Left Panel). Their average $H\alpha$ luminosity is 2.7×10^{31} erg s^{-1} or $\sim 10^{-2}$ $L_\odot$. We have also determined the equivalent width of the $H\alpha$ emission line of these objects (Fig. 4.41 – Right Panel) and have classified as bona fide PMS stars all those with $W_{eq} < -20$ Å (or < -50 Å for stars with $T_{eff} > 10,000K$). These conditions guarantee that our sample is free from contamination due to the chromospheric activity of older objects or to the rotational winds of Be stars. A total of 694 objects satisfy these conditions.

By comparing the locations of these objects in the H-R diagram with the PMS evolutionary models of the Pisa group for metallicity $Z = 0.002$ (Fig. 4.42 – Left Panel), we derived masses and ages for 680 bona fide PMS stars. Masses range from 0.4 $M_\odot$ to 4 $M_\odot$, with an average value of ~ 1 $M_\odot$. The ages show a clear bimodal distribution with two peaks at ~ 1 Myr and ~ 20 Myr and very few objects around ~ 8 Myr, revealing the presence of two distinct but equally populous generations of stars (De Marchi et al. [2011a]).

The size of our PMS sample, and its spread in age and mass, allowed us to study the evolution of the mass accretion rate as a function of stellar parameters. Regardless of the mass of the star, we find that the mass accretion rate decreases with roughly the square root of age, which is ~ 3 times slower than what is currently predicted by models of viscous disc evolution, and that the more massive stars have a systematically higher mass accretion rate in proportion to their mass. Our analysis indicates that, at least in low metallicity environments, a considerable amount of mass is accreted during the PMS phase, and that the PMS evolution of moderate-mass stars (< 2 $M_\odot$) should be reconsidered and recalculated taking into account the high $\dot{M}_{acc}$ values, since for a given MS mass the evolutionary time needed to reach the ZAMS will be longer than what is currently estimated by models that assume $\dot{M}_{acc} = 0$ after the first few 10^4 yr (De Marchi et al. [2011a]).

We used age and other physical parameters of the PMS stars with active $H\alpha$ accretion to study

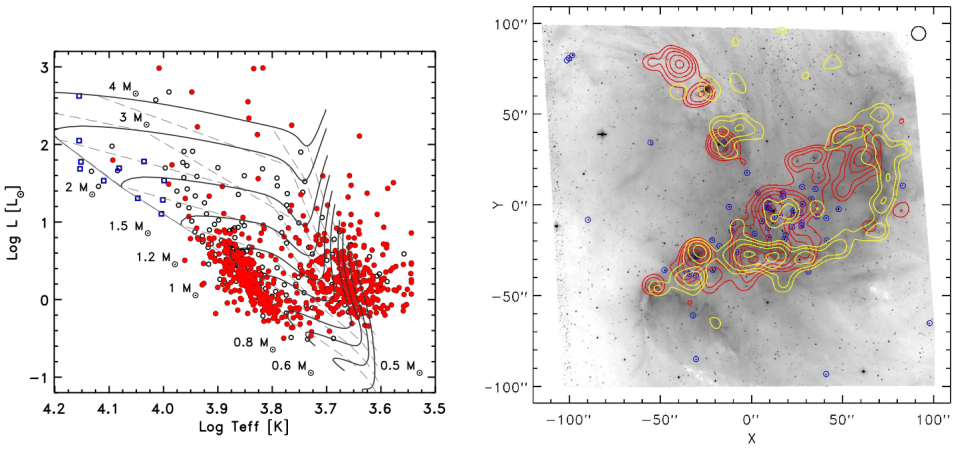

Figure 4.42: *Left Panel*: Hertzsprung-Russel diagram of the PMS candidate stars with active accretion, as derived from their $H\alpha$ excess. Thick solid lines show the evolutionary tracks from the Pisa group (Degl'Innocenti et al. [2008]; Tognelli et al. [2011]) for metallicity $Z = 0.002$ and masses from $0.5\,M_\odot$ to $4\,M_\odot$, as indicated. The corresponding isochrones are shown as thin dashed lines, for ages of 0.125, 0.25, 0.5, 1, 2, 4, 8, 16 and 32 Myr from right to left. *Right Panel*: Spatial density distribution of young (< 7 Myr; red lines) and old (> 7 Myr; yellow lines) PMS stars in NGC 346, overlaid on a negative HST/ACS $H\alpha$ image of the region. The (0,0) position in this figure corresponds to $RA = 0^h59^m8^s$, $DEC = -72^o10'32''$ (J2000), while North is up and East to the left. Blue circles mark the position of young (< 7 Myr) massive stars brighter than $-2 \times 10^4\,L_\odot$.

how SF proceeded in the region of NGC 346 in the last ~ 30 Myr (De Marchi et al. [2011b]). Except for the regions near the centre of NGC 346, the stars belonging to the two generations have very different spatial distributions: $\sim 1/3$ of the older generation occupies an arc-like gas structure to the south and west of NGC 346 that had previously been interpreted as the ionization front caused by the OB stars at its centre. Although the morphology of the arc could have suggested a case of triggered star formation, this is clearly not a viable option since the central massive stars are at least $10 - 20$ Myr younger than the objects on the arc and cannot have triggered their formation (Fig. 4.42 – Right Panel). The compact distribution of older PMS stars along the arc-like structure suggests that they have formed there from the gas that is still visible and have not (yet) been affected by the massive OB stars at the centre of NGC 346. This picture is consistent with the very low velocity dispersion ($< 3\,\mathrm{kms}^{-1}$) of the ionized gas.

Finally we once again note that, with the exception of the most central regions, there is no correspondence between the positions of young PMS stars and massive O-type stars of similar age, suggesting that the conditions (and possibly also the mechanisms) for their formation must be rather different (Panagia et al. [2000]; De Marchi et al. [2011b]).

Summary & Conclusions

We used both a standard synthetic CMD method and a novel technique to identify bona fide PMS stars with active accretion to investigate how SF has been progressing - in space and time - in NGC 346, the site of most intense SF in the SMC. Both methods indicate that NGC 346 experienced different regimes of SF over several tens of Myr.

The youngest regions show an intriguing deficiency of massive stars, either suggestive of an evolution of the initial mass function with time, with the youngest sub-clusters not having had sufficient time to build the more massive stars yet, or that high and low-mass stars may form through different mechanisms.

Bibliography

Bessell, M., Castelli, F., Plez, B. 1998, A&A, 333, 231
Bollatto, A.D. 2007, ApJ, 655, 212
Cignoni, M., Degl'Innocenti, S., Prada Moroni, P.G., & Shore, S.N. 2006, A&A, 459, 783

Cignoni, M., et al. 2009, AJ, 137, 3668
Cignoni, M., & Tosi, M. 2010, Adv. Astron, 2010, 158568
Cignoni, M., Tosi, M., Sabbi, E., Nota, A., Gallagher, J.S. 2011, AJ, 141, 31
Contursi, A., et al. 2000, A&A, 362, 310
Degl'Innocenti, S., Prada Moroni, P. G., Marconi, M., Ruoppo, A. 2008, Ap&SS, 316, 25
De Marchi, G., Panagia, N., &Romaniello, M. 2010, ApJ, 715, 1
De Marchi, G., Panagia, N., Romaniello, M., Sabbi, E., Sirianni, M., Prada Moroni, P.G., Degl'Innocenti, S. 2011a, ApJ (accepted), astro-ph/1104.44942
De marchi, G., Panagia, N., Sabbi, E. 2011b, ApJ (accepted), astr-ph/1106.5780
Dolphin, A. E., Walker, A. R., Hodge, P. W., Mateo, M., Olszewski, E. W., Schommer, R. A., & Suntzeff, N. B. 2001, ApJ, 562, 303
Evans, C., Lennon, D., Smartt, S., Trundle, C. 2006, A&A, 456,623
Gouliermis, D.A., Chu, Y.-H., Henning, T., Brandner, W., Gruendl, R.A., Hennekemper, E., Hormuth, F. 2008, ApJ, 688, 1050
Hennekemper, E., Gouliermis, D., Henning, T., Brandner, W., Dolphin, A., 2008, ApJ, 672, 914
Massey, P., Parker, J.W., Garmany, C.D. 1989, AJ, 539, 197
McCumber, M. P., Garnett, D. R., & Dufour, R. J. 2005, AJ, 130, 1083
Noël, N. E. D., Aparicio, A., Gallart, C., Hidalgo, S. L., Costa, E., & Méndez, R. A. 2009, ApJ, 705, 1260
Panagia, N., Romaniello, M., Scuderi, S., & Kirshner, R. P. 2000, ApJ, 539, 197
Rubio, M., Contursi, A., Lequeux, J., Probst, R., Barba, R., Boulanger, F., Cesarsky, D., Maoli, R. 2000, A&A, 359, 1139
Sabbi, E. et al. 2007, AJ, 133,44
Sabbi, E., et al. 2008, AJ, 135, 173
Sabbi, E., et al. 2009, ApJ, 703, 721
Simon, J. et al. 2007, ApJ, 327
Tognelli, E., Prada Moroni, P., Degl'Innocenti, S. 2011, A&A, (submitted)
Tolstoy, E., Hill, V., & Tosi, M. 2009, ARA&A, 47, 371
Tosi, M., Greggio, L., Marconi, G., & Focardi, P. 1991, AJ, 102, 951

4.14 The Brown Dwarf Population in Nearby Star-Forming Regions

Aleks Scholz[1], K. Muzic[2], V. Geers[3], R. Jayawardhana[2], M. Tamura[4], P. Dawson[1], and T. P. Ray[1]

[1] School of Cosmic Physics, Dublin Institute for Advanced Studies, 31 Fitzwilliam Place, Dublin 2, Ireland
[2] Department of Astronomy & Astrophysics, University of Toronto, 50 St. George Street, Toronto, ON M5S 3H4, Canada
[3] Institute for Astronomy, ETH Zurich, Wolfgang-Pauli-Strasse 27, 8093 Zurich, Switzerland
[4] National Astronomical Observatory, Osawa 2-21-2, Mitaka, Tokyo 181, Japan

Abstract

We present results from a survey program to investigate the population of brown dwarfs in a number of star-forming regions. In the framework of the SONYC project (Substellar Objects in Nearby Young Clusters) we have surveyed three regions (NGC 1333, ρ-Ophiuchus, Chamaeleon-I) and identified ~ 30 new young VLM objects. In addition, we found 19 new high-confidence members of the Upper Scorpius region, most of them likely to be substellar. Among the new brown dwarfs are a few planetary-mass objects, including one with spectral type $\sim$ L3, which puts its mass at ~ 6 M_{Jup} – one of the lowest mass free-floating objects identified thus far. In NGC 1333 we present a census of 51 VLM members by combining our work with literature studies. The spatial distribution of these objects is indistinguishable from the total population of Class I/II objects in this cluster. In comparison with other nearby star-forming regions, NGC 1333 harbours an unusually large number of substellar objects (relative to the number of low-mass stars). If confirmed, this is a sign of environmental differences in the formation of brown dwarfs.

Introduction

As of today, we do not understand which physical processes set the object mass at the low-mass end of the Initial Mass Function (IMF), including the substellar domain at $M < 0.08$ $M_\odot$ (~ 80 M_{Jup}) (Bonnell et al. [2007]). Possible candidates include dynamical ejections from multiple systems or disks, turbulent fragmentation, gravitational fragmentation in a cluster potential, and photoerosion of cores in the radiation fields of OB stars (Whitworth et al. [2007]). Not all these options will be available in every star-forming region; i.e. one way of distinguishing between the proposed scenarios is to look for environmental differences in the number and properties of brown dwarfs. This is only one area of research where detailed studies of young brown dwarfs are relevant; others include the physics of accretion, the dissipation of the circumstellar disks and envelopes, as well as the growth of dusty solids in disks, a problem closely linked with planet formation.

The pre-requisite for tackling all these issues is to carry out surveys to identify large, unbiased, and well-characterised samples of brown dwarfs in diverse star-forming regions. Such surveys reduce issues with low-number statistics, provide the best possible candidates for detailed follow-up studies, and allow us to investigate environmental effects. Thus far, however, the available brown dwarf samples are incomplete, particularly at the low-mass end (< 20 M_{Jup}) and subject to observational biases. In this contribution we discuss our survey programs to tackle these problems and to establish a census of brown dwarfs.

The surveys

In this paper we mainly focus on results from the survey program SONYC – short for Substellar Objects in Nearby Young Clusters. The goal of SONYC is to provide a census of brown dwarfs down to ~ 5 M_{Jup}

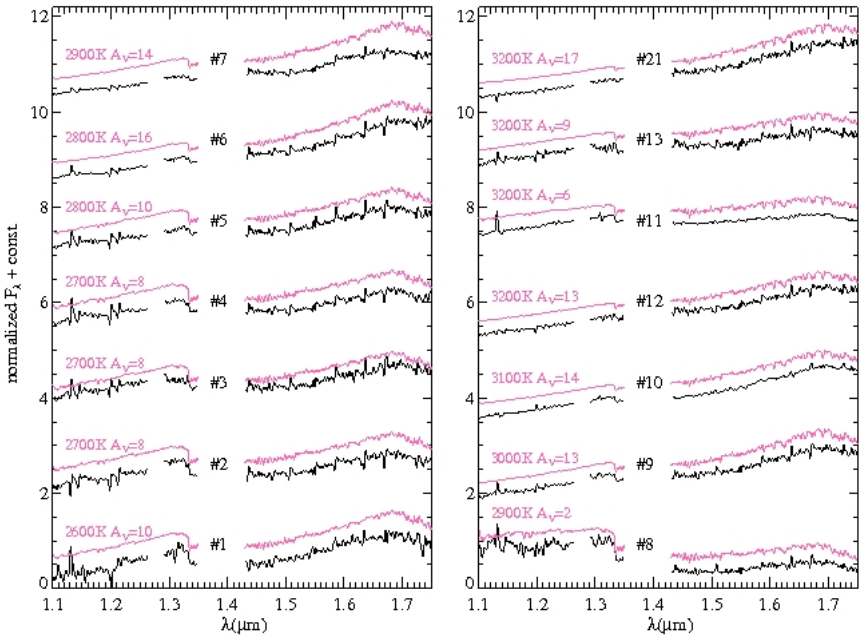

Figure 4.43: Low-resolution near-infrared spectra obtained with FMOS for confirmed very low-mass members of the ρ-Oph star-forming region (from Muzic et al., in prep.). The observed spectra are shown in black; the best-matching model spectra from the AMES-DUSTY series are plotted in pink.

for a number of star-forming regions within 300 pc. The primary method of detecting the sources is deep broadband imaging in the optical and near-infrared wavelength domain. Thus, we select objects based on their photospheric spectral energy distribution, in contrast to other surveys which look for mid-infrared excess due to a disk (Allers et al. [2006]) or narrow-band absorption features (Burgess et al. [2009]).

Broadband surveys in regions with significant extinction are not particularly selective, i.e. follow-up spectroscopy is mandatory to confirm the photometric candidates as young very low-mass (VLM) objects. For this purpose, SONYC uses multi-object facilities at Subaru (MOIRCS, FMOS) and ESO/VLT (VIMOS). Particularly well-suited for this project is FMOS, a near-infrared, low-resolution fibre spectrograph covering a field-of-view of 30 arcmin (Kimura et al. [2010]). In Fig. 4.43 we plot FMOS spectra for confirmed VLM objects in the ρ-Oph star-forming region, showing the broad H_2O absorption features typical for objects later than $\sim$ M3. Overplotted in pink are AMES-DUSTY model spectra (Allard et al. [2001]) which are used to estimate the effective temperatures.

In the framework of SONYC we have carried out imaging and spectroscopy in three regions (NGC 1333, ρ-Ophiuchus, Chamaeleon-I) and are in the process of observing a fourth one (Lupus-3). In Cha-I we have not found yet new substellar objects, indicating that the current census (Luhman [2007]) is mostly complete down to ~ 8 M_{Jup} and $A_V \leq 5$ mag (Mužić et al. [2011]). The number of missing VLM members down to these limits is below ~ 7, i.e. $\leq 3\%$ of the total cluster population. In ρ-Oph we find 10 new VLM sources. We estimate that the number of the missing objects in our survey area (~ 0.33 deg^2 centered on the main core L1688) is about 10, down to masses of 0.003 – 0.03 $M_\odot$ for $A_V = 0 - 15$ mag (Geers et al. [2011]), see also Muzic et al., in preparation. The most relevant results from NGC 1333 are discussed in next Section.

In a complementary project, we have made use of data from the Galactic Cluster Survey, a part of UKIDSS, to search for brown dwarfs in the southern part of the Upper Scorpius (UpSco) OB association. Most areas in UpSco are not significantly affected by extinction; in addition the members show substantial proper motions, which greatly facilitates their identification. Based on colour-magnitude diagrams and proper motions, we find 19 new high-confidence members in an area of 12 deg^2 with masses between 0.01 and 0.09 $M_\odot$, i.e. most of them are likely to be substellar. This work is discussed in detail in Dawson et al. (2011, submitted to MNRAS).

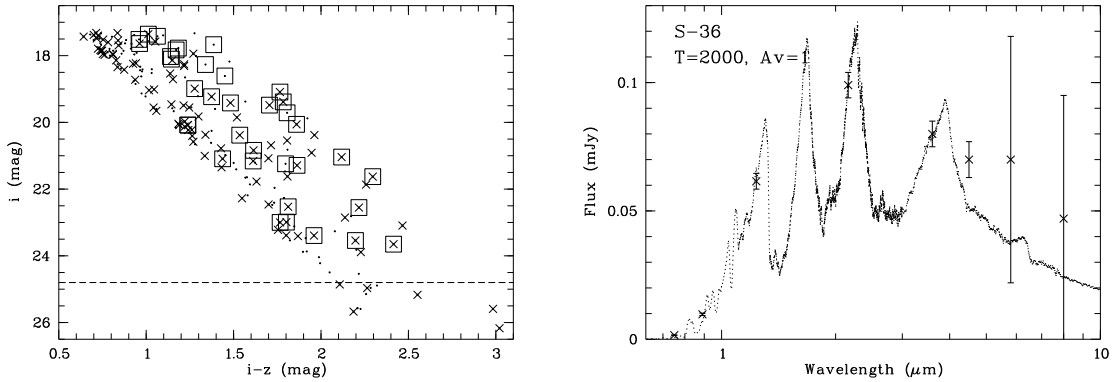

Figure 4.44: *Left panel*: (*i*, *i-z*) colour magnitude diagram for the NGC 1333 candidates identified from the photometric survey published in Scholz et al. [2009]. Objects for which we have obtained follow-up spectroscopy are marked with crosses, objects confirmed as VLM objects (by us or others) with squares. *Right panel*: Spectral flux distribution for SONYC-NGC1333-36, the coolest object identified thus far in NGC 1333, in comparison with a DUSTY model spectrum (Allard et al. [2001]). For this source we estimate an effective temperature of ~ 2000 K, corresponding to a mass of ~ 6 M_{Jup}. (from Scholz et al., in prep.)

NGC 1333

NGC 1333 is a ~ 1 Myr old compact cluster in the Perseus star-forming region (Gutermuth et al. [2008]). We carried out a photometric survey in the bands *izJK* using Suprime-Cam and MOIRCS at the Subaru telescope, covering ~ 0.25 deg^2. Using MOIRCS and FMOS we obtained spectra for about 100 candidates selected from the (*i*, *i-z*) colour magnitude diagram (Fig. 4.44, left panel). In addition, we made use of the Spitzer catalogue from the 'Cores to Disks' Legacy program (Evans et al. [2009]) and verified a few objects with *J*- and *K*-band detection and mid-infrared colour excess. Based on our spectroscopy we find 21 new likely brown dwarfs and confirm many previously known VLM members.

In particular we find a few objects with spectral types of M9 or later, i.e. their masses are likely below 0.02 $M_\odot$. Our previous claim of a deficit of planetary-mass objects in this cluster (Scholz et al. [2009]) does not hold after more extensive analysis. The coolest object in our sample has an approximate spectral type of L3 and an effective temperature of ~ 2000 K. In comparison with theoretical isochrones, this puts its mass at ~ 6 M_{Jup} – one of the lowest mass free-floating objects identified thus far (Fig. 4.44, right panel). In total, the cluster harbours 51 confirmed objects with spectral type M5 or later and/or effective temperature below 3200 K, among them probably about 30 – 40 brown dwarfs. This is currently one of the largest and best characterised samples of substellar objects in the literature. The full census of brown dwarfs in NGC 1333 is published and discussed in Scholz et al. (in prep.); here we provide a brief summary.

In Fig. 4.45, left panel, we show the spatial distribution of the VLM members in NGC 1333 (squares), in comparison with the population of Class I/II YSOs in the cluster (crosses), which has been identified from Spitzer images by Gutermuth et al. [2008]. Since these objects are mostly stars, we are probing here the mass dependence of the spatial distribution. The VLM objects are strongly clustered around the center of NGC1333, similar to the YSOs. The fraction of objects with distance from the cluster center of $d < 0.1$, $0.1 < d < 0.2$ and $d > 0.2$ deg is 65, 35, 0% for the VLM objects and 67, 26, 6% for the Class I/II objects – which is consistent within the statistical uncertainties. Similarly, the average distance from the cluster as well as the scatter in the positions is comparable in the two samples. Thus, Class I/II objects and VLM objects in NGC 1333 are indistinguishable in terms of their spatial distribution.

In particular, we can exclude the existence of a substantial VLM population at distances > 0.2 deg from the cluster center, corresponding to ~ 1 pc at the distance of NGC 1333. Although we took spectra for 31 candidates outside this range, none of them was confirmed. This puts an upper limit of $\sim$2 km/s on the relative spatial velocities between brown dwarfs and the total cluster population, which can potentially be used to constrain scenarios for dynamical ejections of brown dwarfs at an early stage of their evolution.

Based on our survey we estimate that the total number of brown dwarfs in NGC 1333 with masses

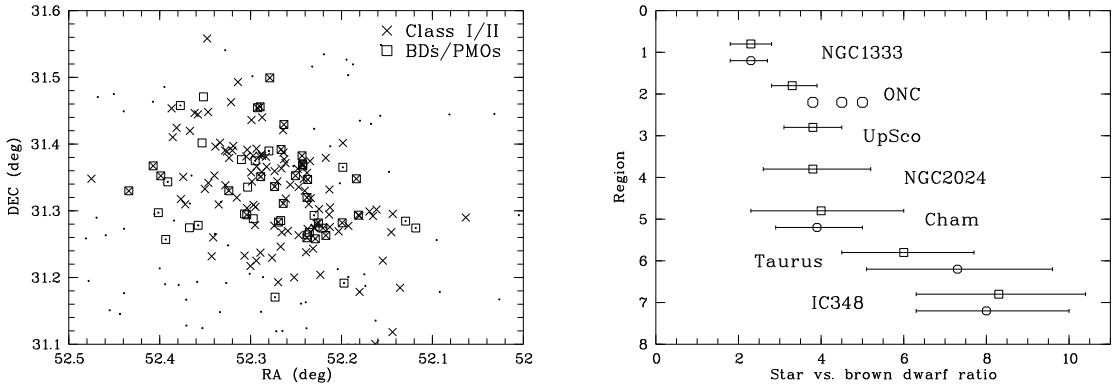

Figure 4.45: *Left panel*: Spatial distribution of VLM objects (spectral type ≥M5) in NGC1333 (squares) in comparison with the distribution of Class I/Class II objects (Gutermuth et al. [2008]). All candidates from our iz survey are shown as dots. *Right panel*: Ratio between the number of stars (0.08 – 1.0 $M_\odot$) and the number of brown dwarfs (0.03 – 0.08 $M_\odot$ for several star-forming regions (squares, the circles show the ratio for slightly different mass ranges). The data has been taken from our work for NGC 1333, Dawson et al. (2011) for UpSco, and Andersen et al. [2008] for the remaining regions. Errorbars have been calculated consistently using the prescription by Cameron [2010]. (from Scholz et al., in prep.)

of 0.03 – 0.08 $M_\odot$ is approx. 30. This includes an estimate of the number of objects not identified yet. From the Spitzer survey by Gutermuth et al. [2008] we find that the number of low-mass stars in NGC1333 with $0.08 < M < 1.0$ $M_\odot$ is around 70. Combining the two numbers yields a star vs. brown dwarf ratio of 2.3 ± 0.5. In Fig. 4.45, right panel, we compare this value with previously published star vs. brown dwarf ratios for other star-forming regions (plotted with squares). For this plot we have re-computed the 1σ confidence intervals using the prescription by Cameron [2010]. NGC 1333 has by far the lowest ratio, i.e. the largest number of brown dwarfs (relative to the number of low-mass stars). In particular, the ratio is significantly lower than in regions like IC 348 and Taurus.

At face value, the figure indicates environmental differences in the formation of brown dwarfs. It is conceivable that more brown dwarfs are formed in NGC 1333 due to turbulent fragmentation (Padoan & Nordlund [2004]) or due to gravitational fragmentation in the cluster potential (Bonnell et al. [2008]). We also note that based on the current numbers regions with OB stars (UpSco, ONC, NGC 2024) appear to have a larger number of brown dwarfs (relative to the number of low-mass stars) than regions without (Taurus, IC 348). This could be due to the additional effect of photoerosion of cores in the vicinity of massive stars (Whitworth & Zinnecker [2004]).

While the currently available results provide interesting hints, the numbers are not good enough yet to give unambiguous evidence for environmental effects on the substellar IMF. The numbers shown above could still be affected by systematic errors which are not taken into account in the statistical confidence intervals, for example survey incompleteness or inconsistencies in the object selection. These findings, in particular the numbers in NGC 1333 and IC 348, definitely need independent confirmation by other methods and with larger samples. In any case, these early results illustrate that deep surveys in star-forming regions have the potential to provide meaningful constraints on theoretical scenarios for the formation of low-mass stars and brown dwarfs.

Acknowledgments

The research was supported in part by grants from the Science Foundation Ireland (no. 10/RFP/AST2780) to AS and from the Natural Sciences and Engineering Research Council (NSERC) of Canada to RJ. We would like to thank the Subaru staff for their generous assistance.

Bibliography

Allard, F., Hauschildt, P. H., Alexander, D. R., Tamanai, A., & Schweitzer, A. 2001, ApJ, 556, 357
Allers, K. N., Kessler-Silacci, J. E., Cieza, L. A., & Jaffe, D. T. 2006, ApJ, 644, 364

Andersen, M., Meyer, M. R., Greissl, J., & Aversa, A. 2008, ApJ Lett., 683, L183
Bonnell, I. A., Clark, P., & Bate, M. R. 2008, MNRAS, 389, 1556
Bonnell, I. A., Larson, R. B., & Zinnecker, H. 2007, in Protostars and Planets V, ed. B. Reipurth, D. Jewitt, & K. Keil, 149–164
Burgess, A. S. M., Moraux, E., Bouvier, J., et al. 2009, A&A, 508, 823
Cameron, E. 2010, ArXiv e-prints
Evans, N. J., Dunham, M. M., Jørgensen, J. K., et al. 2009, ApJS, 181, 321
Geers, V., Scholz, A., Jayawardhana, R., et al. 2011, ApJ, 726, 23
Gutermuth, R. A., Myers, P. C., Megeath, S. T., et al. 2008, ApJ, 674, 336
Kimura, M., Maihara, T., Iwamuro, F., et al. 2010, PASJ, 62, 1135
Luhman, K. L. 2007, ApJS, 173, 104
Mužić, K., Scholz, A., Geers, V., Fissel, L., & Jayawardhana, R. 2011, ApJ, 732, 86
Padoan, P. & Nordlund, Å. 2004, ApJ, 617, 559
Scholz, A., Geers, V., Jayawardhana, R., et al. 2009, ApJ, 702, 805
Whitworth, A., Bate, M. R., Nordlund, Å., Reipurth, B., & Zinnecker, H. 2007, in Protostars and Planets V, ed. B. Reipurth, D. Jewitt, & K. Keil, 459–476
Whitworth, A. P. & Zinnecker, H. 2004, A&A, 427, 299

4.15 The IACOB Project: Synergies for the Gaia Era

Sergio Simón-Díaz[1,2], M. Garcia[1,2], A. Herrero[1,2], J. Maíz Apellániz[3], & I. Negueruela[4]

[1] Instituto de Astrofísica de Canarias, E-38200 La Laguna, Tenerife, Spain.
[2] Departamento de Astrofísica, Univ. de La Laguna, E-38205 La Laguna, Tenerife, Spain.
[3] Instituto de Astrofísica de Andalucía, CSIC, Apdo. 3004, E-18080 Granada, Spain.
[4] Dpto. de Física, Ingeniería de Sistemas y teoría de la Señal. Escuela Politécnica Superior. Univ. Alicante, Apdo. 99, E-03080 Alicante, Spain.

Abstract

The *IACOB spectroscopic survey of Galactic OB stars* is an ambitious observational project aimed at compiling a large, homogeneous, high-resolution database of optical spectra of massive stars observable from the Northern hemisphere. The quantitative spectroscopic analysis of this database, complemented by the invaluable information provided by Gaia (mainly regarding photometry and distances), will represent a major step forward in our knowledge of the fundamental physical characteristics of Galactic massive stars. In addition, results from this analysis will be of interest for other scientific questions to be investigated using Gaia observations. In this contribution we outline the present status of the *IACOB spectroscopic database* and indicate briefly some of the synergy links between the IACOB and Gaia scientific projects.

Introduction

The Gaia mission will gather a complete astrometric, photometric and spectroscopic dataset of over one billion stars. Its instrument performance (see e.g., Prusti [2011]) is designed to provide information about proper motions, radial velocities, photometric variability, distances, interstellar reddening, rotational velocities, atmospheric parameters, and element abundances of the observed stars. The Gaia observations will hence definitely challenge many aspects of our present view of the stellar component in the Milky Way.

While Gaia photometric and spectroscopic observations will allow a proper characterization of the stellar properties of late-B and cooler stars (including abundances), a similar study in the case of O and early-B type stars will be somewhat limited. On the one hand, the Balmer jump (planned to be observed by the Blue Photometer) is less accurate as indicator of the stellar temperature in this type of stars than in the case of cooler stars. On the other hand, as illustrated in Fig. 4.46, the spectral range observed by the Radial Velocity Spectrometer is almost empty of spectral features which could be used to determine rotational velocities, and stellar parameters/abundances (contrarily to the optical range). Although Gaia observations will allow to distinguish between early/mid-O, late-O, and early-B type stars, a proper (accurate) determination of the stellar parameters will require combining these observations with optical spectra (see more details in Section *Quantitative spectroscopic analyses of massive stars in the Milky Way*).

Complementing the Gaia database with optical spectroscopic observations of O and early-B stars is hence of crucial importance for any Gaia scientific project involving stellar parameters and/or abundances of massive stars. Some examples in the context of this conference include the full characterization of the IMF of stellar clusters (also accounting for the high-mass tail), the study of the impact of massive stars on the formation and dynamical evolution of young stellar clusters and associations, or the investigation of self-pollution by SNe Type II products in stellar associations with signatures of triggered star formation.

Although originally motivated by scientific drivers not directly related to Gaia[4], large (on going) optical spectroscopic surveys of O and B-type stars such as GOSSS (P.I. Maíz Apellániz), OWN (P.I. Barbá), NoMaDS (P.I. Pellerin), IACOB (P.I. Simón-Díaz), and IACOB-sweg (P.I. Negueruela) will become very valuable in the Gaia era. All these surveys, initially independent, are now coordinated and

[4]The GREAT (Gaia Research for European Astronomy Training) networking programme also plans to observe massive stars in selected clusters as part of more general long term spectroscopic surveys preparing and following Gaia (see Blomme et al. [2011]).

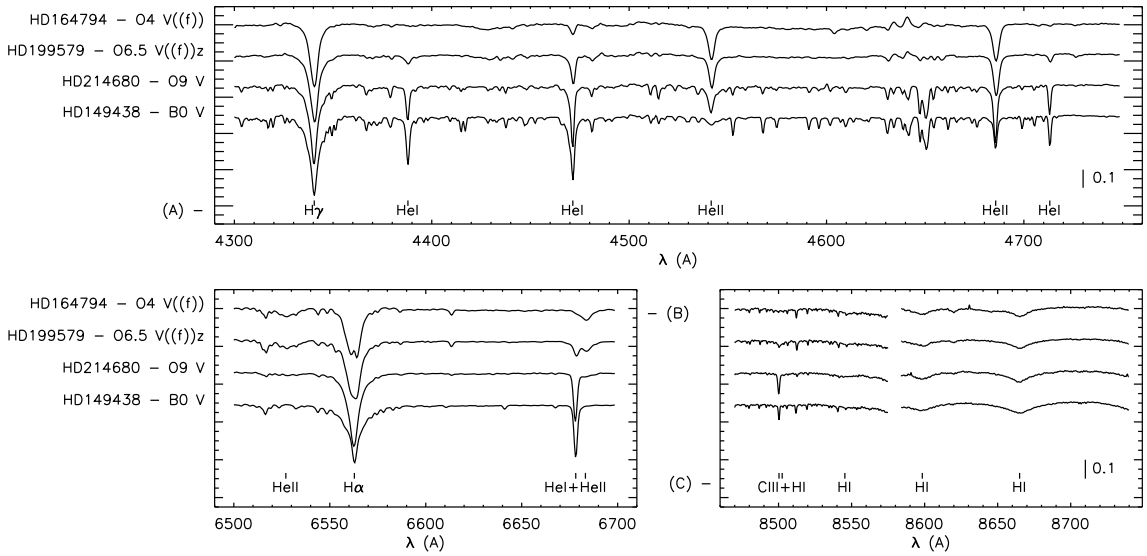

Figure 4.46: *IACOB-sweg* spectra of four representative O stars in the optical (panels A and B) and Gaia (panel C) spectral ranges. Contrary to the optical range, the Gaia range is almost empty of stellar features in the case of O and early B-type stars. Note that the small narrow lines in the Gaia range (appart from the C II line) are telluric.

the corresponding spectroscopic databases are planned to be made public in the future for their maximum exploitation in different scientific contexts.

This contribution concentrates on the *IACOB spectroscopic database* and its scientific exploitation, specially remarking some of the synergy links between the IACOB and Gaia scientific projects. Notes on the other surveys can be found elsewhere (e.g. Barbá et al. [2010]; Sota et al. [2011]; Maíz Apellániz et al. [2011]).

The IACOB project

The *IACOB project* (P.I. Simón-Díaz) aims at progressing in our knowledge of Galactic massive stars using a large, homogeneous, high-quality spectroscopic dataset and modern tools for the quantitative spectroscopic analysis of O and B-type stars. The project is divided into six main working packages. The first one is devoted to the compilation of the *IACOB spectroscopic database of Northern Galactic OB stars*, a very important piece of the project. The other five refer to the scientific exploitation of this unique database of high-resolution spectra, covering several aspects of interest in the massive star research:

WP-1: The *IACOB spectroscopic database*
WP-2: Line-broadening in OB stars
WP-3: Quantitative spectroscopic analyses
WP-4: Abundances in OB-type stars
WP-5: Binary/multiple systems
WP-6: massive stars and the ISM

The number of studies planned to be developed in the framework of the IACOB project (i.e. using spectra from the IACOB database) is large. At present, we are concentrating our efforts on the investigation of the so-called *macroturbulent* broadening affecting the line-profiles of massive stars and its possible connection to stellar pulsations (e.g. Simón-Díaz et al. [2010]), on the revision of rotational velocities of Galactic OB stars, and on the accurate determination of the stellar and wind parameters of the single O and B stars in the sample. Some IACOB spectra have also been used to investigate the degree of chemical (in)homogeneity of B-type stars in the Ori OB1 association (Simón-Díaz [2010]; Nieva & Simón-Díaz [2011]), or to provide a firm comfirmation of the presence of a third massive star component in the σ Ori AB system (Simón-Díaz, Caballero & Lorenzo [2011]).

Gaia observations will have a definite importance in some of the outcomes of the IACOB project (mainly regarding WP3). In addition, the analysis of spectra from the IACOB database (in combination with Gaia observations) will provide unvaluable information for other scientific projects studying our Galaxy and/or some of its components. Some examples of the synergies between IACOB and Gaia will be provided in Section *Quantitative spectroscopic analyses of massive stars in the Milky Way*, but first

we briefly summarize the present status and some future prospects of the *IACOB database*.

The IACOB spectroscopic database: updates and future prospects

The first spectra for the *IACOB spectroscopic database* were obtained with the FIES instrument attached to the Nordic Optical Telescope (NOT) in El Roque de los Muchachos Observatory (La Palma, Spain) in November 2008. Since then, and up to August 2011, we have compiled $\sim$1000 spectra of over 200 bright Galactic OB stars with $\delta \geq$-25 deg. The present version of the database (v2.0) is mainly built on the IACOB v1.0 (Simón-Díaz et al. [2011a]) plus the following updates: (1) the number of observed stars and compiled multi-epoch spectra has increased during 14 new observing nights from 105 and 720 to 204 and 984, respectively; (2) the database is now complete up to $V = 8$ mag in the case of O-type stars; (3) the number of observed B0 – B2 stars has also increased (now also including giants, and not only dwarfs and supergiants).

New observations are already scheduled with FIES for September 2011. We plan (1) to observe fainter O stars (up to $V = 9$ mag) with a somewhat lower resolution (R = 23 000), (2) to increase the number of B-type stars in the database, (3) to obtain at least 3 epochs for the whole sample, and (4) to follow up some of the detected binary/multiple systems.

Since June 2011 (and planned to be completed in November 2011) the *IACOB database* also counts on a new supplement (*IACOB-sweg*, P.I. I. Negueruela). These new observations, obtained with the HERMES spectrograph attached to the Mercator telescope in La Palma, extend further to the red (up to 9000 Å) than the FIES spectra. They were planned to investigate the spectroscopic behaviour of MK standards with spectral types earlier than B9 in the Gaia range for a optimal future exploitation of the Gaia spectra of this type of stars.

Quantitative spectroscopic analyses of massive stars in the Milky Way

As discussed in the Introduction, and illustrated in Fig. 4.46 the Gaia spectroscopic observations will be empty of spectral features which could be used to extract information about the fundamental physical parameters of OB-type stars. The situation is different when we consider the optical spectral range. The quantitative spectroscopic analysis of this spectral range makes it possible to determine the rotational velocities, effective temperatures, gravities and abundances of these stars (see e.g. the recent review by Martins [2011], and references therein). When the optical analyses are complemented with the information provided by other spectroscopic diagnostics (mainly the UV) we can also constrain the wind properties of the analyzed stars.

Nowadays we count with very powerful tools, such as advanced stellar atmosphere codes and stellar evolution models, which have allowed us to make a remarkable progress in our knowledge of the physical and wind properties of massive stars (see review by Puls [2008]). The outcome of the quantitative spectroscopic analysis of medium and high resolution optical spectra of Galactic OB-type stars by means of modern stellar atmosphere codes is now accepted to have reached a high degree of reliability (viz. Herrero et al. [2002]; Repolust et al. [2004]; Lefever et al. [2007]; Markova & Puls [2008]; Simón-Díaz [2010]; Nieva & Przybilla [2010]). However, it is important not to forget that our interpretation of these results may be clearly biased in some cases, mainly due to observational limitations.

The first point refers to the stellar luminosities, radii and masses. To obtain these fundamental parameters we need to combine the derived spectroscopic parameters with information about the distance and extinction to the star. At present, the distance to most massive stars in our Galaxy are poorly constrained and hence luminosities, radii and masses resulting from our analyses are somewhat uncertain in many cases. Table 4.4 illustrates how critical is this point in the case of the O9 V star 10 Lac (d $\sim$ 580 pc). Fortunately, this situation will change very soon thanks to Gaia.

The second point refers to binarity/multiplicity. Most or all massive stars are suspected to be born as part of multiple systems (see e.g. Zinnecker & Yorke [2007]; Mason et al. [2009]; and references therein). Many of these binary/multiple systems remain still unresolved; therefore, it would not be so strange to find studies of massive stars in which its multiple nature has not been detected (since these are based on single-epoch spectroscopic and photometric observations) and consequently the derived stellar parameters are erroneous.

Finally, even in isolated objects, other secondary properties such as mass-loss rate and rotation also have an important impact on stellar evolution of massive stellar objects (Meynet & Maeder [2000]); while it would be desirable to consider a sample of isolated stars large enough to investigate in a systematic

Table 4.4: Results from the analysis of 10 Lac (O9 V) assuming the present accuracy in distance, photometry and stellar parameters. The uncertainties in R, L, and M due to error propagation of the uncertainties in stellar parameters ($T_{\rm eff}$ and $\log g$) and distance are indicated separately. The later one (in brackets) clearly dominates. We need more accurate distances.

d =589±79 pc (13%)	Megier et al. [2009]	$T_{\rm eff}$ = 35000±600 K	
$m_{\rm v}$ =4.879±0.008	Maíz Apellániz et al. [2004]	$\log g$ = 3.87±0.10 dex	
$(B-V)$ = -0.201±0.010	Maíz Apellániz et al. [2004]		
$(B-V)_0$ = -0.27	Martins & Plez [2006]	$R/R_\odot$ = 7.52±0.09	[±1]
$A_{\rm v}$ = 0.214±0.03		$\log(L/L_\odot)$ = 4.88±0.02	[±0.12]
$M_{\rm v}$ = -4.15±0.30		$M/M_\odot$ = 16±3	[±5]

manner the effect of all these parameters, the number of objects analyzed up to now in a consistent way is still limited.

Quantitative spectroscopic analyses of multi-epoch, large sample observations of Galactic OB stars (combining spectroscopy, photometry, and accurate distance determinations) are hence one of the next important steps to improve our knowledge of massive stars and clarify some of the gaps that still remain in this important field of Astrophysics. The *IACOB project* is following this approach in the case of Galactic stars. At present, we are performing the analysis of the stars included in the *IACOB spectroscopic database* following an automatic best-fit strategy based on a extensive grid of synthetic HHe spectra computed with the FASTWIND stellar atmopshere code (see details in Simón-Díaz et al. [2011b]). As a results of this analysis, the project will provide a complete database of stellar parameters of Galactic OB stars homogeneously determined. As commented above, the use of accurate distances and multi-band photometry will be of crucial importance to complete the stellar parameters determined spectroscopically with luminosities, radii, and masses. In this sense, Gaia observations will come right on time.

The final aim of the IACOB spectra and the associated database of stellar parameters (including also rotational velocities and abundances) is to increase the amount of observational constraints which may help to advance in some of the still outstanding problems in the field of massive stars. In addition, they can be used to study e.g. the kinematics of some of the Galactic OB clusters and associations, or the impact that massive stars have on the formation of other stellar objects (via their strong winds and ionizing fluxes). Finally, we plan to provide the spectral energy distributions (SEDs) predicted by the FASTWIND code for all the analyzed stars so they can be then used in the study of the interstellar extinction along different line of sights (when combined with the observed SEDs provided by Gaia).

Acknowledgments

SSD kindly acknowledge the staff at the Nordic Optical Telescope for their professional competence and always useful help during the observing nights. Financial support by the Spanish Ministerio de Ciencia e Innovación under projects AYA2008-06166-C03-01 and AYA2010-21697-C05-05. AYA2010-21697-C05-04, and by the Gobierno de Canarias under project PID2010119. This work has also been partially funded by the Spanish MICINN under the Consolider-Ingenio 2010 Program grant CSD2006-00070: First Science with the GTC (`http://www.iac.es/consolider-ingenio-gtc`).

Bibliography

Barbá, R. H., Gamen, R., Arias, J. I., et al. 2010, RMxAA Conf. Series, 38, 30
Blomme et al., 2011 (in prep.)
Herrero, A., Puls, J., & Najarro, F. 2002, A&A, 396, 949
Lefever, K., Puls, J., & Aerts, C. 2007, A&A, 463, 1093
Maíz Apellániz, J., Walborn, N. R., Galué, H. Á., & Wei, L. H. 2004, ApJS, 151, 103
Maíz Apellániz, et al. 2011 (in prep.)
Markova, N., & Puls, J. 2008, A&A, 478, 823
Martins, F., & Plez, B. 2006, A&A, 457, 637
Martins, F. 2011, Bulletin de la Societe Royale des Sciences de Liege, 80, 29
Mason, B. D., Hartkopf, W. I., Gies, D. R., et al. 2009, AJ, 137, 3358

Megier, A., Strobel, A., Galazutdinov, G. A., & Krełowski, J. 2009, A&A, 507, 833
Meynet, G., & Maeder, A. 2000, A&A, 361, 101
Nieva, M.-F., & Przybilla, N. 2010, Hot and Cool: Bridging Gaps in Massive Star Evolution, 425, 146
Nieva, M.-F., & Simón-Díaz, S. 2011, A&A, 532, A2
Prusti, T. 2011, EAS Publications Series, 45, 9
Puls, J., Urbaneja, M. A., Venero, R., et al. 2005, A&A, 435, 669
Puls, J. 2008, IAU Symposium, 250, 25
Repolust, T., Puls, J., & Herrero, A. 2004, A&A, 415, 349
Simón-Díaz, S. 2010, A&A, 510, A22
Simón-Díaz, S., Herrero, A., Uytterhoeven, K., et al. 2010, ApJL, 720, L174
Simón-Díaz, S., Castro, N., Garcia, M., et al. 2011, BSRSL, 80, 514
Simón-Díaz, S., Caballero, J. A., & Lorenzo, J. 2011, ApJ (in press), arXiv:1108.4622
Simón-Díaz, S., Castro, N., Herrero, A., et al. 2011 (in prep.)
Sota, A., Maíz Apellániz, J., Walborn, N. R., et al. 2011, ApJS, 193, 24
Zinnecker, H., & Yorke, H. W. 2007, ARA&A, 45, 481

4.16 Probing the Mass Accretion Process in the Magellanic Clouds

Loredana Spezzi[1], G. De Marchi[1], N. Panagia[2], A. Sicilia-Aguilar[3], and B. Ercolano[4]

[1] European Space Agency (ESTEC), PO Box 299, 2200 AG Noordwijk, The Netherlands
[2] Space Telescope Science Institute, 3700 San Martin Drive, Baltimore, MD 21218
[3] Max-Planck-Institut für Astronomie, Königstuhl 17, 69117 Heidelberg, Germany
[4] Ludwig-Maximilians-Universitaet, University Observatory Munich, Scheinerstr. 1, D-81679 München, Germany

Abstract

We present a multi-wavelength study of three star-forming regions, spanning the age range 1 – 14 Myrs, located between the 30 Doradus complex and the supernova SN1987A in the Large Magellanic Cloud (LMC). We use a novel self-consistent method to reliably identify pre-main sequence (PMS) objects actively undergoing mass accretion and estimate their stellar properties and mass accretion rate ($\dot{M}$). Our study provides important hints on the mass accretion process of young stars in low-metallicity environments, so far poorly investigated.

Introduction

The mass accretion rate ($\dot{M}$) of young stars is a key parameter to constrain the models of both star and planet formation. $\dot{M}$ is an indicator of the amount of gas and dust in the inner circumstellar disk and, as such, it is affected by the disk structure and evolution as well as by the formation and migration of planets (see, e.g., Calvet et al. [2000]). However, the measure of $\dot{M}$ is very challenging because it requires medium to high resolution spectroscopy of individual young objects. As a result, the data collected so far are limited to nearby (d $\lesssim$ 1 – 2 kpc) star-forming regions with essentially solar metallicity (e.g. Padgett [1996]).

Recently, De Marchi et al. [2010] presented a novel method to identify pre-main sequence (PMS) objects actively undergoing mass accretion and determine their $\dot{M}$. This method relies solely on HST photometry and allows us to overcome the limitations affecting the techniques based on spectroscopy. We have now started a pilot project aiming at applying this technique to the existing and extensive HST photometry of star-forming regions in the Milky Way (MW) and the MCs. In this paper we present the results of this study in the Large Magellanic Cloud (LMC). Because of its relative proximity (51.4 $\pm$ 1.2 kpc; Panagia [1991]; Panagia et al. [1991]) and low metal content (Z = 0.007; Maeder et al. [1999]; and references therein), the LMC is a very interesting test case for star formation studies and, specifically, for mass accretion studies, because it offers a unique opportunity to study a resolved accreting stellar population in an environment with a chemical composition different than the MW (Z $\approx$ 0.018; see Esteban & Peimbert [1995]).

Data sample

We selected three 162×162 arcsec^2 areas in the LMC located between the 30 Doradus star-forming complex and the supernova SN1987A (Fig. 4.47). These observations were performed from February 1999 to November 2003 with the Wide Field Planetary Camera 2 (WFPC2) of the HST using the f606w (V), f656n (Hα) and f814w (I) filters. The three fields were selected following two basic criteria: i) exposure time long enough to allow the detection of objects down to 0.8 – 1 M$_\odot$ at the distance of LMC in the three filters; ii) different environmental conditions, such as vicinity to OB stars and amount of interstellar gas and dust, in order to study the behaviour of $\dot{M}$ in regions expected to be site of different star formation events.

The basic data set used for this paper was retrieved from the HST archive at the Canadian Astronomy Data Centre (CADC). The sources extraction and photometry was performed on the stacked

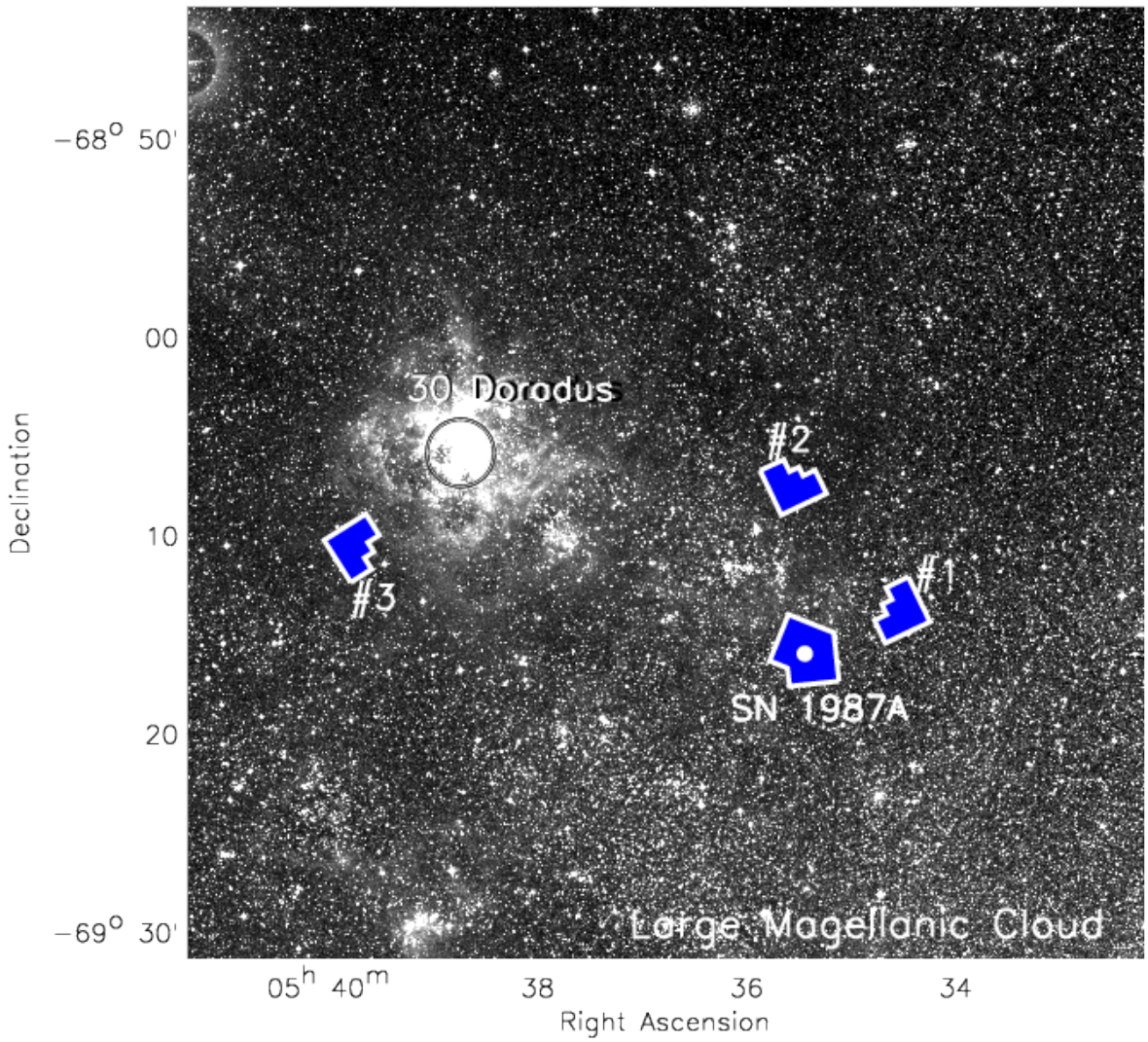

Figure 4.47: R-band image of a 40×40 arcmin^2 area in the LMC from the Sloan Digital Sky Survey. The polygons display the four regions observed with HST/WFPC2 analyzed in this paper. The position of 30 Doradus star-burst cluster and the supernova SN1987A are also indicated.

images using the SExtractor 2.5 tool by Bertin & Arnouts [1996]. Following the prescriptions of the HST Data Handbook for the WFPC2 (Baggett et al. [2002])[5], we adopted a 0.5 arcsec aperture radius for magnitude extraction and then calibrated the instrumental magnitudes to the VEGAMAG photometric.

Selection of PMS stars and measure of $\dot{M}$

We select PMS stars in each of the four fields and determine their mass accretion rates using narrow-band Hα and broad-band V and I dereddened photometry, as described in De Marchi et al. [2010]. We use the median (V-Hα) dereddened colour of stars with small ($\leq$ 0.1) photometric errors in the three (V, I and Hα) bands, as a function of (V-I), to define the reference template with respect to which the excess Hα emission is sought. We select a first sample of stars with excess H? emission by considering all those with a (V-Hα) colour above that of the reference line by 4 times their intrinsic photometric uncertainty. Then we derive the equivalent width of the Hα emission (EW$_{H\alpha}$) from the measured colour excess. We finally consider as bona fide PMS stars those objects with EW$_{H\alpha>}$ 20 Å and V-I > 0; this allows us to clean our sample from possible contaminants (i.e. older stars with chromospheric activity and Ae/ Be stars, respectively). We derive the effective temperature (T$_{eff}$), radius (R$_\star$) and luminosity (L$_\star$) of our bona fide PMS stars from their dereddened (V-I) colour and V magnitude. We adopt the distance of 51.4 kpc

[5]http://www.stsci.edu/instruments/wfpc2/Wfpc2_dhb/WFPC2_longdhbcover.html

to the LMC and use the tabulation of HST/WFPC2 photometry as a function of T_{eff} by Bessel et al. [1998]. Mass ($M_\star$) and age of each star are then derived by comparing its $L_\star$ and T_{eff} with expectations from the theoretical evolutionary models for PMS stars calculated on purpose by P. G. Prada Moroni for the metallicity of the LMC (Z = 0.007). The mass accretion rate is finally derived from the free-fall equation as:

$$\log \dot{M}(M_\odot/yr) = -7.39 + \log \frac{L_{acc}}{L_\odot} + \log \frac{R_\star}{R_\odot} - \log \frac{M_\star}{M_\odot} \tag{4.5}$$

where L_{acc} is the energy released by the accretion process, directly proportional to the Hα luminosity (Dahm [2008]).

For a more detailed description of this method we refer the reader to the original paper by De Marchi et al. [2010].

Results: Magellanic Clouds vs. Milky Way

We identified and determined the mass accretion rates for 298 bona fide PMS stars in our field #1, 347 in our field #2 and 193 in our field #3. Adding the 106 PMS stars characterized by De Marchi et al. [2010] in the field around the supernova SN1987A, we end up with a sample of about 1000 bona fide PMS stars in the LMC with masses between 0.5 and 6 $M_\odot$ and ages between ∼1 and 20 Myr, thereby increasing by a factor of five the current sample of PMS stars with a measured $\dot{M}$. Our sample represents also the largest $\dot{M}$ dataset for low-metallicity stars presented so far. The majority of our PMS stars (∼ 94%) have masses below 2 $M_\odot$, i.e. in the T Tauri star range. The remaining ∼ 6% are Herbig Ae/Be stars.

Using this large sample of PMS stars with $\dot{M}$ measured in a homogeneous way, we investigate the dependency of $\dot{M}$ on stellar mass, age and metallicity, in relation with the proposed mechanisms of disk dispersal. The conclusions of our study are as follows:

- In the mass range 1 – 2 $M_\odot$, the $\dot{M}$ of PMS stars in the LMC increases with stellar mass as $\dot{M} \propto M_\star^b$ with $1 \lesssim b \lesssim 1.6$, i.e. slightly slower than the second power law found for galactic PMS stars in the same mass regime;
- We find that the typical $\dot{M}$ of PMS stars in the LMC is higher than for galactic PMS stars of the same mass, independently of their age;
- Considering the caveats of isochronal age and $\dot{M}$ estimates, the typical difference in $\dot{M}$ between the MCs and our MW appear to be about an order of magnitude;
- Currently available models of disk evolution/dispersal support the hypothesis that the higher $\dot{M}$ measured in the LMC might be a consequence of its lower metallicity with respect to our MW;
- The sample of PMS populations studied in the LMC shows a variety of behaviours with respect to disk photo-evaporation due to external radiation fields. In some of the observed regions, we find clear evidence that circumstellar disks have been eroded by photo-evaporation caused by nearby massive stars, while in other regions there is no evidence of such an effect. We ascribe the lack of a global trend to contamination/statistical effects;

In order to clarify these issues, improved modelling/calculations of disk dispersal at low-metallicity are needed, as well as observations of slightly older (e.g. 30 – 50 Myr) low-metallicity regions than those presented in this paper.

Acknowledgments

We thank A. Natta, L. Testi and G. Beccari for the many useful discussions and suggestions. We are grateful to M. Romaniello for making his tool for calculating stellar masses and ages available, and to P.G. Prada Moroni for providing unpublished PMS evolutionary models for the metallicity of the LMC. This publication makes extensive use of data products from the HST archive at the Canadian Astronomy Data Centre (CADC), operated by the National Research Council of Canada with the support of the Canadian Space Agency.

Bibliography

Baggett, S., et al. 2002, in HST WFPC2 Data Handbook, v. 4.0, ed. B. Mobasher, Baltimore, STScI
Bessel, M.S., Castelli, F., & Plez, B. 1998, A&A, 333, 231
Bertin, E., & Arnouts, S. 1996, A&A Supp., 117, 393
Calvet, N., Hartmann, L. & Strom, E. 2000, in "Protostars and Planets", eds V. Mannings, A. Boss, S. Russell (Tucson: University of Arizona Press), 377
Dahm, S. 2008, AJ, 136, 521
De Marchi, G., Panagia, N., & Romaniello, M. 2010, ApJ, 715, 1
Esteban, C., & Peimbert, M. 1995, Revista Mexicana de Astronomia y Astrofisica Conference Series, 3, 133
Maeder, A., Grebel, E.K., & Mermilliod, J.-C. 1999, A&A, 346, 459
Padgett, D. 1996, ApJ, 471, 847
Panagia, N. 1991, in "New Views of the Magellanic Clouds", IAU Symp. 190, eds. Y.-H. Chu, N. Suntzeff, J. Hesser, D. Bohlender (San Francisco: ASP), 549
Panagia, N., Gilmozzi, R.,Macchetto, F., Adorf, H.-M. & Kirshner, R. P. 1991, ApJ, 380, L23

4.17 Do All O Stars Form in Star Clusters?

Carsten Weidner[1], V. V. Gvaramadze[2,3,4], P. Kroupa[2], and J. Pflamm-Altenburg[2]

[1] Scottish Universities Physics Alliance (SUPA), School of Physics & Astronomy, University of St Andrews, North Haugh, St Andrews, Fife KY16 9SS, Scotland, UK
[2]Argelander-Institut für Astronomie (Sternwarte), Auf dem Hügel 71, D-53121 Bonn, Germany
[3]Sternberg Astronomical Institute, Moscow State University, Universitetskij Pr. 13, Moscow 119992, Russia
[4]Isaac Newton Institute of Chile, Moscow Branch, Universitetskij Pr. 13, Moscow 119992, Russia

Abstract

The question whether or not massive stars can form in isolation or only in star clusters is of great importance for the theory of (massive) star formation as well as for the stellar initial mass function of whole galaxies (IGIMF-theory). While a seemingly easy question it is rather difficult to answer. Several physical processes (e.g. star-loss due to stellar dynamics or gas expulsion) and observational limitations (e.g. dust obscuration of young clusters, resolution) pose severe challenges to answer this question. In this contribution we will present the current arguments in favour and against the idea that all O stars form in clusters.

Introduction

Besides huge efforts observationally and theoretically, the question how massive stars (m $>$ 10 $M_\odot$) form has not been answered satisfactory yet. Amongst others, two main theories of the formation of massive stars have been put forward. One theory being the monolithic collapse of very massive and dense cores (McKee & Tan [2003]; Krumholz [2006]) into a single star or a binary. As this theory has no requirements for the surroundings of such cores, it allows the formation of isolated O stars without a star cluster associated to them. However, the question how the isolated massive core can form remains open. The other important theory is competitive accretion, where massive stars form in the dense centres of star clusters (Bonnell et al. [1997]) and therefore it does not predict isolated O stars.

Shown in Fig. 4.48 is a compilation of star clusters from the literature and the most-massive stars in them (Weidner & Kroupa [2006]; Weidner et al. [2010]). The Figure shows a tight correlation between the mass of the most-massive star, $m_{\rm max}$, and the mass of the cluster, $M_{\rm ecl}$. Especially for massive clusters this $m_{\rm max}$-$M_{\rm ecl}$ relation is well below what is expected when randomly sampling stars (red solid line) from a stellar initial mass function (IMF). If the formation of massive stars is independent of their natal environment, the $m_{\rm max}$-$M_{\rm ecl}$ relation should be well described by random sampling. The existence of a non-trivial $m_{\rm max}$-$M_{\rm ecl}$ relation is therefore direct evidence against the formation of O stars in isolation.

But if all O stars are formed in star clusters why do we indeed observe O stars in the Galactic field?

Massive field stars

Massive field stars are OB stars that are not members of any currently known star cluster, OB association or star-forming region. So far about 20 – 30% of all Galactic O stars are in the field (Gies [1987]). These stars can be separated into two groups:

- $\sim$ 25% are high-velocity OB stars (typical $>$ 30 km/s; runaway stars; Blaauw [1961]; Gies [1987]),
- $\sim$ 75% are low-velocity ($\leq$ 30 km/s) OB stars.

But have these massive field stars formed in isolation or could they originate from star clusters?

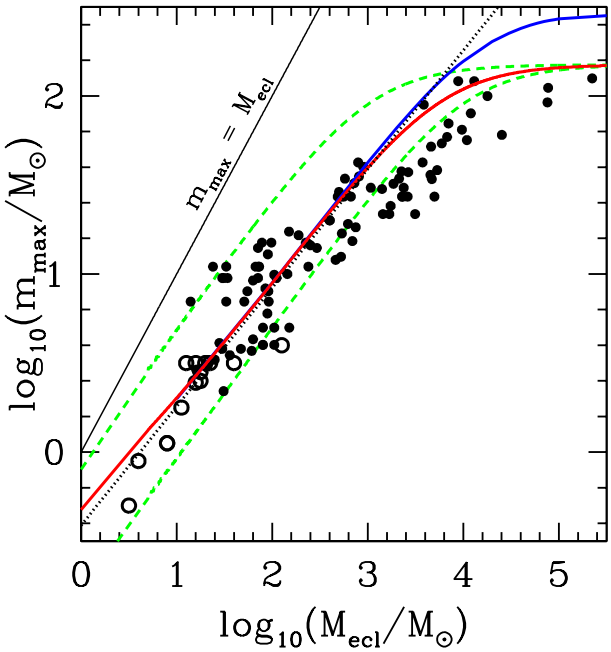

Figure 4.48: Most-massive star ($m_{\rm max}$) in a cluster versus the stellar mass of the young dynamically unevolved "embedded" cluster ($M_{\rm ecl}$). The filled dots are observations compiled by Weidner et al. [2010], while the open circles are new data from Kirk & Myers [2011]. The solid lines through the data points are the medians expected for random sampling when using a fundamental upper mass limit, $m_{\rm max*}$, of 150 $M_\odot$ (lower solid, red line) and $m_{\rm max*} = 300$ $M_\odot$ (upper solid, blue line; Crowther et al. [2010]). The dashed lines are the 1/6 and 5/6th quantiles which encompass 66% of the most-massive stars if they are randomly sampled from an IMF with an upper mass limit of 150 $M_\odot$. The dotted line shows the prediction for a relation by Bonnell et al. [2003] from numerical models of molecular clouds with less than 10000 $M_\odot$. The thin solid line marks the limit where a cluster is just made out of one star.

The origin of runaway OB stars

Generally, high velocity massive field OB stars (runaway stars) originate from two mechanisms:

- Disruption of a short-period binary after a supernova explosion (Blaauw [1961]; Stone [1991]),
- or by three- or many-body interactions in star clusters (Poveda et al. [1967]; Gies & Bolton [1986]).

Recently, this picture has been expanded by a third mechanism which combines the previously known two ones. In the two-step ejection mechanism, a binary of two O stars is ejected and then later the more massive star in the binary explodes as a supernova, shooting the secondary in a random direction and changing its velocity, too (Pflamm-Altenburg & Kroupa [2010]). Such stars can not be traced back to their parent star cluster and will be mistakenly identified as high-mass stars formed in isolation.

Runaway stars can be observationally identified by several direct and indirect methods. The direct methods are based on detection of high ($>$ 30 km/s) peculiar transverse and/or radial velocities via proper motion measurements (e.g. Blaauw [1961]; Moffat et al. [1998]; Mdzinarishvili & Chargeishvili [2005]; Tetzlaff et al. [2010]) and spectroscopy (e.g. Massey et al. [2005]; Evans et al. [2006]; Evans et al. [2010]), respectively. The indirect indications of the runaway nature of some field OB stars are the large ($>$ 200 pc) separation of these stars from the Galactic plane (e.g. Blaauw [1961]; Blaauw [1993]) and the presence of bow shocks around them (e.g. Gvaramadze & Bomans [2008]; Gvaramadze et al. [2010]; Gvaramadze et al. [2011]). Fig. 4.49 shows an example of such a bow shock.

Figure 4.49: Bow shock in front of ζ Ophiuchi. Credit: NASA/JPL-Caltech/WISE team.

The origin of low-velocity field OB stars

For low-velocity massive field stars several different origins are possible:

- They formed in isolation,
- they are the low-velocity tail of the ejected stars,
- their true 3D-velocity has not been determined correctly and they are unrecognised runaways,
- they are members of undetected or dissolved star clusters,
- they are blue stragglers, either directly ejected as such or formed from merged ejected binaries.

It is important to note that a two-step ejection can slow down or stop runaway OB stars (Pflamm-Altenburg & Kroupa [2010]) and therefore make them look like low-velocity field OB stars.

Furthermore, the definition of runaway stars is misleading. The typical velocity of 30 km/s used to separate runaways from low-velocity stars is an observational definition and not necessarily a typical ejection velocity of stars from a star cluster. Shown in Fig. 4.50 is the distribution of escape velocities of all ejected stars form a series of 100 N-body calculations of 500 binaries over 5 Myr. A high-velocity tail certainly exists but in such low-mass clusters these are not massive stars. In all 100 N-body calculations 30 stars ($\sim$ 10% of the massive stars, each individual cluster has only 3 stars above 10 $M_\odot$) with masses above 10 $M_\odot$ have been ejected within 5 Myr. But their escape velocities are only between 7 and 14 km/s. However, they still travel between 1 and 50 pc after their escape within the 5 Myr (Weidner et al. [2011]).

High-mass star formation in isolation?

From an originally proposed fraction of 4% of O stars formed in isolation (de Wit et al. [2004]; de Wit et al. [2005]) careful back-tracking of individual stars (Schilbach & Röser [2008]) could reduce this percentage to 2%. Further studies of the five remaining candidates revealed that two of them have bow shocks and are therefore ejected stars, too (Gvaramadze & Bomans [2008]). This reduces the fraction of O stars formed in isolation to 1% (Weidner et al. [2011b], submitted). But it should be noted that of the three remaining candidates two cases (HD 193793 and HD 202124) haven't been studied for bow shocks so far. And while in the case of HD 124314 no bow shock has been found it is important to note that bow shocks are only formed under certain circumstances. Furthermore, does the two-step ejection method predicts

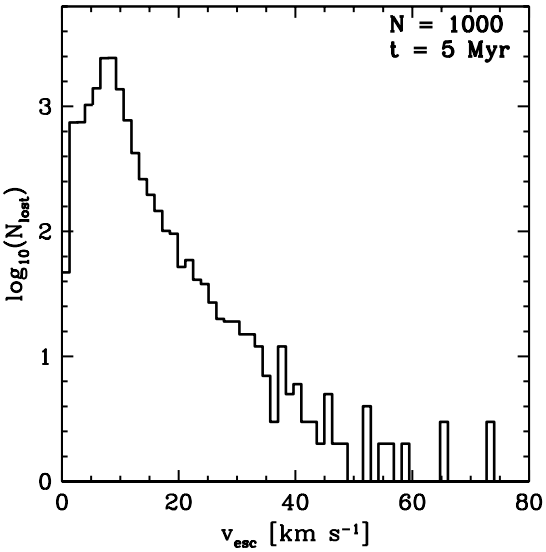

Figure 4.50: Velocity distribution of all stars (including low-mass stars) escaped after 5 Myrs from 100 star cluster calculations starting with 500 binaries ($M_{\rm cluster} \sim 340$ M$_\odot$) each (Weidner et al. [2011]). Note that the velocity distribution and the escape fraction depends strongly on the initial stellar density of the cluster (see the contribution by Pflamm-Altenburg these proceedings).

between 1 and 2% of apparently isolated O stars which can not be tracked back to their natal cluster (Pflamm-Altenburg & Kroupa [2010]).

To conclude, there is no significant evidence for massive stars formed in isolation.

Acknowledgments

VVG acknowledges financial support from the Deutsche Forschungsgemeinschaft.

Bibliography

Blaauw, A. 1961, Bull. Astron. Inst. Netherlands, 15, 265
Blaauw, A. 1993, in Astronomical Society of the Pacific Conference Series, Vol. 35, Massive Stars: Their Lives in the Interstellar Medium, ed. J. P. Cassinelli & E. B. Churchwell, 207–+
Bonnell, I. A., Bate, M. R., Clarke, C. J., & Pringle, J. E. 1997, MNRAS, 285, 201
Bonnell, I. A., Bate, M. R., & Vine, S. G. 2003, MNRAS, 343, 413
Crowther, P. A., Schnurr, O., Hirschi, R., et al. 2010, MNRAS, 408, 731
de Wit, W. J., Testi, L., Palla, F., Vanzi, L., & Zinnecker, H. 2004, A&A, 425, 937
de Wit, W. J., Testi, L., Palla, F., & Zinnecker, H. 2005, A&A, 437, 247
Evans, C. J., Lennon, D. J., Smartt, S. J., & Trundle, C. 2006, A&A, 456, 623
Evans, C. J., Walborn, N. R., Crowther, P. A., et al. 2010, ApJ, 715, L74
Gies, D. R. 1987, ApJS, 64, 545
Gies, D. R. & Bolton, C. T. 1986, ApJS, 61, 419
Gvaramadze, V. V. & Bomans, D. J. 2008, A&A, 490, 1071
Gvaramadze, V. V., Kroupa, P., & Pflamm-Altenburg, J. 2010, A&A, 519, A33+
Gvaramadze, V. V., Pflamm-Altenburg, J., & Kroupa, P. 2011, A&A, 525, A17+
Kirk, H. & Myers, P. C. 2011, ApJ, 727, 64
Krumholz, M. R. 2006, ApJ, 641, L45
Massey, P., Puls, J., Pauldrach, A. W. A., et al. 2005, ApJ, 627, 477
McKee, C. F. & Tan, J. C. 2003, ApJ, 585, 850
Mdzinarishvili, T. G. & Chargeishvili, K. B. 2005, A&A, 431, L1
Moffat, A. F. J., Marchenko, S. V., Seggewiss, W., et al. 1998, A&A, 331, 949

Pflamm-Altenburg, J. & Kroupa, P. 2010, MNRAS, 404, 1564
Poveda, A., Ruiz, J., & Allen, C. 1967, Boletin de los Observatorios Tonantzintla y Tacubaya, 4, 86
Schilbach, E. & Röser, S. 2008, A&A, 489, 105
Stone, R. C. 1991, AJ, 102, 333
Tetzlaff, N., Neuhäuser, R., Hohle, M. M., & Maciejewski, G. 2010, MNRAS, 402, 2369
Weidner, C., Bonnell, I. A., & Moeckel, N. 2011, MNRAS, 410, 1861
Weidner, C. & Kroupa, P. 2006, MNRAS, 365, 1333
Weidner, C., Kroupa, P., & Bonnell, I. A. 2010, MNRAS, 401, 275

Chapter 5

Star Clusters as Probes of Galactic Structure

5.1 Star Formation, Feedback and the Assembly of the Milky Way

Jorge Peñarrubia[1]

[1] Institute of Astronomy & Kavli Institute for Cosmology, University of Cambridge, Madingley Road, Cambridge, CB3 0HA, UK

Abstract

The formation of galaxies in our current cosmological paradigm, Cold Dark Matter (CDM), is still an open issue. CDM model predictions appear in tension with observations regarding (i) the existence of bulge-less galaxies and the relatively high angular momentum of spiral galaxies at a fixed mass (the so-called "angular momentum catastrophe"), (ii) the apparent overabundance of bound substructures expected in CDM haloes (the "missing satellite problem"), and (iii) the absence of centrally-divergent density profiles (the so-called dark matter cusps) in the inner regions of galaxies (the "core/cup problem"). A consensus is emerging wherein the formation of stars from a gaseous medium and the effect of stellar evolution on the ISM and on the surrounding dark matter appear as both a theoretical challenge and a promising solution to several problems faced by CDM.

Introduction

The Milky Way is and will ever be the best known galaxy in the Universe, and as such represents a key system to unravel the physical processes that lead to the formation of galaxies as well as to test a plethora of predictions from the current cosmological paradigm (Cold Dark Matter, hereafter CDM).

However, comparisons to cosmological models tend to be inconclusive for the simple reason that observations refer to baryonic material, whereas most CDM simulations only consider dark matter. The complexities introduced by baryons are two-fold: on the one hand, star formation and supernova feedback still lack theoretical understanding, which introduces considerable theoretical *largesse* in description of the physical processes taking place in dark matter haloes. On the other, those processes tend to occur on scales that are poorly resolved in N-body cosmological simulations, which impedes a self-consistent numerical approach to the problem.

A remedy is typically found in what has been called 'sub-grid physics', which implement semi-

analytical prescriptions for stellar processes that take place on unresolved scales. Their goal is to reproduce in a phenomenological way what is observed in galaxies. The downside of this approach is clear: although by tuning the semi-analytical prescription of baryonic physics these models might satisfactorily describe observations, that would not necessarily validate our cosmological model.

And yet, in spite of the considerable theoretical freedom introduced by sub-grid models, some fundamental properties of spiral galaxies are still in clear tension with CDM predictions. In particular, three problems remain particularly challenging: (i) *the angular momentum catastrophe*, (ii) *the missing satellite problem* and (iii) *the core-cusp problem*.

This talk offers an overview of these issues. It will be shown that the physical processes that govern the formation and evolution of stars on a parsec scale may be indeed key to solve these problems. Yet, one should bear in mind that the formation of stars and the impact of their evolution on the ISM medium are still open topics in Astronomy. In this regard, detailed observations of star-forming regions and the effect of SNe on the ISM are key to successfully incorporate star formation/feedback processes in cosmological hydrodynamical simulations of galaxy formation, as well as to determine whether or not the tensions between CDM expectations and observational data reflect a fundamental problem for our cosmological paradigm, or simply arise from our limited understanding of the formation and evolution of stars and their impact on the gaseous medium that surround them.

The angular momentum catastrophe

Navarro & Steinmetz [2000] showed that spiral galaxies formed in cosmological simulations of structure formation rotate too slowly when compared with observations of external galaxies. Puzzlingly, their simple recipe for star formation, radiative cooling, UV background and feedback from evolving stars was able to reproduce the slope of the Tully-Fisher relationship, although it failed to provide a correct normalization. In particular, the specific angular momentum of stellar discs $\lambda_J \equiv |J|E^{1/2}/(GM^{5/2})$, where $|J|$ is the total angular momentum, $|E|$ is the gravitational energy and M the halo mass, predicted by these models at a specific galaxy mass was around one order of magnitude lower than observed.

Interestingly, Navarro & Steinmetz [2000] realized that the feedback prescription had a limited impact on the results. Only models with extreme feedback were able to bring the mass and angular momentum of spiral galaxies into accord with hierarchical galaxy formation models. Given the paucity of galaxies undergoing violent star formation/feedback processes at low redshift, these authors concluded that the empirical correlation between mass and angular momentum shown by disc galaxies may arise at early epochs of the Universe.

Springel & Hernquist [2003] performed a more complex modelling of star formation/supernova feedback that describes the multi-phase structure of star-forming gas on a few parsec scale, finding that the morphology of disc galaxies was not affected by galactic winds. The resulting spiral galaxies still possessed a massive bulge in the centre because low-angular-momentum baryons and dark matter sink to the centres of galaxies through accretion and repeated mergers.

Recently, Governato et al. [2010] have shown that bulge-less galaxies can be obtained in self-consistent hydrodynamical simulations by adopting new supernova feedback recipes. In these models strong outflows from supernovae remove low-angular-momentum gas in the accreted satellite galaxies, which inhibits the formation of bulges and decreases the dark-matter density to less than half of what it would otherwise be within the central kiloparsec of the spiral galaxy. Interestingly, violent supernova feedback also helps to increase the specific angular momentum of the galactic discs. The simulated galaxies form rotationally supported discs with realistic exponential scale-lengths and fall on both the I band and baryonic Tully-Fisher relations.

It appears therefore that the solution to the mismatch between observations of spiral galaxies and CDM expectations hinges on an even more thorny problem, that is the formation of stars from a gaseous medium and the effect of stellar evolution on the ISM.

The missing satellite problem

CDM predicts an initial fluctuation spectrum with power that continues down to small scales as $P(k) \propto k^{-1}$, which in turn yields a mass function of dark matter haloes that rises steeply towards low masses as $dN/dm \propto m^{-1.9}$. A significant fraction of these haloes survive as gravitationally self-bound units long after falling into more massive haloes. As pointed out forcefully by Klypin et al. [1999] and Moore et al. [1999], the predicted number of sub-haloes within a Milky Way-like galaxy halo greatly exceeded the

then known numbers of Milky Way or Local Group dwarf satellites, when sub-haloes and observed dwarfs were matched based on velocity dispersion or corresponding circular velocity Kauffmann et al. [1993]. This discrepancy between predicted and observed numbers has become known as the "missing satellite problem."

For a fixed intial power-spectrum of fluctuations, there existe only one possible remedy to explain the scarcity of low-mass structures in the Universe: there must be one or several astrophysical mechanisms that suppress star formation in low-mass haloes so that they do not become observable dwarf satellites; photo-heating by the meta-galactic UV background is an attractive mechanism because it naturally introduces a cutoff at approximately the correct velocity scale (see e.g. Bullock et al. [2000]). Another less appealing possibility is that the numerous dwarf companions of the Milky Way actually exist but have been missed by observational searches. This has been explored in some detail by Koposov et al. [2009] and Tollerud et al. [2008].

Independently of whether the subhaloes are visible or not, the predictions from CDM simulations of structure formation are indeed striking: we expect of the order of 10^{12} subhaloes with masses within 10^{-6}–10^{8} $M_{\odot}$ lingering in a Milky Way-size halo (Diemand et al. [2005a]). To date, only a couple of dozens have been detected.

The core/cusp problem

Cold Dark Matter (CDM) haloes produced in collision-less cosmological N-body simulations follow a nearly universal mass-density profile that diverges toward the centre as $\lim_{r\to 0}\rho(r) \propto r^{-\gamma}$ with $\gamma \geq 1$, forming a so-called 'cusp' (Dubinski & Carlberg [1991], Navarro et al. [1996, 1997] ('NFW' hereafter), Moore et al. [1998], Klypin et al. [2001], Diemand et al. [2005b], Springel et al. [2008]). Many observations aim to test this scenario by using the measured motions of dynamical tracers in galaxies to constrain slopes of the underlying dark matter density profiles (e.g., Moore [1994]; Flores & Primack [1994a]; de Blok & McGaugh [1997]; Salucci & Burkert [2000]; McGaugh et al. [2001]; Simon et al. [2005], de Blok and references therein 2010).

Remarkably, most tests tend to favour the presence of constant-density ("cored") dark matter profiles in the central regions of gas-rich spiral galaxies (Flores & Primack [1994b]; Moore [1994]; Gentile et al. [2005]) and in low-surface-brightness galaxies (McGaugh et al. [2001]; Simon et al. [2005]; de Blok [2010]). Within the framework of ΛCDM, numerical models that simulate the formation and evolution of galaxies have suggested that cusps can be transformed into cores of kpc scale either as a result of violent gas expulsion driven by supernova explosions (Navarro et al. [1996]; Read & Gilmore [2005]; Governato et al. [2010]), angular momentum transfer to the central dark matter through supernova-induced bulk gas motions (Mashchenko et al. [2008]) or the accretion of dense stellar clusters (El-Zant et al. [2001]; Tonini et al. [2006]). Thus, tests of the prevailing paradigm should be ideally performed in galaxies where the dynamical role of baryons can be neglected throughout their evolution.

Owing to their extremely large dark matter content, small spatial sizes, low luminosities and absence of gas, dwarf spheroidal galaxies (dSphs) are the best known objects to study how dark matter is distributed on the smallest galactic scales (Gilmore et al. [2007]). The Milky Way has at least twenty-five known dSphs, although recent estimates suggest that the true number may be closer to a couple of hundreds (Tollerud et al. [2008]; Koposov et al. [2009]) after accounting for the limitations imposed by our current technological capabilities. The estimated content of dark matter with respect to the number of stars (the so-called mass-to-light ratio, M/L) is the highest among all galaxy types, and it ranges from a few dozens to over a thousand. Stars, therefore, provide a negligible contribution to the galaxy mass and can be considered as simple kinematic tracers of the underlying dark matter potential.

Previous studies of the way mass is distributed in dwarf spheroidal galaxies have led to contradictory results. For example, the presence of globular clusters in the Fornax dSph (Goerdt et al. [2006]), or the existence of cold substructures in the Ursa Minor dSph (Kleyna et al. [2003]), may be indirect evidence for the existence of central dark matter cores. However, the mass-size relationship exhibited by the Milky Way dSphs (Walker et al. [2009]) appears to favour cuspy halo models (Peñarrubia et al. [2010]). Unfortunately, a *direct* inference of the mass distribution in pressure-supported systems is severely hampered by the degeneracy existing between measured line-of-sight velocity and the enclosed mass. In galaxies where stars have a radially/tangentially biased velocity distribution, the amount of dark matter would artificially appear larger/smaller than in the isotropic case. This degeneracy can only be erased by measuring the internal 3D velocities of individual stars, which is due to their remote distances beyond our technological capabilities.

However, recent dynamical analysis have shown that the mass-anisotropy degeneracy can be broken at one particular radius: the half-light radius, $R_{\rm half}$, which encompasses half of the stars in the galaxy. This arises from the observational fact that the velocity dispersion profiles of dSphs do barely change with radius, i.e. they are "flat" (Walker et al. [2007]). Under this condition the mass enclosed within $R_{\rm half}$ is independent of (i) the anisotropy profile of the stellar velocity distribution, and more importantly (ii) the assumed dark matter halo profile (Walker et al. [2009]; Wolf et al. [2010]).

Recently, Walker & Peñarrubia [2011] have suggested that in dSphs that contain at least two chemo-dynamically distinct stellar populations (Tolstoy et al. [2004]; Battaglia et al. [2006, 2011]) this finding offers the possibility to measure the mass enclosed at two different radii within the same dark matter halo. The slope of the halo mass profile follows immediately. The accuracy of the slope measurement strongly depends on the ability to separate stars according to their likelihood to belong to one or another component, as well as distinguishing Milky Way forground contaminants. These authors introduce a MCMC method that uses measurements of stellar positions, velocities and spectral indices to distinguish two dSph stellar sub-components and to estimate half-light radii and velocity dispersions of both sub-components. A worth-noting remark is that this method operates directly on spectroscopic data and does not invoke a dark matter halo model. Applying the MCMC method to published Magellan/MMFS data Walker & Peñarrubia [2011] were able to distinguish two stellar sub-components in the Fornax and Sculptor dSphs, for which a slope $\Gamma \equiv \Delta \log M / \Delta \log r = 2.61^{+0.43}_{-0.37}$ and $\Gamma = 2.95^{+0.51}_{-0.39}$ was respectively measured. As shown in Fig. 5.1 these values are consistent with cored dark matter haloes of constant density over the central few hundred parsecs and rule out NFW-like ($d \log M / d \log r \leq 2$ at all radii) cusps with significance $\geq 96\%$ and $\geq 99\%$, respectively.

These results therefore show that the core/cusp problem previously detected in spiral galaxies with $L/L_{\odot} \sim 10^9$–10^{10} actually extends to dwarf spheroidal galaxies with $L/L_{\odot} \sim 10^6$–10^7. As in the previous Sections, one wonders whether baryonic matter is at the helm of the absence of CDM cusps in central regions of dwarfs. Unfortunately, assessing the importance of the dynamical interplay between baryonic and dark matter is even more challenging in dSphs than in more massive galaxies: first, because of the extreme numerical resolution that hydrodynamic codes must reach in order to resolve the sizes of dSphs in self-consistent simulations of galaxy formation, and second, because the results rely heavily on the prescriptions adopted for the complex physical processes (star formation, violent supernova feedback, gas outflows and cooling, photoionization and heating from the cosmic UV background, ram stripping ... etc) that are thought to govern baryonic dynamics in low-mass haloes at very high redshift (Mashchenko et al. [2008]; Governato et al. [2010]; Sawala et al. [2010]), but which remain poorly understood and observed to date.

Hierarchical galaxy formation to link them all

Given that the density profile of dark matter haloes in CDM is close to universal, the absence of dark matter cusps in dSphs can only be understood within CDM if baryonic processes shaped the mass distribution currently observed in these systems. Since spiral galaxies form hierarchically, that is through the accretion and ultimate merger of smaller satellite galaxies, it follows that star formation/feedback mechanisms taking place in dSphs at high redshift are key ingredients for the formation of the Milky Way.

This issue was examined by Peñarrubia et al. [2010], who studied the effects of changing the inner density profile of satellite galaxies on the overall properties of the satellite galaxy population that survive to the present. In particular these authors studied the influence of dark matter cusps and cores on the evolution of satellite galaxies driven by tides, and explored whether the satellite population around spirals may retain information on the inner structure of dark matter haloes.

Peñarrubia et al. [2010] showed that the resilience of satellite galaxies to tides increases extraordinarily with the slope of the inner halo profile, γ. A remarkable result was that satellite models with $\gamma \geq 1.0$ cannot be fully disrupted by the tidal field of the parent galaxy, and always retain a bound remnant, even after losing more that 99.99% of mass to tides. In contrast, satellites with cored haloes $\gamma = 0.0$ may undergo full tidal disruption if their orbits bring them in the vicinity of the disc.

The strong dependence between the cuspiness of the satellite density profile and the survivability of satellite galaxies to tidal mass stripping introduces clear differences in the current number and properties of the satellite galaxy population. Peñarrubia et al. [2010] carried a quantitative study by running ten different realizations of merger trees that describe the hierarchical formation of a spiral galaxy with a mass similar to that of the MW. These realizations were re-run adopting different values of γ as well as

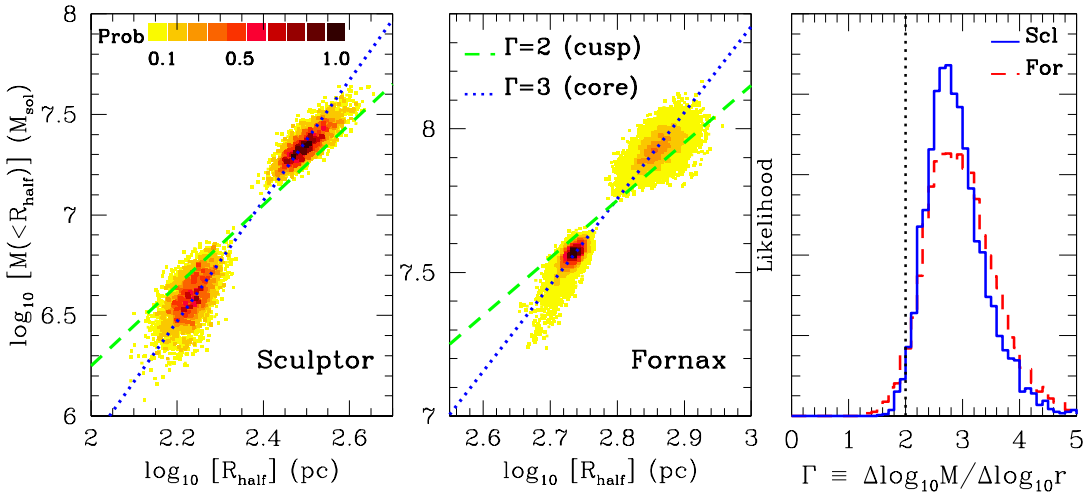

Figure 5.1: *Left and middle panels*: Mass estimated at the half-light radii for each of the components of the Sculptor and Fornax dwarf galaxies (see Walker & Peñarrubia [2011]). *Right panel*: Probability distribution of the logarithmic slope of the halo mass profiles in the Fornax and Sculptor dSphs. The vertical dotted line marks the maximum (i.e., central) value of the halo mass slope typically found within the context of CDM simulations ($\gamma = 1$; $\Gamma \leq 2$). Based on these empirical constraints for Fornax and Sculptor we rule CDM cusps with confidence 93% and 97%, respectively.

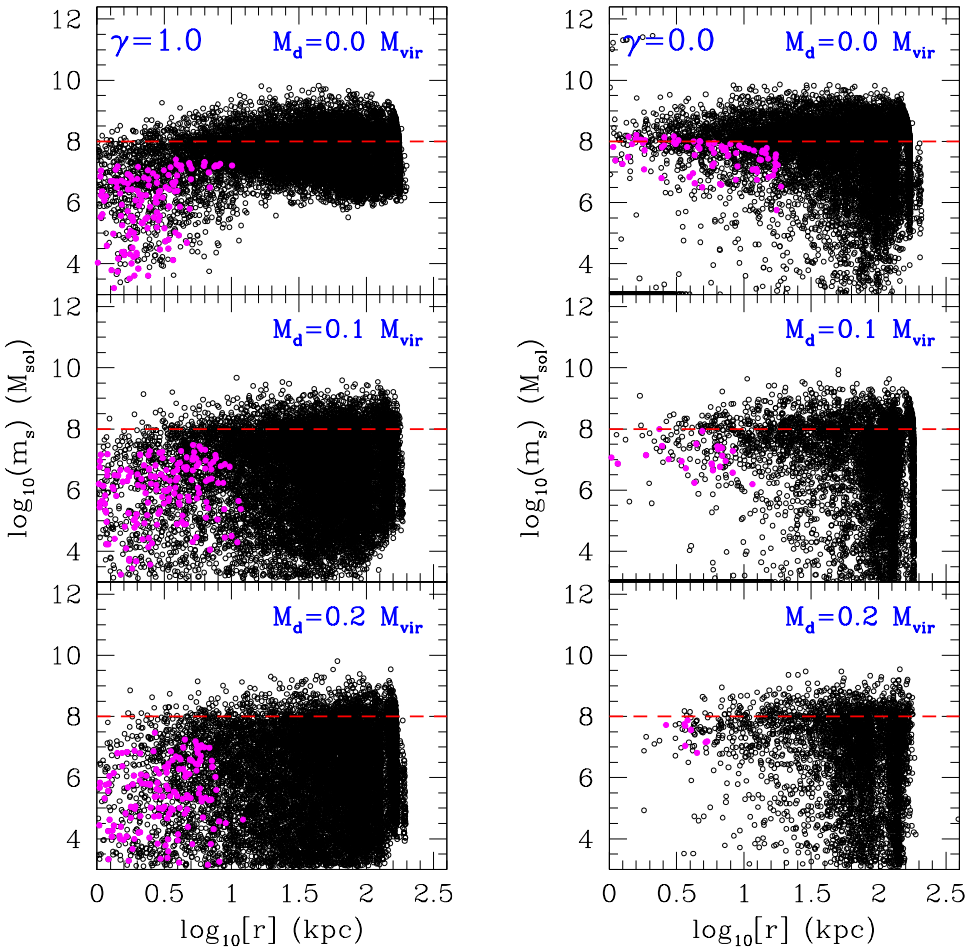

Figure 5.2: Satellite mass versus Galactocentric radius at $z = 0$ for satellite models with $m_s(z_{\rm acc}) > 10^8$ M$_\odot$ (see Peñarrubia et al. [2010] for details). Satellites follow a mass density profile that scale in the inner-most regions as $\rho(r) \propto r^{-\gamma}$. These models consider two values for the power-law index: a 'cuspy' profile $\gamma = 1$ (NFW), and a 'cored' profile with $\gamma = 0$. This Figure stacks the satellite models from ten different realizations of a host galaxy with $M_{\rm vir} = 10^{12}$ M$_\odot$ and $r_{\rm vir} = 210$ kpc at $z = 0$, i.e. representative of the mass and size of the Milky Way halo. The effect of mass stripping can be clearly appreciated, as all subhaloes have masses *above* the dashed lines at their time of accretion. Closed symbols denote satellites that were accreted into the host halo with virial masses above 10^8 M$_\odot$ at $z > 6$ (the so-called *fossils of re-ionization*). Note that injecting a baryonic disc in the host galaxy models at $z = 2$ has the effect of depleting the number of fossils of re-ionization if haloes are cored ($\gamma = 0.0$). If haloes are cuspy ($\gamma = 1.0$), however, the main effect is an increase in the mass scatter at a fixed galactocentric radius.

disc-to-halo mass ratios, $M_d/M_{\rm vir}$. The fact that only a small fraction of subhaloes may be "luminous" is accounted by only considering those that fall into the host with masses above 10^8 $M_\odot$, which is typically considered as the minimum halo mass for which star formation may occur.

The results are summarized in Fig. 5.2. A few interesting points can be gleaned from that Figure. First, the net effect of tides is to decrease the average mass of satellite galaxies at all Galactocentric radii. Increasing the mass of the host disc clearly magnifies this effect: the average bound mass drops by a factor ~ 10 after injecting a disc component in the host with $M_d/M_{\rm vir} = 0.1$, and a factor ~ 30 for $M_d/M_{\rm vir} = 0.2$ (see also D'Onghia et al. [2010]). Second, the present number of satellite galaxies that are accreted before re-ionization (full dots) puts strong constraints on the inner profile of dark matter haloes. Our models predict that a MW-like galaxy may contain ~ 15 of these galaxies orbiting within the central 20 kpc if $\gamma = 1.0$, in very good agreement with recent results from the Aquarius team (Gao et al. [2009]). The number of these systems, however, quickly drops to zero in models that assume a cored halo profile and host disc component with $M_d \geq 0.1 M_{\rm vir}$. These systems may be singled out by anomalous metallicity patterns, and thus represent an interesting observational case to unravel the inner structure of haloes. Third, in models that adopt a cored dark matter halo profile, discs efficiently deplete the inner regions of the host from satellites. In contrast, cuspy satellites can survive in the inner-most regions of spiral galaxies even after losing large fractions of their original mass to tides, which may have important observational consequences for the detection of dark matter annihilation signals in gamma-ray surveys. The presence of dark matter cores in satellite galaxies may thus alleviate the "missing satellite problem".

This Figure also suggests that the number and spatial distribution of the stellar streams that Gaia may be able to detect in the inner regions of the Milky Way will be fairly sensitive to the presence of dark matter cusps in satellite galaxies. Currently it is unclear whether the absence of dark matter cusps in the Fornax and Sculptor dSphs is a result of a baryonic process, such as violent gas expulsion induced by stellar feedback (e.g. Navarro et al. [1996]). If that is indeed the case and the presence of dark matter cores extends to the whole dSph population, the results shown in Fig. 5.2 suggests that both the smooth and the clumpy components of the stellar halo of the Milky Way may retain key information on the inner structure of the satellite galaxies.

Summary

In our current cosmological paradigm the formation of spiral galaxies is still not fully understood. In spite of the strong theoretical efforts undertaken in the last decade, three fundamental problems still abide: (i) *The angular-momentum catastrophe.* Spiral galaxies formed in cosmological hydrodynamical simulations predict the formation of a centrally concentrated stellar bulge and a cuspy dark-matter profile. This is at odds with observations of *bulgeless* spiral galaxies. In addition, these simulations cannot reproduce fundamental scaling relationships observed in spiral galaxies, such as the Tully-Fisher relation. Galaxies in CDM simulations appear too concentrated and rotate too slowly to conform with observations. (ii) *The missing satellite problem.* A decade ago cosmological simulations of increasingly higher resolution were used to demonstrate that virialized regions of CDM haloes are filled with a multitude of dense, gravitationally-bound clumps. These dark matter subhaloes are central regions of haloes that survived strong gravitational tidal forces and dynamical friction during the hierarchical sequence of merging and accretion via which the CDM haloes form. Comparisons with observations revealed that there is a glaring discrepancy between abundance of subhaloes and luminous satellites of the Milky Way and Andromeda as a function of their bound mass within a fixed aperture. (iii) *The core/cusp problem.* The rotation velocity associated with dark matter in the inner parts of disc galaxies is observed to increase approximately linearly with radius. This solid-body behaviour can be interpreted as an indication of the presence of a central core in the dark matter distribution (de Blok [2010] and references therein). Recently, Walker & Peñarrubia [2011] have shown that this result extends to at least two dwarf spheroidal galaxies, which are approximately 100 – 1000 times fainter than the typical low-surface brightness disc galaxies. These results are again in tension with CDM, which predicts a close-to-universal dark matter density profile that diverges as $\rho \propto r^{-1}$ in the central regions (e.g. NFW).

A concensus is emerging wherein the ability of CDM to conform to observations hinges on understanding the processes that drive the formation and evolution of stars. A number of baryonic processes have been proposed to explained the observed mismatches between CDM predictions and observations, e.g. supernova-driven gas outflows may be able under certain conditions to remove the dark matter cusp in satellites. Gas outflows from satellites in turn reduce the amount of gas accreted in the inner regions of spirals, which may explain the existence of bulge-less galaxies (Governato et al. [2010]). As shown by

Peñarrubia et al. [2010], satellites with a cored density profile are much more prone to tidal disruption than those with cusps, which considerably alleviates the missing satellite problem.

We may thus be facing a cosmological paradigm in which processes taking place on a *sub-parsec* scale determine the overall formation and evolution of galaxies on *kiloparsec* scales. Unfortunately, the numerical resolution required to study these processes self-consistently is still prohibitive. This has led to cosmological simulations that use semi-analytical recipes to describe the formation of stars and the impact of stellar evolution/supernova processes on the surrounding gaseous medium with parameters that are poorly constrained theoretically. Indeed, most simulations fit those free parameters *a posteriori* in oder to match observational data. A more consistent approach may be found in semi-analytic models that are calibrated with local observations of star-forming regions, and observations of the ISM properties in regions where recent supernovae events occurred. This gap will probably be breached in a near future, as it appears to be the only remedy to ease important tensions in our current cosmological paradigm.

Acknowledgments

I would like to thank the Instituto de Astrofísica de Andalucía for their invitation to attend this conference and their generosity.

Bibliography

Battaglia, G., Tolstoy, E., Helmi, A., et al. 2011, MNRAS, 411, 1013
Battaglia, G., Tolstoy, E., Helmi, A., et al. 2006, A&A, 459, 423
Bullock, J. S., Kravtsov, A. V., & Weinberg, D. H. 2000, ApJ, 539, 517
de Blok, W. J. G. 2010, Advances in Astronomy, 2010
de Blok, W. J. G. & McGaugh, S. S. 1997, MNRAS, 290, 533
Diemand, J., Moore, B., & Stadel, J. 2005a, Nat, 433, 389
Diemand, J., Zemp, M., Moore, B., Stadel, J., & Carollo, C. M. 2005b, MNRAS, 364, 665
D'Onghia, E., Springel, V., Hernquist, L., & Keres, D. 2010, ApJ, 709, 1138
Dubinski, J. & Carlberg, R. G. 1991, ApJ, 378, 496
El-Zant, A., Shlosman, I., & Hoffman, Y. 2001, ApJ, 560, 636
Flores, R. A. & Primack, J. R. 1994a, ApJ Lett., 427, L1
Flores, R. A. & Primack, J. R. 1994b, ApJ Lett., 427, L1
Gentile, G., Burkert, A., Salucci, P., Klein, U., & Walter, F. 2005, ApJ Lett., 634, L145
Gilmore, G., Wilkinson, M. I., Wyse, R. F. G., et al. 2007, ApJ, 663, 948
Goerdt, T., Moore, B., Read, J. I., Stadel, J., & Zemp, M. 2006, MNRAS, 368, 1073
Governato, F., Brook, C., Mayer, L., et al. 2010, Nat, 463, 203
Kauffmann, G., White, S. D. M., & Guiderdoni, B. 1993, MNRAS, 264, 201
Kleyna, J. T., Wilkinson, M. I., Gilmore, G., & Evans, N. W. 2003, ApJ Lett., 588, L21
Klypin, A., Kravtsov, A. V., Bullock, J. S., & Primack, J. R. 2001, ApJ, 554, 903
Klypin, A., Kravtsov, A. V., Valenzuela, O., & Prada, F. 1999, ApJ, 522, 82
Koposov, S. E., Yoo, J., Rix, H.-W., et al. 2009, ApJ, 696, 2179
Mashchenko, S., Wadsley, J., & Couchman, H. M. P. 2008, Sci, 319, 174
McGaugh, S. S., Rubin, V. C., & de Blok, W. J. G. 2001, AJ, 122, 2381
Moore, B. 1994, Nat, 370, 629
Moore, B., Governato, F., Quinn, T., Stadel, J., & Lake, G. 1998, ApJ Lett., 499, L5+
Moore, B., Quinn, T., Governato, F., Stadel, J., & Lake, G. 1999, MNRAS, 310, 1147
Navarro, J. F., Eke, V. R., & Frenk, C. S. 1996, MNRAS, 283, L72
Navarro, J. F., Frenk, C. S., & White, S. D. M. 1997, ApJ, 490, 493
Navarro, J. F. & Steinmetz, M. 2000, ApJ, 538, 477
Peñarrubia, J., Benson, A. J., Walker, M. G., et al. 2010, MNRAS, 406, 1290
Read, J. I. & Gilmore, G. 2005, MNRAS, 356, 107
Salucci, P. & Burkert, A. 2000, ApJ Lett., 537, L9
Sawala, T., Scannapieco, C., Maio, U., & White, S. 2010, MNRAS, 402, 1599
Simon, J. D., Bolatto, A. D., Leroy, A., Blitz, L., & Gates, E. L. 2005, ApJ, 621, 757
Springel, V. & Hernquist, L. 2003, MNRAS, 339, 289
Springel, V., Wang, J., Vogelsberger, M., et al. 2008, MNRAS, 391, 1685
Tollerud, E. J., Bullock, J. S., Strigari, L. E., & Willman, B. 2008, ApJ, 688, 277

Tolstoy, E., Irwin, M. J., Helmi, A., et al. 2004, ApJ Lett., 617, L119
Tonini, C., Lapi, A., & Salucci, P. 2006, ApJ, 649, 591
Walker, M. G., Mateo, M., Olszewski, E. W., et al. 2007, ApJ Lett., 667, L53
Walker, M. G., Mateo, M., Olszewski, E. W., et al. 2009, ApJ, 704, 1274
Walker, M. G. & Peñarrubia, J. 2011, ArXiv e-prints
Wolf, J., Martinez, G. D., Bullock, J. S., et al. 2010, MNRAS, 406, 1220

5.2 Open Issues in the Evolution of the Galactic Disks

Gerard Gilmore[1,2], and H. M. Asiri[2]

[1] Institute of Astronomy, Madingley Road, Cambridge, UK
[2] Astronomy Department, Faculty of Science, King Abdulaziz University, Saudi Arabia

Abstract

Galactic disks pose a fascinating challenge both to observe and to understand. No realistic *ab initio* formation models exist, so we are led by observations. However, many key physical processes affecting dynamics and chemical evolution can be isolated in kinematic and abundance data. Thus progress can be made by focussing on specific challenges with appropriate observations. We review some of the most topical here.

Introduction

The standard ΛCDM universe model is impressively consistent with a wide range of observations on large spatial scales (Komatsu *et al.* [2011]). Our understanding of the formation and evolution of galaxies in the ΛCDM context however remains very incomplete. Late-type spirals, like the Milky Way, in particular are extremely difficult to understand in the canonical hierarchical clustering paradigm (Shen *et al.* [2010]; Kormendy *et al.* [2010]). Recent detailed numerical simulations which attempt to form Milky Way-like galaxies require adoption of implausibly extreme and/or unusual conditions in the early history of the galaxy. A recent example among many is Guedes *et al.* [2011], whose most observationally-plausible model requires an extreme star formation threshold, inconsistent with observations. More generally, Stewart *et al.* [2009] provide a detailed analysis of the challenges facing consistency between the best current models of late-type galaxies and observations. The primary challenge is that paradigmatic galaxy formation is necessarily hierarchical, with continuing mergers and accretion events for long times. Such mergers damage or destroy thin disks, forming bulges and/or thick disks. Thin disks should be rather rare and rather young. However, thin disks are observed to be common and old. Stewart *et al.* [2009] conclude "Our results raise serious concerns about the survival of thin disk dominated galaxies within the current paradigm for galaxy formation in a ΛCDM universe". On smaller scales the challenges which models face in reproducing either the numbers (the Satellite problem), or the physical properties, of dwarf galaxies are well known. Recent sophisticated models include those of Sawala *et al.* [2011] and Parry *et al.* [2011], which both conclude that current simulations differ by more than an order of magnitude from observations of real galaxies.

It remains unclear as yet to what extent the models lack an adequate approximation to the dominant physics, or if there is a problem in a common assumption, or both. The most likely common assumption to be inconsistent with the Universe is the extrapolation of the CDM power spectrum as a featureless structure-free power-law to arbitrarily small scales. There are many observational studies which show that small-scale dark matter potentials are cored rather than cusped (Gilmore *et al.* [2007]). It is plausible that the many challenges remaining in the standard model of particle physics imply a complex spectrum of elementary particles making up Dark Matter. Changing underlying assumptions in formation models in this way, led by observation, does however open a rich possible parameter space for exploration, which requires even richer observations to guide the process. We may conclude, as usual, that observations lead the way towards improved understanding. Progress in quantifying the observed properties of galaxies, and the Galaxy, and tensioning observations against (the limitations of) models, is the way in which our knowledge and understanding makes progress.

The observational properties of galaxy disks, including that of the Milky Way have been reviewed most recently by van der Kruit and Freeman [2011]. Earlier major reviews which remain valuable include Gilmore, Wyse, and Kuijken [1989] and Freeman and Bland-Hawthorn [2002].

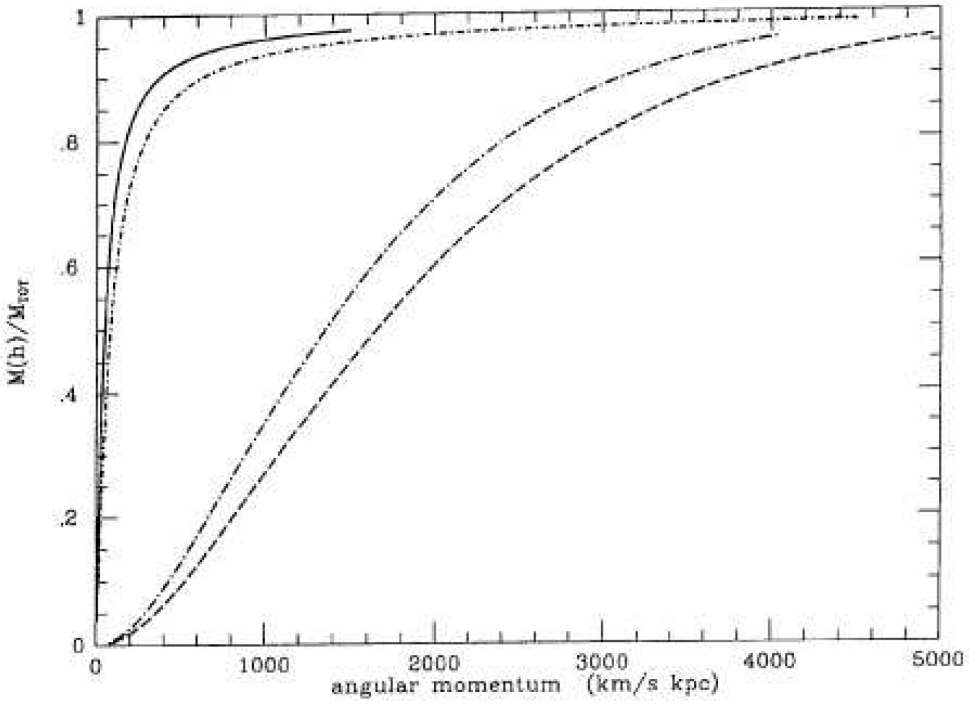

Figure 5.3: Normalized angular momentum distributions for the bulge (solid curve), the $r^{1/4}$ spheroid (short-dashed-dotted curve), the thick disk (long-dashed-dotted curve), and the thin disk (long-dashed curve).

Galactic Thick Disks

Thick disks seem to be a universal stellar population in disk galaxies. The extensive HST survey of Yoachim and Dalcanton [2006] showed that thick disks are present in all, or nearly all, disk galaxies. These thick disks make up typically 10 percent of the light of luminous (Milky Way-like) galaxies, and rather more, up to 50 percent, in lower luminosity systems. Interestingly, thick disk radial scale lengths are similar to those of the galactic thin disk, suggesting an association. Yoachim and Dalcanton [2006] further find that the thick disk stellar populations are typically old. Apparently thick disk formation is a normal aspect of the early formation of disk galaxies, an observation which requires explanation.

The Milky Way has a thick disk (Gilmore and Reid [1983]) with superficially rather typical properties. The stellar population which makes up the thick disk is apparently exclusively old, with age of order 12 Gyr, comparable to that of the metal-rich globular clusters (Unavane, Wyse, and Gilmore [1996]; Jofre and Weiss [2011]). The old age of thick disk stars is apparent even by visual examination of colour-magnitude diagrams from SDSS photometry of high-latitude fields (de Jong *et al.* [2010]), where the sharp blue edge to the colour distribution is apparent.

This is a surprising result. As noted in the introduction, canonical hierarchical galaxy formation models have significant mergers continuing up to times corresponding to redshifts of order unity. These significant mergers should heat thin disks into thick disks, so that a wide age range in thick disks, and a bias to young ages in surviving thin disks, is anticipated (Kazantzidis *et al.* [2008], but see also Moster *et al.* [2010] for the importance of hard to model gas in these simulations).

Although thick disks are at least as old as the oldest stars which can be categorised as thin disk stars, there are structural similarities between thick and thin disks. Yoachim and Dalcanton [2006] establish these in external galaxies. In the Milky Way it has been known for some time that the distribution function of specific angular momentum of the Galaxy's stellar populations shows that the thick and thin disks are in some way similar, while both the Bulge and the halo are systematically different, though similar to each other (Wyse and Gilmore [1992]). The Wyse and Gilmore [1992] results are shown in Fig. 5.3. These results illustrate again the fundamental connection between thin disk and thick disk formation. The connection, if any between thick/thin disk and halo/bulge formation however remains problematic (Wyse and Gilmore [1992]).

Evolutionary relationships are potentially complicated, given that, in addition to two types of disk,

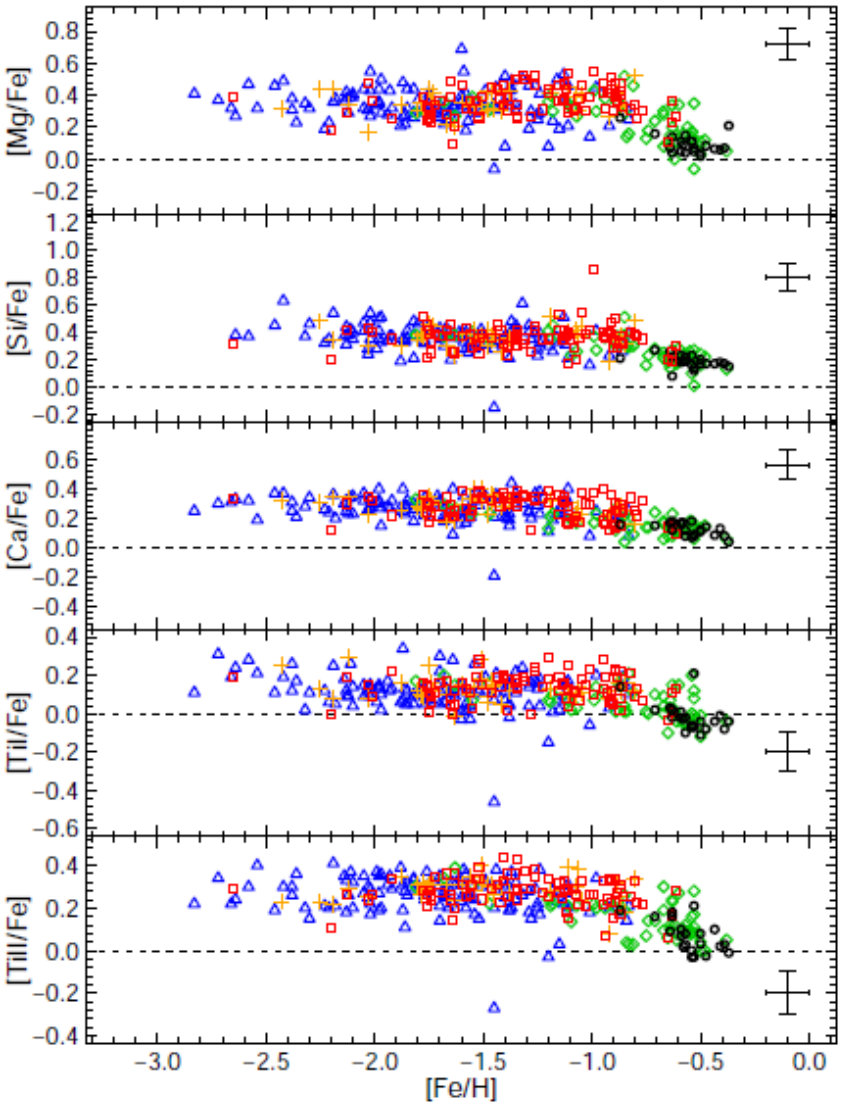

Figure 5.4: The distribution of element ratios in a large sample of thick disk stars (red squares), and some halo (blue triangles) and thin disk stars (green), from a follow-up of the RAVE survey (Ruchti *et al.* [2011]). The stars are allocated to populations using kinematic criteria. Two features are worthy of emphasis: the thick disk stars extend to very low abundances; and the halo and thick disk stars obey the same correlation, with little scatter.

"thick" and "thin", there are at least two types of bulge, "classic" and "pseudo", Kormendy and Kennicutt [2004], with the "pseudo-bulge" being itself closely related to the thin disk (Fisher and Drory [2011], see also Kormendy and Barentine [2010]), and probably formed from it by secular evolution. In this picture, thick disks predate thin disks which predate (pseudo-)bulges.

Thick disk chemical abundances

The volume-complete chemical element distributions functions as a function of kinematics, age, etc, or more simply, as a function of stellar populations, remain very poorly determined. The true distribution functions, sampled with understood bias, are primary data in understanding the coupled evolution of star formation locations and rates, gas flows, and later dynamical mixing (Wyse and Gilmore [1995]; Gilmore, Wyse, and Jones [1995]; Gilmore and Wyse [1998]). In spite of substantial recent progress, such as SEGUE and RAVE, (eg Burnett *et al.* [2011], there is much to learn about the basic properties of Galactic stellar populations from the forthcoming large spectroscopic surveys, such as Gaia-ESO, HERMES, and APOGEE.

Most spectroscopic projects to date have been optimised to study the extremes of the distribution functions, eg, the very many surveys for very metal-poor stars, or very metal-rich stars. These surveys

are however delivering impressive science. Among the most active relatively unbiassed surveys at present is RAVE (Steinmetz *et al.* [2006]; Siebert *et al.* [2011]). Among the specific follow-up studies from RAVE, one has determined accurate chemical element abundance ratios for a large sample of stars with thick disk kinematic population assignment (Ruchti *et al.* [2010, 2011]). The fundamental result from this impressive study is shown in Fig 5.4. The striking feature is the similarity of thick disk and halo populations down to very low metallicity. This has important implications for invariance of the early stellar high-mass Initial Mass Function (IMF, cf Gilmore and Wyse [1991]) and the scale length of ISM mixing at early times. The extension of the metallicity distribution function to low values reduces the need for a significant precursor population (halo??) to pre-enrich the ISM which formed the thick disk. This further establishes the thick disk as a very early population in the galaxy. The thin disk, by contrast, lacks metal-poor stars (the infamous "G-dwarf problem"), and so cannot be among the first stellar populations to form in the proto-Galactic potential. Rather, the thick disk provides a natural explanation as thin-disk precursor, resolving the G-dwarf problem. The low metallicity of the (tail of) the thick disk is consistent with its old age (see above), and shows that radially very extended high-angular momentum populations existed at very early times (cf also Burnett *et al.* [2011]).

The Thin Disk

The immediate solar neighbourhood has been studied rather well, using field stars (e.g. Fuhrmann [2011]), while many star-count studies over many years have determined the approximate structural properties of the thin (and thick) disk (e.g. de Jong *et al.* [2010]). Among the more interesting current topics are the issue of radial chemical abundance gradients, the true dispersion in chemical abundances as a function of Galactocentric radius, and the big challenge of disk secular evolution.

The age-metallicity distribution function remains poorly determined, largely since ages for significant samples of (especially old) stars are extremely difficult to determine. We await Gaia precision distances with eager anticipation, to really advance on this front. In the interim however star clusters are a valuable probe. More cluster ages, metallicities and distances are highly desirable.

Clusters are also a valuable probe of galactocentric radial gradients. ISM studies, complemented by analyses of massive stars with good distances (Cepheids, and such like) suggest a fairly significant radial gradient is present today. Are these gradients also present in older stars? This question is of key importance in determining the importance of flows ("galactic fountains") driven by star formation, in the evolution of the disk. It is also key to test if secular evolution is important in the outer parts of the Galactic disk. Knowing both the amplitude of any radial abundance gradient, and the width of the local abundance distribution function, provides potentially interesting constraints on radial stellar mixing. Especially so if this information for old stars is feasible.

Secular evolution must be important in the thin disk. The disk is a mix of asymmetric time-dependent structures (spiral arms, bars,...) which perturb stellar (and cluster) orbits. These structures are especially important in the inner galaxy, apparently leading to pseudo-bulge formation, as noted above. There have been many recent suggestions that the secular evolution may be so strong it also significantly affects the outer Galaxy (Sellwood and Binney [2002]; Schönrich and Binney [2009]; Loebman *et al.* [2011]). Only much improved observational limits, of both chemical abundances and the types of orbits which stars occupy as a function of age, can test these models. While we await Gaia, star clusters are the best option for progress here, since all of age, metallicity and distance can be determined.

Summary

We lack a predictive model of galaxy formation. Available models are so far from consistency with observation, and are so *ad hoc*, that we progress by observing. Fortunately, precision observations and large surveys are happening, with even better to come in the next few years, culminating with Gaia.

Thick disks provide robust evidence that large high-angular momentum disks were ubiquitous in the early universe. These disks are more extended vertically than are thin disks. Why? Did the disks form thick, or were they thickened?

Thin disks are common, radially large and vertically thin. Why have they not been destroyed by hierarchical mergers and accretions? Thin disks evolve secularly. In their inner regions this process is dominant. How important is it at much greater radii?

These - and many more - questions are the focus of current and new major surveys, where we confidently anticipate new progress, and new questions.

Bibliography

Burnett, B., Binney, J., Sharma, S., Williams, M., Zwitter, T., Bienayme, O, Bland-Hawthorn, J., Freeman, K.C., Fulbright, J., Gibson, B., Gilmore, G., Grebel, E.K., Helmi, A., Munari, U., Navarro, J.F., Parker, Q.A., Seabroke, G.M., Siebert, A., Siviero, A., Steinmetz, M, Watson, F.G., and Wyse, R.F.G.: 2011, *ArXiv e-prints*, arXiv:1107.1256.

Fisher, D.B. and Drory, N.: 2011, *Astrophys. J.* **733**, L47.

Freeman, K. and Bland-Hawthorn, J.: 2002, *Annual Review of Astronomy and Astrophysics* **40**, 487.

Fuhrmann, K.: 2011, *Monthly Notices of the Royal Astronomical Society* **414**, 2893.

Gilmore, G. and Reid, N.: 1983, *Monthly Notices of the Royal Astronomical Society* **202**, 1025.

Gilmore, G., Wyse, R.F.G., and Kuijken, K.: 1989, *Annual Review of Astronomy and Astrophysics* **27**, 555.

Gilmore, G. and Wyse, R.F.G.: 1991, *Astrophys. J.* **367**, L55

Gilmore, G., Wyse, R.F.G., and Jones, J.B.: 1995, *The Astronomical Journal* **109**, 1095.

Gilmore, G. and Wyse, R.F.G.: 1998, *The Astronomical Journal* **116**, 748.

Gilmore, G., Wilkinson, M.I., Wyse, R.F.G., Kleyna, J.T., Koch, A., Evans, N.W., and Grebel, E.K.: 2007, *Astrophys. J.* **663**, 948.

Guedes, J., Callegari, S., Madau, P., and Mayer, L.: 2011, *ArXiv e-prints*, arXiv:1103.6030.

Jofre, P. and Weiss, A.: 2011, *ArXiv e-prints*, arXiv:1105.2022.

de Jong, J.T.A., Yanny, B., Rix, H.-W., Dolphin, A.E., Martin, N.F., and Beers, T.C.: 2010, *Astrophys. J.* **714**, 663.

Kazantzidis, S., Bullock, J.S., Zentner, A.R., Kravtsov, A.V., and Moustakas, L.A.: 2008, *Astrophys. J.* **688**, 254.

Kormendy, J. and Kennicutt, R.C., Jr.: 2004, *Annual Review of Astronomy and Astrophysics* **42**, 603.

Kormendy, J., Drory, N., Bender, R., and Cornell, M.E.: 2010, *Astrophys. J.* **723**, 54.

Kormendy, J. and Barentine, J.C.: 2010, *Astrophys. J.* **715**, L176.

Komatsu, E., Smith, K.M., Dunkley, J., Bennett, C.L., Gold, B., Hinshaw, G., Jarosik, N., Larson, D., Nolta, M.R., Page, L., Spergel, D.N., Halpern, M., Hill, R.S., Kogut, A., Limon, M., Meyer, S.S., Odegard, N., Tucker, G.S., Weiland, J.L., Wollack, E., and Wright, E.L.: 2011, *The Astrophysical Journal Supplement Series* **192**, 18.

Loebman, S.R., Roškar, R., Debattista, V.P., Ivezić, Ž., Quinn, T.R., and Wadsley, J.: 2011, *Astrophys. J.* **737**, 8.

Sawala, T., Guo, Q., Scannapieco, C., Jenkins, A., and White, S.: 2011, *Monthly Notices of the Royal Astronomical Society* **413**, 659.

van der Kruit, P.C. and Freeman, K.C.: 2011, *ArXiv e-prints*, arXiv:1101.1771.

Moster, B.P., Macciò, A.V., Somerville, R.S., Johansson, P.H., and Naab, T.: 2010, *Monthly Notices of the Royal Astronomical Society* **403**, 1009.

Parry, O.H., Eke, V.R., Frenk, C.S., and Okamoto, T.: 2011, *ArXiv e-prints*, arXiv:1105.3474.

Ruchti, G.R., Fulbright, J.P., Wyse, R.F.G., Gilmore, G.F., Bienaymé, O., Binney, J., Bland-Hawthorn, J., Campbell, R., Freeman, K.C., Gibson, B.K., Grebel, E.K., Helmi, A., Munari, U., Navarro, J.F., Parker, Q.A., Reid, W., Seabroke, G.M., Siebert, A., Siviero, A., Steinmetz, M., Watson, F.G., Williams, M., and Zwitter, T.: 2010, *Astrophys. J.* **721**, L92.

Ruchti, G.R., Fulbright, J.P., Wyse, R.F.G., Gilmore, G.F., Bienaymé, O., Bland-Hawthorn, J., Gibson, B.K., Grebel, E.K., Helmi, A., Munari, U., Navarro, J.F., Parker, Q.A., Reid, W., Seabroke, G.M., Siebert, A., Siviero, A., Steinmetz, M., Watson, F.G., Williams, M., and Zwitter, T.: 2011, *Astrophys. J.* **737**, 9.

Schönrich, R. and Binney, J.: 2009, *Monthly Notices of the Royal Astronomical Society* **396**, 203.

Sellwood, J.A. and Binney, J.J.: 2002, *Monthly Notices of the Royal Astronomical Society* **336**, 785.

Shen, J., Rich, R.M., Kormendy, J., Howard, C.D., De Propris, R., and Kunder, A.: 2010, *Astrophys. J.* **720**, L72.

Siebert, A., Williams, M.E.K., Siviero, A., Reid, W., Boeche, C., Steinmetz, M., Fulbright, J., Munari, U., Zwitter, T., Watson, F.G., Wyse, R.F.G., de Jong, R.S., Enke, H., Anguiano, B., Burton, D., Cass, C.J.P., Fiegert, K., Hartley, M., Ritter, A., Russel, K.S., Stupar, M., Bienaymé, O., Freeman, K.C., Gilmore, G., Grebel, E.K., Helmi, A., Navarro, J.F., Binney, J., Bland-Hawthorn, J., Campbell, R., Famaey, B., Gerhard, O., Gibson, B.K., Matijevič, G., Parker, Q.A., Seabroke, G.M., Sharma, S.,

Smith, M.C., and Wylie-de Boer, E.: 2011, *The Astronomical Journal* **141**, 187.
Steinmetz, M., Zwitter, T., Siebert, A., Watson, F.G., Freeman, K.C., Munari, U., Campbell, R., Williams, M., Seabroke, G.M., Wyse, R.F.G., Parker, Q.A., Bienaymé, O., Roeser, S., Gibson, B.K., Gilmore, G., Grebel, E.K., Helmi, A., Navarro, J.F., Burton, D., Cass, C.J.P., Dawe, J.A., Fiegert, K., Hartley, M., Russell, K.S., Saunders, W., Enke, H., Bailin, J., Binney, J., Bland-Hawthorn, J., Boeche, C., Dehnen, W., Eisenstein, D.J., Evans, N.W., Fiorucci, M., Fulbright, J.P., Gerhard, O., Jauregi, U., Kelz, A., Mijović, L., Minchev, I., Parmentier, G., Peñarrubia, J., Quillen, A.C., Read, M.A., Ruchti, G., Scholz, R.-D., Siviero, A., Smith, M.C., Sordo, R., Veltz, L., Vidrih, S., von Berlepsch, R., Boyle, B.J., and Schilbach, E.: 2006, *The Astronomical Journal* **132**, 1645
Stewart, K.R., Bullock, J.S., Wechsler, R.H., and Maller, A.H.: 2009, *Astrophys. J.* **702**, 307.
Unavane, M., Wyse, R.F.G., and Gilmore, G.: 1996, *Monthly Notices of the Royal Astronomical Society* **278**, 727.
Yoachim, P. and Dalcanton, J.J.: 2006, *The Astronomical Journal* **131**, 226.
Wyse, R.F.G. and Gilmore, G.: 1992, *The Astronomical Journal* **104**, 144.
Wyse, R.F.G. and Gilmore, G.: 1995, *The Astronomical Journal* **110**, 2771.

5.3 Strömgren Photometry of the Bulge: the Baade's Window and the Globular Cluster NGC 6522

Annalisa Calamida[1], G. Bono[2], C. E. Corsi[1], G. Iannicola[1], V. Ripepi[3], B. Anthony-Twarog[4], B. Twarog[4], M. Zoccali[5], R. Buonanno[2], S. Cassisi[6], I. Ferraro[1], F. Grundahl[7], A. Pietrinferni[6], and L. Pulone[1]

[1] Osservatorio Astronomico di Roma/INAF
[2] Università di Roma Tor Vergata
[3] Osservatorio Astronomico di Capodimonte/INAF
[4] University of Kansas
[5] Pontificia Universidad Católica de Chile
[6] Osservatorio Astronomico di Collurania/INAF
[7] Department of Physics and Astronomy, Aarhus University

Abstract

We present $Ca - uvby$ Strömgren photometry of the Baade's Window, including the Galactic globular cluster NGC 6522. We separate field and cluster stars by adopting colour–colour planes and proper motions. We then estimate the global metallicity of red-giants (RGs) in NGC 6522 by using a new theoretical metallicity calibration of the Strömgren index hk presented in Calamida et al. (2011). We find that metallicities estimated by adopting the hk index and the Ca–y colour are systematically more metal-rich than metallicities estimated with hk and the b–y, v–y and b–y colours. Current evidence indicate that the hk metallicity index is affected not only by the Ca abundance, but also by another source of opacity.

Introduction and data reduction

The study of the Milky Way bulge is fundamental to understand the star formation history of the Galactic spheroid. The Milky Way bulge is indeed dominated by metal-rich old stars ($t > 10$ Gyr, Zoccali et al. [2003]). Their metallicity distribution is centered on solar metallicity and span a range from $[Fe/H] \sim$ -1.5 to 0.5 dex, based on the high-resolution spectroscopy of $\sim$ 800 stars (Zoccali et al. [2008], hereafter ZO08). These evidence would support a scenario in which the bulge formed very quickly ($t < 1$ Gyr) at the early stages of the Galaxy formation, and then accreted material from the disk (Zoccali et al. [2006], ZO08).

Furthermore, the Baade's window, where the extinction is lower ($E(B-V) < 0.6$ mag), includes NGC 6522, which is classified as a bulge metal-intermediate Galactic globular cluster (GGC, $[Fe/H] \sim$ -1.3/-1.2 dex). For this region ZO08 collected high-resolution spectroscoy for $\sim$ 200 red-giants (RGs) and $\sim$ 200 red clump stars. The two samples show the same metallicity distribution centered on solar metallicity and with most of the stars in the range -1.0 $< [Fe/H] <$ 0.7 dex (see Fig. 8 in ZO08).

We collected a set of *Ca-uvby* Strömgren images centered on the Baade's and the Blanco's windows and we plan to provide metallicity distributions based on the hk Strömgren index for a significant sample of bulge RGs. The advantage of applying a Strömgren metallicity calibration to this data set is the possibility to estimate the metallicity of thousands of RGs in this region at the same time. With this study we would be able to eventually confirm the presence of a metallicity gradient in the bulge, as suggested by ZO08. The drawback is that our new theoretical metallicity calibration of the hk index (Calamida & et al. [2011], hereafter CA11) is only valid in the range -2.7$< [Fe/H] <$-0.6 dex. We then apply the calibration to a significant sample of NGC 6522 candidate RGs, to constrain the metal content of this GGC.

Ca-uvby Strömgren images were collected with the 1.54m Danish Telescope (ESO, La Silla) and the DFOSC camera in July 2000. The pointing was centered on the Baade's Window ($\alpha = 18^h$:03^m:34^s, δ = -30°:04':10"), including NGC 6522. We secured a total of 16 images ($4y, 4b, 2v, 2Ca, 2u$), with exposure times ranging from 60s (y) to 1000 s (Ca), and seeing between $\sim$ 1.2 arcsec and $\sim$ 1.6 arcsec. The reader interested in the details of data reduction and calibration is referred to CA11. The final photometric

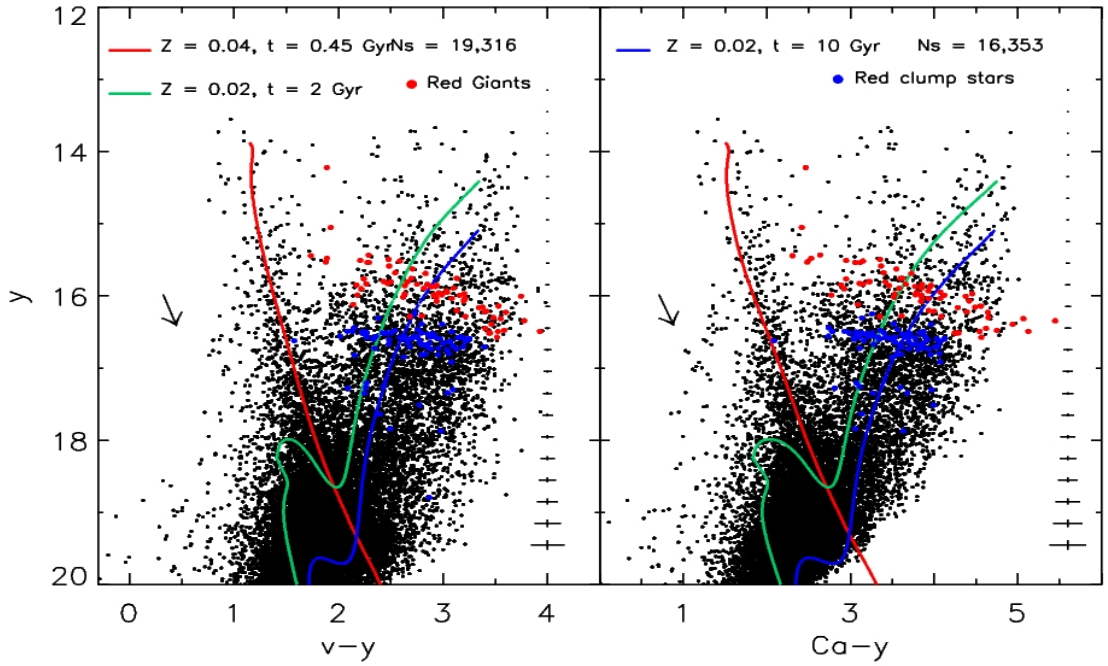

Figure 5.5: y, v–y and y, Ca–y CMDs for stars in the Baade's Window. Stars are selected in position and in photometric accuracy (see text for more details). Error bars display intrinsic errors in colour and in magnitude, while the arrows show the reddening directions. The red solid line shows an isochrone for $t = 0.45$ Gyr and $Z = 0.04, Y = 0.303$, while the green and blue solid lines show two isochrones for the same chemical composition, $Z = 0.02, Y = 0.273$, and $t = 2$ and $t = 10$ Gyr, respectively. Red and blue dots mark red-giant and red-clump stars observed spectroscopically by Zoccali et al. [2008].

catalogue includes $\sim$ 80,000 stars with an accuracy of $\sigma_y < 0.1$, $\sigma_{v-y} < 0.2$ mag at $y \approx 20$ mag. The accuracy of the calibration is ~ 0.02 mag for the y, b, v bands and ~ 0.05 mag for the Ca, u bands.

Fig. 5.5 shows the y, v–y (left panel) and y, Ca–y (right) Colour-Magnitude Diagrams (CMDs) of the Baade's Window. We exclude most of the stars belonging to NGC 6522 by selecting only objects with distances from the cluster center ($\alpha = 18^h{:}03^m{:}34^s$, δ = -30°:02':02") larger than 6 arcmin. Stars are then selected in photometric accuracy according to the "separation index"[1]

In order to validate the absolute calibration we compare our photometry with theoretical predictions. We assume a mean distance of $\sim$ 5 kpc for the foreground thin disk stars according to the simulations by Schultheis and using the Besancon Galaxy model (Robin et al. [2003], see ZO08 for more details), and a distance modulus of $\mu_0 = 13.91$ and a mean reddening of $E(B-V) = 0.55$ for bulge stars (Barbuy et al. [1998]). The extinction coefficients for the Strömgren colours are estimated by applying the Cardelli et al. [1989] reddening relation and $R_V = A_V/E(B-V) = 3.13$ (Barbuy et al. [1998]). We find: $E(b-y) = 0.69 \times E(B-V)$, $E(v-y) = 1.31 \times E(B-V)$, $E(u-y) = 1.82 \times E(B-V)$ and $E(Ca-y) = 1.46 \times E(B-V)$.

The red solid line shows an isochrone for $t = 0.45$ Gyr and $Z = 0.04, Y = 0.303$, while the green and blue solid lines show two isochrones for the same chemical composition, $Z = 0.02, Y = 0.273$, and different ages, $t = 2$ Gyr and $t = 10$ Gyr, respectively. Red and blue dots show RG and red-clump stars observed spectroscopically by ZO08. Isochrones are from the BASTI data base and are based on α-enhanced ([α/Fe] = 0.4) evolutionary models (Pietrinferni et al. [2006]). Evolutionary prescriptions were transformed into the observational plane using atmosphere models computed assuming α-enhanced mixtures. Data plotted in Fig. 5.5 indicate that theory and observations, within the errors, agree quite well both with the thin disk main sequence ($1.0 \lesssim (v-y) \lesssim 2.5$ mag, $14 \lesssim y \lesssim 20$ mag, red solid line) and the bulge and thick disk sequences ($2.0 \lesssim (v-y) \lesssim 3.5$ mag, $14 \lesssim y \lesssim 18$ mag, green and blue solid lines). The spread of the sequences is mostly due to photometric errors and to the presence of differential reddening, but also to depth differences of the stars.

Fig. 5.6 shows the same CMDs but for NGC 6522: only stars with distances from the cluster center in the range 0.65 - 1.65 arcminutes are plotted. The cluster center is excluded due to crowding,

[1]The "separation index" quantifies the degree of crowding (Stetson et al. [2003]).

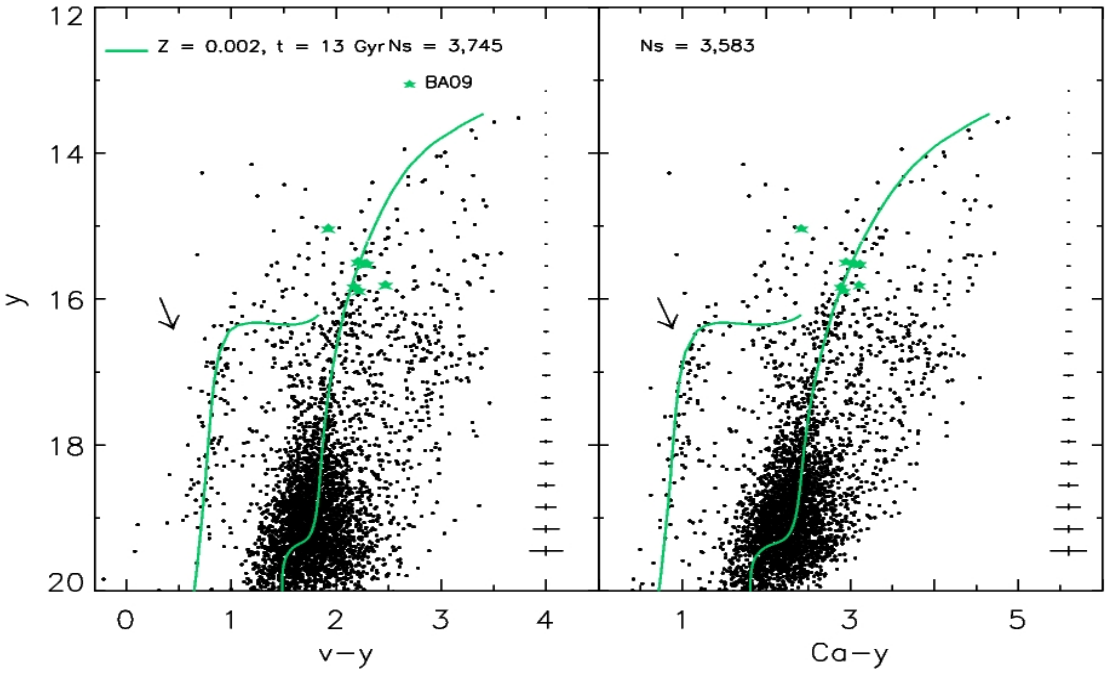

Figure 5.6: Same as Fig. 5.5 but for NGC 6522. The green solid lines show an isochrone for $t = 13$ Gyr and $Z = 0.002, Y = 0.248$ and the predicted ZAHB for $Z = 0.002$, while the green stars mark the eight cluster red-giants observed spectroscopically by Barbuy et al. [2009].

but stars up to about 1.5 the half-light radius ($r_h = 1.0$', Harris [2003]) are selected (CA11). The green solid lines show an isochrone for $t = 13$ Gyr and $Z = 0.002, Y = 0.248$ and the predicted Zero Age Horizontal Branch (ZAHB) for $Z = 0.002$. The eight green stars are RGs with high-resolution spectra collected with FLAMES/GIRAFFE at the VLT (ESO, Barbuy et al. [2009], hereafter BA09). Note that theory and observations agree quite well and give [Fe/H] $\sim$ -1.3 dex for NGC 6522, in agreement with the spectroscopic estimate [Fe/H] $\sim$ -1.2 dex by BA09, converted to the Zinn & West [1984] metallicity scale (CA11).

Metallicity distribution

We select NGC 6522 RGs by star position as in first Section, in magnitude ($y < 18.0$ mag), in photometric accuracy ($\sigma(v,b,y) < 0.03$ and $\sigma(Ca) < 0.02$ mag), and in surface gravity ($[c] = (u-v) - (v-b) - 0.2 \times (b-y) < 0.35$ mag), ending up with 51 RGs. A further selection is performed by using the proper motions by Sumi et al. [2003] and imposing $-2 < pm(\alpha) < 6$ and $-2 < pm(\delta) < 2$ mas/yr (CA11). The final sample includes 28 candidate cluster RGs.

Photometric metallicities are estimated by adopting the new theoretical calibration by CA11 based on the Strömgren hk index. To unredden the hk index we adopt $E(hk) = -0.155\,E(b–y)$ (Anthony-Twarog et al. [1991]).

The panels of Fig. 5.7 show the photometric metallicities of the 28 candidate RGs estimated adopting the Metallicity–Index–Colour relations based on hk_0 and the $b–y$, $Ca–y$, $u–y$ unreddened colours plotted versus metallicities estimated with the hk_0, $v–y$ relation. The eight RGs in common with BA09 are marked with a red star. Metallicity estimates based on the hk_0, $b–y$ and on the hk_0, $u–y$ relations agree quite well with those based on the hk_0, $v–y$ relation ($< \Delta([\mathrm{M/H}]_{\mathrm{by,\ uy}} - [\mathrm{M/H}]_{\mathrm{vy}}) > \simeq 0.0 \pm 0.02$ and $\simeq -0.01 \pm 0.02$ with $\sigma = 0.26$ and 0.19 dex, respectively.) On the other hand, the metallicity estimates based on the hk_0, $Ca–y$ relation are on average ≈ 0.3 dex more metal-rich than those based on the hk_0, $v–y$ relation. The difference might be due to the fact that the hk_0, $Ca–y$ relation is more sensitive to the Ca abundance and, in turn, to the α-element abundance, than the other relations.

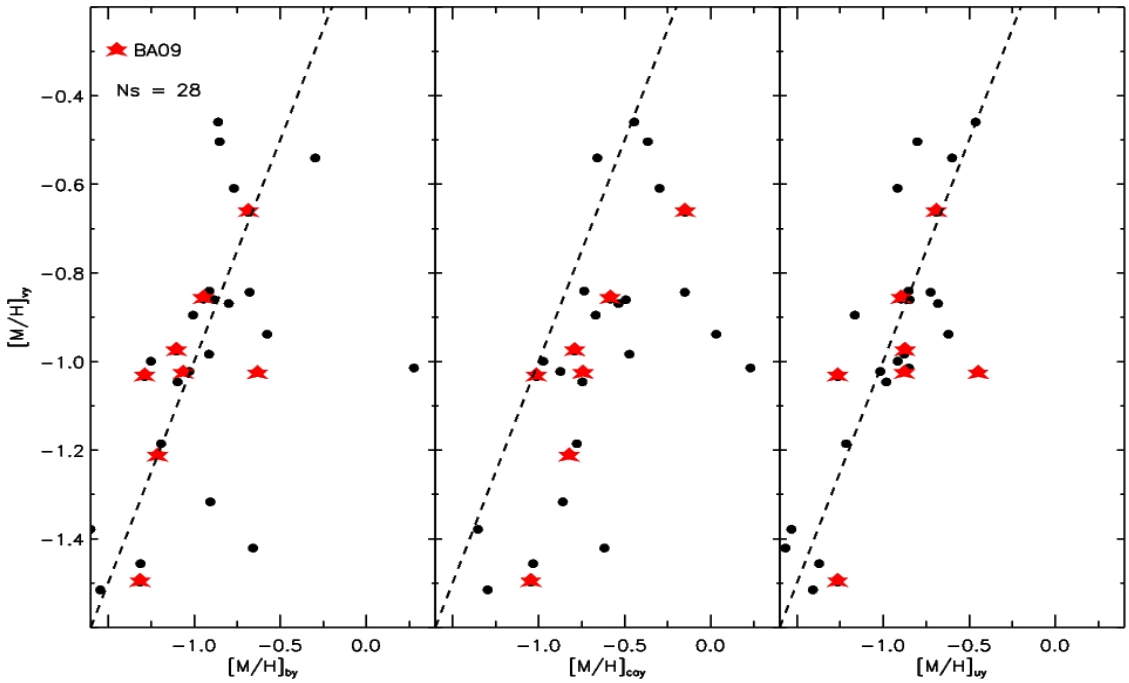

Figure 5.7: Photometric metallicities of 28 candidate RGs of NGC 6522 estimated adopting the Metallicity–Index–Colour relations hk_0, b–y_0, Ca–y_0, u–y_0 ($[\mathrm{M/H}]_{by}, [\mathrm{M/H}]_{cay}, [\mathrm{M/H}]_{uy}$) versus metallicities estimated with the hk_0, v–y_0 relation ($[\mathrm{M/H}]_{uy}$). The eight RGs with spectroscopic measurements from BA09 are marked as red stars.

Conclusions and future perspectives

We presented $Ca-uvby$ Strömgren photometry of the Baade's Window, including the GGC NGC 6522. We separated field and cluster stars and estimated the global metallicity of candidate RGs in NGC 6522 by using a new theoretical metallicity calibration of the hk index. We find that metallicities estimated by adopting the hk index and the Ca–y colour are systematically more metal-rich than metallicities estimated with the hk index and the b–y, v–y and b–y colours. The hk index is then affected not only by the Ca abundance, but also by another source of opacity.

We now plan to perform a new α-enhanced theoretical calibration of the Strömgren index m_1 up to solar metallicities, to constrain the metallicity distribution of bulge RGs and red clump stars. We then plan to match Strömgren data with z, y, J, H, K-band photometry of the bulge from the VVV public survey project (VISTA, ESO, http://vvvsurvey.org/). The optical-NIR colour-colour planes will allow us to better disentangle the different components present in the observed field of view (thin/thick disk, bulge stars). We will then test the adoption of different intermediate- and broad-band colour-colour planes in order to study the metallicity and the age distribution of these stars.

Bibliography

Anthony-Twarog, B. J., Twarog, B. A., Laird, J. B., & Payne, D. 1991, AJ, 101, 1902
Barbuy, B., Bica, E., & Ortolani, S. 1998, A&A, 333, 117
Barbuy, B., Zoccali, M., Ortolani, S., et al. 2009, A&A, 507, 405
Calamida, A. & et al. 2011, ApJ Lett.
Cardelli, J. A., Clayton, G. C., & Mathis, J. S. 1989, ApJ, 345, 245
Harris, W. E. 2003, in Extragalactic Globular Cluster Systems, ed. M. Kissler-Patig, 317–+
Pietrinferni, A., Cassisi, S., Salaris, M., & Castelli, F. 2006, ApJ, 642, 797
Robin, A. C., Reylé, C., Derrière, S., & Picaud, S. 2003, A&A, 409, 523
Stetson, P. B., Bruntt, H., & Grundahl, F. 2003, PASP, 115, 413
Sumi, T., Eyer, L., & Woźniak, P. R. 2003, MNRAS, 340, 1346
Zinn, R. & West, M. J. 1984, ApJS, 55, 45
Zoccali, M., Hill, V., Lecureur, A., et al. 2008, A&A, 486, 177
Zoccali, M., Lecureur, A., Barbuy, B., et al. 2006, A&A, 457, L1

Zoccali, M., Renzini, A., Ortolani, S., et al. 2003, A&A, 399, 931

5.4 The Milky Way Nuclear Star Cluster

Roberto Capuzzo-Dolcetta[1], F. Antonini[2], and A. Mastrobuono-Battisti[1]

[1] Dep. of Physics, Sapienza, Univ. di Roma, Italy
[2] Dep. of Physics, Rochester Institute of Technology, Rochester, USA

Abstract

In the center of the Milky Way, as well as in many other galaxies, a compact star cluster around a very massive black hole is observed. One of the possible explanations for the formation of such Nuclear Star Clusters is based on the 'merging' of globular clusters in the inner galactic potential well. By means of sophisticated N-body simulations, we checked the validity of this hypothesis and found that it may actually have been the one leading to the formation of the Milky Way Nuclear Star Cluster.

Introduction

The existence of very compact star clusters around the centers of many galaxies is well ascertained, nowadays. These clusters, called Nuclear Star Clusters (NSCs) are among the densest star clusters observed, with effective radii of a few pc and central luminosities up to 10^7 $L_\odot$. Recently, the study of dense stellar systems has raised new interest because of the discovery, in an ever increasing number of galaxies, of compact nuclei in form of stellar resolved systems and/or NSCs which are now known to be present in galaxies across the whole Hubble sequence and not only in the dE, N galaxies (Bekki & Graham [2010]). A radial profile and velocity structure for a NSC can be determined only for the Milky Way NSC which is close enough that it can be resolved into individual stars. The Milky Way NSC has an estimated mass of 10^7 $M_\odot$, and it hosts a massive black hole whose mass, 4.3×10^6 $M_\odot$, is uniquely well determined.
The formation mechanism of nuclear star clusters is unknown. Two competing models are possible. In the gas model, a NSC can form from the gas that migrates to the center of the galaxy where it then forms stars. A variety of scenarios have been proposed to account for the required fast radial inflow of gas into the galactic center, including the magneto-rotational instability in a differentially rotating gas disk, tidal compression in shallow density profiles or dynamical instabilities. Alternatively, in the merger model, massive clusters migrate to the center via dynamical friction and merge to form a dense nucleus (Tremaine et al. [1975]; Capuzzo-Dolcetta [1993]). Observations of NSCs in dE galaxies suggest that the majority, but not all, dE nuclei, could be the result of packing mass in form of orbitally decayed globular clusters (GCs) (Lotz et al. [2004]). Numerical simulations have also shown that the basic properties of NSCs, including their shape, mass density profile, and mass-radius relation are reproduced in the merger model under a variety of explored conditions (Capuzzo-Dolcetta et al. [2008a,b]; Hartmann et al. [2011]).

The Milky Way nuclear cluster

As we said, a NSC is present in the central region of the Milky Way. For obvious reasons, it is the only NSC which can be resolved into individual stars in spite of its high density (Schödel et al. [2007]); moreover, detailed kinematic studies exist that allow a precise determination of the mass of the central black hole, $M_{BH} = 4.3 \times 10^6$ $M_\odot$. Moreover, the relaxation time at Sgr A* influence radius is robustly estimated as 20 – 30 Gyr (Merritt [2010]) suggesting there has not been time for a Bahcall-Wolf cusp to rise. This is consistent with the almost flat density distribution of late type stars within 0.5 pc from the center (Buchholz et al. [2009]). As stated in the Introduction, at least two competing models are possible for the formation of the MW NSC. These mechanisms must account for the observed evidence of the MW NSC, i.e.: a mass of the NSC $M_{NSC} \sim 10^7$ $M_\odot$, a density profile with a *core* of about 0.5 pc and decreasing as $r^{-1.8}$ up to $r \simeq 30$ pc. Out of 30 pc there is a large nuclear stellar and molecular disk of approximately the same radius.

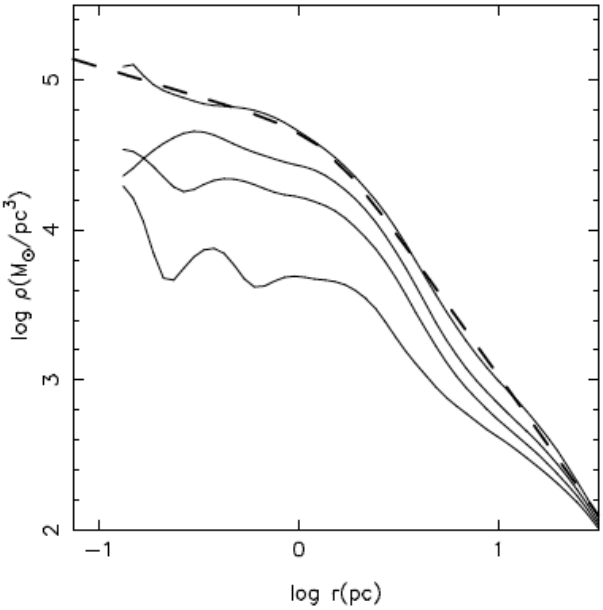

Figure 5.8: Spatial profile of the central NSC after 3, 6, 9 and 12 mergers. The central density grows with time. The dashed line is the fit to the NSC profile obtained at the end of the entire simulation using a broken power law model.

Globular cluster merging and MW NSC formation

We modeled the final evolution of a set of massive GCs which decayed in the inner region of the Milky Way due to the dynamical friction braking exerted by the galactic stellar field. The details of the computations and the extended presentation and discussion of results are given in Antonini et al. [2011]; here we give just a brief summary.
Our Galaxy, likely triaxial in its inner part, is dense enough to make the orbits of GCs with mass around 10^6 $M_\odot$ to decay (by dynamical friction) to the inner 50 pc in a time significantly shorter than a Hubble time. We thus consider 12 such GCs and their final evolution toward a merger state studied via N-body simulations of their motion in the inner region of the Milky Way, represented self-consistently as a set of N particles. The N body galactic environment is sampled from a shallow ($\rho \propto r^{-1/2}$) cusp; the contribution of the central massive black hole is also considered. Simulations are done with both the high precision, parallel PhiGRape (Harfst et al. [2007]) and NBSymple (Capuzzo-Dolcetta et al. [2011]) codes running on the RIT Grape cluster and on the CPU+NVIDIA TESLA C2050 platform in Roma, Sapienza.

Results

The merging occurs rather quickly: after about 20 crossing times the resulting system attains a quasi equilibrium configuration, as it is shown by the almost steady time profile of Lagrangian radii. This corresponds to a slowly evolving (via relaxation) super stellar cluster (SSC) which oscillates around the massive black hole. Fig. 5.8 shows the growth with time of the spatial density profile after the various merger events. The core structure is conserved. Fig. 5.9 (left panel) gives the comparison between the surface density of the 12 GCs merger and the underlying galactic stellar profile. The kinematic properties of the merger system are resumed by the Fig. 5.9 (right panel), which shows the presence of a tangentially biased zone, intermediate between an inner (close to the massive BH, $r \leq 0.3$ pc) and an outer ($r \geq 40$ pc) isotropic region. This tangential anisotropy grows with the number of infalls. This may be an important signature of the modes of NSC formation.

The SSC has a density which is not far from the sum of the individual GC densities, so that the projected density profile in the nuclear region is remarkably similar to that of the Milky Way NSC. The final NSC morphology is nearly oblate with a value $T \sim 0.2$ for the triaxiality parameter.

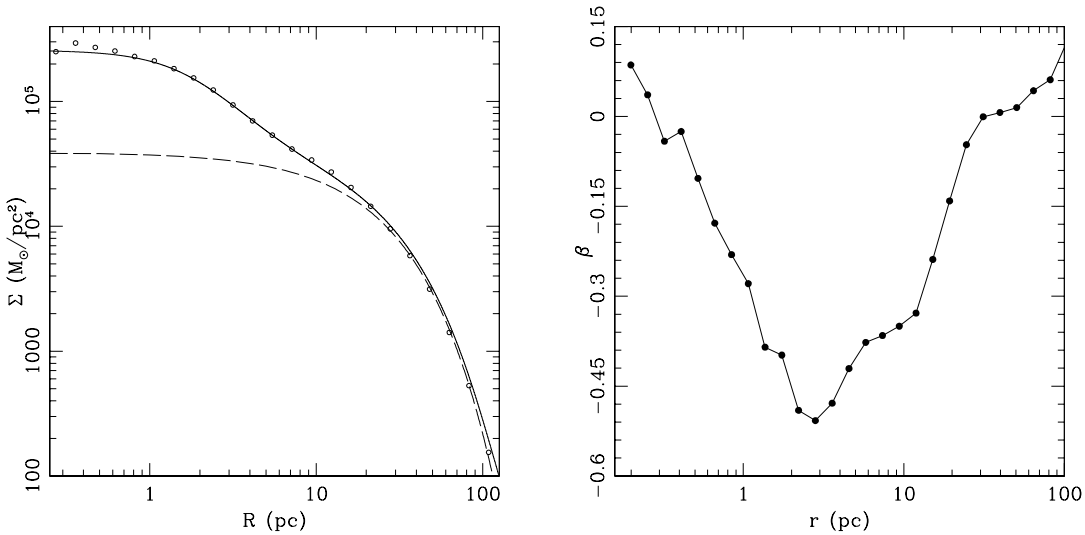

Figure 5.9: *Left panel*: projected density profile of the merged system at the end of the simulation (solid line). Dashed line refers to the galactic density profile. *Right panel*: radial behaviour of the anisotrophy parameter $\beta = 1 - \sigma_t^2/\sigma_r^2$.

Conclusions

As already shown by previous papers (Capuzzo-Dolcetta [1993]; Capuzzo-Dolcetta et al. [2008a,b]) the dynamical friction dragging of massive globular clusters toward the galactic center is a viable explanation of the local high densities. The novelty of this work is the inclusion in the simulations of a massive black hole in the galactic center. Its role, although important in the vicinity of its influence radius, does not alter the general characteristics of the merger event of a set of GCs falling to the center. The merger reaches a sort of quasi-steady state, slowly evolving due to internal relaxation which is partly affected by the presence of the massive black hole. With regard to the Milky Way nuclear cluster, it is relevant noting how the original 'core' profile of the GCs (the NSC building blocks) is maintained for a time long enough to justify the core actually observed in the MW NSC. Moreover, the outward profile radial slope, $\rho \propto r^{-2}$, of the merger system is in good agreement (within 30 pc from the center) with the observed MW NSC profile. Surely, an even more stringent answer to the question of the MW NC formation will come from a high resolution, well extended in time, numerical study of the secular evolution of the merger remnant as well as from a detailed study of the expected observed stellar population (both in progress).

Bibliography

Antonini, F., Capuzzo-Dolcetta, R., Mastrobuono-Battisti, A., & Merritt, D. 2011, in preparation
Bekki, K. & Graham, A. W. 2010, ApJ, 714, 313
Buchholz, R. M., Schödel, R., & Eckart, A. 2009, A&A, 499, 483
Capuzzo-Dolcetta, R., 1993, ApJ, 415, 616
Capuzzo-Dolcetta, R., Miocchi, P., 2008a, MNRAS, 388, L69
Capuzzo-Dolcetta, R., Miocchi, P., 2008b, ApJ, 681, 1136
Capuzzo-Dolcetta, R., Mastrobuono-Battisti, A., Maschietti, D., 2011, NewAstron, 16, 284
Harfst, S., Gualandris, A., Merritt, D., Spurzem, R., Portegies Zwart, S., & Berczik, P. 2007, NewAstron, 12, 357
Hartmann, H., Debattista, V. P., Seth, A., Cappellari, M., & Quinn, T. R., 2011,
Lotz J. M., Miller B. W., Ferguson H. C., 2004, ApJ, 613, 262
Merritt, D., 2010, ApJ, 718, 739
Schödel, R., Eckart, A., Alexander, T., et al. 2007, A&A, 469, 125
Tremaine, S. D., Ostriker, J. P., & Spitzer, L., Jr. 1975, ApJ, 196, 407

5.5 Mass Segregation and Elongation of the Starburst Cluster Westerlund 1

Mario Gennaro[1], W. Brandner[1], A. Stolte[2], and T. Henning[1]

[1] Max-Planck-Institut für Astronomie, Königstuhl 17, 69117, Heidelberg, Germany
[2] Argelander Institut für Astronomie, Auf dem Hügel 71, 53121, Bonn, Germany

Abstract

Massive stellar clusters are the best available laboratories to study the mass function of stars. Based on NTT/SofI near-infrared photometry, we have investigated the properties of the massive young cluster Westerlund 1. From comparison with stellar models, we derived an extinction $A_{K_S} = 0.91 \pm 0.05$ mag, an age $\tau = 4 \pm 0.5$ Myr and a distance $d = 4.0 \pm 0.2$ kpc. The total mass is $M_{\mathrm{Wd\,1}} = 4.91^{+1.79}_{-0.49} \times 10^4 M_\odot$. We performed a 2D study of the cluster's IMF and of its density profiles. From both IMF slope variations and stellar density, we find evidence of mass segregation. For a cluster with $\sim 10^5$ stars, this is not expected at such a young age as the result of two-body relaxation alone. We also confirm previous findings on the elongation of Westerlund 1; assuming an elliptical density profile, we found an axis ratio of a:b = 3:2. Rapid mass segregation and elongation could be well explained as the results of subclusters merging during the formation of Westerlund 1.

Introduction

Westerlund 1 (Wd 1) is among the most massive young clusters in the Local Group. Recent studies have revived interest in this cluster, discovered already 50 years ago (Westerlund [1961]). Several of these studies focus on the rich population of massive stars that are spectroscopically identified as Wd 1 members (e.g. Clark et al. [2005]; Negueruela & Clark [2005]; Crowther et al. [2006]; Negueruela et al. [2010]). Among this population it has been possible to find Wolf-Rayet stars, evolved OB stars, and short-lived transitional objects like Luminous Blue Variables and Yellow Hypergiants. Wd 1 is the only case in which such a rich population of these very rare objects is observable. This makes Wd 1 one of the most important templates for understanding the evolution of very massive stars after they leave the main sequence. Given the high extinction towards Wd 1 of $A_V \sim 10 - 12$ mag (Piatti et al. [1998]) the intermediate- and low-mass stellar population is best studied using near-infrared observations (Brandner et al. [2008]).

With the present estimates of its mass –from 5×10^4 to $1.5 \times 10^5 M_\odot$– and age –from 3 to 6 Myr– (see Clark et al. [2005]; Crowther et al. [2006]; Brandner et al. [2008]; Mengel & Tacconi-Garman [2009]; Negueruela et al. [2010]), Wd 1 represents probably the best template in the Milky Way to understand the cluster mode of star formation that can be observed in other galaxies, like the Antennae Galaxies, where Super Star Clusters with masses larger $10^5 M_\odot$ have been detected (see e.g. Whitmore et al. [2010]).

In addition to the study of the intriguing formation scenario of such massive extragalactic clusters, Wd 1 may also serve as a template to understand the interplay between evolution of massive stars and dynamical processes that may lead to the formation of stable, bound and relaxed globular clusters. Given its mass, Wd 1 may indeed be able to retain a substantial fraction of its initial stellar population, even though, according to Muno et al. [2006], it has probably undergone ~ 65 supernova events. These, in addition to stellar winds and ionizing radiation from the most massive stars, have dispersed the residual gas reservoir of the cluster, decreasing the gravitational binding energy of the system. If massive enough to resist disruption, Wd 1 will eventually turn into a closed, virialized system.

We focus our attention on the study of Wd 1 mass function, degree of mass segregation and shape. These macroscopic properties are, in turn, related to the formation history of Wd 1, its dynamical evolution and its interactions with the rest of the Galaxy.

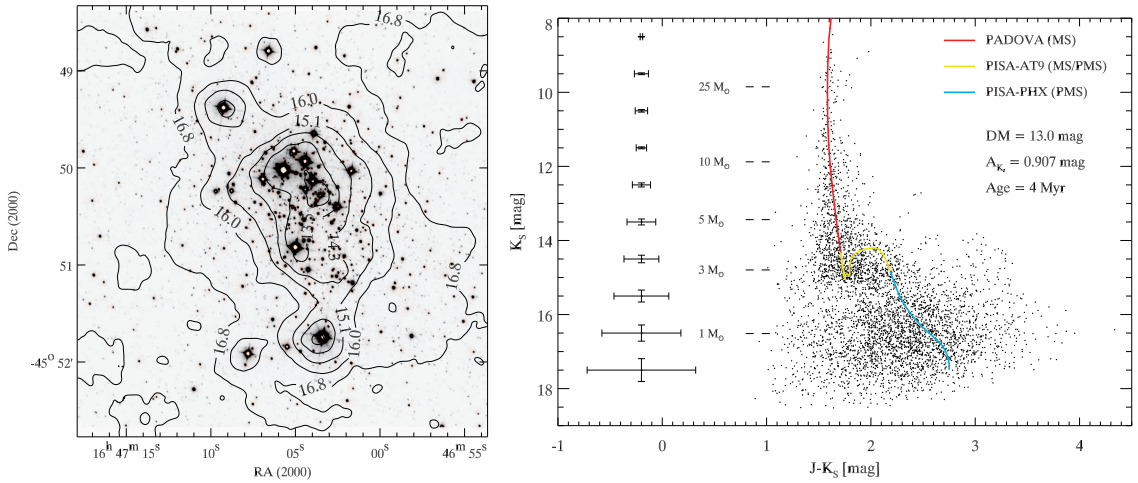

Figure 5.10: *Left:* SOFI K_S band image of Wd 1. Superimposed are K_S 50% completeness contours. The labels correspond to the K_S magnitudes at which 50% completeness is reached. *Right:* clean CMD of Wd 1 with superimposed best-fit isochrone. Adopted models are a combination of Padova models (Marigo et al. [2008]) and Pisa models (Degl'Innocenti et al. [2008]). The latter have been transformed into the observational plane using ATLAS9 (Castelli & Kurucz [2003]) and PHOENIX (Brott & Hauschildt [2005]) spectra.

The data

NTT/SofI J and K_S broad band observations of Wd 1 (RA(2000) = $16^h47^m03^s$, Dec(2000) = $-45°50'37''$) and of a nearby comparison field -offset by ≈ 7 arcmin to the East and ≈ 13 arcmin to the South of Wd 1- were retrieved from the ESO archive (PI: J.Alves). Data reduction was performed using the `eclipse` routines (Devillard [2001]). PSF-fitting photometry was derived using `IRAF/DAOPHOT` (Stetson [1987]). Photometric zero points and colour terms were computed by comparison of instrumental magnitudes of relatively isolated, bright sources with counterparts in the 2MASS Point Source Catalogue (Skrutskie et al. [2006]).

The cluster colour magnitude diagram

To obtain a correct cluster mass function and for the analysis of Wd 1 density profile, it is necessary to derive appropriate incompleteness corrections and to estabilish membership of the detected stars. The main source of incompleteness in our case is crowding, which severely affects seeing limited observations (Eisenhauer et al. [1998]). The effects of crowding on the detection of point sources change according to two quantities: the average stellar density and the magnitude contrast between the given point source and its neighbours. Both of these quantities may not follow a radially symmetric or regular distribution. Using artificial star experiments we built -for each photmetric band 'j'- a completeness function:

$$\mathcal{C}_j \equiv \mathcal{C}(M_j|x, y, \mu) \quad ;$$

where μ is the actual value of the magnitude (in the M_j band) and (x, y) the position at which completeness is evaluated. It is then possible to associate an incompleteness correction to each star for each photometric band.

A visualization of the completeness pattern for Wd 1 is shown in Fig. 5.10, left panel. We display the K_S band image of the cluster with superimposed 50% completeness magnitude-loci. The contours are labeled with the corresponding values of K_S magnitudes for which completeness drops to 50 %. Such contours follow the general distribution of stars, but also show peaks around the brightest stars, as expected; from the figure it is clear that completeness distribution of Wd 1 is not radially symmetric.

After calculating completeness correction, the observed population of stars has been cleaned by field stars contamination using a newly developed statistical approach (see Gennaro et al. [2011] for more details).

The clean colour-magnitude diagram (CMD) is shown in Fig.5.10, right panel. From isochrone fitting an extinction of $A_{K_S} = 0.91 \pm 0.05$ mag was derived. The cluster age and distance were also estimated from model superposition to be $\tau = 4.0 \pm 0.5$ Myr and $d = 4.0 \pm 0.2$ kpc respectively.

Mass function and total mass of Wd 1

Given our best-fitting isochrone we used a maximum-likelihood approach to determine the mass of the member stars. The probability density distribution of the stellar mass for a star with observed magnitudes $\mu = (J, K_{\rm S})$ is given by:

$$p(m) = \frac{1}{2\pi|\mathbf{\Sigma}_*|^{1/2}} \times \exp\left\{-\frac{1}{2}\left[\mathbf{M}(m) - \mu_*\right]^T \mathbf{\Sigma}_*{}^{-1}\left[\mathbf{M}(m) - \mu_*\right]\right\}, \tag{5.1}$$

where $\mathbf{\Sigma}$ is the correlation matrix of the observed magnitude errors and $\mathbf{M}(m)$ are the model-predicted magnitudes as a function of mass. Given the $p_i(m)$ -for each star in Wd 1- we define the observed cluster's Mass Function as:

$$\frac{{\rm d}N(m)}{{\rm d}m} = \sum_i \frac{1}{\mathcal{C}_{J_i}} \times \frac{1}{\mathcal{C}_{K_{{\rm S}\,i}}} \times p_i(m) \tag{5.2}$$

where C_{J_i} and $C_{K_{{\rm S}\,i}}$ are the completeness factors for the i-th star. By fitting a single power-law to the observed mass function in the mass range $m[M_\odot] \in [3.5, 27]$ we obtain $\gamma = 2.44^{+0.20}_{-0.08}$, slightly steeper than an ordinary Salpeter/Kroupa IMF. For the normalization constant we found $\mathcal{A} = 1.22^{+0.56}_{-0.14} \times 10^4$. The best values and uncertainty of γ and $\mathcal{A}$ are evaluated by using a bootstrap technique. Given the couple of values (γ_i, A_i) obtained from a single boostrap sample, it is possible to associate to them a value of the total mass and total number of stars for Wd 1. We extrapolate the power law with index γ_i in the range $m[M_\odot] \in [0.5, 120]$. For masses below 0.5 $M_\odot$ and down to the hydrogen burning limit, i.e., 0.08 $M_\odot$ we used the Kroupa IMF slope for this stellar regime, with a $\gamma = 1.3$. Given the distribution of $N_{tot,i}$ and $M_{tot,i}$ from the bootstrap samples, the total number of stars is $N_{\rm tot} = 1.04^{+0.60}_{-0.18} \times 10^5$ while the total mass of the cluster is estimated to be $M_{\rm tot} = 4.91^{+1.79}_{-0.49} \times 10^4$ $M_\odot$.

Using the MS turn-off mass and the identified post-MS member, by extrapolation of a Kroupa IMF down to lower masses, Clark et al. [2005] found a somewhat higher value for the total mass of $\sim 10^5 M_\odot$. From radial velocity measurements of ~ 10 stars Mengel & Tacconi-Garman [2009] determine an even larger gravitational mass of Wd 1, $M_{dyn} = 1.5^{+0.9}_{-0.7} \times 10^5 M_\odot$, under the hypothesis of virial equilibrium. These findings have been recently questioned by Cottaar et al. [2011, presented in this same conference] who also use radial velocities to estimate the mass of Wd 1. The latter results are in much better agreement with our photometric estimate of Wd 1 total mass.

Morphology of Wd 1

Several recent studies indicate that Wd 1 is elongated (see e.g. Muno et al. [2006]). Brandner et al. [2008] assuming an elliptical shape with a and b as semi-major and semi-minor axis respectively, found an ellipticity of the cluster, $\eta = 1 - \frac{b}{a} = 0.19$, when stars with masses in the range 10 to 32 $M_\odot$ were considered. The value slightly decreases to $\eta = 0.15$ using masses between 3.5 and 10 $M_\odot$. Our 2D incompleteness mapping enables an unbiased study of the cluster's 2D density distribution. We built number density maps for Wd 1 and found out that these density profiles are always elongated. Hence we decided to fit the profiles by using an elliptical generalization of the Elson et al. [1987] profile.

The eccentricity values we obtain from the fit are almost constant for the different mass ranges adopted, with an axis ratio $a : b = 3 : 2$. Our results clearly reveal the elongated distribution of Wd 1 stars with masses between ≈ 3 and ≈ 30 $M_\odot$. An other finding is that the semimajor axis of the elliptical density distribution decreases with mass almost like $1/\log(m)$. This points to the fact that massive stars are more centrally concentrated. MOreover we note that Wd 1's direction of elongation lies very close to the Galactic Plane.

The deviation from the spherical cluster shape must be explained either by unusual initial conditions still reflected in the present cluster appearance or by some interaction with the rest of the Galaxy. We evaluate whether tidal effects in the Galactic central field could be responsible for the Wd 1 shape. Under the simplifying assumption of a circular restricted 3-body problem, with primary mass at the Galactic Centre position and secondary at the cluster centre, we find that the distance of the inner Lagrangian point from Wd 1 centre is $r_L = 12$ pc. This estimate is a lower limit, since it was assumed that all the mass of the Galaxy is confined within the orbit of Wd1. Consequently, it is clear that Wd 1 is far from filling its Roche lobe, while we measure elongation already on a scale of ~ 1 pc from the cluster core. Hence tidal distortion is unlikely the reason for the elongation of Wd 1.

A net angular momentum of the giant molecular cloud forming Wd 1 or a formation of Wd 1 out of two or more subclusters might either be responsible for its elongated shape. Differential galactic rotation exerts a shear on molecular clouds which might lead to a net angular momentum. According to a recent study by Ballesteros-Paredes et al. [2009], however, galactic shear and tides have rather strong effects on initially elongated clouds, eventually quenching star formation and disrupting the clouds. Hence differential rotation is an unlikely source for the elongation of Wd 1. An other intriguing possibility would be a "hierarchical" formation scenario, with merging of two or more smaller subclusters. The existence of a non-negligible fraction of possible binary clusters is supported by observations (see e.g. de la Fuente Marcos & de la Fuente Marcos [2008]). A hierarchical organization of the ISM and of young stellar groups and clusters is indeed observed on many scales [Elmegreen, 2009].

Conclusions

We have presented an analysis of near-infrared data for the intermediate- and low-mass stellar population of the massive young cluster Westerlund 1.

We investigated the cluster's IMF slope using a new approach to stellar mass determination. The information on magnitude errors and their correlation has been used to derive the mass-probability-distribution for each star, given the best-fit isochrone. The completeness-corrected IMF has a slope of $\gamma = 2.44^{+0.20}_{-0.08}$, slightly steeper than the Salpeter or Kroupa IMF; this slight discrepancy could be partially reconciled if we consider that, for the sake of simplicity, we are neglecting the influence of (unknown) undetected binarity, hence our quoted error is probably an underestimate of the total, statistical plus systematic error (Maíz Apellániz [2009]). From the IMF slope and its normalization constant we found a total mass for the cluster of $M_{\mathrm{Wd\,1}} = 4.91^{+1.79}_{-0.49} \times 10^4$ M$_\odot$.

The spatially varying completeness, combined with the probabilistic mass determination, enabled us to investigate the spatial variations of the Mass Function. The Wd 1 starburst cluster is mass segregated, with massive stars more centrally concentrated. Other indications of mass segregation come from the analysis of the stellar density distribution. In order to study the 2D density distribution as a function of stellar mass, we fitted 2D elliptical profiles. This analisys revealed a tight dependency of the ellipses semi-major axis length on mass: $a(m) \propto 1/\log(m)$. Given the young age of Wd 1, its global mass segregation cannot be explained by simple 2-body relaxation. Interestingly, from the density distribution analysis, we found that Wd 1 is elongated along the Galactic Plane with an axis ratio $a : b = 3 : 2$. The mass segregation and the elongation together hint at a formation scenario involving the merging of multiple subclusters formed almost coevally in the parental giant molecular cloud.

Bibliography

Ballesteros-Paredes, J., Gómez, G. C., Pichardo, B., & Vázquez-Semadeni, E. 2009, MNRAS, 393, 1563
Brandner, W., Clark, J. S., Stolte, A., et al. 2008, A&A, 478, 137
Brott, I. & Hauschildt, P. H. 2005, in ESA Special Publication, Vol. 576, The Three-Dimensional Universe with Gaia, ed. C. Turon, K. S. O'Flaherty, & M. A. C. Perryman, 565
Castelli, F. & Kurucz, R. L. 2003, in IAU Symposium, Vol. 210, Modelling of Stellar Atmospheres, ed. N. Piskunov, W. W. Weiss, & D. F. Gray, 20
Clark, J. S., Negueruela, I., Crowther, P. A., & Goodwin, S. P. 2005, A&A, 434, 949
Crowther, P. A., Hadfield, L. J., Clark, J. S., Negueruela, I., & Vacca, W. D. 2006, MNRAS, 372, 1407
de la Fuente Marcos, R. & de la Fuente Marcos, C. 2008, ApJ, 672, 342
Degl'Innocenti, S., Prada Moroni, P. G., Marconi, M., & Ruoppo, A. 2008, Ap&SS, 316, 25
Devillard, N. 2001, in Astronomical Society of the Pacific Conference Series, Vol. 238, Astronomical Data Analysis Software and Systems X, ed. F. R. Harnden Jr., F. A. Primini, & H. E. Payne, 525
Eisenhauer, F., Quirrenbach, A., Zinnecker, H., & Genzel, R. 1998, ApJ, 498, 278
Elmegreen, B. G. 2009, in Globular Clusters - Guides to Galaxies, ed. Richtler, T. & Larsen, S., 87
Elson, R. A. W., Fall, S. M., & Freeman, K. C. 1987, ApJ, 323, 54
Gennaro, M., Brandner, W., Stolte, A., & Henning, T. 2011, MNRAS, 412, 2469
Maíz Apellániz, J. 2009, Ap&SS, 324, 95
Marigo, P., Girardi, L., Bressan, A., et al. 2008, A&A, 482, 883
Mengel, S. & Tacconi-Garman, L. E. 2009, Ap&SS, 324, 321
Muno, M. P., Law, C., Clark, J. S., et al. 2006, ApJ, 650, 203
Negueruela, I. & Clark, J. S. 2005, A&A, 436, 541

Negueruela, I., Clark, J. S., & Ritchie, B. W. 2010, A&A, 516, A78
Piatti, A. E., Bica, E., & Claria, J. J. 1998, A&AS, 127, 423
Skrutskie, M. F., Cutri, R. M., Stiening, R., & et al. 2006, AJ, 131, 1163
Stetson, P. B. 1987, PASP, 99, 191
Westerlund, B. 1961, PASP, 73, 51
Whitmore, B. C., Chandar, R., Schweizer, F., et al. 2010, AJ, 140, 75

5.6 Improved Distances to Several Galactic OB Associations

Nadejda Kaltcheva[1] **and V. Golev**[2]

[1] Department of Physics and Astronomy, University of Wisconsin Oshkosh, 800 Algoma Blvd., Oshkosh, WI 54901, USA (kaltchev@uwosh.edu)
[2] Department of Astronomy, Faculty of Physics, St Kliment Ohridski University of Sofia, 5 James Bourchier Blvd., BG-1164 Sofia, Bulgaria (valgol@phys.uni-sofia.bg)

Abstract

Based on *uvbyβ* photometry we study the structure of several Galactic star-forming fields. Lac OB1 is a compact association at 520 ± 20 pc spatially correlated with a region of intense HII emission in Sh2-126. Lodén 112 is a compact OB group at 1630 ± 82 pc, probably connected to an extended feature of OB stars located toward the Carina tangent. The field toward Car OB1 is complex and likely contains apparent concentrations representing parts of long segments of the Carina arm projected along the line of sight. Within the classical Mon OB2 association we separate a relatively compact group at 1.26 kpc, that is spatially correlated to the Monoceros Loop SN remnant.

Introduction

The Galactic OB-associations offer a unique opportunity to study the influence of massive stars on the interstellar matter. A reconstruction of the star formation history of many Galactic fields should be possible once the spatial distribution of the young stars is reliably determined. Despite the extensive efforts to improve and unify the distances to the young stellar groups in the Milky Way (MW), discrepancies still remain in the published studies for a large number of fields. Many of the present distance estimates are based to a large extent on preliminary distance calibrations, broad-band photometry, or absolute magnitudes (M_V) obtained via spectral and luminosity type (MK classification). On the other hand, the *uvbyβ* photometric system provides M_V and colour excess determinations for early-type stars in excellent agreement with the *Hipparcos* parallaxes (Kaltcheva & Knude [1998]).

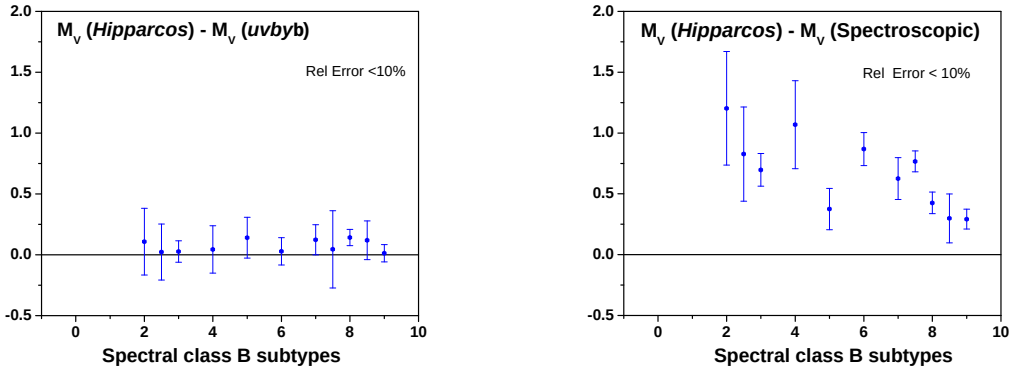

Figure 5.11: Comparisons of *uvbyβ* M_V (left) and MK-based M_V (right) to the *Hipparcos*-based M_V.

Fig. 5.11 represents the comparison of *uvbyβ* M_V and MK-based M_V to the *Hipparcos*-based M_V, pointing out to a possible over-estimation of stellar distance when relying on a MK-based determination. Since the distances to the Galactic OB associations are based mainly on individual stellar distances and rarely on main-sequence fitting, applying *uvbyβ* photometry should lead to a significant improvement for many OB groups in the MW.

Our deriving of *uvbyβ* photometric distances utilizes the intrinsic colour calibrations of Crawford [1978] and Kilkenny & Whittet [1985] and the luminosity calibration of Balona & Shobbrook [1984]

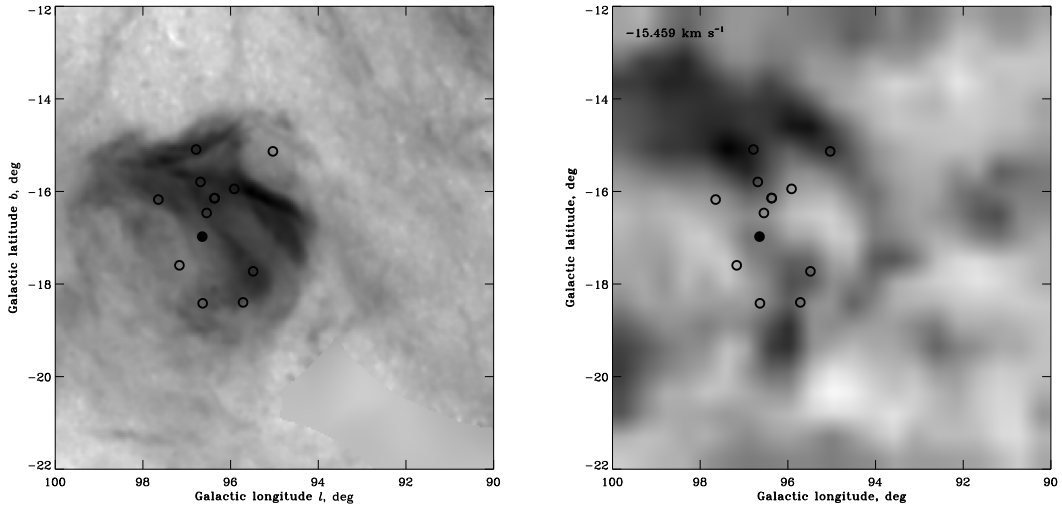

Figure 5.12: The stars of Lac OB1 overploted on the distribution of the HII emission in Sh2-126 (left) and HI (right). 10 Lac is shown with filled symbol.

and takes into account possible stellar emission and mis-classification (Kaltcheva & Hilditch [2000]). The expected errors for one star are about 12 % for luminosity classes III-IV and about 18-20 % for luminosity classes I and II. Photometric *uvbyβ* distances derived in this way provide the same impression of the star-forming field's structure as the improved *Hipparcos* parallaxes (cf. Kaltcheva & Makarov [2007]).

In this contribution we present improved distance estimates for four Galactic OB associations.

Lac OB1

Lac OB1 (Lac OB1b, Blaauw [1958]) is a nearby notable clustering of early-type stars near 10 Lacertae that initially gained attention because of the expanding motion of its members. Based on the derived *uvbyβ* photometric distances used in conjunction with the photometric diagrams we identify Lac OB1 as a compact group of 12 low-reddened main-sequence stars located at a distance 520 ± 20 pc in the direction $l = 96.4°, b = -16.6°$ (see Kaltcheva [2009] for details). The available radial velocity and proper motion measurements support the impression that this is a real group. For these 12 stars, the recalculated *Hipparcos* parallaxes (van Leeuwen [2007]) are in excellent agreement with the photometric *uvbyβ* parallaxes. The photometric distance of the O9V star 10 Lac (HD 214680) is estimated to be 715^{+107}_{-92} pc. Although this estimate is considerably larger than the one based on *Hipparcos*, the agreement for these stars is better with the recomputed *Hipparcos* parallax (van Leeuwen [2007]) which yields a distance of 529^{+70}_{-50} pc in comparison to the original *Hipparcos* estimate of 325^{+82}_{-55} pc.

Fig. 5.12 presents the distribution of HII intensity in units of Rayleighs and brightness temperature distribution of HI at velocity channel −15.5 km/s toward Lac OB1, with Lac OB1 stars superimposed. Here and on all further figures the HII data are taken from Finkbeiner [2003] via the *SkyView* interface (McGlynn et al. [1998]), and the HI data are taken from Leiden/Argentine/Bonn (LAB) Survey of Galactic HI (Kalberla et al. [2005]). A correlation of the stars' location with the regions of intense HII emission in Sh2-126 (Sharpless [1959]) is noticeable. On the other side, the distribution of neutral hydrogen shows a deficiency (most obvious in the selected velocity channel), also correlating with the location of the stars (see also Cappa De Nicolau & Olano [1990]).

The field of Lodén 112

Lodén 112 is identified as a poor, but compact cluster candidate. Based on *uvbyβ* photometry we obtained true DM = 11.06 ± 0.12(s.e.) and average colour excess $E(b-y) = 0.5 \pm 0.03$(s.e.) (Kaltcheva & Golev [2011]). This corresponds to a distance of 1630 ± 82 pc, which is significantly smaller than the presently adopted 2500 pc (WEBDA). In our *uvbyβ* sample there are several other early B stars located at that exact distance. The photometric distances and available proper motions allowed us to identify a group of about 10 early B stars that could represent a new OB association at coordinates $282° < l < 285°$,

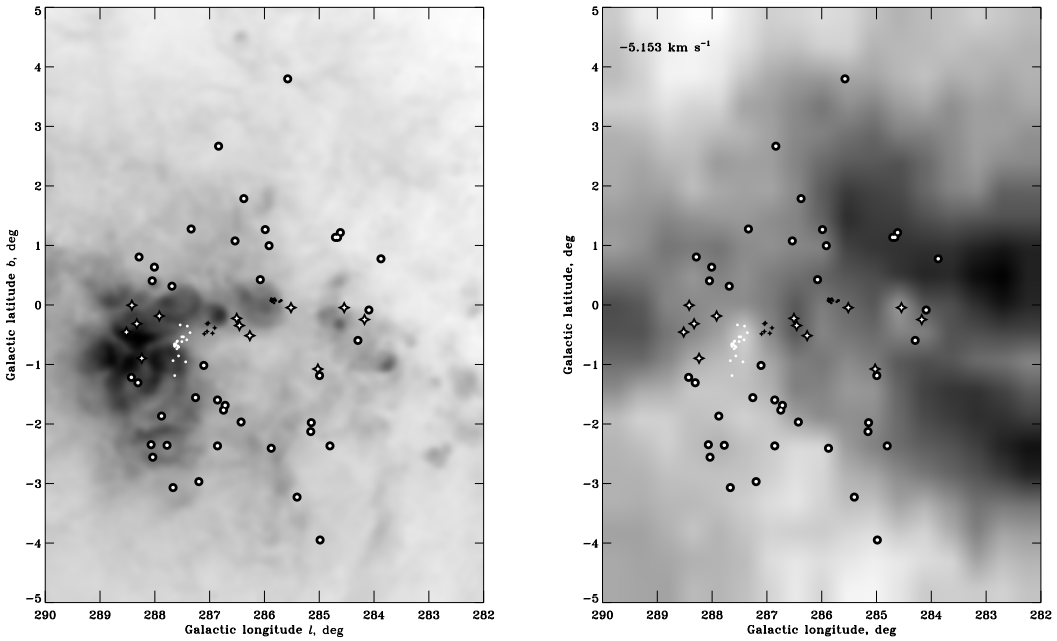

Figure 5.13: The stars in the Car OB1 field overplotted on the distribution of the HII emission (left) and the HI velocity chanel image at $v = -5$ km/s (right).

$-2^\circ < b < 2^\circ$ which appears to be connected to Lodén 112 cluster candidate (see a poster by Kaltcheva & Golev at this meeting for more details).

Car OB1

According to Humphreys [1978] the Car OB1 association is located at 2.5 kpc toward $284^\circ < l < 288^\circ$, $-2.2^\circ < b < 0.9^\circ$ and has an average radial velocity of −5 km/ (see Melnik & Dambis [2009]). In their revision of the list of Galactic OB associations (Melnik & Efremov [1995]) break down Car OB1 into five groups at distances between 2.2 and 2.8 kpc. Fig. 5.13 presents the HI velocity chanel image at $v = -5$ km/s and the distribution of HII toward Car OB1. Only stars intrinsically brighter than −3 mag with $uvby\beta$ distances available are shown. Different symbols are used to denote the apparent groups that could be separated based on our sample. The group marked with white dots (23 stars) is located at average coordinates $l = 287.56^\circ$, $b = -0.67^\circ$ in direction of the Car 1E group from the list of Melnik & Efremov [1995], in the vicinity of η Car. According to the distances obtained here, these stars are spread out between 2204 and 6404 pc, with an average of 3728 ± 956 pc. Another apparent concentration (small black plus-symbols, six stars) is found at $l = 287.01^\circ$, $b = -0.41^\circ$ and an average distance of 3308 ± 2090 pc. The significant spread in distance suggests that these are not physical groups. The third apparent grouping, marked with black dots (16 stars), is found at $l = 285.83^\circ$, $b = 0.071^\circ$ (this is Car 1B of Melnik & Efremov [1995]). These stars are well grouped at 2583 ± 70(s.e.) pc (see Kaltcheva & Scorcio [2010] for more details). It seems that these apparent groups are located along the edge of the Carina arm. The apparent field stars along the edge of the arm are marked with large star-symbols whereas the other field stars are marked with large circles.

This region has a complex structure and does not harbour just one stellar association. It is highly likely that some of the apparent concentrations represent parts of long segments of the Carina arm projected along the line of sight near the Carina tangent.

Mon OB2

In light of the growing importance of Northern Monoceros in the study of star formation, precise distance estimates to the apparent structures of young stars in the field are most important for a variety of reasons. Northern Monoceros is dominated by the Rosette Nebula, thought to be spatially correlated to the young open cluster NGC 2244 and the large Mon OB2 association (Ruprecht [1996]). Precise $uvby\beta$ stellar distances and reddening are derived for a sample of more than 200 O-B9 stars in a 12 × 12 deg^2

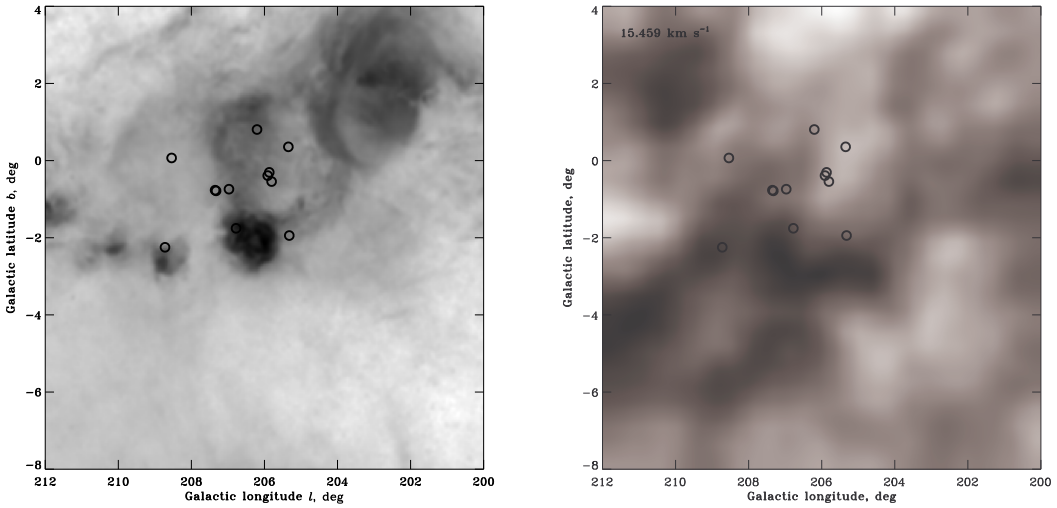

Figure 5.14: The field of Mon OB2. The stars of the group at 1.26 kpc are overploted on the distribution of the HII emission (left) and the HI velocity chanel image at $v = 15.5$ km/s (right).

field centered on NGC 2244 Kaltcheva et al. [2010]. According to this sample, the classical Mon OB2 association, previously thought to be at 1.6 kpc, is represented by a relatively compact group at 1.26 kpc in the vicinity of NGC 2244 and a layer of massive stars between 1.5 and 3 kpc spread across the entire field.

Fig. 5.14 presents the distribution of HII toward the group at 1.26 kpc and the HI velocity chanel image at 15.5 km/s (at which the lack of HI in the vicinity of this group is more obvious). New estimations of the temperature, brightness, spectral index, and distance to the Monoceros Loop SN remnant were recently reported by Borka Jovanovic et al. [2009]. They stressed the influence of molecular cloud on Monoceros SN remnant and calculated a distance of 1250 ± 190 pc to the Loop. This new distance estimate is in excellent agreement with the distance to the group at 1.26 kpc.

Concluding Remarks

As already mentioned, a better understanding of the phenomena associated with the interaction between young massive stars and their surrounding ISM in the fields of the Galactic OB associations should be possible once their structure is reliably established. A multi-wavelength approach analyzing the distribution of the massive OB stars, ionized and neutral material, and that of the interstellar dust would allow us to better understand the different components of the ISM and the interactions among them.

Acknowledgments

This work is supported by the National Science Foundation grant AST-0708950. N.K. acknowledges support from the SNC Endowed Professorship at the University of Wisconsin Oshkosh. V.G. acknowledges support by the Bulgarian National Science Research Fund grants DO 02-85/2008 and DO 02-362/2008. This research has made use of the SIMBAD database, operated at CDS, Strasbourg, France. We acknowledge the use of NASA's *SkyView* facility (http://skyview.gsfc.nasa.gov) located at NASA Goddard Space Flight Center McGlynn et al. [1998].

Bibliography

Balona, L. A. & Shobbrook, R. R. 1984, MNRAS, 210, 375
Blaauw, A. 1958, AJ, 63, 187
Borka Jovanović, V. & Urošević, D. 2009, AN, 330, 741
Cappa De Nicolau, C. E. & Olano, C. A. 1990, Rev. Mexicana Astron. Astrof., 21, 269
Crawford, D. L. 1978, AJ, 83, 48
Humphreys, R. M. 1978, AJSS, 38, 309

Finkbeiner, D. P. 2003, ApJS, 146, 407
Kalberla, P.M.W., Burton, W.B., Hartmann, D., Arnal, E.M., Bajaja, E., Morra, R., Poeppel, W.G.L. 2005, A&A, 440, 775
Kaltcheva, N. 2009, PASP, 121, 1045
Kaltcheva, N. & Golev, V. 2011, in preparation
Kaltcheva, N. & Hilditch, R. 2000, MNRAS, 312, 753
Kaltcheva, N., Kuchera, A., Hathaway, C. 2010, AN, 331, 384
Kaltcheva, N. & Knude, J., 1998, A&A, 337, 178
Kaltcheva, N. & Makarov, V. 2007, ApJ, 667L, 155
Kaltcheva, N. & Scorcio, M. 2010, A&A , 514, A59
Kilkenny, D. & Whittet, D. C. B. 1985, MNRAS, 216, 127
Melnik, A. M. & Dambis, A. K. 2009, MNRAS, 400, 518
Melnik, A. M. & Efremov, Yu. N. 1995, AstL, 21, 10
McGlynn, T., Scollick, K., White, N. 1998, in *New Horizons from Multi-Wavelength Sky Surveys*, Proc. of the 179th Symp. of the IAU, held in Baltimore, USA Aug 26-30, 1996, Kluwer Academic Publishers, edited by B. J. McLean, D. A. Golombek, J. J. E. Hayes, & H. E. Payne, p. 465
Ruprecht, J. 1966, Trans. IAU 12B, 350
Sharpless, S. 1959, ApJS, 4, 257
van Leeuwen, F. 2007, Hipparcos, the new reduction of the raw data (Dordrecht:Springer)

5.7 The Orbital Motion and Formation of Star Clusters in the Centre of the Galaxy

Andrea Stolte[1], M. Morris[2], A. Ghez[2], W. Clarkson[3], B. Hußmann[1], N. McCrady[4], J. R. Lu[5], and K. Matthews[6]

[1] Argelander Institut für Astronomie, Auf dem Hügel 71, 53121 Bonn, Germany
[2] Division of Astronomy and Astrophysics, UCLA, 430 Portola Plaza, Los Angeles, CA 90095-1547, USA
[3] Department of Astronomy, Indiana University, Bloomington, 727 East 3rd Street, Swain West 319, Bloomington, IN47405-7105, USA
[4] Department of Physics and Astronomy, University of Montana, 32 Campus Drive, Missoula, MT 59812, USA
[5] Astronomy Department, California Institute of Technology, 1200 E. California Blvd., MC 249-17 Pasadena, CA 91125, USA
[6] Caltech Optical Observatories, California Institute of Technology, MS 320-47, Pasadena, CA 91225, USA

Abstract

We have derived the Quintuplet cluster's orbital motion from three epochs of ground-based, diffraction-limited observations. The orbital velocity is higher than the expected circular velocity in the central molecular zone. The orbit of the cluster was integrated in the Galactic centre potential, and a possible location of the cluster origin is identified. The comparison with the Arches orbit suggests that massive star clusters form at the tangent point of the bar's minor axis. This is consistent with recent simulations of molecular material streaming into the inner Galaxy and fueling the central molecular zone due to the forces exerted by the bar potential.

Introduction

The Arches and Quintuplet clusters are young (2 – 4 Myr), massive ($\sim 10^4$ $M_\odot$) stellar clusters located at projected distances of 26 and 32 pc from the Galactic centre, respectively. Narrowband images conducted as part of the central molecular zone Paschen α survey (Wang et al. [2010], Dong et al. [2011]) reveal a bright ionisation rim surrounding the Quintuplet cluster. This cluster harbours a rich Wolf-Rayet popuplation, and is host to the Pistol star, which is argued to be one of the most massive stars in the Galaxy (Yungelson et al. [2008]). With their location in the inner Galaxy, however, the Arches and the Quintuplet cluster are exposed to the severe tidal field in the central region of the bulge, which contributes to their rapid dispersal, possibly on timescales as short as 10 – 20 Myr (e.g., Kim et al. [2000], Portegies Zwart et al. [2002]). These young, compact Galactic centre clusters are unique testbeds for cluster formation and evolution – and dissolution – in the central regions of spiral galaxies.

The orbital motion of the Quintuplet cluster

Ground-based adaptive optics systems provide astrometric measurements with milli-arcsecond precision. These diffraction-limited imaging observations can be used to obtain proper motion membership information in clusters out to distances of 8 kpc, and hence are capable to deliver a reliable membership criterion for star clusters residing near the Galactic centre. In addition, the orbital motions of these clusters can be probed in the case that the cluster motion is sufficiently distinct from the motion of the surrounding field population.

We have combined a first epoch of VLT/NAOS-CONICA images obtained in 2003 with two epochs of Keck/NIRC2 observations taken in 2008 and 2009. Stellar positions were derived using multiple-star PSF fitting with the crowded-field PSF photometry tool starfinder (Diolaiti et al. [2000]). The first two epochs were geometrically mapped onto the 2009 Keck/NIRC2 epoch as this epoch has the highest sensitivity and spatial resolution due to its excellent AO correction. A low-order polynomial is fitted as

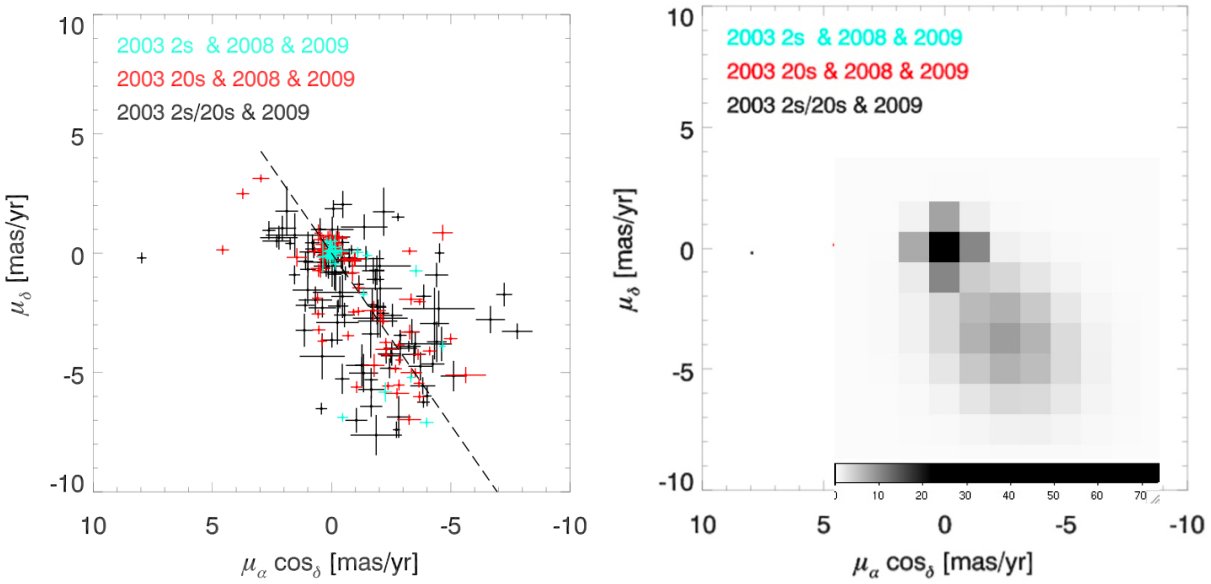

Figure 5.15: Proper motion diagram of sources in the Quintuplet field in the cluster reference frame (left panel). The dashed line depicts the orientation of the Galactic plane. Cluster member candidates cluster tightly around the origin, while field stars are predominantly moving along the Galactic plane. The right panel shows the density fit to the proper motion distribution. Cluster and field are depicted as spherical and ellipsoidal Gaussians, respectively.

the transformation matrix. By referencing all stars to the 2009 epoch, the proper motions are measured in the cluster reference frame. The mapping is carried out iteratively, starting from bright stars known to be cluster members, such that field star motions do not influence the transformation. After matching of all three epochs, the combined proper motion uncertainties are below 1 mas/yr for all but five sources, and typical uncertainties are in the range $0.2 < \sigma_{astrom} < 0.5$ mas/yr. Individual proper motions for each star can be obtained under the assumption of linear motion over the short time period of six years covered by the astrometric observations, which substantially reduces the proper motion uncertainties and allows for a cleaner separation between cluster and field stars. The corresponding proper motion diagram is shown in Fig. 5.15. Cluster member candidates are located around the origin in the cluster reference frame, while field stars are widely distributed. The direction of the Galactic plane is shown as the dashed line, and field star candidates are trailing the cluster parallel to the Galactic plane. Under the assumption of random motions in the inner Galactic bulge, the apparent asymmetric motion of field stars along the plane *in the cluster reference frame* provides evidence that the Quintuplet cluster is moving parallel to the Galactic plane with a velocity higher than the characteristic stellar velocity along this line of sight.

The difference between the tightly condensed cluster population in the proper motion plane and the field star motions spread along the Galactic plane allows us to derive the orbital motion of the Quintuplet cluster with respect to the field. We fit two 2-dimensional Gaussian distributions to the density map of the cluster and the field in the proper motion plane (Fig. 5.15, left panel). The distance between the two peaks provides an estimate of the cluster motion, $\mu_{clus} = 4.5 \pm 1.3$ mas/yr or 172 ± 50 km/s at an assumed distance of 8 kpc. The uncertainty is taken to be the size of the binning box used to obtain the number density map. When combined with the known radial velocity of 130 km/s (Figer et al. [1999]), the orbital motion of the Quintuplet cluster is derived to be $v_{3D} = 215 \pm 50$ km/s. This motion is larger than the typical motions of clouds on circular orbits in the central molecular zone, where radial maps suggest that motions of dense molecular clouds are limited to $v_{circ} \leq 120$ km/s (see, e.g., Dame et al. [2001]). Following the procedures in Stolte et al. [2008], we use the three measured velocity components of the Quintuplet to model the cluster orbit in the gravitational potential of the Galaxy (Fig. 5.16). The high cluster motion leads to non-circular, nested rosetta-like orbits. The peri-galacticon distance depends on the unconstrained present-day line-of-sight distance to the Quintuplet cluster. Despite the fact that the orbits of the Arches and Quintuplet clusters in this approximated inner-Galaxy potential depend sensitively on the exact direction of the three motion vectors, a certain area emerges where both clusters might have formed. In Fig. 5.16, which displays the orbits as viewed from above the Galactic plane, this area is located in the upper left quadrant, corresponding to the far side of the central molecular zone. These potential points of origin indicate that the clouds entering the central molecular zone have preferred entry points where they are rapidly converted into stars.

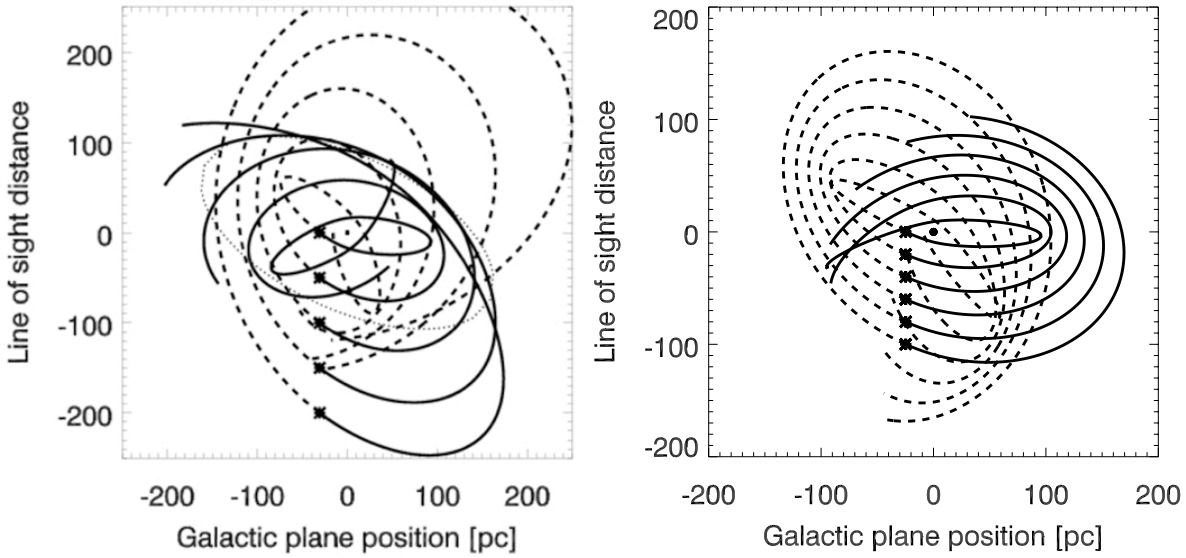

Figure 5.16: Orbital motion of the Quintuplet cluster as viewed from above the Galactic disc (left panel). The direction towards the Sun is at the bottom. The three velocity components and the cluster's current projected position are used as starting points from where the orbit is integrated forwards and backwards in time in the Galactic centre potential following the prescription in Stolte et al. [2008]. Comparison with the Arches orbital motion (right panel) indicates a likely origin of both clusters in the left quadrant behind the Galactic centre, as viewed from the Sun. This region is consistent with a formation locus of Galactic centre star clusters near the x1-x2 orbital transition.

Formation scenarios of Galactic centre (and other galaxies' centres) star clusters

In external galaxies, circumnuclear rings with young star clusters are found in numerous barred systems (Mazucca et al. [2008]). One particularly striking example is NGC 613, where a sequence of young star clusters with ages between 2 and 10 Myr is located in a well-defined circumnuclear ring (Böker et al. [2008]). This led the authors to introduce the "pearls on a string" scenario, where clusters emerge during collisions of infalling gas at the end-points of a possible inner bar. These exceptional locations, where gas from larger radii can spiral in to fuel a circumnuclear ring (the central molecular zone in the Galaxy), are pre-destined areas where collisions can lead to intense cluster formation. Such preferred "points of cluster origin", if they exist in the inner Milky Way, might explain the very similar orbits of the Arches and Quintuplet clusters.

Recently, N-body or sticky particle simulations including star formation and/or feedback effects (Kim et al. [2011], Rodriguez-Fernandez & Combes [2008], Namekata et al. [2008]), suggest that the required influx of molecular material can explain all the young star clusters presently observed in the central molecular zone. In addition, the simulations indicate highly efficient cluster formation at the transition point between the x1 and x2 orbits, which might correspond to the end point of an inner bar (Rodriguez-Fernandez & Combes [2008]). If these simulations allow for the collisional formation of massive clusters with non-circular orbital velocities, they would provide for the first self-consistent explanation of the origin of the Arches and Quintuplet clusters in the Galaxy's central molecular zone.

In this scenario, the Arches and Quintuplet clusters would form at the transition point where instreaming material from x1 orbits collides with central molecular zone clouds on x2 oribts. In a broader context, the simulations of Kim et al. [2011] additionally provide an explanation for the formation of the Red Supergiant clusters discussed by Maria Messineo during this meeting (see also Messineo et al. [2008], Figer et al. [2006]). The origin of these young, massive clusters might then be located at the end points of the major axis of the Galactic bar, while the nuclear clusters form at the end points of the minor axis, as depicted in Fig. 5.17. These modes of star formation suggest that the bar potential plays a major role in massive star cluster formation in the Milky Way, as is indeed observed in nearby extragalactic barred galaxies as well (Mazzuca et al. [2008], and references therein).

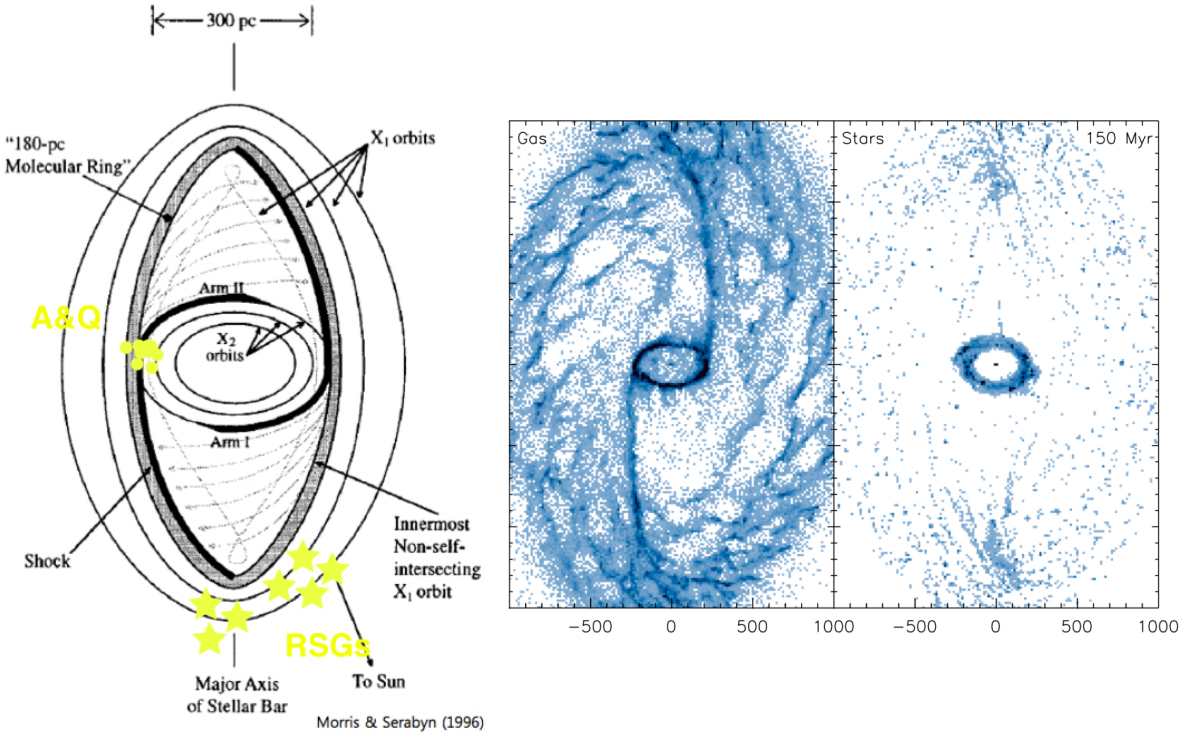

Figure 5.17: Sketch of the x1 and x2 orbital zones in the Galactic bar adopted from Morris & Serabyn [1996]. The orbital motions of the Quintuplet and Arches clusters are consistent with a formation locus near the tangent point where instreaming x1 clouds might collide with molecular material on x2 orbits forming the central molecular zone. In contrast to these innermost clusters, the red supergiant clusters are suggested to form at the end-point of the long axis of the bar in this scenario (see also Rodriguez-Fernandes & Combes [2008], Namekata et al. [2008], Kim et al. [2011]). A comparison of this scetch to the star formation simulations with feedback by Kim et al. [2011, right panels] is particularly striking, as the predicted locations of cluster formation from instreaming matieral match the observationally derived points of origin very well.

Acknowledgments

We thank the organisers for bringing together such an interesting group of people from various areas of cluster research, providing the pathway for exciting discussions. AS acknowledges support from the DFG Emmy Noether program that enables this research, and for UCLA's continuous support. We are grateful to the support teams on both the VLT and Keck telescopes, and to the Hawai'ian people for enabling observations from such an exceptional mountain.

Bibliography

Böker, T., Falc'on-Barroso, J., Schinnerer, E., et al. 2008, AJ, 135, 479
Dame, T. M., Hartmann, D., Thaddeus, P. 2001, ApJ, 547, 792
Diolaiti, E., Bendinelli, O., Bonaccini, D., et al. 2000, A&AS, 147, 335
Dong, H., Wang, Q. D., Cotera, A., et al. 2011, MNRAS, accepted, arXiv/1105.1703
Figer, D. F., McLean, I. S., Morris, M. 1999, ApJ, 514, 202
Figer, D. F., MacKenty, J. W., Roberto, M., et al. 2006, ApJ, 643, 1166
Kim, S. S., Figer, D. F., Lee, H. M., Morris, M. 2000, ApJ, 545, 301
Kim, S. S., Saitoh, T. R., Jeon, M., et al. 2011, ApJ *Letters*, 735, 11
Mazzuca, L. M., Knapen, J. H., Veilleux, S., Regan, M. W. 2008, ApJS, 174, 337
Messineo, M., Figer, D. F., Davies, B., et al. 2008, ApJ *Letters*, 683, 155
Morris, M. & Serabyn, E. 1996, ARA&A, 34, 645
Namekata, D., Habe, A., Matsui, H., Saitoh, T. 2009, ApJ, 691, 1525
Portegies Zwart, S. F., Makino, J., McMillan, S. L. W., Hut, P. 2002, ApJ, 565, 265

Rodriguez-Fernandez, N. J. & Combes, F. 2008, A&A, 489, 115
Stolte, A., Ghez, A. M., Morris, M., et al. 2008, ApJ, 675, 1278
Wang, Q. D., Dong, H., Cotera, A., et al. 2010, MNRAS, 402, 895
Yungelson, L. R., van den Heuvel, E. P. J., Vink, Jorick S., et al. 2008, A&A, 477,223

Chapter 6

Surveys Pre and Post Gaia

6.1 Spectroscopic and Photometric Surveys of the Milky Way and its Stellar Clusters in the Gaia Era

Sofia Feltzing[1]

[1] Lund Observatory, Department of Astronomy and Theoretical Physics, Box 43, SE-221 00 Lund, Sweden

Abstract

This contribution to the *Stellar Clusters & Associations: A RIA Workshop on Gaia* deals with surveys of stars, in particular spectroscopic surveys, with attention to their impact on cluster studies, and their connection with Gaia. I review some of the scientific reasons why we want large spectroscopic surveys, and what requirements these put on the instrumentation. Then I turn to a review of the current and future instrumentation that will enable us to complement Gaia's excellent distances and proper motions with the desired ground-based spectroscopy to obtain additional radial velocities and elemental abundances of high quality. This is a very fast moving area with several new surveys using existing and future multi-object spectrographs on 4- and 8-meter telescopes. As things change rapidly it is difficult to give adequate information on all these projects, but with the inclusion of links to the relevant websites the reader should be able to follow the latest developments as they unfold.

Surveying the Milky Way and its stellar components

In the past the Milky Way was surveyed to find our place in the Universe. Shapley [1918b,a] showed, using globular clusters, that the Sun's position in the Galaxy is not in any privileged central part but indeed quite far from the centre, towards the outer 1/3 of the stellar disk. Later studies focused on the oldest stars in order to figure out how old the Milky Way and its stars are. This enabled much work on the stellar populations in the Milky Way and provided constraints on theories of galaxy formation in general (e.g. Eggen et al. [1962]). A good overview to our understanding of the Milky Way through large surveys and to the future prospects at the time is provided in the proceedings of the Joint Discussion 13 at the 26th IAU General Assembly (Corbally et al. [2006]; in particular the contribution by Wyse [2006], see the footnote for where to access the articles)[1].

Today, we survey our Galaxy to find out how the Milky Way fits in the general framework of galaxy formation and evolution provided by ΛCDM (e.g. Springel et al. [2008, 2005]). Or rather, we wish to

[1]The table of content and all pdf-files are available at `http://sait.oat.ts.astro.it/MSAIt770406/index.html`

use the Milky Way as a testbed for such models. The examples of this approach are many. Interesting examples include House et al. [2011], Sales et al. [2009], and Abadi et al. [2003]. A striking example of the interplay between observations and theory is provided by the prediction that the number of, then, known dwarf spheroidal galaxies (dSph) around the Milky Way was at least an order of magnitude too low as compared with the then current predictions from the state-of-the-art ΛCDM modelling (Moore et al. [1999]). At the time, about ten dSph galaxies were known (Mateo [1998]). This lead to much work studying if, for example, star formation could be inhibited in small dark matter haloes, thus providing a solution such that they would never start shining with stellar light. The Sloan Digital Sky Survey (SDSS, Adelman-McCarthy et al. [2006]) later provided a deep, multi-band, photometric survey of a significant portion of the sky. Vasily Belokurov and colleagues analyzed this material and quickly found several more dSph, which were also confirmed spectroscopically, i.e., that the systems have a common radial velocity and are not just asterisms on the sky (Belokurov et al. [2007, 2009]). A particularly difficult example is given by the Hercules dSph (**?**Adén et al. [2009]). An extrapolation from these, and subsequent investigations, points to the possibility that the Milky Way might actually be surrounded by almost as many dSph as predicted by ΛCDM. However, along the way many important lessons about galaxy formation and evolution have been learnt. Grebel [2011] provides a concise update on the theoretical as well as the observational studies tackling this problem.

Freeman & Bland-Hawthorn [2002] reviewed the prospects of identifying, with the help of *chemical tagging*, individual regions of star formation in the Galaxy. The chemical tagging concept builds on the understanding that all stars form in clusters and that each cluster should have a unique signature, not only in age but also in elemental abundances. The ability to identify unique groups of stars in this way is challenging – requiring very large spectroscopic surveys – and has lead to the proposal that underpins the HERMES project. We will return to the topic of chemical tagging and elemental abundances in next Sections.

Stellar clusters

Stellar clusters are an intrinsic part of any galaxy and provide vital clues to as diverse subjects as star-formation, stellar evolution, nucleosynthesis, understanding dynamical interactions between stars, and galactic formation and evolution. In many galaxies they are the most luminous individual objects that we can study also at very large distances. They can be used to constrain the formation histories of galaxies and put constraints on models of galaxy formation and evolution (Brodie & Strader [2006]; Harris [1991]). In the Milky Way, the two major classes of stellar clusters, open and globular, span a large range of ages and metallicities thus having the potential to play the role to constrain the formation and evolution of our Galaxy. The globular cluster population in the Milky Way contains only old clusters (Marín-Franch et al. [2009]; De Angeli et al. [2005]; Rosenberg et al. [1999]). They divide into mainly two groups as concerns ages – the largest subset, containing only old clusters with very little spread in ages and a younger subset of clusters (a couple of billion years difference at the most) which are, based on their position within the Galaxy and chemical and kinematic properties, interpreted as being accreted from other systems, such as the Sagittarius dSph galaxy (Law & Majewski [2010]). In other galaxies, e.g., the Large Magellanic Cloud, there are both old and young globulars (e.g. Colucci et al. [2011]). The open cluster population in the Milky Way mainly span younger ages, although there are open clusters as old as 10 Gyr (see Dias et al. [2002] with its associated data base[2]). The globular clusters have a broad range of metallicities with two distinct peaks (something which is common to many galaxies, Harris et al. [2006]), but they do not cover very metal-poor stars (below –2.2 dex) nor stars with solar metallicities or higher (Zinn [1985]; Harris [2010])[3]. The open clusters span metallicities higher than about −0.5 dex (e.g., the compilation in Magrini et al. [2009], and the work by Friel et al. [2010]).

The different ranges in metallicities and ages for the two cluster populations is also reflected in (and connected with?) their spatial distributions. The globular clusters in the Milky Way mainly reside in a roughly spherical distribution. Kinman [1959] indicated that the globular cluster system in the Milky Way is composed of two kinematically distinct sub-groups with differing metallicities. The study by Zinn [1985] then later clearly showed that the more metal-rich globulars, [Fe/H] > –0.8, are centrally concentrated, whilst the less metal-rich globulars (in fact the majority of all the globulars in the Milky Way) form a

[2]The data base is available, together with links to many other open cluster catalogues, at `http://www.astro.iag.usp.br/~wilton/`

[3]Note that this is a new update on the *Catalog of Milky Way Globular Clusters* by W.E. Harris. The full data base can be found at `http://physwww.mcmaster.ca/~harris/Databases.html`

much more extended, spherical system. These metal-poor globulars are thought to be associated with the stellar halo, although some of them are likely accreted from other, smaller, galaxies. Palomar 12 is one such example (Dinescu et al. [2000]; Law & Majewski [2010]). Forbes & Bridges [2010] discuss additional associations of globulars with dSph galaxies. For the metal-rich globulars sub-divisions into bulge and disk clusters have been discussed (see examples in, e.g., Minniti [1995]; Zinn [1996]; Harris [1998]) but such divisions remain an open subject. For example, Bica et al. [2006] found that the metal-rich globulars have a spherical distribution, whilst Dinescu et al. [2003] found that at least one of them (NGC 6528) is, based on its kinematics, associated with the bar. This points to the necessity of getting more and better kinematic data also for globulars in order to understand the globular cluster system. In a series of important papers, Dana Casetti-Dinescu and collaborators (Casetti-Dinescu et al. [2010], and references therein) have painstakingly derived the proper motions and space velocities for by now 34 globulars using the Southern Proper Motion Program data, steadily improving our understanding of the dynamics of the system. Very few globulars appear to be genuinely associated with the stellar disks. In fact most globular clusters are too metal-poor to be associated with the disks. The so far only, confirmed, disk globular is NGC 5927 for which the full 3D kinematic information shows it to have an essentially disky orbit (Casetti-Dinescu et al. [2007]). The cluster has a metallicity, [Fe/H] = –0.37, as well as elemental abundances, e.g., Ca is enhanced relative to Fe, that naturally associate it with the thick disk (Simmerer et al., a study of 7 HB stars in the cluster, to be submitted).

Studies of elemental abundances in globular clusters is a large subject that was recently reviewed in detail by Gratton et al. [2004]. The globulars do in general follow the abundance trends of the major stellar populations in the Milky Way, however, there is increasing evidence that there are aspects of "clusterness" that might set their stars apart from the stars normally observed in the field, e.g., they show Na-O anti-correlations which are not seen in the field stars (see, e.g., Carretta et al. [2009a,b]; Marino et al. [2011]) and more and more clusters are shown to have multiple stellar populations also based on their colour-magnitude diagrams (e.g. Piotto et al. [2007]). The discovery of which has resulted in much theoretical work and deepening our understanding of star formation and evolution (see, e.g., D'Ercole et al. [2011]). A good example of how an existing survey can be used to tackle a new problem is given by Lardo et al. [2011] who used publicly available photometry from SDSS to trace the two populations (UV-red and UV-blue) in globular clusters (cores excluded) and find that radial variations in the populations are present. This is feasible as the survey covers the cluster outskirts very well, till they dissolve into the field population, something that is not always feasible with dedicated programs.

Open clusters is a much larger subject than globular clusters. In particular since the clusters include young and heavy stars. Thus rare evolutionary stages can be studied in detail. The reader is directed to other contributions to this workshop for more details on the massive and young stars. Spectroscopic surveys will naturally have a large impact on the study of those rare evolutionary stages, however, I will limit myself to aspects of the open clusters that mainly concerns them as birthplaces of field stars, tracers of Galactic chemical evolution, structure, and dynamics.

In total we know of more than 1800 open clusters detected in the visual (Dias et al. [2002], and subsequent updates). For those about 50% have an age estimate (Moitinho [2010]). In addition there are about 700 clusters detected in the near infra-red. For the about 200 open clusters with abundance estimates the most striking feature is probably the Galactic radial gradient in metallicity that they trace. Currently, very few other tracers are able to deliver well determined metallicities combined with good distance estimates (for the open clusters distances come from isochrone fitting). It appears that the disk as traced by the open clusters shows a steadily declining [Fe/H] as a function of galacto-centric distance, until it reaches a floor at about 10 – 12 kpc (Friel et al. [2010]; Bragaglia [2010]). Similar observations are not readily available for large data-sets in the field. A recent example of a small study of field giants shows, however, the same floor in metallicity (Bensby et al. [2011]). In addition, the abundance trends found in the open cluster population appear to follow the abundances found in the thin disk very well, as shown in Friel et al. [2010] where they compare the [O/Fe] as a function of [Fe/H] with the data for kinematically selected thin and thick disk stars (Bensby et al. [2004]).

Over the last few decades several studies and small and large surveys of both globular and open clusters in the Milky Way have been undertaken. In spite of all these efforts, there is still scope for very large and comprehensive surveys of stellar clusters. For example, only about 10% of the known $\sim$ 1800 open clusters have metallicity estimates available in the literature (Moitinho [2010]). While about half of them have distances, ages, and reddening estimated. For the globular clusters the situation is somewhat more robust with 1/3 of the >150 known globulars having metallicity estimates. Large area coverage not only in photometry but also in spectroscopy is clearly desirable.

Clusters and the underlying field populations

While the globular clusters appear to essentially trace the spheroidal components of the Milky Way, the Galactic bulge and halo, the open clusters reside in the disk. Essentially all open clusters have $|b| < 20°$ (see, e.g., Figure 1 in Moitinho [2010]). Thus the globulars trace the older parts, both the metal-poor halo and the metal-rich bulge, of the Milky Way, whilst the open clusters trace the younger stellar disk. The question then arises – Are these just "spatial coincidences" or do the cluster systems truly trace the underlying field population and can they tell us something about how those stellar components of the Milky Way formed and evolved?

First, it might be interesting to consider if the populations of stellar clusters as we know them today are representative samplings of the underlying, full cluster populations. The answer to this is related to how we discover stellar clusters. For example, it is much easier to find a stellar system in parts of the sky that are less crowded and/or have low extinction. The stellar disk has, especially at the very lowest latitudes, a very large extinction, reaching many magnitudes towards the central parts of the Galaxy. How the presence of extinction influences our ability to find and study open clusters in the disk is illustrated in Fig. 2 in Moitinho [2010] which shows how the known open clusters nicely traces the low extinction areas in the first quadrant. Photometric searches in near infra-red surveys, such as 2MASS, have revealed many clusters hidden to surveys in the optical (e.g. Froebrich et al. [2007]). The need for spectroscopic follow-up to confirm clusters against asterisms is further discussed in Bica & Bonatto [2011]. The photometric near infra-red VVV survey (see page 316) has already discovered 96 new infra-red open clusters and stellar groups. These cluster candidates are mainly faint and compact and are younger than 5 Myr (Borissova et al. [2011]). The high extinction of these new clusters, up to 20 mag in V, show how important it is to have near infra-red surveys to fully explore the cluster population that resides in the plane. In addition, for open clusters there is a clear tendency that more detailed studies have concentrated on the brighter or more well-populated clusters where the colour-magnitude diagrams are better populated (Moitinho [2010]). In summary, we have only begun to scrape the surface of the properties of the open cluster system. Nevertheless, the open clusters, which clearly are currently forming within the stellar disk, are more likely directly related to the field population as such than the globulars are. It is worth pointing out that also globular clusters are found in the near infra-red surveys (e.g. Bonatto & Bica [2008]). It will be interesting to see if the gap in, e.g., age and mass between the two sets of clusters will diminish or remain thanks to the new clusters found.

As discussed earlier, some globular clusters are likely accreted from other galaxies and are thus fossil records of other stellar populations than those in the Milky Way. It is in this context that good elemental abundances become interesting. We expect the abundance trends or patterns to be different for different systems (Tolstoy et al. [2009]). This has, for example, been used in a wide range of studies of the Sagittarius dSph, its associated stellar clusters, and streams to pin down their common origin (e.g. Cohen [2004]; Sbordone et al. [2005, 2007]; Monaco et al. [2007]; Mottini & Wallerstein [2008]).

Stars form in clusters of varying sizes. Lighter clusters are anticipated to dissolve into the surrounding field on a short timescale. Olin Eggen was perhaps the first to investigate the so called moving groups (see, e.g., Eggen [1996, 1966]). He identified a number of such groups based on their common space motions. Improvement in data, in particular the advent of the Hipparcos catalogue (Perryman & ESA [1997]) which enabled the calculation of reliable space velocities, has re-ignited the interest in this field. A number of moving groups have been re-assessed and several new ones have been found (examples include Klement [2010]; Bobylev et al. [2010]; Famaey et al. [2007]; Arifyanto & Fuchs [2006]; Barrado y Navascues [1998]). However, dynamical investigations indicate that some of the moving groups are kinematic features rather than dissolved stellar clusters (Dehnen [2000]). If we assume that the stars were actually born together then they should not only have a common age but also share the abundance pattern. Thus spectroscopic abundance analysis to obtain elemental abundances is necessary to check if it is a cluster or a dynamical feature. De Silva et al. [2007] showed that HR 1614 is indeed a dissolved cluster with the stars sharing a common abundance pattern. The Hercules stream on the other hand was shown to just sample both thin as well as the thick disk abundances and ages, with a rather broad distribution in [Fe/H] proving its origin to be, most likely, the local dynamical effects of the bar (Bensby et al. [2007]). The prospects of Gaia to improve our understanding of the stirring by the bar and spiral arms, and the connection to moving groups and dissolving stellar clusters in terms of Galactic evolution is further discussed in, e.g., Antoja et al. [2011] and Bovy [2010].

Also globular clusters lose stars which populate the field. Prominent streams have been detected, e.g., for Palomar 14 and 5 (Sollima et al. [2011]; Odenkirchen et al. [2001], respectively).

Surveys to complement and enhance Gaia

Gaia[4] will observe a billion objects down to $G \simeq 20$[5]. Gaia will, apart from parallaxes and proper motions, provide photometric information for all objects enabling astrophysical classification (e.g., star or quasar) and the determination of physical variables (e.g., effective temperatures, photometric redshift). For the 150 million stars brighter than $G \simeq 16$ the on-board spectroscopic instrument will in addition provide radial velocities. For even brighter stars, $G \simeq 12$ which corresponds to about 5 million stars, the spectrograph will in addition give interstellar reddening, atmospheric parameters, and rotational velocities. It will provide elemental abundances for tho two billion brightest stars ($G \simeq 11$). This leaves almost 90% of the stars observed by Gaia without radial velocity estimates and even more stars without any additional astrophysical information. Such information can be obtained from ground-based observations using efficient, multi-fibre spectrographs on 4- and 8-m class telescopes.

That Gaia needs to be complemented with ground-based observations has long been recognized. For example the ESA-ESO Working group on galactic populations, chemistry and dynamics set out the challenges and priorities already in their report 2008 (Turon et al. [2008b,a]), where they especially recognized the importance of powerful multi-object spectrographs with high multiplex. ASTRONET's[6] consultations reach the same conclusions and their report concluded: "It is crucial to supplement the Gaia data-set with dedicated ground-based spectroscopic programmes, in order to obtain the radial velocity and detailed chemical abundances for fainter stars."

Depending on what scientific questions are being asked the requirements on the derived abundances will differ. If for example we want to figure out which clusters belong to the Sagittarius dSph galaxy we may only need an internal precision of about 0.1 – 0.2 deg, while if we want to identify individual stars that belong to a dispersed stellar cluster we may need an internal precision in our measurements of about 0.05 deg or less. The latter can readily be referred to as the chemical tagging suggested by Freeman & Bland-Hawthorn [2002] while the former is better referred to as a chemical labelling, a term introduced by Vanessa Hill. It is important to make these distinctions because what you can learn from the various types of measurements differs significantly and has a straightforward, direct impact on the design of stellar spectroscopic surveys. Very high precision within a study is often reached by studying stars that in all respects are very similar in their stellar parameters and only differ in age and elemental abundances. Selecting only similar types of stars for the survey is a technique that has been successfully employed many times. Good examples include Edvardsson et al. [1993], Fuhrmann [2011], Bensby et al. [2004]. Recently, the same methodology has been used to identify solar twins (Meléndez et al. [2010]).

A summary of the necessary requirements on the equipment, based on actual science cases, was set out by a working group inside GREAT-ESF[7]. In the resulting document[8] we concluded that the best synergies with the on-board instrumentation on Gaia would be provided with the following three broad sets of instruments:

1. Low resolution spectroscopy for completion of the $6D$ phase space information for stars with $16 < V < 20$.
2. $R = 20000$ spectroscopy of metal-poor disk and halo stars, giants as well as dwarfs, and stars in nearby dwarf galaxies. This mode will enable observations of stars at very large distances (4-m class telescopes).
3. $R = 40000 - 60000$ multi-fibre and perhaps single slit spectroscopy of selected populations of metal-rich stars, e.g. disk and (outer) bulge (4- and 8-m class telescopes).

This is a very exciting time when some of these thoughts are put into practice through a number of efforts. Below, some of the most relevant projects are discussed.

[4]Gaia's science performance is available at `http://www.rssd.esa.int/index.php?project=GAIA&page=Science_Performance`. The numbers on these web pages are predicted to be robust until the mission flies, and no further updates will be given.

[5]Gaia magnitudes are in the white-light G-band which covers $\sim 330 - 1050$ nm.

[6]ASTRONET was created by a group of European funding agencies in order to establish a long-term roadmap for European astronomy. The report *Science Vision for European astronomy* is available at `http://www.astronet-eu.org/-Science-Vision-`.

[7]GREAT-ESF is the Gaia Research for European Astronomy Training. Funding from ESF provides for meetings and visits. Its web-site is `http://www.ast.cam.ac.uk/ioa/GREAT/` and its wiki is at `http://camd08.ast.cam.ac.uk/Greatwiki/GreatHome`

[8]The latest version,April 2010, is available here

The Gaia-ESO Survey

The Gaia-ESO Survey is the result of the community's response to ESO's call for public spectroscopic surveys. The final proposal was for 3000 hr on FLAMES-UVES on VLT/UT2 to obtain radial velocities and elemental abundances for $> 10^5$ stars and > 100 stellar clusters covering all the major stellar components of the Milky Way. It has a fully stand-alone science case and will provide the first homogeneous overview of the distributions of kinematics and elemental abundances in the Milky Way. It is also designed to, later, take advantage of the Gaia astrometry.

The FLAMES-UVES spectrographs provide a unique opportunity to probe the Galactic components both locally in very high detail as well as on a larger scale with still very good elemental abundances. The FLAMES spectra will enable the determination of individual elemental abundances in each star, yield precise radial velocities for a $4D$ kinematic phase-space, and map both kinematic gradients as well as abundance – phase-space structure throughout the Galaxy. The high-resolution fibres in the UVES spectrograph will be used to obtain high signal-to-noise spectra for a few thousand dwarf stars within 2 kpc providing a complete census of the distribution functions for the elemental abundances present in the old disk.

The Gaia-ESO Survey will be the first homogeneous spectroscopic survey of a statistically significant sample of stellar clusters. Encompassing clusters with ages from 10^6 up to 10^9 yr, in different environments, with different richnesses and cluster masses, and different galacto-centric positions. For each cluster the survey will provide a "complete" stellar sample based on detailed chemistry as well precise kinematics. In addition it will also provide measures of stellar activity, quantitative mass-loss estimates for early-type stars, and refined memberships for cluster members.

An important aspect of this survey is the homogeneous abundance scale for stellar cluster and field stars. Thus enabling a truly differential study between the field the clusters are embedded in and the clusters themselves. Combined with the accurate velocity determinations for the stellar clusters this will lead to a deeper understanding of how the field is populated with stars from dispersing stellar clusters.

The Gaia-ESO Survey includes more than 300 astronomers across Europe and is PIed by Gerry Gilmore and Sofia Randich. The survey will have its own dedicated web-space at `www.gaia-eso.eu`.

Selected instruments and their associated surveys

Currently, a number of multi-fibre spectrographs are either being commissioned, being built, or are undergoing studies. All of these are of direct relevance to the Gaia mission. In addition, many photometric surveys provide valuable data that will enhance the Gaia results. For instance, SkyMapper [9] has a filter system that is designed to be sensitive to stellar metallicity and gravity. This will complement the Gaia data with photometric metallicities for all stars too faint to get good metallicities from the on-board instruments. The SkyMapper filters roughly follow the Strömgren photometric system for which good metallicities can be derived for a range of stellar evolutionary stages (see, e.g., Adén et al. submitted; Casagrande et al. [2011]; Adén et al. [2011]; Árnadóttir et al. [2010]). We may also foresee important complementarity to the Gaia from the photometric VISTA surveys, already operational and including the VISTA Variables in The Via Lactea (VVV) [10] multi-epoch public survey which will build a high resolution $3D$ map of the Galactic bulge including stellar variability (Minniti et al. [2010]). The Galactic bulge is notoriously difficult to study due to the high and variable reddening. Thus the VVV will be a necessary complement to Gaia, which is not optimized for studies in such crowded regions with very high extinction. The variability studies will also add an interesting time dimension, enabling asteroseismology to be carried out on red giants. With such data also red giant branch stars can have their ages determined, something that is impossible without the very accurate masses provided by asteroseismology. Of the current surveys the Sloan Digital Sky Survey (SDSS) is probably the one with the largest impact so far. The combination of its large photometric data base and basic stellar parameters derived from low-resolution spectra (see, e.g., Lee et al. [2011, 2008]) with the Gaia parallaxes and proper motions will very quickly result in new insights into the formation and evolution of the Milky Way. Other photometric surveys of interest includes Pan-STARSS[11] and Large Synoptic Survey Telescope (LSST, Ivezic et al. [2008]). LSST can be thought of as a deep extension Gaia. Gaia's error in proper motion at $r \sim 19$ is 0.1 mas/yr. This is LSST's smallest error and it performs to the same precision down to about $r = 21$ (see further discussions

[9] More about the project, including the filter curves, can be found at http://msowww.anu.edu.au/skymapper/

[10] The survey wiki is available at `http://mwm.astro.puc.cl/mw/index.php/Main_Page`

[11] More information as its surveys progress can be found at `http://pan-starrs.ifa.hawaii.edu/public/`

on the synergy between Gaia and LSST in, e.g., Jurić & Ivezić [2011]).

RAVE (the Radial Velocity Experiment) is an on-going spectroscopic survey obtaining radial velocities with an accuracy of about 2 km/s for up to a million stars. The spectra cover, as for Gaia, the Ca II triplet region. Elemental abundances for the RAVE stars have been derived from these as well as from follow-up spectra (e.g. Ruchti et al. [2010]; Fulbright et al. [2010]). Other recent, interesting results, showing the value of large, comprehensive spectroscopic data-sets, concern, e.g., the detection of young, moving groups (Kiss et al. [2011]). Further examples can be found in the publication lists and news items on their web page[12].

APOGEE is part of SDSS-III[13], which also includes the Baryon Oscillation Spectroscopic Survey (BOSS) as well as the MARVELS search for exo-planets, and the Sloan Extension for Galactic Understanding and Exploration 2 (SEGUE-2). The survey starts 2011. The spectrograph has 300 fibres, a wavelength coverage of $1.52 - 1.69$ μm, and a resolution of about 20 000. Over a period of four years it will obtain spectra (S/N=100) for 100 000 red giant stars down to $H = 13.5$ selected from 2MASS. From these spectra abundances for more than 15 elements will be derived as well as velocities with errors on the order of 0.5 km/s. The survey will observe around 200 stellar clusters, including 17 calibrating cluster. Of the calibrating clusters 12 are open clusters and 5 globular clusters (Frinchaboy et al. [2010]). APOGEE is planning to work together with CoRoT and Kepler (KASC) to combine the good mass estimates for red giant branch stars provided by the space missions from asteroseismology with the detailed elemental abundances from APOGEE. The accuracy of the mass estimate is improved by the good abundance determinations. Combined, they will yield reliable ages for stars on the red giant branch. A task that otherwise is virtually impossible due to the very closely packed isochrones in this evolutionary phase.

HERMES is a multi-fibre spectrograph to operate on the 3.9 m Anglo-Australian telescope (AAT). The instrument will use the existing 2dF optical fibre positioner to place the 400 fibres over the two-degree field of view. The Galactic Archeology with HERMES (GALAH [14]) project starts in 2013. Observations are carried out in four wavelength ranges in the visible covering 25 different species, including all the major nucleosynthetic channels. The resolution is relatively high at 30 000 with an option for even higher resolutions. The survey is limited to stars brighter than V=14. Even so, it will provide a very important first "all-sky" complement to Gaia delivering high quality elemental abundances for almost a million stars without elemental abundances directly measured using the Gaia-spectra. GALAH will use open and globular clusters for calibrating purposes as well as some very metal-poor stars to provide calibrations below the canonical –2.2 deg, where the globulars stop.

4MOST is a proposed multi-object fibre spectrograph with a very high multi-plex to go on one of ESO's 4-meter class telescope. The object is to provide Gaia and *eROSITA* with the necessary ground-based spectroscopy. The baseline is for a 1500 fibres with 3 deg^2 field-of-view with a goal of 3000 fibres over a 5 deg^2 field-of-view. The spectrograph has a low resolution mode for obtaining radial velocities and rough stellar parameters and a high resolution mode for chemical labelling. Examples of the Milky Way science that will be done with 4MOST include detailed studies of moving groups, dynamical structures as well as dissolving clusters, out to about 10 kpc. Hipparcos data allows us to study these features out to about 200 pc and does not allow for strong constraints on the bar and spiral arms (Antoja et al. [2011]; Minchev et al. [2010]). Its high-resolution survey will obtain chemo-dynamical data for more than 10^6 stars which allows, e.g., for studies of radial abundance gradient, i.e. the build up of the stellar disk, radial migration, formation of the thick disk etc. All open clusters will be thoroughly covered and the examples given above will allow for an even deeper understanding of the connection between the field and the clusters. A sub-survey aims at looking for truly large samples of the most metal-poor stars known. The instrument is undergoing a detailed phase A study and is PIed by Roelof de Jong (AIP)[15].

[12] `http://www.rave-survey.aip.de/rave/`

[13] `http://www.sdss3.org/` and `http://www.sdss3.org/surveys/apogee.php`

[14] `http://www.aao.gov.au/HERMES/GALAH/Home.html`. A useful presentation is also available at `http://www.aao.gov.au/HERMES/ScienceWorkshop/Talks/gds.pdf`.

[15] A presentation of the many science goals and the various design concepts was given at the GREAT-ESF meeting in Brussels 2011. It is available here.

MOONS is a proposed multi-fibre spectrograph operating in the near infra-red on the VLT employing 500 fibres over a field of view of 500 arcmin^2. The science goals include Gaia follow-up and several extra-galactic science cases. From the point of view of Galactic Archeology and Gaia its major advantage over many other instruments is the combination of observations in the near infra-red with an 8-meter telescope. Thus it will provide a necessary complement to, e.g., Gaia's radial velocities in the inner disk and Galactic bulge region. MOONS is also the ideal instrument to do spectroscopic follow-up and confirmation of cluster candidates found by photometric surveys in the near infra-red, as exemplified by the new results from the VVV survey (Borissova et al. [2011]). The instrument is undergoing a detailed phase A study and is PI:ed by Michele Cirasuolo (Edinburgh).

WEAVE is a proposed multi-fibre spectrograph for the 4 m William Herschel Telescope on La Palma. The design includes about 1000 fibres within a 2° field of view at the lower resolution of 5000 to, from the point of view of Gaia follow-up, provide radial velocities with an accuracy of less than 5 km/s for stars with $17 < V < 20$ and a high-resolution mode with R=20 000 for abundance determinations for stars (Balcells et al. [2010])[16]. The instrument would, e.g., be ideal to characterize halo streams through chemical labelling, where a relatively low surface density maps well to the field of view and fibre density.

Guoshoujing Telescope (formerly LAMOST[17]) has a 5 deg field of view and 4000 optical fibres. It is currently working in a low resolution mode but updates to a higher resolution are foreseen. It covers the wavelength regions of 370 – 590 nm and 570 – 900 nm. The Guoshoujing Telescope telescope has its own, proposed, open cluster survey, LOCS (Chen et al. [2009]), to, e.g., look at abundance gradients in the Galactic disk.

Concluding remarks

Although it is reasonably feasible to compare the major properties of a Milky Way galaxy formed in a ΛCDM simulation with the overall results from current photometric and spectroscopic surveys e.g., SDSS, SEGUE, RAVE) it is far from straightforward to constrain the models with the available data, mainly for two reasons: 1) the resolution in the models is too low to allow the investigation of the small scale features that we actually see in a real galaxy, 2) the selection of targets in the observational studies is either not well understood/documented or not optimized for the particular question of interest. Future surveys, especially the massive spectroscopic surveys operating after Gaia will be able to have very good selection criteria combined with almost exhaustive coverage of a given stellar population, hence enabling a more detailed comparison with models.

The several examples of past studies of the Milky Way and its stellar components given in this review show the need for large spectroscopic surveys to enable a full disentangling of the formation processes involved in shaping our Galaxy. Indeed, with the combination of Gaia's distances and proper motion and a ground based massive follow-up providing the $6D$ phase-space as well as the multi-dimensional abundance and age space we will finally be able to start testing the models for real (compare, e.g., the proposed tests in Sales et al. [2009] which are only feasible with this new data). In addition, prepare to find the unexpected. This means, be ambitious also when it comes to the elemental abundances and aim for abundance errors smaller than 0.05 deg (internally) in order to find and tag also the small building blocks of our Galaxy, i.e. the open clusters.

Acknowledgments

I would like to thank the organizers of the excellent workshop "Stellar Clusters & Associations: A RIA Workshop on Gaia" for a very nice meeting and their generous hospitality during the conference.

Bibliography

Abadi, M. G., Navarro, J. F., Steinmetz, M., & Eke, V. R. 2003, ApJ, 597, 21

[16]The project's web page is at `http://www.ing.iac.es/weave/`

[17]Their official web site is at `http://www.lamost.org/website/en`

Adelman-McCarthy, J. K., Agüeros, M. A., Allam, S. S., et al. 2006, ApJS, 162, 38
Adén, D., Eriksson, K., Feltzing, S., et al. 2011, A&A, 525, A153
Adén, D., Feltzing, S., Koch, A., et al. 2009, A&A, 506, 1147
Antoja, T., Figueras, F., Romero-Gómez, M., et al. 2011, ArXiv:1106.1170
Arifyanto, M. I. & Fuchs, B. 2006, A&A, 449, 533
Árnadóttir, A. S., Feltzing, S., & Lundström, I. 2010, A&A, 521, A40
Balcells, M., Benn, C. R., Carter, D., et al. 2010, in Society of Photo-Optical Instrumentation Engineers (SPIE) Conference Series, arXiv:1008.0600, Vol. 7735
Barrado y Navascues, D. 1998, A&A, 339, 831
Belokurov, V., Walker, M. G., Evans, N. W., et al. 2009, MNRAS, 397, 1748
Belokurov, V., Zucker, D. B., Evans, N. W., et al. 2007, ApJ, 654, 897
Bensby, T., Alves-Brito, A., Oey, M. S., Yong, D., & Meléndez, J. 2011, ApJ Lett., 735, L46
Bensby, T., Feltzing, S., & Lundström, I. 2004, A&A, 415, 155
Bensby, T., Oey, M. S., Feltzing, S., & Gustafsson, B. 2007, ApJ Lett., 655, L89
Bica, E. & Bonatto, C. 2011, A&A, 530, A32
Bica, E., Bonatto, C., Barbuy, B., & Ortolani, S. 2006, A&A, 450, 105
Bobylev, V. V., Bajkova, A. T., & Mylläri, A. A. 2010, Astronomy Letters, 36, 27
Bonatto, C. & Bica, E. 2008, A&A, 479, 741
Borissova, J., Bonatto, C., Kurtev, R., et al. 2011, ArXiv:1106.3045
Bovy, J. 2010, ApJ, 725, 1676
Bragaglia, A. 2010, in SF2A-2010: Proceedings of the Annual meeting of the French Society of Astronomy and Astrophysics, ed. S. Boissier, M. Heydari-Malayeri, R. Samadi, & D. Valls-Gabaud , 335
Brodie, J. P. & Strader, J. 2006, ARA&A, 44, 193
Carretta, E., Bragaglia, A., Gratton, R., & Lucatello, S. 2009a, A&A, 505, 139
Carretta, E., Bragaglia, A., Gratton, R. G., et al. 2009b, A&A, 505, 117
Casagrande, L., Schönrich, R., Asplund, M., et al. 2011, A&A, 530, A138
Casetti-Dinescu, D. I., Girard, T. M., Herrera, D., et al. 2007, AJ, 134, 195
Casetti-Dinescu, D. I., Girard, T. M., Korchagin, V. I., van Altena, W. F., & López, C. E. 2010, AJ, 140, 1282
Chen, L., Gao, X. H., & Zhao, J. L. 2009, in IAU Symposium: Open clusters and the radial abundance gradient of Galactic disc, ed. J. Andersen, J. Bland-Hawthorn, & B. Nordström, Vol. 254, 15
Cohen, J. G. 2004, AJ, 127, 1545
Colucci, J. E., Bernstein, R. A., Cameron, S. A., & McWilliam, A. 2011, ApJ, 735, 55
Corbally, C., Bailer-Jones, C., Giridhar, S., & Lloyd Evans, T. 2006, Mem. Soc. Astron. Ital., 77, 1026
De Angeli, F., Piotto, G., Cassisi, S., et al. 2005, AJ, 130, 116
De Silva, G. M., Freeman, K. C., Bland-Hawthorn, J., Asplund, M., & Bessell, M. S. 2007, AJ, 133, 694
Dehnen, W. 2000, AJ, 119, 800
D'Ercole, A., D'Antona, F., & Vesperini, E. 2011, MNRAS, 736
Dias, W. S., Alessi, B. S., Moitinho, A., & Lépine, J. R. D. 2002, A&A, 389, 871
Dinescu, D. I., Girard, T. M., van Altena, W. F., & López, C. E. 2003, AJ, 125, 1373
Dinescu, D. I., Majewski, S. R., Girard, T. M., & Cudworth, K. M. 2000, AJ, 120, 1892
Edvardsson, B., Andersen, J., Gustafsson, B., et al. 1993, A&A, 275, 101
Eggen, O. J. 1966, Transactions of the International Astronomical Union, Series B, 12, 432
Eggen, O. J. 1996, AJ, 112, 1595
Eggen, O. J., Lynden-Bell, D., & Sandage, A. R. 1962, ApJ, 136, 748
Famaey, B., Pont, F., Luri, X., et al. 2007, A&A, 461, 957
Forbes, D. A. & Bridges, T. 2010, MNRAS, 404, 1203
Freeman, K. & Bland-Hawthorn, J. 2002, ARA&A, 40, 487
Friel, E. D., Jacobson, H. R., & Pilachowski, C. A. 2010, AJ, 139, 1942
Frinchaboy, P., Zasowski, G., Jackson, K., et al. 2010, in JENAM 2010, Joint European and National Astronomy Meeting
Froebrich, D., Scholz, A., & Raftery, C. L. 2007, MNRAS, 374, 399
Fuhrmann, K. 2011, MNRAS, 414, 2893
Fulbright, J. P., Wyse, R. F. G., Ruchti, G. R., et al. 2010, ApJ Lett., 724, L104
Gratton, R., Sneden, C., & Carretta, E. 2004, ARA&A, 42, 385
Grebel, E. K. 2011, ArXiv:1103.6234
Harris, W. E. 1991, ARA&A, 29, 543
Harris, W. E. 1998, in Astronomical Society of the Pacific Conference Series, Vol. 136, Galactic Halos, ed. D. Zaritsky, 33

Harris, W. E. 2010, ArXiv:1012.3224
Harris, W. E., Whitmore, B. C., Karakla, D., et al. 2006, ApJ, 636, 90
House, E. L., Brook, C. B., Gibson, B. K., et al. 2011, MNRAS, 885
Ivezic, Z., Tyson, J. A., Acosta, E., et al. 2008, ArXiv:0805.2366
Jurić, M. & Ivezić, Ž. 2011, in EAS Publications Series, Vol. 45, EAS Publications Series, 281–286
Kinman, T. D. 1959, MNRAS, 119, 559
Kiss, L. L., Moór, A., Szalai, T., et al. 2011, MNRAS, 411, 117
Klement, R. J. 2010, A&AR, 18, 567
Lardo, C., Bellazzini, M., Pancino, E., et al. 2011, A&A, 525, A114
Law, D. R. & Majewski, S. R. 2010, ApJ, 718, 1128
Lee, Y. S., Beers, T. C., An, D., et al. 2011, ArXiv:1104.3114
Lee, Y. S., Beers, T. C., Sivarani, T., et al. 2008, AJ, 136, 2022
Magrini, L., Sestito, P., Randich, S., & Galli, D. 2009, A&A, 494, 95
Marín-Franch, A., Aparicio, A., Piotto, G., et al. 2009, ApJ, 694, 1498
Marino, A. F., Villanova, S., Milone, A. P., et al. 2011, ApJ Lett., 730, L16
Mateo, M. L. 1998, ARA&A, 36, 435
Meléndez, J., Schuster, W. J., Silva, J. S., et al. 2010, A&A, 522, A98
Minchev, I., Boily, C., Siebert, A., & Bienayme, O. 2010, MNRAS, 407, 2122
Minniti, D. 1995, AJ, 109, 1663
Minniti, D., Lucas, P. W., Emerson, J. P., et al. 2010, New Astronomy, 15, 433
Moitinho, A. 2010, in IAU Symposium, ed. R. de Grijs & J. R. D. Lépine, Vol. 266, 106–116
Monaco, L., Bellazzini, M., Bonifacio, P., et al. 2007, A&A, 464, 201
Moore, B., Ghigna, S., Governato, F., et al. 1999, ApJ Lett., 524, L19
Mottini, M. & Wallerstein, G. 2008, AJ, 136, 731
Odenkirchen, M., Grebel, E. K., Rockosi, C. M., et al. 2001, ApJ Lett., 548, L165
Perryman, M. A. C. & ESA, eds. 1997, ESA Special Publication, Vol. 1200, The HIPPARCOS and TYCHO catalogues. Astrometric and photometric star catalogues derived from the ESA HIPPARCOS Space Astrometry Mission
Piotto, G., Bedin, L. R., Anderson, J., et al. 2007, ApJ Lett., 661, L53
Rosenberg, A., Saviane, I., Piotto, G., & Aparicio, A. 1999, AJ, 118, 2306
Ruchti, G. R., Fulbright, J. P., Wyse, R. F. G., et al. 2010, ApJ Lett., 721, L92
Sales, L. V., Helmi, A., Abadi, M. G., et al. 2009, MNRAS, 400, L61
Sbordone, L., Bonifacio, P., Buonanno, R., et al. 2007, A&A, 465, 815
Sbordone, L., Bonifacio, P., Marconi, G., Buonanno, R., & Zaggia, S. 2005, A&A, 437, 905
Shapley, H. 1918a, PASP, 30, 42
Shapley, H. 1918b, ApJ, 48, 154
Sollima, A., Martínez-Delgado, D., Valls-Gabaud, D., & Peñarrubia, J. 2011, ApJ, 726, 47
Springel, V., Wang, J., Vogelsberger, M., et al. 2008, MNRAS, 391, 1685
Springel, V., White, S. D. M., Jenkins, A., et al. 2005, Nat, 435, 629
Tolstoy, E., Hill, V., & Tosi, M. 2009, ARA&A, 47, 371
Turon, C., Primas, F., Binney, J., et al. 2008a, The Messenger, 134, 46
Turon, C., Primas, F., Binney, J., et al. 2008b, ESA-ESO Working Group on Galactic Populations, Chemistry and Dynamics, Tech. rep.
Wyse, R. F. G. 2006, Mem. Soc. Astron. Ital., 77, 1036
Zinn, R. 1985, ApJ, 293, 424
Zinn, R. 1996, in Astronomical Society of the Pacific Conference Series, Vol. 92, Formation of the Galactic Halo...Inside and Out, ed. H. L. Morrison & A. Sarajedini, 211

6.2 First Results from *Herschel* on Nearby Clouds

Philippe André[1], A. Men'shchikov[1], V. Könyves[1], D. Arzoumanian[1], N. Peretto[1], and P. Palmeirim[1]

[1] Laboratoire AIM, CEA Saclay, IRFU/Service d'Astrophysique, F-91191 Gif-sur-Yvette

Abstract

The *Herschel* Space Observatory offers a unique opportunity to improve our understanding of the formation of stellar clusters and associations. We summarize the first results from the Gould Belt survey, one of the largest key projects with *Herschel*. Our early findings confirm the existence of a close relationship between the prestellar core mass function (CMF) and the stellar initial mass function (IMF). The *Herschel* images also reveal a rich network of filaments in every interstellar cloud and suggest an intimate connection between the filamentary structure of the ISM and the formation process of prestellar cores and protostars. Altogether, the *Herschel* results favour a scenario in which interstellar filaments and prestellar cores represent two fundamental steps in the star formation process: First, large-scale magneto-hydrodynamic turbulence generates a complex web of filaments in the ISM; second, the densest filaments grow and fragment into prestellar cores (and ultimately protostars) via gravitational instability. In this picture, a (proto)stellar cluster forms when a massive filament becomes globally gravitationally unstable and undergoes large-scale collapse.

Introduction: The *Herschel* Gould Belt Survey

The observational objective of the *Herschel* Gould Belt survey (André & Saraceno [2005], André et al. [2010]) is to image the bulk of nearby ($d \lesssim 500$ pc) molecular clouds, mostly located in Gould's Belt (e.g. Guillout [2001]), at 6 wavelengths between 70 μm and 500 μm. The total surface area covered by the survey will exceed 160 deg^2 (cf. http://gouldbelt-herschel.cea.fr/ for the list of all target regions). This will provide complete samples of prestellar cores and Class 0 protostars with well characterized luminosity and mass functions in most nearby star-forming regions. The main scientific goals are to clarify the nature of the relationship between the prestellar core mass function (CMF) and the stellar IMF (cf. Section below) and to elucidate the physical mechanisms responsible for the formation of prestellar cores out of the diffuse interstellar medium (cf. Section *The key role of filaments in the core formation process* and Section *Conclusions: Toward a universal scenario for core and star formation?*). Two extreme regions among a sample of 15 nearby cloud complexes were selected for imaging during the science demonstration phase of *Herschel* in October 2009: the Polaris Flare and the Aquila Rift. While the Polaris flare field is a high-latitude *translucent* cloud with little to no star formation at $d \sim 150$ pc (e.g. Heithausen et al. [2002]), the Aquila field is a very active star-forming complex at $d \sim 260$ pc (e.g. Gutermuth et al. [2008]). Our initial results for these two regions are summarized in next Section and the Section below and discussed in more detail in 6 papers published in the A&A special issue on *Herschel* (André et al. [2010], Könyves et al. [2010], Bontemps et al. [2010], Miville-Deschênes et al. [2010], Men'shchikov et al. [2010], Ward-Thompson et al. [2010]).

First results on the CMF–IMF connection

Briefly, more than 300 starless cores but no protostars were detected with *Herschel* in the Polaris field (~ 8 deg^2). The locations of the Polaris starless cores in a mass versus size diagram show that they are ~ 2 orders of magnitude less dense than self-gravitating isothermal Bonnor-Ebert spheres and therefore cannot be gravitationally bound. The mass function of these unbound starless cores peaks at an order of magnitude smaller mass than the stellar IMF (André et al. [2010]). In contrast, more than 200 (Class 0 & Class I) protostars could be identified in the *Herschel* images of the whole (~ 11 deg^2) Aquila field (Bontemps et al. [2010]), along with a total of 541 starless cores ~ 0.01 – 0.1 pc in size (see Fig. 6.1 (top)

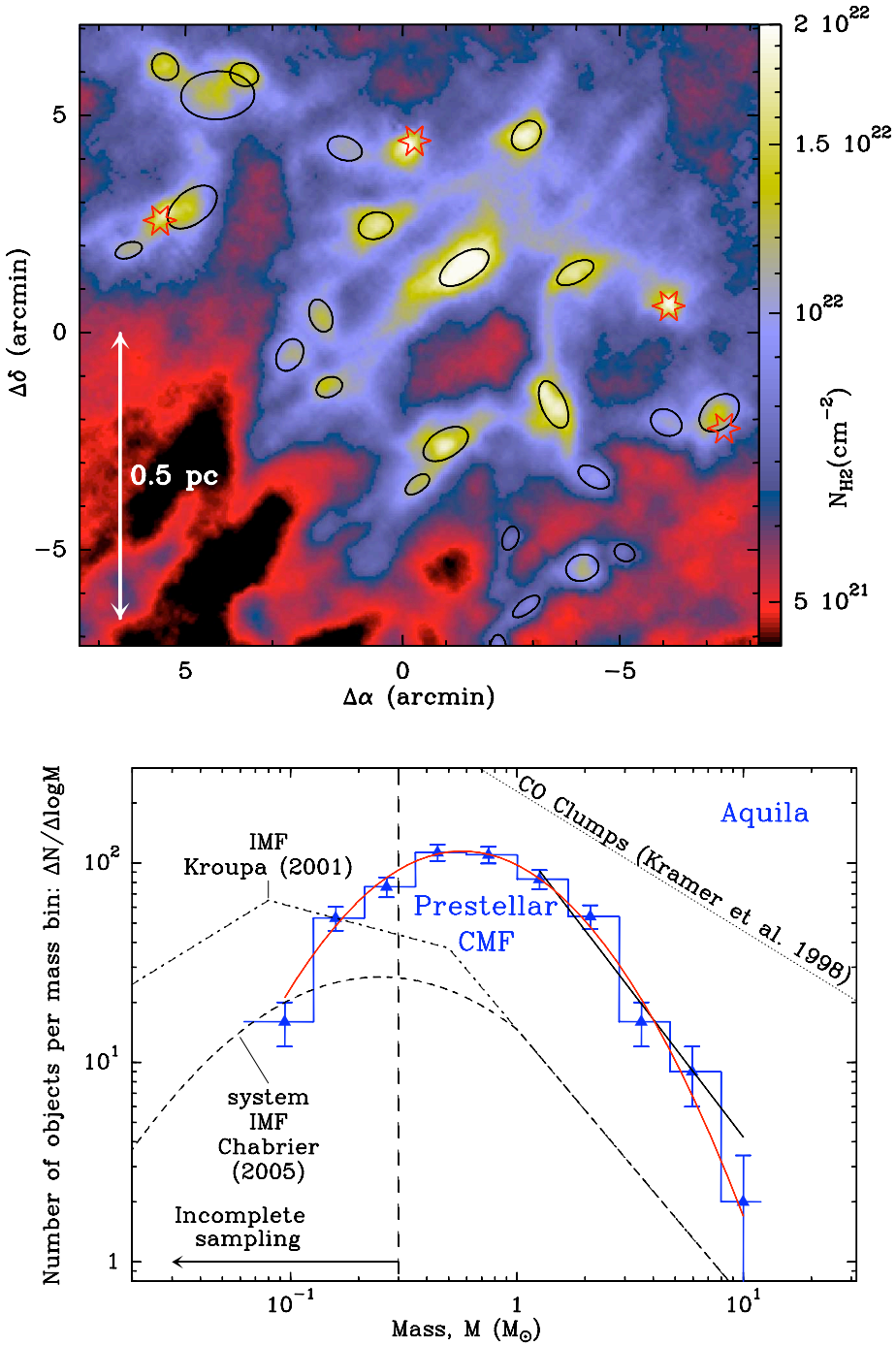

Figure 6.1: *Top*: Close-up column density image of a small subfield in the Aquila Rift complex showing several candidate prestellar cores identified with *Herschel* (adapted from Könyves et al. [2010]). The black ellipses mark the major and minor FWHM sizes determined for these cores by the source extraction algorithm *getsources* (Menshchikov et al. [2010], [2011]). Four protostellar cores are also shown by red stars. The effective resolution of the image is $\sim$ 18 arcsec or $\sim$ 0.02 pc at $d \sim 260$ pc. *Bottom*: Core mass function (blue histogram with error bars) of the 541 candidate prestellar cores identified with *Herschel* in Aquila (André et al. [2010] and Könyves et al. [2010]). The IMF of single stars (corrected for binaries – e.g. Kroupa [2001]), the IMF of multiple systems (e.g. Chabrier [2005]), and the typical mass spectrum of CO clumps (e.g. Kramer et al. [1998]) are shown for comparison. A log-normal fit to the observed CMF is superimposed (red curve); it peaks at ~ 0.6 M$_\odot$.

for some examples). Most ($> 60\%$) of these 541 starless cores lie close to the loci of critical Bonnor-Ebert spheres in a mass versus size diagram, suggesting that they are self-gravitating and prestellar in nature (Könyves et al. [2010]). The CMF derived for the entire sample of 541 starless cores in Aquila is well fit by a log-normal distribution and closely resembles the IMF (Fig. 6.1 (bottom) – Könyves et al. [2010]; André et al. [2010]). The similarity between the Aquila CMF and the Chabrier [2005] system IMF is consistent with an essentially one-to-one correspondence between core mass and stellar system mass ($M_{\star \rm sys} = \epsilon_{\rm core}\, M_{\rm core}$). Comparing the peak of the CMF to the peak of the system IMF suggests that the efficiency $\epsilon_{\rm core}$ of the conversion from core mass to stellar system mass is between ~ 0.25 and ~ 0.4 in Aquila, depending on whether one considers the reduced sample of the best 341 candidate prestellar cores or the entire sample of all 541 starless cores (see discussion in Könyves et al. [2010]).

The early results of the *Herschel* Gould Belt survey therefore confirm the existence of a close relationship between the prestellar CMF and the stellar IMF, using data with already a factor of ~ 2 to 9 better counting statistics than earlier ground-based studies (cf. Motte, André, Neri [1998]; Johnstone et al. [2000]; Stanke et al. [2006]; Alves et al. [2007]; Enoch et al. [2008]). The efficiency factor $\epsilon_{\rm core}$ may be attributed to mass loss due to the effect of outflows during the protostellar phase (Matzner & McKee [2000]). While the results from the entire Gould Belt survey will be necessary to fully characterize the nature of the CMF–IMF relationship, our early findings seem difficult to reconcile with models in which competitive accretion plays a key role in shaping the distribution of stellar masses (e.g. Bate & Bonnell [2005]). They are in much better agreement with the gravo-turbulent fragmentation picture (e.g. Larson [1985]; Klessen & Burkert [2000]; Padoan & Nordlund [2002]; Hennebelle & Chabrier [2008]). In any event, the *Herschel* observations clearly suggest that one of the keys to the problem of the origin of the IMF lies in a good understanding of the formation mechanism of prestellar cores. This is true even if additional processes, such as rotational subfragmentation of prestellar cores into binary/multiple systems during collapse, probably also play an important role and may help to populate the low-mass end of the IMF (e.g. Bate et al. [2003]; Goodwin et al. [2008]).

The key role of filaments in the core formation process

The high quality and dynamic range of the *Herschel* images are such that they provide key information on both dense cores on small (< 0.1 pc) scales *and* the structure of the parent background cloud on large (> 1 pc) scales. In particular, one of the most spectacular early findings made with *Herschel* is the ubiquitous presence of long ($>$ pc scale) filamentary structures in the cold interstellar medium and the apparently tight connection between the filaments and the formation process of dense cores (e.g. André et al. [2010]; Men'shchikov et al. [2010]; Molinari et al. [2010]). Remarkably, filaments are omnipresent even in diffuse, non-star-forming complexes such as the Polaris translucent cloud (cf. Fig. 6.2 (top) – Miville-Deschênes et al. [2010]; Ward-Thompson et al. [2010]). Moreover, in any given cloud complex, *Herschel* imaging reveals a whole network of filaments (see Fig. 6.2), making it possible to characterize their properties in a statistical manner. Detailed analysis of the radial column density profiles derived from *Herschel* data shows that the filaments are characterized by a very narrow distribution of central widths with a typical FWHM value of ~ 0.1 pc (cf. Fig. 6.3 (top) – Arzoumanian et al. [2011]). A plausible interpretation of this characteristic width of interstellar filaments is that it corresponds to the sonic scale below which interstellar turbulence becomes subsonic in diffuse, non-star-forming gas (cf. Padoan et al. [2001]; Federrath et al. [2010]).

The observed correspondence between the filaments and the spatial distribution of compact cores is also remarkable (see Fig. 6.2 (bottom) and Men'shchikov et al. [2010]), suggesting that *dense cores form primarily along filaments*. More precisely, the prestellar cores identified with *Herschel* are preferentially found within the *densest filaments* with masses per unit length exceeding ~ 15 $M_\odot$/pc and column densities exceeding $\sim 7 \times 10^{21}$ cm^{-2} (André et al. [2010] and Fig. 6.2 (bottom)). In the Aquila region, for instance, the distribution of background cloud column densities for the prestellar cores shows a steep rise above $N_{\rm H_2}^{\rm back} \sim 5 \times 10^{21}$ cm^{-2} (cf. Fig. 6.3 (bottom)) and is such that $\sim 90\%$ of the candidate bound cores are found above a background column density $N_{\rm H_2}^{\rm back} \sim 7 \times 10^{21}$ cm^{-2}, corresponding to a background visual extinction $A_V^{\rm back} \sim 8$. The *Herschel* observations of the Aquila Rift complex therefore strongly support the existence of a column density or visual extinction threshold for the formation of prestellar cores at $A_V^{\rm back} \sim 5 - 10$, which had been suggested based on earlier ground-based studies of, e.g., Taurus and Ophiuchus (cf. Onishi et al. [1998]; Johnstone et al. [2004]). In the Polaris flare, our results are also consistent with such an extinction threshold since the observed background column densities are all below $A_V^{\rm back} \sim 8$ and there are no examples of bound prestellar cores in this cloud. Moreover, the

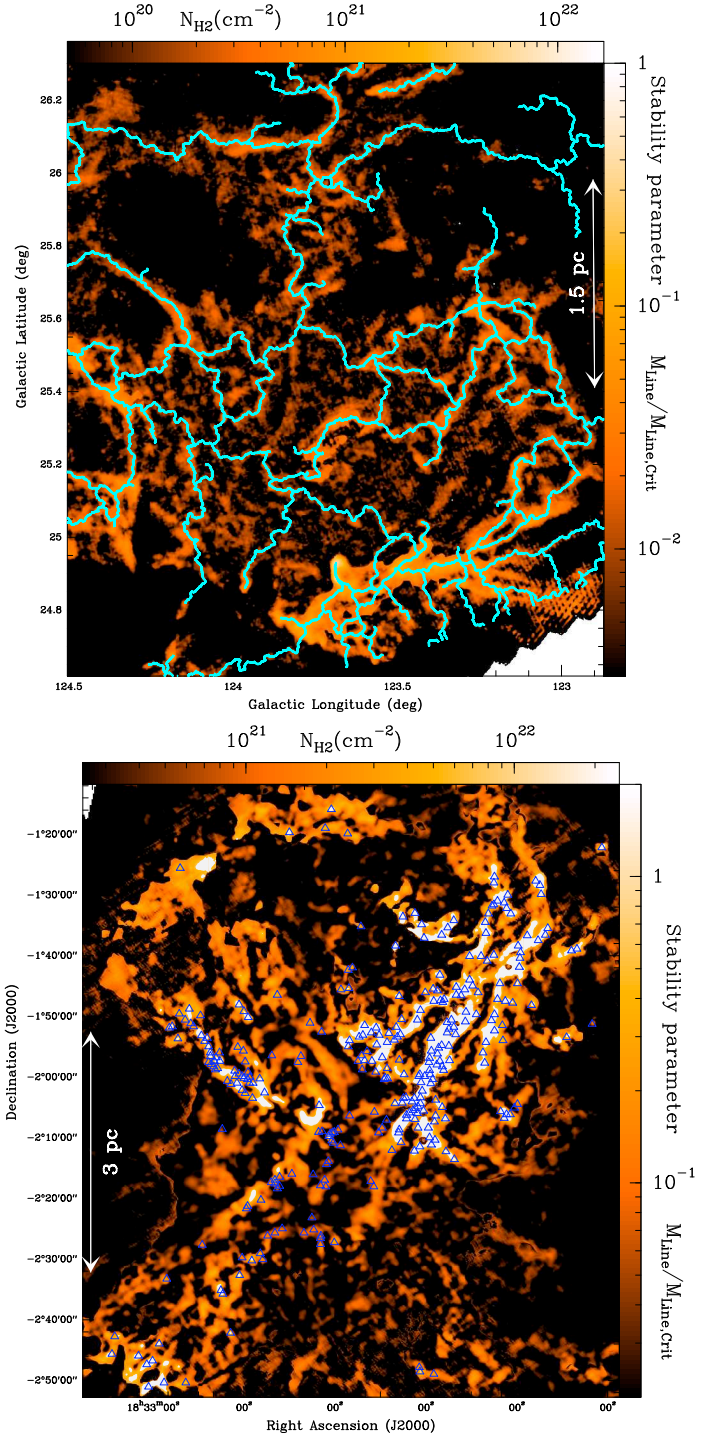

Figure 6.2: Column density maps of two subfields in Polaris (top) and Aquila (bottom) derived from *Herschel* data (André et al. [2010]). The contrast of the filaments has been enhanced using a curvelet transform (cf. Starck et al. [2003]). The skeleton of the filament network identified in Polaris with the DisPerSE algorithm (Sousbie [2011]) is shown in light blue in the upper panel. Given the typical width ~ 0.1 pc of the filaments (Arzoumanian et al. [2011] – see Fig. 6.3 (top)), these maps are equivalent to *maps of the mass per unit length along the filaments*. The areas where the filaments have a mass per unit length larger than half the critical value $2\,c_s^2/G$ and are thus likely gravitationally unstable have been highlighted in white. The bound prestellar cores identified by Könyves et al. [2010] in Aquila are shown as small blue triangles in the bottom panel; there are no bound cores in Polaris.

Herschel results provide an *explanation* of this threshold in terms of the filamentary structure of molecular clouds. Given the typical width ~ 0.1 pc measured for the filaments (Arzoumanian et al. [2011]; see Fig. 6.3 (top)), the threshold at $A_V^{\rm back} \sim 8$ or $\Sigma_{\rm gas}^{\rm back} \sim 130$ $M_\odot\,{\rm pc}^{-2}$ corresponds to within a factor of < 2 to the critical mass per unit length $M_{\rm line,crit} = 2\,c_s^2/G \sim 15$ $M_\odot$/pc required for the hydrostatic equilibrium of isothermal filaments (cf. Ostriker [1964]; Inutsuka & Miyama [1997]), where $c_s \sim 0.2$ km/s is the isothermal sound speed for a typical gas temperature $T \sim 10$ K. Thus, the core formation threshold approximately corresponds to the *threshold above which interstellar filaments are gravitationally unstable*. Prestellar cores are only observed above this threshold because they form out of a filamentary background and only the supercritical, gravitationally unstable filaments with $M_{\rm line} > M_{\rm line,crit}$ are able to fragment into bound cores (cf. André et al. [2010] and Fig. 6.2 (bottom)).

Conclusions: Toward a universal scenario for core and star formation?

The *Herschel* results summarized in Section *First results on the CMF–IMF connection* and Section *The key role of filaments in the core formation process* provide key insight into the core formation process. They led André et al. [2010] to favour a scenario according to which the formation of prestellar cores occurs in two main steps. First, large-scale magneto-hydrodynamic (MHD) turbulence generates a whole network of filaments in the ISM (cf. Padoan et al. [2001]); second, the densest filaments fragment into prestellar cores by gravitational instability (cf. Inutsuka & Miyama [1997]).

That the formation of filaments in the diffuse ISM represents the first step toward core/star formation is suggested by the filaments *already* being omnipresent in a gravitationally unbound, non-star-forming cloud such as Polaris (cf. Fig. 6.2 (top), Men'shchikov et al. [2010], and Miville-Deschênes et al. [2010]). This indicates that interstellar filaments are not produced by large-scale gravity and that their formation must precede star formation. It is also consistent with the view that the filamentary structure results primarily from the dissipation of large-scale interstellar turbulence (cf. Padoan et al. [2001]; Hily-Blant & Falgarone [2007], [2009]). In this view, interstellar filaments correspond to dense, post-shock stagnation gas associated with compressed regions between interacting supersonic flows. One merit of this picture is that it accounts for the characteristic ~ 0.1 pc width of the filaments as measured with *Herschel* (cf. Fig. 6.3 (top): the typical thickness of shock-compressed structures resulting from supersonic turbulence in the ISM is expected to be roughly the sonic scale of the turbulence or precisely ~ 0.1 pc in diffuse interstellar gas (cf. Larson [1981] and discussion in Arzoumanian et al. [2011]).

The second step appears to be the gravitational fragmentation of the densest filaments with supercritical masses per unit length ($M_{\rm line} > M_{\rm line,crit}$) into self-gravitating prestellar cores (André et al. [2010] – cf. previous Section). Indeed, in active star-forming regions such as the Aquila complex, most of the prestellar cores identified with *Herschel* are concentrated within supercritical filaments (cf. Fig. 6.2 (bottom)). In contrast, in non-star-forming clouds such as Polaris, all of the filaments have subcritical masses per unit length and only unbound starless cores are observed but no prestellar cores nor protostars (cf. Fig. 6.2 (top)).

Interestingly, the peak of the prestellar CMF at ~ 0.6 $M_\odot$ as observed in the Aquila complex (cf. Fig. 6.1 (bottom)) corresponds to the Jeans or Bonnor-Ebert mass $M_{\rm BE} \sim 0.6\,M_\odot \times (T/10\,{\rm K})^2 \times \left(\Sigma/150\,M_\odot\,{\rm pc}^{-2}\right)^{-1}$ within marginally critical filaments with $M_{\rm line} \approx M_{\rm line,crit} \sim 15$ $M_\odot$/pc and surface densities $\Sigma \approx \Sigma_{\rm gas}^{\rm crit} \sim 150\,M_\odot\,{\rm pc}^{-2}$. Likewise, the median spacing ~ 0.08 pc observed between the prestellar cores of Aquila roughly matches the thermal Jeans length within marginally critical filaments. All of this is consistent with the idea that gravitational fragmentation is the dominant physical mechanism generating prestellar cores within the filaments. Furthermore, a typical prestellar core mass of ~ 0.6 $M_\odot$ translates into a characteristic star or stellar system mass of ~ 0.2 $M_\odot$, assuming a typical efficiency $\epsilon_{\rm core} \sim 30\%$ (cf. Seccion *First results on the CMF–IMF connection*). Therefore, our *Herschel* findings strongly support Larson [1985]'s interpretation of the peak of the IMF in terms of the typical Jeans mass in star-forming clouds. Naively, one would expect gravitational fragmentation to result in a narrow prestellar CMF sharply peaked at the median thermal Jeans mass. However, a broad CMF resembling the log-normal shape of the IMF (e.g. Fig. 6.1 (bottom)) can be produced if turbulence has generated a field of initial density fluctuations within the filaments in the first place (cf. Inutsuka [2001]). Overall, our results suggest that the gravitational fragmentation of supercritical filaments produces the prestellar CMF which, in turn, accounts for the log-normal "base" (cf. Bastian et al. [2010]) of the IMF. It remains to be seen, however, whether the bottom end of the IMF and the Salpeter power-law slope at the high-mass

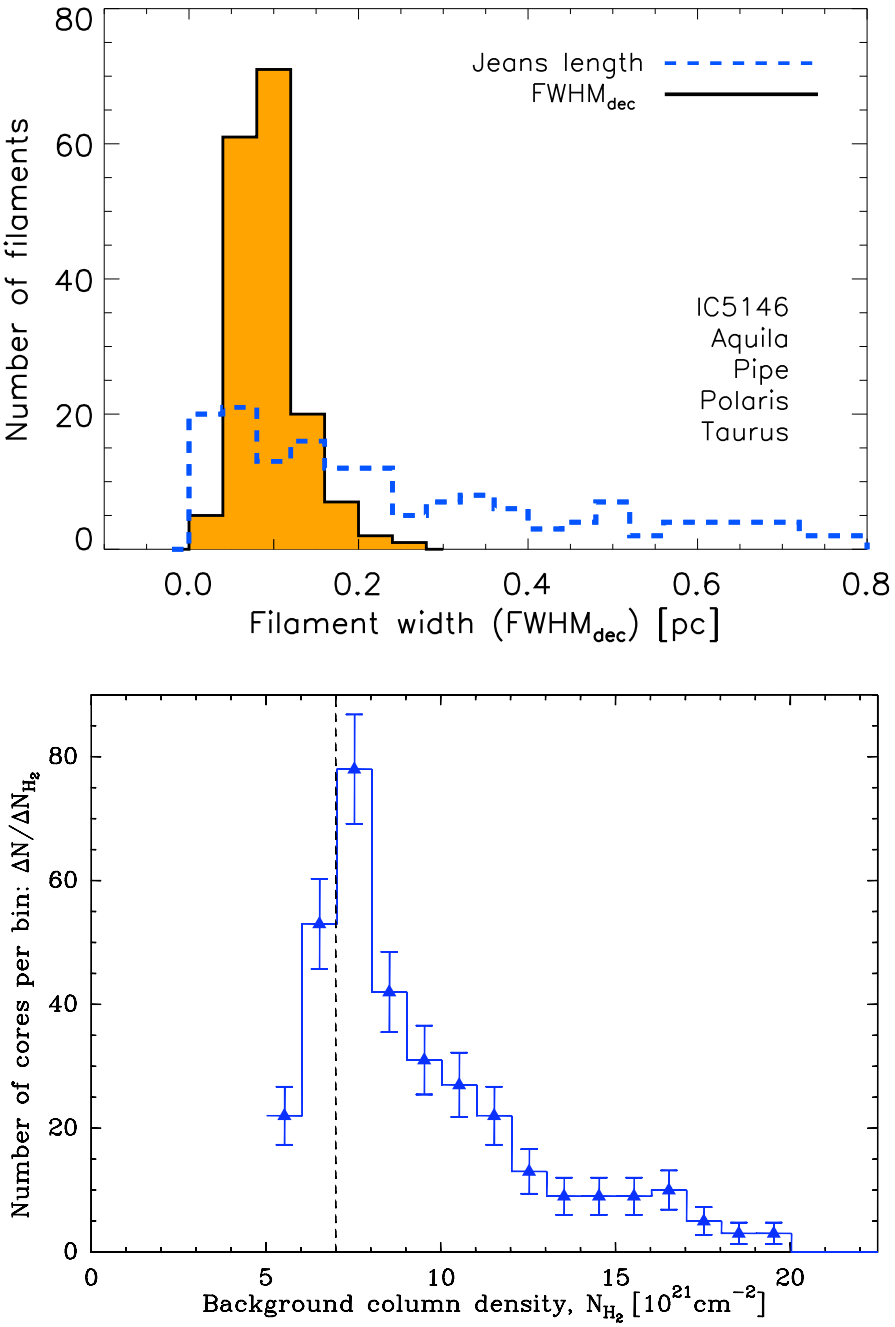

Figure 6.3: *Top*: Histogram of deconvolved FWHM widths for a sample of 169 filaments in 5 nearby regions, all observed with *Herschel* (at effective spatial resolutions ranging from $\sim$ 0.01 pc to $\sim$ 0.04 pc) and analyzed in the same way. The distribution of filament widths is narrow with a median value of 0.09 pc and a standard deviation of 0.04 pc. In contrast, the distribution of Jeans lengths corresponding to the central column densities of the filaments (blue dashed histogram) is much broader. (Adapted from Arzoumanian et al. [2011]). *Bottom*: Distribution of background column densities for the candidate prestellar cores identified with *Herschel* in the Aquila Rift complex. The vertical dashed line marks the column density or extinction threshold at $N_{\rm H_2}^{\rm back} \sim 7 \times 10^{21}$ cm^{-2} or $A_V^{\rm back} \sim 8$ (also corresponding to $\Sigma_{\rm gas}^{\rm back} \sim 130$ M$_\odot$ pc^{-2}).

end can be explained by the same mechanism.

In this scenario, a (proto)stellar cluster would form when a massive, supercritical filament becomes globally gravitationally unstable and undergoes large-scale, coherent collapse. Possible examples are provided by NGC2264-C in Mon OB1 (Peretto et al. [2006], [2007]), Serpens-South in Aquila (Gutermuth et al. [2008]; Maury et al. [2011]), and DR21 in Cygnus X (Schneider et al. [2010]).

The realization that prestellar core formation occurs primarily along gravitationally unstable filaments also has potential implications for our understanding of star formation on global Galactic and extragalactic scales. Remarkably, the critical line mass of a filament, $M_{\rm line,crit} = 2\,c_s^2/G$, depends only on gas temperature (i.e., $T \sim 10$ K for the bulk of molecular clouds, away from the immediate vicinity of massive stars) and is modified by only a factor of order unity for filaments with realistic levels of magnetization (cf. Fiege & Pudritz [2000]). This may set a quasi-universal threshold for star formation in the cold ISM of galaxies at ~ 15 M$_\odot$/pc in terms of filament mass per unit length, or ~ 150 M$_\odot$ pc^{-2} in terms of gas surface density. Indeed, recent near-/mid-infrared studies of the star formation rate as a function of gas surface density in both Galactic and extragalactic cloud complexes (e.g. Heiderman et al. [2010]; Lada et al. [2010]) show that the star formation rate tends to be linearly proportional to the mass of dense gas above a surface density threshold $\Sigma_{\rm gas}^{\rm th} \sim 120$ – $130\ M_\odot\,{\rm pc}^{-2}$ and drops to negligible values below $\Sigma_{\rm gas}^{\rm th}$ (see Gao & Solomon [2004] for external galaxies). Note that this is the *same* threshold as found with *Herschel* for the formation of prestellar cores (cf. previous Section and Fig. 6.3 (bottom)). Moreover, the relation between the star formation rate SFR and the mass of dense gas $M_{\rm dense}$ above the threshold is estimated to be $SFR = 4.6 \times 10^{-8}$ M$_\odot$ yr^{-1} $\times (M_{\rm dense}/M_\odot)$ by Lada et al. [2010]), which is close to the relation $SFR = 2 \times 10^{-8}\,M_\odot\,{\rm yr}^{-1} \times (M_{\rm dense}/M_\odot)$ found by Gao & Solomon [2004]. Both of these values are very similar to the star formation rate per unit solar mass of dense gas of $0.15 \times 0.3/10^6 \sim 4.5 \times 10^{-8}$ M$_\odot$ yr^{-1} that we may derive based on *Herschel* in the Aquila complex by considering that only $\sim 15\%$ of the cloud mass above the column density threshold is in the form of prestellar cores, that the local star formation efficiency at the level of an individual core is $\epsilon_{\rm core} \sim 30\%$ (cf. Seccion *First results on the CMF–IMF connection*), and that the typical lifetime of the Aquila cores is $\sim 10^6$ yr (Könyves et al., in prep.). Despite relatively large uncertainties, the agreement with the extragalactic value of Gao & Solomon [2004] is surprisingly good, implying that the star formation scenario sketched above may well apply to the ISM of all galaxies.

To summarize, the *Herschel* results suggest that it may be possible to understand both the IMF and the global rate of star formation in galaxies by studying the physics of how dense structures (e.g. filaments, cores) form and grow in the ISM of our own Galaxy.

Bibliography

Alves, J. F., Lombardi, M., & Lada, C. J. 2007, A&A, 462, L17

André, P. , & Saraceno, P. 2005, in The Dusty and Molecular Universe: A Prelude to *Herschel* and ALMA, ESA SP-577, p. 179

André, Ph., Men'shchikov, A., Bontemps, S. et al. 2010, A&A, 518, L102

Arzoumanian, D., André, Ph., Didelon, P. et al. 2011, A&A, 529, L6

Bastian, N., Covey, K.R., & Meyer, M.R. 2010, ARA&A, 48, 339

Bate, M. R., & Bonnell, I. A. 2005, MNRAS, 356, 1201

Bate, M. R., Bonnell, I. A., & Bromm, V. 2003, MNRAS, 339, 577

Bontemps, S., André, Ph., Könyves, V. et al. 2010, A&A, 518, L85

Chabrier, G. 2005, in The Initial Mass Function 50 years later, Eds. E. Corbelli et al., p.41

Enoch, M. L., Young, K. E., Glenn, J., Evans, N. J. et al. 2008, ApJ, 684, 1240

Federrath, C., Roman-Duval, J., Klessen, R.S., Schmidt, W., & Mac Low, M.-M. 2010, A&A, 512, A81

Fiege, J.D., & Pudritz, R.E. 2000, MNRAS, 311, 85

Gao, Y., & Solomon, P. 2004, ApJ, 606, 271

Goodwin, S. P., Nutter, D., Kroupa, P., Ward-Thompson, D., Whitworth, A. P. 2008, A&A, 477, 823

Guillout, P. 2001, in From Darkness to Light, Eds. T. Montmerle & P. André, ASP Conf. Ser., 243, p. 677

Gutermuth, R.A., Bourke, T.L., Allen, L.E. et al. 2008, ApJ, 673, L151

Heiderman, A., Evans, N.J., Allen, L.E. et al. 2010, ApJ, 723, 1019

Heithausen, A. et al. 2002, A&A, 383, 591

Hennebelle, P., & Chabrier, G. 2008, ApJ, 684, 395

Hily-Blant, P., & Falgarone, E. 2007, A&A, 469, 173

Hily-Blant, P., & Falgarone, E. 2009, A&A, 500, L29
Inutsuka, S.-I. 2001, ApJ, 559, L149
Inutsuka, S-I, & Miyama, S.M. 1997, ApJ, 480, 681
Johnstone, D., Wilson, C.D., Moriarty-Schieven, G. et al. 2000, ApJ, 545, 327
Johnstone, D., Di Francesco, J., & Kirk, H. 2004, ApJ, 611, L45
Könyves, V., André, Ph., Men'shchikov, A. et al. 2010, A&A, 518, L106
Kramer, C., Stutzki, J., Rohrig, R., Corneliussen, U. 1998, A&A, 329, 249
Kroupa, P. 2001, MNRAS, 322, 231
Lada, C.J., Lombardi, M, & Alves, J. 2010, ApJ, 724, 687
Larson, R.B., 1981, MNRAS, 194, 809
Larson, R.B. 1985, MNRAS, 214, 379
Matzner, C.D., & McKee, C.F. 2000, ApJ, 545, 364
Maury, A., André, Ph., Men'shchikov, A., Könyves, V., & Bontemps, S. 2011, A&A, in press (astro-ph/1108.0668)
Men'shchikov, A., André, Ph., Didelon, P. et al. 2010, A&A, 518, L103
Men'shchikov, A. et al. 2011, in preparation
Miville-Deschênes, M.-A., Martin, P.G., Abergel, A. et al. 2010, A&A, 518, L104
Molinari, S., Swinyard, B., Bally, J. et al. 2010, A&A, 518, L100
Motte, F., André, P., & Neri, R. 1998, A&A, 365, 440
Onishi, T., Mizuno, A., Kawamura, A. et al. 1998, ApJ, 502, 296
Ostriker, J. 1964, ApJ, 140, 1056
Padoan, P. & Nordlund, A. 2002, ApJ, 576, 870
Padoan, P., Juvela, M., Goodman, A.A., & Nordlund, A. 2001, *ApJ*, 553, 227
Peretto, N., André, P., & Belloche, A. 2006, A&A, 445, 979
Peretto, N., Hennebelle, P., & André, P. 2007, A&A, 464, 983
Schneider, N., Csengeri, T., Bontemps, S., Motte, F., Simon, R., Hennebelle, P., Federrath, C., & Klessen, R. 2010, A&A, 520, A49
Sousbie, T., 2011, MNRAS, 414, 350
Stanke, T., Smith, M. D., Gredel, R., & Khanzadyan, T. 2006, A&A, 447, 609
Starck, J. L., Donoho, D. L., Candès, E. J. 2003, A&A, 398, 785
Ward-Thompson, D., Kirk, J.M., André, P. et al. 2010, A&A, 518, L92

Chapter 7

Tertulias

7.1 Birth, Evolution and Death of Stellar Clusters

Richard de Grijs[1]

[1] Kavli Institute for Astronomy and Astrophysics, Peking University, Yi He Yuan Lu 5, Hai Dian District, Beijing 100871, China

Abstract

Using our recently improved understanding of star cluster physics, we are now within reach of answering a number of fundamental questions in contemporary astrophysics. Star cluster physics has immediate bearing on questions ranging from the physical basis of the stellar initial mass function – Do any O-type stars form in isolation? What is the relative importance of stochastic (random) star formation versus competitive accretion? – to the build-up of the most massive clusters – Does the cluster mass function differ in different types of galaxies? How and why do the most massive star clusters form in small dwarf galaxies and what does that imply for the build-up of larger cluster samples? What are the main observables one could (or should) use to try and distinguish among the various star- and cluster-formation scenarios? Newly emerging theoretical insights, novel high-quality observational data and the advent of the next generation of observational facilities offer significant promise to reach satisfactory and robust answers to the key outstanding questions in this field.

Preamble: Tertulias

When I was first approached to lead a main 'Tertulia' during the *RIA workshop on Stellar Clusters and Associations*, I was rather puzzled by the invitation, to say the least. Although this expression may be commonplace to some, it is not outside of the Spanish-speaking diaspora. Fortunately, our trusted friend Wikipedia[1] offered answers: tertulias were originally informal, social literary or artistic get-togethers, particularly in Latin cultural contexts, often (but not always) held in public places. In relation to this conference, however, the organisers meant me to chair an open discussion on outstanding questions in contemporary star cluster-related astrophysics. In the following, I aim at setting the scene for the discussion that followed, which I attempt to summarise in general terms. The lively exchange of new (and some old) ideas that ensued led, I believe, to a general broadening of participants' perspectives – in the true sense of the traditional tertulia.

[1] http://en.wikipedia.org/wiki/Tertulia

Outline of key emerging questions

Stars do not form in isolation, at least for stellar masses above ~ 0.5 $M_\odot$. In fact, 70 – 90% of stars may form in star clusters or associations (cf. Lada & Lada [2003]). Star formation results from the fragmentation of molecular clouds, which in turn seems to preferentially lead to star cluster formation. Over time, their member stars become part of the general field stellar population. Star clusters are thus often stated as being among the basic building blocks of galaxies.

Using our improved understanding of star cluster physics, we are now within reach of answering a number of fundamental questions in contemporary astrophysics, ranging from the formation and evolution of galaxies to the details of the process of star formation itself. These two issues are the backbone of research in modern astrophysics. They lead to new questions (for a detailed discussion, see de Grijs [2010]), including:

- How is star cluster formation triggered and how does it proceed?

What is the role of ambient or internal pressure? Which other internal and/or external factors affect star cluster formation and longevity? Can we set constraints on the minimum requisite star formation efficiency? Is star cluster formation a distinct mode of star formation or simply part of a broad spectrum of star formation modes?

- Do star clusters really represent the basic building blocks of galaxies?

How does the star cluster mass distribution relate to the turbulent properties of the interstellar medium (ISM)? Does initial substructure play a role? Is there a physically important difference between star formation in a 'fractal' ISM versus in clustered mode? Are mergers of smaller components a viable way to form more massive clusters? If so, what are the constraints implied for the relevant parameter space (e.g., velocity dispersions, half-mass radii, etc.?)

- How is the stellar mass distribution established?

Although the stellar initial mass function (IMF) seems fairly universal, we still do not know what establishes its well-known (multiple) power-law shape. What are the roles and the formation scenario(s) of massive versus low-mass stars and the importance of feedback? How are stellar and cluster IMFs related and how are they affected by the underlying star formation history?

- How do environmental conditions affect further cluster formation?
- How do quiescent galaxies form extremely massive clusters?

What is the role of galaxy dynamics? Does it depend on a cluster's position in a given galaxy or on the galaxy type? How are the results affected by variations in the star formation efficiency, or are we simply witnessing stochastic cluster formation? What triggers the formation of the most massive clusters?

These (and other) questions form the basis of much research in numerous fields in contemporary astrophysics: after all, star formation is one of the pivotal physical processes underlying most of astrophysics. Significant progress has been made in past decades, yet we still have a long way to go before all of the key questions will have been answered satisfactorily and sufficiently robustly to stand the test of time.

New advances in both theoretical and observational approaches may be required. Are the main theoretical (modelling) challenges preventing the next step towards a change in our understanding of star and star cluster formation processes related to limitations in hardware or techniques? Are currently available instruments sufficient to reach these lofty goals, or will new facilities – including Gaia, the Atacama Large Millimetre Array (ALMA), the *James Webb Space Telescope*, the Large Synoptic Survey Telescope, or any flavour of extremely large telescope – be essential? Do we need higher spatial resolution than currently routinely attainable or perhaps larger fields of view, or a combination of both – and is this feasible?

Are star clusters indeed basic galactic building blocks?

The question as to what constitutes a characteristic scale in star formation comes down to our understanding of the way in which stars appear to form in a self-similar, hierarchical ('fractal') fashion. Observationally, we find a wide range in the gas distribution and star formation properties in regions of active star formation (e.g., Bressert et al. [2010]), where what we tend to call 'clusters' are the loci in which many stars form together in the basic, underlying hierarchical scenario. Gaia may well be instrumental in refining our understanding of the scales on which star formation occurs in the Milky Way.

Turbulent molecular clouds form clusters in the denser regions, where filaments might cross. Star formation occurs along such filaments, usually in small groups ('knots'), which is shown beautifully by recent observations with *Herschel*. This is sometimes referred to as the distributed mode of star formation, but it is an integral part of the power-law distribution of structures. Clusters, or 'spatially and temporally correlated star formation' follow a power-law distribution of mass at a given time. One can start building galaxies from that Ansatz.

In some places, large numbers of stars are formed at roughly the same time. These loci are easily identified as star clusters. At other times, star formation proceeds in a more distributed mode, upon which the individual knots merge and also form structures we identify as star clusters. Gaia will likely find a lot of evidence of distributed star formation, where most stars never originated in clusters. The European Space Agency's mission will, therefore, be key in distinguishing between these models.

Superficially, it appears that two somewhat different views are prevalent in the community, apparently advocating the extremes of our ideas of how stars form and the structures resulting from that process. Proponents of one viewpoint would argue that star formation occurs in a spatially confined, clustered mode, while their counterparts support the full hierarchical picture. However, as long as proponents of the tenet that star clusters are the basic building blocks from which galaxies form take their view down to the lowest-mass, often embedded clusters (which includes the distributed population of young stars), these apparent differences are merely semantic.[2]

In essence, therefore, it is not important whether the star formation process forms a dense cluster, an embedded cluster or an association. What matters is whether star formation is correlated: are star formation events quantised? Is there any length scale that is special and unique? If so, clusters of a given size and/or mass may well be the basic building blocks of galaxies. However, if star formation is hierarchical, this implies that there is no unique timeframe or spatial scale on which star-forming clumps are absolutely correlated. In the latter case, star clusters and associations are not unique; instead, they simply represent a continuous distribution. In extragalactic environments, at least, on spatial scales in excess of 5 pc there is no specific length scale (e.g., Bastian et al. [2009], [2011]).

However, there is a unique scale at the bottom of the fractal distribution in both the stellar and gas distributions, i.e., that of a dense core: ~ 0.1 pc. This is the scale of individual stars, which we could potentially resolve with ALMA or – for nearby star-forming regions – the Plateau de Bure interferometer. This is of a similar order as the scale of subsonic turbulence. In addition, the IMF exhibits a peak at stellar masses between ~ 0.5 and 1 $M_\odot$, which also implies a characteristic *mass* scale.

From this discussion, the following hypothesis naturally results. The fundamental galactic building blocks are units of star formation of a few tenths of a parsec across, distributed according to a mass spectrum that is a power law down to a few $M_\odot$. If one were to distribute this kind of structure throughout a region of a galaxy according to a model of what the ISM looks like – essentially a fractal distribution – and then let it evolve dynamically, the result would enable us to derive which fraction of stars is found in distributed versus clustered mode. The null hypothesis of a scale-free star formation process can thus be either verified or discarded.

In a hierarchical scenario, this picture would be created by a turbulence power spectrum that is self-similar. However, even in such an ISM there is a definite scale, i.e., the scale on which the turbulence is injected into the ISM – and this differs among galaxies because of variations in the perturbing mechanism. One cannot have correlated structures on scales that are larger than the scales on which the energy is injected. In Holmberg 2, a dwarf galaxy, Dib & Burkert [2005] found that the structures are correlated on a very large scale of ~ 6 kpc. In the Galaxy, Dib et al. [2009] found that the orientations of molecular clouds are spatially correlated on scales of a few 100 pc. This may be related to some instability in the outer Galaxy, because it is on the order of the scales of supernova remnants which evolve in a low-pressure

[2] At the meeting, this was effectively summarised by Pavel Kroupa, who commented – in response to an argument proposed by Simon Goodwin – that "[w]hat I said is essentially what you said, just a bit more mathematical."

environment. The conclusion is, therefore, that at least on large scales there must also be a characteristic spatial scale.

From the preceding discussion, it seems that asking whether star clusters are basic galactic building blocks is a matter of semantics. More interesting, perhaps, is understanding why, when and how star formation happens. Star clusters tell us about stellar populations, the conditions in molecular clouds and the gas at the time of their formation.

How is the stellar mass distribution established?

Do any O-type stars form in isolation?

Can O-type stars form in complete isolation? The answer to this question is intimately linked to our understanding of where the IMF comes from and how it fits in with the cluster mass–maximum stellar mass relation (e.g., Weidner et al. [2010], and references therein). If the (molecular cloud) core mass function is the origin of the stellar mass function, then at the top end of the core mass function a very massive core may occasionally be formed because of stochastic effects (although note that observations are affected by small-number statistics). In very rare circumstances, this core will not fragment and collapses into one single massive object. For this to happen, the core needs to be warm so that it does not fragment, although a small cluster could form at the same place as well. In this case, the term 'isolated O stars' does not imply that no other stars can form nearby. On the contrary, a small cluster, possibly containing an O-star binary, might form, but the IMF is simply not fully sampled: it may contain a single O star, a few G stars, and possibly one B star, for instance.

If, on the other hand, the process of competitive accretion dominates, large cores will fragment into many objects. In this case, the starting point consists of cores with masses of around 1 $M_\odot$. These allow formation of a few objects per core, some of which may then accrete additional mass. Proponents of this scenario assume that most of the stellar mass function is set by the core mass function, and most cores do not grow very massive. All cores start small and if there is not much ambient gas, none can grow big. The only way in which a massive core can develop is if there is a lot of ambient gas present and a few objects can accrete a significant fraction of that gas. Competitive accretion naturally leads to the cluster mass–maximum stellar mass relationship.

In reality, a combination of processes is likely responsible for the final stellar mass distribution. For instance, in 30 Doradus (the largest HII region in the Local Group), competitive effects must have played a very significant role, but in associations this may be a different side of the same coin. Perhaps we should instead ask the question as to how frequently one or the other mode of star formation dominates.

In the first scenario outlined above, the core mass function sets the stellar mass function. In the latter case, however, one cannot really predict the resulting mass function, yet the observed mass functions are very similar. So, the simple question is whether we can quantify any differences: Are there measurable differences between the mass functions of cores and stars?

What sets the initial mass function?

The IMF and core mass function appear very similar in terms of their morphology (except, perhaps, at the high-mass end), but this result depends on the implicit assumption of one-to-one mapping from cores to stars. However, we definitely observe cores (e.g. B59: Covey et al. [2010]) that are single, do not exhibit any substructure or fragmentation, but contain 20 stars. Therefore, the scenario in which we shift the core mass function to the stellar mass function (modulo the star formation efficiency, usually assumed to be $\sim 30\%$) depends on some assumption as to how this efficiency acts on individual cores. We have at least one example where the peak should shift by more than a factor of 3. This problem is difficult to solve, because once the stellar mass function can be measured, significant stellar evolution is (and has already been) proceeding, while cores represent the very early, almost unevolved stages of star formation.

In an alternative approach, one may explore differences in the mass functions at the high-mass end, where any differences will be most pronounced. Based on observations of a statistically large number of clusters, it is very difficult to show that the observed, strict relationship between the mass of the most massive star and that of its parent cluster is valid under any circumstances. However, if one were to observe the formation of a single massive star, that would represent a significant deviation from that relationship. Therefore, if a truly isolated O star were found (i.e., an exception to the rule), there would be

at least one case in which competitive accretion has not worked, thus providing support for the stochastic sampling theory.

In observational terms, let us compare Taurus, a region of active star formation harbouring a mass of some 10^3 – 10^4 $M_\odot$, and NGC 3603, a larger star-forming region. In essence, the random sampling scenario implies that a collection of molecular material composed of Taurus-like units equivalent to that of a large cluster would never produce a massive star. However, proponents of the idea of competitive accretion would argue that a large number of Taurus-like units *do* lead to the formation of massive stars. This apparent conflict may disappear if it were a simple matter of scaling up one's star-forming regions. If one considers Orion, for instance, the morphology is always the same, exhibiting numerous filaments and clumps – just like the structure of Taurus. Scaling this kind of hierarchical structure up leads to configurations resembling Orion A. Alternatively, small sections of Orion A at high resolution look exactly like Taurus or the Pipe Nebula.

An alternative approach to the conundrum of massive-star formation may be found in considering the ratio between the number of massive to low-mass stars in different regions. If we first consider Orion and count the total number of low-mass stars as well as the number of massive stars, and we find that the number of massive stars is underrepresented in the entire Orion area, what do we deduce from this? Similarly, if we explore this ratio in dwarf galaxies, i.e., we count the number of massive stars in a dwarf galaxy with a low star formation rate and we find that there are too few massive stars compared to what we expect from the shape of the 'canonical' IMF, what do we conclude from this, since it is all driven by purely stochastic (random) sampling? The underlying idea of stochastic sampling is that if we add many Taurus–Auriga-like structures to form an Orion-like configuration, we should find an IMF that is more dominated by low-mass stars than expected for a canonical IMF. We can thus either exclude or verify random sampling as a viable star formation scenario.

However, these scenarios may be too simplistic. First, if massive clusters form from hierarchical mergers of subclusters before gas expulsion, then the prestellar clumps in these subclusters do not know *a priori* where they will end up. Why then is there a clear correlation between the maximum stellar mass in a cluster and the total cluster mass? Second, one may wonder whether there are there any clumps that collapse in which the star formation has completely stopped. Instead, star formation is likely ongoing while the clumps collapse and during the early dynamical evolution of the resulting systems. This early collapse occurs on essentially the free-fall timescale, at least in Orion-like clusters (e.g., Allison et al. [2009], [2010]; Yu et al. [2011]). This is corroborated by arguments based on structural parameters: at longer wavelengths (e.g., as seen with the *Spitzer Space Telescope*), star-forming regions are rather filamentary. However, when we consider nearly 'complete' clusters, they are quite spherical but not extremely substructured: collisions of these clumps seem, therefore, quite fast. Perhaps some of these clumps first merge before forming a massive star (e.g., to release angular momentum). One should keep in mind that the entire picture is extremely dynamical; one certainly cannot assume that young star-forming clumps evolve in isolation.

Finally, one should be cautious in linking the stellar mass distribution directly to the star formation process. Although we have assumed in this discussion that the IMF is somehow the result of star formation, it is perhaps better to state that at the end of the star formation process, a near-invariant IMF results. A similar IMF is also observed at the start of the process of star formation. However, one should keep in mind that the start of the fragmentation process may be driven by different physics than that underlying that of star formation itself (i.e., the reasons for the onset of the collapse). As a consequence, depending on how one defines one scale, the resulting clusters and cluster masses may differ, so that the IMF does not carry much or any information about the star formation process.

Binarity

What is the role of multiplicity in high-mass stars? There are numerous examples of significant multiplicity fractions in young (star-forming) environments, e.g. the Orion Nebula's Trapezium system or the young Large Magellanic Cloud (LMC) cluster NGC 1818 (Hu et al. [2010]). Each of the massive Trapezium stars is at least a binary, and there are many more examples. Even based on interferometric submillimetre observations, some Class 0 objects have been found to be multiple.

Let us assume that the power-law stellar mass distribution goes down to very low masses. For stellar masses below ~ 100 $M_\odot$, the population of these objects will not be dynamically processed; it will simply disperse. Given that the IMF is quite invariant, it then follows quite reasonably that the binary populations may also be initially invariant (assuming universal binary properties). One can now calculate

the binary population expected for a galactic field or an entire galaxy, if we understand star formation to the extent we believe we do in the Milky Way, i.e., where the IMF and binary populations are both universal and stars form in power-law structures. One can show that the galactic-field binary population is derived beautifully, because the more massive objects break up the binaries, while the lower-mass objects do not. This leads to an invariant IMF and binary population. One can then predict that dwarf galaxies should have high and starburst galaxies low binary fractions. This could potentially be checked observationally, at least if we could resolve nearby galaxies into individual stars.

What are the conditions for massive-cluster formation?

On larger scales, how do globular clusters (GCs) form? The answer to this question is linked to how environmental conditions affect further cluster formation. Large numbers of massive proto-GCs formed in the past, but why do we not see similar numbers at the present time in the Milky Way? The massive young cluster Westerlund 1 may be a recent example, although it is also possible that it may turn into an open cluster or dissolve into the Galactic field because of its rather extreme environmental conditions. In fact, we have to be careful in making a clear distinction between open and globular clusters. We see young GCs in massive galaxy mergers, and even in spiral disks. Instead of advocating distinct formation mechanisms, we are most likely observing the remnants of a much more varied original population – which may have formed following a variety of mechanisms – of which many members have disappeared because of dynamical evolution. The main physical driver underlying the mass build-up of young star clusters is the star-formation-rate density: higher densities allow a cluster to assemble more mass before star formation ceases.

At least some of the massive globular-like clusters in galaxies like the Milky Way originated in smaller dwarf galaxy companions (including, most likely, ω Centauri), which later merged with the main galaxy dominating the local gravitational potential. This leads to the question as to why we do not observe many of such massive proto-GCs in dwarf galaxies like the Magellanic Clouds. The LMC contains the most significant HII region in the Local Group, 30 Doradus, but it is small by comparison of the structures required to form true GCs. Other nearby dwarf galaxies, including NGC 1569 and NGC 1705, do contain the type of object that may evolve into genuine GCs, however.

How can such small dwarf galaxies host several globular or young massive clusters that contain some 10% of the total mass of these galaxies? Molecular clouds can be larger in dwarf galaxies because of the lower shear and tidal forces in these systems compared to large spiral galaxies. In the Milky Way, molecular cloud masses are of order 10^5 – 10^6 $M_\odot$, while in the LMC they are approximately 10^7 $M_\odot$, for instance. Molecular clouds in galaxies with lower shear can grow larger by agglomeration.

Two other, complementary effects (both related to metallicity) might make clumps and/or giant molecular clouds more massive in galaxies like the Large and Small Magellanic Clouds. In lower-metallicity galaxies, the gas-to-dust coupling occurs at a different density compared to that in higher-metallicity environments. The probability density function is broader and extends to higher densities, because a cloud has to accumulate more mass to shield itself (e.g., Glover & Clark [2011]). Second, lower-metallicity feedback is less effective and allows for more star formation, potentially also resulting in more massive clusters and associations.

The natural question to ask in this context is whether the cloud (and cluster) mass function in dwarf galaxies is different from that in L^* galaxies. Current thinking implies that complete universality is no longer fully supported by the data, but one has to look carefully at where the differences arise. There are no significant differences between the Magellanic Clouds and the Milky Way. On the other hand, despite the small-number statistics affecting these arguments, it is curious that dwarf galaxies like NGC 1569 and NGC 1705 host very massive ($> 10^5$ $M_\odot$) clusters, which are truly outstanding in their respective cluster mass functions.

Ongoing research aimed at addressing the question of the origin of the most massive young and globular clusters has not yet produced a satisfactory answer. The most massive clusters in extragalactic environments are found in merging systems. Observations and theory support many mergers in the young Universe. However, mergers are not necessarily the evolutionary end point of a galaxy: disks can reform within a Gyr, potentially allowing the formation of new populations of GCs at that stage.

Perhaps the most promising approach to addressing the GC formation scenario resides in the use of concrete, observable indicators that can help distinguish the various formation scenarios proposed. Massive ellipticals contain the largest populations of GCs, the most massive GCs and the highest metal-

licities. Dwarf galaxies have very low metallicities, so that it appears unfeasible to merge large numbers of dwarf galaxies to form ellipticals. To understand GC formation, much better metallicity measurements are required. Similarly, better determinations of ages and age spreads are advisable, although they are much harder to obtain. Metallicities – both integrated and of individual stars in resolved, nearby clusters – are the most basic, clearest and most important indicator of how GCs may have formed.

Despite a significant body of recent work in this field, there is no single observation of a subclustered massive proto-GC. Most of our theoretical understanding of the details of massive cluster formation hinge on scenarios involving scaled-up versions of smaller open cluster-like configurations, where we do see clear substructure at early stages. Nevertheless, tantalising objects that might indeed provide clues as to the morphology of forming proto-GCs on small scales include Sagittarius B2 (e.g., Bally [2010]) – observed as part of the Bolocam Galactic Plane Survey – and the embedded massive young clusters in NGC 5253. Further Galactic Plane surveys (e.g., Lucas et al. [2008]; Minniti et al. [2010]) will be instrumental in constraining the early evolutionary properties of such objects.

Although at the present time we do not know of any proto-GCs in the Milky Way, with the possible exception of Westerlund 1, our observational sample is very incomplete: to date, only 14 massive young stellar clusters have been discovered on the near side of the Galaxy, all with masses around 10^4 $M_\odot$. In addition, Davies et al. [2011] recently discovered a 1 Gyr-old, 10^5 $M_\odot$ cluster in the Galactic disk at a distance of only $\sim 2 - 3$ kpc. Indeed, very massive clusters do form occasionally in galactic disks (e.g., Larsen et al. [2001]).

Acknowledgments

It is my great pleasure to thank the organisers of this workshop for the opportunity to shape this tertulia. In addition, I would like to pay tribute to all active participants, without whose contributions we would not have had such a lively exchange of ideas!

Bibliography

Allison, R. J., Goodwin, S. P., Parker, R. J., de Grijs, R., Portegies Zwart, S. F., Kouwenhoven, M. B. N. 2009, ApJ, 700, L99

Allison, R. J., Goodwin, S. P., Parker, R. J., Portegies Zwart, S. F., de Grijs, R. 2010 MNRAS, 407, 1098

Bally, J., Aguirre, J., Battersby, C., Bradley, E. T., Cyganowski, C., Dowell, D., Drosback, M., Dunham, M. K., et al. 2010, ApJ, 721, 137

Bastian, N., Gieles, M., Ercolano, B., Gutermuth, R. 2009, MNRAS, 392, 868

Bastian, N., Weisz, D. R., Skillman, E. D., McQuinn, K. B. W., Dolphin, A. E., Gutermuth, R. A., Cannon, J. M., Ercolano, B., Gieles, M., Kennicutt, R. C., Walter, F. 2011, MNRAS, 412, 1539

Bressert, E., Bastian, N., Gutermuth, R., Megeath, S. T., Allen, L., Evans II, N. J., Rebull, L. M., Hatchell, J., et al. 2010, MNRAS, 409, L54

Covey, K. R., Lada, C. J., Román-Zúñiga, C., Muench, A. A., Forbrich, J., Ascenso, J. 2010, ApJ, 722, 971

Davies, B., Bastian, N., Gieles, M., Seth, A. C., Mengel, S., Konstantopoulos, I. S. 2011, MNRAS, 411, 1386

de Grijs, R. 2010, Phil. Trans. R. Soc. A., 368, 693

Dib, S., & Burkert, A. 2005, ApJ, 630, 238

Dib, S., Walcher, C. J., Heyer, M., Audit, E., Loinard, L. 2009, MNRAS, 398, 1201

Glover, S. C. O., & Clark, P. C. 2011, MNRAS, submitted (arXiv:1102.0670)

Hu, Y., Deng, L., de Grijs, R., Liu, Q., Goodwin, S. P. 2010, ApJ, 724, 649

Lada, C. J., & Lada, E. A. 2003, ARA&A, 41, 57

Larsen, S. S., Brodie, J. P., Elmegreen, B. G., Efremov, Yu. N., Hodge, P. W., Richtler, T. 2001, ApJ, 556, 801

Lucas, P. W., Hoare, M. G., Longmore, A., Schroeder, A. C., Davis, C. J., Adamson, A., Bandyopadhyay, R. M., de Grijs, R., et al. 2008, MNRAS, 391, 136

Minniti, D., Lucas, P. W., Emerson, J. P., Adamson, A., Aigrain, S., Ahumada, A. V., Alonso, M. V., Arias, J. I., et al. 2010, New Astron., 15, 433

Weidner, C., Kroupa, P., Bonnell, I. A. D. 2010, MNRAS, 401, 275

Yu, J., de Grijs, R., Chen, L. 2011, ApJ, 732, 16

7.2 Long Term Surveys Preparing and Following Gaia: What Do We Need?

Sofia Randich[1]

[1] INAF-Osservatorio Astrofisico di Arcetri, Italy

Abstract

The Gaia mission will provide data that will bring us into a new domain of cluster research. However, full exploitation of those data will require complementary and supplementary long term surveys to be carried out. Whilst a few ground-based surveys are already ongoing and/or planned, additional ones will likely be necessary. During the *TERTULIA* different aspects were discussed, including the type and volume of needed datasets, timescales, requirements on parallel theoretical modelling, needs for human resources. This paper presents a subjective summary of the most relevant points touched upon during the discussion.

Introduction

Accurate parallaxes and proper motions provided by the Gaia mission will bring us into a new era of open cluster research. Gaia will be sensitive to stars down to G = 20[3]. It will measure parallaxes and thus distances of *individual* stars in open clusters with a precision better than 1% for clusters closer than $\sim$ 1 kpc and better than 10% for almost the entire open cluster family. Higher accuracies are expected for proper motions[4], yielding a precision in *individual* tangential velocities (V_t) of the order of 10 m/s and below for very nearby clusters, and of the order of $0.2 - 0.3$ km/s for low mass stars in clusters up to $\sim$ 1.5 kpc and up to larger distances for bright O/B stars. Gaia will also provide good photometric information for all objects observed astrometrically, as well as radial velocities (but see below) and spectroscopic characterization for stars down to brighter magnitudes (see also Prusti, these Proceedings).

In summary, Gaia will deliver a dataset, for both known and possibly newly discovered clusters, that will have a huge impact on a large variety of topics; a non-comprehensive list includes internal dynamics, cluster formation, evolution, and destruction; cluster evaporation, population of the thin disc, Galactic dynamics; stellar ages and star formation histories; stellar structure and evolution; cluster orbits, abundance gradients, and thin disc evolution. Several of these topics are indeed discussed in papers in these Proceedings.

Why ground based surveys?

Whereas Gaia will already represent a revolution in cluster science, full exploitation of its potential requires complementary and supplementary surveys from the ground to be carried out. The main reasons for that are summarized below and were proposed as an input to the discussion during the *TERTULIA*.

- Crucially Gaia has limited spectroscopic capability, hence missing a vital third kinematic dimension and having poor chemical discrimination.

  As mentioned, Gaia will deliver radial velocities (RVs) and some spectroscopic characterization. However, the limiting magnitude for RV measurements is considerably brighter than for photometry and astrometry: only stars brighter than $G_{RVS} = 16$ will have a spectroscopic observation. This implies that, whereas 1 billion stars will have astrometry and photometry measurements, only about 150 million stars will have a RV measurement; focusing on clusters, the brighter limit for RVs

[3] G is the Gaia magnitude; the G filter is wide and covers the range between $\sim$ 300 to 900 nm. The corresponding V magnitude depends on the stellar colour.

[4] `http://www.rssd.esa.int/index.php?project=GAIA&page=Science$_$Performance`

corresponds, for each given spectral-type, to smaller cluster distances up to which Gaia will yield a measurement of the RV. Also, and most importantly, the expected accuracy in RV (about 1 km/s at best) is far below that expected for tangential velocities and is not good enough for complete and accurate dynamical studies of clusters. This point is graphically shown in Fig. 7.1. We finally notice that astrophysical information, such as interstellar reddening, atmospheric parameters, and rotational velocities, will only be possible for stars brighter than $G_{RVS} = 12$, while elemental abundances will be delivered for stars brighter than $G_{RVS} = 11$. In other words, the large majority of stars, even in the closest clusters, will not have this key information from Gaia and will thus lack full characterization;

- Photometry from Gaia, although of very high accuracy, might not be good enough for detailed studies of cluster colour-magnitude diagrams and stellar evolution; for these an accuracy at the milli-mag level even for faint stars is needed, in order to better classify the stars in terms of gravity, reddening, and temperature;
- Gaia will have little sensitivity to red and low-mass stars, brown dwarfs, and planetary mass objects in clusters; clearly, complementary astrometric data would be needed to sample the full cluster populations;
- Several new clusters, associations, and moving groups will be detected by Gaia, as well as new members in known clusters (particularly in the halos), binaries, peculiar objects, etc. Appropriate spectroscopic and possibly photometric follow-up of these targets will certainly be required, to fully characterize them.

Starting from these preliminary considerations, the discussion at the *TERTULIA* focused on a variety of different, but related aspects. A summary is given in the following sections.

What data are needed? When?

Observational data. There was a general consensus that, in order to complement Gaia, both accurate photometric (in the optical and near-infrared) and spectroscopic datasets are needed. Photometric monitoring surveys should also be considered. Stars in young clusters are photometrically variable at the level of one hundredth–one tenth of a magnitude; thus, if those variations cannot be characterized, having milli-mag accuracy in photometry would be useless. Whilst the agreed priority is on spectroscopy, if one can afford it, also photometric monitoring should hence be performed. This would indeed allow recovering good magnitudes, exploring variability, and getting rotation periods, that are much better than projected rotational velocities. To this aim, large telescopes are not needed and 1-1.5m class telescopes would be sufficient. There are several such telescopes around the world, some of them are robotic, and could be employed to monitor clusters.

As mentioned, the number of stars for which Gaia will deliver RVs is a small fraction (15%) of the stars that will have an astrometric measurement; hence, in principle, one would like to get as much spectroscopy as possible from the ground. Since this does not look feasible, everybody agreed that the size of the complementary datasets should instead follow from the science requirements. In other words, the requirement are in science, not in volume. Whilst some specific scientific issues would need relatively small samples, others would require a much more comprehensive dataset to supplement Gaia.

Science also should drive the requirements on the accuracy of the ground based data. After the required dataset is identified, one should then evaluate whether getting it is realistic or not and whether this requires adjustments of instrumentation and/or methods. Finally, the point was made that devoted instrumentation and specific telescopes, working for several years, both in the Northern and Southern hemispheres, would be needed to carry out these surveys. A community effort in that direction is encouraged.

As for the sample selection, complementary observational programs should initially be tuned on what is known before first Gaia releases -this is actually the strategy of the Gaia-ESO Survey (see below); then, one should build in the programmes as Gaia starts providing more information for the clusters. Even the first astrometric releases will provide proper motions allowing a huge improvement in membership knowledge of nearby clusters. This implies that, although final accuracies will not be reached before 2018, there will already be much information to exploit with intermediate data. In other words, the timescales for acquiring the complementary datasets should follow different steps, because Gaia is also going to produce more releases at different times. Some datasets from the ground (e.g., accurate RVs in

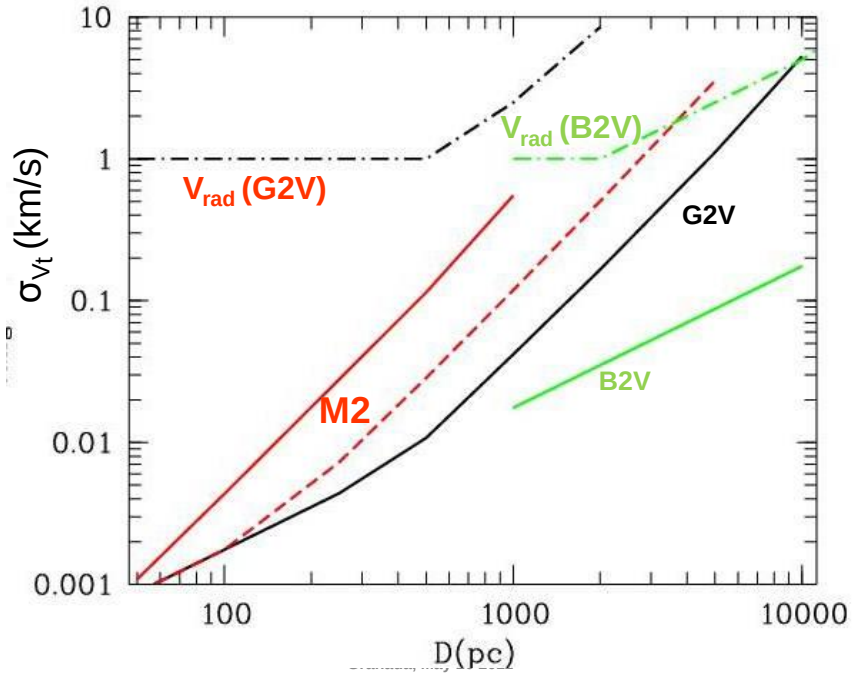

Figure 7.1: Expected accuracy in Gaia tangential velocities -from proper motions- as a function of cluster distance, for different stellar types. The green and black solid lines refer to a B2V and G2V spectral-types; the red solid and dashed lines instead represent a main-sequence and a few Myr old M2 stars, respectively. For comparison, dot-dashed lines instead denote the expected accuracy in radial velocity from Gaia for a B2V (green) and G2V (black) spectral-types.

the closest clusters) must be provided in the horizon of 2015 – 2016, while others can be done later.
Theoretical models. A complementary, but crucial aspect was addressed; namely, the need of theoretical models to interpret the data. Specifically, the point was made that updated and reliable stellar evolutionary models are required to interpret extremely accurate HR diagrams of clusters delivered by Gaia plus photometric and spectroscopic characterization. For example, without adequate stellar models, one cannot indeed derive stellar masses and ages. A sample of well characterized binaries, to calibrate the models, would also be very useful.

With respect to the second point it was stressed that Gaia will yield both astrometric and photometric binaries; therefore, calibration material will be largely available from Gaia already. As to stellar models, it was announced that there are concrete plans to publish a large set of updated Geneva models. These should be available within the next two years, will cover stellar masses from 0.5 to 120 $M_{\odot}$ as well as a large interval of metallicities, and will include non-standard processes, such as rotation, gravity waves, etc.

As discussed during several talks at the meeting, significant progress has been made in N-body simulations of clusters. Those simulations now just need to be compared to statistically significant, homogeneous, and reliable sets of data, providing both positions and velocities –the full 6D phase space– with comparable precisions.
Human and financial resources. During the discussion the concern was raised about the need of human resources to analyze and scientifically exploit both Gaia data and those coming from ground based surveys. Crucially, jobs both at the post-doc and higher level are needed. It was noted that in the US post-doc programs associated to space missions have been running since long, like e.g. the Hubble or Chandra Post-docs. The question was raised whether there would be any possibility to have Gaia post-docs. The answer is that ESA does not fund science, while member states should support the science exploitation. The GREAT network indeed represents a very good example of community organization in preparation to Gaia.

Following a specific question, the strategy and organization for the Gaia data analysis was briefly reviewed. It was stressed that we may learn from this, and that, hopefully, there should be a transfer of knowledge in handling of future ground based data.

Running surveys and future plans

A review of current ongoing photometric and spectroscopic surveys is given in the paper by Feltzing in these Proceedings. Specific surveys are also presented and discussed in the contributions by Bouy (Dance survey), Feltzing/Bragaglia (Gaia-ESO Survey), Drew (Galactic plane Hα surveys), Covet/James (LSST).

During the *TERTULIA* it was further noted that in the time frame of 2016 – 2017 a variety of large scale surveys, such as LSST, SkyMapper, VISTA, and UKIDSS, will provide photometry for most of the Gaia stars in the optical and near-infrared ranges, both in the Northern and Southern Hemispheres. Although these will certainly help, it seems however that higher accuracy surveys (at the milli-magnitude level) will still be needed to make full use of the Gaia data. Also, most of these surveys start at the 15^{th} magnitude, thus missing the information on the brighter stars in nearby open clusters. Whilst SkyMapper is planning a short integration survey that should reach the 6th magnitude, it won't cover the full Northern Hemisphere. Bright optical surveys making use of the five Sloan filters and allowing the coverage of the full range of magnitude, from 5th to 20th magnitude, seem desirable.

On the spectroscopic side, two very big surveys are currently underway, the combination of which have produced about 1.5 million spectra. Specifically, the RAVE survey has yielded good astrophysical spectra of bright stars. The other one, Segue, has also provided a very large number of spectra; they are of rather low resolution, and low signal-to-noise ratio, but nevertheless people are learning how to use and scientifically exploit them. Due to the uncertain funding situation, a longer-term continuation of RAVE is not guaranteed. Also, Segue follow-on is currently being discussed. It has to be noted, however, that none of these two surveys specifically focuses on clusters and on supplementing Gaia.

The Gaia-ESO Survey was discussed again. This survey, which will start in January 2012, includes an open cluster survey, specifically aimed to supplement Gaia, by providing very accurate RVs, astrophysical, and chemical characterization for cluster members down to the 19th magnitude in a sample of about 100 clusters. Noticeably, and at variance with other spectroscopic surveys, it will also include a large number of early-type stars. Sample selection in the Gaia-ESO Survey is done in a uniform manner, based on currently known information on membership. A significant fraction of the Gaia-ESO Survey will be completed by the time of the first release of Gaia data; this means that basic astrometry (positions, parallaxes, proper motions) and photometry will be available about within the same time scale as the products of the Gaia-ESO survey. This in turn will allow both the best scientific exploitation of the combined datasets and, at the same time, devising an optimal strategy for planning further spectroscopic surveys.

On the longer time-frame there are currently several proposals for wide field, high multiplex instruments, like BigBoss on the Mayall telescope. Even if not all, some of these proposals will be approved in the near future, will turn into reality, and will thus represent a great opportunity for Gaia follow-up.

Focusing on the European side of the planning, after a decade of work which included both the ESA-ESO planning and the ASTRONET decadal survey and Infrastructure Roadmap, spectroscopic surveys of stellar population are now recognized as the top science priority for the next generation on medium-size telescopes. There is indeed a series of government level commitments to achieve that. In particular, a design study is underway, funded by ESO and lead by AIP-Potsdam, for a wide field, massive spectroscopic capability (3 deg^2 FoV, 3000 fibers), to be put either on the NTT or VISTA. This instrument, 4MOST, should provide in a five year survey $\sim 10^6$ spectra with a resolution R $\sim 20,000$ down to V=16 magnitude and $\sim 20 \times 10^6$ spectra at R = 7,000 down to V = 20. There is indeed good probability that it will be operational in five years. Similarly, but for the Northern hemisphere, there is a proposal for the same type of instrument to be put on the WHT at La Palma. Noticeably, this should be jointly supported by all western national funding agencies.

To summarize, there are very good perspectives for massive spectroscopic surveys to occur in the long term ($\sim$ 10 yr) period. Most obviously, efforts should be made by the cluster community to ensure that open clusters are included in these surveys.

Acknowledgments

I would like to warmly thank all the participants who lively contributed to the discussion.

Chapter 8

Posters Contributions

8.1 An Aladin-Based Search for Proper-Motion Companions to Young Stars in the Local Association, Tucana-Horologium and β Pictoris

Francisco Javier Alonso-Floriano[1], J. A. Caballero[2], and D. Montes[1]

[1] Departamento de Astrofísica y Ciencias de la Atmósfera, Facultad de Física, Universidad Complutense de Madrid, E-28040 Madrid, Spain
[2] Centro de Astrobiología (CSIC-INTA), PO Box 78, E-28691 Villanueva de la Cañada, Madrid, Spain

Abstract

We have used the Aladin sky atlas of the Virtual Observatory to look for new common proper-motion pairs in three young stellar kinematic groups: Local Association ($\tau \sim 10$ – 120 Myr), Tucana-Horologium ($\tau \sim 30$ Myr) and β Pictoris ($\tau \sim 12$ Myr). We have found 9 new and 14 known common proper-motion companions to the 210 investigated stars. With the CAFOS instrument at the 2.2 m Calar Alto telescope, we have investigated in detail one of the new pairs, the HD 143809 AB system, which is formed by a bright G0V primary star and a previously unknown young M1.0–1.5Ve star.

Introduction

Young nearby late-type stars are excellent targets for high-contrast imaging surveys for brown dwarf and planetary companions. Many of these young low-mass stars in the solar neighbourhood belong to stellar kinematics groups with ages younger than the Pleiades, such as the Local Association and its kinematic subgroups (Montes et al. [2001b]; Song et al. [2003]; Zuckerman & Song [2004]). One way of identifying such stars is searching for faint proper-motion companions at wide separations to already-known members in young stellar kinematic groups.

We followed the procedure described by Caballero et al. [2010a] and used a powerful Virtual Observatory tool, the Aladin sky atlas (Bonnarel et al. [2000]), to look for proper-motion companions to stars in the Local Association (LA, $\tau \sim 10$ – 120 Myr), Tucana-Horologium (Tuc-Hor, $\tau \sim 30$ Myr) and β Pictoris (β Pic, $\tau \sim 12$ Myr) stellar kinematic groups.

Analysis

We searched for either primary (i.e., brighter) and secondary (i.e., fainter) companions to 210 nearby young stars in the three different moving groups compiled by Montes et al. [2001b] and Torres et al. [2008]: 116 in LA, 44 in Tuc-Hor, and 50 in β Pic. We used the interactive software Aladin v5 to load 2MASS (Skrutskie et al. [2006]) and USNO-B1 (Monet et al. [2003]) astro-photometric catalogues and cross-matched them in a circular area of radius 30 arcmin centred on each target. Next, we constructed a proper-motion diagram with the Aladin application VOPlot and searched for sources with USNO-B1 proper motions different from those of the target stars by less than 10 mas/yr.

For each proper-motion candidate, we searched the literature for previous claims of membership in multiple systems (e.g., the Washington Double Star catalogue; Mason et al. [2001]) and for better proper-motion determinations (e.g., Tycho-2; Høg et al. [2000]). We derived photometric distances for both primaries and secondaries, based on available spectroscopy or photometry, of the candidate pairs without parallactic distance measurements and discarded those with no coincident values.

Results

Of the 210 investigated stars, we identified 23 multiple system candidates, of which 14 were known common proper-motion companions and 9 were unknown multiple systems (see Table 8.1 and Fig. 8.1).

Table 8.1: The nine unknown proper-motion pairs (SKG indicates the stellar kinematic group).

Name	Sp. type	ρ [arcsec]	θ [deg]	s [kAU]	SKG
HD 82939	G5V	162.28 ± 0.17	121.49 ± 0.07	6.3 ± 0.2	LA
GJ 9303	K7V				
EX Cet	G5V	612.10 ± 0.11	258.66 ± 0.02	14.7 ± 0.3	LA
G 271–110	M3.5V				
HD 143809 A	G0V	86.40 ± 0.11	252.57 ± 0.09	7.1 ± 0.9	LA
HD 143809 B	M1.0–1.5V				
HD 13183	G7V	705.99 ± 0.10	103.761 ± 0.009	36.0 ± 1.2	Tuc-Hor
CD–53 413	G5V				
CD–53 544	K6Ve	22.06 ± 0.08	11.11 ± 0.17	0.93 ± 0.09	Tuc-Hor
AF Hor	M2Ve				
HD 207964 AB	F1III+...	1412.75 ± 0.11	245.020 ± 0.005	64.0 ± 1.9	Tuc-Hor
HD 207575	F6V				
HD 173167	F5V	550.31 ± 0.10	290.244 ± 0.011	29 ± 3	β Pic
TYC 9073–0762–1	M1Ve				
η Tel AB	A0Vn+M7.5V	416.26 ± 0.13	170.691 ± 0.012	20.1 ± 0.2	β Pic
HD 181327	F6V				
HD 199143 AB	F7V+...	325.04 ± 0.08	138.35 ± 0.02	14.8 ± 0.5	β Pic
AZ Cap	K6Ve				

One of nine of them was a suspected multiple system (η Tel AB and HD 181327; Schneider et al. [2006]). At the measured or derived distances, the angular separations of 0.37 to 24 arcmin translate into projected physical separations between 0.0045 and 0.31 pc. Interestingly, some of the proper-motion companions had already been tabulated as members in the same stellar kinematic group as their target stars (e.g., HD 207964 AB and HD 207575 in Tucana-Horologium).

One of the new multiple systems was formed by a young solar analogue and an anonymous high proper-motion red dwarf never described in the literature before, and was subject of a dedicated astrometric, photometric and spectroscopic follow-up study. First, we confirmed the common proper motion of the "HD 143809 AB" system using 11 astrometric epochs separated by over 56 years as in Caballero et al. [2010b]. Next, we collected B, V, R and I images and low-resolution spectra (grating G100) with the CAFOS instrument at the 2.2 m Calar Alto telescope. While the primary is a known G0V star with a high lithium abundance (EW(Li I) = 103 mÅ; López-Santiago et al. [2010]), an estimated age of $\tau \sim$ 80 – 120 Myr and kinematics consistent with membership in the Local Association Montes et al. [2001a], the new companion at $s = 7.1 \pm 0.9$ kAU is an M1.0–1.5Ve star with chromospheric Hα, Hβ and Hγ emission. The heliocentric distance derived from its spectral type and photometry matches the one of the primary measured by *Hipparcos* at $d = 78 \pm 8$ pc. Using this distance, its J-band apparent magnitude (J = 10.35 ± 0.03 mag) and the NextGen models (Baraffe et al. [1998]) for an age of 100 Myr, HD 143809 B has a most probable mass of 0.57 – 0.60 $M_\odot$.

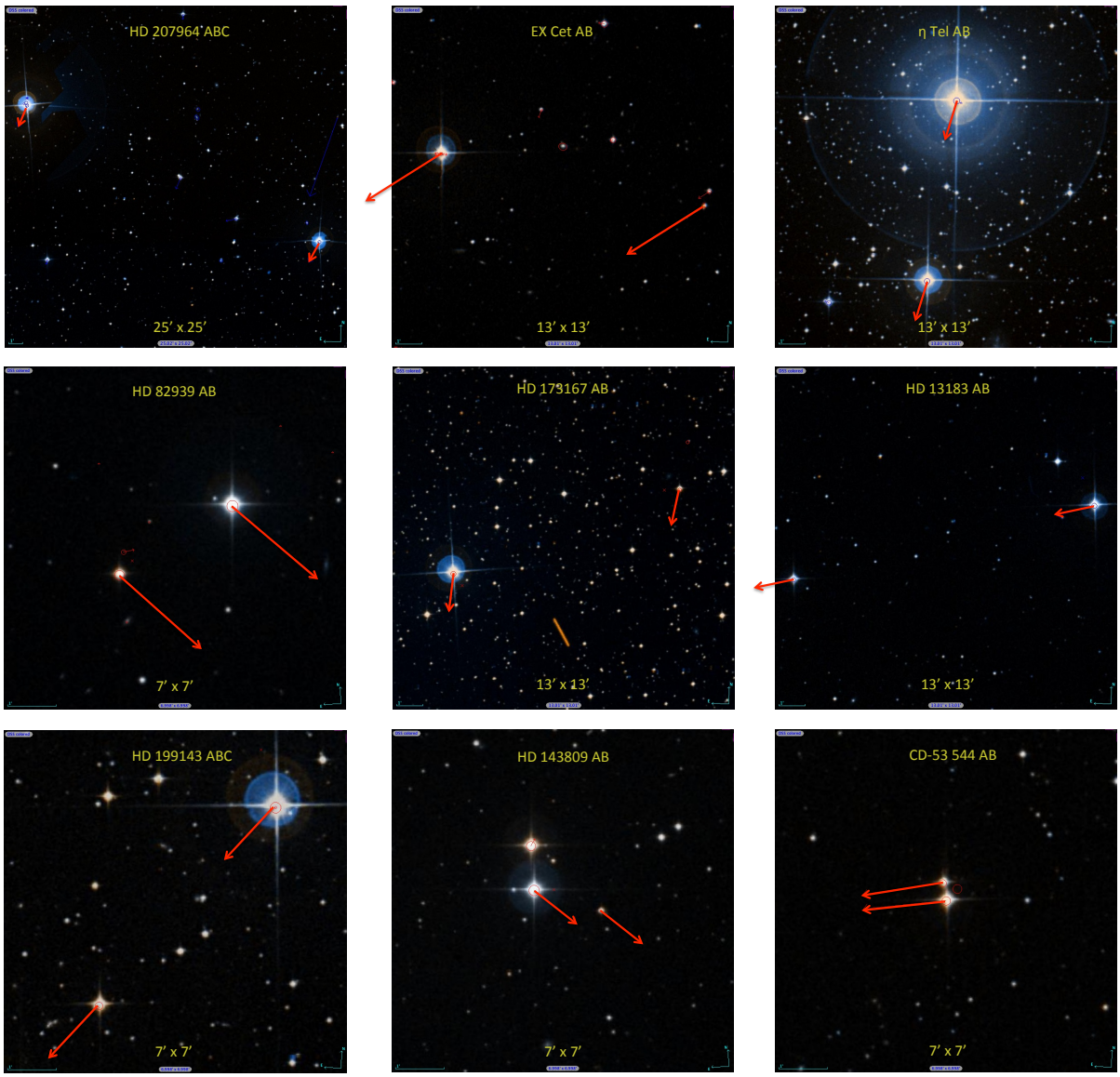

Figure 8.1: False-colour images combining DSS POSSII B_J, R_F and I_N photographic plates of the nine new pairs. Labelled are the multiple system names and field-of-view sizes. North is up and east is to the left. The red arrows show the proper motion.

Acknowledgments

We thank J. Genebriera for providing us unpublished images of the HD 143809 AB system. This research has made use of Aladin. This work is supported by the Universidad Complutense de Madrid, the Spanish Ministerio de Ciencia e Innovación (MICINN) under grant AYA2008-0695, and the Comunidad de Madrid under PRICIT project S2009/ESP-1496 (AstroMadrid).

Bibliography

Baraffe, I., Chabrier, G., Allard, F., & Hauschildt, P. H. 1998, A&A, 337, 403
Bonnarel, F., Fernique, P., Bienaymé, O., et al. 2000, A&A, 143, 33
Caballero, J. A., Miret, F. X., Genebriera, J., et al. 2010a, in Highlights of Spanish Astrophysics V, ed. J. M. Diego, L. J. Goicoechea, J. I. González-Serrano, & J. Gorgas, 379
Caballero, J. A., Montes, D., Klutsch, A., et al. 2010b, A&A, 520, A91
Høg, E., Fabricius, C., Makarov, V. V., et al. 2000, A&A, 355, L27
López-Santiago, J., Montes, D., Gálvez-Ortiz, M. C., et al. 2010, A&A, 514, A97

Mason, B. D., Wycoff, G. L., Hartkopf, W. I., Douglass, G. G., & Worley, C. E. 2001, AJ, 122, 3466
Monet, D. G., Levine, S. E., Canzian, B., et al. 2003, AJ, 125, 984
Montes, D., López-Santiago, J., Fernández-Figueroa, M. J., & Gálvez, M. C. 2001a, A&A, 379, 976
Montes, D., Lopez-Santiago, J., Galvez, M. C., et al. 2001b, MNRAS, 732, 45
Schneider, G., Silverstone, M. D., Hines, D. C., et al. 2006, ApJ, 650, 414
Skrutskie, M. F., Cutri, R. M., Stiening, R., et al. 2006, AJ, 131, 1163
Song, I., Zuckerman, B., & Bessell, M. S. 2003, ApJ, 599, 342
Torres, C. A. O., Quast, G. R., Melo, C. H. F., & Sterzik, M. F. 2008, Handbook of Star Forming Regions, Volume II: The Southern Sky, ASP Monograph Publications, Vol. 5, ed. Reipurth, B., 757
Zuckerman, B. & Song, I. 2004, ARA&A, 42, 685

8.2 Large-Scale Young Gould Belt Stars Across Orion

Katia Biazzo[1], J. M. Alcalá[1], M. F. Sterzik[2], E. Covino[1], A. Frasca[3], and P. Guillout[4]

[1] INAF - Capodimonte Astronomical Observatory
[2] European Southern Observatory (ESO) - Chile
[3] INAF - Catania Astrophysical Observatory
[4] Observatoire Astronomique de Strasbourg, CNRS, UMR 7550, France

Abstract

We report first results on the large-scale distribution of the ROSAT All-Sky Survey (RASS) X-ray sources in a 5000 deg^2 field centered on Orion. Our final aim is to study the properties of different widespread populations in the Orion Complex close to the Gould Belt (GB) in order to trace the star formation history in the solar neighbourhood.

Sample definition and candidate selection

We considered a $\sim$ 5000 deg^2 field centered on Orion and selected in this area $\sim$ 1500 young stellar object (YSO) candidates through X-ray criteria established by Sterzik et al. [1995]. We then selected a $\sim 10 \times 75$ deg^2 strip (see Fig. 8.2) perpendicular to the GB and crossing the Orion star-forming region (SFR), as well as a $\sim 10 \times 10$ deg^2 region at $\alpha = 5^{\rm h}34^{\rm m}$ and $\delta = +22^{\rm o}01'$ with enhanced X-ray space density. Some $\sim$ 200 stars inside the strip turn out to be YSO candidates (Fig. 8.2), while three stellar groups seem to have high X-ray space density: two of them are inside the strip, while the third one is close to $\alpha = 5^{\rm h}34^{\rm m}$ and $\delta = +22^{\rm o}01'$.

Observational data set and candidate characterization

Low-resolution spectroscopy ($R \sim 1\,000$) was obtained with the Boller and Chivens Cassegrain spectrographs attached to the 1.5m telescope of the ESO (Chile) and to the 2.1 m of the Observatorio Astronómico Nacional de San Pedro Mártir (Mexico). High-resolution spectroscopy ($R \sim 30\,000 - 100\,000$) was performed using the FOCES spectrograph attached to the 2.2 m telescope at the Calar Alto Observatory (Spain) and with the Coudé Echélle Spectrometer fed by the 1.5 m CAT telescope (Chile).

Using the low-resolution spectra, we determined spectral types (and effective temperatures) and detected the presence of Hα and lithium line. This allowed us to select very young not-accreting stars (accretion is mainly associated with stars in the Orion SFR). We thus find that all stars located in the Orion region possess lithium stronger than the Pleiades stars of the same spectral type; many of the stars located in the region of the GB have also a strong Li content, but tend to be more similar to that of the Pleiades; and the majority of the field stars have lithium weaker than the Pleiades. From the high-resolution spectroscopy we determined rotational and radial velocity and measured lithium abundance. Preliminary results show that stars in the strip are segregated in three populations: clustered stars in Orion, with ages of 2 – 5 Myr; non-clustered stars in the GB with ages of 5 – 10 Myr; field stars with a wide age spread; while, stars in stellar groups show ages $<$ 20 Myr.

Work in progress and Future perspectives with Gaia

Following the prescriptions given by Biazzo et al. [2011], we are measuring the metallicity of single stars with low $v \sin i$ and observed at high resolution. Two main preliminary results are the following: i) stars with high-Li content show a distribution in agreement with that of young nearby clusters, i.e. close to the solar one; ii) stars with no Li absorption show wide [Fe/H] values, which resemble the distribution of field stars in the solar neighbourhood.

Thanks to the future Gaia mission we will obtain parallaxes for our targets with a precision of 0.014 – 0.070 mas, which will translate into 1 – 7 pc at the Orion distance. This will allow us to derive

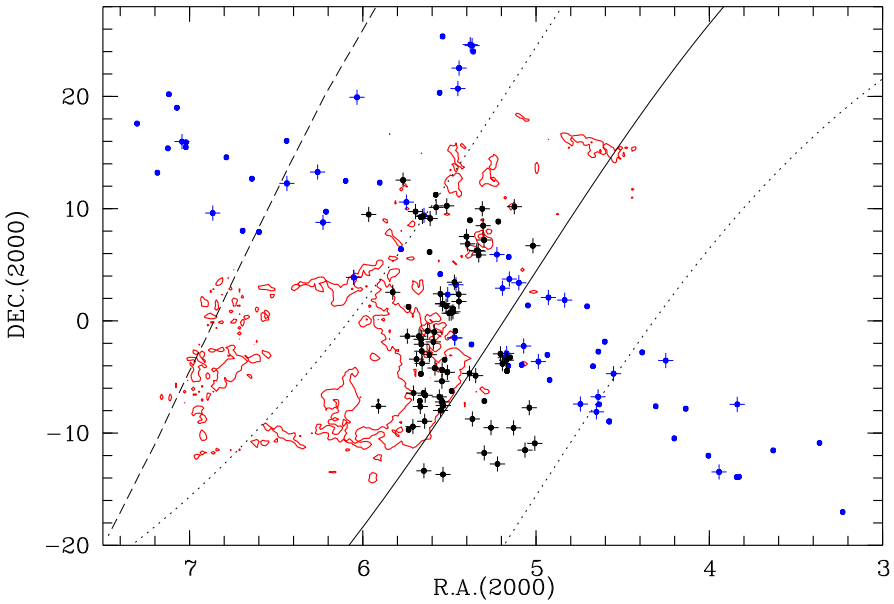

Figure 8.2: Large-scale spatial distribution of our targets in the strip and clumps observed at low and high resolution (blue symbols). The Alcalá et al. [2000] data are also shown with black symbols. Dots represent targets with low-Li content, while dots with crosses are stars with high-Li content. The positions of the three clumps are at ($\alpha = 5^{\rm h}34^{\rm m}$, $\delta = +22^{\rm o}01'$), ($\alpha = 5^{\rm h}07^{\rm m}$, $\delta = -03^{\rm o}20'$), and ($\alpha = 4^{\rm h}30^{\rm m}$, $\delta = -08^{\rm o}$). Solid and dotted lines represent the GB and its limits (Guillout et al. [1998]), while the dashed line represents the Galactic Plane. The CO emission map by Maddalena et al. [1986] is also overlaid in red.

the distance to the individual stars and to place them on the HR diagram with accuracy of 0.7 – 1.4% in $\log(L/L\odot)$. Therefore, Gaia will allow us to definitively establish the nature of the widespread population of young stars on a Galactic scale.

Bibliography

Alcalá, J. M., Covino, E., Torres, G. et al. 2000, A&A, 353, 186
Alcalá, J. M., Watcher, S., Covino, E. et al. 2004, A&A, 416, 677
Biazzo, K., Randich, S., Palla, F., Briceño, C. 2011, A&A, 530, 19
D'Antona, F., Mazzitelli, I. 1997, MSAIt, 68, 807
Guillout, P., Sterzik, M. F., Schmitt, J. H. M. M., Motch, C., Nauhäuser, R. 1998, A&A, 337, 113
Maddalena, R. J., Morris, M., Moscowitz, J., Thaddeus, P. 1986, ApJ, 303, 375
Soderblom, D. R., Jones, B. F., Balachandran, S. et al. 1993, AJ, 106, 1059
Sterzik, M. F., Alcalá, J. M., Nauhäuser, R., Schmitt, J. H. M. M. 1995, A&A, 297, 418

8.3 Observing Brown Dwarfs in the Magellanic Cloud Star-Forming Regions with the E-ELT

Annalisa Calamida[1], F. Comeron[2], and H. Zinnecker[3]

[1] Osservatorio Astronomico di Roma (INAF), Italy
[2] ESO
[3] NASA-Ames, USA

Abstract

We present the results of near-infrared imaging simulations of young star-forming regions in the Magellanic Clouds to be observed with the European Extremely Large Telescope (E-ELT). The simulated J, H, K-band images show that we should be able to obtain nearly complete samples of young brown dwarfs above the deuterium burning limit ($M > 13$ M$_{Jup}$) in low-mass star-forming regions in the Clouds. Moreover, very young giant planet-mass objects in the Clouds should be detectable with the E-ELT under favourable conditions.

Magellanic Cloud brown dwarfs in the E-ELT Design Reference Mission

One of the projects proposed as part of the E-ELT Design Reference Mission (DRM) is the determination of the low-mass luminosity function down to the giant planet-mass regime in low-metallicity star-forming regions of the Large Magellanic Cloud (LMC, $[Fe/H] = -0.33$ dex) and the Small Magellanic Cloud (SMC, $[Fe/H] = -0.75$ dex, Romaniello et al. [2008]). Typical low-mass star-forming regions of the solar neighbourhood, such as Lupus 3 or ρ-Ophiuchi, would subtend an angle of ~ 2" at the distance of the Clouds, thus being appropriate for Laser Tomography Adaptive Optic (LTAO) observations, which would provide nearly diffraction-limited, deep near-infrared (NIR) imaging of the whole stellar and sub-stellar content of the cluster. In order to explore the detectability of the lowest-mass objects we simulate very young clusters similar to those found in the solar vicinity, without massive stars ($M < 2$ M$_\odot$) able to significantly ionize the gas, as this would dramatically increase the NIR background brightness via free-free emission. The challenge of the observations is the high density of objects (~ 20 objects/arcsec^2) and the fact that the members of the star-forming region cover a wide range in magnitudes, from $K \sim 18$ to $K \sim 30$ mag.

We simulate J, H, K-band images assuming different zenith distance values, in order to assess how much the location of the telescope will influence the observations, and different instrument pixel scales and stellar densities. We assume a distribution of stellar masses drawn from Chabrier [2003] initial mass function truncated at 2 M$_\odot$. Stars are randomly distributed over the 2"×2" extent of the cluster and masses are transformed to J, H, K absolute magnitudes using a $t = 5$ Myr isochrone from Baraffe et al. [2003]. A distance modulus of 18.5 mag is added plus a random extinction for each star. Variable background is introduced in some cases. All the simulations are performed adopting the technical assumptions of the official DRM data base (http://www.eso.org/sci/facilities/eelt/science/drm/tech_data). Fig. 8.3 shows a composite J, H, K simulated image of a young star-forming region in the LMC.

We then perform crowded field photometry on the simulated images and compare the recovered luminosity function with the input one, in order to verify if giant planet-mass objects can be detected and measured with sufficient accuracy, i.e. $S/N > 5$ (see Fig. 8.4).

Conclusions

Our simulations show that nearly complete samples of young brown dwarfs above the deuterium burning limit ($M > 13$ M$_{Jup}$) can be obtained in the Magellanic Cloud low-mass star-forming regions with E-ELT, and even giant planet-mass objects may be detected if the cluster nebulosity is sufficiently faint.

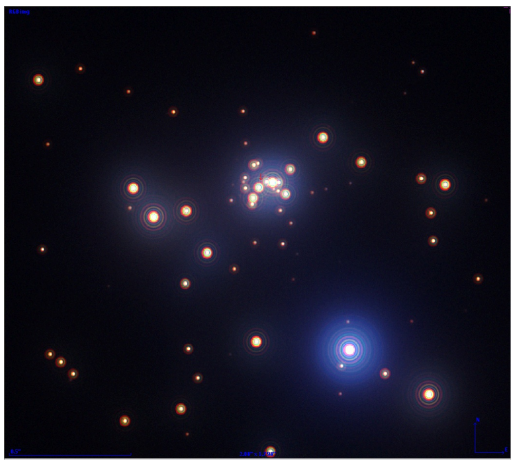

Figure 8.3: Composite J, H, K-band image of a low-mass star-forming region in the LMC, as observed with E-ELT and LTAO. 100 objects are simulated with masses in the range 5 $M_{Jup} < M < 2$ $M_\odot$, randomly distributed in a field of view of 2×2 arcsec^2 (0.5×0.5 pc^2).

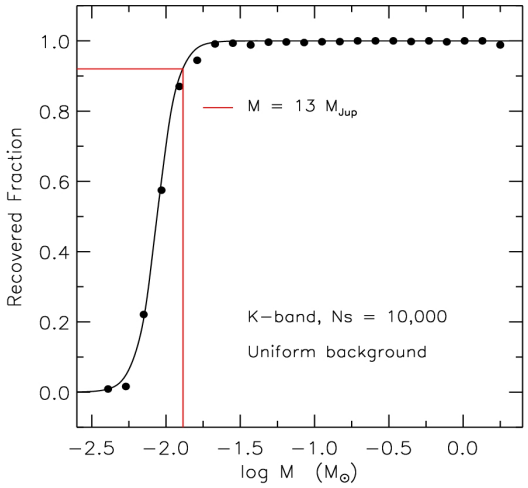

Figure 8.4: Recovered fraction of stars versus the input mass in steps of 0.12 $M_\odot$. The completeness function is overplotted as a solid line. The red line indicates the deuterium burning limit, $M = 13$ M_{Jup}, where the recovered fraction of objects is $\sim 90\%$.

Bibliography

Baraffe, I., Chabrier, G., Barman, T. S., Allard, F., & Hauschildt, P. H. 2003, A&A, 402, 701
Chabrier, G. 2003, PASP, 115, 763
Romaniello, M., Primas, F., Mottini, M., et al. 2008, A&A, 488, 731

8.4 Gaia's View of Clusters: A Case Study of R136 in the Large Magellanic Cloud

Jos H. J. de Bruijne[1] **and G. De Marchi**[1]

[1] Research and Scientific Support Department of the European Space Agency, Postbus 299, NL-2200 AG, Noordwijk, The Netherlands (jdbruijn and gdemarchi "at" rssd.esa.int)

Abstract

Gaia will observe thousands of open clusters in the galactic disk but will also reach clusters in the Magellanic Clouds. We present a case study of the massive cluster R136, the central ionising star cluster of the Tarantula nebula (30 Doradus) in the Large Magellanic Cloud (LMC). Through simulations using the on-board object-detection software in combination with a cluster membership list based on deep HST images, we find that, even in this massively crowded environment, Gaia detects stars down to $20^{\rm th}$ mag. The main sequence of the cluster, as well as the field-star red clump, are representatively sampled.

Summary

Fig. 8.5 shows an "image" of a Gaia (Lindegren et al. [2008]; de Bruijne et al. [2010]) astrometric AF2 CCD of the R 136 cluster, generated using the Gaia Instrument and Basic Image Simulator (GIBIS) based on a user-supplied source list. The latter is based on HST WFC3/UVIS images (6,848 seconds in F555W $\sim$ Johnson V and 10,656 seconds in F814W $\sim$ Cousins I) taken as part of the WFC3 Early-Release Science programme. The source list extracted from these images extends beyond $V = 25$ mag and contains 22,081 stars (De Marchi et al. [2011]). The associated object density is 11×10^6 stars deg^{-2}. The density of objects with $G < 20$ mag – the Gaia faint limit for astrometry and photometry – is 1.4×10^6 stars deg^{-2}. The source list has been extended – to 69,166 stars – with a representative background sample of stars to cover an area equal to the Gaia CCD height and spanning 4.0 sec of Gaia scanning time. The green boxes in Fig. 8.5 indicate 2,829 observation windows allocated by the on-board software for one particular transit of the field of view. Fig. 8.6 shows the completeness limit of Gaia as well as the colour-magnitude diagram of the observed sources. It is clear that, even in this uniquely crowded environment, Gaia will easily detect stars down to $20^{\rm th}$ magnitude. The cluster main sequence, and even field-star red clump giants, are representatively sampled down to the faint survey limit.

Acknowledgments

This work has made use of GIBIS, developed by Carine Babusiaux and collaborators within the Gaia Data Processing and Analysis Consortium and deployed by the Centre National d'Études Spatiales, as well as of the Gaia Video Processing Algorithms prototype, developed by EADS Astrium SAS. Carmen Blasco kindly provided support with running GIBIS and interpreting the results.

Bibliography

de Bruijne, J., Kohley, R., & Prusti, T. 2010, in Presented at the Society of Photo-Optical Instrumentation Engineers (SPIE) Conference, Vol. 7731, Society of Photo-Optical Instrumentation Engineers (SPIE) Conference Series

De Marchi, G., Paresce, F., Panagia, N., et al. 2011, ArXiv e-prints

Lindegren, L., Babusiaux, C., Bailer-Jones, C., et al. 2008, in IAU Symposium, Vol. 248, IAU Symposium, ed. W. J. Jin, I. Platais, & M. A. C. Perryman, 217–223

Panagia, N., Gilmozzi, R., Macchetto, F., Adorf, H.-M., & Kirshner, R. P. 1991, ApJ, 380, L23

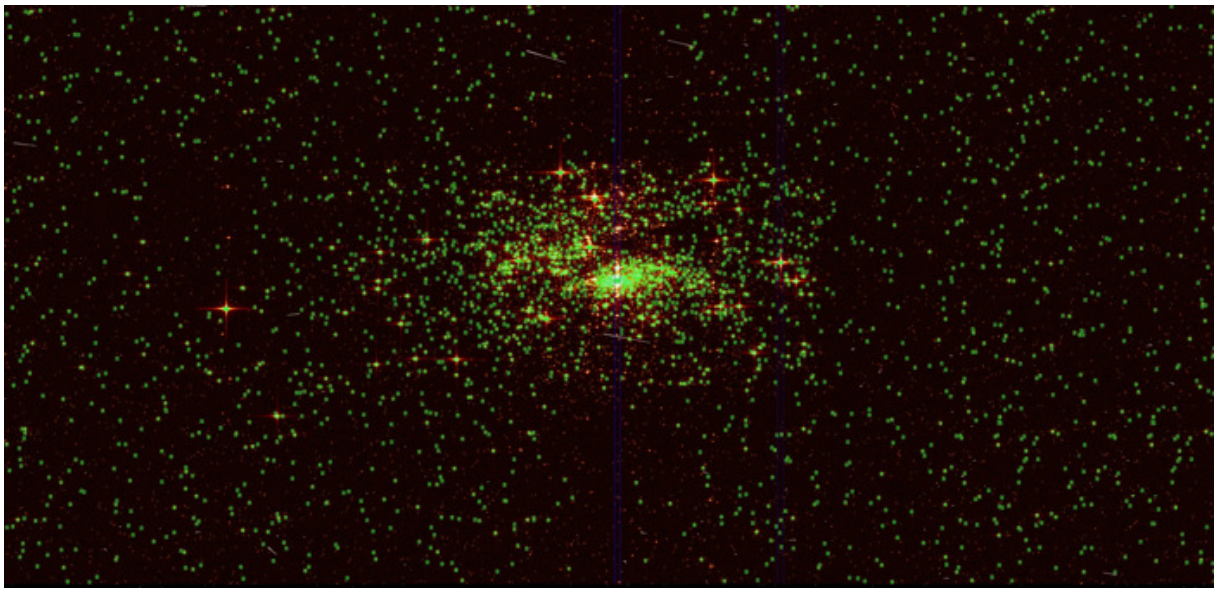

Figure 8.5: "Image" of a Gaia astrometric AF2 CCD of the R136 cluster and surroundings (the full-resolution version is available here). The image measures 240 × 350 arcsec^2, i.e., 1,966 across-scan Gaia pixels "vertically" – equal to a full CCD height – and 4,096 along-scan Gaia pixels "horizontally", corresponding to 4.0 sec of scanning time or $\sim$ 60 pc at the distance of the LMC (Panagia et al. [1991]). The green boxes indicate 2,289 observation windows allocated by the on-board software for one particular transit of the field of view. Gaia's two telescopes have non-rectangular apertures, with an aspect ratio 3:1. The associated point-spread function is matched by the non-rectangular pixels, which have an aspect ratio 1:3. The image renders non-rectangular pixels as square, which explains the "vertically" flattened shape of the cluster.

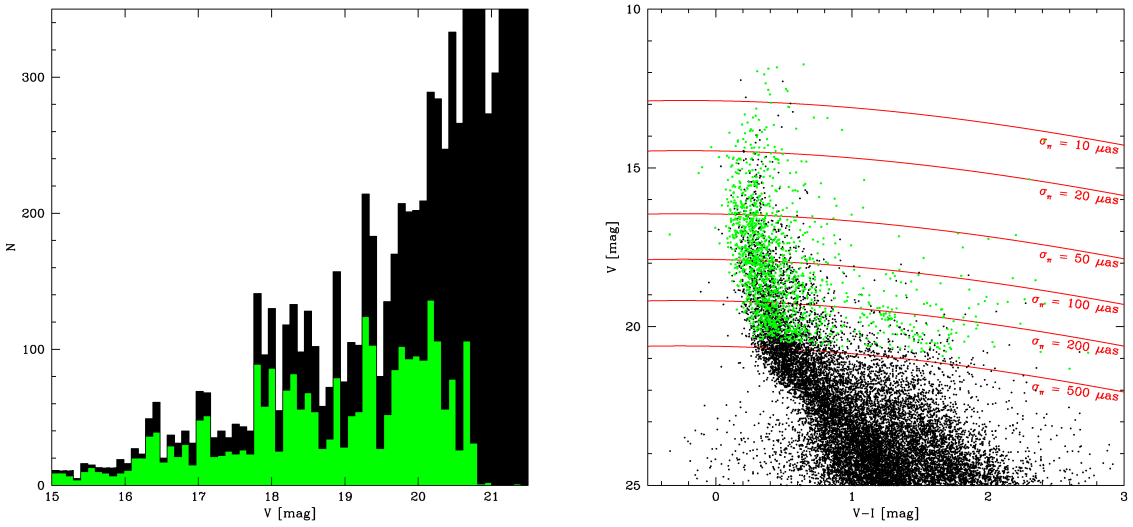

Figure 8.6: Gaia's on-board object-detection software successfully assigns observation windows to 2,829 sources, corresponding to a density of 437,000 stars deg^{-2}. The number of sources observed, however, is substantially larger as a result of close-bye companions which are contained in the windows albeit not counted in the number 2,829. *Left*: Johnson V magnitude histograms for all sources in the field (black) and for those stars which were assigned astrometric observation windows in the AF2 CCD (green) for one particular transit of the field of view. Gaia's on-board object-detection software operates in the Gaia white-light G band, which is redder than Johnson V. The Gaia faint limit $G = 20$ mag hence translates into a fainter limit in V for most (reddened) stars. The incompleteness for stars brighter than $G = 20$ mag is essentially caused by the extreme stellar density of the field. The completeness at the end of the five-year mission will be drastically improved since the ~ 70 transits of this field occur with different scanning orientations. *Right*: Johnson V versus Johnson V minus Cousins I colour-magnitude diagram showing all sources in the field (black) and those stars which were assigned astrometric observation windows in the AF2 CCD (green). The cluster main sequence is sampled down to $G = 20$ mag. Field red-clump giants – around $V = 20$ mag and dispersed between $V - I = 1$ and 2 mag due to differential reddening – are also reached by Gaia. The red lines indicate loci of constant end-of-mission parallax errors for individual stars. Typical annual-proper-motion errors are half the size of parallax errors. At the distance of the LMC, 10 μas yr^{-1} corresponds to 2 km/s.

8.5 Mining the Sky for "Isolated" Very Young Stars

Patrick Guillout[1], A. Frasca[2], D. Montes[3], F.-X. Pineau[1], A. Klutsch[3], E. Marilli[2], and N. Grosso[1]

[1] Observatoire Astronomique de Strasbourg, CNRS, UMR 7550, France
[2] INAF - Osservatorio Astrofisico di Catania, Italy
[3] Universidad Complutense de Madrid, Dpto. de Astrofísica, Spain

Abstract

Accreting young stars whose origin cannot be unmistakably linked to standard stellar birthplaces are extremely rare and also challenging candidates for the commonly accepted theory of stellar formation. We present preliminary results of optical observations conducted on "isolated" stars showing strong near- and far-infrared excesses that could be due to circumstellar discs. We acquired high-resolution optical spectra allowing us to investigate in detail their nature and physical parameters. We concluded that 5 of our targets are very young stars, with ages of around 10 Myr or even younger. They offer the opportunity to study the stage between transition and debris circumstellar discs and may help to shed new light on atypical formation processes of stars and planets in low-mass clouds.

Introduction

Accreting T Tauri stars (TTSs) whose origin cannot be unmistakably linked to standard stellar nurseries (i.e. in loose associations) are extremely rare. Discovering "isolated" very young stars with ages of around 10 Myr is extremely important for studying phenomena related to planet formation, especially in the gap between 3 and 50 Myr respectively covered by star-forming regions (SFRs) and open clusters near the zero-age-main sequence.
Thanks to statistical multivariate analysis methods, developed for the automatic classification of XMM-Newton X-rays sources (Pineau et al. [2011]), we have constructed the RASS-Stars catalogue (RSC). The RSC encompasses the RasTyc sample and extends it by a factor 3 or so, with good identification of active young stars down to $V = 18$ mag. Moreover, the correlation of the RSC with the AKARI/IRC mid-infrared (IR) all-sky survey (S9W filter) (Ishihara et al. [2010]) offers the opportunity to search for "isolated" and possibly accreting stars.

Searching for accreting "isolated" very young stars

We used colour-colour diagrams to select, a priori, young stellar objects from the cross-correlation of the RSC and AKARI catalogues. In the $(B-V)$ vs. $(V-S9W)$ diagram (Fig. 8.7, left panel), stars showing IR excess (red dots) which could originate from dust emission (see an example in Fig. 8.7, middle panel) are clearly visible on the right side of the major sequence. Among those ones with no reference in the literature, we identified 13 stars visible from the north hemisphere. Although some of them are close to known SFRs whose they could be accreting TTS members, a few of them are located in sky region devoid of dense interstellar matter. We also note that TW Hya and TYC4496-780-1 (Guillout et al. [2010]) were part of the selection, which makes us confident regarding the effectiveness of our selection method.

High-resolution optical spectra were acquired to discriminate young stars from older ones thanks to spectral features. Among the 13 field stars initially selected, 5 exhibit a large Hα emission profile and high-lithium abundance (see an example in Fig. 8.7, right panel) typical of TTSs. High-lithium content is now widely accepted as a youth criteria and according to the concept of the magnetospheric accretion model, the large Hα line width (several hundred km/s) is indicative of large-scale gas flow while the inverse P Cygni profile traces gas infall. They also show strong Hα variability like observed in TTSs. Based on these observational criteria, they are classified as likely accreting TTSs and their ages estimated to be 5 - 10 Myr. Although not strictly isolated, all are located several degrees apart from the cores of SFRs in their vicinity. Additional photometric observations will better constrain the SED. SED modelling will

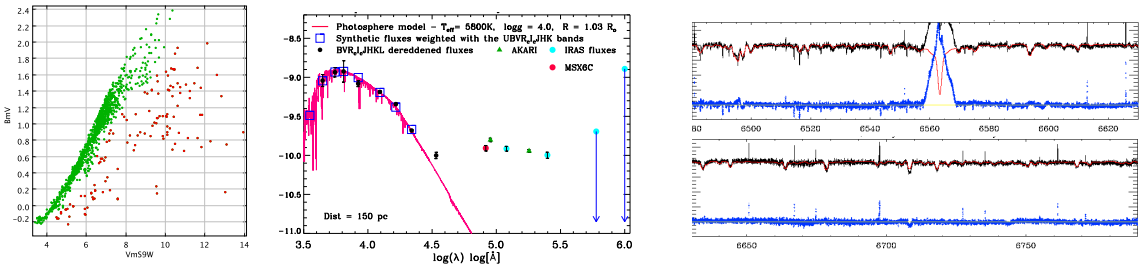

Figure 8.7: *Left panel*: 13 stars showing IR excess (red dots) were selected from colour-colour diagram. *Middle panel*: Spectral energy distribution (SED) for one of the targets. *Right panel*: High-resolution spectra in the Hα (upper panel) and Lithium (lower panel) regions. The blue line displays the spectrum resulting of subtraction of the synthetic star (red line).

then allow us to constrain the stellar parameters and the properties of the circumstellar disc, and derive an age from evolutionary tracks. Finally, the kinematics should shed light on their origin and possible relation with the closest SFRs, young associations or moving groups.

Bibliography

Pineau, F.-X., Motch, C., Carrera, F., et al. 2011, A&A, 527, A126
Ishihara, D., Onaka, T., Kataza, H., et al. 2010, A&A, 514, A1
Guillout, P., Frasca, A., Klutsch, A., et al., 2010, A&A, 520, A94

8.6 Origin of Extended Star Clusters

Narae Hwang[1]

[1] National Astronomical Observatory of Japan, Tokyo 181-8588, Japan

Abstract

We have discovered new extended star clusters (ESCs) in a nearby dIrr galaxy NGC 6822. These clusters are the nearest sample of ESCs available to date. The key characteristic of ESCs is their large size compared to typical globular clusters even though the two cluster populations are rather similar in terms of other parameters, i.e., colour and luminosity. Several scenarios have been suggested to explain the formation of ESCs. However, the currently known ESCs may be a mixture of populations with heterogenous formation histories. Future observational and theoretical studies are expected to better constrain the origins of ESCs as well as to increase their sample size.

Observational Characteristics of ESCs

ESCs are one of the new cluster populations being discovered with the advance of observational studies of star clusters. They are characterized by a relatively large size, that is, the half-light radii $R_h \gtrapprox 10$ pc, compared to typical globular clusters (GC) with $R_h \sim 2 - 3$ pc. Some examples may include faint fuzzy clusters discovered in SB0 type galaxies (Brodie & Larsen [2002]; Hwang & Lee [2006]) and extended clusters found in the halo of M 31 (Huxor et al. [2005, 2011]). Even in the Milky Way galaxy, there are rather extended GCs found in the outer halo (van den Bergh & Mackey [2004]). The ESCs in dwarf galaxies had not been known until the discovery of new ESCs in an isolated dIrr galaxy NGC 6822 (Hwang et al. [2005, 2011]). Those new ESCs in NGC 6822 are the nearest sample of ESCs available to date (D $\approx$ 500 kpc).

Another noteworthy characteristic of ESCs is their spatial distribution. It is shown that the ESCs in NGC 6822 are preferentially aligned along the old stellar halo that lies almost perpendicular to the HI disk like structure (see Fig. 8.8 in Hwang et al. [2011]). Faint fuzzy clusters in NGC 5195 and M 51 also exhibit elongated spatial distribution, which is not followed by red compact clusters (Hwang & Lee [2006, 2008]). This elongated distribution of ESCs is different from the one reported for faint fuzzy clusters in NGC 1023 that are usually found in the galaxy disk (Larsen & Brodie [2000]). For ESCs in M 31, no distinct spatial distribution is apparent. However, it is suggested that many ESCs in M 31 appear to be associated with stellar streams in the halo (Collins et al. [2009]; Huxor et al. [2011]).

Scenarios at the moment

Fig. 8.8 shows the correlations between R_h and M_V of various types of objects including GCs, LMC, UCDs (ultra compact dwarfs), DGTOs (dwarf globular transition objects), UFDs (ultra faint dwarfs), dSph galaxies, as well as ESCs in M 31, M 33, and NGC 6822. There are at least two important points to note. Firstly, ESCs are found in almost every type of galaxies ranging from dwarfs (e.g., NGC 6822, Scl-dE1) to giant spirals (e.g., M 31) and ellipticals (e.g., NGC 5128). Secondly, there are two subclasses of ESCs with different luminosity: one with $M_V < -9.4$ and the other with $M_V > -8.0$. The bright ESCs are found to occupy the common parameter space with UCDs or DGTOs, while the faint ESCs extend toward UFDs.

Various scenarios for the origins of those ESCs have been proposed and some reviews on each scenario and exemplary ESCs are given in Hwang et al. [2011]. A brief summary is as follows: (1) Remnants or cores of tidally stripped dwarf galaxies may form ESCs. (2) Collisions of two or more star clusters in star cluster complexes or super-star clusters may make ESCs. (3) Star clusters are born in various sizes and some ESCs may survive the disruption under the weak tidal field. (4) Another scenario very recently pointed out by Gieles et al. [2011] is that slow expansion of initially compact clusters under

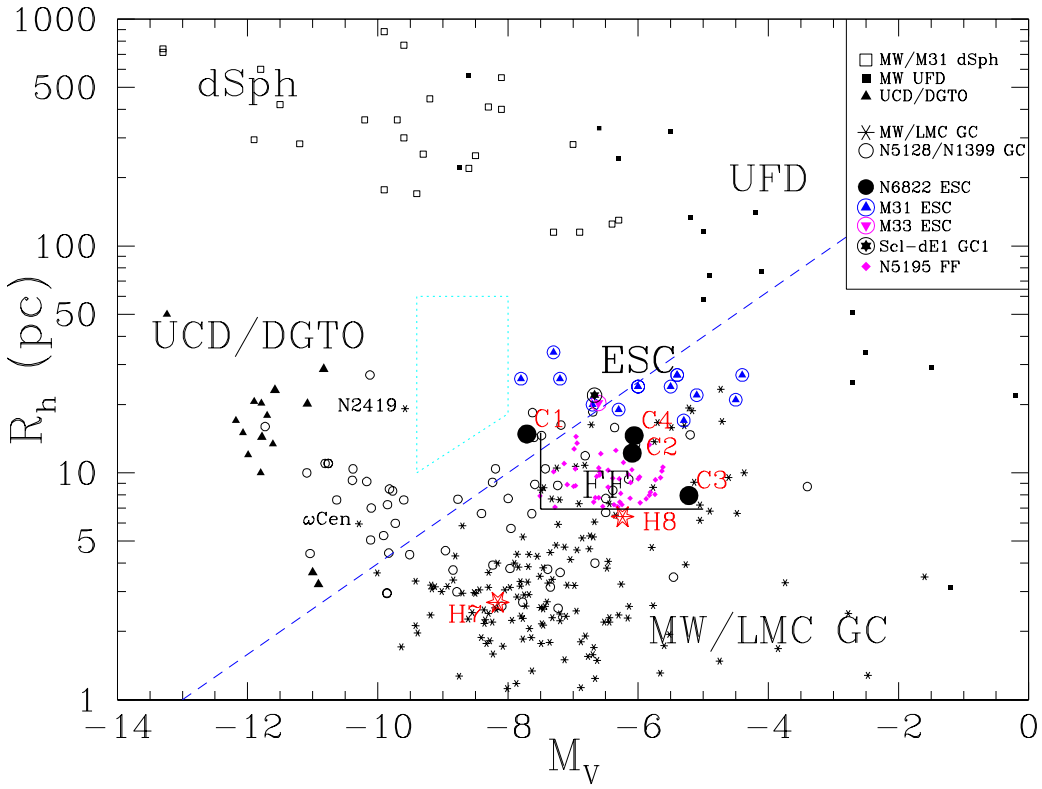

Figure 8.8: M_V vs. half light radii (R_h) diagram of GCs including the Galactic GCs and LMC GCs (van den Bergh & Mackey [2004]), ESCs including M 31 ESCs (Huxor et al. [2005, 2011]), M 33 ESC (Stonkutė et al. [2008]), Scl-dE1 ESC (Da Costa et al. [2009]) as well as NGC 6822 ESCs (Hwang et al. [2011]). Bright and faint ESCs are separated by a box in dotted lines at the center. Please refer to Hwang et al. [2011] for more details.

the tidal field may have produced ESCs whose size evolution can be explained by adopting a line of constant relaxation time in the mass-radius diagram.

Usually, bright ESCs could be the remnant of disrupted dwarf galaxies or the multiple star cluster collisions, while faint ESCs may have evolved under the optimal tidal field to survive or to expand to their current forms. But no observational evidence is available yet to justify such dichotomy and/or to prefer any scenario over the others. However, every scenario involves the tidal interactions and/or mergers on the scale of star clusters or galaxies that should be the major physical drivers that make ESCs.

For the better understanding and clarification of the ESCs and their possible use for the galaxy evolution studies, future observations with improved photometric depth and spectral resolution as well as wider spatial coverage are required. In view of this expectation, Gaia will play a crucial role to survey even more ESCs in the Milky Way and to reveal their true nature and origin.

Acknowledgments

I acknowledge invaluable collaborations with Myung Gyoon Lee, Hong Soo Park, Won-Kee Park, and Sang Chul Kim in the course of the study on ESCs in NGC 6822. I also thank Mark Gieles for bringing my attention to the cluster relaxation and expansion for the ESC formation.

Bibliography

Brodie, J. P. & Larsen, S. S. 2002, AJ, 124, 1410
Collins, M. L. M., Chapman, S. C., Irwin, M., et al. 2009, MNRAS, 396, 1619
Da Costa, G. S., Grebel, E. K., Jerjen, H., Rejkuba, M., & Sharina, M. E. 2009, AJ, 137, 4361
Gieles, M., Heggie, D. C., & Zhao, H. 2011, MNRAS, 413, 2509
Huxor, A. P., Ferguson, A. M. N., Tanvir, N. R., et al. 2011, MNRAS, in press (arXiv:1102.0403)

Huxor, A. P., Tanvir, N. R., Irwin, M. J., et al. 2005, MNRAS, 360, 1007
Hwang, N. & Lee, M. G. 2006, ApJ Letters, 638, L79
Hwang, N. & Lee, M. G. 2008, AJ, 135, 1567
Hwang, N., Lee, M. G., Lee, J. C., et al. 2011, ApJ, in press (arXiv:1106.2878)
Hwang, N., Lee, M. G., Lee, J. C., et al. 2005, in IAU Colloq. 198: Near-fields cosmology with dwarf elliptical galaxies, ed. H. Jerjen & B. Binggeli, 257–258
Larsen, S. S. & Brodie, J. P. 2000, AJ, 120, 2938
Stonkutė, R., Vansevičius, V., Arimoto, N., et al. 2008, AJ, 135, 1482
van den Bergh, S. & Mackey, A. D. 2004, MNRAS, 354, 713

8.7 The First Multi–Colour Photometry of Three ASCC Clusters

Evrim Kiran[1,*] **and G. Taş**[1]

[1] Ege University, Science Faculty, Astronomy and Space Science Department, Bornova - İzmir, Türkiye

Abstract

In this work, we present the first comprehensive photometry of the three open clusters (ASCC 31, 111 and 112) listed in the open clusters catalogue published by Kharchenko et al. [2005]. Plotting the data in colour-magnitude and colour-colour diagrams, and using the main sequence fitting method we estimated the distance modules of 9.3, 10.62 and 9.7 and the distances 724, 1330 and 871 pc for ASCC 31, ASCC 111 and ASCC 112 clusters, respectively. Using theoretical isochrones taken from related literature (e.g. Schaerer et al. [1993]; Mowlavi et al. [1998]; Schaller et al. [1992]) we computed the ages as follows; in the order mentioned above log (t) = 9.14, 6.09 and 8.00 of these open clusters.

Introduction

Kharchenko et al. [2005] revealed that some star groups which seem dispersed in the sky actually likely constituted a star cluster combining Hipparcos photometry with all catalogue data given in the literature on proper motion, radial velocity and position studies, and they published a new open cluster catalogue. This catalogue contains 130 clusters listed together with their kinematics and photometric parameters. In this study, we present the results of our photometric study of three open clusters, namely ASCC 31, ASCC 111 and ASCC 112, listed in this new catalogue. The galactic and equatorial coordinates of these clusters taken from the open cluster database WEBDA[1] are listed in Table 8.2.

Table 8.2: The galactic and equatorial coordinates of three open clusters observed for this work.

Cluster	b (∘)	l (∘)	RA (2000) (h, m, s)	DEC (2000) (∘, ′, ″)
ASCC 31	210.89	+3.69	07 00 53	+03 30 00
ASCC 111	74.26	+2.08	20 11 13	+37 27 00
ASCC 112	87.47	+9.30	20 16 26	+52 05 59

These three open clusters were observed at the Ege University Observatory using the 40-cm MEADE LX200 GPS Schmidt-Cassegrain telescope and Apogee Alta-U42 2048 × 2048 CCD in BVRI filters. The total field of view is $27.65 \times 27.65\ mm$ ($764.4\ mm^2$). The reductions of the CCD images were made by using MaXimDL program. SA 98 and SA 109 standard areas from Landolt [1992] were used for the standard calibration of the cluster data.

Results and Discussions

The colour-colour diagrams (CCDs) and colour-magnitude diagrams (CMDs) were used to estimate the photometric parameters of the clusters and to determine their new possible members. The stars which have the same colour excess were adopted as other possible members of cluster. After that, we determined the total absorption using $R = A_V/E(B-V) = 3.1$ given by Fitzpatrick [1999]. The distance moduli of the clusters were determined by using the main sequence fitting method. Then, we calculated the average distance moduli for ASCC 31, ASCC 111 and 112 as $(m_0 - M)_V$ = 9.3, 10.62 and 9.7, respectively, and also the distances of the clusters were estimated as d = 724, 1330 and 871 pc in the same order mentioned above using the distance module equation, $(m_0 - M)_V$= -5 + 5 log d.

*e-mail: evrimkiran@mail.ege.edu.tr

[1] http://www.univie.ac.at/webda/navigation.html

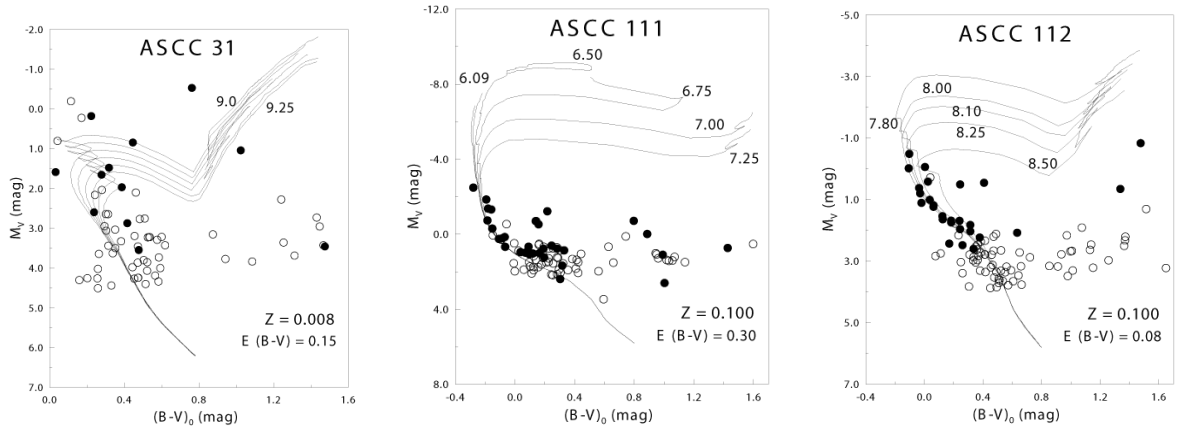

Figure 8.9: The best isochrones for ASCC 31, ASCC 111, and ASCC 112 are shown here. The isochrones are labelled in log age (yr). Z amd E(B-V) refer to metallicity and reddening of the clusters.

We tried to estimate the ages of clusters included in this study using isochrones for a wide range mass and metallicity taken from Schaller et al. [1992], Schaerer et al. [1993], Mowlavi et al. [1998]. Later, we searched for the most suitable fits trying isochrones with different metallicities for this age range. The best match for ASCC 31 was achieved for the values of Z = 0.008 and log (t) = 9.14. The same procedure was carried out also for ASCC 111 and ASCC 112, and the best fits for an age and metallicity were accomplished with the values of log (t) = 6.09, Z = 0.10, and log (t) = 8.00, Z = 0.10, respectively. Fig. 8.9 shows the best combinations with the observational data.

Table 8.3: Estimated parameters for the clusters ASCC31, ASCC 111, and ASCC112

Cluster	$(m-M)_0$ (mag)	Distance (pc)	Age ($\times 10^6$ years)	Reference
ASCC 31	9.30	724	1 380	This work
	9.36	600	427	Kharchenko et al. [2005]
ASCC 111	10.62	1330	1.23	This work
	11.95	1600	11	Kharchenko et al. [2005]
ASCC 112	9.70	871	126	This work
	8.95	550	141	Kharchenko et al. [2005]

The parameters derived in this study are listed in the Table above with the corresponding literature values for comparison. As seen in Table 8.3, there are some differences between our results and the literature. We made a comparison between the isochrones that we used and suitable isochrones for parameters given by Kharchenko et al. [2005] in Fig. 8.9 to better understand what causes the differences. The reason of these differences might be that our study is not limited to the observational data published in the literature and that availability of multi-colour photometric data of many stars in a wide region in sight of view presents an observational opportunity to find out the new cluster members. This means, we obtained a main sequence whose limits are specified well by using the stars observed in a wide magnitude and spectral type range and thus a more complete cluster CMD.

When we examine CCDs and CMDs, we can see that there have been many stars which have the same photometric features and which settled in diagrams in conformity with the members listed by Kharchenko et al. [2005]. Unfortunately, there are no kinematics studies or radial velocity measurements for these stars. It is an important issue to study radial velocities of these possible members. On the other hand, the spectroscopic determination of metallicities, temperatures, and luminosity class of these objects is necessary for a comparison with our photometric results.

Acknowledgments

This study was supported by the project of 2007/FEN/015. The authors would like to thank the staff of Ege University Observatory for their help during observation nights.

Bibliography

Fitzpatrick, E. L. 1999, PASP, 111, 63
Kharchenko, N. V., Piskunov, A. E., Röser, S., Schilbach, E., Scholz, R.-D. 2005, A&A, 440, 403
Landolt, A. 1992, AJ, 104, 340
Mowlavi, N., Schaerer, D., Meynet, G., Bernasconi, P. A., Charbonnel, C., Maeder, A. 1998, A&AS, 128, 471
Schaerer, D., Meynet, G., Maeder, A., Schaller, G. 1993, A&AS, 98, 523
Schaller, G., Schaerer, D., Meynet, G., Maeder, A. 1992, A&AS, 96, 269

8.8 The Field of Lodén 112

Nadejda Kaltcheva[1] and V. Golev[2]

[1] Department of Physics and Astronomy, University of Wisconsin Oshkosh, 800 Algoma Blvd., Oshkosh, WI 54901, USA (kaltchev@uwosh.edu)
[2] Department of Astronomy, Faculty of Physics, St Kliment Ohridski University of Sofia, 5 James Bourchier Blvd., BG-1164 Sofia, Bulgaria (valgol@phys.uni-sofia.bg)

Abstract

Based on the available $uvby\beta$ photometry of OB stars in the longitude range 281° to 285° in the Galactic disk, we identify a feature of young stars at 1630±82 pc, that is probably connected to the compact cluster candidate Lodén 112 and the open cluster IC 2581. This feature seems to be spatially correlated to RCW 48 and RCW 49 and several other smaller HII regions.

Introduction

The field between the OB groups in Vela ($262° < l < 268°$) and Car OB1 ($284° < l < 288°$) is not known to be dominated by any prominent OB association (see Humphreys [1978], Melnik & Efremov [2006]). The longitude range 283° - 284° is thought to correspond to a tangential direction of a large segment of the Carina arm in both the 3- and 4-arm models of the grand design of the Milky Way (Russeil [2003]). Our study is based on $uvby\beta$ photometric distances and provides new insights on the apparent groupings and layers toward $281° < l < 285°$ in the Galactic disk. This field clearly stands apart from the extended HII features toward Car OB1 and contains several prominent HII regions.

Results

Our sample includes a number of OB stars with very similar luminosities according to the $[c_1]$ vs. $[m_1]$ classification diagram (Stromgren [1966]) (Fig. 8.10, left). Among them, 5 stars belong to the poor but very compact cluster candidate Lodén 112. Two other stars are assigned to the relatively young cluster IC 2581, and the rest are apparent field stars. According to the $uvby\beta$ photometric distances all OB stars in this sample show a very small spread in distance, thus forming a structure at 1630 ± 80 pc. This new estimate is significantly smaller than the presently adopted distance of 2500 pc to Lodén 112 (WEBDA database). These OB-stars are located toward the prominent HII regions RCW 48 and RCW 49 and several smaller HII fields and could represent a new OB association at coordinates $282° < l < 285°$, $-2° < b < 2°$ (Fig. 8.10, right), containing the compact cluster candidate Lodén 112 and IC 2581 (more details can be found in Kaltcheva & Golev [2011]).

Acknowledgments

This work is supported by the National Science Foundation grant AST-0708950. N.K. acknowledges support from the SNC Endowed Professorship at the University of Wisconsin Oshkosh. V.G. acknowledges support by the Bulgarian National Science Research Fund grants DO 02-85/2008 and DO 02-362/2008. This research has made use of the SIMBAD database, operated at CDS, Strasbourg, France. We acknowledge the use of NASA's *SkyView* facility (http://skyview.gsfc.nasa.gov).

Bibliography

Finkbeiner, D. P. 2003, ApJS, 146, 407
Humphreys, R. M. 1978, AJSS, 38, 309
Kaltcheva, N., & Golev, V. 2011, in preparation

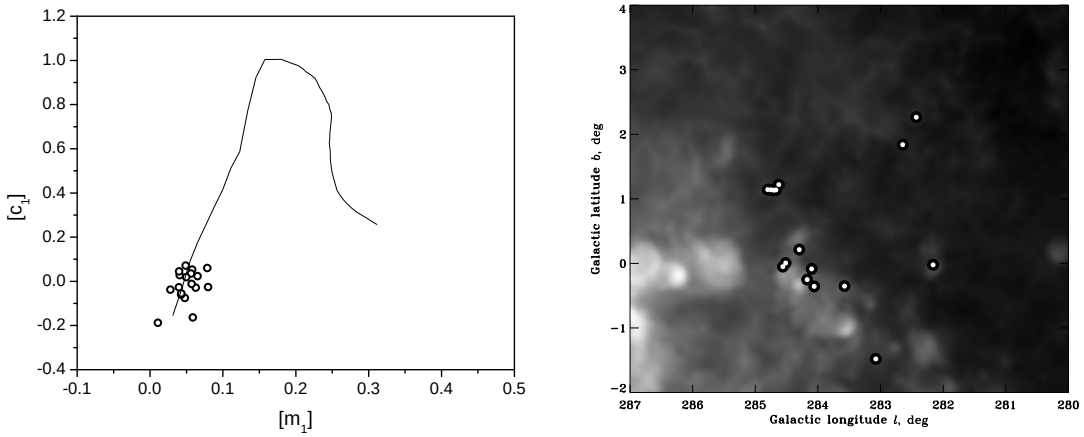

Figure 8.10: *Left*: the classification photometric diagram for the OB stars in the sample. *Right*: same stars overplotted on the distribution of the HII emission in the region Finkbeiner [2003] obtained via *SkyView* VO interface (McGlynn et al. [1998]).

McGlynn, T., Scollick, K., White, N. 1998, in *New Horizons from Multi-Wavelength Sky Surveys*, Proc. of the 179th Symp. of the IAU, held in Baltimore, USA Aug 26-30, 1996, Kluwer Academic Publishers, edited by B. J. McLean, D. A. Golombek, J. J. E. Hayes, & H. E. Payne, p. 465

Melnik, A. M., & Efremov, Yu. N. 1995, AstL, 21, 10

Russeil, D. 2003, A&A, 397, 133

Strömgren, B. 1966, ARA&A, 4, 433

8.9 Young Stars Towards the CO Cepheus Void

Alexis Klutsch[1], D. Montes[1], P. Guillout[2], A. Frasca[3], F.-X. Pineau[2], N. Grosso[2], E. Marilli[3] and J. López Santiago[1]

[1] Universidad Complutense de Madrid, Dpt. de Astrofísica, Facultad C.C. Físicas, Spain
[2] Observatoire Astronomique de Strasbourg, CNRS, UMR 7550, France
[3] INAF - Osservatorio Astrofisico di Catania, Italy

Abstract

[a] Once mixed in the galactic plane stellar population, young stars are virtually indiscernible from older ones. In the *RasTyc* sample, we nevertheless discovered 4 lithium-rich field stars that are located within a few degrees from each other on the celestial sphere and near the *Cepheus-Cassiopeia* complex. They form a homogeneous group of T Tauri stars. To discover some new comoving companions, we selected optical counterparts of ROSAT All-Sky Survey X-ray sources cross-identified with late-type stars around these 4 young stars thanks to multivariate analysis methods. Our recent intermediate- and high-resolution spectroscopic observations of this sample allowed us to discover additional lithium-rich sources. From the analysis of their spectra, we found that 6 of our young star candidates have similar physical and kinematical properties as those of the 4 comoving T Tauri stars. Moreover they are all located inside or close to the CO Cepheus void. They have properties rather similar to those of members of the TW Hydrae association, although they are slightly older and placed in the northern hemisphere. These young stars in the field are of great importance to give new insight into the process of stellar formation outside standard star-forming regions.

[a]The printed version of the poster presented during this workshop is available at this URL.

Introduction

Guillout et al. [2010] discovered a group of four comoving T Tauri stars (TTS) towards the *Cepheus-Cassiopeia* complex. Although this sky area is rich in CO molecular regions and dark clouds, the stars are projected in front of a region devoid of interstellar matter. Klutsch et al. [2010] selected 162 *young star candidates* to search for new members of this group. We also included all TTS discovered by Tachihara et al. [2005] located in this region to determine their kinematics and find a possible connection with ours.

Preliminar results

We identified 24 sources displaying a strong lithium line. We applied the ROTFIT code (Frasca et al. [2006]) to estimate astrophysical parameters. Using the spectral subtraction technique, we measured their lithium equivalent width, EW(Li), from the residual spectrum obtained with ROTFIT. Till now, 8 targets have an EW(Li) higher than that of Pleiades cluster stars (Fig. 8.11, left panel). We derived kinematics of all lithium-rich sources (Fig. 8.11, right panel). Among them, 6 sources are good young comoving candidates, 5 of which are located in the CO Cepheus void. That seems to confirm the existence of a link between the TTS discovered towards this region, where 15 stellar X-ray sources turn to be rich in lithium.

Acknowledgments

This work was supported by AstroMadrid (CAM S2009/ESP-1496), Universidad Complutense de Madrid, and the Spanish Ministerio de Ciencia e Innovación (MICINN) under grants AYA2008-00695 and AYA2008-06423-C03-03. Part of this study is supported by the Italian Ministero dell'Istruzione, Università e Ricerca (MIUR), and the Région Alsace.

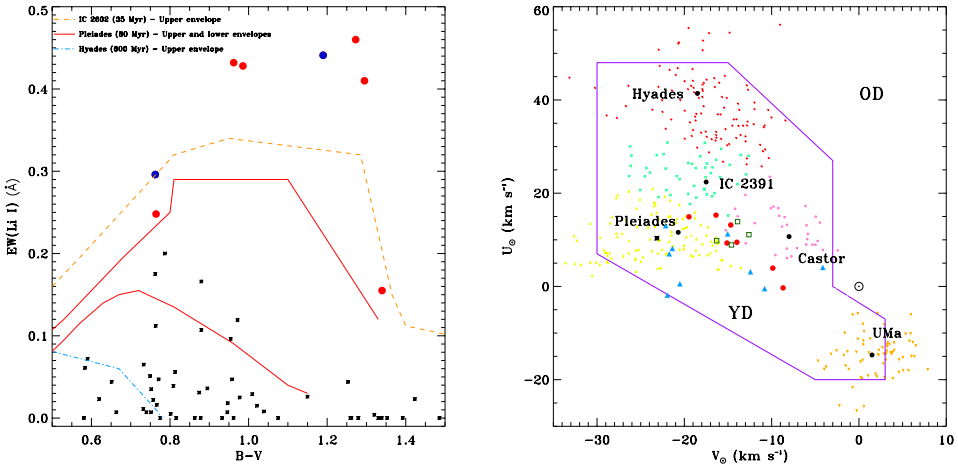

Figure 8.11: *Left panel*: Li I λ6707.8 line equivalent width versus $B-V$ colour index for the selected sources. 6 of our candidates (red circles) and 2 Tachihara's TTS (blue circles) are above the Pleiades lithium upper envelope. *Right panel*: U-V kinematic diagram for all our lithium-rich candidates. The stars for which we already derived the astrophysical parameters are showed with red circles. We use blue triangles and open squares for the remaining candidates and the original TTS, respectively.

Bibliography

Frasca, A., Guillout, P., Marilli, E., et al. 2006, A&A, 454, 301
Guillout, P., Frasca, A., Klutsch, A., Marilli, E., & Montes, D. 2010, A&A, 520, A94
Klutsch, A., Montes, D., Guillout, P., et al. 2010, ArXiv e-print: 1012.1979
Tachihara, K., Neuhäuser, R., Kun, M., & Fukui, Y. 2005, A&A, 437, 919

8.10 Stellar Clusters in M 31 from PHAT: Comparing Young Cluster Properties using UV and Resolved Stars

Jacob Simones[1], J. Dalcanton[2], A. Dolphin[3], L. C. Johnson[2], A. C. Seth[4], E. Skillman[1], D. R. Weisz[2], B. Williams[2], and the PHAT Collaboration

[1] Minnesota Institute for Astrophysics, 116 Church Street SE, Minneapolis, MN 55455, USA
[2] Department of Astronomy, Box 351580, University of Washington, Seattle, WA 98195, USA
[3] Raytheon, 1151 E. Hermans Road, Tucson, AZ 85706, USA
[4] Harvard-Smithsonian Center for Astrophysics, 60 Garden Street, Cambridge, MA 02138, USA

Abstract

The Panchromatic Hubble Andromeda Treasury (PHAT) offers a rich set of multi-wavelength observations with which to study the resolved stellar populations of clusters in M 31. We present colour-magnitude diagrams (CMDs) of young clusters and measure integrated near-ultraviolet (NUV) fluxes from GALEX imaging. We briefly discuss plans to determine cluster ages and masses through CMD analysis leading to NUV flux estimates.

Introduction, Science Progress, and Future Work

The Panchromatic Hubble Andromeda Treasury (PHAT) is a program to observe a large portion of M 31 with the Hubble Space Telescope for more than 800 orbits (Dalcanton [2011], in preparation; Johnson [2011], in these proceedings). This multi-wavelength survey (ultraviolet through the near-infrared) includes optical coverage by the Advanced Camera for Surveys in the F475W and F814W filters, with which we are able to resolve individual members of clusters in the disk of M 31. By analyzing the colour-magnitude diagrams (CMDs) of these clusters, we will be able to determine their ages and masses, which will then lead to estimates of integrated ultraviolet fluxes. We present our progress toward this goal.

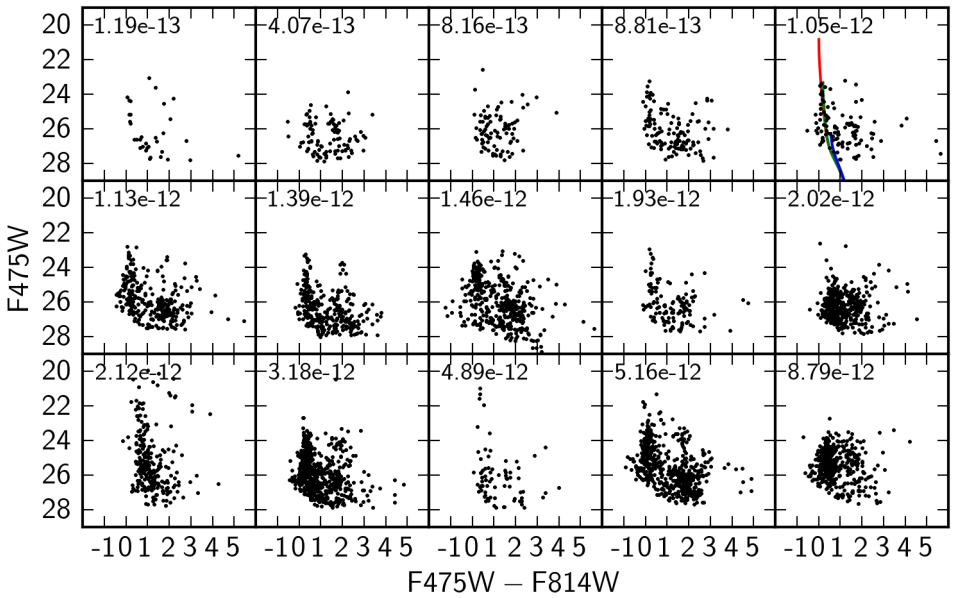

Figure 8.12: CMDs and NUV fluxes (erg s^{-}1 cm^{-}2) of M 31 clusters. 5, 50, and 500 Myr MS isochrones (red, green, and blue) are shown in the upper right panel.

Fig. 8.12 shows optical CMDs of the PHAT photometry for a sample of young clusters identified in the PHAT survey. For each cluster, we measured the total count rate within the visual radius in the near-ultraviolet (NUV) images of GALEX's Deep Imaging Survey (Martin et al. [2005]), applying the aperture corrections given by Morrissey et al. [2007]. Count rates were converted to physical fluxes (erg

s^{-1} cm^{-2}) using the standard GALEX conversion recipes[1], and are reported in each panel of Fig. 8.12. NUV flux traces main sequence (MS) stars, as expected, but it does not appear to correlate monotonically with the total number of MS stars (indicating the total star formation over roughly the last Gyr at this depth).

We are currently investigating applying MATCH, a CMD fitting program for computing star formation histories (Dolphin [2002]), to the PHAT photometry as a means of estimating cluster ages and masses, assuming simple stellar populations (see Weisz [2011] in these proceedings). The derived ages and masses will be used in conjunction with spectral synthesis models to estimate integrated NUV fluxes for our cluster sample. This will make an interesting comparison with the fluxes measured directly from GALEX.

Bibliography

Dalcanton, J. 2011, in preparation
Dolphin, A. E. 2002, MNRAS, 332, 91
Johnson, L. C. 2011, in this proceedings
Martin, D. C., Fanson, J., Schiminovich, D., et al. 2005, ApJ, 619, L1
Morrissey, P., Conrow, T., Barlow, T. A., et al. 2007, ApJS, 173, 682
Weisz, D. 2011, in this proceedings

[1]See http://galexgi.gsfc.nasa.gov/docs/galex/FAQ/counts_background.html.

8.11 Using Open Clusters to Study Mixing in Low- and Intermediate-Mass Stars

Rodolfo Smiljanic[1]

[1] European Southern Observatory, Garching bei München, Germany

Abstract

In many evolutionary stages, low- and intermediate-mass stars show signs of mixing of the surface material with material from the interior. To account for all the details revealed by the observations it is necessary to include non-standard physical processes in the models (e.g. atomic diffusion and rotation-induced mixing). The study of mixing in stars of different masses, ages, and chemical composition helps to identify and constrain these processes. In this sense, stars in open clusters are the ideal targets. All stars in one given cluster have the same age and chemical composition, and their masses can be well estimated. By studying many clusters, one can separate and trace the effects of these different parameters.

The early main sequence

Lithium and beryllium burn at low but different temperatures (2.5×10^6 K and 3.5×10^6 K, respectively). Their abundances can be used to study mixing in the outer layers of stars (see e.g. Smiljanic et al. [2010], and references therein). Observations of stars in young clusters (from $\sim$ 10 to 100 Myr) have shown that pre-main sequence (PMS) models predict too much Li depletion. In addition, there is a significant spread in Li abundances among late-G and K dwarfs which is connected to rotation, i.e. fast-rotating stars have higher Li abundances than slow-rotating ones (see e.g. Balachandran et al. [2011], and references therein).

Beryllium has been studied in far fewer stars than Li has. In Smiljanic, Randich & Pasquini [2011, submitted] we derived Be abundances in ten G- and K-type main-sequence stars of the open clusters IC 2391 and IC 2602 ($\sim$ 50 Myr). As these stars have just arrived on the main sequence, any change in Li and Be should have taken place during the PMS.

All stars have, within the uncertainties, the same Be abundances even though their Li abundances differ by almost one order of magnitude. This confirms what is expected by the models; Be abundances are not affected by mixing during the PMS in stars between $0.80 \leq M/M_{\odot} \leq 1.20$. Comparing our Be abundances with those of other young clusters from the literature, we confirm that Be depletion in stars cooler than $\sim$ 5600 K increases with age. The depletion is stronger for smaller masses. As stars with ages of 50 and 150 Myr do not show Be depletion, we conclude that the depletion in older stars happens during the main sequence, in agreement with Randich et al. [2007].

The Li-Be dip

The so-called Li-dip is a strong decrease in the Li abundance seen in main-sequence stars in a small temperature range around 6700 K. It was first found by Boesgaard & Tripicco [1986] in the Hyades. Be was also found to be depleted in these stars (see e.g. Smiljanic et al. [2010], and references therein).

In Smiljanic et al. [2010] we derived Be abundances along the whole evolutionary sequence of the cluster IC 4651 ($\sim$ 1.7 Gyr). A well defined LiBe-dip was found (Li abundances from Pasquini et al. [2004]). The hydrodynamical models of Charbonnel & Lagarde [2010] reproduce well the observed behaviour of Li and Be over the whole temperature range. The hot side of the dip requires models with atomic diffusion, and transport of angular momentum and chemicals by meridional circulation and shear turbulence. In the cool side of the dip, the models also take into account extraction of angular momentum by internal gravity waves.

The red giant branch

Abundances of C, N, O, and the $^{12}C/^{13}C$ in low-mass giants, before the bump were found to be in good agreement with theoretical predictions. However, after the bump an additional mixing event takes place resulting in further abundance changes [see e.g. Smiljanic et al., 2009, and references therein].

In Smiljanic et al. [2009] we derived C, N, O, Na, and $^{12}C/^{13}C$ in 31 giants, with $1.7 \leq M/M\odot \leq 3.1$, of 10 open clusters. We found that the well-known trend of decreasing carbon ratio with decreasing mass is not so well defined, but shows a significant scatter. The decrease of $^{12}C/^{13}C$ can be explained by the action of thermohaline mixing while the scatter might be partially explained by a dispersion in the initial rotation velocities of the stars (Charbonnel & Lagarde [2010]). The lowest values found are however difficult to explain. New homogeneous analyses are needed to confirm and better constrain these results.

Bibliography

Balachandran, S. C., Mallik, S. V., & Lambert, D. L. 2011, MNRAS, 410, 2526
Boesgaard, A. M. & Tripicco, M. J. 1986, ApJL, 302, L49
Charbonnel, C. & Lagarde, N. 2010, A&A, 522, A10+
Pasquini, L., Randich, S., Zoccali, M., et al. 2004, A&A, 424, 951
Randich, S., Primas, F., Pasquini, L., Sestito, P., & Pallavicini, R. 2007, A&A, 469, 163
Smiljanic, R., Gauderon, R., North, P., et al. 2009, A&A, 502, 267
Smiljanic, R., Pasquini, L., Charbonnel, C., & Lagarde, N. 2010, A&A, 510, A50

8.12 The AMBRE Project: Looking for Stellar Clusters in FEROS Archived Spectra

Clare C. Worley[1], P. de Laverny[1], A. Recio-Blanco[1], V. Hill[1], and G. Kordopatis[1]

[1] Université de Nice Sophia Antipolis, CNRS (UMR 6202), Observatoire de la Côte D'Azur, Cassiopée, B.P.4229, 06304 Nice Cedex 04, France

Abstract

The goal of AMBRE, a joint project between ESO and the Observatoire de la Cote d'Azur, is to provide a homogeneous determination of the stellar parameters for the archived spectra of the FEROS, HARPS, UVES and Flames/GIRAFFE spectrographs. These parameters will be made available to the astronomical community via the ESO Archive. The analysis of the FEROS spectra is now complete and the analysis of the UVES and HARPS spectra is underway (Worley et al. [2011a]). Here we have extracted FEROS stellar samples that correspond kinematically to ten open galactic clusters and compared the MATISSSE (Recio-Blanco et al. [2006]) chemical properties of these samples to the typical literature values for these stellar populations.

Galactic Metallicity Gradient

The AMBRE Project presents a unique opportunity to exploit a large pre-existing spectral dataset ($\sim$ 250,000 spectra) for global information outside the original goals of the individual observing programmes. The analysis of the FEROS archived spectral dataset (as for the remaining archived datasets) has resulted in a homogeneous determination of stellar parameters for a large sample of stellar spectra ($\sim$ 20,000 spectra corresponding to $\sim$ 7000 stars).

The FEROS archived spectra were explored for stars within open galactic clusters. Cluster members were identified kinematically by: selection within 0.5 deg of cluster centre; and selection within 2 km/s of cluster radial velocity. We discarded those clusters for which only one star was found, resulting in 56 stars (72 spectra) over 10 open clusters. For each cluster sample the mean values of metallicity ([M/H]), effective temperature (T_{eff}), surface gravity (log g) and alpha element abundances ([α/Fe]) were calculated from the AMBRE:FEROS results. Fig. 8.13a compares the WEBDA (Mermilliod [1995]) metallicity ([Fe/H]) with the AMBRE:FEROS [M/H] for each of the 10 clusters. There is reasonable agreement for six clusters, although the uncertainties are, in general, on the order of 0.1 dex for both datasets.

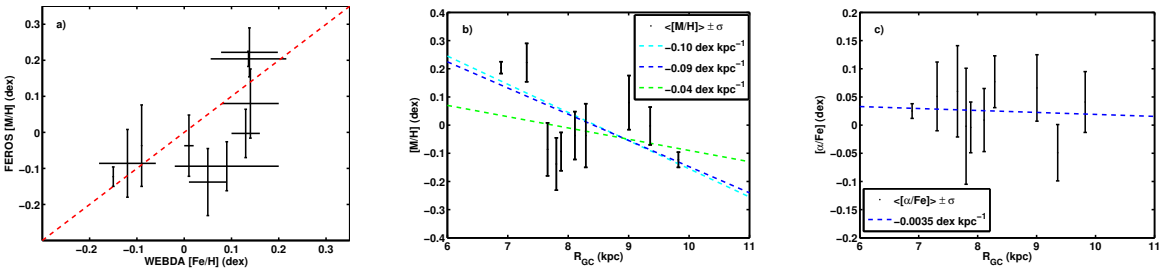

Figure 8.13: a) Comparison of the WEBDA metallicities ([Fe/H]) with the mean [M/H] AMBRE:FEROS values for each cluster. b) Galactocentric distance against $\langle$[M/H]$\rangle$ with lines of best fit. c) Galactocentric distance against $\langle[\alpha/\mathrm{Fe}]\rangle$ with line of best fit.

Fig. 8.13b shows the trend of [M/H] against galactocentric distance (R_{GC}) for the open clusters. The line of best fit has a gradient of -0.09 ± 0.04 dex kpc^{-1} compared to gradients of -0.10 dex kpc^{-1} and -0.04 dex kpc^{-1} from other studies. Fig. 8.13c shows the trend of [α/Fe] against R_{GC} for the open clusters with a line of best fit gradient of -0.0035 ± 0.02 dex kpc^{-1}.

The stellar components of each open cluster have the same origin and initial chemical composition, but clusters range over ages and locations in the galaxy, hence they can be used to test our theories of galaxy formation and evolution. Using 39 old open clusters Friel et al. [2002] determined a metallicity gradient of -0.06 $\pm$ 0.01 dex kpc^{-1}, while Chen et al. [2009] used 1020 clusters compiled from open cluster

catalogues to derive a value of -0.058 dex kpc^{-1}, both of which are in reasonable agreement with the gradient determined here. Gradients derived from Cepheids and galactic disk populations range in value from -0.1 to -0.04 dex kpc^{-1} (Haywood [2008]) (see Fig. 8.13b). This is a well observed relation showing that the results from this homogeneous determination using MATISSE are consistent and very promising for probing galactic relations on a large scale. The investigation of [α/Fe] with galactocentric distance found no significant gradient.

The analysis of the FEROS archived spectra, in this first phase of the AMBRE Project, is now complete. The analyses of the UVES and HARPS archived datasets are now underway. By expanding the sample of stellar clusters using the other instrumental datasets, and also determining heavy element abundances, a comprehensive comparison of the chemical abundance and metallicity distributions of stellar clusters will be made.

Acknowledgments

The authors would like to acknowledge the financial support of ESO, CNES and OCA. This research has made use of the WEBDA database, operated at the Institute for Astronomy of the University of Vienna, and also the SIMBAD database, operated at CDS, Strasbourg, France.

Bibliography

Chen, L., Gao, X. H., & Zhao, J. L. 2009, in IAU Symposium, Vol. 254, IAU Symposium, ed. J. Andersen, J. Bland-Hawthorn, & B. Nordström, 15P–+

Friel, E. D., Janes, K. A., Tavarez, M., et al. 2002, AJ, 124, 2693

Haywood, M. 2008, MNRAS, 388, 1175

Mermilliod, J.-C. 1995, in Astrophysics and Space Science Library, Vol. 203, Information: On-Line Data in Astronomy, ed. D. Egret & M. A. Albrecht, 127–138

Recio-Blanco, A., Bijaoui, A., & de Laverny, P. 2006, MNRAS, 370, 141

Worley, C. C., Recio-Blanco, A., de Laverny, P., Hill, V., & Bijaoui, A. 2011, in preparation

8.13 Cluster-Host Relations: A Tool to Study Star Formation Modes in Galaxies?

Angela Adamo[1], E. Solva-Villa[2] , N. Bastian [3], and S. Larsen[2]

[1] Department of Astronomy, Stockholm University, Oscar Klein Center, AlbaNova, Stockholm SE-106 91, Sweden
[2] Utrecht University
[3] Excellence Cluster Universe, Garching, Germany

Abstract

Star clusters are a common product of star-forming galaxies and their properties can be used to study the formation history of the host systems. It has been observed that galaxy mergers enhance the mean star formation rate (SFR) and produce more numerous and more massive clusters than quiescent spirals. Observed empirical relations between the properties of young star clusters (luminosity or cluster formation efficiency) and the mean SFR in the host support this scenario. We present the relations and test their validity using M 83 as a test-case.

Cluster-host relations: a tool to study star formation modes in galaxies?

Angela Adamo[1], Esteban Silva-Villa[2], Nate Bastian[3], & Søren Larsen[2]

1) adamo@astro.su.se, Stockholm University; 2) Utrecht University; 3) Excellence Cluster Munich

Star clusters are a common product of star-forming galaxies and their properties can be used to study the formation history of the host systems. It has been observed that galaxy mergers enhance the mean star formation rate (SFR) and produce more numerous and more massive clusters than quiescent spirals. Observed empirical relations between the properties of young star clusters (luminosity or cluster formation efficiency) and the mean SFR in the host support this scenario. We present the relations and test their validity using M83 as test-case.

2. The cluster formation efficiency (Γ=CFR/SFR; Bastian 2008) is a measure of the fraction of star formation happening in clusters (cluster formation rate - CFR). Goddard et al. (2010) found a trend between Γ and Σ_{SFR}. The environmental conditions of the host galaxy (expressed by Σ_{SFR}) determine the efficiency of the cluster formation. BCGs follow the trend (colour dots in the plot, Adamo et al. 2011) while the Silva-Villa& Larsen (2011) galaxies scatter around the relation (open squares). Which uncertainties are affecting this relation?

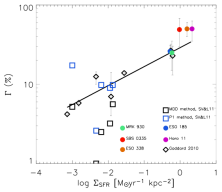

Uncertainties:
1)How is star and cluster formation estimated?
2)How does sample selection affect the results?
3)Are cluster numbers overestimated?

M83 is a face-on, nearby (~5 Mpc) spiral galaxy. It represents an ideal target to test cluster-host relations

1. The fraction of light in U band contributed by the young clusters with respect to the total luminosity of the host – $T_L(U)$ – is correlated with the surface star formation density (Σ_{SFR}, Larsen &Richtler, 2000). The relation holds also for galaxies with high Σ_{SFR} as showed b the overplotted blue compact galax sample (BCGs; Adamo et al. 2011).

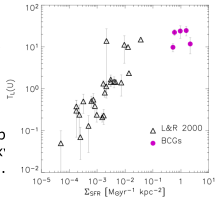

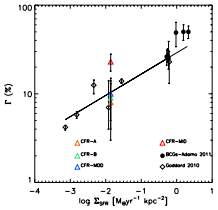

5. **Work in progress:** The relation holds and is consistent with a scenario in which cluster lifetimes are mass dependent. If the lifetimes do not depend on mass, a factor of 2 higher CFR is required.

3. ***M83 Cluster sample*** is a combination of 2 data sets covering a large fraction of the galaxy. 1) Sliva-Villa&Larsen(2011) included only compact sources, older than 10 Myr, and brighter of M_V <-4.6; 2) Bastian et al. (2011) included only compact sources, dynamically bound (Gieles&Portegies Zwart, 2011).

M83 SFR has been estimated with 2 methods:1) Given the total far-IR luminosity ($L_{FIR;}$ Kennicutt 1998) → present SFR(L_{FIR}); 2) Using colour-magnitude diagrams of resolved stellar populations, the star formation history in the last 100 Myr has been recovered (Silva-Villa &Larsen, 2011) → averaged SFR(CMD)

Γ=CFR/SFR [%]	present SFR (L_{FIR})	averaged SFR (CMD)
CFR-A (<10 Myr)	0.08	
CFR-B (10-100Myr)		0.10
CFR-MDD (10-100 Myr)		0.09
CFR-MID (10-100 Myr)		0.23

Mass dependent disruption (MDD) suggests that low mass clusters disrupt faster than their high mass counterparts due to interactions with the galactic environment.
Mass independent disruption (MID) suggests a scenario where ~90 % of clusters are destroyed each age dex, independently of their masses.

4. ***M83 CFR*** has been estimated under different assumptions. ***CFR-A:*** using young star clusters of age <10 Myr and assuming they have been formed with a power-law mass function of index -2, the total mass is estimated extrapolating the amount contained in low mass (undetected) clusters. ***CFR-B:*** same assumptions but the final CFR is a mean of the values estimated each 0.2 dex in age up to 100 Myr. ***CFR-MDD*:*** The CFR is estimated by fitting the observed cluster luminosity function (of clusters in age range 10-100 Myr), assuming a Schechter mass function and a MDD scenario. ***CFR-MID*:*** same conditions as the previous case but a different disruption scenario (MID) is used.

Conclusions
1) The observed trends in panel 1 and 2 suggest that the physical conditions of the interstellar medium in merger systems is different than in quiescent spiral galaxies. The former typically show higher SFRs and cluster formation efficiencies.
2) BCGs are dwarf merger systems with environmental physical properties comparable to luminous IR galaxies and spiral starburst nuclei.
3) Test-cases such as M83 are needed to test the validity of these relations and how uncertainties (sample selection, host distance, model assumptions) can affect the results.
4) The validity of the cluster-host relations is a powerful tool to test important physical processes affecting cluster evolution, e.g. cluster disruption scenarios. Our M83 analysis suggests that mass dependent disruption can better reproduce the expected trends. However, we point out that a similar analysis on different targets has produced different results (see Silva-Villa&Larsen, 2011). More data are needed to put better constraints on the results.

References:
Adamo et al. 2011, MNRAS accepted
Bastian 2008, MNRAS
Bastian et al. 2011, submitted to MNRAS
Kennicutt 1998, ARA&A
Gieles & Portegies Zwart 2011, MNRAS
Goddard et al. 2010, MNRAS
Larsen & Richtler 2000, A&A
Silva-Villa & Larsen 2011, A&A

*See Silva-Villa&Larsen (2011) for the latter 2 methods.

8.14 New Membership Study on the Corona of the Open Cluster M 67

Lola Balaguer Núñez[1], C. Jordi[1,2], J. L. Muiños[3], D. Galadí-Enríquez[4], and E. Masana[1,2]
[1] Universitat de Barcelona. ICC-UB. IEEC. Barcelona. Spain
[2] Institut de Ciències del Cosmos. ICC-IEEC. Barcelona. Spain
[3] Real Instituto y Observatorio de la Armada, San Fernando, Cádiz, Spain
[4] Centro Astronómico Hispano Alemán. CAHA. Almería. Spain

Abstract

A new deeper and wider astrometric study of the open cluster M 67, covering an area of about 2×1.4 deg^2 and down to 17 mag in r' has been accomplished with new data from the Meridian Circle of San Fernando CMASF at El Leoncito (Argentina). We derive properties for 2738 stars fainter, and in a wider area, than any previous precise survey in the cluster region. Proper motions are then used to determine the membership probabilities of stars in the region, applying parametric and non-parametric approaches to cluster/field segregation. Adding photometric criteria, we obtained a preliminary list of 557 probable member stars, up to a distance of 0.96 deg from the cluster center. These are preliminary results of our work that will lead us to the most complete study of its structure, dynamics and mass segregation up to date.

New Membership Study on the Corona of the Open Cluster M67

L. Balaguer-Núñez[1,2], C. Jordi[1,2], J. L. Muiños[3], D. Galadí-Enríquez[4], E. Masana[1,2]

1. Dpt. d'Astronomia i Meteorologia, Universitat de Barcelona, Barcelona, Spain
2. Institut de Ciències del Cosmos ICC - IEEC, Barcelona, Spain
3. Real Instituto y Observatorio de la Armada, San Fernando, Spain
4. Centro Astronómico Hispano Alemán CAHA, Almeria, Spain

ABSTRACT

A new deeper and wider astrometric study of the open cluster M67, covering an area of about 2°x1.4° and down to 17 magnitude in r' has been accomplished with new data from the Meridian Circle of San Fernando CMASF at El Leoncito (Argentina). We derive properties for 2738 stars fainter and, in a wider area, than any previous precise survey in the cluster region. Proper motions are then used to determine the membership probabilities of stars in the region, applying parametric and non-parametric approaches to cluster/field segregation. Adding photometric criteria, we obtained a preliminary list of 557 probable member stars, up to a distance 0.96° from the cluster center. These are preliminary results on our work that will lead us to the most complete study of its structure, dynamics and mass segregation up to date.

1. New Proper Motions Study

New absolute proper motions for 2738 stars have been calculated on the basis of new measurements made with the Meridian Circle of San Fernando CMASF at El Leoncito (Argentina). First epoch data have been taken from plates POSSI (1951.9) measured with two different machines: APM (median σ_{RA} = 0".27, σ_{DEC} = 0".31) and USNO-A.2 (median σ_{RA} = 0".25, σ_{DEC} = 0".29) catalogues, with averaged positions when the star is present in both catalogues. The second epoch is taken from CMC14 (2001 for this zone) and the new measurements taken with CMASF (2010, see errors top left graph in the figure below). When the three epochs where available a linear fit was used. For stars with no intermediate data (CMC14 2001) nominal errors of the proper motions are larger (see bottom left graph in the figure below). Final data cover an area of 2°x1.4° with approximate magnitude limits 9 < r'< 17. To check for magnitude trends in proper motions we have plotted (see right figure) our selection of cluster members as red circles. We find no trend with magnitude.

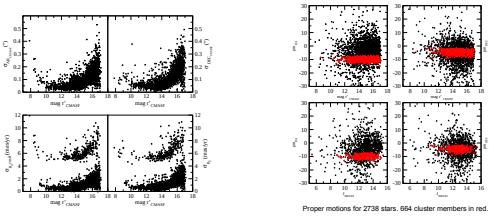

Proper motions for 2738 stars. 664 cluster members in red.

2. Membership Probabilities

The parametric approach: we assume the existence of two populations in the vector-point diagram (VPD): cluster and field. A circular Gaussian model is adopted for the cluster distribution while a bivariate (elliptical) Gaussian describes the field. We apply a 9-parametric Gaussian model following Balaguer-Núñez et al (2004b, 2005, 2007). Our implementation takes into account the individual errors of the proper motions measurements (Zhao & He 1990).

	n_c	$\mu_\alpha cos\delta$	μ_δ	σ_c	$\sigma_{\mu\alpha cos\delta}$	$\sigma_{\mu\delta}$	ρ
M 67	0.260	-9.82	-4.40	1.31			
	±0.011	± 0.08	± 0.09	±0.05			
Field		-3.69	-5.28		+7.57	6.99	-0.14
		± 0.04	± 0.18		± 0.01	± 0.10	±0.01

Distribution parameters and their uncertainties: n_c measures the volume of the cluster frequency function, $\mu_\alpha cos\delta$ and μ_δ are then mean absolute proper motions, σ_c and $\sigma_{\mu\alpha cos\delta}$ and $\sigma_{\mu\delta}$ are the dispersions of the Gaussians fitted to the cluster and field distributions, and ρ is the correlation for the field function. The units of μ and σ are mas yr^{-1}.

The non-parametric approach: we perform an empirical determination of the frequency functions, ψ, from the VPD without relying on any previous assumption about their profiles (Balaguer-Núñez et al 2004b, 2005, 2007; Galadí-Enríquez et al. 1998). In the area occupied by the cluster, the ψ is made up from two contributions: cluster and field. To disentangle the two populations, we studied the VPD for the area outside a circle centred on the cluster. The maximum of the cluster PDF is located at $(\mu_\alpha cos\delta, \mu_\delta)$ = (-9,9 ± 0.2, -4.6 ± 0.2) mas yr^{-1}

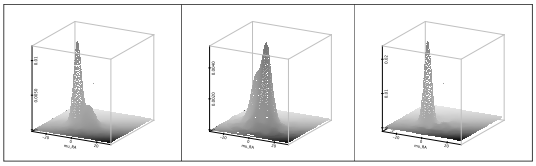

Empirical PDFs in the VPD. Left: ψ_{c+f} mixed sample from the inner circle of 35' centred on the point of maximum spatial density of stars. Centre: ψ_f field population from outside this circle. Right: ψ_c cluster population of M67.

Membership probabilities are computed for both approaches (see histogram below). The non-parametric technique yields an expected number of cluster members from the integrated volume of the cluster frequency function in the VPD areas of high cluster density. The expected number of cluster members in this VPD area is 577. Sorting the sample in order of decreasing membership probability, the first 577 are the most probable members. The minimum value for the non-parametric probability (for the 577th star) is P_{NP} = 0.803. Accepting the same volume for the parametric approach gives us P_P = 0.68. We accept as members those classified as such by at least one of the methods. This way we get a list of 664 members,

3. Comparison with UCAC3 Proper Motions

We compare our absolute proper motions with those of the latest release UCAC3 (Zacharias et al. 2009), as well as repeat the check on the magnitude trend using our selection of cluster members (in red). We can see that for magnitude J_{2MASS} fainter than 13.5 UCAC3 proper motions for the cluster members show a trend with magnitude (as happened with UCAC2 release for J_{2MASS} fainter than 12). The use of proper motion data from UCAC3 catalogue should be carefully performed to avoid systematics.

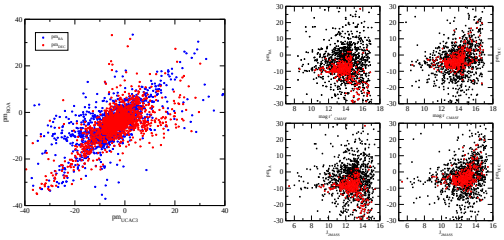

4. Colour - magnitude diagrams

The area covered by our proper motions study is well suited by the 1.92°x1.92° BATC photometry (Fan et al. 1996) as can be seen in green in the left figure below. The segregation of members based on proper motions isdata, that is described in Sec. 2, was photometrically refined on the BATC colour-magnitude diagram shown in the central panel of the figure below. From the common 579 member stars, 557 (marked in red) are photometrically compatible. We divide this selection of members in four annular areas to study the corresponding CM diagrams (see figures below).

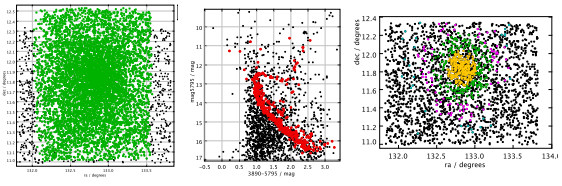

5. Studies on the Corona of M67

The area covered by our new wider and deeper cluster segregation study allow us to improve our knowledge of the corona of M67. These are only the first results on a complete study of its structure. We will be able to derive structural parameters and discuss the spatial dependence of the luminosity and mass functions. We will analyze the spatial distribution of mass functions and the cluster mass segregation, as well as the dynamical implications in a forthcoming paper.

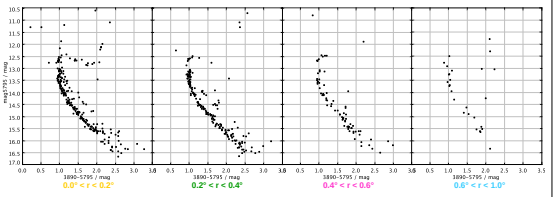

8.15 Finding Early-type Stars in the Gaia Catalogue

Ronny Blomme[1]
[1] Royal Observatory of Belgium

Abstract

The Gaia satellite will provide accurate parallaxes and photometry (330 – 1000 nm) for 1 billion stars down to magnitude 20. In addition, spectra (847 – 874 nm) will be taken for 150 million stars down to magnitude 16.
Among those targets, there will be a large sample of O and B type stars. According to the Besançon Universe model (Jordi & Carrasco [2007], ASPCS 364, 215), about 900,000 B stars should be observed. About one sixth of these stars (Briot & Robichon [2004], ESA SP-576, 561) are expected to have parallaxes with a relative precision better than 3%.
This large number will enable us, for the very first time, to perform unbiased statistical analyses and high-accuracy luminosity determinations based on a homogeneous dataset. It will also allow us to study the dynamics of the open clusters in which these stars are formed.

Finding Early-type Stars in the Gaia Catalogue

Ronny Blomme

Royal Observatory of Belgium, Brussels, Belgium

The Gaia Satellite

The Gaia satellite will provide accurate parallaxes and photometry (330 – 1000 nm) for 1 billion stars down to magnitude 20. In addition, spectra (847 – 874 nm) will be taken for 150 million stars down to magnitude 16.

Among those targets, there will be a large sample of O and B type stars. According to the Besançon Universe model (Jordi & Carrasco, 2007, ASPCS 364, 215), about 900,000 B stars should be observed. About one sixth of these stars (Briot & Robichon 2004, ESA SP-576, 561) are expected to have parallaxes with a relative precision better than 3%.

This large number will enable us, for the very first time, to perform unbiased statistical analyses and high-accuracy luminosity determinations based on a homogeneous dataset. It will also allow us to study the dynamics of the open clusters in which these stars are formed.

The A_V – T_{eff} Degeneracy

Bailer-Jones (2010, MNRAS, 403, 96) pointed out the A_V – T_{eff} degeneracy that will be present in the Gaia photometric data.

As can be expected, a unique determination of interstellar extinction (A_V) and effective temperature (T_{eff}) is not possible, due to the noise in the data.

But the errors are much larger than may be naively expected, especially for early-type stars.

The figure shows UBVRI simulated photometry (S/N=10) of a 25,000 K star with A_V=3.1.

When we try to fit these simulated observations (to within the error bars) we find that *temperatures ranging from 5,500 to 40,000 K all provide a good fit!*

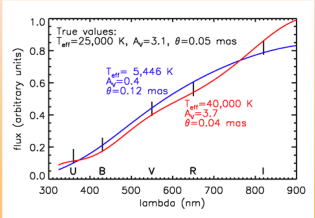

A Possible Solution

The equation relating emitted flux (F_ν) and flux received at Earth (f_ν) is:

$$f_\nu = F_\nu(T_{\mathrm{eff}}) \left(\frac{R_*}{D}\right)^2 10^{-0.4\,A_\lambda}$$

with R_* the radius, D the distance to the star, $\theta = 2R_*/D$ the angular diameter and A_λ the interstellar extinction at wavelength λ.

In the degeneracy, the three parameters (T_{eff}, A_λ, θ) play a role. Constraining them will break the degeneracy.

Gaia will also give us the distance to the star. But this will not be sufficient to break the degeneracy, as we also need to know the radius.

A possible solution is to use a relation between T_{eff} and R_* (e.g. the relation valid on the ZAMS). This allows us to break the degeneracy, but of course, the result will be wrong if the star is not on the ZAMS.

A more sophisticated version of this idea was proposed by Bailer-Jones (2011, MNRAS 411, 435). In a Bayesian model, a prior is used that contains information about the probability of finding a star in a certain part of the Hertzsprung-Russell diagram (HRD).

Using this prior will result in more likely T_{eff} values, i.e. those corresponding to more populated areas of the HRD.

Early-type stars, however, are not in the more populated areas. Applying this technique would skew them towards lower temperatures.

What About the Early-type Stars?

To find the early-type stars among the 1 billion Gaia targets, we therefore need to try another approach.

One possibility is to use external photometric data with higher precision, from the large surveys that are currently running, or are planned for the near future.

Adding a few high-precision data to a set of lower-precision data considerably reduces the degeneracy.

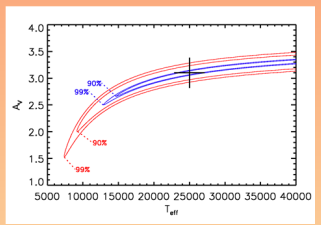

The figure shows the 90 and 99 % confidence intervals for the (T_{eff}, A_V) determination. The correct solution is given by the cross.

The red curves take into account only the simulated Gaia photometric data with 10% precision.

The blue curves also use the Gaia data, but add UBV photometric data with 0.5% precision. This tightens the confidence region, leading to a better T_{eff} determination.

Using high-precision external data improves the T_{eff} determination, but it is not sufficient.

Another approach is to use the fact that most early-type stars occur in clusters.

Knowledge of distances, proper motions (and possibly radial velocities) will allow the clusters to be recognized.

The assumption that the extinction is similar in the whole cluster (which is certainly not always true!) will allow us to break the degeneracy.

Conclusion

- Gaia will provide us with a enormous amount of data about early-type stars.
- It will, however, not be easy to recognize these early-type stars among the 1 billion Gaia targets.
- Careful planning and testing of different approaches is required to see how best to find these early-type stars.

8.16 Stellar Clusters in LIRGs: IC 1623 and NGC 2623

Clara Cortijo-Ferrero[1], **R. M. González Delgado**[1], **E. Pérez**[1]
[1] Instituto de Astrofísica de Andalucía - CSIC, Spain

Abstract

We present the analysis of Hubble Space Telescope multiwavelength imaging data (from UV to NIR) for two LIRGs: IC 1623 and NGC 2623. Using SPs synthesis models we have found that both LIRGs are mainly composed by intermediate age and young stellar components. The extinction is significant, with the highest values in the nuclear regions.
Very young off-nuclear star-forming regions have been found in both LIRGs that could be related to the enhancement of the SF during the first encounter of the merger.
We also present the preliminary analysis of GTC OSIRIS Tunable Filters imaging data for NGC 2623, that reveal the presence of very young clusters (1 – 10 Myr) in the outskirts of NGC 2623, at more than 19 kpc from the galaxy center.

Stellar Clusters in Luminous Infrared Galaxies: IC 1623 and NGC 2623

Clara Cortijo-Ferrero
clara@iaa.es

Rosa M. González Delgado
rosa@iaa.es

Enrique Pérez
eperez@iaa.es

(IAA, CSIC)

Abstract

We present the analysis of Hubble Space Telescope multiwavelength imaging data (from UV to NIR) for two LIRGs: IC1623 and NGC2623. Using SPs synthesis models we have found that both LIRGs are mainly composed by intermediate age and young stellar components. The extinction is significant, with the highest values in the nuclear regions.

Very young off-nuclear star forming regions have been found in both LIRGs that could be related to the enhancement of the SF during the merger first encounter.

We also present the preliminary analysis of GTC OSIRIS Tunable Filters imaging data for NGC 2623, that reveal the presence of very young clusters (1-10 Myr) in the outskirts of NGC2623, at more than 19 Kpc from the galaxy center.

Introduction

Luminous and Ultraluminous Infrared Galaxies (LIRGs and ULIRGs, respectively) have bolometric luminosities larger than 10^{11} and 10^{12} $L_{\odot}$, respectively. They are rare in the local universe, but they were very luminous in the past and they are the most significant contributors to the infrared galaxy population at redshifts larger than 1 (Pérez-González et al. 2005).

Within the hierarchical model it is believed that galactic merger (U)LIRGs could generate starburst processes (SBs) that would feed a central AGN. The final stage, once the gas has been dissipated, is the formation of elliptical galaxies. In other words, we want to investigate the evolutionary sequence: (U)LIRGs ➧ post-SBs QSOs ➧ QSOs ➧ ellipticals.

In this work we present a photometric study of the stellar populations in two LIRGs: IC1623 and NGC2623, using HST images. In the future we are planning to perform the same analysis in a larger sample of LIRGs and post-SBs QSOs, for which we have HST high resolution multiwavelength imaging but also integral field spectroscopy (IFS-VIMOS-PMAS) data.

Data: HST images

LIRGs: They have been selected from the IRAS Revised Bright Galaxy sample with log L_{IR} > 11.3 $L_{\odot}$. They belong to the GOALS project (Armus et al. 2009) that combines data from NASA's Spitzer, Chandra, Hubble and GALEX observatories.

Images: We have analyzed HST archival images from UV to NIR. Also Spitzer IRAC bands images are available.

IC 1623

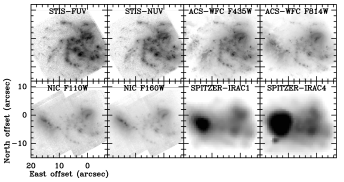

IC 1623 is a gas-rich, nearby interacting system composed by 2 galaxies, IC 1623E and IC 1623W, which are in the pre-merger close binary stage (IIIb) of interaction, following Veilleux et al. classification. The west component dominates the emission in the UV and optical, whereas the eastern component, totally extinguished in the UV is dominating the brightness in the IR, as seen in NICMOS and SPITZER images.

NGC 2623

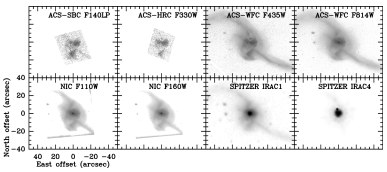

NGC2623 is in the merger (IV) interaction stage of Veilleux et al. classification. Its nucleus, quite faint and extended in UV and optical images becomes very bright and point-like in NICMOS and SPITZER images.

Moreover, this galaxy has a large, very young star forming region, south of the nucleus, UV bright and formed by ~100 stellar clusters.

OSIRIS Tunable Filters @ GTC: NGC 2623

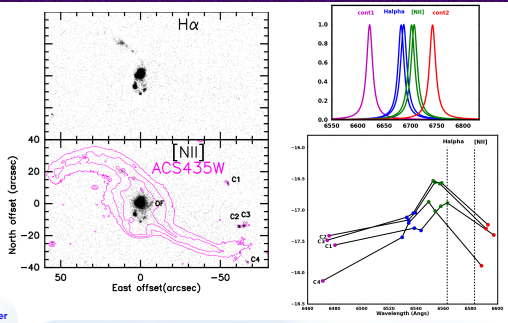

We have OSIRIS Tunable Filter imaging data in 6 narrow bands, covering Hα and [NII] λ6583. We have obtained the Hα and [NII] emission line images (continuum subtracted). Their morphologies are similar with several differences:

-The four bright clusters (C1,C2,C3, C4), appear in [NII] and HST ACS-WFC images but not in Hα.

-The outflow-like structure (OF) in the [NII] image nuclear region, also absent in Hα.

From the SEDs of C1 to C4 clusters we have found their emission peaks in [NII] image consistent with being Ho (in the OSIRIS FOV the TF wavelength varies with the distance to the center of the CCD).

The intense Hα emission suggests that these should be very young clusters (1-10 Myr), which are located in the outskirts of the galaxy, more than 19 kpc away from the centre, and moving with velocities from -80 to -500 km/s with respect to it.

Method and Results

Clusters IC 1623

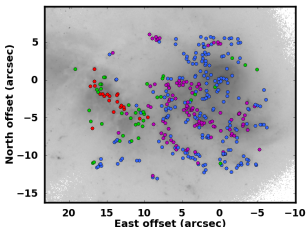

Method

- We have performed aperture photometry on the stellar clusters detected in the HST images to compare their colours with those of Bruzual and Charlot (2003) SSPs models and determine the stellar population properties (age, extinction and masses).
- For clusters detection, we have developed a simple program that uses IRAF DAOFIND algorithm. To clean false detections we have performed photometry for all detected clusters, and selected only those with S/N>50 in the ACS-WFC images. Finally, we have detected around 360 and 180 clusters in IC 1623 and NGC 2623 respectively.
- Model colours have been computed with SYNPHOT software using a Salpeter initial mass function and Calzetti extinction law. We have compared our data with solar metallicity SSPs models covering a large range in ages, from 1 Myr to 10 Gyr and 3 possible extinction values from Av=0-2 mag.
- Clusters are plotted with a 4 colour scheme, from the bluest to the reddest clusters (magenta, cyan, green, red) as seen in the colour-colour diagrams.
- In addition, we have also estimated the mass range of the clusters by comparing their absolute magnitudes in NICMOS 1.6 μm band with the models.

Clusters NGC 2623

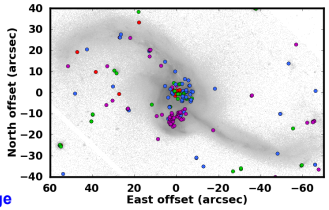

Age

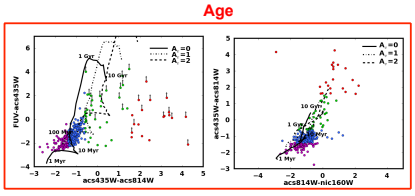

Mass

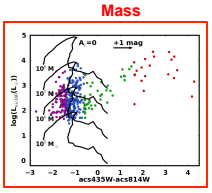

Age

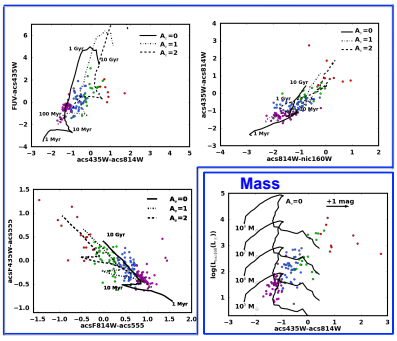

Mass

Conclusions

- Stellar population in IC1623: IC1623W clusters are consistent with young ages between 1-10 Myr and small extinctions of 0-1 mag. From IR-optical diagrams, IC1623 clusters are consistent with young to intermediate ages and higher extinctions (2-4 mag).
- Stellar population in NGC 2623: The circumnuclear region is consistent with young to intermediate SPs from 1 Myr to 1Gyr and extinction between 1-2 mag. At the nucleus the extinction is higher, up to 3 mag. The star forming region located south of the nucleus, is formed by very young clusters between 1-10 Myr, with about 1mag of extinction.
- We find no significant differences between the SPs in our LIRGs and previous works of ULIRGs, Rodríguez Zaurín et al. (2009)
- We have found very young (1-10 Myr) clusters in both LIRGs, even though they are in a different merger evolutionary stage. Could this be related to the enhancement of the SF during merger first encounter?
- The extinction values are around 0-2 mag, with the highest values in the nuclear regions.
- In our LIRGs the mass range of the clusters lies between 10^{5}–10^{7} $M_{\odot}$
- With GTC OSIRIS TF imaging data, we have found very young clusters (1-10Myr) (named as C1, C2, C3 and C4 in the figure) in the outskirts of NGC2623, at more than 19 Kpc from the center. This is also confirmed by HST data. We have estimated that these clusters are moving at velocities between -80 and -500 km/s with respect to the galaxy center.

References

- Armus et al. 2009, PASP, 121, 559
- Bruzual G., Charlot S. 2003, MNRAS, 344, 1000
- Calzetti D. et al. 2000, ApJ, 533, 682
- Pérez-González P. et al. 2005, ApJ, 630, 8
- Veilleux S. et al. 2002, ApJS, 143, 315
- Rodríguez-Zaurín J. et al. 2009, MNRAS, 400, 1139
- Rodríguez-Zaurín J. et al. 2010, MNRAS, 403, 1317

8.17 Evidence for Triggered Star Formation in the Open Cluster Stock 8

Amparo Marco[1], **I. Negueruela Díez**[1], **C. González Fernández**[1]
[1] Universidad de Alicante, Spain

Abstract

We present a deep study of the area surrounding the open cluster Stock 8, consisting of infrared photometry of the cluster area, wide area Strömgren photometry of its surroundings and spectroscopy of OB stars. Stock 8 seems to be emerging from its parental cloud, with a significant fraction of the stars still embedded. The most massive stars have spectral types B0 - 1. The geometry of the region suggests triggering by nearby O type stars. We study the connection of other small clusters in the neighbourhood with this main star-forming group.

Evidence for triggered star formation in the open cluster Stock 8

Amparo Marco-Tobarra, Ignacio Negueruela-Díez and Carlos González-Fernández, University of Alicante, Spain
amparo.marco@ua.es; ignacio.negueruela@ua.es; carlos.gonzalez@ua.es

Introduction: *Stock 8* is a poorly studied open cluster in the constellation *Auriga*, associated to the *HII* region *IC417*. A region of high stellar concentration immediately adjacent to the *HII* region has been studied by a few authors, most recently by Jose et al. (2008, MNRAS 384, 1675). There are, however, many early type stars in the neighbourhood, and the actual extent of the cluster has not been explored. We have chosen this area as part of a sample to study sequential star formation and the possible role of triggering in massive cluster formation.

Data: We obtained *Strömgren uvbyβ* photometry of the regions marked with red squares (the area generally called *Stock 8* and two nearby stellar concentrations which turn out to be real clusters) with the Jacobus Kapteyn Telescope in 2003. We obtained spectroscopy of bright catalogued OB stars in the area with the 1.5 m telescope at OHP in 2002. We obtained deep *JHK* photometry of stars associated with *IC417* with the Telescopio Nazionale Galileo in 2008.

Preliminary Results: We find two new open clusters approximately 20' North of *Stock 8* and not associated with nebulosity. Both clusters are located at the same distance as the population of unobscured stars in *Stock 8* (d ~ 2.2 kpc). The infrared images reveal a large population of heavily obscured sources, in part spatially coincident with the early type stars in *Stock 8*. The geometry of the area suggest that star formation is triggered by the luminous O8 II(f) star *HD 35633*. The spectral type of this object suggest an age > *2* Myr for the OB population, while the presence of deeply embedded bright sources indicates that star formation is likely still going on inside *IC417*.

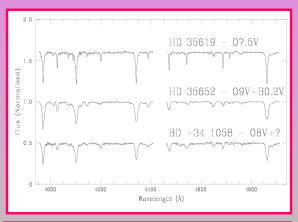

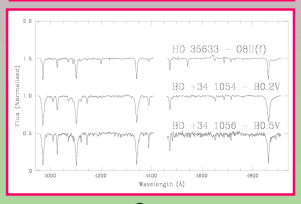

SPECTRA OF THE STARS

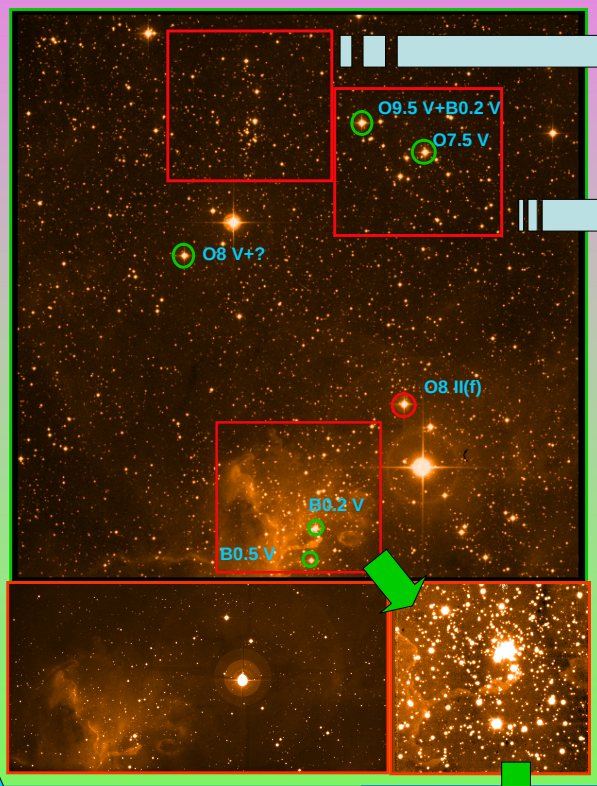

New Open Cluster called:

ALICANTE 12

New Open Cluster called:

ALICANTE 11

M_V/c_0 diagram for stars in Stock 8 (yellow open circles), Alicante 11 (green open circles) and Alicante 12 (red open circles). The three populations are consistent with a single distance and can be fitted with the ZAMS from Perry et al. (1987, PASP 99, 1184) displaced to DM=11.7 (~2.2 kpc)

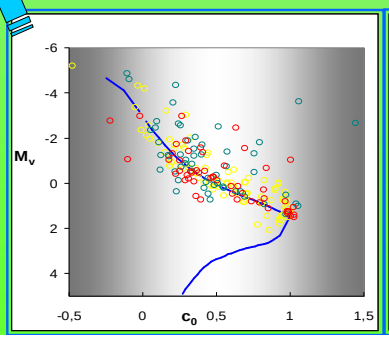

$K_S/(J-K_S)$ diagram for Stock 8

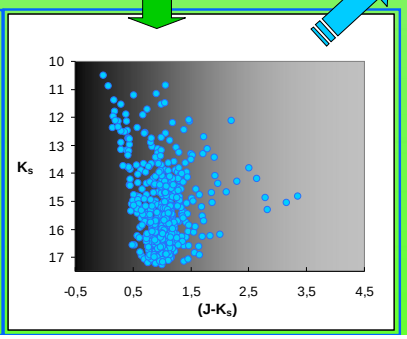

8.18 Searching for the Perseus Arm in the Anticenter Direction

Maria Monguió[1], **P. Grosbøl**[2], **F. Figueras**[1]
[1] Universitat de Barcelona, Spain
[2] European Southern Observatory, Garching, Germany

Abstract

Here we propose a two step approach to provide new insights on the outer spiral arm pattern of the Milky Way: 1) a Strömgren photometric survey to map the stellar space density of moderate young type stars tracing the Perseus arm, and 2) a spectroscopic survey to determine the velocity perturbation due to the density wave through accurate radial velocities (RV). First reduced preliminary data suggest an overdensity around 1.5 – 2 kpc, probably associated with the Perseus arm. Results from this project will present a significant step towards mapping the spiral structure between the second and the third galactic quadrant, where the determination of kinematic distances is not possible.

Searching for the Perseus arm in the anticenter direction

M. Monguió[1], P. Grosbøl[2], F. Figueras[1]

(1) Dept. d'Astronomia i Meteorologia and IEEC-UB, ICC-Barcelona University

(2) European Southern Observatory

contact: mmonguio@am.ub.es

Abstract

Here we propose a two step approach to provide new insights on the outer spiral arm pattern of the Milky Way: 1) a Strömgren photometric survey to map the stellar space density of moderate young type stars tracing the Perseus arm, and 2) a spectroscopic survey to determine the velocity perturbation due to the density wave through accurate radial velocities (RV). First reduced preliminary data suggest an overdensity around 1.5-2kpc, probably associated with the Perseus arm. Results from this project will present a significant step towards mapping the spiral structure between the second and the third galactic quadrant, where the determination of kinematic distances is not possible.

Mapping the space density using uvbyβ photometry: Photometric survey

We have almost completed a 8□º deep Strömgren uvbyHβ photometric survey for stars up to u~20 with the Wide Field Camera (WFC) at the Isaac Newton Telescope (INT), La Palma. Target stars must be old enough to respond to the potential perturbation, but young enough to still have small intrinsic velocity dispersion. B5-A3 stars (σ<15 km/s according to Aumer and Binney, 2009) are optimal for our studies. Strömgren photometry is the natural system to identify these stars and to compute accurate individual distances for them (10-15% accuracy). Data from February 2009 run (3□º) has been fully reduced and analyzed. Preliminary results (see Fig.4) seems to indicate an stellar overdensity around 1.5-2kpc. We estimate that this overdensity detection is in the range of 2-3σ. Adding the double amount of stars obtained during January 2011 run we expect to be close to the five sigma detection. Our WFC/INT photometric survey of B5-A3 stars (~300 stars/□º) is the catalog for which the spectroscopic targets are being selected.

Observational Program:

There successful observational runs have been developed:

1) February 2009: 3□º up to u~19 already reduced and analyzed.

2) January 2011: 5□º up to u~20 are being reduced.

3) February 2011: two bright nights, devoted to increase the sample for the first kiloparsec bins, where low statistics and saturation problems prevented us to reach the five sigma detection.

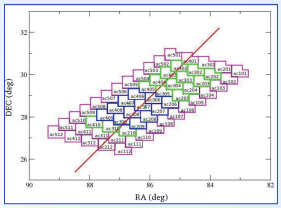

Figure 1: RA-DEC plot with the already observed WFC fields. In blue, data from 2009 (1), in green, data from January 2011 (2), in pink, data from February 2011 (3). Central point is at (l,b)=(180.5, -0.25), following the warp and avoiding high extinction regions. Red line shows latitude b=-0.25.

Completeness:

The Strömgren u filter defines the limiting magnitude of our sample.

We checked that 2009 data allow us to ensure completeness only up to 2.2 kpc (u~19.5) for A3 stars. We did that comparing with a deeper region we used as a standard field. During 2011 observations we increased the exposure times to ensure completeness up to u=20, so up to 2.5kpc for A3V stars (see figure 2).

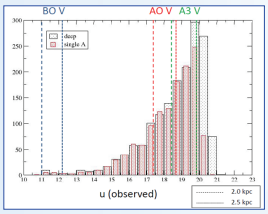

Figure 2: In red: histogram of the stars for which a mean u magnitude has been derived following our reduction strategy. In gray: histogram showing the limiting u magnitude reached in the deep field (seven pointings have been stacked previous to magnitude derivation). Vertical lines show the apparent magnitude for different type stars at 2 and 2.5kpc.

Results:

Distances, extinction and physical parameters have been obtained using the method from Jordi et al. 1997.

• From the distance histogram of B5-A3 stars we detect a possible overdensity around 1.5-2kpc (see figure 4).

•The extinction vs. distance plot (see figure 3) shows a change in the slope. This tendency, if confirmed, will be consistent with a main dust lane on the inner side of the arm. In a standard density wave picture, this suggests that the co-rotation of the spiral pattern is outside this radius.

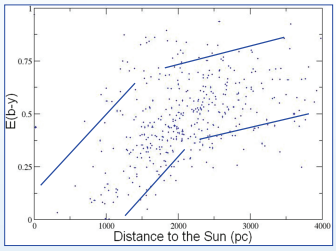

Figure 3: Extinction vs. distance plot.

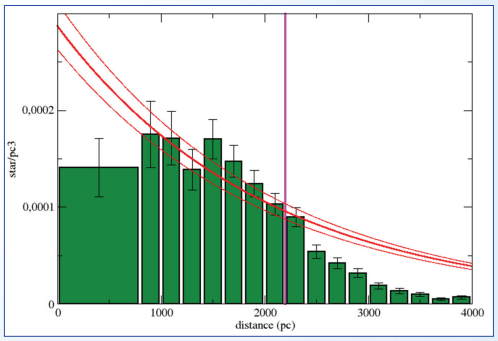

Figure 4: Stellar density distribution of B5-A3 stars in the anticenter direction from 3□º (~900 stars). One sigma error bars are shown. Histogram complete up to 2.2 kpc, (pink vertical line). An exponential disk density law (red line) with scale length of 2 kpc have been plotted for comparison. As a zero point of the exponential law we used (2.87 ± 0.24)·10^{-4} stars/pc^3 at the Sun position, as obtained by Murray et al. 1997 from Hipparcos data.

The data suggest an overdensity around 1.5-2kpc, probably associated to the Perseus arm.

Data is being reduced to increase the limiting magnitude and the statistics.

Velocity perturbation due to the spiral pattern: Spectroscopic survey

Accurate radial velocities for young B5-A3 stars are needed to trace the radial kinematic perturbation due to the Perseus arm in the anticenter direction. This direction allows us to minimize the influence of galactic rotation. The radial velocity perturbation due to the spiral pattern is rather uncertain and is expected to be small (amplitude A=2.5-5 km/s, e.g. Fernández. et al 2001), so this impose an important constrain on the accuracy required in our radial velocity survey. Even if the real perturbation is smaller than expected, we will be able to set an upper limit. In order to develop that survey we are using AF2/WYFFOS at the William Herschel Telescope (WHT), La Palma. A high resolution grating has been selected to reach the 3-5 km/s accuracy.

Obtained data

In November 2011 we already observed spectra for ~600 stars (data is being reduced). A second epoch is needed to identify binary stars. It is important to mention that, although the completeness in the photometric survey is a critical issue, the kinematic sample do not need to be complete in distance, we simply need to have enough stars in each bin to statistically detect the spiral radial perturbation.

Simulations

We developed some simulations in order to establish the number of stars needed to achieve the detection of the perturbation and the RV accuracy required. The steps followed are:

1) We use the distance distribution of the stars from the photometric sample (3□º).

2) We model the kinematic effect of the spiral arm with a sinusoidal as a function of distance: **RV=A(1-cos(r/D$_{sp}$))**, where:

A is the amplitude of the kinematic perturbation.

r is the heliocentric distance for each star obtained from the photometric sample.

D$_{sp}$ is the distance between the Sun and the expected locus of the Perseus arm (~2kpc, see above). The Sun is placed near the interarm region.

3) We add an intrinsic radial velocity dispersion as a function of the spectral type following Aumer and Binney (2009).

4) We add an observational gaussian error in radial velocity σ=5km/s (upper limit).

5) We add a 10% error in distance.

From several statistical tests we concluded that, to reach a 3σ detection of a 2.5km/s amplitude perturbation, radial velocity data for 800 stars is required. We should also take into account that some of the observed stars will be binary (30% according to Evans et al. 2010) so we have increased the observing target list to 1000 stars.

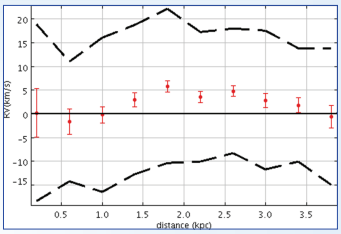

Figure 5: Simulation of the kinematic perturbation due to the spiral arm with A=2.5km/s and 800 stars. Dots are the mean velocity for each 0.5kpc distance bin with its error of the mean (error bar). Standard deviation is shown in dashed black lines. We assume Perseus at 2 kpc and the Sun near the interarm region. We randomly add to each star an intrinsic velocity dispersion, an observational error in RV of 5km/s and a 10% error in the photometric distance.

References

1) Kinematics and history of the solar neighbourhood revisited, Aumer, M.; Binney, J., 2009, MNRAS, 397, 1286

2) The VLT-FLAMES Tarantula Survey, Evans, C. J.; Bastian, N.; Beletsky, Y., et al., 2010, IAUS, 266, 35.

3) Kinematics of young stars, II. Galactic spiral structure, Fernández, D., Figueras, F., Torra, J., 2001, A&A, 372, 833

4) An analysis of the currently available calibrations in Strömgren photometry by using open clusters, Jordi, C.; Masana, E.; Figueras, F.; Torra, J., 1997, A&AS, 123, 83

5) The Luminosity Function of Main Sequence Stars within 80 Parsecs , Murray, C.; Penston, M.; Binney, J.; Houk, N., 1997, ESASP, 402, 485

6) Spectral Classification Through Photoelectric Narrow-Band Photometry , Strömgren, B., 1966 ARA&A, 4, 433

8.19 The Role of Environment in Star Formation: Young Clusters forming in Isolation

Dawn Peterson[1], **L. Allen**[2], **R. Gutermuth**[3], **T. Bourke**[1]
[1] Harvard-Smithsonian Center for Astrophysics, Cambridge
[2] National Optical Astronomy Observatory (NOAO)
[3] University of Massachusetts at Amherst

Abstract

We present preliminary results from a study of a large sample of Bok globules that have been observed with the NASA Spitzer Space Telescope. We identify and classify young stellar objects using Spitzer and near-infrared 2MASS photometry, and will present the ratio of Class I to Class II YSOs in each of the regions. In addition, near-infrared extinction maps will be presented.
The stellar populations will be used, along with the known gas masses of these clouds to estimate the fraction of the gas from a molecular cloud that typically ends up as stars. The initial conditions for the formation of a single star, binary or cluster of stars can be constrained, and with an estimate of the age from theoretical models, the time it takes a star (or a cluster of stars) to form can also be constrained, as well as the timescales for the various evolutionary states. Bok globules are unique because they are simple environments, free from the confusing effects of winds and external turbulence that are often seen in young clusters embedded within larger, star-forming complexes. As part of our study, we will compare these simple structures, which span a wide range of evolutionary states, with more complex bright-rimmed clouds, which are strongly influenced by nearby O and B stars, ultimately studying the role of environment in star formation.

The Role of Environment in Star Formation: Young Clusters forming in Isolation

Dawn Peterson[1], Lori Allen[2], Rob Gutermuth[3], Tyler Bourke[1]

1-Harvard-Smithsonian Center for Astrophysics, 2-NOAO, 3-University of Massachusetts at Amherst

Spitzer Observations

- Spitzer observations of the Bok globules were taken from several programs, including the "Young Cluster Survey," a guaranteed time observation (GTO), a general observer (GO) program specifically targeting Bok globules known to show signs of star formation by PI Peterson, and the "Lonely Cores" GO program (PI Bourke). A few isolated fields were also taken from the archive.
- The fields were observed with IRAC, in all four bands, and with at least the 24 micron MIPS band. For the near-infrared photometry, 2MASS was used.
- YSO candidates were identified from color-magnitude and color-color diagrams, using the "Cluster Grinder" IDL program written by R. Gutermuth.

(Right): 2MASS extinction maps for a few of the Bok globules in our sample are shown. These extinction maps, which show a field approximately 20' square around each Bok globule, were created using a nearest-neighbor method using H-K colors (Gutermuth et al. 2005, ApJ 632, 397).

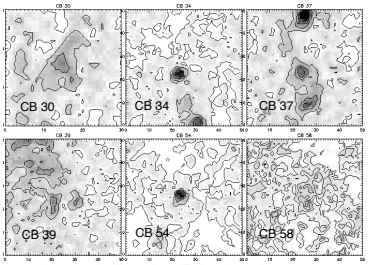

Sample of Bok Globules

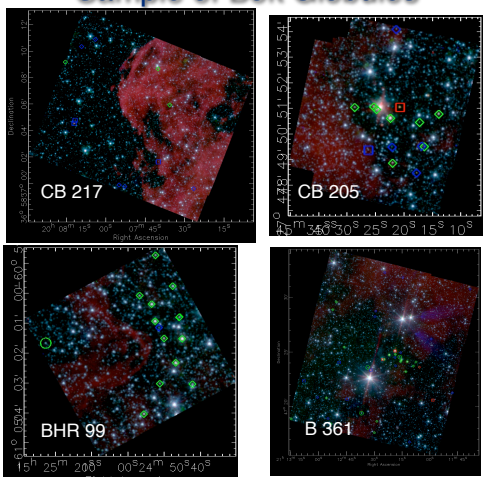

As an example, we show 4 Bok globules above. The color images are created from 3.6 micron (blue), 4.5 micron (green), 8.0 micron (red) IRAC images. YSO candidates are shown as the following: Class I (red squares and diamonds), Class II (green diamonds; green circles are possible 'transition disks'), and PAH (blue diamonds), and AGN (blue squares) 'vermin.'

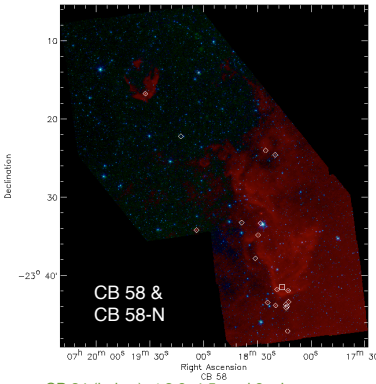

CB 58 and CB 58-N(left) This image is 3.6, 4.5, and 24 micron MIPS: Class I (squares) and Class II (diamonds) overlaid.

Next steps:

1) Compare stellar content with the mean/peak column densities for each Bok globule
2) Determine what fraction of Class I's surveyed for outflows have one
3) Compute surface densities for sources with good distances

CB 34 (below) at 3.6, 4.5, and 8 micron with 850 micron SCUBA data overlaid (from the archive). Class I (squares) and Class II (diamonds) sources are also overlaid. Image inset: DSS Blue (blue), IRAC 3.6 (green), IRAC 8 micron (red).

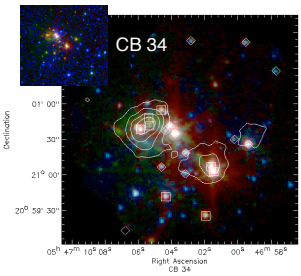

CB 34 (below) 2MASS extinction map in inverse greyscale and extinction contours Av = [2, 4, 6]. Class I (squares) and Class II (diamonds) sources are overlaid.

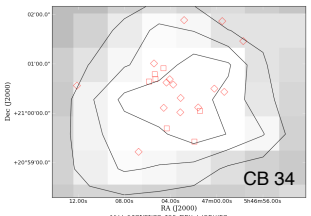

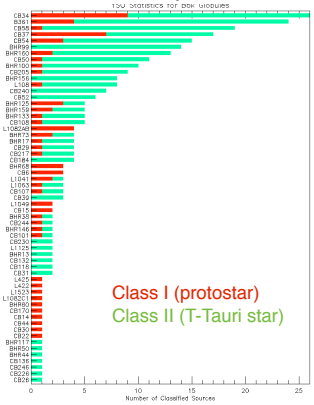

Ratio of Class I to Class II Sources

For each of the Bok globules, we counted the number of Class I and Class II candidates selected by Cluster Grinder and tabulated them (right). CB 34 appears to be an anomaly for Bok globules, with the highest number of YSOs and highest Class I/Class II ratio, i.e. it has a high rate of star formation. CB 58 (shown above) has a large number of Class II sources compared with Class I, and, along with its morphology, appears to be more like a bright-rimmed cloud than Bok globule.

Note: I would like to thank Mac Singularity (http://www.macsingularity.org) for the suggestion to use iWork Pages for this poster and for the basis template.

8.20 The Mistery of the Floating Stars around W3(OH)

Carlos G. Román-Zúñiga[1], **G. Megías Vázquez**[2,3], **J. Alves**[4], **E. A. Lada**[5]
[1] Instituto de Astronomía, Sede Ensenada, Universidad Nacional Autónoma de México
[2] Universidad de Sevilla, Spain
[3] Instituto de Astrofísica de Andalucía - CSIC, Granada, Spain
[4] University of Vienna
[5] University of Florida

Abstract

The W3 molecular cloud is a region of massive star formation with 3 distinct cluster populations. Deep near-infrared observations of the region southeast of W3 OH may indicate the presence of a low surface density component which could not be coeval with the W3 OH clusters. We discuss the plausibility of a distributed population in W3.

The Mistery of the Floating Stars Around W3(OH)

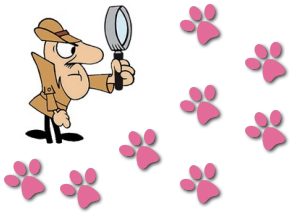

Carlos Román Zúñiga (IAUNAM)
Guillermo Megías (U. Sevilla-IAA)
Joao Alves (U. Vienna)
Elizabeth Lada (U. Florida)

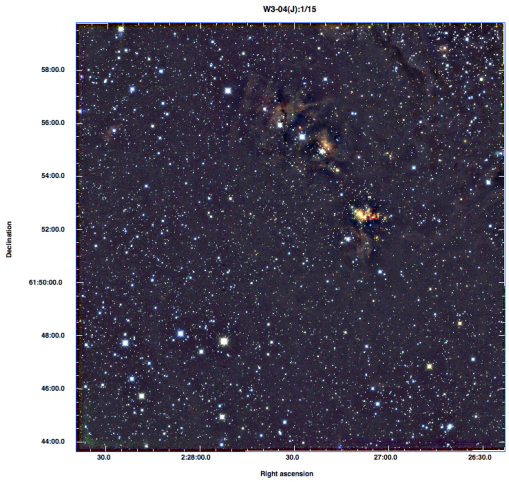

Calar Alto 3.5m JHK images reveal W3(OH) region in unprecedented detail. We selected this field for a study of the distribution of sources in and around W3(OH). With aid of mid-IR (Spitzer, WISE) catalogs we distinguish a number of young sources spread SE of the cluster chain. What are these sources? Could we have evidence for a distributed (non-cluster) population?

W3(OH) is a young stellar cluster with massive star formation, possibly the most recent in a 3-generation event which includes W3-Main and IC 1795. The W3(OH) cluster host an archetypical UCHII region and a group of maser sources. Studies have revealed at least one more association north of W3(OH), forming a chain of clusters. Deep NIR images also reveal a few more possible small embedded groups.

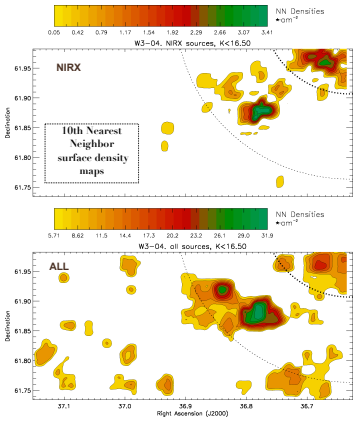

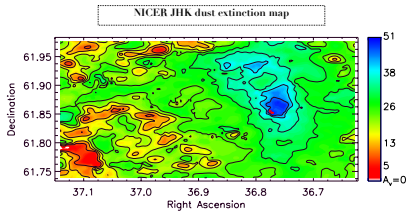

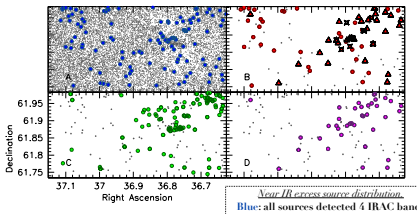

Near IR excess source distribution.
Blue: all sources detected 4 IRAC bands
Red: JHKL excess stars; Class I/II
Green: JHK excess stars
Magenta: hybrid NIR-MIR excess criteria

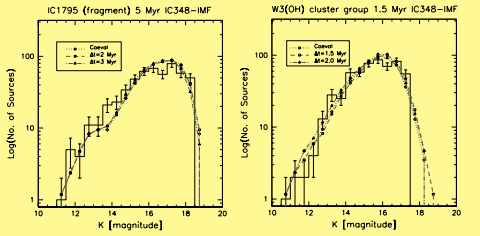

KLF median age fits. We made models of artificial embedded clusters (Muench et al 2001) over a sequence of ages (0.5 to 12 Myr) and compared the K band luminosity functions to obtain possible ages for the populations in the field. We used extinction and IRX fraction distributions according to each region, and a Trapezium-like IMF. The age of IC 1795 East fit well with a 5±2 Myr cluster (in good agreement with literature), the age of the W3(OH) cluster chain fit well with a 1.5±0.5 Myr cluster (as expected for a recent episode) and the bottom region, to the East of W3(OH) resulted into a significant population (over background) whose KLF can be fit well with a cluster model of 8±2 Myr. Could there be a population of small, dispersed groups from an older episode around W3(OH)?

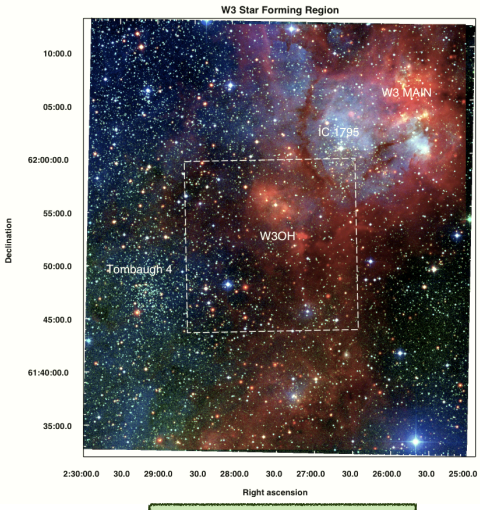

W3 is a complex region, where different episodes of formation mix in a rich cluster environment. In addition, open clusters like Tombaugh (8 Gyr, 3.95 kpc) lie nearby. A full scale study of the region, combining information from past and present multiwavelength

8.21 The Galactic O-Star Spectroscopic Survey (GOSSS). First results: A new O-Type classification atlas.

Alfredo Sota Ballano[1], J. Maíz Apellániz[1], R. H. Barbá[2], N. R. Walborn[3], E. Alfaro Navarro[1], R. C. Gamen[4], N. I. Morrell[5], J. I. Arias[2], and M. Penadés Ordaz[1]
[1] Instituto de Astrofísica de Andalucía - CSIC, Spain
[2] Departamento de Física, Universidad de La Serena, Benavente 980, La Serena, Chile
[3] Space Telescope Science Institute, 3700 San Martin Drive, Baltimore, MD 21218, USA
[4] Instituto de Astrofísica de La Plata-CONICET, Paseo del Bosque s/n, 1900 La Plata, Argentina
[5] Las Campanas Observatory, Observatories of the Carnegie Institution of Washington, La Serena, Chile

Abstract

The Galactic O-Star Spectroscopic Survey (GOSSS) is a project that is observing all known Galactic O stars with B < 13 (~ 2000 objects) in the blue-violet part of the spectrum with R ~ 2500. It is based on v2.0 of the Galactic O star catalogue (v1, Maíz Apellániz et al. [2004]; v2, Sota et al. [2008]). We have completed the first part of the main project. Here we present a new O-type classification atlas, which supersedes previous versions.

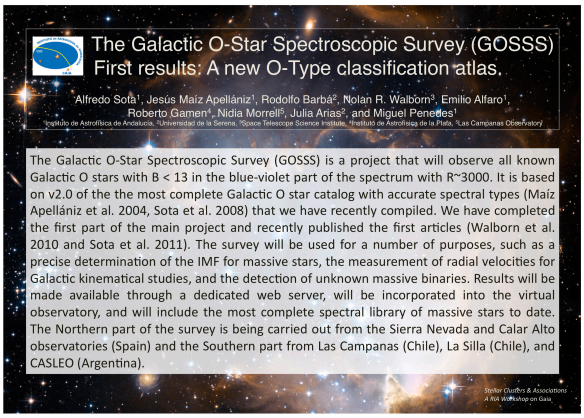
The Galactic O-Star Spectroscopic Survey (GOSSS)
First results: A new O-Type classification atlas.
Alfredo Sota[1], Jesús Maíz Apellániz[1], Rodolfo Barbá[2], Nolan R. Walborn[3], Emilio Alfaro[1], Roberto Gamen[4], Nidia Morrell[5], Julia Arias[2], and Miguel Penedes[1]
[1]Instituto de Astrofísica de Andalucía, [2]Universidad de la Serena, [3]Space Telescope Science Institute, [4]Instituto de Astrofísica de la Plata, [5]Las Campanas Observatory
The Galactic O-Star Spectroscopic Survey (GOSSS) is a project that will observe all known Galactic O stars with B < 13 in the blue-violet part of the spectrum with R~3000. It is based on v2.0 of the the most complete Galactic O star catalog with accurate spectral types (Maíz Apellániz et al. 2004, Sota et al. 2008) that we have recently compiled. We have completed the first part of the main project and recently published the first articles (Walborn et al. 2010 and Sota et al. 2011). The survey will be used for a number of purposes, such as a precise determination of the IMF for massive stars, the measurement of radial velocities for Galactic kinematical studies, and the detection of unknown massive binaries. Results will be made available through a dedicated web server, will be incorporated into the virtual observatory, and will include the most complete spectral library of massive stars to date. The Northern part of the survey is being carried out from the Sierra Nevada and Calar Alto observatories (Spain) and the Southern part from Las Campanas (Chile), La Silla (Chile), and CASLEO (Argentina).
Stellar Clusters & Associations
A RIA Workshop on Gaia

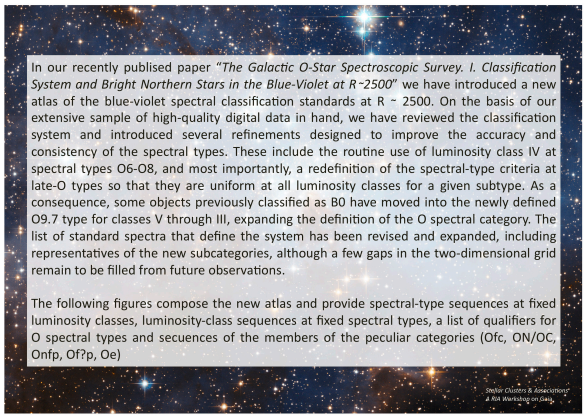
In our recently publised paper "*The Galactic O-Star Spectroscopic Survey. I. Classification System and Bright Northern Stars in the Blue-Violet at R ~2500*" we have introduced a new atlas of the blue-violet spectral classification standards at R ~ 2500. On the basis of our extensive sample of high-quality digital data in hand, we have reviewed the classification system and introduced several refinements designed to improve the accuracy and consistency of the spectral types. These include the routine use of luminosity class IV at spectral types O6-O8, and most importantly, a redefinition of the spectral-type criteria at late-O types so that they are uniform at all luminosity classes for a given subtype. As a consequence, some objects previously classified as B0 have moved into the newly defined O9.7 type for classes V through III, expanding the definition of the O spectral category. The list of standard spectra that define the system has been revised and expanded, including representatives of the new subcategories, although a few gaps in the two-dimensional grid remain to be filled from future observations.
The following figures compose the new atlas and provide spectral-type sequences at fixed luminosity classes, luminosity-class sequences at fixed spectral types, a list of qualifiers for O spectral types and secuences of the members of the peculiar categories (Ofc, ON/OC, Onfp, Of?p, Oe)
Stellar Clusters & Associations
A RIA Workshop on Gaia

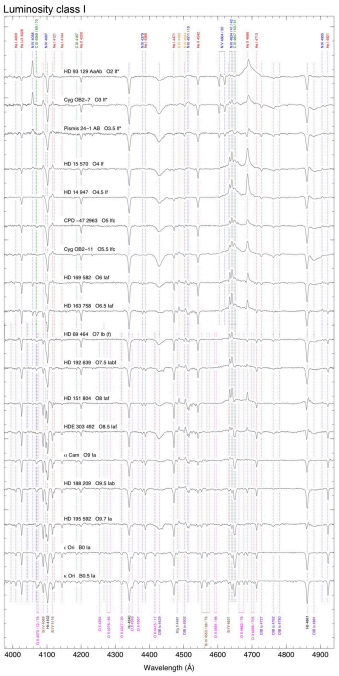
Luminosity class I
Wavelength (Å)

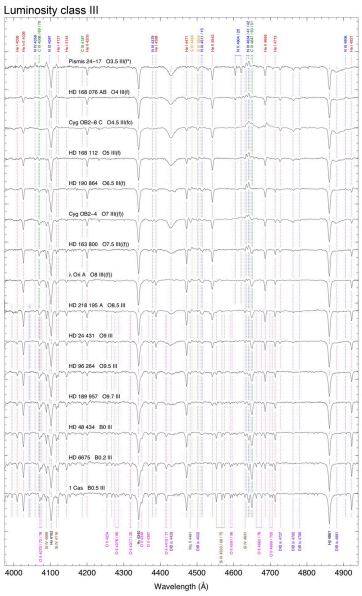
Luminosity class III
Wavelength (Å)

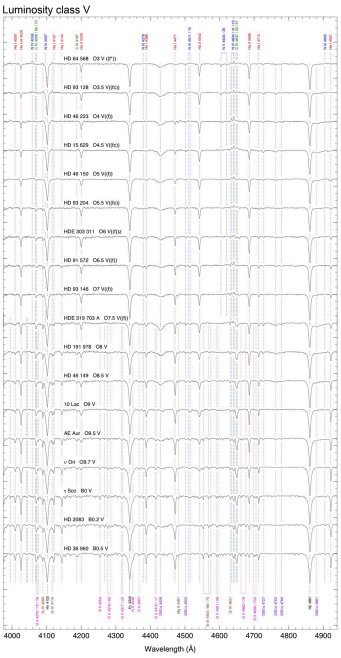
Luminosity class V
Wavelength (Å)

8.22 Chemical Tagging of Stellar Kinematic Groups: The Hyades Supercluster

Hugo M. Tabernero[1], D. Montes[1], J. I. González Hernández[2]
[1] Universidad Complutense de Madrid (UCM), Spain
[2] Instituto de Astrofísica de Canarias (IAC), Spain

Abstract

Stellar Kinematic Groups are kinematical coherent groups of stars which may share a common origin. These groups spread through the Galaxy over time due to tidal effects caused by galactic rotation and disk heating, however some chemical information remains unchanged.
The aim of chemical tagging is to show that abundances of every element in the analysis must be homogeneous between members. We have studied the case of the Hyades Supercluster in order to compile a reliable list of members (FGK stars) based on chemical tagging information.
This information has been derived from high-resolution echelle spectra obtained during our surveys of late-type stars. For selected northern stars of the Hyades Supercluster, stellar atmospheric parameters (Teff, log(g), ξ and [Fe/H]) have been determined using an automatic code which takes into account the sensibility of iron EWs measured in the spectra.
We have derived absolute abundances consistent with galactic abundance trends reported in previous studies. The chemical tagging method has been applied with a carefully differential abundance analysis of each candidate star, using a well-known member of the Hyades cluster as reference.

Chemical Tagging of Stellar Kinematic Groups: The Hyades Supercluster

H.M. Tabernero[1], D. Montes[1], J.I. González Hernández[1,2]

[1]Dpto. Astrofísica, Universidad Complutense de Madrid (UCM), Spain.
[2]Instituto de Astrofísica de Canarias (IAC), Spain.

Abstract

Stellar Kinematic Groups are kinematical coherent groups of stars which might share a common origin. These groups spread through the Galaxy over time due to tidal effects caused by galactic rotation and disk heating, however the chemical information survives. The aim of chemical tagging is to show that abundances of every element in the analysis must be homogeneous between members. We have studied the case of the Hyades Supercluster in order to compile a reliable list of members (FGK stars) based on chemical tagging information. For a total of 61 stars from the Hyades Supercluster, stellar atmospheric parameters ($T_{\rm eff}$, log *g*, ξ and [Fe/H]) have been determined using an own-implemented automatic code (*StePar*) which takes into account the sensibility of iron *EWs* measured in the spectra. We have derived absolute abundances consistent with galactic abundance trends reported in previous studies. The chemical tagging method has been applied with a carefully differential abundance analysis of each candidate member of the Hyades Supercluster, using a well-known member of the Hyades cluster as reference (vB 153). We find a **41 %** of membership candidates based on the differencial abundance analysis, proving that the Hyades Supercluster can not originate solely from the Hyades Cluster.

Sample selection

The sample was selected using kinematical criteria in ***U***, ***V*** galactic velocities taking a dispersion of ≈10 km/s around the core velocity of the group (Montes et al. 2001). We had taken also additional candidates and spectroscopic information about some of these stars from López-Santiago et al. (2010), Martinéz-Arnáiz et al. (2010), and Maldonado et al. (2010). Some exoplanet host star candidates are also taken from Montes et al. (2010).

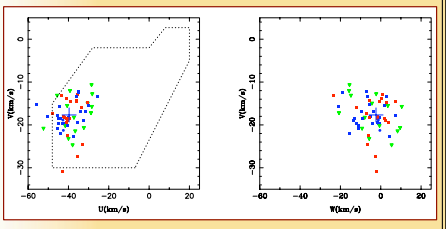

Fig. 1: *U, V, W* velocities for late-type stars candidate members of the Hyades Supercluster (Tabernero et al. 2011). Blue points are the final selected member stars. Red points are stars compatible with Hyades Fe abundance (but not for other elements), and the green ones not compatible. BZ Cet and V683 Per Hyades cluster members are denoted with circle blue points. The big blue cross indicates the core velocity of the Hyades Supercluster (Montes et al. 2001).

Observations

The spectroscopic observations (see Fig. 2) were obtained at the 1.2 m *Mercator* Telescope in La Palma in January, May and November 2010 with *HERMES*, a high resolution echelle spectrograph. The spectral resolution is 85000, the wavelength range covers from 3800 to 8750 Å. Our S/N ranges from 70 to 300 (160 on average) in the *V* band. A total of **92** stars have been observed. In this contribution only single stars (from F6 to K4.) have been analyzed, being **61** in total.

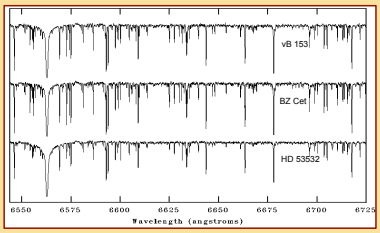

Fig. 2: High resolution spectra for some representative stars of our sample (see Table 1).

Stellar parameters

Stellar atmospheric parameters ($T_{\rm eff}$, log *g*, ξ and **[Fe/H]**) have been determined with a own-developed code (*StePar*, see Tabernero et al. 2011) which iterates until the slopes of χ *vs* log(*e*(Fe I)) and log(*EW*/λ) *vs* log(*e*(Fe I)) where zero and imposing ionization equilibrium: log(*e*(Fe I)) = log(*e*(Fe II)). Fig. 3 shows the $T_{\rm eff}$ and log *g* histogram for the stars analyzed (The obtained values for representative stars are given in Table 1).

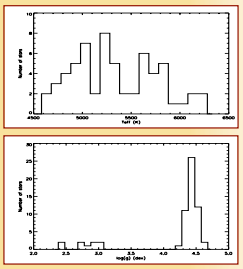

Fig. 3: $T_{\rm eff}$ and log*g* histogram of the sample.

Abundance determination

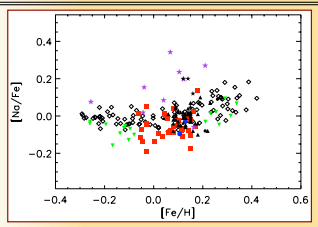

Fig. 4: [Na/Fe] *vs* [Fe/H]: open diamonds represent the thin disk data (González Hernández et al. 2010), black filled triangles represent Hyades cluster data (Paulson et al. 2003). Red points are our stars compatible with Hyades Fe abundance, and the green ones not compatible. BZ Cet and V683 Per Hyades cluster members are marked with blue circles. Purple starred points represent the giant stars. Black starred points are the candidates selected stars in De Silva et al. (2011), black circles are those selected in Pompéia et al. (2011).

Absolute abundances have been calculated using the equivalent width (*EW*) method in a line-by-line basis. Line lists were taken from (González Hernández et al. 2010) and the *EW* measured with the *ARES* code (Sousa et al. 2007). Abundance analysis was carried out with the *MOOG* code (Sneden 1973) using our determined atmospheric parameters and a solar spectrum taken with the same instrumental configuration. Our abundance trends seem to be consistent with the thin disk solar analogs (González Hernández et al. 2010) as shown in Figs. 4 and 5. Representative abundances are given in Table 1.

Name	$T_{\rm eff}$(K)	log *g*	ξ (km/s)	[Fe/H]	[Na/H]	[Mg/H]	[Si/H]	[Ca/H]
vB 153	5235 ± 36	4.45 ± 0.11	1.14 ± 0.06	0.06	-0.04	-0.04	0.13	0.09
BZ Cet	5035 ± 37	4.38 ± 0.11	0.98 ± 0.08	0.11	0.09	0.09	0.25	0.15
HD 53532	5698 ± 17	4.56 ± 0.05	1.10 ± 0.03	0.12	0.08	0.03	0.18	0.22

Table 1: Example table of determined **parameters** and **abundances** as well as the typical parameter errors. **vB 153** is the Hyades cluster reference star used in the differential analysis, **BZ Cet** is a Hyades cluster confirmed member, and **HD 53532** is a Hyades Supercluster candidate star that satisfies chemical homogeneity.

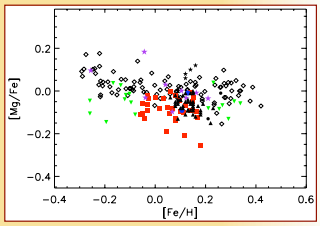

Fig. 5: As Fig. 4, for [Mg/Fe] vs [Fe/H].

Differential abundances

Differential abundances **Δ[X/H]** have been determined by comparison with a reference star known to be member of the Hyades cluster (**vB 153**) in a line-by-line basis (see Paulson et al. 2003 and De Silva et al. 2006). We have computed the differential abundances for the following elements: **Fe**, **Na**, **Mg**, **Al**, **Si**, **Ca**, **Sc**, **Ti**, **V**, **Cr**, **Mn**, **Co**, and **Ni**, the most representative of them are shown in Figs. 6 to 10. A first candidate selection within the sample has been determined by applying a 1-rms rejection for the **Fe** abundance results. In this subsample another 1-rms diagnostic has been applied in order to prove homogeneity in each element (see Figs. 7 to 10).

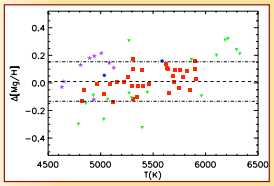

Fig. 7: As Fig. 6, for Δ[Mg/H] vs $T_{\rm eff}$.

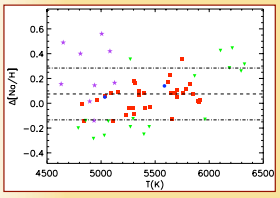

Fig. 8: As Fig. 6, for Δ[Na/H] vs $T_{\rm eff}$.

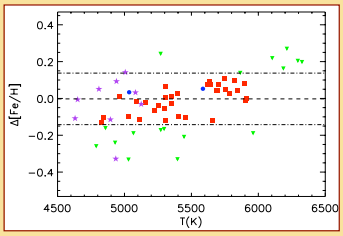

Fig. 6: Δ[Fe/H] differential abundance vs $T_{\rm eff}$. Dashed-dotted lines represent 1-rms level for the Hyades cluster. The dashed line represents the median abundance. Red points are accepted as a preliminary selection of candidates, while green ones are rejected. The Hyades cluster member BZ Cet and V683 Per are marked with **blue points**. Purple starred points represent the giant stars.

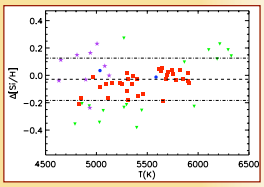

Fig. 9: As Fig. 6, for Δ[Si/H] vs $T_{\rm eff}$.

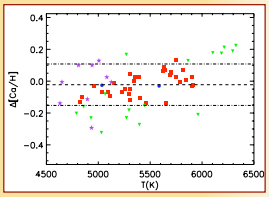

Fig. 10: As Fig. 6, for Δ[Ca/H] vs $T_{\rm eff}$.

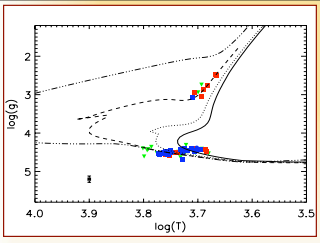

Fig. 11: Spectroscopic log $T_{\rm eff}$ vs log *g* for the candidate stars. We have employed the Yale-Yondale ischrones (Demarque et al. 2004) for Z=0.025 and 0.1, 0.7, 4 and 13 Gyr (from left to right). Mean error bars are represented at the right bottom. Blue points are the final selected member stars. Red points are stars compatible with Hyades Fe abundance (but not for other elements), and the green ones not compatible. BZ Cet and V683 Per Hyades cluster members are denoted with circle blue points.

Conclusions

We have computed the stellar parameters and their uncertainties for 61 single Hyades Supercluster candidate stars, after that we have obtained the chemical abundances of 12 elements, and the differential abundances. From the chemical tagging analysis we have found that 25 stars from the original sample are homogeneous in abundances for all the elements we have considered (a **41 %** of the sample), 5 stars fail to be homogeneous in one element. The selected stars are consistent (within the error bars) with the Hyades age (0.7 Gyr, see Fig. 11). A more detailed analysis to check consistency between the different age indicators and the chemical homogeneity is in progress.

References

- Demarque, P., et al. 2004, ApJS, 155, 667
- De Silva G.M., et al. 2006, ApJ, 131, 455
- De Silva G.M., et al. 2011, MNRAS, in press (arXiv:1103.2588)
- González Hernández J.I., et al. 2010, ApJ, 720, 1592
- López-Santiago J., et al. 2010, A&A, 514, A97
- Maldonado J., et al. 2010, A&A, 521, A12
- Martinéz-Arnáiz R., et al. 2010, A&A, 520, A79
- Montes D., et al. 2001, MNRAS, 328, 45
- Montes D., et al. 2010, ASP Conf. Ser., 430, 507
- Paulson D.B., et al. 2003, ApJ, 125, 3185
- Pompéia ,et al. 2011, MNRAS, in press (arXiv:1101.2583)
- Sneden C. 1973, PhD Dissertation
- Sousa S.G., et al. 2007, A&A, 469, 783
- Tabernero H.M., et al. 2011, A&A, submitted

Acknowledgments: This work was supported by the Universidad Complutense de Madrid (UCM), the Spanish Ministerio de Ciencia e Innovación (MCINN) under grant AYA2008-000695, and "The Comunidad de Madrid under PRICIT project S2009/ESP-1496 (AstroMadrid).

8.23 Kinematic Determination of the Luminosity Function in the Solar Neighbourhood

Belén Vicente[1,2], **F. Garzón**[1,3], **A. Cabrera-Lavers**[1]
[1] Instituto de Astrofísica de Canarias (IAC), La Laguna, Tenerife, Spain
[2] Instituto de Astrofísica de Andalucía - CSIC, Granada, Spain
[3] Universidad La Laguna, Tenerife, Spain

Abstract

The luminosity function is not only crucial to know stellar density distribution in space, and thus to know the structure of the Galaxy, but it allows the determination of the stellar mass function using the mass-luminosity relationship.
The luminosity function and mass function are fundamental to the understanding of star formation and the evolution of the Milky Way. It is customary to assume that the luminosity function in the solar neighbourhood, which can be obtained directly from precise star counts, well represents that of the Galactic disk, if not over the whole Galaxy and external galaxies of similar morphological type.
Under this assumption, we simply need to calculate in the solar vicinity and then move it to the disk area of interest. In this regard, the larger the sample used for the determination the more reliable the extrapolation to galactic studies.
We have determined the luminosity function in the solar neighbourhood up to 200 pc considering the proper motions as distance estimators. We used the parameter "reduced proper motion" (Luyten [1938]) for calibration of the apparent magnitudes to absolute ones.
This calibration must be done with kinematically similar populations, i.e., they share the same velocity distribution. So, prior to calculating the luminosity determination we used the SKY model (Wainscoat et al. [1992]) to separate stars with different kinematic evolution in our catalogue.
As our kinematical database, we used the CdC-SF Catalogue (Vicente et al. [2010]), which has proper motion precision similar to that of Hipparcos but up to much fainter magnitudes (V = 15). Such a rich data allow getting the luminosity function for distances greater than those identified so far by extending existing results. Having stars at greater distances implies that we can get information covering the bright field of the luminosity function. Also, a larger sample with smaller proper motions produces a luminosity function that is more adapted to the real Galaxy model thanks to a smaller correction factor.

Kinematic determination of the luminosity function in the neighborhood

Belén Vicente [1,2], F. Garzón [1,3], A. Cabrera-Lavers [1]

(1) Instituto de Astrofísica de Canarias (IAC), La Laguna, Tenerife, Spain
(2) Current address: Instituto de Astrofísica de Andalucía (IAA-CSIC), Granada, Spain
(3) Universidad La Laguna, Tenerife, Spain

AIMS

The luminosity function is crucial to know the structure of the galaxy as well as allowing the determination of the stellar mass function, two functions essential to know the star formation and evolution of the galaxy.

At present, all studies of the local luminosity function, the distance limit studied is given by the limiting magnitude of stars with accurate proper motions and distances.

In this work we have determined the luminosity function in the solar neighborhood up to 200 pc, whereas the proper motions as estimates of distances, using the method of mean absolute magnitudes.

SAMPLE TO STUDY

The sample chosen to determine the LF is out from the galactic plane and is complete (Fig. 1):

- spatially (260° < l < 340°, 45° < b < 60°)

- photometrically (Ks ≤ 12, less sensitive to extinction)

- kinematically (μ ≥ 0.03 "/ year)

Kinematic database: CdC-SF catalogue (Vicente et al. 2007, 2010), with precise proper motions similar to that of Hipparcos up to V = 16 and uniformity of data.

Photometric database: CdC-SF includes JHKs photometry from 2MASS catalogue (Cutri et al. 2003)

The detemination of the H-M regression to calibrate, we use the Hipparcos catalogue (ESA 1997) which includes trigonometric parallax up to V = 8.

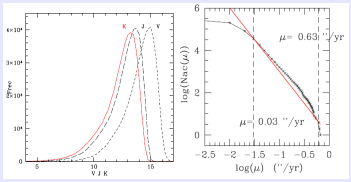

Fig. 1

(a) Magnitude distribution of the CdC-SF stars.

(b) Proper motion distribution of CdC-SF. Densities follow the law N (μ) ~ μ^{-3}. We consider completeness 0.03 "/year ≤ μ ≤ 0.63"/year.

MEAN ABSOLUTE MAGNITUDES METHOD

The parameter **H, reduced proper motion** (Luyten 1938), defined similarly to the absolute magnitude M, it is used as a statistical estimator M:

$$\left.\begin{aligned} M_\lambda &= m + 5 - 5\log d \\ H_\lambda &= m + 5 + 5\log\mu \\ \mu &= \frac{V_t}{4{,}74\ d} \end{aligned}\right\} \Rightarrow M = H_\lambda + 3.38 - 5\log V_t$$

Proper motion is directly related to the absolute magnitude M, **if Vt is independent of M**. So, with a sample of stars with the same distribution we have

Vt = a + b <M> H

Determined the relationship <M> = a + b H with calibration stars, we can obtain absolute magnitudes for all stars in our sample.

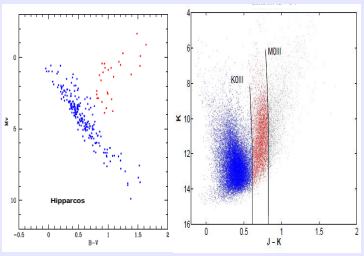

Fig. 2 Photometric separation of populations with similar kinematic: dwarf (blue) and giants (red):

(a) Hipparcos HR diagram and manual stellar classification.

(b) Color-magnitude diagrams of CdC-SF and dividing traces in a field near the galactic plane as example.

PROCEDURE

Luminosity Function: number of stars Φ (M) per unit of magnitude and volume.

The application of the Luyten's method to transform apparent magnitudes into absolute required to have a group of stars that share the same velocity distribution.

This separation of populations with similar kinematics performed following the photometric criteria, because dwarfs and giants have a different cinematic history:

- Separation of the calibration stars of Hipparcos has done manually (Fig. 2a)

- In our sample, the separation is done using theoretical traces given by the SKY model (Wainscoat et al. 1992). An example is shown in Fig. 2b.

RESULTS

We obtained the calibration equations to relate the proper motion reduced with the absolute magnitude (Fig. 3), and are as follows:

$$DWARFS: \quad M_K = -2.91\,(\pm 0.45) + 0.74\,(\pm 0.06) H_K \,;\, \sigma_M = 0.97$$
$$GIANTS: \quad M_K = -5.27\,(\pm 0.67) + 1.33\,(\pm 0.20) H_K \,;\, \sigma_M = 0.67$$

Malmquist bias and Lutz-Kelker corrections were found to be negligibles.

We have determined the Luminosity Function up to 200 pc (Fig. 4). It agrees perfectly with the transformation, in the K band, calculated by Mamon & Soneira (1982) from the semi-empirical Luminosity Function of Bahcall & Soneira (1980).

In case of dwarfs stars (Fig. 4a), there is a deficit of faint and near stars that are not included in our catalogue CdC-SF due to its construction itself (Fig. 5). In the future, we will add high proper motion catalogs to solve this problem.

For giant stars (Fig. 4b), not just our data agree very well, but extending to the current observations.

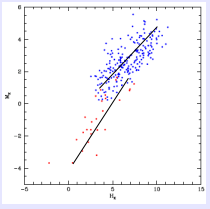

Fig. 3 H-M linear relations used for calibration, different for each type of population. Fitting has been made by least squares weighted according to the observational errors.

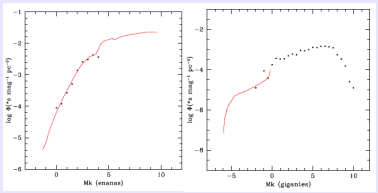

Fig. 4 Transformation of stellar luminosity function into JHK band (Mamon & Soneira 1982) of the analitical function determinated visual band (Bahcall & Soneira 1980), for giants (left) and dwarfs (right).

REFERENCES

- Bahcall, J. N. & Soneira, R. M. 1980, ApJ 238, 17
- Cutri, R.M et al. 2003, NASA/IPAC Infrared Science Archive
- ESA 1997, SP 1200
- Luyten, W. J. 1938, MNRAS 98, 677
- Mamon, G. A. & Soneira, R. M. 1982, ApJ 255, 181
- Vicente, B., Abad, C. & Garzón, F. 2007, A&A 471, 1077
- Vicente , B., Abad, C., Garzón, F. & Girard, T. 2010, A&A 510, 78
- Wainscoat, R. J. 1992, ApJS 83, 111

Contact : Belén Vicente, bvicente@iaa.es

8.24 A Detailled 2D Spectroscopic Study of the Central Region of NGC 5253

Ana Monreal-Ibero[1,2], **José M. Vílchez**[1], **J. Walsh**[2], **C. Muñoz-Tuñón**[3]
[1] Instituto de Astrofísica de Andalucía - CSIC, Granada, Spain
[2] European Southern Observatory
[3] Instituto de Astrofísica de Canarias (IAC), Spain

Abstract

We present Integral Field Spectroscopy observations of NGC 5253, a very nearby (d $\sim$ 3.8 Mpc) HII galaxy. This type of observations allows the detailed study of the interplay between gas, dust and stars. Here, we will focus on recent results related to the cause of the local enrichment of nitrogen found for this galaxy as well as on its kinematics. In particular, for the first time we show maps with the velocities derived from H_α and [NII] in a starburst galaxy. Further details on these and other issues can be found in Monreal-Ibero et al. [2010], A&A, 517A, 27.

A detailed 2D spectroscopic study of the central region of NGC5253

A. Monreal-Ibero[1,2], J. M. Vílchez[1], J. Walsh[2], C. Muñoz-Tuñón[3]

[1]IAA-CSIC, [2]ESO, [3]IAC

Abstract:

We present Integral Field Spectroscopy observations of NGC5253, a very nearby (d~3.8 Mpc) HII galaxy. These type of observations allows the study in detail of the interplay between gas, dust and stars. Here, we will focus on recent results related with the cause of the local enrichment of nitrogen found for this galaxy as well as on its kinematics. In particular, we show for the first time maps with between the velocities derived from Hα and [NII] in an starburst galaxy. Further details on these and other issues can be found in Monreal-Ibero et al. 2010, A&A, 517A, 27.

1. The galaxy

NGC5253 is an Irr galaxy located in the Centaurus A/M83 group suffering a starburst triggered by an encounter with M83. Its clusters in the central region have masses of 2-120x10^3 $M_\odot$ and ages ~1-120 Myr (Harris et al. 2004, ApJ, 603, 503). In the nucleus, there are two very massive SSCs separated by 0.4" (Alonso-Herrero et al. 2004, ApJ, 612, 222). This galaxy presents a local increase in the abundance of nitrogen whose cause has not been fully clarified.

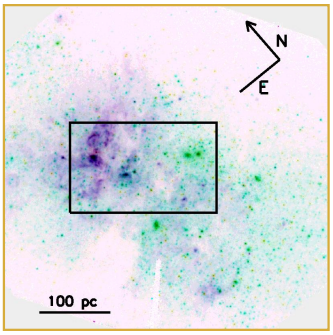

2. The observations

Data were obtained with FLAMES (Pasquini et al. 2002, The Messenger, 101, 1) at at the VLT, using the ARGUS mode with a sampling of 0.52"/lens (f.o.v.=11.5"x7.3"). We used the L682.2 and L479.7 gratings which provide with resolutions of 13700 and 12000, covering respectively the spectral ranges of 6440-7180Å and 4500-5080Å.

Fig 1. False color image in filters F435W (blue), F658N (magenta) and F814W (green) with the area covered by FLAMES data overplotted as a rectangle.

3. Extra nitrogen, Wolf-Rayets and HeII

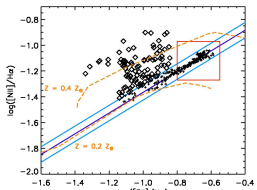

Fig 2. [SII]/Hα vs. [NII]/Hα diagram. The red box contains the data utilized to determine our normal [SII]/Hα-[NII]/Hα relation. Data above and below the 3-σ level were represented with diamonds and crosses. The expected line ratios for HII regions with Z=0.2$Z_\odot$ and Z=0.4$Z_\odot$ and ages in the range of 2-6 Myr (Dopita et al. 2006) are over-plotted for comparison.

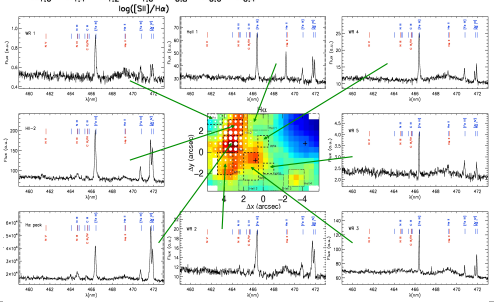

Fig 3. *Central map:* Spaxels with [NII]/Hα line ratio above the 3- σ level on top of our Hα map. Size of the white circles is proportional to the excess in [NII]/Hα. Dashed and dotted lines delimit the apertures utilized to extract the spectra with Wolf-Rayet and nebular HeII features. The position of the three peaks of continuum emission are marked with crosses. *Surrounding ring:* Spectra showing the Wolf-Rayet features. The positions of the nebular emission lines have been indicated with blue ticks and labels, while those corresponding to Wolf-Rayet features appear in red.

Extra N, as deduced from the excess in [NII]/Hα, is found up to ~60 pc from the maximum pollution. WR features are distributed over a larger area and associated with young stellar clusters. He^{++} was detected in areas not coinciding, in general, with those with WR features or extra nitrogen.

4. Kinematics

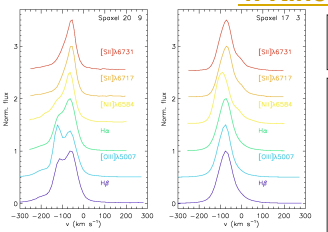

Fig 4. Two examples showing the complexity of the profiles for the main emission lines.

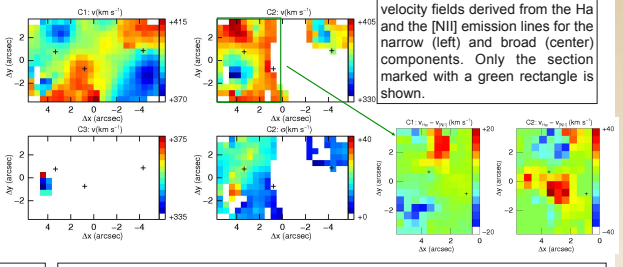

Fig 5. *2x2 panel on the left:* Kinematical information derived from the Hα emission line. Left: Velocity field for the two nqrrow components. Right: Velocity field (upper) and velocity dispersion map (lower) for the broad component. *2x1 panel on the right*: Difference between the velocity fields derived from the Ha and the [NII] emission lines for the narrow (left) and broad (center) components. Only the section marked with a green rectangle is shown.

Up to three emission components were needed to reproduce the line profiles. One of them, associated with the giant HII region, presents supersonic widths and [NII] and [SII] lines shifted up to 40 km/s with respect to Hα. Similarly, one of the narrow components presents offsets in [NII] of <20km/s. This is the first time that maps providing such offsets for a starburst galaxy have been presented.

(based on Monreal-Ibero et al. 2010, A&A, 517A, 27)

8.25 Molecular Hydrogen Outflows and their Exciting Sources in Ophiuchus

Miaomiao Zhang[1,2], W. Brandner[1], H. Wang[2], Th. Henning[1], R. Gredel[1]
[1] Max Planck Institute for Astronomy, Germany
[2] Purple Mountain Observatory, China

Abstract

We performed a deep search for molecular hydrogen outflows (MHOs) toward the ρ Ophiuchi molecular cloud, covering an area of ~ 0.11 deg^2. In total, six new MHOs are discovered and 30 known MHOs are detected, too. Using previously-published H_2 images, we measured proper motions for H_2 features in 29 outflows and associated them with 22 young stellar objects (YSOs). Among 22 outflow sources, there are 12 ($\sim 54.5\%$) Class II sources, which means that we detected many low power jets from more evolved classical T Tauri stars. About 35% Class I sources and 25% Class II sources drive H_2 outflows, which indicates that the lifetime of H_2 outflows should be roughly approximate to the evolutionary time scale of low-mass young stars.

Molecular hydrogen outflows and their exciting sources in Ophiuchus

M. Zhang[1,2]; W. Brandner[1]; H. Wang[2]; Th. Henning[1]; R. Gredel[1]

[1]Max Planck Institute for Astronomy, Germany; [2]Purple Mountain Observatory, China

Abstract

We performed a deep search for molecular hydrogen outflows (MHOs) towards the ρ Ophiuchi molecular cloud, covering an area of ~ 0.11 deg^2. In total, six new MHOs are discovered and 30 known MHOs are detected, too. Using previously-published H_2 images, we measured proper motions for H_2 features in 29 outflows and associated them with 22 young stellar objects (YSOs). Among 22 outflow sources, there are 12 (~54.5%) Class II sources, which means that we detected many low power jets from more evolved classical T Tauri stars. About 35% Class I sources and 25% Class II sources drive H_2 outflows, which indicates that the lifetime of H_2 outflows should be roughly approximate to the evolutionary time scale of low mass young stars.

The project

This work is part of the project which aims to understand the dynamic characteristic of outflows in Ophiuchus. Its objectives include:

- To obtain jet radial velocity information with the VLT/CRIRES.
- To obtain jet proper motions with multi-phase astrometry from NTT/SOFI.
- To determine independently the flow orientation and the shock physics with models.

The data

The *observations* are conducted using ESO NTT/SOFI. Data reduction uses IRAF packages and proper motion measurements use the cross-correlation method suggested by Davis et al. (2009).

Log of observations

Year	PID	H_2	Ref
2000	65.I-0576(A)	480s	Gómez et al. (2003)
2001	67.C-0284(A)	600s	Khanzadyan et al.(2004)
2007	79.C-0717(B)	1260s	this work

The region

left, background: 2MASS K band image; gray, green, red boxes: the coverage of *SofI* (2007), *SofI* (2001) and *SofI* (2000) observations, respectively; filled circles: YSOs
right, the background: *SofI* (2007) H_2 mosaic; gray contours: continuum emission at 1.1mm; green triangles: millimeter sources; squares and pluses: MHO features; blue circles: YSOs.

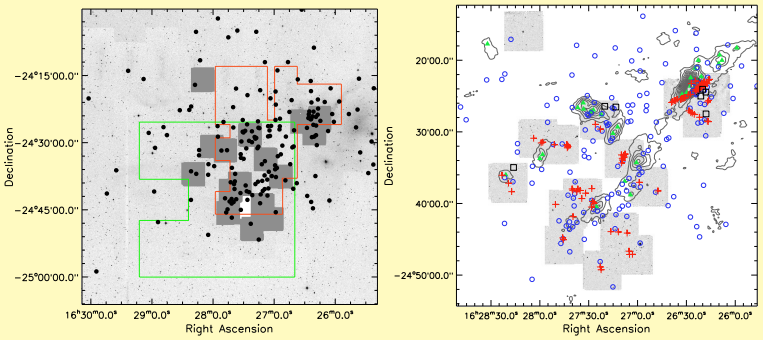

Results

This figure shows the PMs of some MHOs. Most of MHOs in this region are driven by VLA 1623, a well-known Class 0 source. The red triangles mark the positions of MHO features and the solid arrow label their proper motions. Note that the dashed lines represent the errors of PA. Pink circles mark YSOs, green diamonds mark sub-millimeter sources and blue squares label millimeter sources.

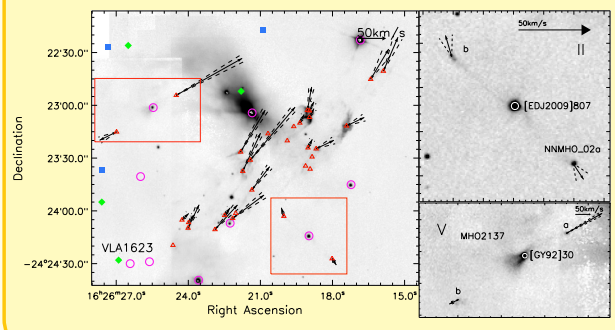

Discussion

Histogram shows the number of YSOs and outflow sources with a given value of spectral index (α): *Left* for Ophiuchus and *right* for Orion A. Open columns represent all YSOs and black columns represent outflow sources. Compared to Orion A, we detected many low power jets from T Tauri stars in Ophiuchus. We also estimate that about about 36.8% Class I sources and about 23.4% (this fraction is corrected considering the extinction and the detection sensitivity) Class II sources drive H_2 outflows in Ophiuchus. We note that these two values are approximately the same considering the statistical errors. Hence, the fraction of YSOs driving H_2 outflows seems to be independent of the evolutionary age of the driving sources.

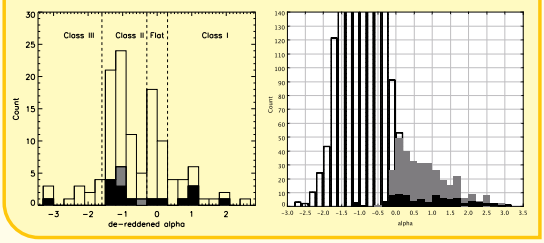

Summary

- We detected 6 new and 30 known molecular hydrogen outflows (MHOs) with NTT/SOFI images in Ophiuchus.
- We obtained the proper motions of 29 MHOs (typical value is 30-120 mas/yr or 15-70 km/s) using multi-phase astrometry from NTT/SOFI images.
- We identified 22 likely exciting sources for 29 MHOs based on the MHO morphology and PM analysis.
- We detected about 12 low power jets from Class II sources, which indicates that outflows are prevalent for extended periods of time living of low mass star formation.
- We estimated that ~35% Class I sources and ~25% Class II sources drive H_2 outflows, which indicates that the lifetime of H_2 outflows should be roughly approximate to the evolutionary time scale of low mass young stars in Ophiuchus.

Future Work

- Analyze the dynamic and physical properties of these outflow together with the radial velocity information obtained from VLT/CRIRES.
- As an outflow sample to study jet formation through high-resolution astrometric observations such as VLTI/GRAVITY.

References

[1] C. J. Davis et al. 2009, A&A, 496, 153
[2] M. Gómez et al. 2003, AJ, 126, 863
[3] T. Khanzadyan et al. 2004, A&A, 426, 171

Index